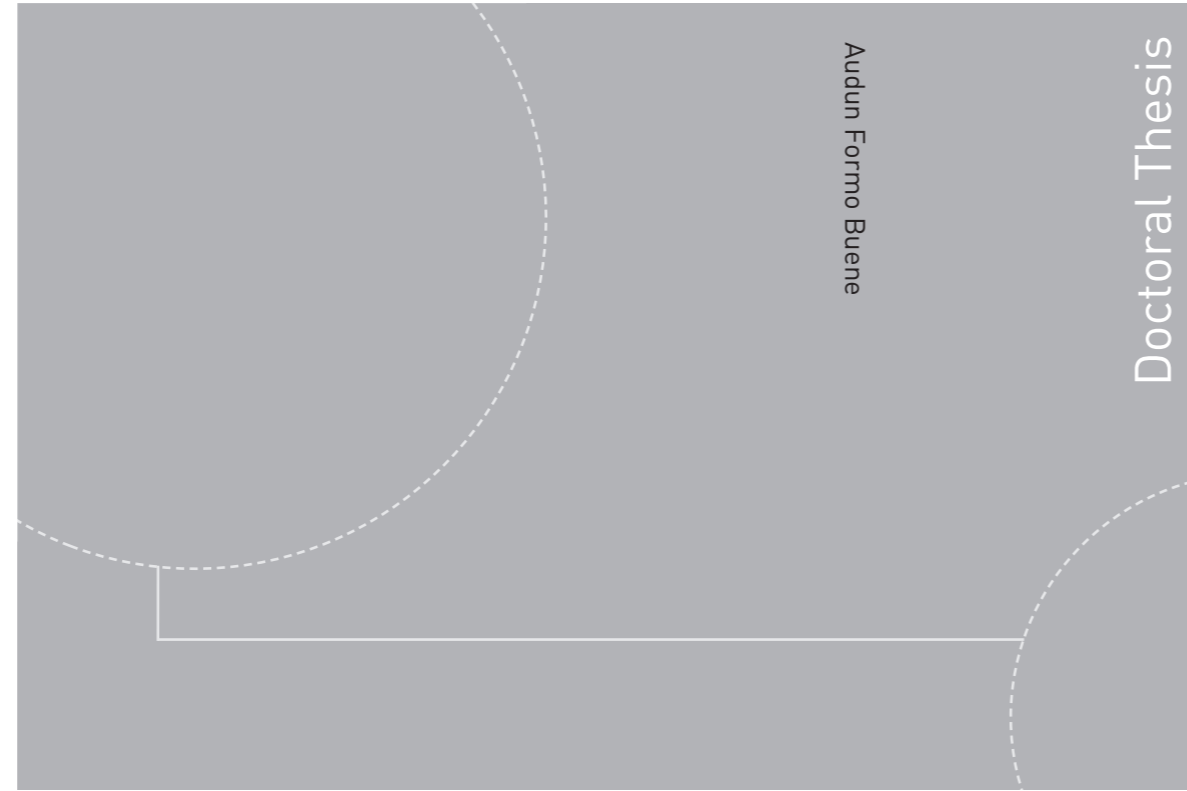


ISBN 978-82-326-4104-8 (printed version)  
ISBN 978-82-326-4105-5 (electronic version)  
ISSN 1503-8181



Doctoral theses at NTNU, 2019:254

Audun Formo Buene

**Molecular Engineering and  
Photovoltaic Evaluation of  
Phenothiazine and Triarylamine Dyes  
for Dye-Sensitized Solar Cells**

Audun Formo Buene

# Molecular Engineering and Photovoltaic Evaluation of Phenothiazine and Triarylamine Dyes for Dye-Sensitized Solar Cells

Thesis for the degree of Philosophiae Doctor

Trondheim, September 2019

Norwegian University of Science and Technology  
Faculty of Natural Sciences  
Department of Chemistry



Norwegian University of  
Science and Technology

**NTNU**

Norwegian University of Science and Technology

Thesis for the degree of Philosophiae Doctor

Faculty of Natural Sciences

Department of Chemistry

© Audun Formo Buene

ISBN 978-82-326-4104-8 (printed version)

ISBN 978-82-326-4105-5 (electronic version)

ISSN 1503-8181

Doctoral theses at NTNU, 2019:254



Printed by Skipnes Kommunikasjon as

## ACKNOWLEDGEMENTS

This thesis is the result of four years of work at the Department of Chemistry at the Norwegian University of Science and Technology (NTNU) from August 2015 to July 2019 under the supervision of professor Bård Helge Hoff, associate professor Odd Reidar Gautun and professor Bjørn Kåre Alsberg. In addition, during the autumn of 2018 I had a truly wonderful research stay at the Laboratory of Photomolecular Science (LSPM) at École Polytechnique Fédérale de Lausanne (EPFL) under the supervision of professor Anders Hagfeldt. The PhD funding was provided by the Faculty of Natural Sciences, while the Department of Chemistry financed the stay in Switzerland and a lot of the laboratory equipment.

Moving from medicinal chemistry to the field of organic photovoltaics is no small step, and I have to thank Bård for entering this field with me and supporting me all the way. I am grateful for the liberty you have given me in pursuing crazy ideas, and the motivation and encouragement in the moments when it has been most needed. A huge thank you also goes to Odd for fruitful discussions on chemistry and all the good stories. In addition, I would like to thank the award-winning scientist PhD student David Moe Almenningen for taking over the management of the solar lab and for excellent help with Paper VI. Thank you to Bjørn Kåre Alsberg for being such a visionary and starting the idea of the Centre of Organic Electronic Materials at NTNU, you are missed. I also want to thank associate professor Solon Economopoulos for all the help in buying equipment and setting up the solar cell lab, in addition to instructions on electrochemistry. To Anders Hagfeldt, who invited me to EPFL for a research stay in the LPI/LSPM laboratories, and to the rest of my friends in Lausanne, thank you for making it such a fruitful and memorable stay.

I am grateful to all my colleagues at the Department of Chemistry. Starting a new field of research requires a lot of effort also from technical staff and others. Thank you for your patience and enthusiasm about the new solar cell lab, it has made a big difference. A special mention has to go to staff engineer Roger Aarvik, for relentlessly providing a steady flow of chemicals to the solar cell lab, wonderful stories and perpetual optimism, thank you.

To my friends through nine years in Trondheim, thank you for making this such a joyful and memorable time! To the past, present and future members of the Hoff/Sundby family research group and members of the new solar cell lab; thank you for creating

a superb social and scientific environment, both inside and outside the laboratories.

To my family, thank you for always being there for me. Without your continuous support and encouragement, this thesis would be a pretty dreary spectacle.

# CONTENTS

<b>Abstract</b>	<b>VII</b>
<b>Sammendrag</b>	<b>IX</b>
<b>List of Publications</b>	<b>XI</b>
<b>Abbreviations</b>	<b>XIII</b>
<b>Symbols</b>	<b>XV</b>
<b>Preface</b>	<b>1</b>
<b>1 Introduction part I: Application</b>	<b>5</b>
1.1 Energy consumption and production . . . . .	5
1.2 Solar energy . . . . .	6
1.3 Solar cells . . . . .	8
1.4 Dye-sensitized solar cells . . . . .	11
1.4.1 Working principles . . . . .	12
1.4.2 Components . . . . .	14
1.4.3 Other devices based on DSSC architecture . . . . .	19
1.5 DSSC characterization . . . . .	22
1.5.1 <i>J-V</i> characteristics . . . . .	22
1.5.2 Incident photon-to-electron conversion efficiency (IPCE) . . . . .	24
1.5.3 Charge extraction and electron lifetime measurements . . . . .	26
1.5.4 Component characterization . . . . .	28
<b>2 Introduction part II: Sensitizers</b>	<b>33</b>
2.1 Metal-free sensitizers . . . . .	34
2.2 Phenothiazine sensitizers . . . . .	36
2.2.1 Common synthetic routes . . . . .	38
2.2.2 Dyes based on analogues of phenothiazine . . . . .	40
2.2.3 Synthesis of phenothiazine scaffolds . . . . .	41
2.3 Photovoltaic performance of phenothiazine sensitizers . . . . .	43
2.4 Triarylamine sensitizers . . . . .	51

2.5	Suzuki cross-coupling . . . . .	53
2.5.1	Mechanism . . . . .	53
2.5.2	Selectivity . . . . .	56
2.5.3	Challenges . . . . .	57
2.6	Miyaura borylation . . . . .	57
2.7	Buchwald–Hartwig amination . . . . .	58
2.8	Knoevenagel condensation . . . . .	60
<b>3</b>	<b>Results and Discussion of Papers</b>	<b>63</b>
3.1	Summary of Papers I–V . . . . .	63
3.1.1	Paper I . . . . .	63
3.1.2	Paper II . . . . .	64
3.1.3	Paper III . . . . .	68
3.1.4	Paper IV . . . . .	69
3.1.5	Paper V . . . . .	70
3.2	Synthesis . . . . .	71
3.2.1	3,7-Dibromo-10-hexyl-10 <i>H</i> -phenothiazine route . . . . .	71
3.2.2	7-Bromo-10-hexyl-10 <i>H</i> -phenothiazine-3-carbaldehyde route . . . . .	72
3.2.3	7-Bromo-2-chloro-10-hexyl-10 <i>H</i> -phenothiazine route . . . . .	73
3.2.4	3,7-Dibromo-10-aryl-10 <i>H</i> -phenothiazine route . . . . .	73
3.2.5	Synthesis of reference sensitizers . . . . .	74
3.3	Photovoltaic summary from Paper I–V . . . . .	76
3.4	Paper VI: CDCA-substituted triarylamine dyes . . . . .	79
3.4.1	Synthesis strategy . . . . .	79
3.4.2	Photovoltaic performance . . . . .	83
<b>4</b>	<b>Materials and Methods</b>	<b>85</b>
4.1	Materials . . . . .	85
4.1.1	Fluorine-doped tin oxide glass . . . . .	85
4.1.2	Titania pastes . . . . .	85
4.1.3	Electrolytes . . . . .	86
4.1.4	Reference sensitizers . . . . .	87
4.2	Methods and equipment . . . . .	87
4.2.1	Electrochemistry setup . . . . .	87
4.2.2	Screenprinting . . . . .	89
4.2.3	Annealing oven . . . . .	90
4.2.4	Sealing machine and drybox . . . . .	90
4.2.5	Solar simulator setup . . . . .	91
4.2.6	IPCE setup . . . . .	94
4.2.7	Absorption and emission measurements . . . . .	95

---

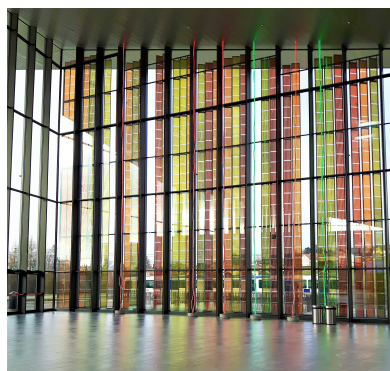
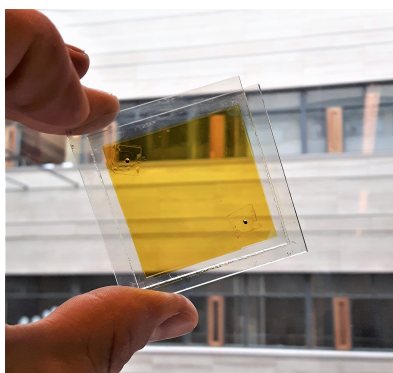
4.2.8	Dye loading measurements . . . . .	95
4.2.9	Device fabrication . . . . .	97
<b>5</b>	<b>General Conclusion and Further Work</b>	<b>99</b>
5.1	Summary . . . . .	99
5.2	Future development . . . . .	100
5.2.1	DSSC field in general . . . . .	100
5.2.2	Phenothiazine sensitizers . . . . .	102
	<b>References</b>	<b>103</b>
	<b>Paper I</b>	<b>117</b>
	<b>Paper II</b>	<b>161</b>
	<b>Paper III</b>	<b>207</b>
	<b>Paper IV</b>	<b>247</b>
	<b>Paper V</b>	<b>281</b>
	<b>Paper VI</b>	<b>311</b>





## ABSTRACT

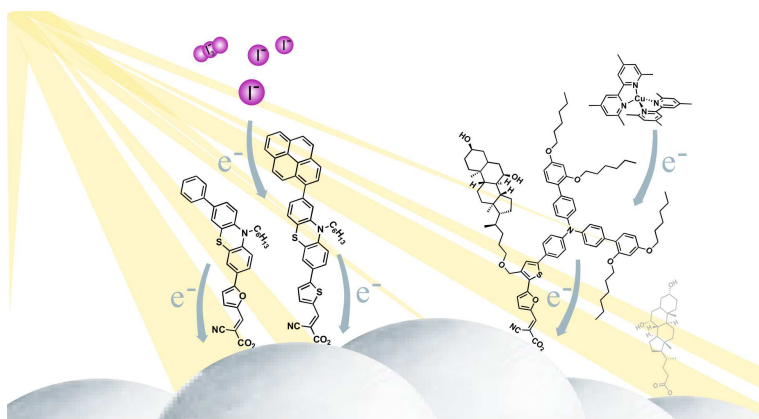
The climatic consequences of rising CO<sub>2</sub> emissions have been well understood since the seminal work of Svante Arrhenius in 1896. Through his correlation of global temperature and atmospheric CO<sub>2</sub> concentrations, he predicted quite accurately the temperature rise we are now experiencing over 120 years later. Even at the time, burning of coal was recognized as a major contributor to the increasing CO<sub>2</sub> concentrations. Hence, the idea of anthropogenic global warming is by no means a new concept. However, we are now beginning to see the real consequences of the changing climate; sea levels are rising, glaciers melting and permafrost thawing. The Earth is currently balancing on a climatic knife's edge, but there is still time to react and correct the course. As a matter of immediacy, humanity must cut hard in the use of fossil fuels and rely on hydroelectric, nuclear, wind, tide or solar energy. As one of numerous solar cell technologies, dye-sensitized solar cells (DSSC) are a promising low-cost alternative.



DSSCs are fabricated from widely available and inexpensive materials in an energy efficient process. They are incredibly efficient in conditions when conventional solar cells are not, can be made flexible, of tunable color, and semi- or possibly even fully transparent. The major hurdle to overcome for the DSSC technology is improving the efficiency through developing the light harvesting properties of the dye molecules. The "family tree" of sensitizer classes has grown large over its 20+ years of development, with metal-complexes and metal-free organic dyes further branching into a myriad of different sub-classes. The primary focus of this thesis is phenothiazine sensitizers. Through molecular engineering of the dye structures, we aimed to understand the behaviour and develop the photovoltaic performance of such sensitizers in dye-sensitized solar cells.

In Papers I-V, we investigated a number of aspects related to the phenothiazine scaffold, such as finding the most suitable  $\pi$ -spacers and auxiliary donors. We found the five-membered  $\pi$ -spacers such as thiophene and furan vastly superior to six-membered alternatives, and with regards to the contribution of auxiliary donors, only a very modest performance enhancement was found. The fundamental substitution geometry of the phenothiazine sensitizers has been made more diverse by the development of novel geometries, rivaling the conventional 3,7 substitution pattern. The photophysical properties of one of the most efficient phenothiazine sensitizers was considerably improved by the introduction of a furan  $\pi$ -spacer, and we also uncovered highly suspicious efficiency data for the phenothiazine sensitizer with the highest claimed power conversion efficiency.

Aggregation inhibition by chenodeoxycholic acid was the main topic of the last part of the thesis, covered in Paper VI. A significant amount of synthetic work was performed to attach a chenodeoxycholic substituent covalently onto the  $\pi$ -spacer of a triarylamine dye. This approach enhanced the photovoltaic performance by improving the overall distribution of anti-aggregation moieties, leading to a higher quality dye/co-adsorbent monomolecular layer on the photoanodes.



### Keywords:

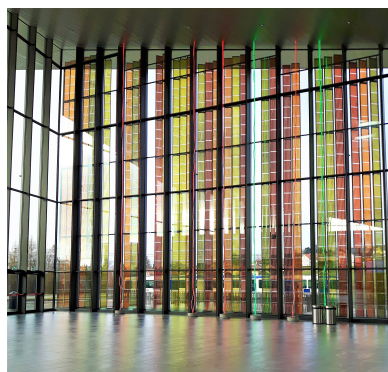
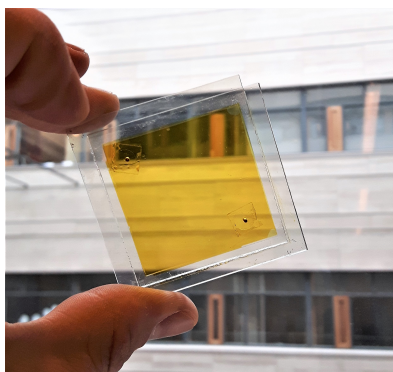
*Dye-sensitized solar cells, phenothiazine sensitizers, triarylamine sensitizers, organic synthesis, novel geometries, new design concepts, anti-aggregation moieties.*

---

The photographs above show the very first dye-sensitized solar cell fabricated at NTNU with dye **AFB-7**, and the glass facade of the Swiss Tech Convention Center at EPFL, covered with 300 m<sup>2</sup> of dye-sensitized solar cells.

## SAMMENDRAG PÅ NORSK

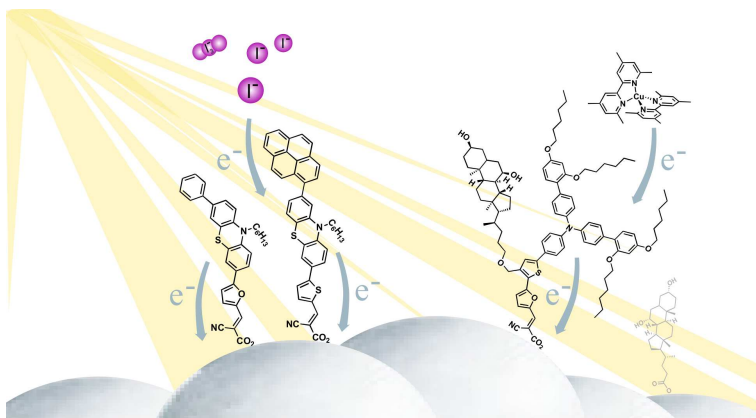
De klimatiske konsekvensene av økende CO<sub>2</sub> utslipp har vært godt kjent siden Svante Arrhenius' tidlige forskning i 1896. Han korrelerte global temperatur og atmosfærisk CO<sub>2</sub>-konsentrasjon, og gav nøyaktige estimater på den temperaturøkningen vi nå opplever over 120 år senere. Selv på den tiden ble brenning av kull nevnt som en av hovedårsakene til de økende mengdene av CO<sub>2</sub> i atmosfæren, så menneskeskapt global oppvarming er is eg selv ikke et nytt begrep. Likevel er det ikke før nå vi virkelig ser alvorlige konsekvenser som økte havnivåer, isbreer som smelter og permafrost som tiner. Jorden balaserer nå en på en klimatisk knivsegg, men det er fortsatt tid til å korrigere kursen. For å få det til, må vi i umiddelbar fremtid kutte hardt i forbruket av fossilt brensel og ta i bruk vann-, kjerne-, vind- og tidevannkraft i tillegg til solenergi. Som en av mange solcelleteknologier er fargestoff-sensiterte solceller (DSSC) et lovende, kostnadseffektivt alternativ.



Disse solcellene kan lages med lett tilgjengelige og billige materialer i en lite energikrevende prosess. De kan være utrolig effektive under forhold hvor konvensjonelle solceller ikke er det, kan lages fleksible, ha forskjellige farger og kan lages delvis eller fullstendig gjennomsiktige. Den største utfordringen for utviklingen av denne teknologien er å øke effektiviteten, noe som kan oppnås ved å forbedre lysfangstegenskapene til fargestoffmolekylene. I løpet av de over 20 årene siden teknologien første ble presentert har familietreet av fargestoff vokst stort. Hovedklassene metallkomplekserte og metallfrie fargestoff har dannet grunnlaget for et villniss av underklasser. Hovedfokuset i denne doktorgraden har vært fenotiazin-baserte fargestoff. Gjennom molekylær design på fargestoffstrukturene er målet å kunne forstå fargestoffenes oppførsel, samt utvikle deres fotovoltaiske ytelse i fargestoff-sensiterte solceller.

I artiklene I-V undersøkte vi en rekke aspekter ved fenotiazinkjernen, som å finne passende  $\pi$ -spacere og hjelpeonorgrupper. Vi fant at femringede heterosykliske  $\pi$ -spacere som tiofen og furan var betydelig overlegne seksringede alternativer og for hjelpeonorgruppene fant vi at de bidro med kun en liten økning i ytelse. Vi har også utvidet stoffklassen ved å introdusere nye grunnleggende substitusjonsmønstre for fenotiazinfargestoff, med ytelse på linje med den konvensjonelle 3,7-geometrien. De fotofysiske egenskapene til et av de mest effektive fenotiazinfargestoffene har blitt forbedret ved å inkludere en furan  $\pi$ -spacer. I tillegg har vi avdekket høyst urovekkende effektivitetsdata for fenotiazinfargestoffet med den høyest rapporterte effektivitet i DSSC.

Hindring av fargestoffaggregering med gallesyren chenodeoxycholic acid var hovedtema for siste del av avhandlingen, beskrevet i artikkel VI. Et betydelig syntesearbeid ble gjort for å feste chenodeoxycholic acid kovalent til  $\pi$ -spaceren på triarylaminfargestoffer. Denne strategien økte den fotovoltaiske ytelsen ved å forbedre fordelingen av anti-aggregeringsenheter som igjen gav høyere kvalitet av det monomolekulære laget av fargestoff/additiv på fotoanoden.



#### Nøkkelord:

*Fargestoffsensiterte solceller, fenotiazinfargestoffer, triarylaminfargestoffer, organisk syntese, nye fargestoffgeometrier, nye designkonsepter, anti-aggregeringsenheter.*

Bildene over viser den aller første fargestoffsensiterte solcellen laget på NTNU med fargestoffet **AFB-7**, i tillegg til fasaden på Swiss Tech Convention Center på EPFL, dekket av 300 m<sup>2</sup> med fargestoffsensiterte solceller.

---

# PUBLICATIONS AND CONTRIBUTIONS

## Scientific Publications

### Paper I

*Effect of  $\pi$ -linkers on phenothiazine sensitizers for dye-sensitized solar cells*

Audun Formo Buene, Nora Uggerud, Solon P. Economopoulos, Odd R. Gautun and Bård Helge Hoff

Dyes and Pigments, **2018**, Volume 151, Page 263-271.

### Paper II

*Auxiliary donors for phenothiazine sensitizers for dye-sensitized solar cells - How important are they really?*

Audun Formo Buene, Eline Ekornhol Ose, Ane Garborg Zakariassen, Anders Hagfeldt and Bård Helge Hoff

Journal of Materials Chemistry A, **2019**, Volume 7, Page 7581-7590.

### Paper III

*A comprehensive experimental study of five fundamental phenothiazine geometries increasing the diversity of the phenothiazine dye class for dye-sensitized solar cells*

Audun Formo Buene, Anders Hagfeldt and Bård Helge Hoff

Dyes and Pigments, **2019**, Volume 169, Page 66-72.

### Paper IV

*Effect of furan  $\pi$ -spacer and triethylene oxide methyl ether substituents on performance of phenothiazine sensitizers in dye-sensitized solar cells*

Audun Formo Buene, Nanna Boholm, Anders Hagfeldt and Bård Helge Hoff

New Journal of Chemistry, **2019**, Volume 43, Page 9403-9410.

### Paper V

*Experimental study comparing the 3,7 and 3,8 substitution geometry of phenothiazine sensitizers for DSSC*

Audun Formo Buene, Mats Christensen and Bård Helge Hoff

Submitted to Dyes and Pigments.

**Paper VI**

*First Report of CDCA-Substituted Dyes for DSSC Improving Efficiency through Reduced Aggregation*

Audun Formo Buene, David Moe Almenningen, Anders Hagfeldt, Odd Reidar Gauntun and Bård Helge Hoff

Manuscript in preparation.

**Conference Contributions****OKV31 - Organic Chemistry Winter Meeting 2016**

Skeikampen, Norway

Poster, *Route Selection in Preparation of Phenothiazine Dyes*

**Center for Organic Electronic Materials (COREM) Seminar 2016**

Trondheim, Norway

Oral presentation, *Synthesis of Phenothiazine-based Dyes for Dye-Sensitized Solar Cells*

**OKV32 - Organic Chemistry Winter Meeting 2017**

Skeikampen, Norway

Oral presentation, *Synthesis of Phenothiazine-based Dyes for Dye-Sensitized Solar Cells*

**F $\pi$ 13 - 13<sup>th</sup> International Symposium on Functional  $\pi$ -Electron Systems**

Hong Kong

Poster, *Development of Phenothiazine-based Dyes for Dye-Sensitized Solar Cells*

**OKV34 - Organic Chemistry Winter Meeting 2019**

Skeikampen, Norway

Oral presentation, *Phenothiazines in dye-sensitized solar cells: Some good news and some bad news*

**Dyename conference 2019 - DSSC strikes on**

Uppsala, Sweden

Oral presentation, *First Report of CDCA-Substituted Dyes for DSSC Improving Efficiency through Reduced Aggregation*

# ABBREVIATIONS

AFM	Atomic force microscope
AM	Air Mass
APCE	Absorbed photon to current conversion efficiency
aq	Aqueous
ASTM	American Society for Testing and Materials
BINAP	2,2'-bis(Diphenylphosphino)-1,1'-binaphthyl
BMII	1-Butyl-3-methylimidazolium iodide
bpy-pz	6-(1 <i>H</i> -Pyrazol-1-yl)-2,2'-bipyridine
CB	Conduction band
CDCA	Chenodeoxycholic acid
CE	Counter electrode
CV	Cyclic voltammetry
dba	Dibenzylideneacetone
DMF	Dimethylformamide
DMSO	Dimethyl sulfoxide
DPP	Diketopyrrolopyrrole
dppf	1,1'-Bis(diphenylphosphino)ferrocene
DPV	Differential pulse voltammetry
DSSC	Dye-sensitized solar cell
EDOT	3,4-Ethylenedioxythiophene
EPFL	École polytechnique fédérale de Lausanne
eq.	Equivalent
FF	Fill factor
FTO	Fluorine-doped tin oxide
HOMO	Highest occupied molecular orbital
HPLC	High-performance liquid chromatography
HTM	Hole transport material
ICT	Internal charge transfer
IMPS	Intensity-modulated photocurrent spectroscopy
IMVS	Intensity-modulated photovoltage spectroscopy
IoT	Internet of things
IPCE	Incident-photon-to-current-conversion efficiency
IR	Infrared
IUPAC	International union of pure and applied chemistry
<i>I-V</i>	Current-voltage
<i>J-V</i>	Current density-voltage
LHE	Light harvesting efficiency
LUMO	Lowest unoccupied molecular orbital
MBI	1-Methylbenzimidazole
MIDA	<i>N</i> -Methyliminodiacetic acid
MLCT	Metal-to-ligand charge transfer



---

MS	Mass spectrometry
NBS	<i>N</i> -Bromosuccinimide
NHE	Normal hydrogen electrode
NMR	Nuclear magnetic resonance
NREL	National renewable energy laboratory
PCE	Power conversion efficiency
PEDOT	Poly(3,4-ethylenedioxythiophene)
PL	Photoluminescence
PSC	Perovskite solar cell
PTZ	Phenothiazine
PV	Photovoltaic
SEM	Scanning electron microscope
SHE	Standard hydrogen electrode
SPhos	2-Dicyclohexylphosphino-2',6'-dimethoxybiphenyl
SQE	Sensitizer quantum efficiency
ssDSSC	Solid state dye-sensitized solar cell
TBAOH	Tetrabutylammonium hydroxide
TBP	4- <i>tert</i> -Butylpyridine
TCO	Transparent conductive oxide
TEOME	Triethylene oxide methyl ether
TFSI	bis(Trifluoromethanesulfonyl)imide
TGA	Thermogravimetric analysis
THF	Tetrahydrofuran
tmby	4,4',6,6'-tetramethyl-2,2'-bipyridine
TPA	Triphenylamine
TW	Terawatt
UV	Ultraviolet
XPhos	2-Dicyclohexylphosphino-2',4',6'-triisopropylbiphenyl

---

# SYMBOLS

$C_x$	Concentration of species $x$
$D$	Dye/sensitizer
$D^*$	Excited dye
$D^+$	Dye cation
$e^-$	Electron
$E_{1/2}$	Half-wave potential
$E_F$	Fermi level
$E_{0-0}$	Zero-zero excitation energy
$E_{CB}$	Conduction band energy
$eV$	Electron volt
$F$	Faraday constant
$Fc$	Ferrocene ( $Fe(C_5H_5)_2$ )
$h\nu$	Photon energy
$J_{max}$	Current density at maximum power point
$J_{SC}$	Short-circuit current density
$k_B$	Boltzmann constant
$\lambda$	Wavelength
$\nu$	Solar cell efficiency
$\Phi_{cc}$	Charge collection efficiency
$\Phi_{inj}$	Injection efficiency
$\Phi_{reg}$	Regeneration efficiency
$P_{in}$	Incident power
$P_{max}$	Maximum power point/output
$q$	Elementary charge
$Q_{OC}$	Extracted charge
$R$	Gas constant
$T$	Temperature
$\tau_e$	Electron lifetime
$\tau_{tr}$	Electron transport time
$V_{max}$	Potential at maximum power point
$V_{OC}$	Open-circuit voltage



# PREFACE

This thesis is constructed as a collection of the papers published by the author during the PhD work. All the published papers and manuscripts can be found in the appendices of this thesis. As the first PhD thesis produced in Norway within the field of dye-sensitized solar cells, extra care has gone into describing the field of dye-sensitized solar cells, in *Introduction part 1*. The chapter called *Introduction part 2* focus on phenothiazine sensitizers for DSSCs, while the *Materials and Methods* chapter describes the process of device fabrication and characterization. The *Results and Discussion* tries to link the findings of the different appended papers, while an overall summary and outlook can be found in the chapter called *General Conclusion and Further Work*.

## Declaration of authorship

**Paper I** Nora Uggerud synthesized and characterized four dyes, including precursors. Audun F. Buene synthesized the remaining seven dyes and did all device fabrication and characterization. Solon Economopoulos performed the electrochemical measurements. The paper was written by Audun F. Buene with input from all co-authors. Odd R. Gautun and Bård H. Hoff supervised the work and helped in writing the publication.

**Paper II** Ane G. Zakariassen synthesized and characterized one dye, including precursors. Eline E. Ose synthesized and characterized five dyes, including precursors. Audun F. Buene synthesized the remaining five dyes and did all device fabrication and characterization. Anders Hagfeldt supervised the electron lifetime experiments, discussion and writing about these measurements. The paper was written by Audun F. Buene with input from all co-authors. Bård H. Hoff supervised the work and helped in writing the publication.

**Paper III** Audun F. Buene did all synthesis, characterization and device fabrication. Anders Hagfeldt supervised the electron lifetime experiments, discussion and writing about these measurements. The paper was written by Audun F. Buene with input from all co-authors. Bård H. Hoff supervised the work and helped in writing the pub-

lication.

**Paper IV** Nanna Boholm synthesized the dyes, including precursors. Audun F. Buene did all photophysical experiments, device fabrication and characterization. Anders Hagfeldt supervised the electron lifetime experiments, discussion and writing about these measurements. The paper was written by Audun F. Buene with input from all co-authors. Bård H. Hoff supervised the work and helped in writing the publication.

**Paper V** Mats Christensen, Eline Ekornhol Ose and Audun F. Buene each synthesized two dyes and their intermediates. Mats Christensen did the photophysical and electrochemical measurements, while Audun F. Buene did the dye loading, device fabrication and characterization. Audun F. Buene also wrote the manuscript with input from all co-authors. Bård Helge Hoff supervised the work and helped in writing the manuscript.

**Paper VI** David Moe Almenningen synthesized the reference dyes, while Audun F. Buene synthesized the CDCA-dyes and precursors. Audun F. Buene also did all photophysical characterization, electrochemistry, device fabrication and characterization. Audun F. Buene wrote the manuscript with input from all co-authors. Anders Hagfeldt supervised the electron lifetime experiments, discussion and writing about these measurements. Odd Reidar Gautun and Bård Helge Hoff supervised the work and helped in the writing of the manuscript.

## Aim of the thesis

The main goal of this thesis was to fuse the powers of the strong synthetic organic chemistry community in Trondheim with an environmentally friendly energy-related application requiring a large number of highly specialized organic molecules. The intersection was found to be the field of dye-sensitized solar cells, and that was the starting point for this work. Selecting the phenothiazine sensitizer scaffold came down to supporting a theoretical chemometric interest at NTNU focusing on calculating DSSC device performance, led by Professor Bjørn Kåre Alsberg. Such a large objective had to be approached in portions, so the following set of sub-goals were constructed along the course of the work:

- Develop convenient synthesis routes to phenothiazine sensitizers.
- Establish laboratory facilities for the fabrication and characterization of dye-sensitized solar cells at NTNU.
- Synthesize large data-sets of phenothiazine sensitizers for a number of investigative studies.
- Research stay in a research group with long experience in the field focusing on device fabrication.
- Produce research results illuminating the behavior of the phenothiazine dye class in dye-sensitized solar cells, such as constructing structure-property relationships.
- Implement findings and synthesis techniques from phenothiazines to other dye scaffolds.

In short, the overall goal of this PhD was to initiate experimental research activity on dye-sensitized solar cells at NTNU with phenothiazine dyes as a starting point. From there on, the focus would be to investigate intriguing phenomena as we encountered them.



# INTRODUCTION PART I: APPLICATION

This chapter describes the fundamental theory relevant for the field of dye-sensitized solar cells. It concerns the properties of the sunlight, the development of the photovoltaic technologies and most crucially, the working principles of dye-sensitized solar cells.

## 1.1 Energy consumption and production

Despite the rate of population growth rate slowing down, it is estimated that the World population will pass 11 billion people by 2100, an increase of 45% compared to the 2019 population of 7.7 billion.<sup>1</sup> In addition to this population growth, the energy consumption per capita is also increasing. The sum of these effects is undoubtedly an increased energy demand in the future. Since the industrial revolution, most of the required energy has been produced from fossil fuels such as coal, gas and oil. This has converted the fixed carbon in the ground into atmospheric carbon dioxide (CO<sub>2</sub>), a potent greenhouse gas. These emissions have increased the global temperature by 1.5 °C compared to pre-industrial levels. Consequences include accelerated ice melting, rising sea levels and increasing frequency of freak weather situations. The ideas of climate change and global warming are by no means new, and the first account of the matter was by the Swedish scientist Svante Arrhenius in 1896.<sup>2</sup> He correctly connected the rise in global temperature to the increasing concentration of atmospheric CO<sub>2</sub>, even predicted the climatic consequences.

The only way to meet both the increased energy demand and climate change is to transition to renewable energy sources. Solar, wind, wave, hydroelectric and geothermal are all examples that will help reduce the global temperature rise. Despite the wide range of renewable energy sources, these still only account for 8.4% of the total energy generated in 2017.<sup>3</sup> According to the Paris agreement, 196 countries have committed to limiting the average global temperature rise to 2.0 °C compared to pre-industrial levels.<sup>4</sup> The longer we delay, the faster we will have to make the transition to renewable, sustainable and clean energy.

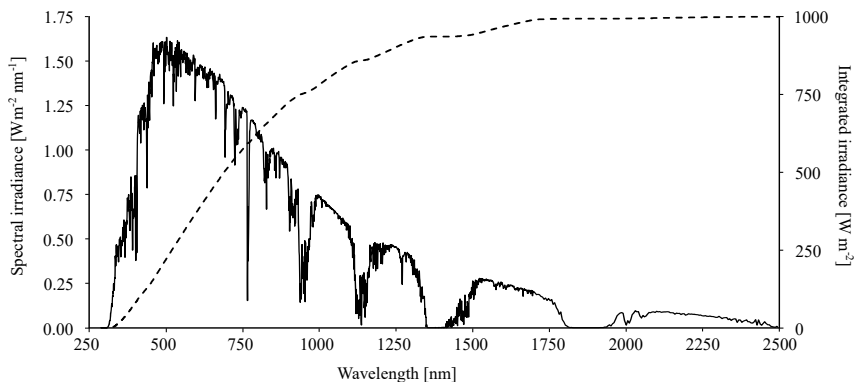
In a discussion on clean energy sources of the future, nuclear energy can not be left out. In a 2007 study in the *Lancet*, a comparison of the health risks, environmen-



tal impact and the cost of a range of different energy sources was made. Surprising to many, nuclear energy is the all-round safest source of energy, for human health and the environment.<sup>5</sup> Still, this technology is plagued by a fear for nuclear accidents, weapons development and waste management. Countries such as Germany and France are in fact closing down their nuclear energy facilities. As a consequence, the development of other sustainable energy sources and storage solutions has to continue with accelerated effort in the near future. Another aspect commonly overlooked is the intermittency of many renewable energy sources, meaning they will only provide energy when the conditions are right. The most probable solution to this problem is the use of coal and gas power plants to fill the gaps, again slowing the transition which is so desperately needed. The development of alternative solutions such as large-scale batteries, pumped hydroelectric energy storage and other ways of storing surplus electrical energy are also highly desirable, and will aid the transition away from fossil-based fuels.

## 1.2 Solar energy

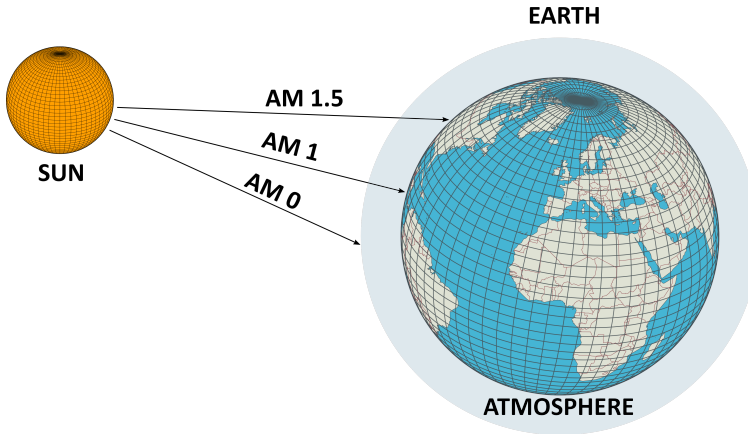
The sun is our closest star, and it is constantly emitting  $3.828 \cdot 10^{26}$  W of energy in all directions.<sup>6</sup> About 0.0000005% of the total solar radiation strikes the Earth, and after 30% is reflected by the atmosphere, the solar energy reaching the ground is still a massive  $1.8 \cdot 10^{17}$  W. Comparing this to the global energy consumption in 2015 of 12.5 TW, it becomes clear that the Earth receives enough solar energy in 40 minutes to cover the energy requirements for a whole year. The only challenge is how best to harvest the solar energy.



**Figure 1.1:** AM 1.5G solar spectrum with integrated irradiance (dashed line). Spectrum from [www.astm.org](http://www.astm.org).

The surface temperature of the sun is 5772 K,<sup>6</sup> and the solar spectrum is very similar to that of a black-body radiating at this temperature. The solar spectrum

reaching the edge of the atmosphere has a spectral shape referred to with an air mass coefficient of zero (AM 0). This is the solar spectrum used for extra-terrestrial photovoltaic applications, such as solar panels fitted to satellites. The American Society for Testing and Materials (ASTM) G-173 AM 0 reference spectrum has a total irradiance of  $1348 \text{ W/m}^2$ , while the AM 1.5G spectrum shown in Figure 1.1 has  $1000 \text{ W/m}^2$ .



**Figure 1.2:** Three common solar spectra are the AM 0, AM 1 and AM 1.5, depending on the relative atmospheric path of the sunlight.

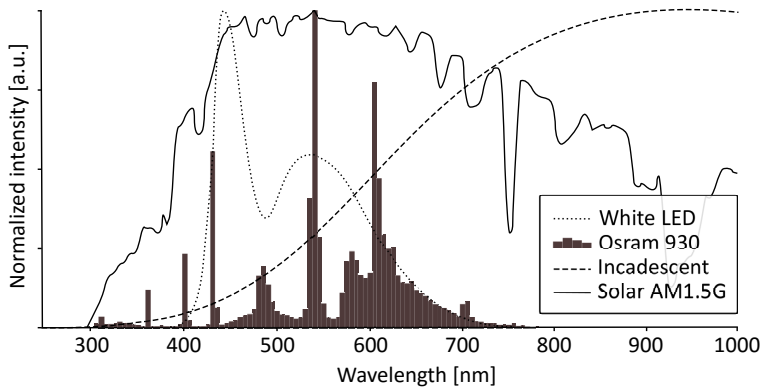
Earth's atmosphere reflects a certain part of the sunlight, and the components of the atmosphere itself will also scatter and absorb some of the radiation. Gases such as ozone, carbon dioxide, oxygen and water vapor all absorb some of the solar spectrum. The amount of radiation they absorb will depend on how much atmosphere the light has to pass through before reaching the surface, called the air mass coefficient, illustrated in Figure 1.2. The zenith angle of the sun (angle away from zenith),  $z$ , determines the air mass coefficient as defined in Equation 1.1, where  $l$  is the light path in the atmosphere,  $l_0$  the shortest possible light path (i.e. zenith atmosphere thickness). An air mass coefficient of 1 corresponds to the solar spectrum at the equator, while AM 1.5 corresponds to a solar zenith angle of approximately  $48^\circ$ , covering most of the mid-latitude countries.

$$\text{AM} = \frac{l}{l_0} \approx \frac{1}{\cos z} \quad (1.1)$$

In the atmosphere there are also a lot of particles scattering the light, resulting in some diffuse light. Consequently, the reference solar spectra are further divided into *direct*, which only reports the direct incident sunlight, and *global* which includes the diffuse light. Direct or global is denoted as a D or G after the air mass coefficient.

The standard measurement conditions for solar cell efficiency testing is 1 sun AM 1.5G illumination, meaning it has a total irradiance of  $100 \text{ mW/cm}^2$  and a spectral shape of AM 1.5 global.<sup>7</sup> Lower intensities than 1 sun are also often used to simulate low-light conditions, still using the AM 1.5G filter.

For indoor applications, no standardized testing conditions have yet been agreed upon.<sup>8</sup> Light emitting diodes (LEDs), fluorescent light tubes and conventional incandescent light-bulbs are all common for indoor lighting applications. The spectral shape from these light sources is very different, as shown in Figure 1.3. Many light sources have highly irregular spectra, such as the more energy-efficient fluorescent light tubes and bulbs now replacing many conventional incandescent light bulbs. Also, within the fluorescent light sources there are large spectral differences. Consequently, when measuring devices under simulated indoor conditions it is important to state the spectral shape and light intensity used.



**Figure 1.3:** Common indoor light sources. Intensities are normalized for easy comparison of intensity distribution.

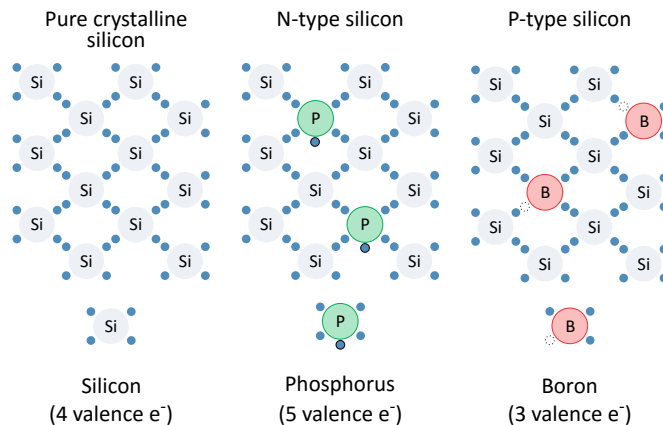
### 1.3 Solar cells

Photosynthesis in plants is by far the most extensive light harvesting mechanism on Earth, storing solar energy in the chemical bonds of the plant material. Man-made technologies such as solar thermal energy and photovoltaics allow the solar energy to be efficiently converted into heat or electricity.<sup>9</sup>

The earliest utilization of solar energy were probably heating of houses, drying of foods and evaporation of water in the production of salt.<sup>10</sup> These are all based on having a material absorb the solar energy, converting it into heat. It was only quite recently that solar energy would be used for other purposes than heat, and the first example was the discovery of the *photovoltaic effect* by Alexandre-Edmond

Becquerel in 1839.<sup>11</sup> The French physicist found that illumination of silver halide coated electrodes immersed in an electrolyte produced a photocurrent, thus reporting the first photoelectrochemical cell. The photovoltaic effect is easily confused with the *photoelectric effect*, but the latter concerns electrons ejected into vacuum, while the photovoltaic effect describes the phenomenon where the electron remains in the material. Interestingly, Becquerel also experimented with color photography in the 1840's, investigating the effect of silver halide sensitization.

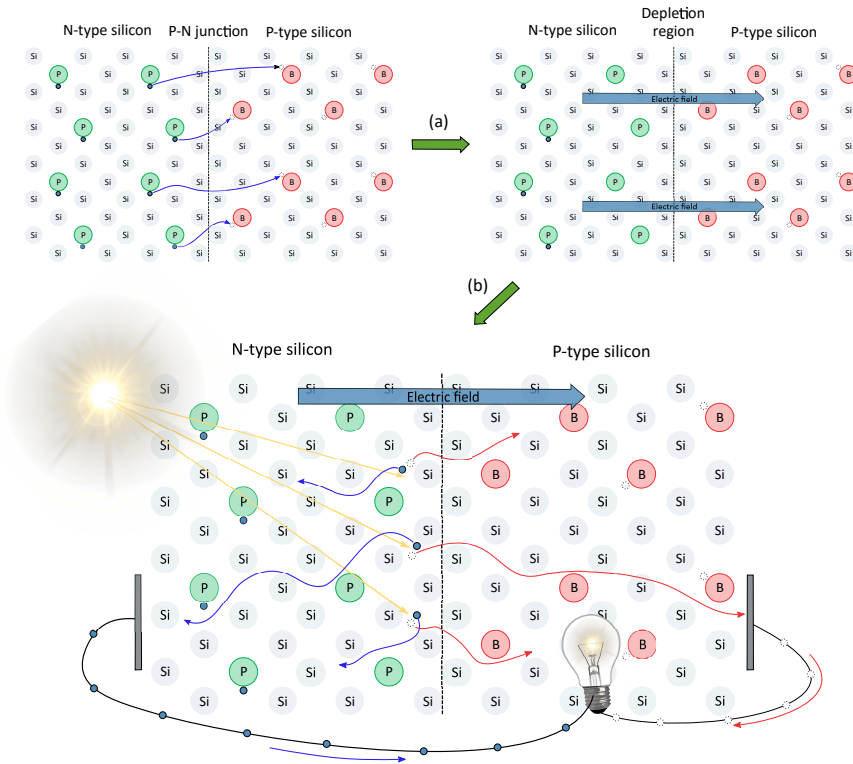
The first photovoltaic solar cell is accredited to the American inventor Charles Fritts, who in 1883 made what is known as the *selenium cell*.<sup>12</sup> This device used the semiconductor selenium, covered with a thin gold layer. The result was a photovoltaic device delivering a photoconversion efficiency of 1%. As early as in 1884, a rooftop array of solar cells were constructed in New York. Sadly, the interest in steam-electric power plants was growing immensely in this decade, steering the electricity generating industry in the direction of fossil fuels such as coal, from the very start.



**Figure 1.4:** Doping of pure silicon can create *n*- and *p*-type silicon with an excess and deficit of electrons, respectively.

The next major development was the discovery of the *p-n junction* by Russell Shoemaker Ohl in 1939.<sup>13</sup> The *p-n junction* is an interface between two phases of a semiconducting material. Ohl realized that the type and amount of impurities in the semiconductors played a very important role in creating a *p-n junction*. The *n side* has an excess of negative charges, while the *p side* has a deficit of negative charges, achieved by a process called doping, essentially adding a controlled amount other elements to the semiconductor, as illustrated for silicon in Figure 1.4. At the boundary between these two materials, charges move and create a permanent electric field, as shown in Figure 1.5. A discovery in 1910 by the Polish scientist Jan Czochralski was

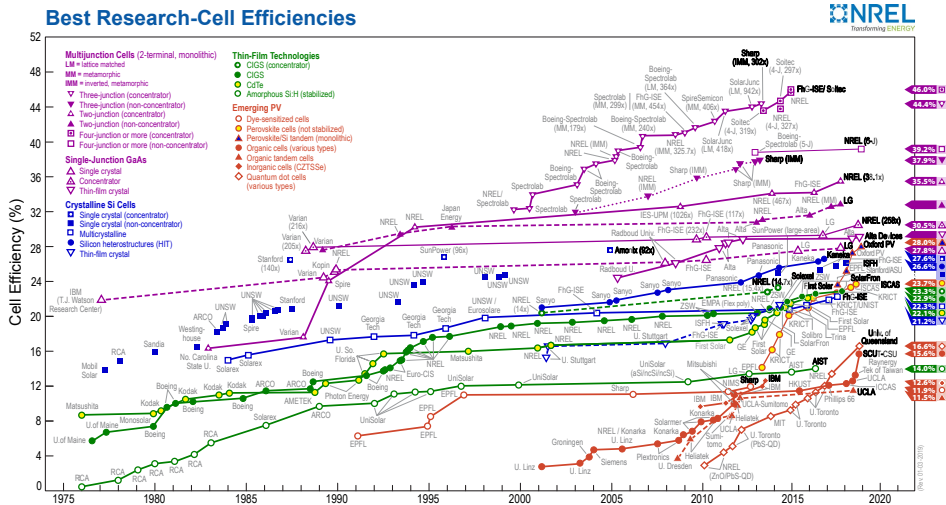
also crucial to the development of silicon solar cells.<sup>14</sup> In the Czochralski process high purity monocrystalline metals and semiconductors could be produced.



**Figure 1.5:** Workings of a p-n junction silicon solar cell. Lattice electrons not shown. (a) The migration of charges across the p-n junction creates an electric field. (b) When photons knock electrons out of the lattice, an electron-hole pair is formed, which is then separated by the electric field and collected in the external circuit.

Supported by the *space race* of the 1950's, the first silicon solar cells were developed by the Bell laboratories in 1954. Since then, the production costs have been cut massively and the efficiencies have also been improved considerably. In addition to the silicon solar cells, a plethora of other technologies have been developed over the last 40 years, as can be seen from Figure 1.6 tracking the record efficiencies of all the photovoltaic technologies from 1976.

The highest performing PV technologies are multi junction silicon solar cells and GaAs solar cells.<sup>15,16</sup> The predominant applications for these technologies are extra-terrestrial, such as satellites and space stations, where the limited available area and low weight are more important than cost. Recently, the efficiency of the perovskite solar cells have progressed very rapidly. First reported in 2009 with an architecture based on the dye-sensitized solar cell,<sup>17</sup> the first real breakthrough came in



**Figure 1.6:** Research-cells efficiency records. This plot is courtesy of the National Renewable Energy Laboratory, Golden, CO. (<https://www.nrel.gov/pv/>, 08.03.2019).

2012 when the liquid electrolyte was replaced by a solid hole-transporting material (HTM).<sup>18,19</sup> The latest push in efficiency was made in March 2019 when NREL certified an efficiency of 24.2% for a perovskite solar cell. (Research not yet published)

## 1.4 Dye-sensitized solar cells

The technology from which the perovskite solar cells evolved is dye-sensitized solar cells (DSSC). First reported in 1991,<sup>20</sup> it caused quite a stir because of the chaotic nature of the working electrode. The developments leading up to the discovery of Grätzel and O'Regan in 1991 started as early as the experiments of Alexandre-Edmond Becquerel in 1839 on the photovoltaic effect.<sup>11</sup> Later, in development of the colour photography, a lot of research on sensitization of silver halide was produced. Further down the years in the late 1960's and early 70's, sensitization of zinc oxide crystals by various dyes was found to produce photocurrents.<sup>21–24</sup> The density of the oxide monolayer was found to be of great significance,<sup>25</sup> and later the focus turned to increasing the available surface area to further increase the total dye loading of the oxides.<sup>26,27</sup> In 1984, Jacques Moser and Michael Grätzel published a study on eosin-sensitized colloidal  $\text{TiO}_2$  particles. The focus of the study was the electron kinetics of the electron injection and recombination processes, and they found the recombination to be 4000 times slower than the injection process.<sup>28</sup> Then in 1991, Grätzel and O'Regan published the first dye-sensitized solar cell employing a high surface area mesoporous  $\text{TiO}_2$  electrode, sensitized with a trimeric ruthenium dye complex,

an iodide/triiodide electrolyte and a counter electrode of conductive glass with a thin coating of platinum.<sup>20</sup>

### 1.4.1 Working principles

The dye-sensitized solar cell is a photoelectrochemical cell, constructed from a working electrode, an electrolyte and a counter electrode. Both the working and counter electrodes are usually made from conductive glass, creating a sandwich construction containing an electrolyte. The working principle of a DSSC is simplified in Figure 1.7. The five-step cycle starts with (1) the dye molecule absorbing a photon and transitioning from the ground state to an excited state. (2) From the excited state the dye molecule can inject an electron into the conduction band of  $\text{TiO}_2$ . (3) Once in the  $\text{TiO}_2$ , the electron can diffuse through the mesoporous layer, be collected in the external circuit and perform electrical work before reaching the counter electrode. (4) The electron will reduce the oxidized redox shuttle species, and finally (5) the reduced redox shuttle diffuses from the counter electrode to the oxidized dye molecule on the  $\text{TiO}_2$  where it transfers the electron back to the dye and the cycle is completed.

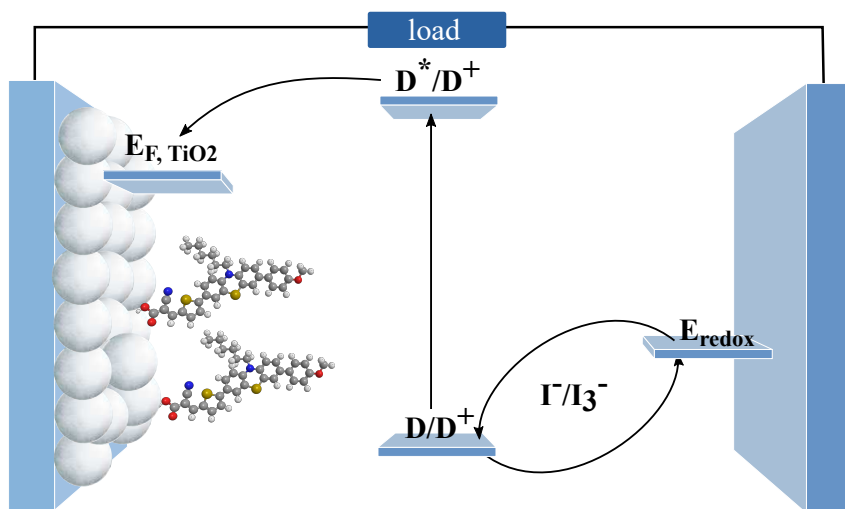
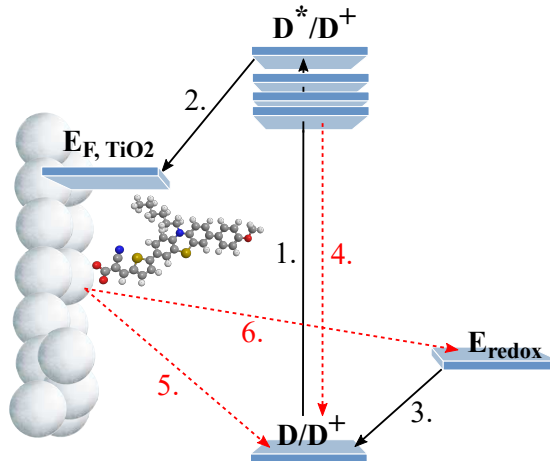


Figure 1.7: Working principle of a dye-sensitized solar cell.

There are many electronic processes happening inside a DSSC, some are favorable and others unfavorable. In general, any process contributing to generating a current in the external circuit between the electrodes is considered favorable. A summary of the main processes is given in Figure 1.8, where black arrows indicate a favorable process and red dashed arrows indicate unfavorable processes.



**Figure 1.8:** Main electronic processes within a DSSC. Favorable processes are given black arrows while unfavorable processes are shown in red. 1) Excitation, 2) injection, 3) regeneration, 4) relaxation, 5) recombination to oxidized sensitizer and 6) recombination to oxidized redox shuttle species.

The first and most important process is naturally the dye molecule harvesting a photon from the sunlight yielding an excited dye molecule ( $D^*$ ), as stated in Equation 1.2.



where  $h\nu$  is the energy of the photon and  $D/D^*$  are the ground state and excited state dye molecules. The injection of an electron into the  $\text{TiO}_2$  can be described as in Equation 1.3



where the excited dye  $D^*$  injects an electron into the  $\text{TiO}_2$  becoming a dye cation  $D^+$ . Last of the favorable reactions is the regeneration of the dye, i.e. transferring an electron from the counter electrode to the dye cation. This is described in Equation 1.4 and 1.5. First the oxidized redox shuttle species is reduced by an electron from the counter electrode before transferring this electron to the dye cation.



A number of unfavorable reactions, also known as dark reactions, take place inside a DSSC, described in Equation 1.6, 1.7 and 1.8. First, relaxation of the excited state ( $D^*$ ) to the ground state ( $D$ ) will produce either heat or a photon of lower energy



in the case of radiative decay.



Secondly, an oxidized redox species may collect an electron from the excited dye molecule, a process competing with the electron injection step.



Finally, the most encountered dark reaction is the transfer of an injected electron from the  $\text{TiO}_2$  to the oxidized redox species.



The dye-sensitized solar cell is one of those unicorn devices where the output really feels larger than the sum of the individual components. The successful interplay between the components is elegant and attractive to researchers across many disciplines. However, optimization of a single component will often require further adjustment of the remaining system to fully harvest the improvement potential.

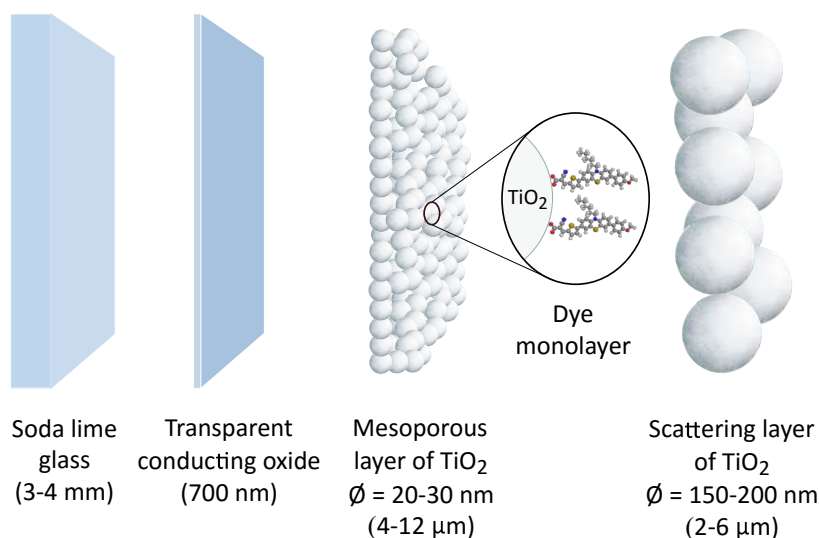
## 1.4.2 Components

An *n-type* dye-sensitized solar cell is constructed from three main components: the photoanode, the counter electrode and the electrolyte. This section will give deeper insight into the construction and workings of these important components.

### Working electrode

The working electrode of a DSSC carries the dye molecules, and in an *n-type* DSSC this is the photoanode. An exploded view of a typical photoanode is shown in Figure 1.9. The basis for the photoanode is soda-lime glass coated with a thin layer of a transparent conducting oxide, usually fluorine-doped tin oxide (FTO) and sometimes indium-doped tin oxide (ITO). This provides structural support, conductivity and transparency. Transparencies of visible light in the range of 80-85% for FTO glass is quite common. Lower sheet resistance comes at a price of lowered transmittance, so a compromise between conductivity and transparency has to be found. Due to the limited transmittance of FTO glass, front-illumination is almost always preferred to back-illumination in DSSCs.

The three main crystalline polymorphs commonly encountered for titanium dioxide are anatase, rutile and brookite. While rutile is the most thermodynamically stable, anatase is the one preferred for use in DSSCs. The higher bandgap of anatase (3.2 eV) yields higher  $V_{\text{OC}}$  compared to the other crystal forms.<sup>29</sup> Brookite is the most difficult polymorph to synthesize in pure form, and despite a few accounts of



**Figure 1.9:** Exploded view of the main parts of the DSSC photoanode.

brookite DSSCs, it is not widely used.<sup>30</sup> Synthesis of anatase nanoparticles is commonly done by hydrolysis of titania precursors such as titanium tetrachloride or titanium tetraisopropoxide.<sup>31,32</sup> The 20-30 nm diameter nanoparticles are made into a paste with additives such as ethyl cellulose and terpinol, which can be applied by screenprinting or doctorblading. The small particle size yields a light absorption layer of nanoparticles which is almost fully transparent, even with a thickness of over 10 microns. The last major component of the photoanode is a scattering layer of large titania particles. This is a way of extending the light path by introducing a layer of larger particles of  $\text{TiO}_2$  which will reflect and scatter any light not initially absorbed. Naturally, if transparent devices are desired, a scattering layer can not be used. The application of a uniformly thick layer of the paste is achieved by screenprinting or doctorblading onto the FTO glass, followed by sintering which burns off residual binders and solvents in addition to creating electrical contact between nanoparticles. Commonly, a thin blocking layer of dense  $\text{TiO}_2$  is usually also found between the FTO and the first layer of active titania. The purpose of this layer is to prevent the electrolyte access to the FTO, a highly undesirable loss-process in these devices. Lastly, to increase the surface area, an ultrathin coating of titania can be applied to the porous layer by the same technique used for the blocking layer, by immersion in aqueous  $\text{TiCl}_4$  and followed by a sintering step.

While  $\text{TiO}_2$  is the most widely used oxide in dye-sensitized solar cells, other oxides have also been studied. Zinc oxide can be synthesized to form nanoparticles, nanorods or other ordered large-surface-area structures. Electrodeposition can be

utilized to grow the ZnO layer directly on the FTO glass as ordered nanostructures. The bandgap and conduction band edge of ZnO are comparable to those of anatase TiO<sub>2</sub> and the electron mobility is higher.<sup>33</sup> A drawback is the low chemical stability, as ZnO is dissolved by acids and bases.<sup>34</sup> Consequently, dyes with carboxylic acid anchoring groups are dissolving the structure during the sensitization process, forming Zn<sup>2+</sup> ions which again may complex and precipitate dyes in the mesoporous structure. Despite the inherent challenges with ZnO DSSCs, devices with up to 7.0% PCE have been reported with nanoparticle ZnO working electrodes sensitized with **N719**.<sup>35</sup> Many other oxides, and combinations of oxides have been tested, such as SnO<sub>2</sub>,<sup>36,37</sup> SrTiO<sub>3</sub>,<sup>38</sup> Nb<sub>2</sub>O<sub>5</sub><sup>39</sup> and Zn<sub>2</sub>SnO<sub>4</sub>.<sup>40,41</sup>

## Dye

The dye is the most important component in a dye-sensitized solar cell, as it is the light harvesting material. It also performs the important task of separating the electron and the associated electron hole, which is crucial for generation of electrical current. In the development of new dyes, the following properties are important to consider:<sup>29</sup>

1. **Absorption properties:** For high efficiency, the absorption of the dye should be broad. High extinction coefficient is very desirable, especially if thin TiO<sub>2</sub> films are required due to diffusion limitations for the redox couple.
2. **Electrochemical properties:** The HOMO and LUMO energies must be compatible with the TiO<sub>2</sub> and redox shuttle, i.e. the HOMO must be found at a more positive potential than the redox potential of the electrolyte and the LUMO must have a more negative potential than the conduction band of TiO<sub>2</sub>.
3. **Molecular requirements:** The dyes need an anchoring group to permanently attach to the TiO<sub>2</sub> surface. Cyanoacrylic acid and benzoic acid are the most common, but also silanes, phosphonic acid and sulfonate anchoring groups are in use.<sup>42</sup> Controlling undesirable aggregation issues in the monomolecular dye layer can be done by anti-aggregation moieties on the dye molecules, or by the addition of additives.
4. **Stability properties:** The dye must be stable during the fabrication process and in the operational environment inside the DSSC, i.e. the dye must be heat-, photo- and electrochemically stable.

### Electrolytes and redox couples

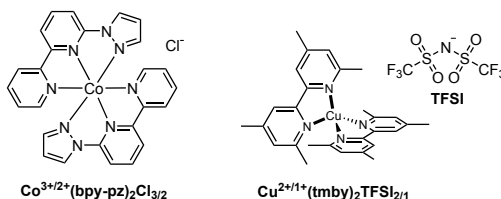
The redox couple completes the circuit by transferring an electron from the counter electrode back to the oxidized dye molecule on the photoanode. A wide array of redox couples are available to the DSSC community.<sup>43,44</sup> The iodide/triiodide couple has been the most widely used electrolyte system in DSSCs.<sup>45</sup> More recently, new redox mediators based on metal complexes with tunable ligands have allowed researchers to minimize the  $V_{OC}$  losses in the dye regeneration process. The copper and cobalt complexes used in this thesis are shown in Figure 1.10.

#### *Iodide / triiodide*

The redox potential of the  $I^-/I_3^-$  electrolyte is 0.35 V vs. the normal hydrogen electrode (NHE).<sup>45</sup> Liquid electrolyte compositions vary, but common additives are lithium iodide, guanidinium thiocyanate, 4-*tert*-butylpyridine and various imidazolium iodides. Common solvents include acetonitrile, valeronitrile and propionitrile. The  $I^-/I_3^-$  couple is still widely used in DSSC research, especially paired with low extinction coefficient dyes requiring  $TiO_2$  layers up to 12  $\mu m$ , thus a redox couple with good diffusion is necessary.<sup>43</sup> This redox couple is also in use in *p*-type<sup>46</sup> and aqueous DSSCs.<sup>47</sup>

#### *Cobalt (II+ / III+)*

While the two-electron  $I^-/I_3^-$  redox shuttle is slow to recombine with electrons in the  $TiO_2$ , a large voltage loss has to be accepted due to mismatch between the  $I^-/I_3^-$  Nernst potential and sensitizer oxidation potential. Cobalt redox couples use organic ligands, and by varying the ligands, the Nernst potential can be tuned.<sup>48</sup> Due to slower diffusion for cobalt complexes, larger  $TiO_2$  particle size and thinner  $TiO_2$  films are preferred compared to devices employing the  $I^-/I_3^-$  electrolyte.<sup>49,50</sup> Aqueous cobalt electrolytes have also been successfully developed.<sup>51,52</sup> By the use cobalt electrolytes,  $V_{OC}$  values in excess of 1000 mV have been reported,<sup>48,53</sup> and highly efficient devices with PCE over 13% have been fabricated.<sup>53,54</sup> Another attractive feature of cobalt complexes is the low light absorption in the visible range, so the redox couple is not competing with the absorption of the sensitizer.<sup>55</sup>



**Figure 1.10:** Structures of the copper and cobalt complexes used in this thesis.

### *Copper (I+/II+)*

Electrolytes based on copper complexes also use organic ligands, and the redox potential is tunable, just as the cobalt electrolytes. However, while the cobalt complexes have large reorganization energies between their  $d^7$  and  $d^6$  spin states, this energy is much lower for copper complexes between  $d^{10}$  and  $d^9$ . Consequently, driving forces as low as 100 mV are needed for efficient dye regeneration, resulting in increased photovoltage.<sup>56</sup> A record open-circuit voltage of 1.14 V has been achieved with a  $[\text{Cu}(\text{dmp})_2]^{+/2+}$  electrolyte,<sup>57</sup> and recently devices delivering 13% PCE under 1 sun and 32% PCE under ambient light were reported with  $[\text{Cu}(\text{tmby})_2]^{+/2+}$ .<sup>58</sup> Solid-state DSSCs have been fabricated by evaporation of solvents from copper-based electrolytes.<sup>59,60</sup> Moreover, tetradentate ligands have been developed for Cu-based redox couples, leading to impressive device stability for 500 hours at full sun irradiation.<sup>61</sup>

### *Other electrolytes*

Many other redox couple systems have been tested in dye-sensitized solar cells, such as those based on polymers<sup>62</sup> or ionic liquids.<sup>63</sup> Crown-ether-complexed iodide salts have been used in solid-state devices.<sup>64</sup> Redox couples based on sulfide/polysulfide,<sup>65</sup> fully organic redox-couples<sup>66</sup> and those based on halides and pseudo halides such as SCN have also been investigated.<sup>43</sup>

### **Counter electrode**

The counter electrode is normally also fabricated from FTO glass. A thin layer catalyzing the electron transfer to the redox couple has to be deposited. For the  $\text{I}^-/\text{I}_3^-$  shuttle, a thin layer of Pt is usually deposited from a platinum precursor solution followed by heating. Other redox couples may require other catalytic surfaces, such as many copper complexes for which electrochemically polymerized 3,4-ethylenedioxythiophene (EDOT polymerized to PEDOT) deposited on FTO glass is a good catalyst.<sup>67</sup>

### 1.4.3 Other devices based on DSSC architecture

During the almost 30 years of DSSC development, the field has widened and many variations in device architecture have evolved. Interweaved and partially overlapping concepts such as *p*-type DSSCs, dye-sensitized photoelectrolysis cells,<sup>68</sup> tandem DSSCs,<sup>69</sup> quantum dot-sensitized solar cells,<sup>70</sup> perovskite solar cells<sup>71</sup> and artificial photosynthesis<sup>72</sup> are all technologies more or less related to dye-sensitized solar cells.

#### *p*-type and tandem DSSC

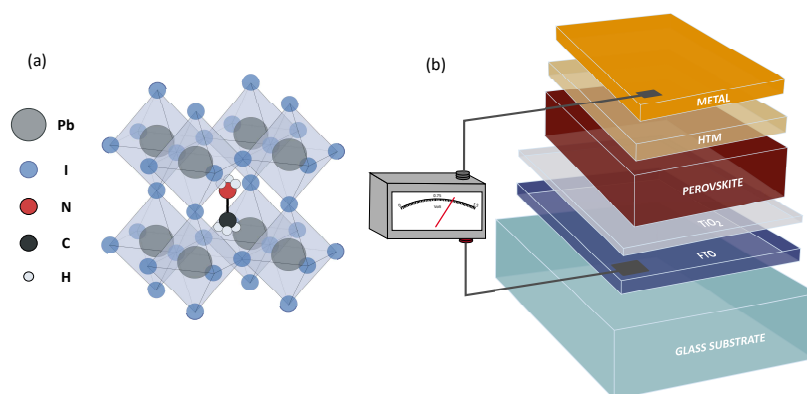
The *p*-type DSSC is essentially a device where everything is inverted compared to the "conventional" DSSC. The cathode is the photoactive electrode where the dye is anchored, and upon photoexcitation, the dye donates an electron to the electrolyte or HTM (in the case of a solid-state *p*-type DSSC).<sup>73</sup> For this purpose NiO is used for dye anchoring, but the efficiencies are so far very limited. The concept of tandem DSSCs was reported as early as in 2000 by Lindquist and coworkers.<sup>74</sup> In a tandem device both electrodes are sensitized, essentially a combination of the working electrodes of an *n*-type and a *p*-type DSSC.<sup>75</sup>

#### Solid-state DSSC (ssDSSC)

With liquid electrolytes there is a constant risk of leakage or evaporation, leading to device failure and release of toxic chemicals in the environment. Solid-state DSSCs can eliminate these issues.<sup>76</sup> The major challenge in ssDSSCs is achieving good charge mobility through the hole transport material (HTM). The chaotic nature of the photoanode usually restricts the penetration depth of traditional hole transport materials such as Spiro-OMeTAD.<sup>77,78</sup> A recent allegedly accidental discovery has perhaps found a solution to this problem. DSSC devices fabricated with liquid copper electrolytes that were left to dry out, were found to be highly efficient even though all the solvent of the electrolyte had evaporated.<sup>59,60</sup> Consequently, the discovery was given the fitting name of *Zombie cells*. In the first report by Freitag et al.,<sup>60</sup> the dye **LEG4** was paired with the liquid  $\text{Cu}^{+/2+}(\text{dmp})_2\text{TFSI}_{1/2}$  electrolyte to give a power conversion efficiency of 6.0%. Surprisingly, after solvent evaporation, the PCE increased to 8.2%, predominantly attributed to increased short-circuit current. In comparison, ssDSSC devices fabricated with Spiro-OMeTAD only gave a PCE of 5.6% in the same study. The phenomenon was confirmed in 2017 by a group from EPFL using a very similar dye (**Y123** differ from **LEG4** in the length of the alkoxy chains on the triarylamine donor), but with a different copper electrolyte. The result was a ssDSSC with 11% efficiency and high reproducibility.<sup>59</sup>

### Perovskite solar cells (PSC)

Around 2009, new light harvesting materials were tested in the architecture of the DSSC, one of which was a perovskite developed by Tsutomu Miyasaka and coworkers in Japan.<sup>17</sup> Their synthetic  $\text{CH}_3\text{NH}_3\text{PbI}_3$  perovskite achieved a power conversion efficiency of 3.81%. From nature, perovskite is the mineral  $\text{CaTiO}_3$ , but any mineral with the same crystal structure and  $\text{ABX}_3$  composition can be described as perovskite. By replacing the cations and anions, the bandgap of the perovskite can be tuned for increased light harvesting. The perovskite not only harvests the sunlight, it also separates the electron-hole pair so they can be collected at the different electrodes. In 2012 the first major efficiency jump took place for PSC, when it was found that only a very thin layer of semiconducting oxide was needed, thus efficiencies of 9-10% were achieved.<sup>18,19</sup> The crystal structure of  $\text{CH}_3\text{NH}_3\text{PbI}_3$  perovskite and the architecture of a conventional PSC are shown in Figure 1.11. At present, lead-based organo halide materials are the focus of the perovskite research, and efficiencies over 24% has recently been certified by NREL.



**Figure 1.11:** (a) Perovskite crystal structure, (b) conventional perovskite solar cell architecture.

While the efficiency improvement of PSCs has continued to reach new heights, there is still much work to be done on the device stability.<sup>79</sup> The perovskites used are inherently sensitive to moisture, so controlling the atmosphere during fabrication and proper sealing for the devices is crucial.<sup>71</sup> Another consequence of poor sealing would be lead contamination. Although the amounts of lead are relatively moderate and reliable encapsulation techniques exist, the fear of lead polluting the environment has driven the development of low-toxicity lead-free perovskite solar cells. The reported PCE values of these devices have so far been below 10% and the most promising alternatives are based on tin, caesium and germanium.<sup>80</sup>

**Non-photovoltaic applications**

Dye-sensitized solar cells are also the basis for a novel distance measurement technique called Focus-Induced Photoresponse distance measurements.<sup>81</sup> The technology is based on DSSCs giving a different current response depending on how focused a beam of incident light is. By using optics and two transparent DSSCs, simple distance measurements and 3D mapping can be done with one light source and one detector. The architecture of dye-sensitized solar cells has also been used for other applications such as dye-sensitized photoelectrolysis cells also referred to as water-splitting technology.<sup>68</sup> Also artificial photosynthesis<sup>72</sup> and solar fuel generation have certain similarities with dye-sensitized solar cells.<sup>82</sup>



## 1.5 DSSC characterization

Reliable characterization of materials and devices is hugely important in the DSSC field, and indeed with any photovoltaic technology. Power conversion efficiency is the ultimate number researchers are reporting and the only number that matters for solar cell records. Therefore, being able to accurately measure and report reliable performance data is essential.<sup>83,84</sup> Accurate measurements of observed trends and phenomena is also of high importance, as these are the basis for further optimization of dyes and devices. Fortunately, there are a number of techniques that can be used to evaluate the performance of solar cells.<sup>85</sup> The use of several techniques will increase the credibility of the efficiency claims.

### 1.5.1 $J$ - $V$ characteristics

The main performance characteristics of a solar cell can be obtained by applying a forward bias voltage across the solar cell under illumination. The potential applied across the cell is varied and the current measured, in what is called a  $J$ - $V$  sweep or  $J$ - $V$  measurement. From the  $J$ - $V$  curve, device characteristics such as the open-circuit voltage ( $V_{OC}$ ), short-circuit current density ( $J_{SC}$ ) and fill factor (FF) are obtained. If measured under darkness, the DSSC will behave as a diode, allowing current to flow in one direction, but not the other. This current is commonly called *dark current* ( $J_{dark}$ ), and can be described by the ideal diode equation (Equation 1.9), where  $J_0$  is the reverse bias saturation current of the diode,  $k_B$  the Boltzmann constant,  $T$  temperature and  $q$  the elementary charge ( $1.602 \cdot 10^{-19}$  C).

$$J_{dark} = J_0(e^{\frac{qV}{k_B T}} - 1) \quad (1.9)$$

However, under illumination a working device will generate a current in the opposite direction of the dark current,  $J_{light}$ . The photocurrent measured in a  $J$ - $V$  sweep is total of these two currents, as shown in Equation 1.10.

$$J_{total} = J_{light} - J_{dark} = J_{light} - J_0(e^{\frac{qV}{k_B T}} - 1) \quad (1.10)$$

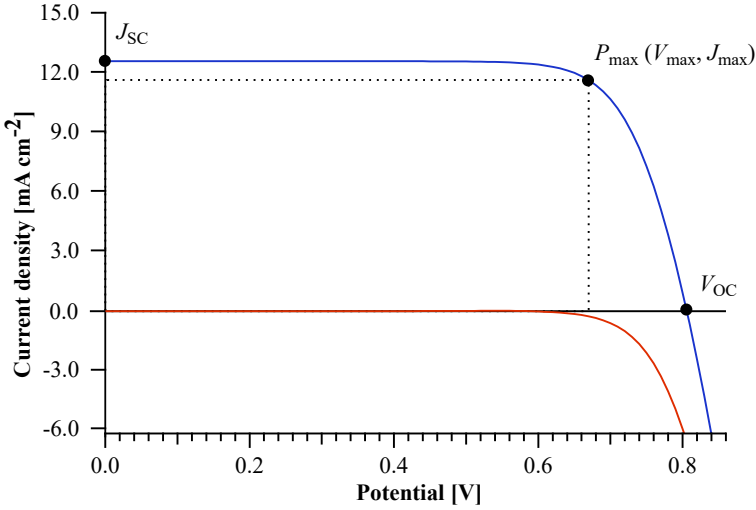
In reality there are a number of factors affecting the performance of a solar cell, that can be included in the equations because they are possible to measure. Firstly, there is the *shunt resistance* ( $R_{shunt}$ ), originating from recombination in the solar cell, in other words, an alternative path for the generated electron which is not contributing to the total photocurrent. A higher  $R_{shunt}$  is always favorable, and the effect of this resistance can be added to the total photocurrent equation by utilizing Ohms law.

$$J_{\text{total}} = J_{\text{light}} - J_{\text{dark}} - J_{\text{shunt}} = J_{\text{light}} - J_0 \left( e^{\frac{qV}{k_B T}} - 1 \right) - \frac{V}{R_{\text{shunt}}} \quad (1.11)$$

Secondly, in a solar cell such as a DSSC, electrons are forced to move through materials and over surfaces, such as  $\text{TiO}_2$  and fluorine-doped tin oxide glass. This acts as a restriction for the electrons, effectively introducing another resistor causing a voltage drop in the device, which is called series resistance ( $R_{\text{series}}$ ). Additionally, all connections such as crocodile clips will add to this resistance. Naturally, it is desirable for the value of  $R_{\text{series}}$  to be as low as possible. Again by using Ohm's law for the drop in voltage caused by the series resistance, the final equation for the photocurrent for the devices may be formulated as in Equation 1.12:

$$J_{\text{total}} = J_{\text{light}} - J_{\text{dark}} - J_{\text{shunt}} = J_{\text{light}} - J_0 \left( e^{\frac{q(V+JR_{\text{series}})}{k_B T}} - 1 \right) - \frac{V + JR_{\text{series}}}{R_{\text{shunt}}} \quad (1.12)$$

From the  $J$ - $V$  sweep under illumination a curve like the example in Figure 1.12 is obtained. From this curve we can directly extract the values for  $V_{\text{OC}}$  and  $J_{\text{SC}}$  as the intersects with the horizontal and vertical axes, respectively. The *fill factor* (FF) is a measure of the ideality of the  $J$ - $V$  curve, and is defined in Equation 1.13. A completely square  $J$ - $V$  curve would have a FF of 1, while values in the range of 0.65 to 0.80 are common for DSSCs.



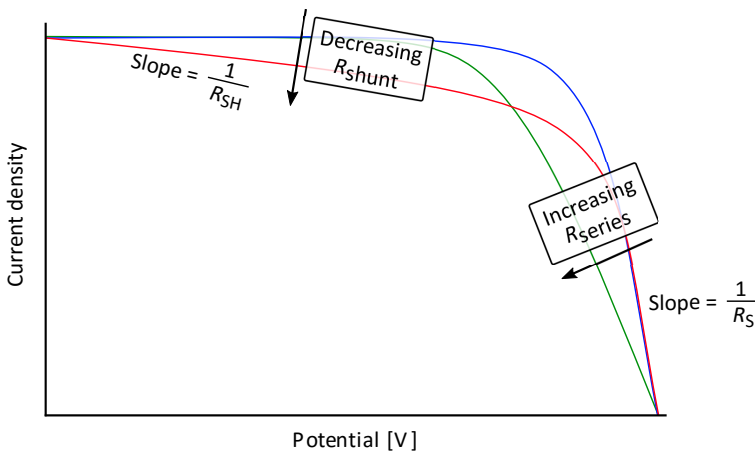
**Figure 1.12:**  $J$ - $V$  curve for **N719** measured under 1 sun AM 1.5G illumination (blue) and under darkness (red). The example data is the  $J$ - $V$  curve for the best performing **N719** device in Paper IV.

$$\text{FF} = \frac{J_{\text{max}} \cdot V_{\text{max}}}{J_{\text{SC}} \cdot V_{\text{OC}}} \quad (1.13)$$

Having extracted the values for  $V_{OC}$ ,  $J_{SC}$  and FF, the power conversion efficiency (commonly abbreviated as PCE or  $\eta$ ) of the device may be calculated from Equation 1.14. This is the ratio of maximum generated electrical power to the incident solar power, hence the intensity of the illumination ( $P_{in}$ ) will also have to be measured reliably. This is usually done with a calibrated reference silicon solar cell.

$$PCE = \frac{P_{max}}{P_{in}} \cdot 100\% = \frac{J_{SC} \cdot V_{OC} \cdot FF}{P_{in}} \cdot 100\% \quad (1.14)$$

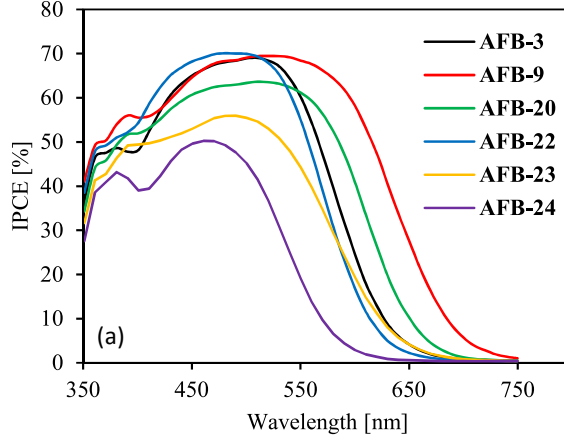
Other useful characteristics may be obtained from the  $J$ - $V$  curve, such as estimates for the  $R_{shunt}$  and  $R_{series}$ . As the shunt resistance decreases, it affects the "flatness" of the  $J$ - $V$  curve near the  $J_{SC}$ , as illustrated in Figure 1.13. Similarly, increased series resistance will make the slope of the  $J$ - $V$  curve close to  $V_{OC}$  less steep. The values of the resistances can be obtained by the inverses of the slopes, i.e.  $R_{series} \approx 1/\text{slope}_{V_{OC}}$  and  $R_{shunt} \approx 1/\text{slope}_{J_{SC}}$ .



**Figure 1.13:** The effect of  $R_{shunt}$  and  $R_{series}$  on the shape of the  $J$ - $V$  curves. High  $R_{shunt}$  and low  $R_{series}$  is favorable. Values of  $R_{shunt}$  and  $R_{series}$  can be found from the inverse of the slopes.

### 1.5.2 Incident photon-to-electron conversion efficiency (IPCE)

The incident photon-to-electron conversion efficiency (IPCE) is another way of measuring the efficiency of a solar cell. Another abbreviation for the same measurement is EQE, short for external quantum efficiency. In this technique, the solar cell is not illuminated by simulated sunlight, but monochromatic light. The IPCE values are simply the ratio of electrons generated to the number of incident photons, per wavelength. The IPCE spectrum will, in contrast to a  $J$ - $V$  curve, give information about at which wavelengths a solar cell is most efficient, as seen in Figure 1.14.



**Figure 1.14:** IPCE spectra of devices with sensitizers **AFB-3**, **9**, **20** and **AFB-22** to **24**. Reprinted from Paper III with permission from Elsevier.

At each wavelength, a  $J_{SC}$  value is recorded from the solar cell. The IPCE value is obtained by dividing the  $J_{SC}$  by the maximum theoretical current, which is the product of the incident light photon flux at the specific wavelength  $\Phi(\lambda)$ , and the elementary charge ( $q$ ), as formulated in Equation 1.15.

$$\text{IPCE}(\lambda) = \frac{J_{SC}}{q \cdot \Phi(\lambda)} = 1240 \cdot \frac{J_{SC}}{\lambda \cdot P_{in}(\lambda)} \frac{[\text{A cm}^{-2}]}{[\text{nm}] [\text{W cm}^{-2}]} \quad (1.15)$$

In devices such as DSSCs, the IPCE can further be explained in terms of the light harvesting efficiency (LHE) of the dye film and the absorbed-photon-to-electron efficiency (APCE). The APCE is the product of the injection efficiency from the dye into the  $\text{TiO}_2$  ( $\Phi_{inj}$ ), the regeneration efficiency ( $\Phi_{reg}$ ) and the charge collection efficiency ( $\Phi_{cc}$ ), see Equation 1.16. LHE is by IUPAC called absorbance and is defined as  $\text{LHE} = (1 - 10^{-A})$ .

$$\text{IPCE}(\lambda) = \text{LHE}(\lambda) \cdot \text{APCE}(\lambda) = \text{LHE}(\lambda) \cdot \Phi_{inj}(\lambda) \cdot \Phi_{reg}(\lambda) \cdot \Phi_{cc}(\lambda) \quad (1.16)$$

The charge collection efficiency is related to what happens to the injected electron in the  $\text{TiO}_2$ . Because of recombination processes, the injected electron will have an average lifetime in the  $\text{TiO}_2$ , called electron lifetime ( $\tau_c$ ). Electron transport through the  $\text{TiO}_2$  is diffusion driven, and the electron transport time ( $\tau_{tr}$ ) is the average transport time from injection to collection. The charge collection efficiency reflects the probability of an electron to be collected in the available electron lifetime, see Equation 1.17.

$$\Phi_{cc} = \frac{\tau_c}{\tau_c + \tau_{tr}} = \frac{1}{1 + \frac{\tau_{tr}}{\tau_c}} \quad (1.17)$$

The monochromatic light intensities used in IPCE measurements are significantly weaker than  $100 \text{ mW/cm}^2$ , and accurate measurement of the light intensity per wavelength is crucial. Calibrated silicon photodiodes with a known responsivity are commonly used for this purpose. Because the wavelength distribution of the solar spectrum is well known, it is in fact possible to integrate a recorded IPCE spectrum over the solar spectrum. Thus, an estimate for the device  $J_{SC}$  can be obtained from Equation 1.18.

$$J_{SC} = \int_{\lambda_1}^{\lambda_2} \frac{\lambda}{1240} \cdot \text{IPCE}(\lambda) \cdot E(\lambda) d\lambda \quad (1.18)$$

where  $E(\lambda)$  is the irradiance per wavelength from the 1 sun AM 1.5G solar spectrum. Under most circumstances this estimate should be within 20% of the  $J_{SC}$  obtained from the  $J$ - $V$  sweep, as suggested by Christians et al. for the closely related field of perovskite solar cells.<sup>86</sup> A large disagreement between the two  $J_{SC}$  measurements is often a clue that there is something wrong with the intensity of the solar simulator and should always be explained or investigated further. There are a few scenarios where the integration of the IPCE spectra does not yield reliable  $J_{SC}$  values, such as when the performance of a device is limited by the diffusion rate of the redox couple. In this case, the lower light intensity during the IPCE measurement will be favourable and an overestimated IPCE curve and also  $J_{SC}$  integration will be obtained.

### 1.5.3 Charge extraction and electron lifetime measurements

Charge extraction and injected electron lifetimes measurements are important for understanding the recombination behaviours of a DSSC. From these measurements, the amount of injected charge, and their average lifetime before recombining with the electrolyte are obtained. Being able to measure these will also yield valuable insight into the inner workings of a device, such as figuring out what is causing observed differences in open circuit voltage. The  $V_{OC}$  of a DSSC is defined as the difference in the quasi-Fermi level of the  $\text{TiO}_2$  and the Nernst potential of the redox shuttle, as given in Equation 1.19. Under darkness, no current is flowing through the device, hence the quasi-Fermi level of the  $\text{TiO}_2$  is equal to the redox shuttle potential. As current starts to flow, trap states in the  $\text{TiO}_2$  are filled and the quasi-Fermi level is shifted towards more negative potentials. This is in fact a common observation, as higher light intensities will often yield higher open circuit potentials in DSSCs.

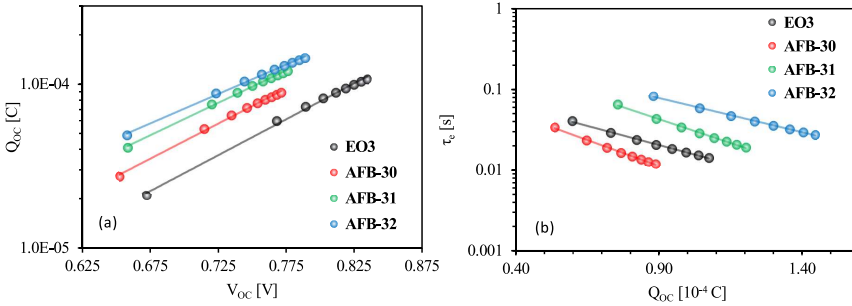
$$V_{OC} = E_{F, TiO_2} - E_{F, redox\ shuttle} \quad (1.19)$$

Further, the quasi-Fermi level of the  $TiO_2$  is defined in Equation 1.20, where the  $E_{CB, TiO_2}$  is the conduction band edge of  $TiO_2$ ,  $k_B$ , the Boltzmann constant,  $T$  temperature while  $n_{CB}/N_{CB}$  is the ratio of electron density to state density in the  $TiO_2$ , i.e. the degree of electron filling.

$$E_{F, TiO_2} = E_{CB, TiO_2} + k_B T \ln \frac{n_{CB}}{N_{CB}} \quad (1.20)$$

Lastly, the  $E_{F, redox\ shuttle}$  can be calculated from Equation 1.21. Here,  $E^\theta$  is the formal redox potential of the couple,  $R$  the gas constant,  $T$  temperature,  $z$  the number of electrons transferred,  $F$  the Faraday constant and  $C_{ox}$  and  $C_{red}$  the respective concentrations of the oxidized and reduced redox species.

$$E_{F, redox\ shuttle} = E^\theta - \frac{RT}{zF} \ln \left( \frac{C_{ox}}{C_{red}} \right) \quad (1.21)$$



**Figure 1.15:** (a) Charge extraction measurements. (b) Electron lifetime measurements. Adapted from Paper IV with permission from the Centre National de la Recherche Scientifique (CNRS) and The Royal Society of Chemistry.

The charge extraction and electron lifetime values will affect the term  $n_{CB}/N_{CB}$  in Equation 1.20. Higher electron lifetimes will increase this term, hence the quasi-Fermi level is shifted upwards, and the  $V_{OC}$  is increased. Equally, higher charge extraction values will be an indication of higher electron filling in the  $TiO_2$ , also lifting the Fermi level and increasing the  $V_{OC}$ . Therefore, being able to measure the injected charge and injected electron lifetime is very valuable, see Figure 1.15 for examples of these plots. A complicating factor is that while the extracted charge ( $Q_{OC}$ ) and electron lifetime ( $\tau_e$ ) influence the  $V_{OC}$ , both are usually measured as a function of  $V_{OC}$ .<sup>87</sup> A solution to this is described in Paper II. It is based on correcting the measurements so that electron lifetimes from different devices are comparable. Any shift in conduction band edge of the  $TiO_2$  can be observed as horizontal shifts of the

charge extraction curves. By adjusting the electron lifetime curves by this relative potential shift, the first term in Equation 1.20 is corrected for. Secondly, we need to make the comparisons of lifetimes at the same potentials, which is done by plotting the  $Q_{OC}$  against the  $\tau_e$ . This requires exponential regression of either of the curves because the voltages obtained for the two measurements are never identical. With the new plot of  $Q_{OC}$  vs.  $\tau_e$ , comparisons of electron lifetimes at the same charge density can be done. Then and only then, can firm statements on differences in electron lifetimes be made.

### 1.5.4 Component characterization

As the DSSC is a closed photoelectrochemical cell, characterization and investigation of individual components is sometimes desirable. A number of the components of a DSSC are possible to characterize separately, prior to device construction. Naturally, the dye molecule is subject to a lot of investigation in order to determine its suitability as a sensitizer for DSSCs. Also the complete photoanodes may be characterized separately, something which is one step closer to device conditions compared to when only investigating the properties of the dyes in solution or as solids.

#### UV-Visible Spectroscopy

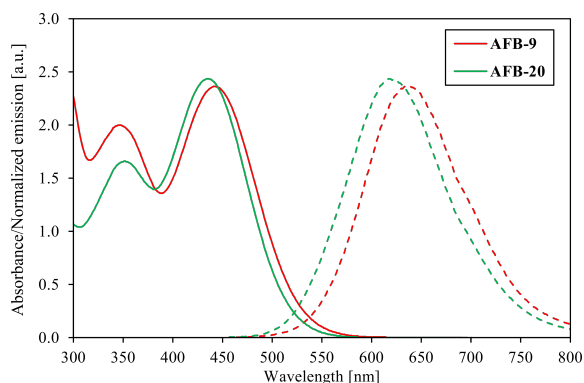
Absorption property measurements in the UV and visible part of the spectrum is very much the workhorse of any dye-focused DSSC laboratory. It provides vital information on how the dyes interact with light of different wavelengths. For some applications, such as DSSCs for indoor use, it is desirable to tailor the absorption properties to the light spectrum of the indoor light. Alternatively, if high efficiency under regular sunlight illumination is the goal, the absorption should cover as many wavelengths as possible. Nonetheless, reliable measurements of UV/Vis absorption is an essential measurement, and important in dye development.

UV/Vis absorption measurements of dyes for DSSCs can be performed in solution, but also while adsorbed onto  $TiO_2$  films on FTO glass. From these measurements, important characteristics such as wavelengths of maximum absorption and molar extinction coefficients can be found. Other characteristics such as dye loading is also measured with UV/Vis absorption spectroscopy.

#### Fluorescence Spectroscopy

In fluorescence spectroscopy, the emission of the molecules is measured when they are illuminated at a specific wavelength, usually their absorption maxima. Fluorescence spectroscopy is also called photo luminescence (PL) spectroscopy or emission spectroscopy. The fluorescence behaviour of dyes is often used for establishing the

optical bandgaps of the sensitizers. The method is based on finding the intersection of the absorption and normalized emission spectra, as shown in Figure 1.16. The wavelength in nanometers is then converted to eV and this is the value for the optical bandgap of the material.<sup>85</sup> An alternative method uses only the absorption onset of the dyes, calculated at 10% of the height of the amplitude of the absorption maximum.<sup>88</sup> The difference between the absorption and emission maxima of the same electronic transition is called the *Stokes shift*. This corresponds to the energy difference between the absorbed and emitted photons due to vibrational relaxation and solvent reorganization.



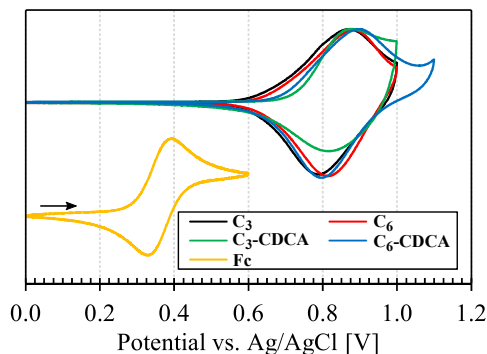
**Figure 1.16:** Absorbance and normalized emission spectra of dyes AFB-20 and AFB-9 in THF solution.

### Cyclic voltammetry

Knowing the optical bandgap is important, but for DSSCs the positions of the HOMO and LUMO levels are equally important, and these can be found from the electrochemical experiment called cyclic voltammetry (CV). Cyclic voltammetry is commonly performed in solution with a three-electrode setup with a working electrode, counter electrode and a reference. A supporting electrolyte is also required, usually an inert salt which is soluble in the solvent of choice. The potential is applied to the working electrode relative to the reference electrode while the current is measured when flowing from the working electrode to the counter electrode.<sup>89</sup> CV measurements are conducted by linearly changing the potential and measuring at which potentials a current signal is observed. By reversing the potential sweep, a full cyclic voltammogram can be recorded, as in Figure 1.17. The signals in the voltammograms correspond to the potentials where the sample undergoes electrochemical oxidation or reduction. Occasionally, both the oxidation and reduction can be found with CV, however it is most common only to obtain the oxidation signal. The energy level of the excited state of the sensitizer is then usually calculated from this ground state po-



tential and the optical bandgap of the dye.



**Figure 1.17:** Normalized cyclic voltammograms adapted from Paper VI. The cyclic voltammogram of ferrocene is shifted downwards for clarity, and the arrow indicates the scan direction.

While solution measurements are most common, CV of dyes adsorbed onto TiO<sub>2</sub> films have recently been developed.<sup>90–92</sup> By virtue of being a chemical reaction, it is expected that the adsorption process will affect the electrochemical behaviour of the dyes. This has indeed been observed for a triarylamine dye reported by Ferdowsi et al., with a difference of almost 200 mV between the solution and TiO<sub>2</sub> experiments.<sup>93</sup> Again, the measurement which is closer to the end application is likely to give the most accurate representation. Another convenient aspect of measuring on TiO<sub>2</sub> films is that the supporting electrolyte used in the CV measurements can be the same electrolyte as used in devices, only without the actual redox species. Cyclic voltammetry is also the method employed to determine the redox potential of the redox couple.

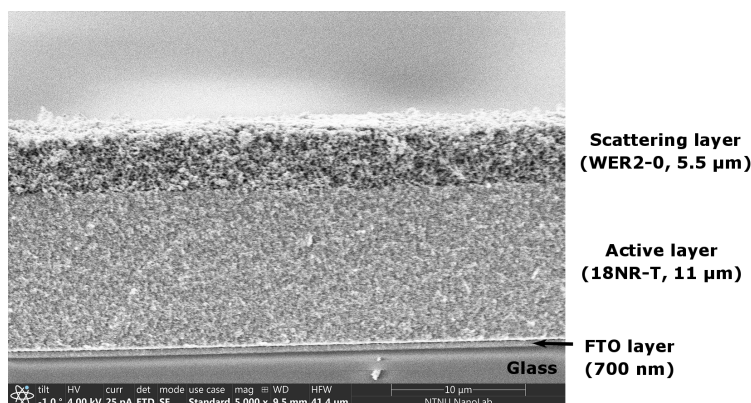
A number of other electrochemical experiments using the same electrochemical setup have been developed, with differential pulse voltammetry (DPV) being one of the more common.<sup>94</sup> The advantage of this technique over standard voltage sweep techniques is it measures only the faradaic currents, so higher sensitivity can be obtained with lower sample concentrations. In regular cyclic voltammetry also non-faradaic currents caused by capacitance are recorded, which do not correspond to any electrochemical reaction, such as oxidation or reduction processes.<sup>89</sup> Additionally, electrochemical techniques such as electrochemical impedance spectroscopy (EIS), intensity-modulated photocurrent spectroscopy (IMPS) and intensity-modulated photovoltage spectroscopy (IMVS) on complete DSSC devices can yield important information on device performance.<sup>95,96</sup> However, these techniques have not been used in this work and will not be covered in any detail.

### Profilometer measurements

In the fabrication of the  $\text{TiO}_2$  electrodes, by either doctorblading or screenprinting, knowing the precise thickness of each layer is important to achieve high reproducibility between devices. A contact profilometer can be compared to a large scale atomic force microscope (AFM). It measures the surface profile with a diamond stylus which is passed over the surface while measuring the profile. With a normal profilometer, surface profiles up to 1 cm in length can be measured, with a height resolution down to 10 nanometers. Paired with being a fast and non-destructive technique, the profilometer is ideal for ensuring the electrodes have the correct thickness of  $\text{TiO}_2$ .

### Scanning electron microscopy

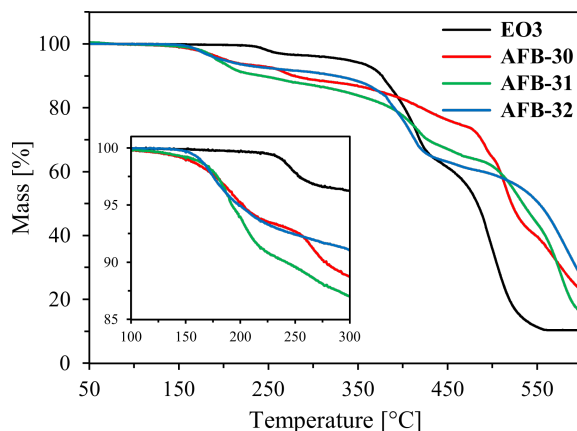
The basis for the scanning electron microscope (SEM) is utilizing the shorter wavelengths of electrons compared to photons in order to greatly increase the magnification of a microscope. By breaking photoanodes and analyzing the cross section by SEM, images such as Figure 1.18 can be captured. With this technique, it is possible to measure the thickness of the various layers. Additionally, SEM will allow the researcher to see features normally not visible with the naked eye, such as the conductive FTO layer but also the ultra thin  $\text{TiO}_2$  blocking layer deposited between the FTO and  $\text{TiO}_2$ . Most SEM instruments will also include other detectors such as Energy-Dispersive X-ray detector (EDX) which can detect the characteristic X-rays of elements when hit by the focused electron beam.



**Figure 1.18:** Cross section SEM image of the  $\text{TiO}_2$  photoanodes used in Paper II. Reproduced from Paper II with permission from The Royal Society of Chemistry.

### Thermogravimetric Analysis

Thermogravimetric analysis (TGA) is a method for determining weight change of a sample during heating. A typical TGA curve reports the sample mass, often given as a percentage of the initial mass, plotted against temperature as seen in Figure 1.19, alternatively time. Most modern TGA instruments also record heat flow, meaning one may simultaneously record thermal events occurring in the sample which are not affecting the sample weight. This technique is called Differential Scanning Calorimetry. As a result, events such as melting and crystallization can be measured alongside events such as combustion and decomposition in a TGA/DSC instrument. Various atmospheres, flow rates and even pressures can be selected, and TGA instruments are often connected to FTIR or mass spectrometers to detect the composition of the decomposition products. In Paper IV, TGA was used to investigate the decarboxylation behaviour of the sensitizers in the study. From TGA it was established the furan  $\pi$ -spacer lowered the decarboxylation temperature significantly compared to the reference sensitizer without furan.



**Figure 1.19:** Thermogravimetric analysis of sensitizers **AFB-30**, **AFB-31**, **AFB-32** and **EO3**. Illustration from Paper IV, reproduced with permission from the Centre National de la Recherche Scientifique (CNRS) and The Royal Society of Chemistry.

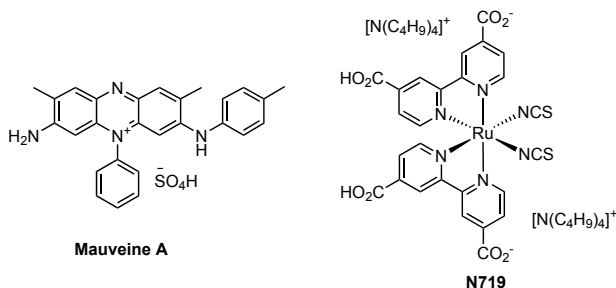
## CHAPTER 2

# INTRODUCTION PART II:

## SENSITIZERS

This aim of this chapter is to give an overview of the history and development of sensitizers for DSSCs. A review of the photovoltaic performance of a selection of phenothiazine sensitizers will also be presented. Because triarylamine dyes were investigated in Paper VI, a small section on the synthesis and performance of these sensitizers is included at the end of this chapter.

For hundreds of years, dyes for fabrics and decorative purposes were either based on minerals or natural dyes. This changed by the accidental discovery of the first synthetic dye, Mauveine (see Figure 2.1), by the 18 year old William Henry Perkin in 1856, while trying to synthesize quinine.<sup>97</sup> While quinine was not synthesized for another 88 years,<sup>98</sup> Mauveine sparked a whole new industry focused around synthetic dyes. The new dye industry grew quickly, and many important developments in chemistry, medicine and other fields have come out of dye laboratories.



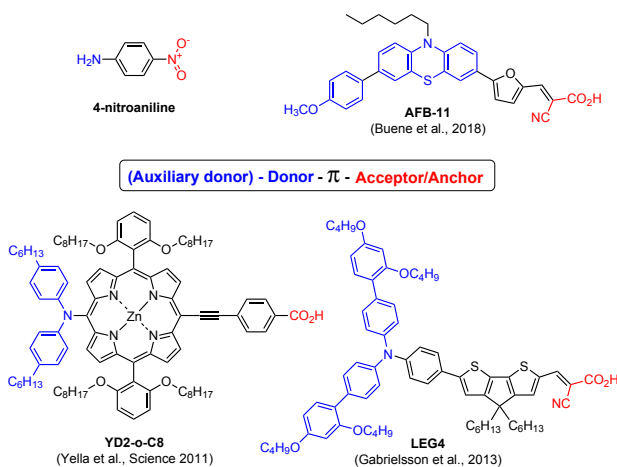
**Figure 2.1:** Structures of *Mauveine A* (one of four structurally very similar components comprising Mauveine) and one of the most popular dyes for dye-sensitized solar cells, **N719**.

In the early days of dye-sensitized solar cells, ruthenium (II) complexes and porphyrins resembling the structure of chlorophyll were in much use.<sup>20,99</sup> Because the absorption of the metal-complex dyes usually cover a large part of the visible spectrum, highly efficient DSSCs can be fabricated, but these sensitizers are also commonly hampered by moderate molar extinction coefficients. This means thick films are needed and this will limit the choice of electrolytes and applications for these sen-

sensitizers. Numerous studies also report on sensitizers extracted from natural sources, often referred to as *natural sensitizers*.<sup>100</sup> While nature is an excellent chemist in many regards, it has not yet synthesized an efficient sensitizer for DSSCs. Many natural dyes have the most wonderful colours, but as sensitizers for DSSCs they usually lack the all-important anchoring group and stability is a reported issue.<sup>101</sup> For natural sensitizers, power conversion efficiencies of 1.7-2.0% have been achieved with extracts from red turnip and pomegranate.<sup>102,103</sup>

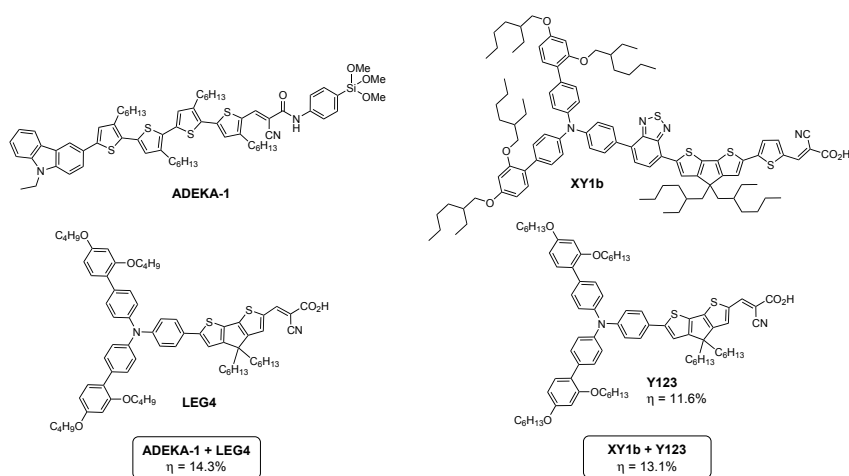
## 2.1 Metal-free sensitizers

Recognizing the flaws with metal-based and natural sensitizers, a new branch of sensitizers started developing, namely the *metal-free sensitizers*.<sup>104,105</sup> Not containing any complexed metal atoms, fully organic sensitizers cannot rely on the same metal-to-ligand charge transfer (MLCT) excitation mechanism. Rather, they are commonly constructed following a push-pull principle promoting an internal charge transfer (ICT) excitation mechanism.<sup>106</sup> This is often referred to as the donor- $\pi$ -acceptor principle, illustrated in Figure 2.2 for a simple push-pull molecule such as 4-nitroaniline,<sup>107</sup> two metal-free sensitizers (**AFB-11** and **LEG4**) and a more complex porphyrin-based sensitizer, **YD2-o-C8**. Sometimes, terms like auxiliary donor or auxiliary acceptor (or both) are used. This usually refers to an additional donating or withdrawing (or both) group attached to the sensitizer, and these systems are commonly abbreviated to D-D- $\pi$ -A or D- $\pi$ -A-A. The terms are inherently vague and are usually further explained in publications.



**Figure 2.2:** Push-pull/donor- $\pi$ -acceptor systems of **AFB-11**,<sup>108</sup> **LEG4**,<sup>109</sup> **YD2-o-C8**,<sup>110</sup> and 4-nitroaniline.

The metal-free dyes have certain advantages, such as a wider array of available chemical reactions in the synthesis of the dyes, more convenient purification processes, compared to the metal-complex dyes such as **N719**<sup>111</sup> (di-tetrabutylammonium cis-bis(isothiocyanato) bis(2,2'-bipyridyl-4,4'-dicarboxylato)ruthenium(II)), see Figure 2.1 for structure. However, while high molar extinction coefficients can be obtained, achieving the same broad light harvesting properties as the metal-based dyes has proved a challenge. Narrow absorption spectra may also be used as an advantage, if several sensitizers with complementary absorption spectra are combined in the devices to cover a larger part of the solar spectrum. Using the dyes shown in Figure 2.3, some of the most efficient devices reported in the literature used this approach, commonly called co-sensitization.<sup>53,58</sup> Kakiage et al. reported in 2015 a co-sensitized system of **LEG4** and **ADEKA-1** achieving a remarkable 14.3% PCE under 1 sun illumination.<sup>53</sup> Cao et al. reported a co-sensitized system of **Y123** and **XY1b** with a novel direct contact device architecture and  $[\text{Cu}^{2+/1+}(\text{tmbpy})_2](\text{TFSI})_{2/1}$  electrolyte, delivering a PCE of 13.1% under 1 sun and a massive 32% under ambient 1000 lux illumination.<sup>58</sup>



**Figure 2.3:** Dyes **ADEKA-1** and **LEG4** co-sensitized by Kakiage et al. to reach 14.3% PCE,<sup>53</sup> and dyes **XY1b** and **Y123** combined by Cao et al. to obtain 13.1% PCE with a copper electrolyte.<sup>58</sup>

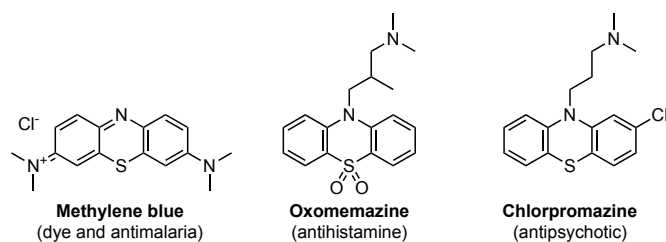
The field of metal-free sensitizers has expanded to include a large number of different dye scaffolds, probably powered by a sense of curiosity and exploration. Over the years, scaffolds including triarylamines,<sup>112</sup> carbazoles,<sup>113</sup> coumarines,<sup>114</sup> oligothiophenes,<sup>115</sup> ullazines,<sup>116,117</sup> squaraine<sup>118</sup> and phenothiazine<sup>119,120</sup> have been investigated. This list is by no means complete, only an example to emphasize the diversity of the sensitizers investigated in the field. The popularity of different scaffolds is like most other topics in science, trending in and out of fashion, much dictated by

other developments in the wider field, such as anti-aggregation additives or novel electrolyte compositions.

## 2.2 Phenothiazine sensitizers

The first example of a phenothiazine-based molecule was the well-known dye and malaria drug *methylene blue*. It was first synthesized by Heinrich Caro and published as part of a patent in 1877 (German Patent No. DE-18771866). Phenothiazine, the main scaffold of *methylene blue* was first reported a bit later, in 1883 by Bernthsen.<sup>121</sup> Initially, research into the phenothiazine class was focused on development of compounds with biological activity for therapeutic uses. *Methylene blue* and derivatives were investigated as antiseptic and anti-malaria agents, while 10*H*-alkyl phenothiazine derivatives were developed as antihistamines, antipsychotic and anti-inflammatory agents.<sup>122</sup> Three examples are given in Figure 2.4. The medicinal applications of the phenothiazine scaffold will not be covered in any further detail in this thesis.

Phenothiazine is a heterocyclic compound essentially comprised of two benzene rings connected by a sulfur and a nitrogen atom. The dihedral angle of the two planes of the benzene rings about the S-N axis is commonly referred to being around 150°, depending on the substituent at the nitrogen atom.<sup>123,124</sup> However, the radical cation of phenothiazine is planar, i.e. a dihedral angle of 180°. <sup>125</sup> As a consequence, a certain reorganization energy has to be considered whenever the phenothiazine backbone is oxidized and reduced.<sup>126–128</sup>

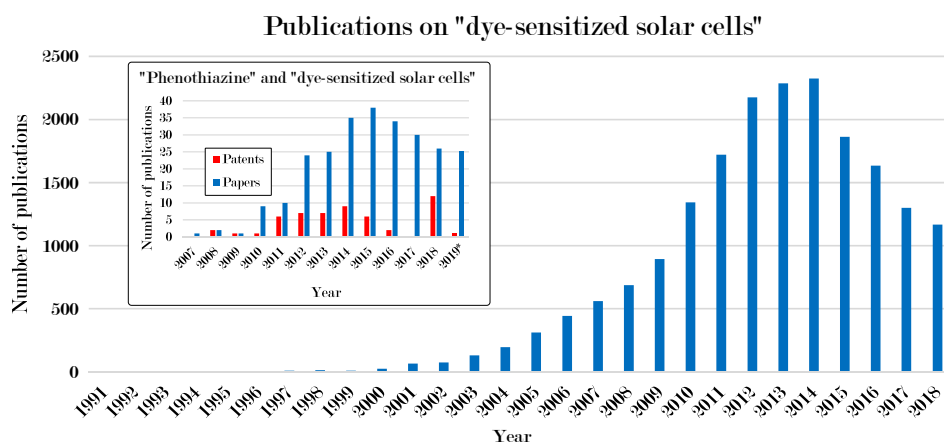


**Figure 2.4:** Structures and uses of Methylene blue, Oxomemazine and Chlorpromazine.

A large amount of research has been performed on sensitizers based on the phenothiazine scaffold for dye-sensitized solar cells.<sup>101,119</sup> A brief literature review for Paper III on SciFinder suggested at least 246 sensitizers have been published in 113 publications, as of 20<sup>th</sup> February 2019. Phenothiazine is sometimes incorporated simply as an electron donating substituent onto other chromophores, such as porphyrins and triaryl amines, or as the main chromophore of the dye. The total structural diversity of all the sensitizers with a phenothiazine component is quite large, but the

structural diversity of the phenothiazine-based dyes is surprisingly narrow, a topic raised in paper III. Another observation with the studies on sensitizers for DSSC is that the sample sets are usually small, often as little as 1-3 sensitizers. Consequently, an opportunity to enter the field of phenothiazine sensitizers arises when producing larger studies of structurally more diverse sensitizers.

The first reports of phenothiazine being used in dye-sensitized solar cells was as electron transport mediators, accelerating the dye regeneration of other sensitizers.<sup>129</sup> Due to their electron donating nature and electrochemical properties, simple phenothiazines were added to the electrolyte to rapidly reduce the oxidized dye before it recombined with an electron from the  $\text{TiO}_2$ .<sup>129</sup> Phenothiazine was in fact also covalently attached, via an alkyl linker, to a ruthenium sensitizer as early as in 1997. Improved lifetime of interfacial charge-separated pairs ( $e_{\text{TiO}_2}^- \text{dye}^+$ ) was achieved.<sup>130</sup>



**Figure 2.5:** Bar plot of number of publications on *dye-sensitized solar cells* per year. Insert shows number of papers and patents per year containing the concepts of *dye-sensitized solar cells* and *phenothiazine*. \*2019 numbers for the period 1.1.19-24.5.19.

Phenothiazine was first used as a sensitizer for DSSC in a 2007 paper by Haining Tian and coworkers.<sup>131</sup> The paper investigated the effect of the cyanoacrylic acid and rhodanine-3-acetic acid anchoring groups as well as looking into the effect of a styrene  $\pi$ -spacer. Since then, a number of journal publications and patents have been published on phenothiazine sensitizers. The bar graph in Figure 2.5 shows the development in number of publications in the DSSC field. The plot only includes papers with the term *dye-sensitized solar cells*. This may cause some inaccuracies in the early years, when this was not an established term for the field as a whole. Following a rapid increase in publications from the early 2000's, the interest has dropped by approximately 50% since 2014. It is natural to associate this drop with the rapid development of the perovskite solar cells field. For phenothiazines in DSSCs,



the bulk of the publications are after 2010 with a clear peak in 2015 followed by the same drop in interest as observed for the DSSC field as a whole. However, something encouraging from the insert in Figure 2.5 is the rise in patents in 2018 and a very promising number of publications already published in the first five months of 2019.

### 2.2.1 Common synthetic routes

On the 10*H*-phenothiazine scaffold there three main reactive sites, C-3, C-7 and the nitrogen atom (N-10). The hydrogen on the nitrogen atom may be removed by a base, and phenothiazine will undergo substitution reactions acting as a nitrogen nucleophile. Phenothiazine will readily react as an amine in the Buchwald cross-coupling,<sup>92,132</sup> and oxidation of the sulfur atom to *S,S*-dioxides readily occurs with peroxy acids<sup>133</sup> and hydrogen peroxide.<sup>134</sup> Sulfide oxidation by *N*-halosuccinimides are surprisingly efficient,<sup>135</sup> and *S*-oxide phenothiazines have been obtained in halogenation reactions with *N*-bromosuccinimide.<sup>136</sup> While substituted nitrogen atoms (-NH<sub>2</sub>, N-HR or -NR<sub>2</sub>) are considered strongly activating and *para*-directing substituents, thioethers (-SR) are only moderately donating. Consequently, nitrogen has the strongest directing properties of the two bridging atoms of phenothiazine, hence electrophilic aromatic substitution occurs predominantly in 3- and 7-positions, *para* to the nitrogen atom.

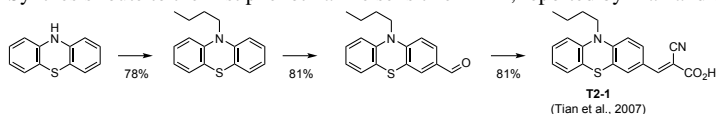
With the reactivity of the phenothiazine scaffold in mind, it is perhaps not surprising that most phenothiazine dyes are extended in the 3-, 7- and 10-directions. Other geometries of phenothiazine dyes requires already functionalized phenothiazine starting materials, the synthesis of those will be covered briefly at the end of this section. A number of synthetic routes have been reported for phenothiazine sensitizers over the years. In Schemes 2.1-2.4, five common synthetic routes are shown leading to literature sensitizers **T2-1**, **P2**, **JH305**, **TLEP-2** and **Z4**. Some main features are prominent for all the routes. Firstly, an alkyl or aryl group is introduced in the 10*H*-position, either with a substitution reaction or a Cu or Pd catalyzed cross-coupling to an aryl halide.

Then, depending on the desired structure of the sensitizers, mono- or dibromination, mono- or di-formylation or mono-formylation followed by bromination is performed to introduce reactive handles in the 3- and 7-positions. The subsequent steps usually introduce auxiliary donors and  $\pi$ -spacers in cross-coupling reactions, or with the Wittig reaction. The latter introduces a potentially isomerizable double bond, and is therefore not extensively used. The widely employed cyanoacrylic acid anchoring group is introduced in a Knoevenagel condensation between an aldehyde and cyanoacetic acid. Ester derivatives are sometimes also used,<sup>137,138</sup> requiring a separate hydrolysis step to yield the finished dye molecule.

The synthesis route to the first phenothiazine sensitizer for DSSC is shown in

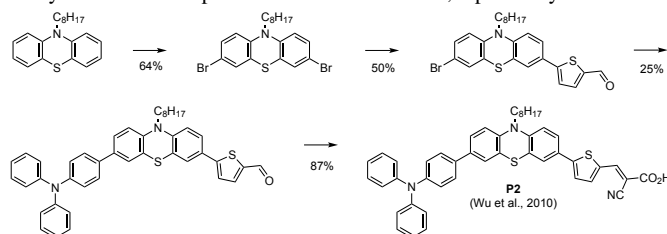
Scheme 2.1. The alkyl chain is first introduced in an  $S_N2$  reaction, before the Vilsmeier formylation was employed for monoformylation. The anchoring group was prepared by the Knoevenagel condensation, yielding **T2-1**. Good yields around 80% for all three steps were reported.

**Scheme 2.1:** Synthesis route to the first phenothiazine sensitizer **T2-1**, reported by Tian and coworkers.<sup>131</sup>



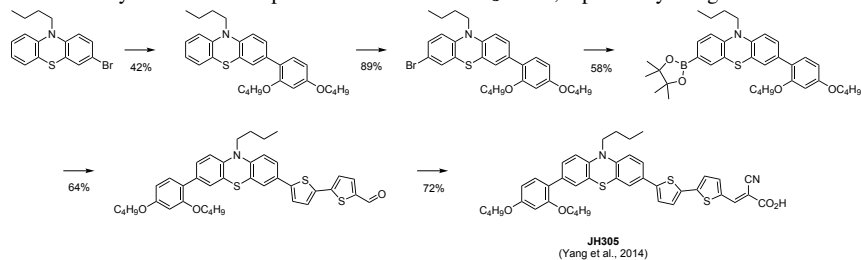
The dye called **P2** is different from **T2-1** in that it has a triphenylamine auxiliary donor and a thiophene  $\pi$ -spacer. Consequently, a different route has to be used, starting from the 10*H*-alkylated phenothiazine, it is dibrominated in 3- and 7-position by molecular bromine, see Scheme 2.2. The symmetric building block which was obtained was then coupled with 1.2 equivalents of 5-formylthienyl-2-boronic acid in a Suzuki cross-coupling in 50% yield. The triphenylamine auxiliary donor was introduced from a boronic acid in a Suzuki cross-coupling before adding the anchoring group to yield dye **P2**.

**Scheme 2.2:** Synthesis route to phenothiazine sensitizer **P2**, reported by Wu and coworkers.<sup>139</sup>

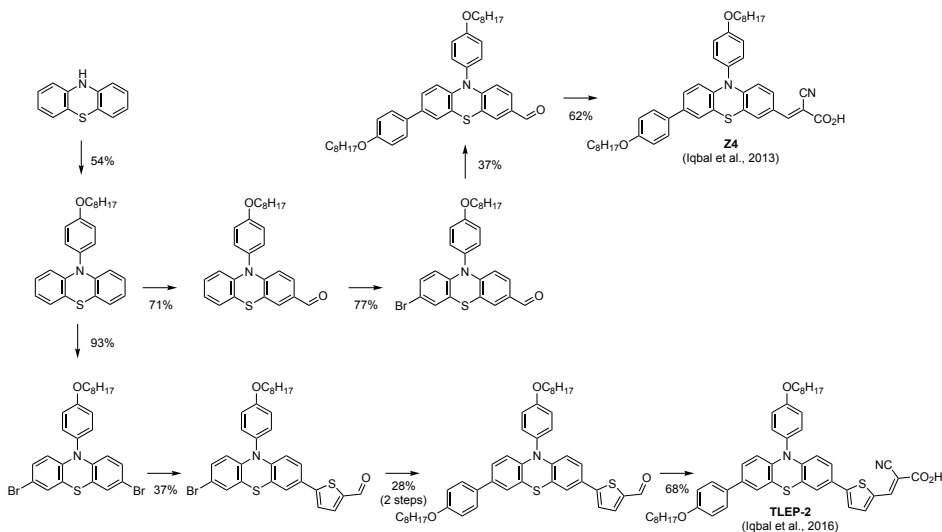


Despite being structurally similar to **P2**, the synthetic route employed towards dye **JH305** is different in that a more stepwise approach was used, see Scheme 2.3. The authors started with 3-bromo-10-butyl-10*H*-phenothiazine, onto which the auxiliary donor was introduced in a Suzuki coupling in a mediocre yield of 42%. Then another bromination of the phenothiazine scaffold by NBS was performed, followed by a lithiation-borylation procedure to introduce a pinacol boronic ester. A subsequent Suzuki coupling with the 2-2'-bithiophene-based  $\pi$ -spacer building block and Knoevenagel condensation gave sensitizer **JH305**.

While alkyl substituents are most common on the nitrogen atom of phenothiazine, a growing number of dyes also use aryls. The dyes **TLEP-2** and **Z4** are examples of this, both prepared by Iqbal et al.<sup>141,142</sup> The first step is a Buchwald coupling of 10*H*-phenothiazine and a 4-alkoxy aryl halide. Dye **Z4**, which has an auxiliary donor but no  $\pi$ -spacer was synthesized in a reaction sequence comprised of monoformyla-

**Scheme 2.3:** Synthesis route to phenothiazine sensitizer **JH305**, reported by Yang and coworkers.<sup>140</sup>

tion, bromination, Suzuki cross-coupling and Knoevenagel condensation. **TLEP-2** is structurally very similar to **Z4**, apart from a thiophene  $\pi$ -spacer which is inserted in the same fashion as for **P2**, onto a symmetric dibrominated phenothiazine building block, as seen in Scheme 2.4. The auxiliary donor is introduced in two steps by borylation and Suzuki cross-coupling, and the Knoevenagel condensation is used to install the anchoring group.

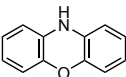
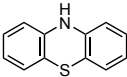
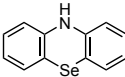
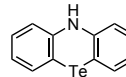
**Scheme 2.4:** Synthesis route to phenothiazine sensitizers **TLEP-2** and **Z4**, reported by Iqbal and coworkers.<sup>141,142</sup>

## 2.2.2 Dyes based on analogues of phenothiazine

Phenoxazine is the structurally closest relative to the phenothiazine class in frequent use, differing only in the 5-position of the scaffold. The selenium and tellurium scaffolds have also been reported, see Figure 2.6. Some well-known dyes such as *Nile red* and *Nile blue* utilize the phenoxazine scaffold. The first report of phenoxazine

sensitizers for DSSCs was in a 2008 patent by Yang et al.<sup>143</sup> While the phenothiazine class has grown large over the years, only 20 journal articles and five patents report phenoxazine sensitizers for DSSCs with the conventional cyanoacrylic acid anchoring group. Recently, a comparative study of two analogous phenothiazine and phenoxazine sensitizers was performed by He et al.<sup>144</sup> The phenoxazine sensitizer was found to be 30% more efficient than the phenothiazine sensitizer, largely attributed to a smaller optical bandgap. To the best of the author's knowledge this is the only comparative study between phenothiazine and phenoxazine sensitizers. A possible reason for the lower interest in phenoxazine dyes could be the lower availability and higher cost of commercial phenoxazine building blocks and derivatives, especially compared to phenothiazine.

No crystallographic data was found for 10*H*-phenoxazine. However, an early study of dipole moments on a selection of heterocyclic compounds by Cullinane and Rees concluded the folding of phenoxazine, if any, had to be small.<sup>145</sup> The flatter structure could be the reason for the bathochromic shift of the phenoxazine dyes relative to phenothiazine, observed by He et al.<sup>144</sup>

				
	Phenoxazine	Phenothiazine	Phenoselenazine	Phenotellurazine
Number of known compounds*	40352	63359	438	78
Benzene plane dihedral angle	≈ 180°	158.5°	149.7°	151.1°
Melting point [°C]	156	185	195	–

**Figure 2.6:** Phenothiazine analogues and their properties. \*Scifinder structure search 07.06.2019.

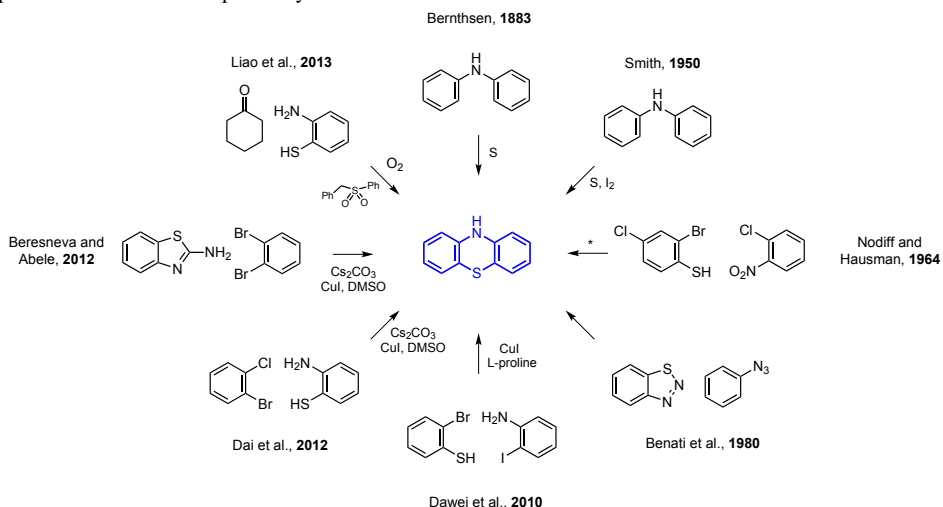
Phenoselenazine and phenotellurazine scaffolds have also been reported and characterized.<sup>146,147</sup> There are only very few examples of compounds with these scaffolds, none of which were prepared for use in dye-sensitized solar cells.

### 2.2.3 Synthesis of phenothiazine scaffolds

Several synthetic protocols have been developed towards phenothiazine-based heterocyclic compounds, and a selection of reactions yielding 10*H*-phenothiazine have been collected in Scheme 2.5. In 1883, the first synthetic procedure to phenothiazine involved the thiocyclization of diphenylamine.<sup>121</sup> Improving on Berntsens protocol, the use of iodine as a catalyst was reported in 1950 by Nathan Smith.<sup>148</sup> Previously reported for phenoxazine synthesis, Nodiff and Hausmann developed the protocol for fusion of bromothiophenols and 2-chloronitrobenzenes by sodium ethoxide, leading to substituted diphenyl sulfides.<sup>149</sup> By reduction of NO<sub>2</sub> followed by formylation,

the subsequent *o*-bromo-*o*-formamidodiphenylsulfide then underwent a Smiles rearrangement to yield 3-chlorophenothiazines. 1,2,3-Benzothiadiazoles have also been used to synthesize phenothiazine in a reaction with phenyl azide reported by Benati et al.<sup>150</sup>

**Scheme 2.5:** Procedures for preparing the phenothiazine scaffold. \* 3-Chloro-10*H*-phenothiazine was the product in the reaction reported by Nodiff and Hausman.<sup>149</sup>



A convenient synthesis route to substituted phenothiazines was yet to be reported until Dawei et al. developed a CuI/L-proline-catalyzed reaction between 2-iodoanilines and 2-bromothiophenols.<sup>151</sup> Dai et al. expanded the scope of this reaction to work with aryl *ortho*-dihalides and 2-aminothiophenols, without the need of a ligand.<sup>152</sup> Further on, the preparation from 2-aminobenzothiazoles and 1,2-dibromobenzene was in 2012 reported by Beresneva and Abele.<sup>153</sup> The last and most recent of the examples was reported by Liao et al. in 2013.<sup>154</sup> In this protocol, substituted phenothiazines were prepared from 2-aminothiophenols and cyclohexanones with molecular O<sub>2</sub>. Using the additives benzyl phenyl sulfone and KI improved the reaction, and a range of substituted phenothiazines were obtained in good yields.

## 2.3 Photovoltaic performance of phenothiazine sensitizers

This section aims to describe the photovoltaic development of the phenothiazine sensitizer class. Two reviews specifically covering phenothiazine sensitizers in DSSC were published in 2016 by Luo et al.<sup>120</sup> and Huang et al.<sup>119</sup> They cover largely the same compounds, but Huang et al. also gives a brief general introduction into synthesis and photovoltaic operation of phenothiazine sensitizers. Both reviews are simply reporting the photovoltaic data with no further processing or discussion of the collected performance data. A selection of phenothiazine sensitizers published between 2007 and 2018 are shown in Figures 2.7-2.10 with the reported photovoltaic performance given in Table 2.1. The sensitizers included are selected to display the diversity of the dyes including the phenothiazine scaffold. A more detailed description of some of the studies is given below, in categories according to the main focus of the studies.

### Studies on the $\pi$ -spacer and anchoring groups

As previously mentioned, the first phenothiazine sensitizers for DSSC were reported in 2007 by Tian et al.<sup>131</sup> In studying the effect of the anchoring group, the cyanoacrylic acid anchoring group was found far superior to the rhodanine-3-acetic acid anchor. Secondly, the paper investigated the effect of a styrene  $\pi$ -spacer for the dye **T2-2**. Surprisingly perhaps, the introduction of the extra styrene moiety affected the light absorption properties negatively and lowered the  $V_{OC}$  by almost 40 mV, also reducing the PCE compared to the simpler dye **T2-1**, shown in Figure 2.7.

The **V7** dye (Figure 2.8) is one of the very few published dyes that have a geometry differing from positions 3, 7 and 10 on the phenothiazine core, however that was not investigated in this study by Marszalek et al.<sup>155</sup> Rather, the study addressed the effect of the  $\pi$ -spacer, very similarly to the seminal study by Tian et al.<sup>131</sup> Again, a massive difference in  $V_{OC}$  of 77 mV in favour of the dye with no  $\pi$ -spacer (**V5**) was reported. Despite this, the broader absorption of **V7**, compared to the reference dye **V5**, increased the  $J_{SC}$  sufficiently for this dye to deliver the highest PCE of the study.

With the sensitizer **P6H2T2A** (Figure 2.7) Yang et al. compared the effect of one versus two  $\pi$ -spacers and anchoring groups.<sup>156</sup> The dianchoring sensitizer had the highest extinction coefficient and most redshifted absorption. However, the additional protonation from the second anchoring group brought the  $V_{OC}$  down resulting in identical PCE compared to the mono-anchored dye.

As the last example in this section, Hart et al. studied the position of the anchoring group on the phenothiazine dye scaffold.<sup>157</sup> **Dye 4** in Figure 2.8 was compared to three dyes with the anchoring group in the 3-position on the phenothiazine backbone. **Dye 4** had the lowest dye loading,  $V_{OC}$  and PCE by a big margin.

### Studies on the auxiliary donor

Kim et al. studied extending the conjugation on the auxiliary donor side of the phenothiazine core by a double bond and a triphenylamine unit, see **D-PTZ-A** in Figure 2.8.<sup>158</sup> Unfortunately, it was not compared to a simpler dye, but by comparing the absorption to that of **T2-1** a redshift of approximately 50 nm can be estimated with comparable extinction coefficients. It should be noted that different work-up procedures may affect the degree of protonation, and subsequently the absorption properties.

The effect of an auxiliary donor was among the topics investigated by Gao et al., with the dye **JY-33** in Figure 2.9.<sup>159</sup> An improvement in PCE of 14% was found when this dye was compared to the analogue without the 4-butoxyphenyl auxiliary donor, despite lower  $\lambda_{max}$ , extinction coefficient and dye loading.

### Studies on anti-aggregation moieties on phenothiazine

Hua et al. published a thorough study on the effects of chain length on the 10*H*-nitrogen atom of phenothiazine sensitizers.<sup>160</sup> The most efficient devices were fabricated with **PT-C6** (Figure 2.8) delivering a PCE of 8.18%. The octyl-substituted dye was also highly efficient, but even longer or shorter chains (C12 or C2) reduced the efficiency.

A very exciting anti-aggregation moiety on a phenothiazine sensitizer was reported by Manfredi et al. for photocatalytic hydrogen generation.<sup>161</sup> They attached glucose derivative through a click-chemistry reaction to a dianchoring phenothiazine sensitizer, creating the dye **PTZ-GLU** in Figure 2.10. The result was enhanced photocatalytic performance with coadsorbents (glucuronic acid), which was not observed with dyes carrying alkyl chains.

### Phenothiazine as auxiliary donor

Dye **TH208** (Figure 2.7) is the thiophene equivalent to **T2-2**, also reported by Tian et al.<sup>162</sup> This phenothiazine dye was compared to the corresponding triphenylamine (**D5**) and tetrahydroquinoline (**C1-1**) dyes. The absorption in solution was identical for **T2-2** and **D5** while **C1-1** was redshifted. The phenothiazine and tetrahydroquinoline dyes were equally efficient at 6.4% PCE, while the TPA dye delivered 6.0%.

Lately the phenothiazine scaffold has been used as a donor along with other chromophores, like in the Bodipy dye **UY7** by Mao et al. in Figure 2.8.<sup>163</sup> Here, the anchoring group as well as the  $\pi$ -spacer unit was investigated. The furan spacer in **UY7** considerably outperformed the thiophene-spacered **UY5** in terms of PCE, for the same dye loading. For the Bodipy dyes very desirable absorption maxima around 550 nm and extinction coefficients over 70000 M<sup>-1</sup>cm<sup>-1</sup> were reported, but very low  $V_{OC}$  values limited the PCE to 5.3% for **UY7**.

The diketopyrrolopyrrole (DPP) unit is much used in dyes and conjugated polymers, known for its narrow absorption at long wavelengths with high extinction coefficients. In the dye **XS3** (Figure 2.8), Sun et al. used DPP with a phenothiazine donor to create a co-sensitizer for filling an absorption gap in a zinc porphyrin sensitizer.<sup>164</sup> Alone, **XS3** delivered an impressive PCE of 8%, and in a co-sensitized system 10.75% PCE was achieved. **XS3** also employ a triple bond to extend conjugation rather than a double bond, which are known to photoisomerize under illumination.

Another group known for redshifting of absorption is squaraine. With dye **SGT-201** in Figure 2.9, Bae et al. used phenothiazine as a donor while investigating various squaraine-based spacers.<sup>165</sup> Strong absorption properties close to the near-IR was achieved, but prominent aggregation resulted 0.9% PCE, which was improved to 2.0% by the addition of CDCA (50 molar eq.).

Lastly, phenothiazine has been used as an auxiliary donor in several zinc porphyrin dyes, as **LG5** in Figure 2.10 is an example of, published by Krishna et al.<sup>166</sup> The focus of the study was studying seven  $\pi$ -spacer/anchor combinations, from which thiophene and cyanoacrylic acid (**LG5**) was found to be most efficient, reaching a PCE of 10.2%.



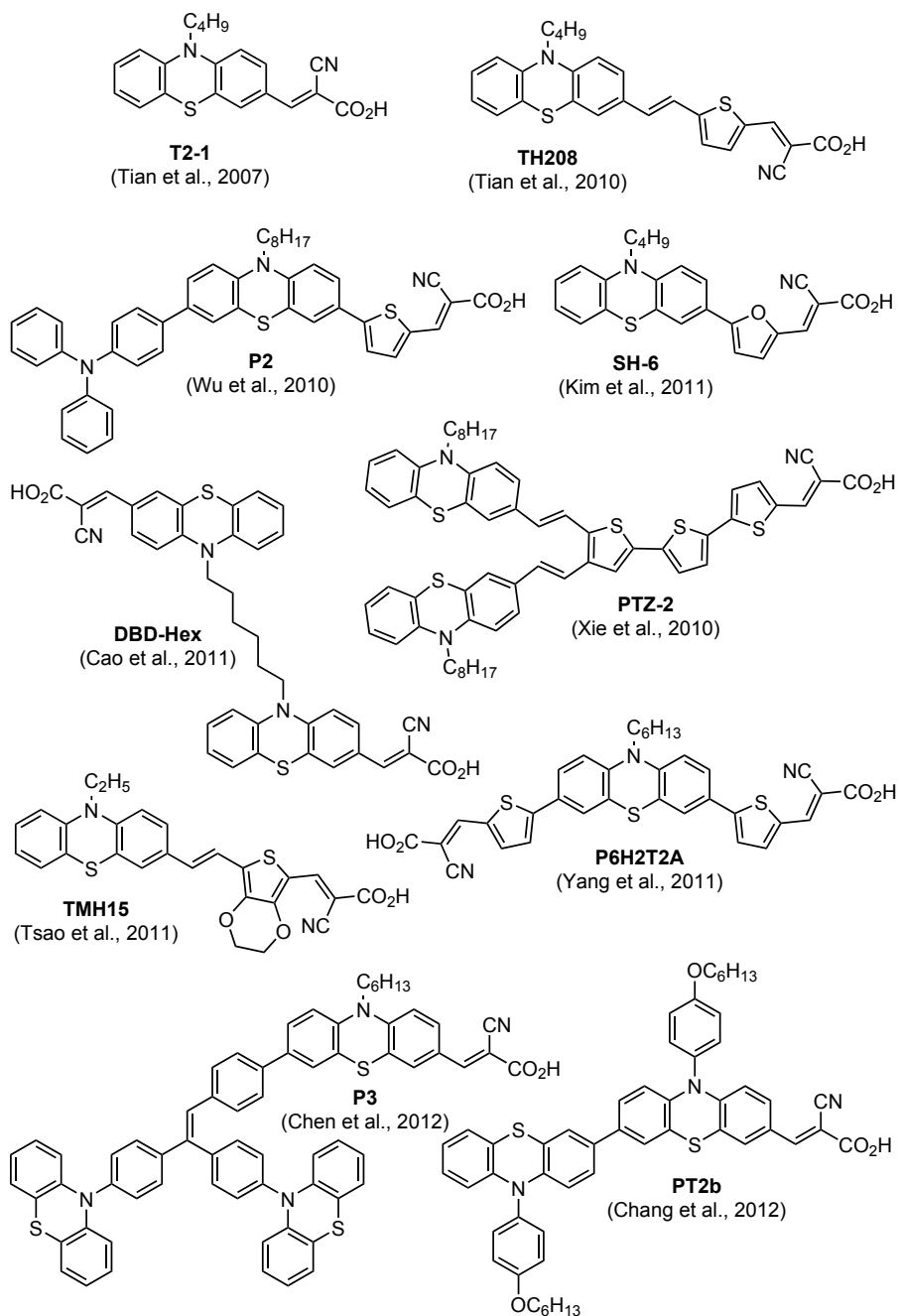


Figure 2.7: A selection of phthalocyanine dyes from 2007-2012.

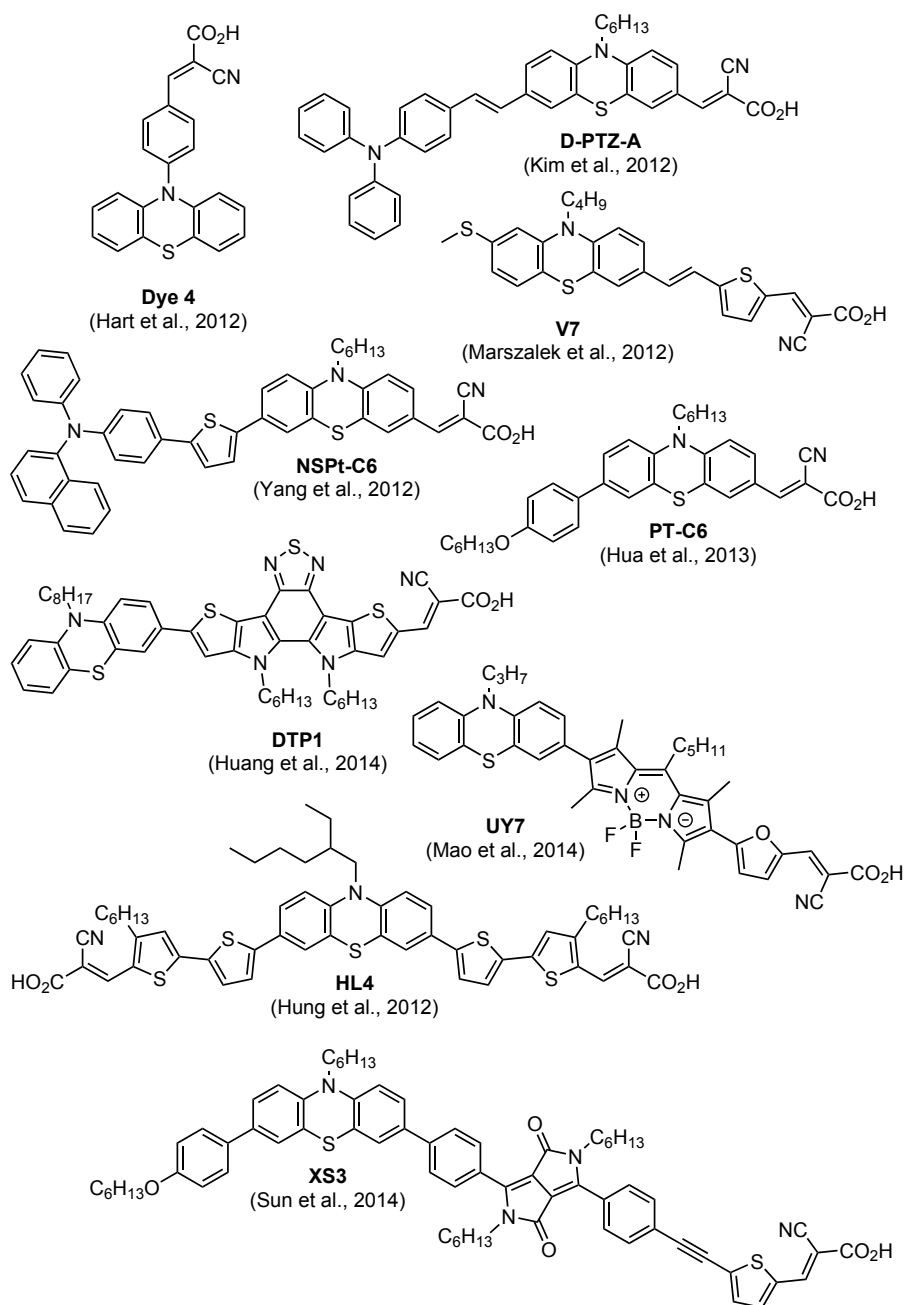
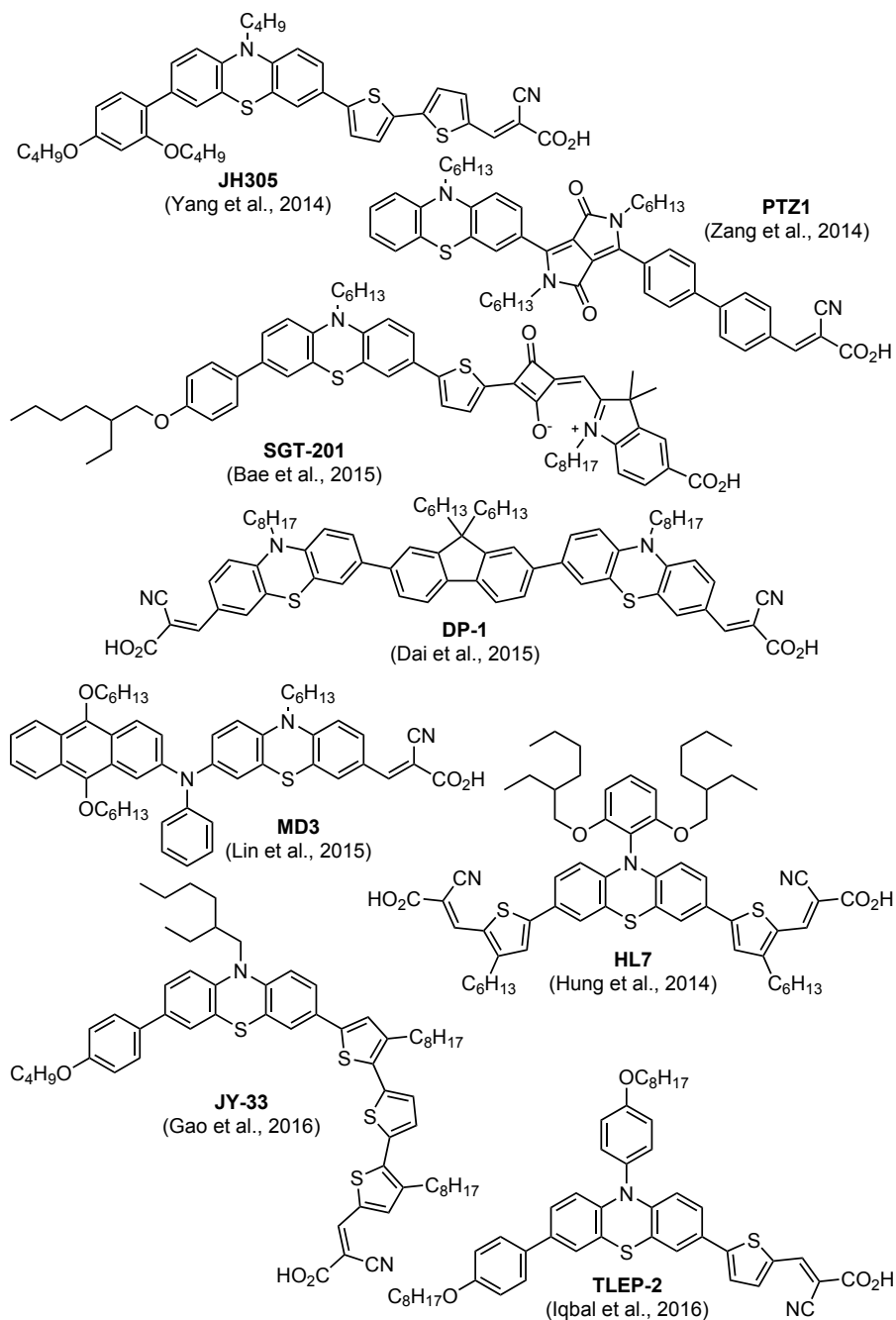
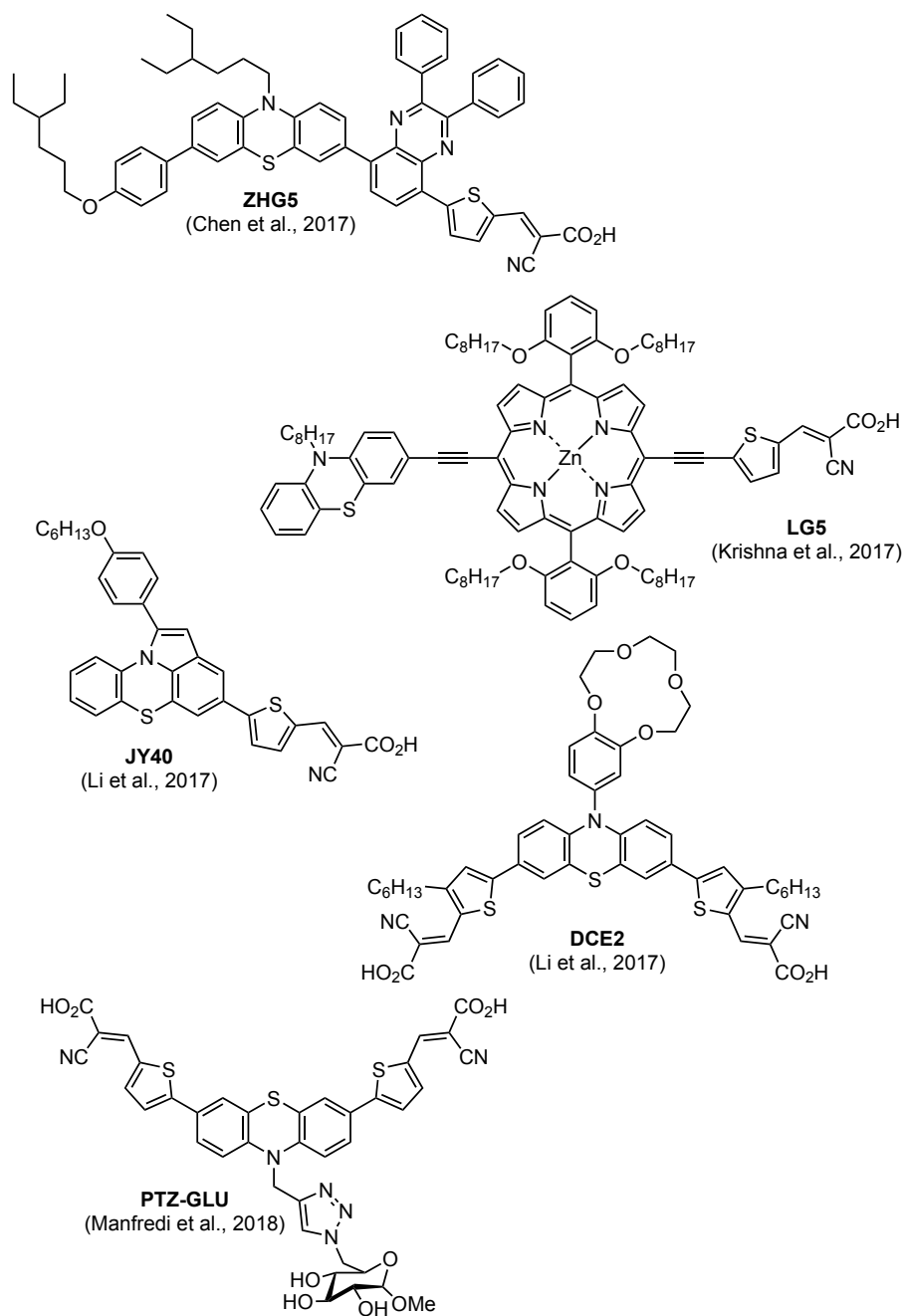


Figure 2.8: A selection of phenothiazine dyes from 2012-2014.



**Figure 2.9:** A selection of phenothiazine dyes from 2014-2016.



**Figure 2.10:** A selection of phenothiazine dyes from 2017-2018.

**Table 2.1:** Photovoltaic performance of a selection of phenothiazine dyes.

Dye name	$J_{SC}$ [mA cm <sup>-2</sup> ]	$V_{OC}$ [V]	FF	PCE [%]	Reference
<b>T2-1</b>	10.9	712	0.71	5.5	Tian et al. <sup>131</sup>
<b>TH208</b>	13.4	685	0.70	6.4	Tian et al. <sup>162</sup>
<b>P2</b>	10.8	592	0.69	4.4	Wu et al. <sup>139</sup>
<b>SH-6</b>	12.2	772	0.70	6.6	Kim et al. <sup>167</sup>
<b>PTZ-2</b>	9.8	662	0.67	4.3	Xie et al. <sup>168</sup>
<b>DBD-Hex</b>	9.3	745	0.68	4.8	Cao et al. <sup>169</sup>
<b>TMH15</b>	15.2	645	0.69	6.7	Tsao et al. <sup>170</sup>
<b>P6H2T2A</b>	11.6	635	0.70	5.2	Yang et al. <sup>156</sup>
<b>P3</b>	12.2	826	0.65	6.6	Chen et al. <sup>171</sup>
<b>PT2b</b>	14.0	820	0.64	7.4	Chang et al. <sup>172</sup>
<b>Dye 4</b>	2.8	620	0.77	1.3	Hart et al. <sup>157</sup>
<b>D-PTZ-A</b>	14.1	746	0.58	6.1	Kim et al. <sup>158</sup>
<b>V7</b>	15.2	691	0.70	7.4	Marszalek et al. <sup>155</sup>
<b>NSPt-C6</b>	14.4	690	0.63	6.2	Yang et al. <sup>173</sup>
<b>PT-C6</b>	15.3	775	0.69	8.2	Hua et al. <sup>160</sup>
<b>DTP1</b>	14.8	642	0.57	5.4	Huang et al. <sup>174</sup>
<b>UY7</b>	13.6	590	0.66	5.3	Mao et al. <sup>163</sup>
<b>HL4</b>	15.9	690	0.67	7.3	Hung et al. <sup>175</sup>
<b>XS3</b>	15.7	748	0.68	8.0	Sun et al. <sup>164</sup>
<b>JH305</b>	16.4	706	0.65	7.5	Yang et al. <sup>176</sup>
<b>PTZ1</b>	11.7	656	0.68	5.2	Zang et al. <sup>177</sup>
<b>SGT-201</b>	6.0	448	0.73	2.0	Bae et al. <sup>165</sup>
<b>DP-1</b>	11.7	726	0.67	5.7	Dai et al. <sup>178</sup>
<b>MD3</b>	15.1	730	0.65	7.1	Lin et al. <sup>179</sup>
<b>HL7</b>	16.2	750	0.68	8.3	Hung et al. <sup>180</sup>
<b>JY-33</b>	17.2	742	0.59	7.5	Gao et al. <sup>159</sup>
<b>TLEP-2</b>	14.9	777	0.63	7.3	Iqbal et al. <sup>142</sup>
<b>ZHG5</b>	12.6	730	0.62	5.6	Chen et al. <sup>181</sup>
<b>LG5</b>	21.0	680	0.71	10.2	Krishna et al. <sup>166</sup>
<b>JY40</b>	13.4	736	0.65	6.4	Li et al. <sup>182</sup>
<b>DCE2</b>	18.2	706	0.69	8.8	Li et al. <sup>183</sup>
	16.0	848	0.75	10.1 <sup>a</sup>	Li et al. <sup>183</sup>
<b>PTZ-GLU<sup>b</sup></b>	-	-	-	-	Manfredi et al. <sup>161</sup>

<sup>a</sup> Cobalt electrolyte<sup>b</sup> Synthesized for Dye-Sensitized Photocatalytic Hydrogen Generation

## 2.4 Triarylamine sensitizers

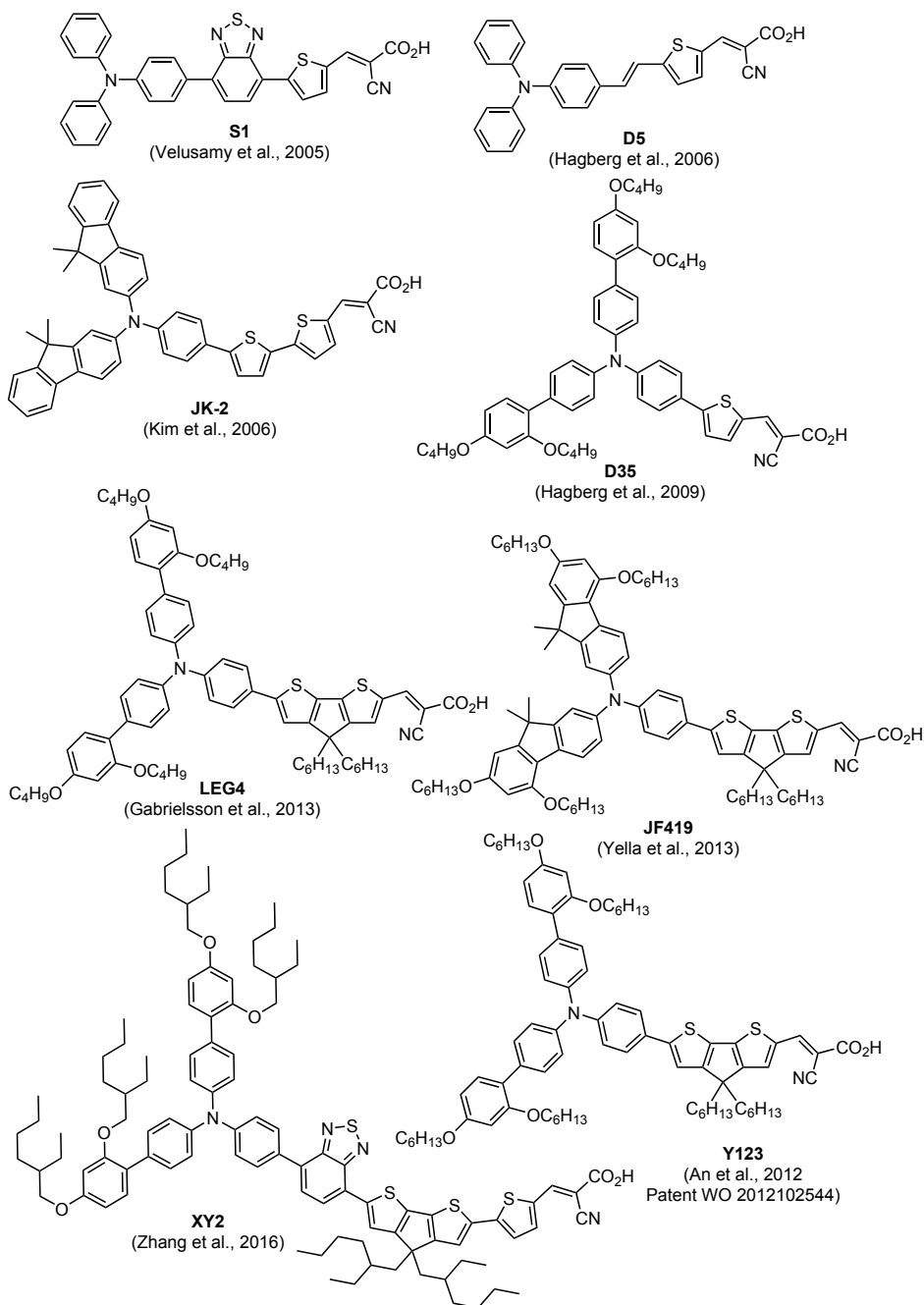
One of the most popular groups of sensitizers in the field of DSSC are the triarylamines. More commonly called triphenylamines, they have been continuously developed since the first report in 2005 by Velusamy et al.,<sup>184</sup> describing the simple triphenylamine dye **S1** in a study comparing benzothiadiazole and benzoselenadiazole. Since then, the number of reported triarylamine sensitizers has grown tremendously. A quick literature search on Scifinder indicates around 3000 triarylamine dyes with the cyanoacrylic acid anchoring group, at the time of writing this thesis. A very limited selection has been included in Figure 2.11, with corresponding photovoltaic performance parameters in Table 2.2.

The triarylamine sensitizers vary enormously in complexity, from the simplest dyes that are prepared in a few steps to highly complex structures. In the triarylamine donor, cross-coupling reactions such as the Buchwald-Hartwig amination and the Suzuki-Miyaura coupling are frequently used. The presence of *para* alkoxy groups is frequently used to red-shift the absorption of sensitizers.<sup>185</sup> Further development found additional alkoxy groups in the *ortho* and *para* positions inhibited recombination with the  $I^-/I_3^-$ <sup>186</sup> and cobalt electrolytes.<sup>187</sup> The 2,4-dialkoxy phenyl units are now common structural elements in many high performance triarylamine dyes.<sup>90,188,189</sup> As for the  $\pi$ -spacer part, so many variations are reported, and coupling reactions are usually a necessity. Because of the loss of orbital overlap between aromatic rings due to ring twist, some  $\pi$ -spacers have polycyclic units, locking the rings into one plane. To obtain such moieties, interesting ring-closing reactions are utilized. The  $\pi$ -spacer of the **LEG4** and **Y123** dyes has been synthesized by cyclization, forming the central ring of the cyclopentadithiophene moiety.<sup>109</sup>

**Table 2.2:** Photovoltaic performance of a selection of triarylamine dyes.

Dye name	$J_{SC}$ [mA cm <sup>-2</sup> ]	$V_{OC}$ [V]	FF	PCE [%] <sup>a</sup>	Reference
<b>S1</b>	10.4	546	0.66	3.8	Velusamy et al. <sup>184</sup>
<b>D5</b>	11.9	660	0.68	5.1	Hagberg et al. <sup>190</sup>
<b>JK-2</b>	14.0	753	0.77	8.0	Kim et al. <sup>191</sup>
<b>D35</b>	13.0	750	0.61	6.0	Hagberg et al. <sup>188</sup>
<b>LEG4</b>	10.9	850	0.74	6.8	Gabrielsson et al. <sup>109</sup>
<b>JF419</b>	16.2	840	0.76	10.3	Yella et al. <sup>192</sup>
<b>Y123</b>	14.6	855	0.70	8.8	An et al. <sup>193</sup>
<b>XY2</b>	10.4	929	0.70	6.9	Zhang et al. <sup>194</sup>

<sup>a</sup> Performance data from the first publication reporting the sensitizer. Many dyes have since been optimized to higher photovoltaic efficiency.



**Figure 2.11:** A selection of important triarylamine dyes from 2005 to 2016.

## 2.5 Suzuki cross-coupling

As most sensitizers for dye-sensitized solar cells have large conjugated carbon-based backbones, the Suzuki coupling is a much treasured tool in dye synthesis. In general, carbon-carbon bond forming reactions are very valuable in organic chemistry.<sup>195</sup> For a long time, researchers had to rely on methodology involving harsh conditions, high temperature or water-sensitive organometallic compounds such as Grignard reagents. While usually reliable reactions, the harsh conditions limited the substrate scope significantly.<sup>196</sup> It was not until the beginning of the 1970's that good reactions for coupling moieties such as aryl, vinyl and alkynyl started emerging. In the center of this development were catalysts of transition metals such as copper, nickel, ruthenium and palladium.<sup>196</sup> The cross-coupling reactions that developed around palladium have become some of the most used methods for carbon-carbon bond formation.<sup>197</sup> The Suzuki cross-coupling is regarded as the most versatile and widely used of the coupling reactions, and its inventor Akira Suzuki was awarded the Nobel Prize in Chemistry in 2010 together with Richard F. Heck and Ei-ichi Negishi, the inventors of their respective named reactions.<sup>198–201</sup>

The Suzuki coupling is the reaction between an organoboron compound and an aryl- or vinyl halide or pseudo halide, facilitated by a palladium catalyst.<sup>200</sup> Some of the most common organoboron compounds includes boranes, boronic esters, boronic acids, trifluoroboronates and MIDA boronate esters.<sup>202,203</sup> A number of attractive features are commonly associated with the Suzuki coupling.<sup>204,205</sup> 1) The great number of commercially available organoboron derivatives and their low toxicity, 2) mild procedures for preparing non-commercial organoboron derivatives exist, 3) very mild conditions, 4) easily removable by-products, both inorganic and organic, 5) extremely wide scope with regards to both major starting materials, 6) the tolerance with respect to different solvents is great, and water is usually tolerated.<sup>206</sup>

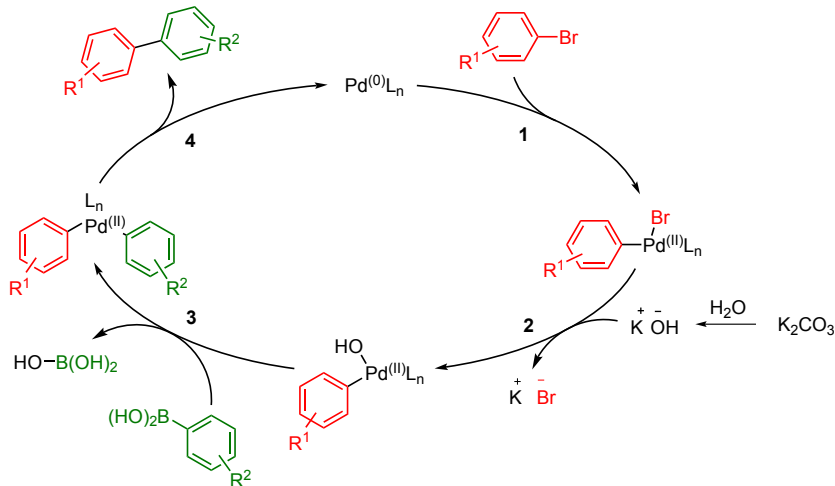
### 2.5.1 Mechanism

The catalytic mechanism of the Suzuki coupling is commonly described proceeding through four steps, oxidative addition, metathesis, transmetalation and reductive elimination, numbered 1-4 in Scheme 2.6.<sup>204,207,208</sup> The inclusion of the metathesis is sometimes debated and occasionally a rearrangement step is included before the reductive elimination. The cycle begins with the formation of the active catalyst, a  $\text{Pd}^0\text{L}_n$  complex, usually from a precursor such as  $\text{Pd}(\text{PPh}_3)_4$  upon dissociation of ligands. Palladium (II) precursors like  $\text{Pd}(\text{OAc})_2$  will spontaneously yield palladium (0) complexes with phosphine ligands.<sup>209</sup> In this process, palladium transitions from a saturated  $d^{10}$  18 electron complex into the active  $d^6$  complex with 14 electrons. The palladium center is then activated for oxidative addition by insertion into the carbon-



halogen bond of the aryl halide. Palladium is formally oxidized to a  $\text{Pd}^{\text{II}}$  species, where it remains until the reductive elimination, when it is returned to  $\text{Pd}^0$  and another cycle may begin.

**Scheme 2.6:** A simplified catalytic cycle for a standard Suzuki cross-coupling.

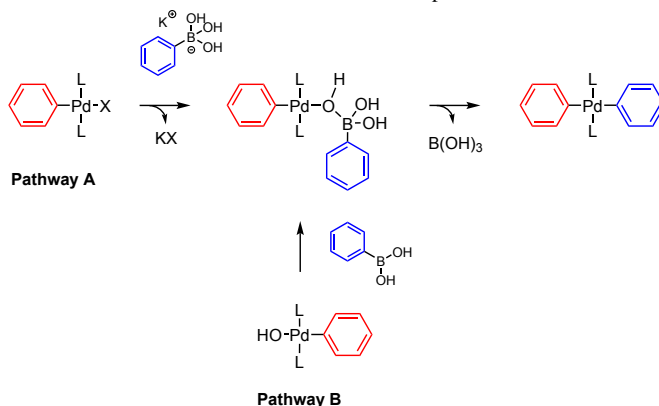


In the *oxidative addition* step, palladium inserts into the carbon-halogen bond of the aryl halide, and palladium is oxidized from  $\text{Pd}^0$  to  $\text{Pd}^{\text{II}}$ . Weaker C-X bonds will increase the rate of this step, in most cases following the order C-I > C-Br > C-Cl > C-F. As a consequence, electron withdrawing groups on the aryl halide will accelerate this step. Similarly, higher electron densities on palladium will also promote the rate of oxidative addition. Adjusting the electron density on the palladium central atom is done by altering the nature of the ligands, and the oxidative addition step may even be reversed by the addition of excess phosphine ligands.<sup>210,211</sup> The oxidative addition is usually claimed to be the rate-determining step of the Suzuki coupling, however a few exceptions have been reported where the transmetalation step is suggested to be rate-determining.<sup>212,213</sup>

The *metathesis* is a much debated step sometimes included in the Suzuki-coupling catalytic cycle. The controversy is related to the role of the base, and two pathways are postulated. Pathway A, also referred to as the 'boronate' pathway, involves the base reacting with the boronic acid to form a four-coordinate boron species, which enters the catalytic cycle in the transmetalation step. In pathway B, also called the 'oxopalladium' pathway, the base replaces the halide of the palladium complex, creating an organopalladium hydroxide R-Pd-OH complex. Here, the four-coordinate boronate species is only formed upon association with the palladium complex, by attack of a Lewis acid present in either of the palladium ligands. Recent evidence

suggest pathway B to be the main pathway, claiming  $\text{Ar-B(OH)}_3^-$  is non-reactive in comparison.<sup>208,214</sup> Thus, the catalytic cycle shown in Scheme 2.6 includes the oxopalladium pathway.

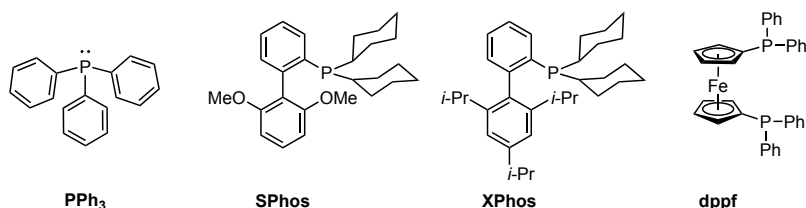
**Scheme 2.7:** The two pathways leading into the transmetalation step with the elusive Pd-O-B intermediate, as reported by Thomas and Denmark.<sup>215</sup> Reductive elimination proceeds from the Ar-Pd-Ar complex.



*Transmetalation* is the process where an organic group is transferred from one metal to another, in the case of the Suzuki coupling, from boron to palladium.<sup>215</sup> While organoboron compounds are electrophilic, the organic moiety of these compounds is slightly nucleophilic.<sup>216</sup> Electron donating substituents will increase the nucleophilicity, thus the rate of transmetalation is accelerated.<sup>217</sup> The two pathways leading into the transmetalation step are shown in Scheme 2.7, as suggested by Thomas and Denmark, who recently reported the isolation and characterization of several pre-transmetalation Pd-O-B intermediates.<sup>215,218</sup>

Lastly, *reductive elimination* is the step where the two organic moieties, from the organo halide and organo boron compounds, are eliminated from the palladium complex.<sup>219</sup> This forms the aryl-aryl coupling and returns the palladium back to oxidation state 0, ready for another catalytic cycle. The main effects on the rate of reductive elimination are electronic effects from the ligands and organic moieties surrounding the palladium center, as well as the steric congestion provided by the bulky ligands.<sup>220</sup>

The earliest catalyst system used in the Suzuki coupling was tetrakis(triphenylphosphine)palladium (0) ( $\text{Pd(PPh}_3)_4$ ), which is still a widely used catalyst.<sup>200</sup> Since then, a bewildering amount of research has been conducted into catalyst systems and reaction conditions for the Suzuki coupling, from the simplest systems imaginable with Pd/C<sup>221,222</sup> to complex graphene oxide/palladium composite catalytic aerogels.<sup>223</sup> Some of the more common ligands encountered in the literature are the biaryl ligands pioneered by Stephen L. Buchwald.<sup>204</sup> Four of the most frequently



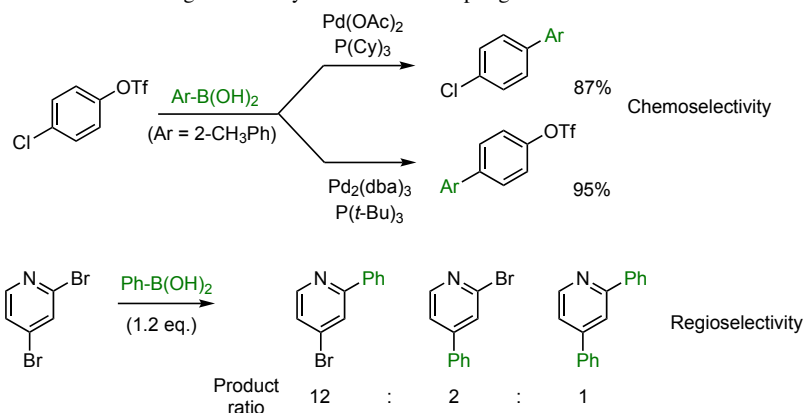
**Figure 2.12:** Common ligands for the Suzuki coupling.

employed ligands are shown in Figure 2.12. SPhos and XPhos have given very active catalytic systems particularly for heteroaromatic systems.<sup>224,225</sup> Further development of XPhos into XPhos 2<sup>nd</sup> generation precatalyst allowed the formation of the catalytic complex to occur under mild conditions, allowing the coupling of unstable boronic acid derivatives commonly prone to decomposition.<sup>226,227</sup> Lastly, the 1,1'-bis(diphenylphosphino)ferrocene (dppf) ligand is much used in the Miyaura borylation, but is also highly efficient in the Suzuki cross-coupling.<sup>228</sup>

### 2.5.2 Selectivity

Selectivity between different halogens (or pseudo halides) available in a substrate is called *chemoselectivity*. Selectivity between the same halogen, but in different positions is called *regioselectivity*, as explained in Scheme 2.8. The general order of reactivity for the aryl halides in the Suzuki coupling follows the order of I > Br > Cl > F, but can be affected by steric or structural properties of the substrates.<sup>216</sup> Selectivity can be tuned by changing the electronic and steric properties of the ligands on palladium.

**Scheme 2.8:** An excellent example of catalyst directed chemoselectivity from Littke et al.<sup>229</sup> and an example from Sicre et al.<sup>230</sup> on regioselectivity in the Suzuki coupling.



Another way of tuning reactions where multiple products may be formed is to alter the ratio of substrate and boronic acid. While this does not affect the selectivity in the coupling, it will affect the product mixture composition. At some point the limiting reactant will run out and the reaction halts at the achieved composition. If the purification of the reaction mixture is optimized and the non-limiting reagent is cheap or easily recovered, this can be a very valuable approach to increase the yield of the desired product.

### 2.5.3 Challenges

Despite the versatility of the Suzuki coupling, in certain situations researchers still run into trouble. Especially coupling of some nitrogen- and sulfur-containing heterocyclic compounds has been challenging.<sup>224</sup> The source of the problem can be related to the instability of the heterocyclic compounds, either as the boronic acid derivative or aryl halide.<sup>231</sup> It can be equally detrimental if either of the starting materials or even the product acts as a catalyst scavenger, complexing and thus inactivating the catalyst from completing the reaction.<sup>232</sup> The use of other coupling protocols may sometimes solve the challenge. The Stille coupling is a very good alternative for tricky reactions involving heterocyclic compounds such as thiophenes.<sup>233,234</sup> Changing the catalyst from palladium to nickel has in some cases given better yields for challenging Suzuki coupling reactions of aryl chlorides.<sup>235,236</sup>

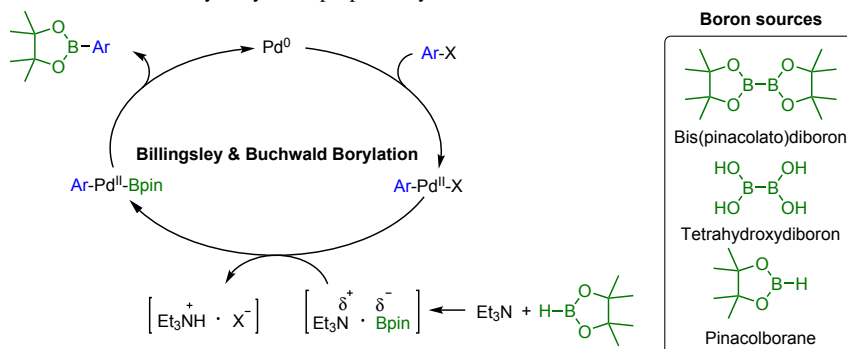
## 2.6 Miyaura borylation

By far the most used borylation protocol of aryl halides is through lithiation.<sup>237,238</sup> While being good reactions, this protocol requires low temperature, flammable bases and the functional group tolerance is limited by the strongly basic conditions. Luckily, an alternative route to these useful compounds has been developed based on palladium catalysis. The *Miyaura borylation* reaction prepares boronic esters from aryl or alkenyl halides.<sup>239</sup>

The catalytic cycle of the borylation is related to that of the Suzuki-Miyaura cross-coupling. In place of a boronic acid, the coupling partner is a diboron reagent such as bis(pinacolato)diboron. Avoiding formation of the Suzuki-Miyaura byproduct during the reaction is achieved by the choice of base, and hard Lewis bases such as potassium acetate or phenoxide are much used.<sup>202</sup> If the boronic acids are required a subsequent hydrolysis was the only solution. However, in 2010 a variant of the same reaction using tetrahydroxydiboron was demonstrated by Molander et al.<sup>242</sup> Using this protocol the boronic acids were obtained directly from aryl halides.<sup>243</sup>

Despite the often high yields and conversions of the Miyaura-borylation, this reaction does not display impressive atom efficiency. Following the transmetalation

**Scheme 2.9:** Plausible catalytic cycle for the palladium catalyzed borylation reaction reported by Billingsley and Buchwald.<sup>240</sup> Catalytic cycle as proposed by Murata et al.<sup>241</sup>

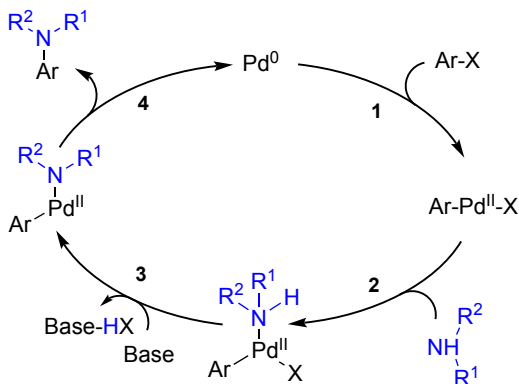


step, the half of the diboron reagent not included in the product is effectively wasted. A solution to this came in 2008 from Billingsley and Buchwald.<sup>240</sup> They reported the successful use of pinacolborane in a palladium catalyzed borylation reaction, yielding pinacol boronic ester products in good yields. Further improvements of atom efficiency in related borylation reactions has been achieved through direct C-H borylation on alkanes with rhenium catalysis<sup>244</sup> and on arenes with iridium-catalysis.<sup>245</sup>

## 2.7 Buchwald–Hartwig amination

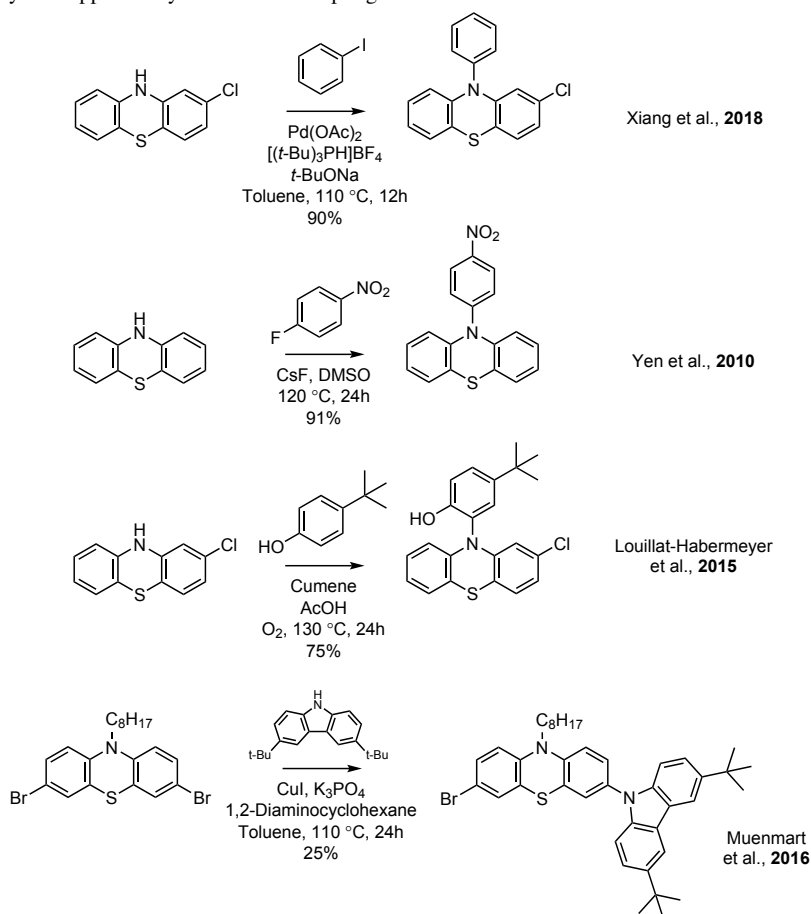
Arylated amines are useful compounds found in applications ranging from pharmaceuticals and natural products to catalyst ligands and organic electronic materials.<sup>246</sup> Hence the development of mild C-N coupling protocols has been a topic of high importance.<sup>247</sup> In 1983, a palladium-catalyzed protocol resembling the Stille reaction was reported for the coupling of  $\text{Bu}_3\text{SnNEt}_2$  to aryl bromides by Kosugi et al.<sup>248</sup>

**Scheme 2.10:** Catalytic cycle for the Buchwald-Hartwig amination. Ligands are omitted.



Hartwig and Buchwald both worked on improving the scope of the reaction reported by Kosugi et al., and in 1995 they independently found that the free amines may be used if a bulky base was added to the reaction.<sup>249,250</sup> This eventually led to the development of what is now called the *Buchwald–Hartwig amination*, where amines can be cross-coupled to aryl halides. Extensive development of ligands and catalyst systems have since then improved the scope of this reaction, now including electronic and sterically challenging substrates.<sup>251–253</sup>

**Scheme 2.11:** Four examples of C–N bond forming reactions involving phenothiazine. From the top: a Buchwald–Hartwig amination,<sup>254</sup> nucleophilic substitution,<sup>255</sup> dehydrogenative amination with a phenol<sup>256</sup> and lastly the copper-catalyzed Ullmann coupling.<sup>257</sup>



The catalytic cycle of the Buchwald coupling involves four steps as illustrated in Scheme 2.10: 1) oxidative addition, 2) coordination of amine to palladium, 3) base-mediated palladium–amide bond formation and 4) reductive elimination. Phe-

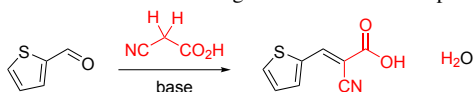
nothiazine readily reacts as the amine in Buchwald coupling with aryl halides<sup>254,258</sup> while the researcher thitherto was limited to the scope of the Ullmann reaction or nucleophilic amination.<sup>255,259,260</sup> Amination on the phenothiazine scaffold may also be done in a dehydrogenative amination with phenols.<sup>256,261</sup> (See Figure 2.11 for examples)

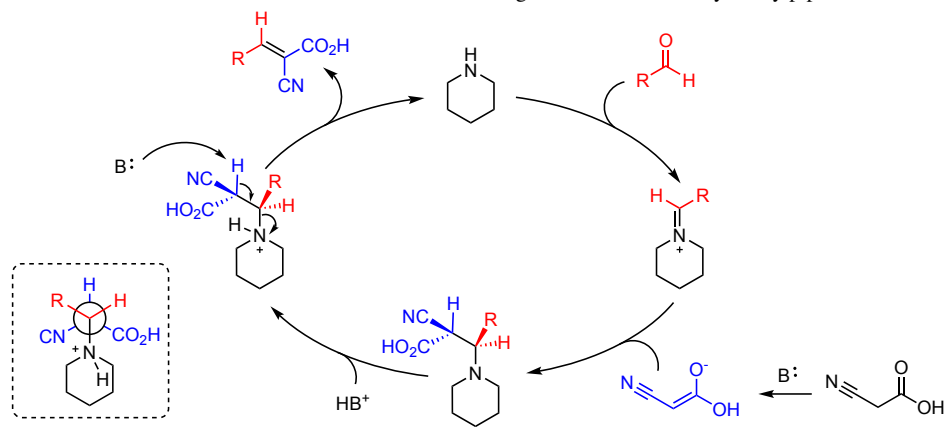
The first catalyst systems employed for the Buchwald coupling used the Pd<sub>2</sub>dba<sub>3</sub> precatalyst and P(*o*-tolyl)<sub>3</sub> ligand.<sup>250</sup> This was a reactive catalyst system, albeit primary amines were incompatible with the protocol leading to dehalogenation and imine formation.<sup>249</sup> Primary amines were however successfully included in the scope when bulky bidentate ligands such as BINAP (2,2'-bis(diphenylphosphino)-1,1'-binaphthyl) and dppf were employed.<sup>262,263</sup> Another development with regards to ligand evolution were the sterically hindered biaryl monodentate phosphine ligands.<sup>264</sup> First introduced by Stephen Buchwalds group, this class of ligands are now extremely common also in other reactions such as the Suzuki coupling and Miyaura borylation.

## 2.8 Knoevenagel condensation

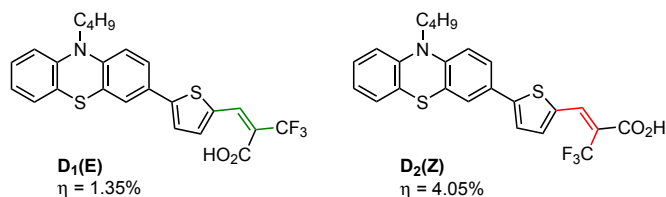
The Knoevenagel condensation is a nucleophilic addition to a carbonyl group with a subsequent elimination of water and the formation of a double bond. The nucleophile is an activated methylene compound and a catalytic amount of base is required, usually ammonium salts, primary or secondary amines, such as piperidine, see Scheme 2.12.<sup>265</sup> The reaction was reported in 1898 by Emil Knoevenagel.<sup>266</sup> In fields such as organic electronics, reactions introducing electron deficient groups while extending a conjugated system are very valuable. Not surprisingly, the Knoevenagel condensation is a favorite reaction among researchers in DSSC research, but also in the field of small molecular acceptor molecules for bulk heterojunction solar cells.<sup>267,268</sup> The mechanism for the Knoevenagel condensation differs based on the conditions, and commonly two major mechanisms are used to explain the reaction. In the first alternative, the role of the base is to deprotonate and thus activate the methylene compound, which subsequently attacks the carbonyl of the aldehyde. In the other mechanism the aldehyde and secondary amine catalyst forms an iminium ion, which is attacked by the activated methylene compound. The second mechanism is illustrated in Scheme 2.13. The Doebner-modification employs pyridine as a catalyst, and through a concerted mechanism the product may directly decarboxylate.

**Scheme 2.12:** Knoevenagel condensation example.



**Scheme 2.13:** Reaction mechanism for Knoevenagel condensation catalyzed by piperidine.

The absolute stereochemistry notation of a double bond, as preferred by IUPAC is the *E-Z* notation. The substituents of the double bond are given priorities according to the Cahn-Ingold-Prelog rules, and the relative position of the substituents with highest priority on either end of the double bond dictates the configuration (*E* for opposite and *Z* for same side). The double bond formed in the Knoevenagel condensation may give rise to both the *E* and *Z* geometric isomers if the activated methylene compound is asymmetric. This is the case for cyanoacetic acid, which is extensively used to prepare the cyanoacrylic acid anchoring group present in the majority of organic sensitizers used in dye-sensitized solar cells. Despite the wide-spread use of this anchoring group, any discussion around the absolute stereochemistry is very rarely included in publications. For DSSC sensitizers, the unanimously reported configuration is the (*E*) isomer. Some work was devoted to this topic in the 90's, and Cho et al. determined by long-range selective proton decoupling  $^{13}\text{C}$  NMR experiments and by X-ray crystallography that the R group of the aldehyde was found *trans* to the carboxylic acid derivative of the methylene compound.<sup>269</sup> Zhang et al. and Maadi et al. later reported similar stereopreference in related systems.<sup>270,271</sup>

**Figure 2.13:** Sensitizers **D<sub>1</sub>(E)** and **D<sub>2</sub>(Z)** reported by Hong et al.<sup>272</sup>



The recent preparation of trifluoromethylacetic acid allowed this reaction to be studied in more detail, with emphasis on the implications on sensitizers for DSSCs. Hong et al. used trifluoromethylacetic acid in a Knoevenagel condensation on 5-bromo-2-thiophenecarboxaldehyde, and obtained a mixture of the (*E*) and (*Z*) isomers.<sup>272</sup> Proceeding with the mixture they were able to separate and obtain both the (*E*) and (*Z*) dye isomers, as shown in Figure 2.13. Note that the Cahn-Ingold-Prelog priority rules here gives  $\text{CF}_3$  priority over  $\text{CO}_2\text{R}$ , and thus the roles of (*E*) and (*Z*) are for this paragraph reversed. The  $^1\text{H}$  NMR shift of the H on the double bond was found at 7.87 ppm for (*E*) and at 8.19 ppm for the (*Z*) isomer. While the photo-physical and electrochemical properties of the two isomers were largely comparable, the photovoltaic performance was very different. The (*E*) isomer delivered a PCE of 4.05% and the (*Z*) isomer a modest 1.35%. Hong et al. postulated the configuration of the double bond affected the binding mode, and as the 'bent' mode of the (*E*) isomer brought the dye cation closer to the  $\text{TiO}_2$  surface, it caused increased electron recombination and lower efficiencies. This was also supported by the considerably lower  $V_{\text{OC}}$  of the (*E*) isomer.

While the Knoevenagel condensation predominantly produces the desirable isomer for dye-sensitized solar cells, this may change during device operation. In a report by Zietz et al., the photoisomerization behaviour of two simple triphenylamine dye was investigated.<sup>273</sup> The conclusion was that the double bond of the cyanoacrylic acid anchoring group is indeed able to photoisomerize when irradiated by visible light. The reverse isomerization was also observed by UV illumination, however not without considerable degradation. Anchored on a semiconductor oxide surface the isomerization was observed, but retarded compared to in solution. Photoisomerization of double bonds has been a concern in dye design for many years,<sup>104</sup> and has been observed in azo dyes,<sup>274</sup> indoline dyes,<sup>275</sup> and triarylamine dyes.<sup>276</sup>

## RESULTS AND DISCUSSION OF PAPERS

This chapter is intended to bring the separate reasoning from the papers together as a whole. First, short summaries of the papers will be given before specific topics spanning several papers will be discussed in separate sections, specifically synthesis and photovoltaic performance across all Papers I-V. A discussion from Paper II on suspicious efficiency data in a phenothiazine DSSC paper will also be covered and elaborated. Despite attempting to cover all the papers, the finest details will still have to be sourced from the original papers, which may be found in the Appendices of this thesis.

Briefly summarized, Paper I-V cover the topics of  $\pi$ -spacers, auxiliary donors and sensitizer geometry for phenothiazine dyes. Our investigations have focused on producing large sample size studies to maximize the confidence in our findings. Paper VI investigates the effect of covalent CDCA substituents on triarylamine dyes.

### 3.1 Summary of Papers I-V

#### 3.1.1 Paper I

The main topic of Paper I was the effect of  $\pi$ -spacers for phenothiazine sensitizers.<sup>108</sup> A robust synthesis route was developed, facilitating a late-stage introduction of the  $\pi$ -spacer moiety, producing a total of 11 sensitizers. Five  $\pi$ -spacers were evaluated in two dye series with different auxiliary donors, in addition to a dye with no auxiliary donor, see Figure 3.1. Considerable trouble was encountered when attempting a Suzuki coupling with 5-formyl-2-thienylboronic acid, and therefore a two-step borylation/Suzuki approach was developed so 5-bromo-2-thiophenecarboxaldehyde could be used as a coupling partner instead. The selection of  $\pi$ -spacers included furan, thiophene, phenyl, *meta*-fluorophenyl and 3,5-difluorophenyl. The fluorine-substituted phenyl-based spacers were included to investigate effects of additional electron withdrawing units. A clear distinction between five- and six-membered  $\pi$ -spacers was found. The five-membered  $\pi$ -spacers outperformed the phenyl-based ones in all photophysical and photovoltaic measurements. For the six-membered dyes, increasing the number of fluorine atoms on the phenyl ring further deteriorated the photovoltaic performance. There are several accounts of thiophene and furan outperform-

ing phenyl as a  $\pi$ -spacer,<sup>166,277,278</sup> however as for the effect of the fluorine-substituted phenyl spacers, opinions are divided. Our findings are supported remarkably well by those of Lin et al.,<sup>279</sup> reporting highly comparable efficiencies for dyes with Ph and PhF spacers, while PhF<sub>2</sub> dramatically decreased the efficiency. Meanwhile, Lee et al. investigated the same series of three spacers, finding the efficiency increased in the order Ph < PhF < PhF<sub>2</sub>.<sup>280</sup>

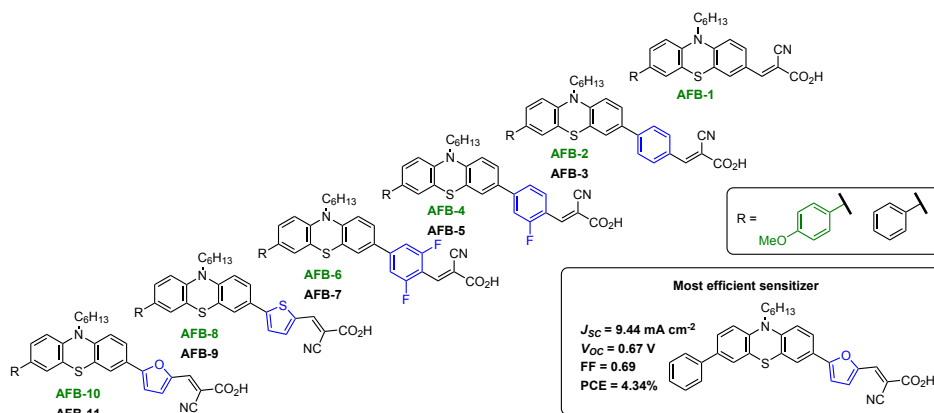


Figure 3.1: Dyes investigated in Paper I.

Surprising at the time, the dye without a  $\pi$ -spacer was inferior only to the furan dyes, predominantly due to a higher  $V_{OC}$  than the dyes with  $\pi$ -spacers. Although not mentioned in our discussion in the paper, this is a common phenomenon for phenothiazine dyes, often reported in similar studies.<sup>92,131,155</sup> Consequently, the performance contribution from the  $\pi$ -linker unit comes at a price of lower  $V_{OC}$ . Lastly, between the two different auxiliary donors used in Paper I, phenyl and 4-methoxyphenyl, no difference in photovoltaic performance could be identified.

### 3.1.2 Paper II

Picking up the curious fact from Paper I that different auxiliary donors did not alter the photovoltaic performance, we designed a study screening a range of auxiliary donors in Paper II.<sup>281</sup> A synthetic route identical to the one developed for the thiophene  $\pi$ -spacer dyes in Paper I was employed, yielding ten sensitizers with different auxiliary donors, see Figure 3.2. Six dyes carried phenyl-based auxiliary donors with various substitution patterns, three with naphthyl-donors and one with a pyrene auxiliary donor. A reference dye with no auxiliary donor was prepared following a similar route, employing a palladium catalyzed dehalogenation protocol to remove the surplus bromine substituent.<sup>282</sup> The various auxiliary donors had a positive effect on the photovoltaic properties, increasing the PCE by 4-11%, with pyrene identified as

the most efficient auxiliary donor. For this sensitizer, the dependence of CDCA on the performance was tested. The optimum performance was found when 10 molar equivalents of CDCA was used in the staining solutions, an enhancement of 27% compared to no co-adsorbent.

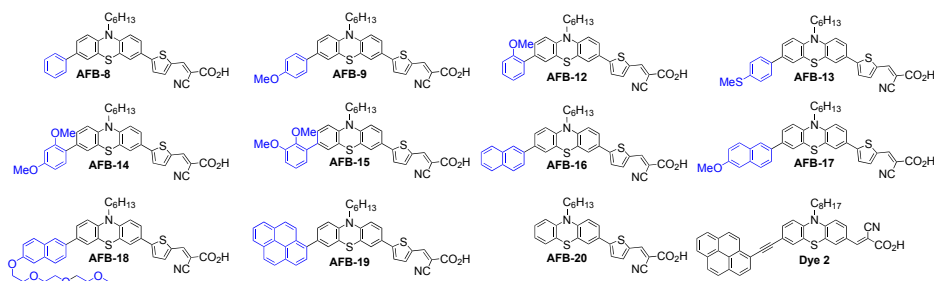


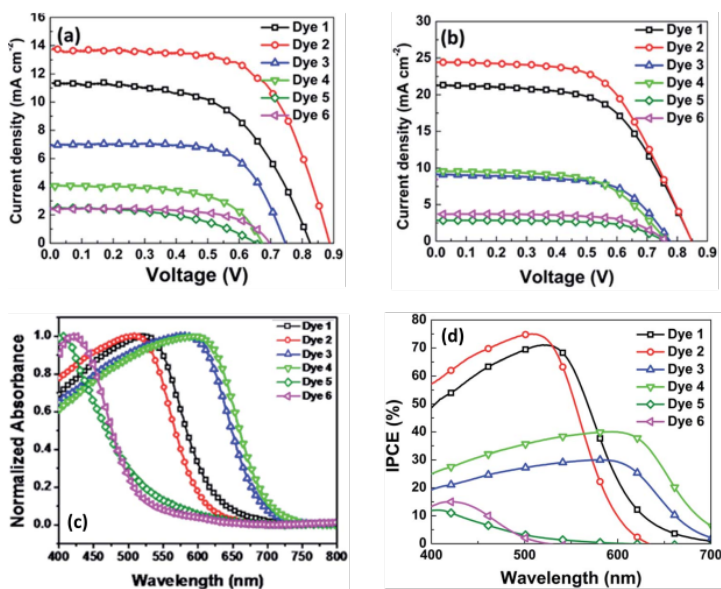
Figure 3.2: Dyes investigated in Paper II.

### Discussion regarding Dye 2 by Nagarajan et al.

Paper II also included the synthesis and evaluation of a sensitizer called **Dye 2** (see structure in Figure 3.2), reported by Nagarajan et al. in 2017.<sup>283</sup> This publication appeared during our work on the pyrene auxiliary donor, and we decided to synthesize the best dye and use it as a state-of-the-art phenothiazine reference. On closer inspection of the published data, we found a number of suspicious performance characteristics. The surrounding discussion in Paper II was a little muted, so the following is a full discussion into why the data reported by Nagarajan et al. was in our eyes, suspicious.

The first thing that caught our attention was the fact that no reference sensitizer was used. For devices with  $I^-/I_3^-$  electrolyte, the reference sensitizer **N719** has been used successfully for years. Due to varying fabrication procedures and materials, the use of reference sensitizers allow rough estimates of different sensitizer systems to be made. Another use of reference sensitizers is as a yardstick for performance, and if the reference performs outside what is commonly reported within the field, it should be further investigated. In our photovoltaic experiments for Paper II, the performance of **Dye 2** was 26% below that of the reference sensitizer **N719**, in identical devices. By assuming the efficiency ratio of **Dye 2** to **N719** would be comparable in devices prepared by Nagarajan et al., the efficiency of **N719** would exceed 16%, which clearly is unrealistic.

Secondly, there was an obvious mismatch between the  $J$ - $V$  characteristics and the published IPCE spectra, see Figure 3.3. The best sensitizer, **Dye 2**, was reported with an average  $J_{SC}$  of  $24.2 \text{ mA cm}^{-2}$ ,  $V_{OC}$  of 856 mV and FF of 0.59, resulting in an average

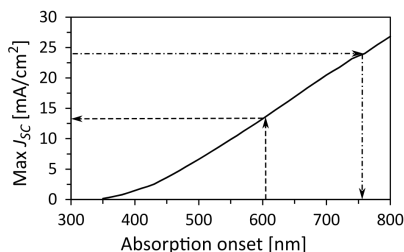


**Figure 3.3:** Original figures from Nagarajan et al. (a)  $J$ - $V$ -sweeps for devices without CDCA, (b)  $J$ - $V$ -sweeps for devices with 10 mM (50 molar equivalents) of CDCA, (c) normalized absorption on  $\text{TiO}_2$  films and (d) IPCE spectra. Reproduced from *J. Mater. Chem. A*, 2017, **5**, 10289–10300 with permission from The Royal Society of Chemistry. (Annotations (c) and (d) have been added by the thesis author.)

PCE of 12.1%. Upon integration of the reported IPCE-spectrum over the AM1.5 G solar spectrum we obtained a moderate  $J_{\text{SC}}$  value of  $7 \text{ mA cm}^{-2}$ . In the closely related field of perovskite solar cells, if  $J_{\text{SC}}$  from the 1 sun measurement and by integration of the IPCE spectra deviates by more than 20%, it should call for further experimental support or explanation.<sup>86</sup> This is also common practice in the dye-sensitized research field. The extremely high  $V_{\text{OC}}$  achieved with an  $\text{I}^-/\text{I}_3^-$  electrolyte consisting of 0.05 M iodine and 0.5 M lithium iodide in propylene carbonate solvent was also a cause for concern. Lithium iodide is a common additive in DSSC electrolytes, contributing with small complexing  $\text{Li}^+$  cations, reducing charge repulsion in the  $\text{TiO}_2$  nanoparticles.<sup>284</sup> However, it also has the effect of lowering the  $V_{\text{OC}}$ , and 856 mV is far superior to the voltages we obtained in Paper II without any LiI in the electrolyte.<sup>285</sup> Excessively high irradiance during the  $J$ - $V$  sweep may explain the high  $V_{\text{OC}}$  with the reported electrolyte. Filling of trap states in the  $\text{TiO}_2$  at high illumination lifts the Fermi level of the  $\text{TiO}_2$  and consequently the  $V_{\text{OC}}$  of the device.<sup>286,287</sup>

Another important aspect to consider is that the AM1.5 G solar spectrum has a finite irradiance, and integration of the solar spectrum will give the maximum obtainable  $J_{\text{SC}}$  for a range of wavelengths. We performed this integration for Paper II, shown in Figure 3.4. Despite the reported absorption onset for **Dye 2** of 530 nm, we used an estimated onset of 605 nm from the reported absorption spectra on  $\text{TiO}_2$  for

our estimates. The conclusion from Figure 3.4 is that even with 100% IPCE in the region where **Dye 2** absorbs light, the reported  $J_{SC}$  and hence PCE are overestimated by a factor of around 2.



**Figure 3.4:** Integration of the AM1.5 G solar spectrum yields the theoretical maximum  $J_{SC}$  attainable from a device at a specific absorption onset. Arrows indicate the maximum  $J_{SC}$  for a sensitizer with an absorption onset of 605 nm and the required absorption onset to achieve a  $J_{SC}$  of 24.2 mA cm<sup>-2</sup>. Reproduced from Paper II with permission from The Royal Society of Chemistry.

Finally, we were struck by the remarkable resemblance between the reported IPCE spectra and the absorption spectra on TiO<sub>2</sub>, see Figure 3.3 (c) and (d). All the six sensitizers have identical onsets and peak positions in both spectra. Characteristics such as a kink in the curves for **Dye 2** around 450 nm is present in both spectra. The intersections between curves of both spectra correspond to the absorbance spectrum simply being the normalized IPCE spectrum. Which spectrum is correct is impossible to determine, but it is beyond doubt the same data set which is used to produce both spectra. It should be noted that the IPCE and absorbance spectra of a DSSC are expected to possess similar features, but the statistical probability of two spectra of six dyes being completely identical is infinitesimal.\*

In a field largely driven by efficiency improvements, it is hugely important to be able to trust the values which are published. This is to a large degree the responsibility of the author, by providing sufficient and coherent evidence of the device performance. Higher efficiency research tends to be published in higher impact factor journals, so a certain responsibility has to be held by the scientific journals. Dye-sensitized solar cells is a field where efficiency improvements of 1-2% are considered breakthroughs. Characterization errors related to device masking and light intensities can easily cause inaccuracies of such magnitudes, resulting in the research data erroneously being interpreted as a major technology improvement. The journals have to increase their requirements to documentation, and when record claims are made, reviewers have to perform the basic calculations needed to assess the credibility of the findings.

\*The two corresponding authors of the paper by Nagarajan et al. have been addressed about the issues raised in Paper II by email 15.01.2018 and 06.04.2018, but no reply has been received.

### 3.1.3 Paper III

The third paper focused on the effect of the basic geometry of phenothiazine sensitizers.<sup>91</sup> In all the known phenothiazine sensitizers (with the exception of two studies by Marszalek et al.<sup>155</sup> and Kim et al.<sup>288</sup>), the scaffold is extended from C-3, C-7 or N-10, often combinations of the three. While these are the most accessible positions for chemistry on the phenothiazine core, alternative substitution patterns could give the sensitizers other, more favourable properties such as higher dye loading on the TiO<sub>2</sub> surface. Conveniently, 2-chloro-10*H*-phenothiazine is commercially available, and bromination produced a novel phenothiazine building block allowing the preparation of sensitizers with geometries like 2,7 and 3,8, following the geometry nomenclature established in Paper III. Sensitizers from the five different geometries (2), (3), (2,7), (3,7) and (3,8) were prepared, in two series with thiophene and phenyl  $\pi$ -spacers, see Figure 3.5.

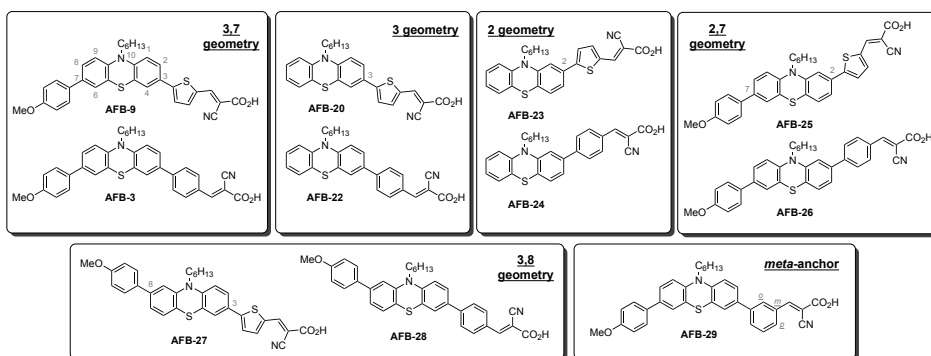


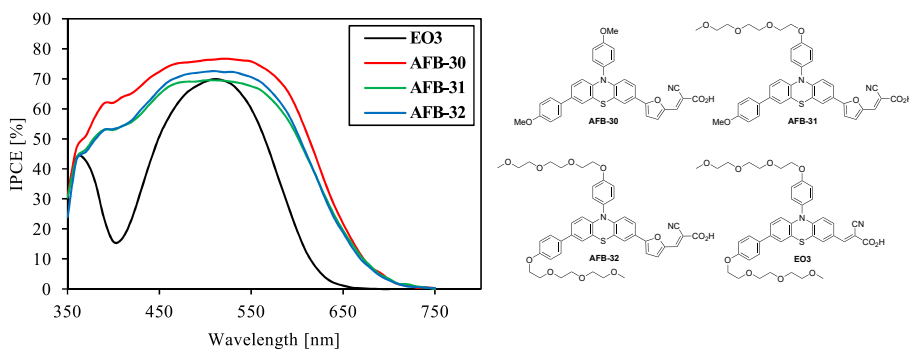
Figure 3.5: Dye geometries included in Paper III.

The structural diversity of the sensitizers in this work resulted in a wide range of photophysical, electrochemical and photovoltaic behaviours. Firstly, the findings from Paper I on the effect of the  $\pi$ -spacer was again observed, with thiophene outperforming phenyl in all the geometries. Thiophene was found to lower (towards more positive potentials) the HOMO-level energies by 20-70 mV, but the largest difference was the lowering of the LUMO-level position by at least 200 mV. A number of conclusions were drawn from the geometry study. Unsurprisingly, the  $\pi$ -spacer moiety on the phenothiazine scaffold should unquestionably be placed in 3-position, *para* to the nitrogen atom of phenothiazine. The photovoltaic performance of the geometries followed the ascending order of:  $2 < 2,7 < 3 < 3,7 \approx 3,8$ . Differing only in the position of the auxiliary donor, the 3,7 and 3,8 geometries were indistinguishable throughout the study. However, in dye loading measurements, the 3,8 geometry displayed increased dye loading by 10%. Although not pursued further in Paper III, this differ-

ence in dye loading could improve the efficiency of the 3,8 dyes beyond those of the conventional 3,7 dyes in the future.

### 3.1.4 Paper IV

Four dyes were prepared for Paper IV,<sup>92</sup> including the literature dye **EO3** reported by Lin et al.<sup>289</sup> **EO3** is one of the highest performing phenothiazine sensitizers with a reported PCE of 9.98% with an organic  $I^-/I_3^-$  electrolyte and 5.97% with novel aqueous  $I^-/I_3^-$  electrolyte. The absorption spectrum of **EO3** is relatively narrow, and the concept for Paper IV was to broaden the absorption by the insertion of the furan  $\pi$ -spacer. Additionally, the synthetic route allowed us to investigate the effect of the triethylene oxide methyl ether (TEOME) chains. In total, three variants of **EO3** were prepared with furan  $\pi$ -spacer and zero, one and two TEOME chains. Thermogravimetric analysis was employed to investigate the decomposition temperatures of the dyes. **EO3** was found to decarboxylate under air at 225 °C, while the presence of the furan moiety reduced this to approximately 150 °C for the AFB dyes.



**Figure 3.6:** IPCE spectrum of devices with sensitizers **EO3** and **AFB-30** to **32**. Adapted from Paper VI with permission from the Centre National de la Recherche Scientifique (CNRS) and The Royal Society of Chemistry.

The introduction of furan red-shifted and improved the absorption of the sensitizers compared to **EO3**, while increasing the number of TEOME chains reduced the dye loading. Electrochemical measurements indicated that the furan group shifted the HOMO level up by approximately 100 mV. In devices, the furan spacer caused a drop in  $V_{OC}$  of 60 mV compared to **EO3**, attributed to a conduction band shift, as the charge density and electron lifetimes of the AFB dyes generally were marginally better than for **EO3**. However, as indicated by a broadening of the IPCE spectra (Figure 3.6), the absorption properties of the novel dyes was improved, and superior efficiencies were the result. The most efficient sensitizer was **AFB-30**, with two methoxy groups in place of TEOME substituents.



### 3.1.5 Paper V

Following up on the loose end from Paper III, where no performance difference could be found between the 3,7 and 3,8 geometries, we decided to increase the sample size in Paper V. Three 3,7-substituted dyes from Papers I and II with phenyl, naphthyl and pyrenyl auxiliary donors were selected. The 3,8-substituted analogues were synthesized, so two sets of three sensitizers could be investigated, see Figure 3.7. The synthesis route employed was identical to the one presented in Paper III. As in Paper II focusing on auxiliary donors, a tight grouping of absorption maxima was found for the various auxiliary donor groups, with no clear distinction between the two geometries. A striking difference between the two geometries can be observed in the electrochemical determination of the HOMO level position. The HOMO level of the 3,8-substituted dyes is found 40-50 mV below those of the 3,7-dyes. The photovoltaic performance for the 3,7 geometry was marginally superior for the phenyl and naphthyl auxiliary donors, while the opposite was the case for the pyrenyl-substituted sensitizers. In this study, increased dye loading for the 3,8-substituted dyes was also observed, meaning the staining conditions likely favour the 3,7-sensitizers. The lower quality of the 3,8-dye monolayer is supported by lower electron lifetime values compared to the 3,7-analogues.

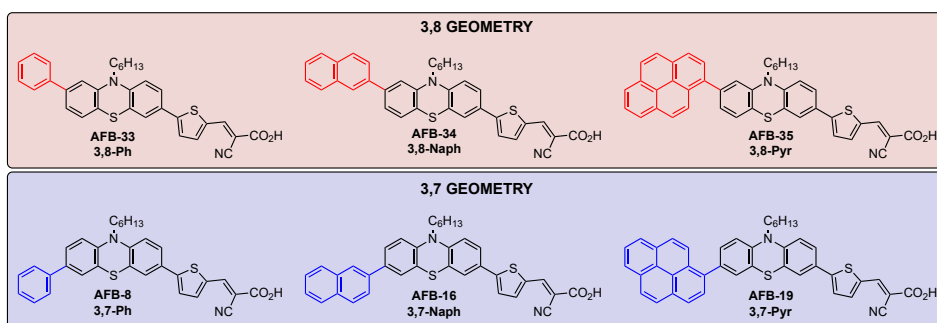
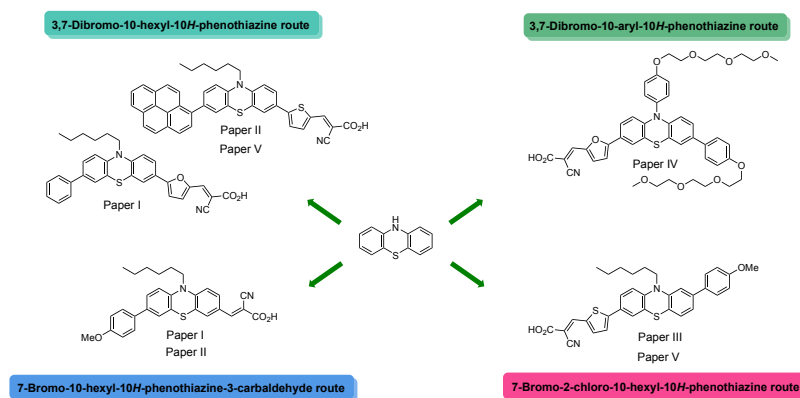


Figure 3.7: Dyes investigated in Paper V.

The increased dye loading is a desirable trait, meaning higher efficiency devices may be obtainable upon optimization of the staining conditions. A small-size sensitizer with narrow absorption properties could also be a valuable co-sensitizer. While conventional phenothiazine dyes are not generally compatible with copper electrolytes in our hands, the novel 3,8-dyes may have sufficiently low-lying HOMO orbital energies for sufficiently fast dye regeneration. This could make these promising co-sensitizers alongside sensitizers with more red-shifted absorption spectra.

## 3.2 Synthesis

In the field of dye-sensitized solar cells, organic chemistry is an indispensable tool. The synthesis and evaluation of novel sensitizers is the backbone of a large portion of the DSSC literature, including the six papers included in this thesis. The main focus has been to find flexible and reliable synthesis routes, so that a range of sensitizers could be prepared using the same procedure. Four main synthesis routes have been used in Papers I-V, as shown in Figure 3.8 with examples of sensitizers obtained through each specific route.



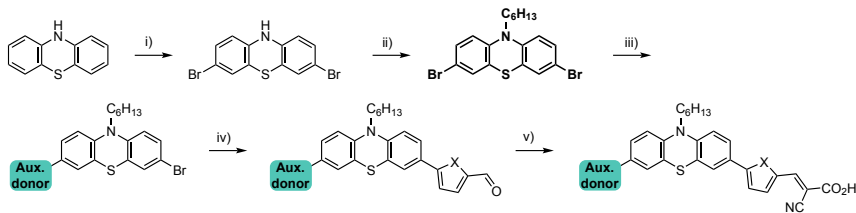
**Figure 3.8:** Four main synthetic routes to the phenothiazine sensitizers studied in Papers I-V.

### 3.2.1 3,7-Dibromo-10-hexyl-10H-phenothiazine route

The route used to the sensitizers of Paper I and II relied on the building block 3,7-dibromo-10-hexyl-10H-phenothiazine which was prepared in two steps from 10H-phenothiazine, see complete sequence in Scheme 3.1. Firstly, the bromination with molecular bromine on phenothiazine was conveniently scaled, so close to 40 gram of product could be obtained by crystallization. The next reaction was alkylation, and even this reaction was possible to purify in up to 13 gram scale using as little as 90 gram silica gel with pure *n*-pentane eluent. By reversing the order of the first two reactions, smaller scales have to be accepted, as the alkyl chains effectively rules out purification of the compounds by crystallization. In introducing the auxiliary donor by Suzuki coupling, a curious situation arose. No selectivity was detected in the coupling, thus the only way of obtaining as much mono-coupled product as possible was by using the boronic acid as limiting reagent. By only using 1.00-1.05 equivalents, a rough distribution of 1:2:1 of starting material:mono-coupled:di-coupled product was obtained. Purification by column chromatography varied in difficulty depend-

ing on the nature of the auxiliary donor. Pyrene undoubtedly gave the most difficult mixtures to separate, presumably due to extensive  $\pi$ - $\pi$  interactions. Introducing the  $\pi$ -conjugated spacers was straight-forward by Suzuki coupling with all boronic acids apart from 5-formyl-2-thienylboronic acid. Without much investigation into the failure, an alternative approach was found. Effectively, the roles of the coupling partners were reversed. Using the palladium-catalyzed borylation reported by Billingsley and Buchwald,<sup>240</sup> the phenothiazinyl bromide was converted to the pinacol boronic ester, which in turn coupled efficiently with 5-bromo-2-thiophenecarboxaldehyde to give the desired products. The anchoring group was introduced by conversion of the aldehyde to cyanoacrylic acid by the piperidine catalyzed Knoevenagel condensation.

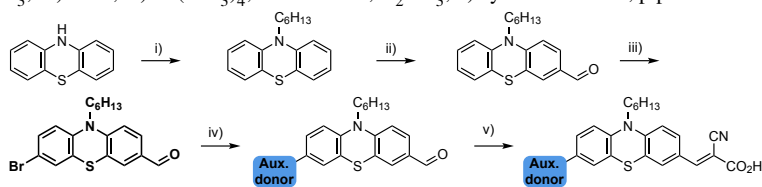
**Scheme 3.1:** 3,7-Dibromo-10-hexyl-10*H*-phenothiazine route. i) Br<sub>2</sub>, ii) NaH, 1-bromohexane, iii) Pd(PPh<sub>3</sub>)<sub>4</sub>, boronic acid, K<sub>2</sub>CO<sub>3</sub>, iv) X = O, C<sub>2</sub>H<sub>2</sub>: Pd(OAc)<sub>2</sub>, SPhos, boronic acid, K<sub>2</sub>CO<sub>3</sub>, X = S: borylation/Suzuki two-step protocol, v) cyanoacetic acid, piperidine.



### 3.2.2 7-Bromo-10-hexyl-10*H*-phenothiazine-3-carbaldehyde route

For sensitizers with the anchoring group directly connected to the phenothiazine scaffold, another approach was needed, see Scheme 3.2. This sensitizer layout is very common, and a number of successful routes have been employed.<sup>290–292</sup> We opted for a route where the first step was alkylation of the phenothiazine nitrogen atom, followed by monoformylation using the Vilsmeier-Haack reaction. While we have had a hard time finding suitable conditions for monohalogenation on this substrate, monoformylation has proceeded smoothly. Similar regioselectivity has previously been reported,<sup>293</sup> presumably due to a reduction of nucleophilicity or undesirable charge repulsion of two ionic iminium intermediates limiting overformylation. Following a bromination by NBS, the *N*-alkyl-3-bromo-7-formylphenothiazine building block is obtained. Further reactions may include attaching an auxiliary donor by Suzuki coupling and the anchoring group by Knoevenagel condensation, as done in Paper I. Naturally, other coupling reactions using aryl halides should be compatible with this building block, and the aldehyde moiety has also been used in the Horner-Wadsworth-Emmons reaction to extend conjugation.<sup>155</sup> By reduction of the aldehyde, the phenothiazine may also be converted into a Wittig reagent as done in the route reported by El-Shishtawy et al.<sup>290</sup>

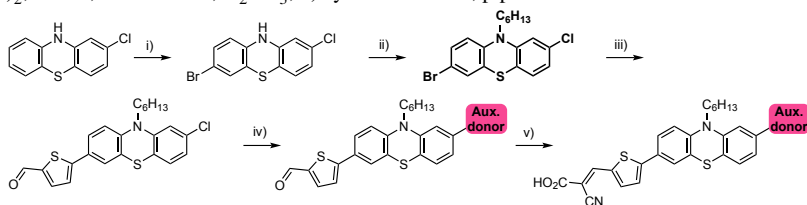
**Scheme 3.2:** 7-Bromo-10-hexyl-10*H*-phenothiazine-3-carbaldehyde route. i) NaH, 1-bromohexane, ii) DMF, POCl<sub>3</sub>, iii) NBS, iv) Pd(PPh<sub>3</sub>)<sub>4</sub>, boronic acid, K<sub>2</sub>CO<sub>3</sub>, v) cyanoacetic acid, piperidine.



### 3.2.3 7-Bromo-2-chloro-10-hexyl-10*H*-phenothiazine route

In order to develop novel phenothiazine geometries, a new building block was required. Thankfully, 2-chloro-10*H*-phenothiazine is commercially available and a superb starting point, see Scheme 3.3. As with the "3,7 N-alkyl route" in Scheme 3.1, bromination by Br<sub>2</sub> in glacial acetic acid was the first step. Unlike in the symmetric case, a mixture of products was formed, with the desirable compound comprising approximately 50 mol% of the crude material. The low regioselectivity in electrophilic aromatic substitution reactions on phenothiazine is a well-known issue, which has been reported a number of times.<sup>151,152,294</sup> Purification by recrystallization from toluene (3-5 times) proved to be effective, yielding the desired product in 31% yield. Despite low regioselectivity and tedious purification, the method was reasonably scalable yielding over 5 grams of the pure product, and the starting material was inexpensive. Alkylation by NaH and an alkyl halide proceeds efficiently, yielding a highly versatile building block towards the synthesis of sensitizers with 2,7 and 3,8 geometries. The advantage of this building block over the 3,7-dibromo analogue is chemoselectivity in the subsequent coupling reaction. In our hands, yields of 71-87% were obtained in the first Suzuki coupling with three different boronic acids, including 5-formyl-2-thienylboronic acid.

**Scheme 3.3:** 7-Bromo-2-chloro-10-hexyl-10*H*-phenothiazine route. i) Br<sub>2</sub>, ii) NaH, 1-bromohexane, iii/iv) Pd(OAc)<sub>2</sub>, SPhos, boronic acid, K<sub>2</sub>CO<sub>3</sub>, v) cyanoacetic acid, piperidine.

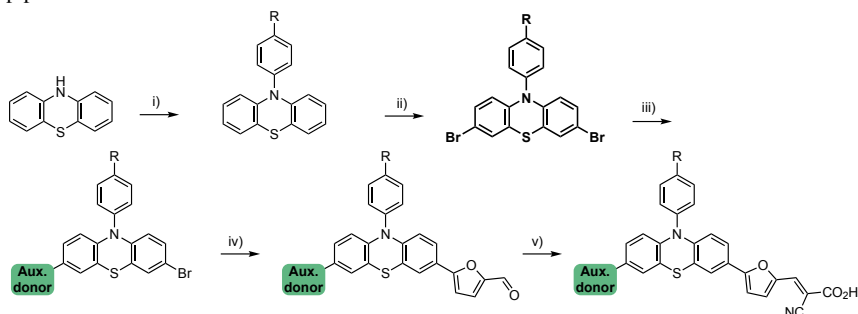


### 3.2.4 3,7-Dibromo-10-aryl-10*H*-phenothiazine route

In paper IV, sensitizers with aryl substituents on the phenothiazine nitrogen were investigated, and consequently another route was required. Introduction of the aryl

moiety was efficiently performed with a Buchwald coupling on 10*H*-phenothiazine, followed by dibromination by NBS, see Scheme 3.4. The aryl moieties used were all substituted in the *para* position, likely to be a contributing factor to the success of the bromination.<sup>295</sup> Upon retrieval of the 3,7-dibromo building block the synthesis of the sensitizers could be performed as described for the 3,7-alkyl derivatives.

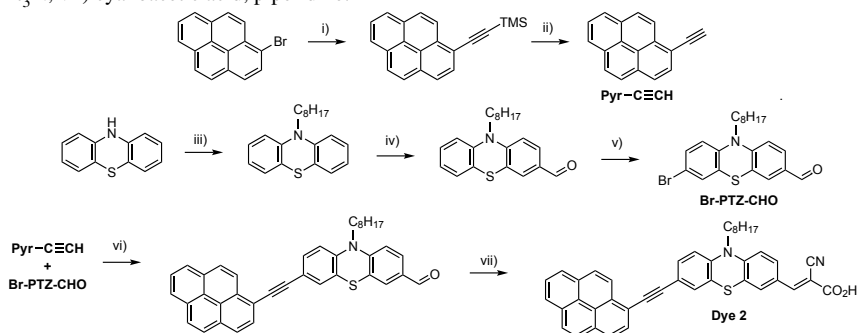
**Scheme 3.4:** 3,7-Dibromo-10-aryl-10*H*-phenothiazine route. i) aryl halide, Pd<sub>2</sub>(dba)<sub>3</sub>, P(Cy)<sub>3</sub>, NaOtBu, ii) NBS, iii) Pd(PPh<sub>3</sub>)<sub>4</sub>, boronic acid, K<sub>2</sub>CO<sub>3</sub>, iv) Pd(OAc)<sub>2</sub>, SPhos, boronic acid, K<sub>2</sub>CO<sub>3</sub>, v) cyanoacetic acid, piperidine.



### 3.2.5 Synthesis of reference sensitizers

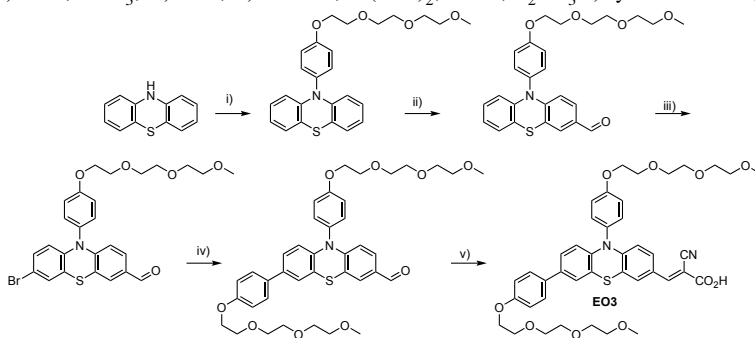
In paper II, the sensitizer **Dye 2** previously reported by Nagarajan et al.<sup>283</sup> was synthesized. This was performed using a route similar to that described for the 7-bromo-2-chloro-10-hexyl-10*H*-phenothiazine-based sensitizers, only an eight carbon alkyl chain was used, see Scheme 3.5. Further, the route differed in that the Sonogashira coupling was used to attach the ethyl pyrenyl auxiliary donor and not the Suzuki coupling.

**Scheme 3.5:** Synthesis route used to **Dye 2**, investigated in Paper II. i) Ethynyltrimethylsilane, PdCl<sub>2</sub>(PPh<sub>3</sub>)<sub>2</sub>, CuI, Et<sub>3</sub>N, ii) NaOH, iii) NaH, 1-bromooctane, iv) DMF, POCl<sub>3</sub>, v) NBS, vi) PdCl<sub>2</sub>(PPh<sub>3</sub>)<sub>2</sub>, CuI, Et<sub>3</sub>N, vii) cyanoacetic acid, piperidine.



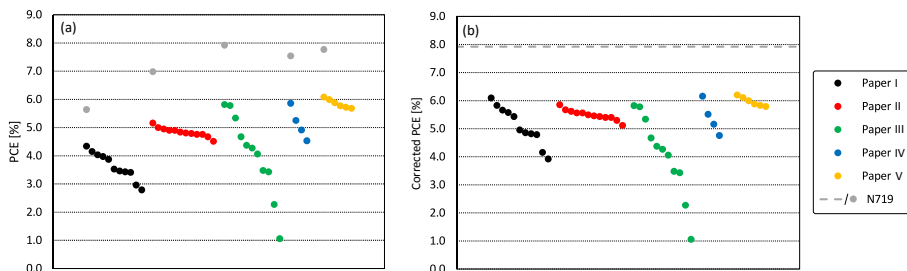
For Paper IV, the literature dye **EO3** was prepared following a route different from the one published by Lin et al.<sup>289</sup> The Buchwald coupling introducing the aryl moiety on the phenothiazine nitrogen atom was used in both protocols. We then performed the Vilsmeier-Haack formylation followed by bromination by NBS, yielding a highly versatile building block, which is not available from the literature protocol. The last steps introduced the auxiliary donor by a Suzuki coupling before the Knoevenagel condensation furnished the anchoring group, see Scheme 3.6.

**Scheme 3.6:** Synthesis route used to **EO3**, investigated in Paper IV. i) aryl halide, Pd<sub>2</sub>(dba)<sub>3</sub>, P(Cy)<sub>3</sub>, NaOtBu, ii) DMF, POCl<sub>3</sub>, iii) NBS, iv) Ar-BPin, Pd(OAc)<sub>2</sub>, SPhos, K<sub>2</sub>CO<sub>3</sub> v) cyanoacetic acid, piperidine.



### 3.3 Photovoltaic summary from Paper I-V

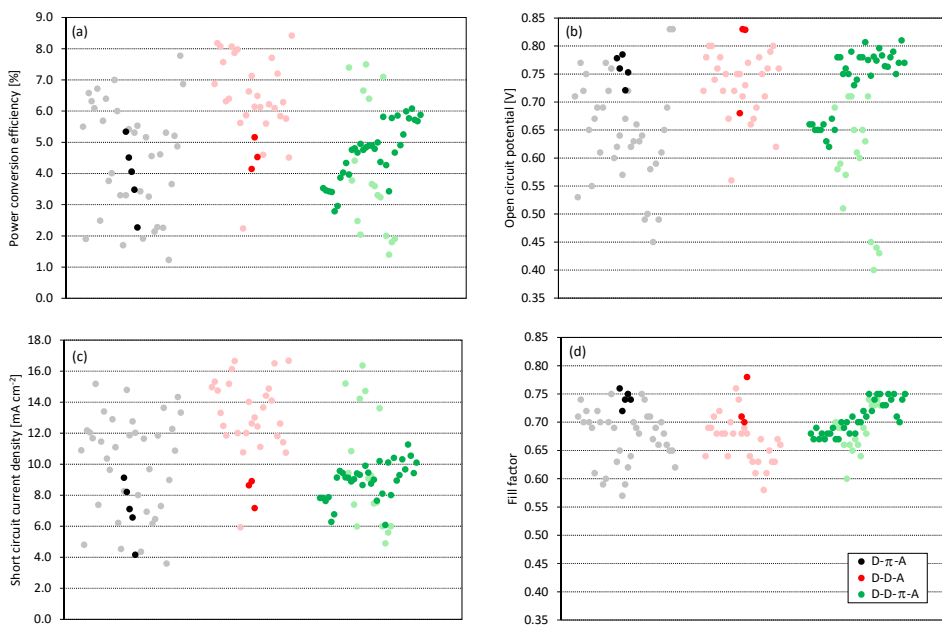
The quality of the fabrication equipment, procedures and materials have all improved throughout the five phenothiazine papers included in this thesis. Naturally, a progression in device performance has followed, as can be seen in Figure 3.9 (a), where all the the power conversion efficiencies from Papers I-V are plotted. The reference sensitizer **N719** has been used in all the papers, allowing the performance of all the sensitizers to be compared by calculating the efficiency ratio  $PCE_{\text{dye}}/PCE_{\text{N719}}$ . This ratio has been calculated for the first five studies of this thesis, and the values scaled to the highest **N719** performance, which was obtained in Paper III. The resulting plot shown in Figure 3.9 (b) suggests the efficiencies of the best performing dyes from each study are in fact very comparable. The use of relative performance rather than absolute performance has been recommended by many researchers within the DSSC field.<sup>44,296</sup> However, particularly the lack of a universal reference sensitizer and electrolyte makes the idea of universally comparable performance data utopic. It can however be very useful for comparing a handful of performance data sets employing similar device conditions.



**Figure 3.9:** (a) Distribution of power conversion efficiency values of phenothiazine sensitizers and **N719** reference devices from Papers I-V. (b) Corrected PCE values. Calculated via the ratio of  $PCE_{\text{dye}}/PCE_{\text{N719}}$  and adjusted to the highest performing **N719** reference across all five publications.

To compare our photovoltaic performance with the rest of the phenothiazine sensitizers published requires a thorough literature review. Fortunately, Luo et al. performed a comprehensive review of the phenothiazine-based DSSC publications in 2016.<sup>120</sup> They grouped the sensitizers into categories depending on the dye structure, such as D-D-A, D- $\pi$ -A and D-D- $\pi$ -A. In Figure 3.10 (a), the photovoltaic characteristics of our sensitizers are plotted together with the collected performance data from Luo et al. It is clear from the plot that the most efficient phenothiazine dyes structure up to 2016 were the dyes with the D-D-A structure, i.e. dyes without any  $\pi$ -spacers. This is predominantly due to the higher  $V_{\text{OC}}$  and  $J_{\text{SC}}$  values reported for these structures, as shown in Figure 3.10 (b) and (c). In terms of the fill factors of the reported devices, no clear differences can be observed from the data selection.\*

The devices reported in the works included in this thesis deliver high  $V_{OC}$  values compared to the rest of the literature, most likely due to the A6141 electrolyte used for Papers II-V not containing any LiI.<sup>297</sup> Also the fill factors of our devices appear to be in the upper part of the distribution. However, the  $J_{SC}$  values of our devices are low compared to the other publications, resulting in our overall PCE values being reasonably average, compared to the other reports.



**Figure 3.10:** Shaded data points are collected by Luo et al. and reported in their review of phenothiazine sensitizers published in 2016.<sup>120</sup> The full colour data points are the average performance values from the devices in Papers I-V.

Throughout Papers I-V we have identified a number of performance characteristics of the phenothiazine sensitizer. For instance, as observed in Paper I, II and IV, and very well illustrated in Figure 3.10 (b), the introduction of  $\pi$ -spacers has a significant negative effect on the  $V_{OC}$  of the devices. The average values for the photovoltaic data collected by Luo et al. are given in Table 3.1, highlighting a difference in  $V_{OC}$  between the D-D-A and D-D- $\pi$ -A of 50 mV. As the introduction of the  $\pi$ -spacers generally improves the absorption properties, lower  $V_{OC}$  will severely limit the performance enhancement associated with this improvement. Even the effect of the auxiliary donor seems to be limited, as the performance characteristics summarized in Figure 3.10

\*Many structures have been reported since 2016, so this is by no means a collection of the entire sensitizer class, but an estimate. Also, the photovoltaic performance improvements of the DSSC field as a whole will likely favor the later publications relative to the earlier publications.



are very similar for the D- $\pi$ -A and D-D- $\pi$ -A sensitizers. This corresponds excellently with the findings from Papers II and III, where we found only a minor contribution by the introduction of auxiliary donors (4-11% improved PCE). The reason for the limited effect of the auxiliary donors is most likely due to the dihedral angle of the phenothiazine scaffold of approximately 30°, restricting the conjugation between the auxiliary donor and the anchoring group and ultimately the TiO<sub>2</sub>. As for the lowered  $V_{OC}$  values, we have been unable to find a suitable explanation, and to the best of our knowledge this has not been previously investigated in the phenothiazine DSSC field. As described in the introduction, the  $V_{OC}$  depends on the Fermi level of the TiO<sub>2</sub>, which is affected by the conduction band position of the TiO<sub>2</sub> and the electron concentration in the TiO<sub>2</sub>. Assuming a  $\pi$ -spacer does not on average affect the dye loading significantly, it is reasonable to conclude the  $\pi$ -spacer affects either the charge injection efficiency or the conduction band position. In our studies, the peak IPCE values are largely comparable between the D-D-A and D-D- $\pi$ -A dyes suggesting the charge injection efficiencies should be comparable, indicating the main effect should be a change of conduction band position, caused by the difference in dye structures.

**Table 3.1:** Average and median photovoltaic performance reported in the review by Luo et al.<sup>120</sup> for phenothiazine dyes with D- $\pi$ -A, D-D-A and D-D- $\pi$ -A dye structures.

Dye structure	$J_{SC}$ [mA cm <sup>-2</sup> ]		$V_{OC}$ [mV]		FF		PCE [%]	
	Average	Median	Average	Median	Average	Median	Average	Median
<b>D-<math>\pi</math>-A</b>	11.0	10.1	645	647	0.69	0.67	4.74	4.49
<b>D-D-A</b>	13.2	13.3	750	732	0.68	0.67	6.36	6.49
<b>D-D-<math>\pi</math>-A</b>	9.1	9.6	600	584	0.69	0.69	3.60	4.04

The explanation of this phenomenon has not been immediately apparent to us, and we have been unable to find any accounts in the literature of research into the issue. Hence, we here present a possible explanation into how the  $V_{OC}$  may be affected by the dye structure. The pKa of acetic acid is 4.75, while that of cyanoacetic acid is 2.45 due to the inductive effect of the nitrile functional group affecting the acidity of the acid. By assuming the donor group of the dye is also affecting the acidity through induction, we can make a guess into the effect of a  $\pi$ -spacer. The introduction of the  $\pi$ -spacer increases the distance between the donor and anchor moieties of the dye, and consequently the pKa of the anchoring group is expected to decrease as the electron donation through induction is reduced. Lower pKa means the compound is a stronger acid, and a corresponding increase in protonation of the TiO<sub>2</sub> during the staining procedure is thus expected.<sup>298</sup> A consequence of this will be a shift of the TiO<sub>2</sub> conduction band towards more positive potentials.

We cannot see any reason why this phenomenon would be exclusive to phenothiazine sensitizers, and more elaborate studies into the pKa and conductive band po-

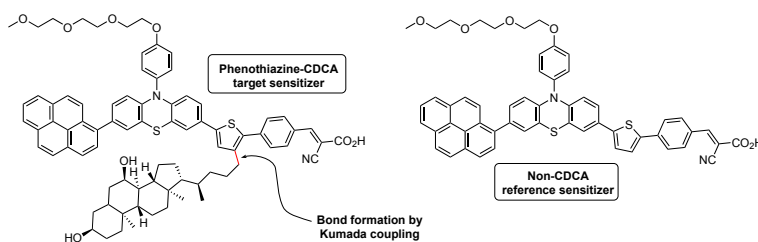
sition of sensitizers are needed to confirm this hypothesis. More device-oriented experiments into the staining procedure and conditions may also illuminate the issue further. To summarize the weak points of the phenothiazine dyes we emphasize the HOMO level position, folded sensitizer scaffold and limited effect of extending the conjugation in the direction of both the donor and acceptor sides of the sensitizers. Accordingly, it is clear that phenothiazines have some inherent structural limitations making the design of highly efficient dyes for DSSC very difficult.

### 3.4 Paper VI: CDCA-substituted triarylamine dyes

Triarylamine dyes were only investigated in Paper VI, and the following discussion will predominantly concern the findings of that paper, and a little about the background. This study did in fact start out as a crazy idea in a notebook. Would it be possible to replace or complement the common anti-aggregation alkyl chains with the most used anti-aggregation additive, chenodeoxycholic acid? We could not find any accounts of this ever being attempted in the 25 years CDCA has been used as an additive, and set to work.

#### 3.4.1 Synthesis strategy

Initially, this paper was also intended to be constructed around phenothiazine sensitizers, incorporating favorable traits identified in Papers I-V while also investigating the effect of the covalent moiety of chenodeoxycholic acid (CDCA). The target molecules in Figure 3.11 were attempted synthesized. MSc Ingunn Schröder worked on an approach for attaching the CDCA moiety to a thiophene using the Kumada coupling.<sup>299</sup> This strategy was terminated when the alkyl halide of the CDCA moiety proved difficult to obtain and thus the Grignard reagent was unavailable. The intended reference dye was however prepared successfully, but it had unimpressive photophysical properties.



**Figure 3.11:** Initial sensitizer design for Paper VI. The bond intended formed by Kumada coupling is highlighted in red.

We suspected the ring twisting between the thiophene and phenyl rings of the  $\pi$ -spacer to be responsible for the low performance, and that the large CDCA moiety would only increase the unfavorable twist. Hence, another approach was needed. Around the same time, we also discovered that the oxidation potentials of our phenothiazine sensitizers were largely incompatible with the redox potentials of novel copper electrolytes recently developed in Uppsala and Lausanne.<sup>44,56,57,300</sup> Due to the novelty of the dye design concept we planned, the use of state-of-the-art electrolytes was desirable over the conventional  $I^-/I_3^-$  electrolytes used for Papers I-V. Consequently, we had to replace the phenothiazine dye scaffold. In a study by Chiykowski et al., the oxidation potential of a triarylamine dye was found 190 mV below that of the analogous phenothiazine dye.<sup>301</sup> Reassuringly, triarylamine dyes are known to be compatible with copper electrolytes, and this scaffold was therefore selected for Paper VI. Next was the challenge of attaching the CDCA moiety to the thiophene unit, which was unsuccessful by coupling chemistry, so a simpler approach was sought. We had already developed chemistry to the CDCA-OH derivative, and to use that in a simple  $S_N2$  reaction with a 2-(bromomethyl)thiophene would yield a stable ether-linkage between the two moieties.<sup>302</sup> Lastly came the hurdle of the second ring of the  $\pi$ -spacer unit, which was preferably smaller than a phenyl ring and conveniently introduced. Earlier experience with the 5-formyl-2-thienylboronic acid suggested strongly against this, especially since it would be fused to another thiophene, a tricky coupling even with simpler substrates. Hence, we landed on the furan moiety, as this was the most efficient moiety in Paper I and in our hands easier to successfully couple to aryl halides. During the synthesis process we decided to further diversify the sensitizers by introducing two different alkoxy chains on the triarylamine donor moiety, namely  $C_3H_7$  and  $C_6H_{13}$ . The two resulting target molecules and their reference non-CDCA sensitizers are shown in Figure 3.12. The

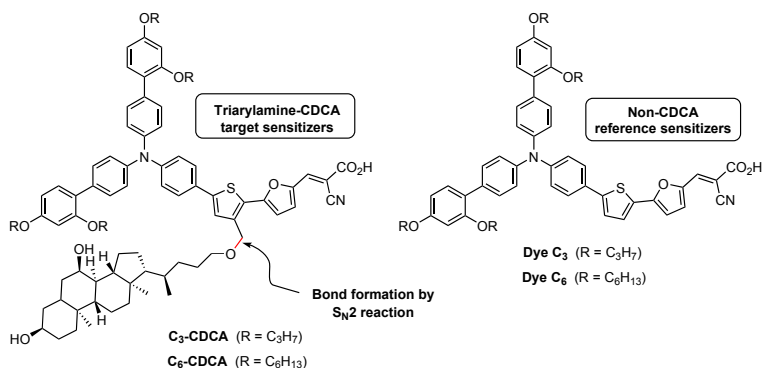


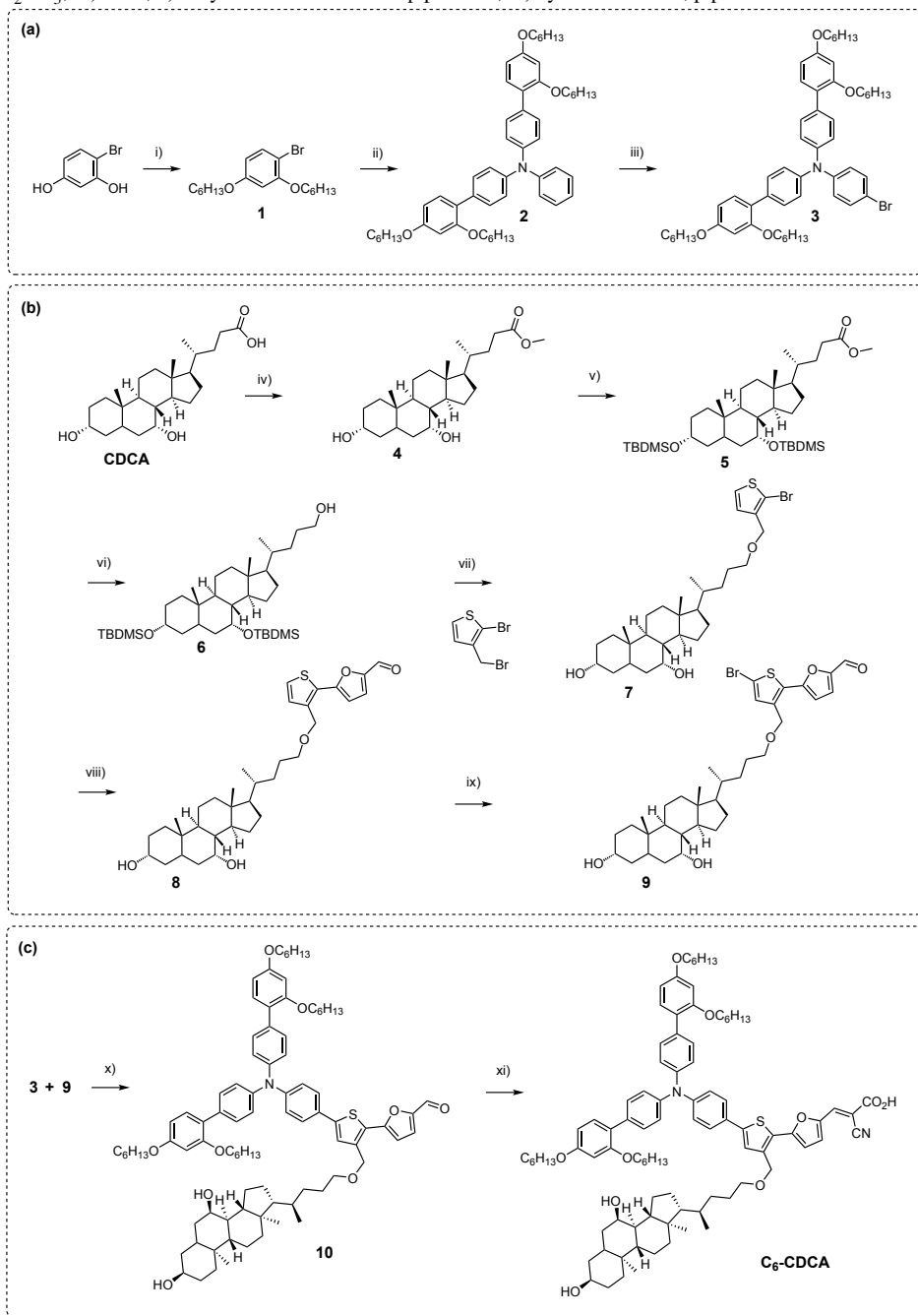
Figure 3.12: The final target molecules for Paper VI.

complete synthesis route with numbering of compounds is given in Scheme 3.7 for dye **C6-CDCA**. The chemistry towards **C3-CDCA** very similar, with the exception that as (2,4-dipropoxyphenyl) boronic acid was commercially available, the first part of the triarylamine synthesis could be shortened by two steps. The synthesis of the donor fragment **3**, previously used in **Y123** started with attachment of hexyl chains to 4-bromoresorcinol. A palladium-catalyzed borylation gave the pinacolboronic ester which was then coupled to 4,4'-dibromotriphenylamine in a Suzuki coupling. A very efficient bromination by NBS gave the brominated **Y123** donor moiety, ready to be coupled to the  $\pi$ -spacer.

The chenodeoxycholic moiety would be attached to the  $\pi$ -spacer as a substituent on the thiophene of the spacer. This part of the synthesis started with converting commercially available chenodeoxycholic acid to the methyl ester **4** in a classic Fischer esterification procedure. Protection of the hydroxyl moieties of CDCA by *tert*-butyldimethylsilyl (TBDMS) groups was a crucial step originally needed for the Kumada approach previously described. TBDMS triflate and 2,6-lutidine ensured complete protection yielding compound **5** as a viscous oil. The next step was reduction of the methyl ester to a primary alcohol by  $\text{LiAlH}_4$ , giving the primary alcohol **6** as a white crystalline solid. The crucial reaction connecting the CDCA moiety to the thiophene was performed with NaH as a base. Subsequent TBDMS deprotection with HCl completed this two-step procedure as the fourth quantitative yield reaction in this sequence, yielding compound **7**. However, as the complexity of the substrates and the reactions increased the yields also suffered. The next step was the Suzuki coupling between the 2-bromothiophene carrying the massive CDCA substituent (**7**) and (5-formylfuran-2-yl)boronic acid. This was for a long time the crux of this synthesis sequence, as the regular system with  $\text{Pd}(\text{OAc})_2/\text{SPhos}$  failed. However, acceptable conversion was finally obtained upon switching the catalyst to  $\text{PdCl}_2(\text{dppf})$ , inspired by the protocol by Bumagin et al.<sup>303</sup> The use of 3 equivalents of boronic acid and short reaction times gave the cleanest reaction mixtures yielding up to 68% of the desired compound **8** after purification. The last reaction, supposed to be a simple bromination by NBS, turned out to be the most challenging of the the sequence. The desired compound **9** was only obtained in humble amounts of up to 25% yield following purification. Although enough material was recovered to finish the synthesis, the last step would be a prime candidate for further reaction optimization. However, due to a severe shortage of time, this was not done.

The fusion of the triarylamine donor **3** and CDCA-substituted  $\pi$ -spacer **9** was performed using the  $\text{Pd}(\text{OAc})_2/\text{SPhos}$  Suzuki coupling system. The Knoevenagel condensation was used to install the cyanoacrylic acid anchoring group, yielding just enough material of the two CDCA-substituted sensitizers to complete the photovoltaic study.

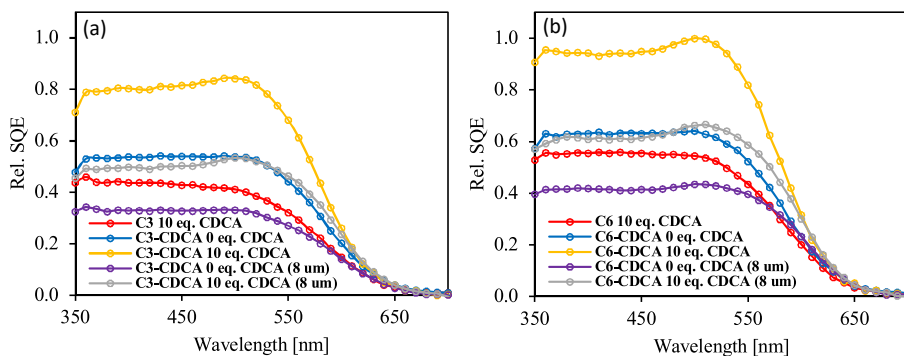
**Scheme 3.7:** Synthesis route to dye **C6-CDCA** in Paper VI. The synthesis towards **C3-CDCA** is completely analogous while the reference sensitizers **C3** and **C6** were prepared with a much simpler thiophene-furan  $\pi$ -spacer. i) 1-bromohexane, KOH, ii) borylation/Suzuki two-step protocol, iii) NBS, iv) methanol,  $\text{H}_2\text{SO}_4$ , v) 2,6-lutidine, TBDMS triflate, vi)  $\text{LiAlH}_4$ , vii) NaH, viii) (5-formylfuran-2-yl)boronic acid,  $\text{PdCl}_2(\text{dppf})$ ,  $\text{K}_2\text{CO}_3$ , ix) NBS, x) borylation/Suzuki two-step protocol, xi) cyanoacetic acid, piperidine.



### 3.4.2 Photovoltaic performance

To our extreme delight, the CDCA substituents did not affect the absorption properties, nor the electrochemical behaviour of the sensitizers. That meant the differences we would find in the photovoltaic properties would be related only to the aggregation properties of the sensitizers or quality of the self-assembled dye/co-adsorbent monolayer. The first stage of the study was to establish how prone to aggregation the reference, non-CDCA dyes were. This was done by screening a number of CDCA co-adsorbent concentrations in the staining solutions. The CDCA dependency was found to be related to the alkoxy chain length, as **C6** was not noticeably affected while for **C3** a clear performance maxima was found for 10 molar equivalents of CDCA. The  $V_{OC}$  was also affected, with dye **C3** delivering 100 mV lower  $V_{OC}$  compared to dye **C6**.

Then we tested the sensitizers with CDCA-substituents, first without additional co-adsorbent CDCA. A striking discovery was that the  $V_{OC}$  of **C3-CDCA** was now comparable to that of dye **C6**, meaning the CDCA substituent improves the compatibility with the copper electrolytes and inhibits recombination from the  $TiO_2$  to the  $Cu^{2+}$  complex. Encouragingly, the PCE values of **C3-CDCA** and **C6-CDCA** were only slightly below those of the optimized non-CDCA sensitizers. The next step was therefore investigating the effect of additional co-adsorbent to **C3/C6-CDCA**. The optimum concentration of 10 equivalents of CDCA was tested, and for **C6-CDCA** this increased the PCE by 10% compared to the best performing conditions for dye **C6**, reaching an average PCE of 6.20%.



**Figure 3.13:** Relative sensitizer quantum efficiency (SQE) spectra from Paper VI, essentially dye loading-adjusted incident photon-to-current conversion efficiency curves. Curves are scaled relative to the highest performing device. Comment of 8  $\mu m$  means 8+4  $\mu m$   $TiO_2$  was used, while no specification implies 4+2  $\mu m$   $TiO_2$  electrodes.

By increasing the thickness of  $TiO_2$  from 4+2  $\mu m$  (active  $TiO_2$  + scattering  $TiO_2$ ) to 8+4  $\mu m$ , another slight increase in performance was observed for both **C3-CDCA** (5.81% PCE) and **C6-CDCA** (6.44% PCE). To assess the quality of the dye monolayer,

we wanted an estimate of the performance contribution per sensitizer molecule. By adjusting the IPCE spectra using the dye loading values, we could obtain a plot we called *sensitizer quantum efficiency* (SQE), shown in Figure 3.13. As a variant of absorbed photon-to-current conversion efficiency (APCE) spectra, these plots better illustrate the performance of the individual sensitizers. It is our opinion that the individual sensitizer performance can be interpreted as a measure of the quality of the dye/co-adsorbent monolayer.

From the SQE spectra it is clear that the combination of a CDCA substituent on the sensitizer, and 10 equivalents of additional CDCA co-adsorbent in the staining solution yields a far superior individual sensitizer performance. We interpret this to indicate that it is not only the amount of co-adsorbent used in the staining process which is important, but also the distribution. An excellent way of ensuring CDCA is evenly distributed among the sensitizer molecules is covalently attaching it to the sensitizers. The conclusion on this anti-aggregation concept is that it could be a highly valuable design tool for the development of future sensitizers.

# MATERIALS AND METHODS

This chapter describes the materials used and methods established in the experimental work for this thesis, including some techniques not used in the publications. A bit of history behind some developments has been included in case it should be needed in the future.

## 4.1 Materials

### 4.1.1 Fluorine-doped tin oxide glass

Fluorine-doped tin oxide (FTO) coated glass for Paper I was TEC8 sourced from DyeSol, Australia. This was used for both working and counter electrodes. For Paper II, TEC 10 FTO glass for the working electrodes was sourced from Sigma Aldrich, while TEC 8 was used for the counter electrodes. For Papers III-VI FTO NSG 10 from Nippon Sheet Group was used for working electrodes, while TEC 15 was used for both platinum and PEDOT counter electrodes.

### 4.1.2 Titania pastes

The titania pastes were predominantly sourced from DyeSol (later GreatCell Solar). For use with  $I^-/I_3^-$  electrolyte, the 18NR-T paste was found to be the most efficient and it was used for Papers I-V. For Paper VI, titania paste 30NR-D from DyeSol was used. This has slightly larger titania particle size, which was compatible with the slower diffusing copper complexes used in the study. The scattering paste employed in all the papers was WER2-O (DyeSol) with a particle size of 200 nm. A transparent titania paste developed by Dyenamo (DN-HP01) was also tested, however it was inferior to 18NR-T and was not used further.



### 4.1.3 Electrolytes

#### Iodide electrolytes

For Paper I an electrolyte composition reported by Joly et al. was used.<sup>304</sup> This electrolyte contained 0.5 M 1-butyl-3-methylimidazolium iodide (BMII), 0.1 M lithium iodide, 0.05 M iodine and 0.5 M *tert*-butylpyridine in acetonitrile.

The devices reported in Paper II-V employed an electrolyte called A6141 reported by Nazeeruddin et al.<sup>297</sup> The composition of this electrolyte was 0.60 M 1-butyl-3-methylimidazolium iodide (BMII), 0.03 M iodine, 0.10 M guanidinium thiocyanate and 0.50 M *tert*-butylpyridine in a mixture of acetonitrile and valeronitrile (85:15, v/v).

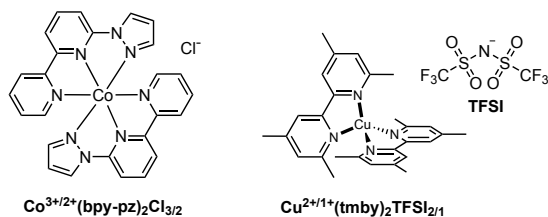
In the optimization ahead of fabricating the devices for Paper I, commercial electrolytes from Solaronix were tested. Iodolytes HI-30, AN-50 and Z-150 were tested, with HI-30 yielding the highest efficiencies. The efficiency for the different electrolytes with **N719** were: Z-150 (3.96%) < AN-50 (4.47%) < HI-30 (5.37%).

#### Cobalt electrolyte

The aqueous  $\text{Co}^{3+/2+}(\text{bpy-pz})_2\text{Cl}_{3/2}$  electrolyte used in Paper IV was first reported by Ellis et al.<sup>52</sup> Electrolyte composition was 0.13 M  $[\text{Co}(\text{bpy-pz})_2]\text{Cl}_2$ , 0.06 M  $[\text{Co}(\text{bpy-pz})_2]\text{Cl}_3$  and 0.8 M 1-methylbenzimidazole (MBI) in deionized water. Cobalt complexes were sourced from Dyenamo. (bpy-pz = 6-(1*H*-pyrazol-1-yl)-2,2'-bipyridine)

#### Copper electrolyte

For Paper VI, a copper electrolyte previously reported by Cao et al. was used.<sup>58</sup> The composition of this electrolyte was 0.09 M  $[\text{Cu}(\text{tmby})_2]\text{TFSI}_2$ , 0.20 M  $[\text{Cu}(\text{tmby})_2]\text{TFSI}$ , 0.1 M lithium bis(trifluoromethanesulfonyl)imide (LiTFSI) and 0.6 M 1-methylbenzimidazole in dry acetonitrile. Copper complexes were sourced from Dyenamo. (tmby = 4,4',6,6'-tetramethyl-2,2'-bipyridine)



**Figure 4.1:** Structures of the copper and cobalt complexes used in this thesis.

#### 4.1.4 Reference sensitizers

Reference sensitizers are important yardsticks between different scientific works on dye-sensitized solar cells. **N719** has long been the reference sensitizer of choice, at least when  $I^-/I_3^-$  electrolytes are used. With copper and cobalt electrolytes other sensitizers compatible with the electrolyte system are more appropriate. For Papers I-V, **N719** was used, together with **RK1** for Paper IV. Papers II and IV included previously published dyes, **Dye 2** by Nagarajan et al.<sup>283</sup> and **EO3** by Lin et al.<sup>289</sup> For Paper VI, the reference sensitizer **D35** was used, previously reported to be compatible with the  $[Cu^{2+/1+}(tmbpy)_2](TFSI)_{2/1}$  electrolyte.<sup>57</sup> The **N719** used in the papers included in this thesis was sourced from DyeSol, **RK1** from Solaronix and **D35** was sourced from Dyanamo. **Dye 2** and **EO3** were prepared at NTNU with synthesis details reported in Papers II and IV.

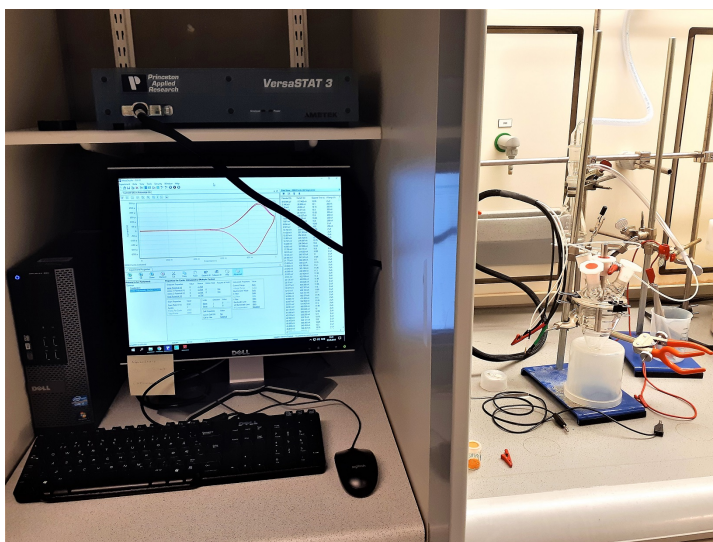
## 4.2 Methods and equipment

### 4.2.1 Electrochemistry setup

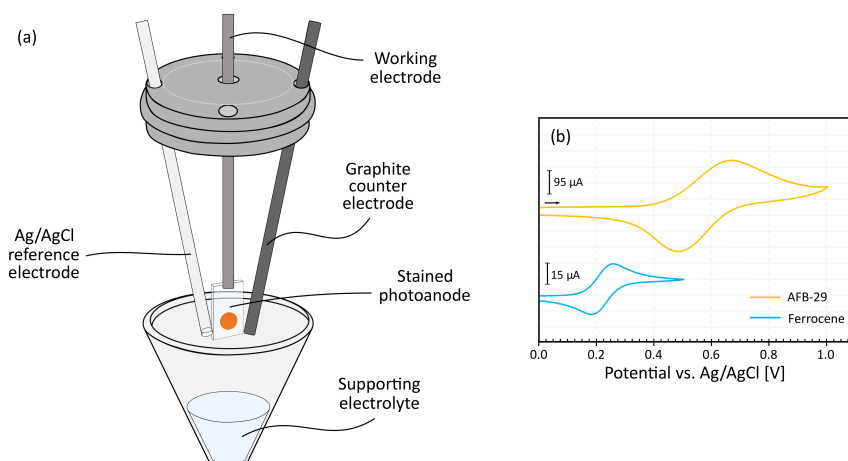
The electrochemical measurements performed at NTNU were performed on a Versa-STAT 3 potentiostat from Princeton Applied Research, as shown in Figure 4.2. The proprietary Versastudio software was used for data acquisition. A basic setup for solution electrochemistry was used for Papers I and II, where platinum wires were used as working, reference and counter electrodes. The area of the counter electrode was maximized by coiling a thin diameter Pt wire into a bundle. Later, for Paper III and IV, an electrochemical setup developed by Nick Vlachopoulos at EPFL was used. This setup comprised a larger electrochemical cell where stained  $TiO_2$  photoanodes could be connected to the working electrode, a graphite rod counter electrode and a pseudo Ag/AgCl reference. Figure 4.3 gives an illustration of what the assembled electrochemical cell looks like. The Ag/AgCl reference contained AgCl in the supporting electrolyte used during the experiments, 0.1 M LiTFSI in dry acetonitrile, separated by a glass frit. The purging nitrogen was first saturated with acetonitrile in a pre-bubbler as this minimized concentration changes due to solvent evaporation from the electrochemical cell.

A similar setup was then constructed in the DSSC laboratory at NTNU, and this was used for the measurements for Paper V and VI. A major difference was the construction of the Ag/AgCl reference electrode. At NTNU a commercial reference electrode was used, which contained Ag/AgCl in an aqueous 3 M NaCl solution, separated from the electrochemical cell. This is not ideal due to water from the reference contaminating the acetonitrile electrolyte, but NaCl can also crystallize in the glass frit when in contact with an organic solvent, blocking the frit completely. However, nei-

ther of these issues are critical in the short term, but in the long term a more stable Ag/AgCl reference should be developed for this characterization technique.



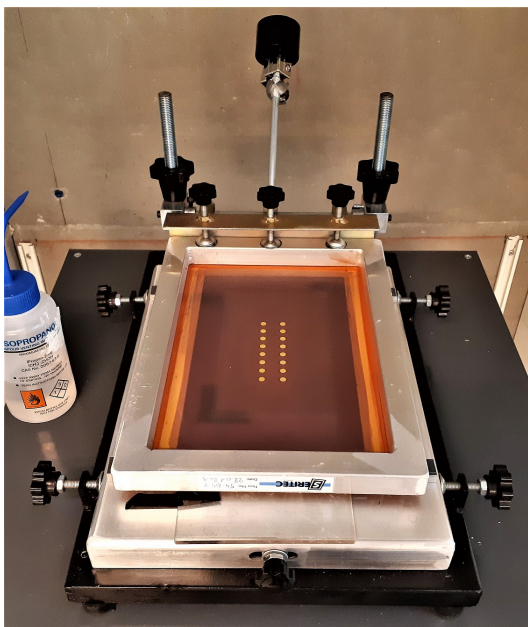
**Figure 4.2:** Electrochemistry setup at NTNU. VersaSTAT 3 potentiostat, Versastudio software and electrochemical cell in the fume hood.



**Figure 4.3:** a) Setup for cyclic voltammetry measurements of stained photoanodes and b) typical cyclic voltammogram.

### 4.2.2 Screenprinting

The most common techniques for deposition of titania pastes for fabrication of photoanodes for DSSCs are screenprinting and doctorblading. While doctorblading will work in a roll-to-roll fabrication process, screenprinting has advantages in that it can also produce small-area electrodes more suitable for research devices. In screenprinting, a mesh is stretched over a frame, and the areas of the mesh not intended for printing are masked by a polymer, completely blocking the gaps in the mesh. The titania paste is then applied to the screen and a tool resembling a wide spatula called a squeegee is used to press the paste through the mesh openings and onto the substrate positioned underneath. By varying the mesh count and filament thickness of the screens, the researcher can achieve different thickness of the printed layers. When the screen is positioned in a rig, several layers can be printed on top of each other with perfect precision.



**Figure 4.4:** Screenprinting setup at the Department of Chemistry, NTNU.

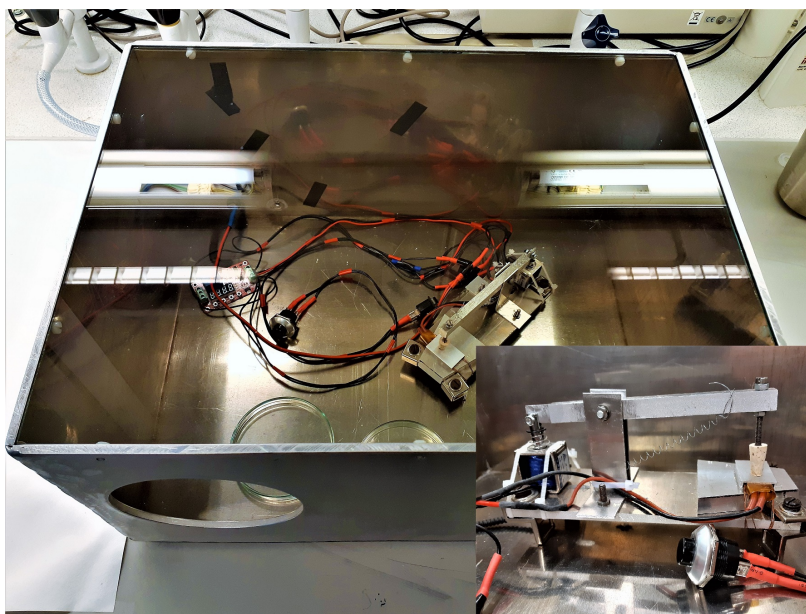
In the work in this thesis, a screen with a 54T mesh from Sefar was found to produce a thickness of  $6.5 \mu\text{m}$ , while a 120T mesh screen gave  $2 \mu\text{m}$  thick films. Multiples of these layers yields photoanodes with suitable thickness for devices with different electrolyte systems. The screens used at EPFL and NTNU were produced by a Swiss company called Seritec Services S.A. The outer dimensions of the frame were  $36 \times 26 \text{ cm}$ , made from  $25 \times 25 \text{ mm}$  aluminium box profile (see Figure 4.4).

### 4.2.3 Annealing oven

Sintering of the photoanodes can be done in several ways. At EPFL, programmable hotplates were used, while at NTNU a programmable furnace is used for the same purpose. The advantage of a hotplate is faster regulation of temperature, while a furnace requires longer temperature ramping times. The furnace installed in the DSSC laboratory at NTNU is a Nabertherm LT 9/12. No comparative study has been performed between the furnace and hotplate, but efficient devices were produced with both sintering methods.

### 4.2.4 Sealing machine and drybox

Proper sealing is very important in fabricating devices of high efficiency and stability. Surlyn has been a favourite sealing polymer used for many years in the DSSC field. A temperature between 80 and 100 °C is required to melt the polymer, and upon cooling a high quality seal is usually obtained. Surlyn can be bought in different thicknesses, hence dictating the distance between the electrodes. Typical Surlyn thicknesses vary from 25-60  $\mu\text{m}$ , and the thickness should be optimized for the electrolyte in question. For  $\text{I}^-/\text{I}_3^-$  electrolytes, larger distances can be tolerated than for metal-complexed redox couples.



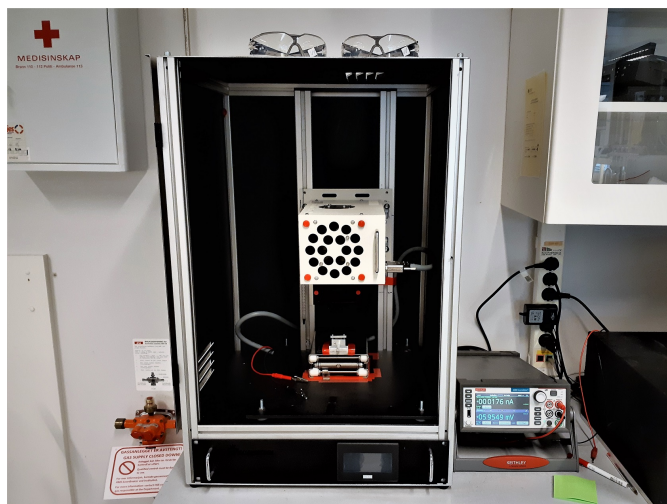
**Figure 4.5:** Sealing drybox setup. Insert shows the homemade sealing machine and remote controlling switch providing pressure and heat for DSSC sealing.

Exposure to high temperatures may degrade sensitizers, and consequently controlling and limiting the heating time during the sealing process is important. At NTNU a device was built for this purpose, as illustrated in Figure 4.5. The heating is supplied by a 12 V, 50 W PTC heat element bought on Ebay, connected to a programmable microcontroller with a relay. With this setup, exact pressure and heating cycles can be programmed, and also be connected to a remote control available to the operator. From experience, moderate pressure on the electrodes while heating provides more efficient sealing in shorter time. A pressure arm tensioned by a spring was built for this purpose. The arm is also connected to an electronic solenoid step motor, so switching pressure on/off can be controlled remotely if desirable. Ensuring as little moisture as possible is present during the sealing process, the entire process is conducted in a drybox. This is simply an aluminium box with a glass lid connected to a compressed gas supply, as seen in Figure 4.5.

#### 4.2.5 Solar simulator setup

The solar simulator is the most important characterization tool in photovoltaic research, providing simulated sunlight of a certain intensity so that reliable device efficiency measurements can be preformed. The solar simulator at NTNU was bought from a Canadian company called Sciencetech, and is of the Model SF300B. This is a low-cost simulator with a rating of ABA for light uniformity, spectral match and temporal stability. This means the spectral match and temporal stability are very high, while the uniformity is slightly compromised and rated to a B. The lamp is a Xenon arc lamp with an expected life-time of up to 1000 hours, and filters are used to alter the spectral shape. The filter fitted to the simulator at NTNU is an AM 1.5 Global filter. The power to the lamp can be controlled with the power source, and one should be aware that the spectral shape can be affected by the power. Consequently, a power setting of 100% corresponding to approximately 283 W is always selected for the measurements. If lower light intensities are required, this should be achieved by using mesh filters rather than altering the power settings, as mesh filters do not alter the spectral distribution of the light. A sourcemeter is required to apply potential to the devices and simultaneously measure the current produced. Keithley sourcemeters are widely used, and at NTNU the model used is 2450. This is remote controlled by a program written in Labview.

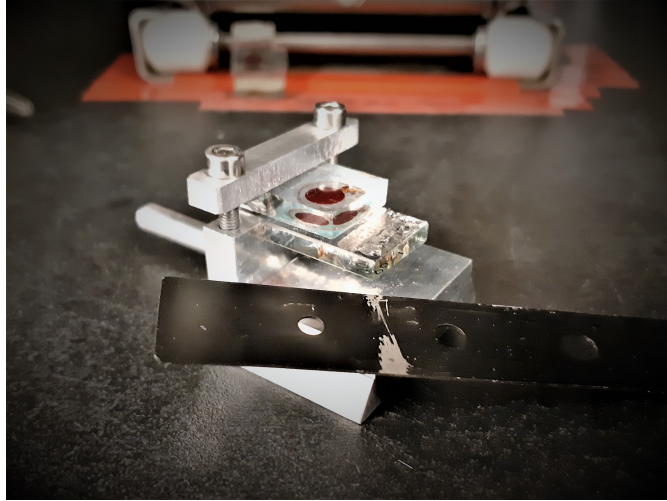
Correct calibration of the light intensity is extremely important, and this requires a reference cell with a known efficiency. The one used in the NTNU lab belongs to the Department of Materials Engineering and is a Newport Reference Cell and Meter (91150V). It is important to calibrate at the same height as the sample holder, and the intensity is calibrated by moving the lamp up or down until a value of 1 sun is reached. Although the total intensity of ambient indoor illumination is quite low (1-



**Figure 4.6:** Solar simulator setup. Scincetech SF300B solar simulator built into a casing fabricated by the NTNU mechanical engineering workshop. Keithley 2450 sourcemeter (right).

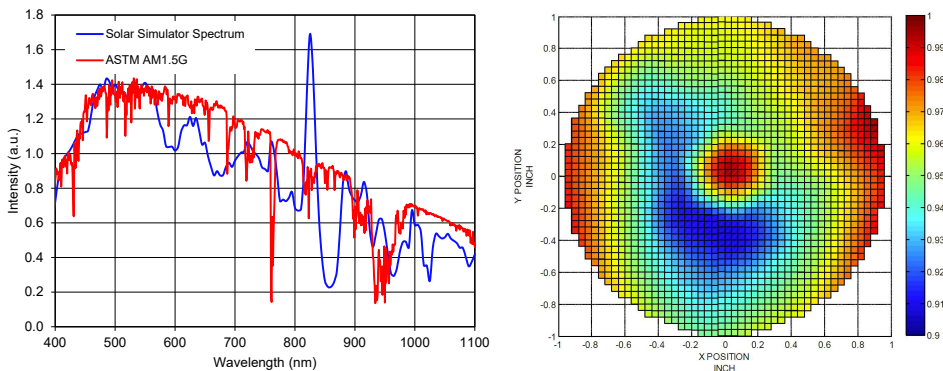
0.01% of 1 sun), covering the IV setup is advantageous for repeatable measurements, as has been done to the NTNU solar simulator in Figure 4.6. It should be noted that calibrating the solar simulator with a reference silicon solar cell does not ensure the spectral shape of the solar simulator is correct, only the irradiance. The solution to this is to calculate a spectral mismatch factor, as described by Snaith.<sup>84</sup>

Lastly, for higher repeatability, a sample holder has been developed based on the system which has been in use at EPFL for many years. The idea is to fix the DSSC into a device which slots into the same position under the collimated light beam of the solar simulator every time. Thus, any errors caused by non-uniformity of the light will be systematic and not affect the relative performances of devices. With this sample holder, shown in Figure 4.7, masking the devices to an accurate area is also straight-forward. The use of a fully opaque mask covering the entire device apart from the active area is essential. A phenomenon called *piping* is the channeling of light in the glass substrate from the sides into the active area, which can be a considerable source of error, causing overestimated efficiency measurements. Snaith characterized a DSSC with 10% PCE (correctly masked and measured) under side-illumination where the same DSSC delivered a PCE of 6.6%, indicating the extent of the problem of light channeling or piping.<sup>305</sup> It is worth noting that reliable reporting of data is just as important as correct acquisition of data. The efficiency variation in a batch of DSSC devices fabricated by the same scientist can easily be 10-15%. It is therefore important to report average values with corresponding standard deviation to correctly describe the whole data set.



**Figure 4.7:** Sample holder with machined mask for  $J$ - $V$  sweeps under the solar simulator. Sample holder ensures correct height and position of the DSSC in the collimated light beam.

While the Xenon lamp can never fully mimic the real sunlight, it is widely accepted as the best substitute available to researchers in the field of photovoltaics. The spectral shape and non-uniformity map of the Sciencetech SF300B solar simulator with the AM 1.5 G spectrum is given in Figure 4.8. The spectral match is quite good in the region most photovoltaic devices operate, but caution should be taken ensuring the sample position in the beam is consistent. With a reported non-uniformity of 4.7%, differences in intensities of almost 10% can be encountered.

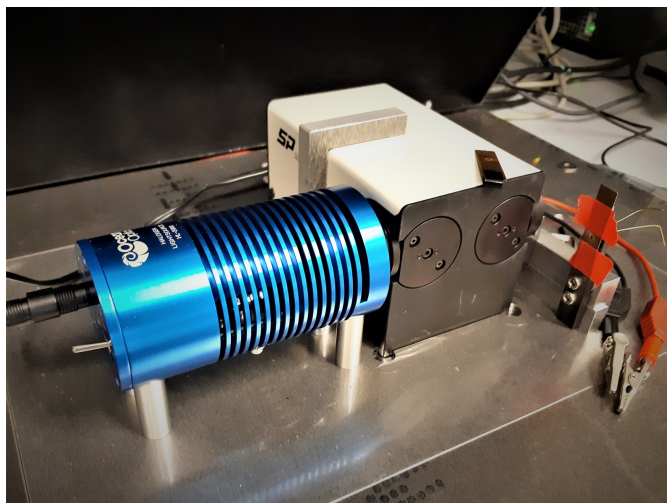


**Figure 4.8:** Spectral shape and non-uniformity map of NTNU's Sciencetech SF300B solar simulator from the Sciencetech QC report.



### 4.2.6 IPCE setup

Incident Photon-to-Current Conversion Efficiency (IPCE) is another important solar cell characterization technique used to determine the device efficiency at different wavelengths of monochromatic light. Commercial systems are available, such as the Arkeo-Ariadne from Cicci Research s.r.l. in use at LPI/LSPM at EPFL. More affordable, and equally accurate systems may be built from cheap components. The system at NTNU (Figure 4.9) is built from a halogen white light lamp from Ocean Optics (HL-2000), in line with a monochromator (Spectral Products CM110) controlled by a program written in Labview by Dr. James Bannock. The current produced by the device is measured with the Keithley 2450.



**Figure 4.9:** IPCE setup. Lamp (left), monochromator (middle) and sample holder for devices and photodiode (right).

As the IPCE values is the ratio of generated electrons to incident photons, knowing the light flux at each wavelength is paramount. This is done with a NIST traceable calibrated photodiode from Thorlabs (FDS100-CAL) with a known responsivity curve (W/nm). Masking of both the reference diode and the device is important in order to obtain the correct measurements. The intensity of the light used for IPCE measurements is very weak, and consequently any stray light from the surroundings will affect the measurements considerably. Hence, a light proof box had to be manufactured for the IPCE setup.

Integration of the recorded IPCE spectra across the AM 1.5G solar spectrum has been done in a number of ways. The website [www.opvap.com](http://www.opvap.com) offers a free online calculator where IPCE data can be integrated and the  $J_{SC}$  value obtained. The author also developed a simple excel sheet which did the same calculations. And lastly,

the commercial IPCE setup in use in the LPI/LSMP facilities at EPFL integrates the IPCE curve continuously while recording the spectra and reports the integrated  $J_{SC}$  value. The calculations are not complex, so all three methods worked equally well.

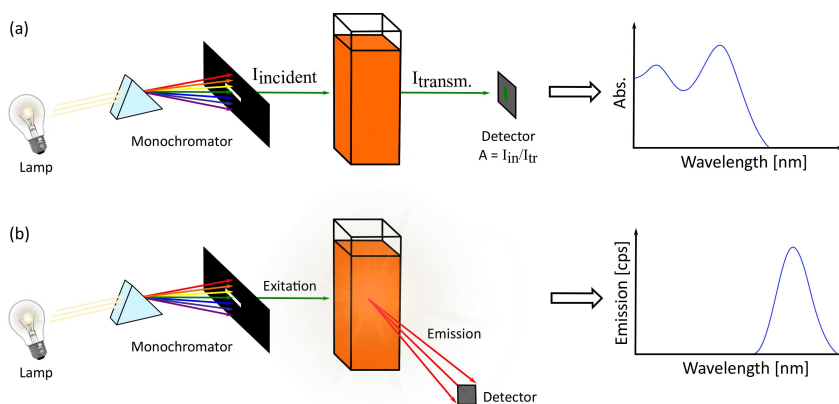
#### 4.2.7 Absorption and emission measurements

Absorption spectra were measured on a Hitachi U-1900 instrument. When absorption measurements of stained  $\text{TiO}_2$  films was performed, these had to be aligned and attached to the cuvette holder so that the entire monochromatic light beam passes through the sample. The principle of absorption measurements is illustrated in Figure 4.10 (a). Essentially the absorption is the difference in light intensity hitting the sample and the transmitted light. Because of any effects from the solvent or cuvette, a background measurement has to be subtracted, which is automatically done for most modern spectrophotometers.

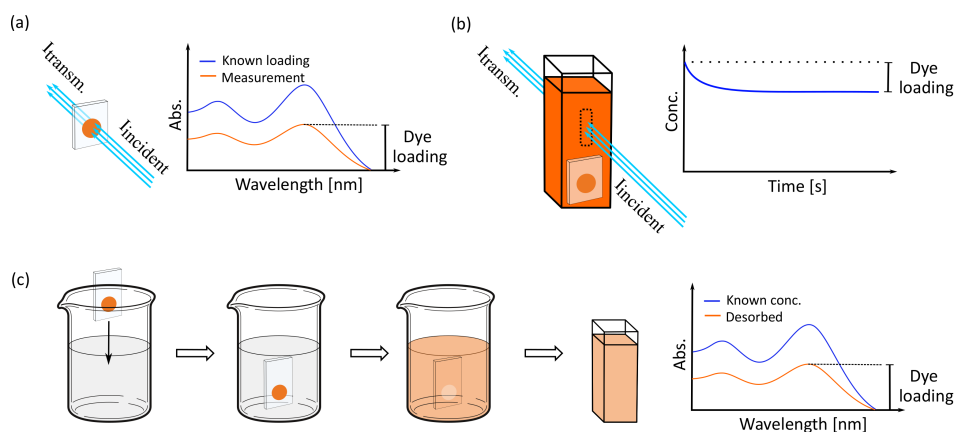
Emission spectra are recorded in a slightly different way than absorption spectra, in that the detector is not in line with the light beam, but perpendicular. The reason for this is to minimize stray light hitting the detector, as only the emitted radiation is of interest. Usually, a sample is illuminated with the wavelength corresponding to the wavelength of maximum absorption of the most red-shifted peak in the absorption spectra. Here, no background measurement is necessary unless the solvent emits in the same region as the sample, and even then a change of solvents should be considered. The emission signal is simply counts per second, i.e. the number of photons detected per second at each wavelength. The principle of emission spectroscopy is shown in Figure 4.10 (b). The instrument used for emission spectroscopy at NTNU is a FS5–TCSPC spectrophotometer instrument from Edinburgh Instruments. It was found for the FS5 instrument that in order to obtain a correct measurement, the correction file should not be used. A Cary Eclipse spectrophotometer was used for the measurements for Papers I-IV and was used to verify the measurements of the FS5 without correction file as the correct spectra.

#### 4.2.8 Dye loading measurements

Dye loading experiments are very important measurements giving information on the number of dye molecules adsorbed on the DSSC photoanode.<sup>306,307</sup> Despite being frequently reported, the experimental details of the dye loading values are often omitted in the publications in the field of DSSCs. A number of different experimental procedures are available to the researcher as illustrated in Figure 4.11, all of which rely on UV/Vis spectrophotometry. The methods can be divided into *direct* and *indirect* measurements of dye loading.



**Figure 4.10:** Working principles of: a) UV/Vis spectrophotometer and b) Fluorescence spectrophotometer.



**Figure 4.11:** Direct and indirect measurements of dye loading.

### *Direct measurement*

Direct measurements of the dye loading can be done by measuring the UV/Vis absorption of a stained electrode, using a non-stained electrode as the blank sample. The challenge with this technique lies in obtaining the extinction coefficient of the sensitizer while anchored on  $\text{TiO}_2$ , but one may also encounter issues when measuring thick films due to high extinction causing very low transmission. Unless an integrating sphere spectrophotometer is used, this technique requires electrodes without a scattering  $\text{TiO}_2$  layer. Consequently, you are not measuring the dye loading on exactly the same electrodes as the ones used for fabricating the devices. Therefore, many researchers favor the indirect measurement procedures.

*Indirect measurements*

There are two main ways of measuring the dye loading indirectly, either by measuring the decrease in staining solution concentration during staining or by desorbing the dye from the photoanode and measure the absorbance of the desorption solution. A challenge with the first measurement would be solvent evaporation during the staining time, but also any aggregation and precipitation of sensitizers in the staining solution will affect the dye loading measurements. If these effects are suppressed, then this procedure will allow for a large number of measurements per electrode and one can easily determine the optimal staining time and rate constants for the adsorption process. For the latter procedure it is important to obtain the correct extinction coefficients, because alkaline desorption solutions are used which will affect the extinction coefficients. The dye loading is usually calculated as mol/cm<sup>2</sup>, which is sufficient as long as dye loading of electrodes of similar thickness is compared. Also small differences in the area of the screen printed electrodes will affect the measurements, so electrodes from the same screen printing batch should always be compared. Ideally, calculating the dye loading as mol/cm<sup>3</sup> of TiO<sub>2</sub> would yield more comparable results between different studies, but this requires very reliable thickness measurements of the TiO<sub>2</sub> electrodes.

In this thesis both the indirect protocols have been tested. Procedure (b) from Figure 4.11 was used for Paper II, but the protocol employing dye desorption was found to be easier and more reliable. Desorption solutions of 100 mM NaOH in ethanol/water (1:1, v/v) and 40 mM tetrabutylammonium hydroxide (TBAOH) in stabilized THF have been used. The first desorption solution was found to desorb the dyes fully in 24-48 hours, depending on the dye. However, a decrease in absorbance of the standard solutions was observed over the same time frame as the desorption time, indicating a stability issue in this system leading to underestimates of the actual dye loading. The TBAOH system was found to desorb the dyes within seconds, allowing for the most reliable measurements of dye loading.

**4.2.9 Device fabrication**

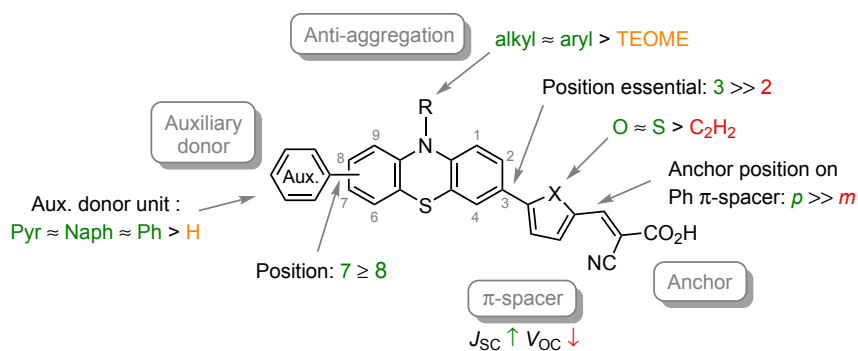
The main device fabrication procedure is described in detail in the individual papers. While the fabrication developed and performance increased from paper I to Paper VI, the overall architecture of the devices stayed the same. The completely different electrolyte system of Paper VI required different counter electrodes and thinner TiO<sub>2</sub> layers.



# GENERAL CONCLUSION AND FURTHER WORK

## 5.1 Summary

This thesis has focused on using organic chemistry as a tool to understand, explore new concepts and develop sensitizers for dye-sensitized solar cells based on the phenothiazine and triarylamine scaffolds. First, convenient synthetic routes to strategic building blocks were developed. Then, sets of sensitizers designed to investigate different aspects of dye design were synthesized. Alongside this, a permanent laboratory for the fabrication and characterization of dye-sensitized solar cells was established at the Department of Chemistry, NTNU. This would not have been possible without valuable knowledge from two short visits and a three-month research stay in the Laboratory of Photonics and Interfaces/Laboratory of Photomolecular Science (LPI/LSPM) at EPFL. This thesis includes six scientific works reporting a total of 36 phenothiazine and four triarylamine sensitizers. All the reported dyes have been evaluated and characterized using a range of electrochemical and spectroscopic methods, in addition to thorough photovoltaic evaluation in dye-sensitized solar cells.



**Figure 5.1:** Structure-PCE relationship for phenothiazine dyes for DSSC compiled based on investigations in Papers I-V.

The chemistry of the phenothiazine scaffold is flexible, and a number of commercially available compounds allow great versatility in dye structures based on phenothiazine. However, several limitations in the photovoltaic performance have become apparent through Papers I-V, as summarized in a structure-PCE relationship in Figure 5.1. The  $\pi$ -spacer is used to extend the conjugation and redshift the absorption properties, and it was established this group had to be positioned *para* to the nitrogen atom of phenothiazine. However, a significant reduction in  $V_{OC}$  was associated with the introduction of  $\pi$ -spacers. Further, the effect of auxiliary donors is extremely limited, and the nature and position of this donor group appears to be of minor importance. This we interpret as a consequence of the folded nature of the phenothiazine scaffold along the S-N axis, restricting the conjugation across the system. Thus, any positive effects from the auxiliary donor side of the sensitizer are significantly impaired. The same folding is also associated with a reorganizational energy cost, upon oxidation of the sensitizer to the flat cation. Lastly, the high HOMO-levels paired with the relatively low extinction coefficients of phenothiazine dyes, make them poor candidates for use with novel electrolyte systems such as those based on copper and cobalt.

The opinions on phenothiazine dyes mentioned above contributed to triarylamine-based dyes being the basis for Paper VI. The introduction of a chenodeoxycholic acid-based substituent, coupled covalently onto the  $\pi$ -spacer of a triarylamine dye, produced high quality monolayers. This effect was attributed to an overall even and controlled distribution of free and covalent anti-aggregation moieties in the dye monolayer.

## 5.2 Future development

### 5.2.1 DSSC field in general

The future of the dye-sensitized solar cell field is not immediately clear, and a number of different directions can be envisioned. An increasing number of new PV technologies have developed alongside the dye-sensitized solar cells, all with inherent advantages and disadvantages. Aesthetically, dye-sensitized solar cells are superior to most other PV technologies due to the tunability in colour and transparency. Devices of high transparency and a wide range of colours can be manufactured, and companies such as H.Glass and Solaronix are already commercializing the technology in this direction. Further development in this field will likely focus on novel high stability dyes with colours desirable for building integration.

Dye-sensitized solar cells have also been proven to be incredibly efficient under indoor illumination, and this is likely to be a field of considerable interest in the future.

Indoors, the spectral shape of the available light is typically completely different to that outside. This favours the relatively narrow and tunable absorption properties of the most common sensitizers, and further development will likely focus on tailoring the dye absorption properties. The use of co-sensitized systems could also be a successful approach, especially under LED illumination, which usually exhibits illumination spectra consisting of a few peaks with narrow wavelength distribution. Apart from the dye, the development of new transparent conduction oxides or similar would allow larger solar cells without the need for metallic contacting grids for charge collection.

The Focused-Induced Photoresponse distance measurement technique was recently introduced. The basis of the measurement technique is the irradiance dependency of the DSSC. In turn, this introduced a completely new application to the field of dye-sensitized solar cells, and other sensor-based applications using the versatile architecture of the DSSC are certainly commercially interesting.

Another group of non-photovoltaic applications include the interweaved fields of dye-sensitized photoelectrolysis devices, water-splitting applications, artificial photosynthesis and solar fuel production. The electrochemical behaviour of the dyes is of huge importance in these field, and development of new dyes targeting these applications is necessary. Because of the inherently difficult process of CO<sub>2</sub> reduction, the development of new catalysts for this purpose would be of interest to the fields of artificial photosynthesis and solar fuels.

There is still a lot of activity within the "conventional" DSSC field. The efficiency of DSSCs can be improved in two ways, either by increasing the amount of light harvested by the sensitizer, or by converting a larger amount of the absorbed photon energy into electrical power. In terms of semiconducting oxides, developing new oxides with more negative Fermi levels would help close the injection gap from the sensitizer LUMO level, thus increasing the  $V_{OC}$ . Tuning of redox shuttle complexes will increase the photovoltage further, and voltages approaching 1.5 V can be within reach with proper tuning. Organic synthesis is an important tool in this field and several exciting concepts involving organic chemistry spring to mind for further development:

- Develop new donor moieties to lower the HOMO levels of the dyes enough to work with copper or cobalt electrolytes with low-lying redox potentials.
- Develop new  $\pi$ -spacers to bring the LUMO level of the sensitizers down while not affecting the HOMO level. This will also redshift the absorption and increase the number of wavelengths the sensitizer will harvest.
- Investigate *in situ* formation of a hole-transport material creating ssDSSC with HTM penetrating the entire TiO<sub>2</sub> layer.



- New ligands for fine tuning of the redox potentials of copper complexes can allow sensitizers with more negative HOMO levels to utilize these electrolytes.

### 5.2.2 Phenothiazine sensitizers

During work with the six papers included in this thesis, we have learned a few lessons, but also come up with some design ideas which may be useful to the wider DSSC community. Firstly, although a few reasonably efficient sensitizers based on phenothiazine have been reported over the years, the author is of the opinion that there is little more to gain from this scaffold in terms of efficiency. Sadly, when looking back into the phenothiazine sensitizer literature, we observe similar unfavorable behaviour has been reported for over a decade. A number of review papers summarizing the field have failed to identify and illuminate these issues. Unfortunately, at least one highly suspicious account of outstanding phenothiazine performance has been published, and is already being cited as a major breakthrough for the phenothiazine sensitizer class. We hope our work has highlighted both the advantages and shortcomings of this sensitizer class in such a way that other researchers may take well informed decisions on further development of the field.

Fortunately, our findings on triarylamine dyes with chenodeoxycholic acid substituents are highly encouraging. The dyes are compatible with novel copper electrolytes, yielding  $V_{OC}$  values in excess of 1000 mV. The CDCA substituent has a profound effect on the performance of the individual dye molecules, yielding highly efficient dye monolayers. Adopting a similar approach for dyes already at the peak of performance, such as **XY1b** and **Y123** would be very interesting to pursue. Additionally, these dyes have fused heterocyclic  $\pi$ -spacers, which can allow for installation of the CDCA substituent in such a way that it cannot induce detrimental ring twisting. Lastly, near-IR dyes such as those based on squaraine and DPP appear to be especially prone to aggregation, and thus would be prime candidates for a study into large covalent anti-aggregation moieties.

## REFERENCES

- [1] United Nations Department of Economic and Social Affairs/Population Division World Population Prospects: The 2017 Revision, Key Findings and Advance Tables.
- [2] Arrhenius, S. *Philos. Mag.* **1896**, *41*, 237–276.
- [3] BP Statistical Review of World Energy (Accessed 13.03.2019); <https://www.bp.com/content/dam/bp/business-sites/en/global/corporate/pdfs/energy-economics/statistical-review/bp-stats-review-2018-full-report.pdf>.
- [4] UNFCCC, Adoption of the Paris Agreement (Accessed 13.03.2019); <https://unfccc.int/resource/docs/2015/cop21/eng/l09r01.pdf>.
- [5] Markandya, A.; Wilkinson, P. *The Lancet* **2007**, *370*, 979–990.
- [6] Williams, D. R. Sun Fact Sheet 2018, NASA Goddard Space Flight Center (Accessed 02.07.2019); <https://nssdc.gsfc.nasa.gov/planetary/factsheet/sunfact.html>.
- [7] Gueymard, C. A.; Myers, D.; Emery, K. *Solar Energy* **2002**, *73*, 443–467.
- [8] Chen, C.-Y. et al. *J. Phys. Chem. Lett.* **2017**, *8*, 1824–1830.
- [9] Blankenship, R. E. et al. *Science* **2011**, *332*, 805–809.
- [10] Szabó, L. The history of using solar energy. 2017 International Conference on Modern Power Systems (MPS). pp 1–8.
- [11] Becquerel, A. *Comptes Rendus Acad. Sci* **1839**, *9*, 145–149.
- [12] Fritts, C. E. *Am. J. Sci.* **1883**, *26*, 465–472.
- [13] Ohl, R. S., Patent US2402662A. 1946.
- [14] Czochralski, J. *Z. Phys. Chem.* **1918**, *92*, 219–221.
- [15] Nayak, P. K.; Mahesh, S.; Snaith, H. J.; Cahen, D. *Nat. Rev. Mater.* **2019**, *4*, 269–285.
- [16] Pakhanov, N. A.; Andreev, V. M.; Shvarts, M. Z.; Pchelyakov, O. P. *Optoel. Instr. Data Proc.* **2018**, *54*, 187–202.
- [17] Kojima, A.; Teshima, K.; Shirai, Y.; Miyasaka, T. *J. Am. Chem. Soc.* **2009**, *131*, 6050–6051.
- [18] Kim, H.-S.; Lee, C.-R.; Im, J.-H.; Lee, K.-B.; Moehl, T.; Marchioro, A.; Moon, S.-J.; Humphry-Baker, R.; Yum, J.-H.; Moser, J. E.; Grätzel, M.; Park, N.-G. *Sci. Rep.* **2012**, *2*, 591–597.
- [19] Lee, M. M.; Teuscher, J.; Miyasaka, T.; Murakami, T. N.; Snaith, H. J. *Science* **2012**, *338*, 643–647.
- [20] O'Regan, B.; Grätzel, M. *Nature* **1991**, *353*, 737–740.
- [21] Namba, S.; Hishiki, Y. *J. Phys. Chem.* **1965**, *69*, 774–779.
- [22] Gerischer, H.; Tributsch, H. *Ber. Bunsenges. Phys. Chem.* **1968**, *72*, 437–445.
- [23] Tributsch, H.; Gerischer, H. *Ber. Bunsenges. Phys. Chem.* **1969**, *73*, 251–260.
- [24] Hauffe, K.; Danzmann, H. J.; Pusch, H.; Range, J.; Volz, H. *J. Electrochem. Soc.* **1970**, *117*, 993–999.

- [25] Nelson, R. C. *J. Phys. Chem.* **1965**, *69*, 714–718.
- [26] Tsubomura, H.; Matsumura, M.; Nomura, Y.; Amamiya, T. *Nature* **1976**, *261*, 402–403.
- [27] Anderson, S.; Constable, E. C.; Dare-Edwards, M. P.; Goodenough, J. B.; Hamnett, A.; Seddon, K. R.; Wright, R. D. *Nature* **1979**, *280*, 571–573.
- [28] Moser, J.; Graetzel, M. *J. Am. Chem. Soc.* **1984**, *106*, 6557–6564.
- [29] Hagfeldt, A.; Boschloo, G.; Sun, L.; Kloo, L.; Pettersson, H. *Chem. Rev.* **2010**, *110*, 6595–6663.
- [30] Xu, J.; Wu, S.; Jin, J.; Peng, T. *Nanoscale* **2016**, *8*, 18771–18781.
- [31] Barbé, C. J.; Arendse, F.; Comte, P.; Jirousek, M.; Lenzmann, F.; Shklover, V.; Grätzel, M. *J. Am. Ceram. Soc.* **1997**, *80*, 3157–3171.
- [32] Zaban, A.; Aruna, S. T.; Tirosh, S.; Gregg, B. A.; Mastai, Y. *J. Phys. Chem. B* **2000**, *104*, 4130–4133.
- [33] Anta, J. A.; Guillén, E.; Tena-Zaera, R. *J. Phys. Chem. C* **2012**, *116*, 11413–11425.
- [34] Rahman, M. U.; Wei, M.; Xie, F.; Khan, M. *Catalysts* **2019**, *9*, 273–284.
- [35] Memarian, N.; Concina, I.; Braga, A.; Rozati, S. M.; Vomiero, A.; Sberveglieri, G. *Angew. Chem. Int. Ed.* **2011**, *50*, 12321–12325.
- [36] Ferrere, S.; Zaban, A.; Gregg, B. A. *J. Phys. Chem. B* **1997**, *101*, 4490–4493.
- [37] Banik, A.; Ansari, M. S.; Qureshi, M. *ACS Omega* **2018**, *3*, 14482–14493.
- [38] Guo, E.; Yin, L. *J. Mater. Chem. A* **2015**, *3*, 13390–13401.
- [39] Guo, P.; Aegerter, M. A. *Thin Solid Films* **1999**, *351*, 290–294.
- [40] Tan, B.; Toman, E.; Li, Y.; Wu, Y. *J. Am. Chem. Soc.* **2007**, *129*, 4162–4163.
- [41] Chen, J.; Lu, L.; Wang, W. *J. Phys. Chem. C* **2012**, *116*, 10841–10847.
- [42] Zhang, L.; Cole, J. M. *ACS Appl. Mater. Interfaces* **2015**, *7*, 3427–3455.
- [43] Wu, J.; Lan, Z.; Lin, J.; Huang, M.; Huang, Y.; Fan, L.; Luo, G. *Chem. Rev.* **2015**, *115*, 2136–2173.
- [44] Saygili, Y.; Stojanovic, M.; Flores-Díaz, N.; Zakeeruddin, S. M.; Vlachopoulos, N.; Grätzel, M.; Hagfeldt, A. *Inorganics* **2019**, *7*, 30–98.
- [45] Boschloo, G.; Hagfeldt, A. *Acc. Chem. Res.* **2009**, *42*, 1819–1826.
- [46] Gibson, E. A.; Le Pleux, L.; Fortage, J.; Pellegrin, Y.; Blart, E.; Odobel, F.; Hagfeldt, A.; Boschloo, G. *Langmuir* **2012**, *28*, 6485–6493.
- [47] Bella, F.; Galliano, S.; Falco, M.; Viscardi, G.; Barolo, C.; Grätzel, M.; Gerbaldi, C. *Chem. Sci.* **2016**, *7*, 4880–4890.
- [48] Yum, J.-H.; Baranoff, E.; Kessler, F.; Moehl, T.; Ahmad, S.; Bessho, T.; Marchioro, A.; Ghadiri, E.; Moser, J.-E.; Yi, C.; Nazeeruddin, M. K.; Grätzel, M. *Nat. Commun.* **2012**, *3*, 631–639.
- [49] Yella, A.; Mathew, S.; Aghazada, S.; Comte, P.; Grätzel, M.; Nazeeruddin, M. K. *J. Mater. Chem. C* **2017**, *5*, 2833–2843.
- [50] Son, Y. J.; Kang, J. S.; Yoon, J.; Kim, J.; Jeong, J.; Kang, J.; Lee, M. J.; Park, H. S.; Sung, Y.-E. *J. Phys. Chem. C* **2018**, *122*, 7051–7060.
- [51] Xiang, W.; Huang, F.; Cheng, Y.-B.; Bach, U.; Spiccia, L. *Energy Environ. Sci.* **2013**, *6*, 121–127.
- [52] Ellis, H.; Jiang, R.; Ye, S.; Hagfeldt, A.; Boschloo, G. *Phys. Chem. Chem. Phys.* **2016**, *18*, 8419–8427.
- [53] Kakiage, K.; Aoyama, Y.; Yano, T.; Oya, K.; Fujisawa, J.-i.; Hanaya, M. *Chem. Commun.*

- 2015**, *51*, 15894–15897.
- [54] Mathew, S.; Yella, A.; Gao, P.; Humphry-Baker, R.; Curchod, B. F. E.; Ashari-Astani, N.; Tavernelli, I.; Rothlisberger, U.; Nazeeruddin, K.; Grätzel, M. *Nat. Chem.* **2014**, *6*, 242–247.
- [55] Bella, F.; Galliano, S.; Gerbaldi, C.; Viscardi, G. *Energies* **2016**, *9*, 384–406.
- [56] Saygili, Y.; Söderberg, M.; Pellet, N.; Giordano, F.; Cao, Y.; Muñoz-García, A. B.; Zakeeruddin, S. M.; Vlachopoulos, N.; Pavone, M.; Boschloo, G.; Kavan, L.; Moser, J.-E.; Grätzel, M.; Hagfeldt, A.; Freitag, M. *J. Am. Chem. Soc.* **2016**, *138*, 15087–15096.
- [57] Saygili, Y.; Stojanovic, M.; Michaels, H.; Tiepelt, J.; Teuscher, J.; Massaro, A.; Pavone, M.; Giordano, F.; Zakeeruddin, S. M.; Boschloo, G.; Moser, J.-E.; Grätzel, M.; Muñoz-García, A. B.; Hagfeldt, A.; Freitag, M. *ACS Appl. Energy Mater.* **2018**, *1*, 4950–4962.
- [58] Cao, Y.; Liu, Y.; Zakeeruddin, S. M.; Hagfeldt, A.; Grätzel, M. *Joule* **2018**, *2*, 1108–1117.
- [59] Cao, Y.; Saygili, Y.; Ummadisingu, A.; Teuscher, J.; Luo, J.; Pellet, N.; Giordano, F.; Zakeeruddin, S. M.; Moser, J. E.; Freitag, M.; Hagfeldt, A.; Grätzel, M. *Nat. Commun.* **2017**, *8*, 15390–15397.
- [60] Freitag, M.; Daniel, Q.; Pazoki, M.; Sveinbjörnsson, K.; Zhang, J.; Sun, L.; Hagfeldt, A.; Boschloo, G. *Energy Environ. Sci.* **2015**, *8*, 2634–2637.
- [61] Hu, M.; Shen, J.; Yu, Z.; Liao, R.-Z.; Gurzadyan, G. G.; Yang, X.; Hagfeldt, A.; Wang, M.; Sun, L. *ACS Appl. Mater. Interfaces* **2018**, *10*, 30409–30416.
- [62] Su'ait, M. S.; Rahman, M. Y. A.; Ahmad, A. *Solar Energy* **2015**, *115*, 452–470.
- [63] Chu, T.-C.; Lin, R. Y.-Y.; Lee, C.-P.; Hsu, C.-Y.; Shih, P.-C.; Lin, R.; Li, S.-R.; Sun, S.-S.; Lin, J. T.; Vittal, R.; Ho, K.-C. *ChemSusChem* **2014**, *7*, 146–153.
- [64] Gao, M.; Wang, Y.; Yi, Q.; Su, Y.; Sun, P.; Wang, X.; Zhao, J.; Zou, G. *J. Mater. Chem. A* **2015**, *3*, 20541–20546.
- [65] Li, L.; Yang, X.; Zhao, J.; Gao, J.; Hagfeldt, A.; Sun, L. *J. Mater. Chem.* **2011**, *21*, 5573–5575.
- [66] Tian, H.; Gabrielsson, E.; Lohse, P. W.; Vlachopoulos, N.; Kloo, L.; Hagfeldt, A.; Sun, L. *Energy Environ. Sci.* **2012**, *5*, 9752–9755.
- [67] Ellis, H.; Vlachopoulos, N.; Häggman, L.; Perruchot, C.; Jouini, M.; Boschloo, G.; Hagfeldt, A. *Electrochim. Acta* **2013**, *107*, 45–51.
- [68] Yun, S.; Vlachopoulos, N.; Qurashi, A.; Ahmad, S.; Hagfeldt, A. *Chem. Soc. Rev.* **2019**, Ahead of print.
- [69] Baranwal, A. K.; Shiki, T.; Ogomi, Y.; Pandey, S. S.; Ma, T.; Hayase, S. *RSC Adv.* **2014**, *4*, 47735–47742.
- [70] Ye, M.; Gao, X.; Hong, X.; Liu, Q.; He, C.; Liu, X.; Lin, C. *Sustain. Energy Fuels* **2017**, *1*, 1217–1231.
- [71] Ansari, M. I. H.; Qurashi, A.; Nazeeruddin, M. K. *J. Photochem. Photobiol. C: Photochem. Rev.* **2018**, *35*, 1–24.
- [72] Zhang, B.; Sun, L. *Chem. Soc. Rev.* **2019**, *48*, 2216–2264.
- [73] Qin, P.; Zhu, H.; Edvinsson, T.; Boschloo, G.; Hagfeldt, A.; Sun, L. *J. Am. Chem. Soc.* **2008**, *130*, 8570–8571.
- [74] He, J.; Lindström, H.; Hagfeldt, A.; Lindquist, S.-E. *Sol. Energy Mater. Sol. Cells* **2000**, *62*, 265–273.

- [75] Odobel, F.; Le Pleux, L.; Pellegrin, Y.; Blart, E. *Acc. Chem. Res.* **2010**, *43*, 1063–1071.
- [76] Benesperi, I.; Michaels, H.; Freitag, M. *J. Mater. Chem. C* **2018**, *6*, 11903–11942.
- [77] Ding, I.-K.; Tétreault, N.; Brillet, J.; Hardin, B. E.; Smith, E. H.; Rosenthal, S. J.; Sauvage, F.; Grätzel, M.; McGehee, M. D. *Adv. Funct. Mater.* **2009**, *19*, 2431–2436.
- [78] Kroeze, J.; Hirata, N.; Schmidt-Mende, L.; Orizu, C.; Ogier, S.; Carr, K.; Grätzel, M.; Durrant, J. *Adv. Funct. Mater.* **2006**, *16*, 1832–1838.
- [79] Editorial, *Nature Energy* **2019**, *4*, 1–1.
- [80] Ke, W.; Kanatzidis, M. G. *Nat. Commun.* **2019**, *10*, 965.
- [81] Pekkola, O.; Lungenschmied, C.; Fejes, P.; Handreck, A.; Hermes, W.; Irle, S.; Lennartz, C.; Schildknecht, C.; Schillen, P.; Schindler, P.; Send, R.; Valouch, S.; Thiel, E.; Bruder, I. *Sci. Rep.* **2018**, *8*, 9208–9216.
- [82] Armaroli, N.; Balzani, V. *Chem. Eur. J.* **2016**, *22*, 32–57.
- [83] Shrotriya, V.; Li, G.; Yao, Y.; Moriarty, T.; Emery, K.; Yang, Y. *Adv. Funct. Mater.* **2006**, *16*, 2016–2023.
- [84] Snaith, H. J. *Nat. Photonics* **2012**, *6*, 337–340.
- [85] Pazoki, M.; Cappel, U. B.; Johansson, E. M. J.; Hagfeldt, A.; Boschloo, G. *Energy Environ. Sci.* **2017**, *10*, 672–709.
- [86] Christians, J. A.; Manser, J. S.; Kamat, P. V. *J. Phys. Chem. Lett.* **2015**, *6*, 852–857.
- [87] Nakade, S.; Kanzaki, T.; Kubo, W.; Kitamura, T.; Wada, Y.; Yanagida, S. *J. Phys. Chem. B* **2005**, *109*, 3480–3487.
- [88] Edvinsson, T.; Li, C.; Pschirer, N.; Schöneboom, J.; Eickemeyer, F.; Sens, R.; Boschloo, G.; Herrmann, A.; Müllen, K.; Hagfeldt, A. *J. Phys. Chem. C* **2007**, *111*, 15137–15140.
- [89] Elgrishi, N.; Rountree, K. J.; McCarthy, B. D.; Rountree, E. S.; Eisenhart, T. T.; Dempsey, J. L. *J. Chem. Educ.* **2018**, *95*, 197–206.
- [90] Hao, Y.; Saygili, Y.; Cong, J.; Eriksson, A.; Yang, W.; Zhang, J.; Polanski, E.; Nonomura, K.; Zakeeruddin, S. M.; Graetzel, M.; Hagfeldt, A.; Boschloo, G. *ACS Appl. Mater. Interfaces* **2016**, *8*, 32797–32804.
- [91] Buene, A. F.; Hagfeldt, A.; Hoff, B. H. *Dyes Pigm.* **2019**, *169*, 66–72.
- [92] Buene, A. F.; Boholm, N.; Hagfeldt, A.; Hoff, B. H. *New J. Chem.* **2019**, *43*, 9403–9410.
- [93] Ferdowsi, P.; Saygili, Y.; Zhang, W.; Edvinsson, T.; Kavan, L.; Mokhtari, J.; Zakeeruddin, S. M.; Grätzel, M.; Hagfeldt, A. *ChemSusChem* **2018**, *11*, 494–502.
- [94] Scholz, F. *ChemTexts* **2015**, *1*, 17–40.
- [95] Kavan, L. *Curr. Opin. Electrochem.* **2017**, *2*, 88–96.
- [96] Ha, S.; Ramanathan, M.; Ramani, V.; Prakash, J. *ECS Trans.* **2011**, *33*, 159–168.
- [97] Seeman, J. *Angew. Chem. Int. Ed.* **2007**, *46*, 1378–1413.
- [98] Woodward, R. B.; Doering, W. E. *J. Am. Chem. Soc.* **1944**, *66*, 849–849.
- [99] Carella, A.; Borbone, F.; Centore, R. *Front. Chem.* **2018**, *6*:481.
- [100] Narayan, M. R. *Renew. Sust. Energ. Rev.* **2012**, *16*, 208–215.
- [101] Ludin, N. A.; Al-Alwani Mahmoud, A. M.; Mohamad, A. B.; Kadhum, A. A. H.; Sopian, K.; Abdul Karim, N. S. *Renew. Sust. Energ. Rev.* **2014**, *31*, 386–396.
- [102] Calogero, G.; Di Marco, G.; Cazzanti, S.; Caramori, S.; Argazzi, R.; Di Carlo, A.; Bignozzi, C. A. *Int. J. Mol. Sci.* **2010**, *11*, 254–267.
- [103] Ghann, W.; Kang, H.; Sheikh, T.; Yadav, S.; Chavez-Gil, T.; Nesbitt, F.; Uddin, J. *Sci.*

- Rep.* **2017**, *7*, 41470–41481.
- [104] Mishra, A.; Fischer, M. K.; Bäuerle, P. *Angew. Chem. Int. Ed.* **2009**, *48*, 2474–2499.
- [105] Lee, C.-P.; Lin, R. Y.-Y.; Lin, L.-Y.; Li, C.-T.; Chu, T.-C.; Sun, S.-S.; Lin, J. T.; Ho, K.-C. *RSC Adv.* **2015**, *5*, 23810–23825.
- [106] Błaszczyk, A. *Dyes Pigm.* **2018**, *149*, 707–718.
- [107] Bureš, F. *RSC Adv.* **2014**, *4*, 58826–58851.
- [108] Buene, A. F.; Uggerud, N.; Economopoulos, S. P.; Gautun, O. R.; Hoff, B. H. *Dyes Pigm.* **2018**, *151*, 263–271.
- [109] Gabrielsson, E.; Ellis, H.; Feldt, S.; Tian, H.; Boschloo, G.; Hagfeldt, A.; Sun, L. *Adv. Energy Mater.* **2013**, *3*, 1647–1656.
- [110] Yella, A.; Lee, H.-W.; Tsao, H. N.; Yi, C.; Chandiran, A. K.; Nazeeruddin, M.; Diau, E. W.-G.; Yeh, C.-Y.; Zakeeruddin, S. M.; Grätzel, M. *Science* **2011**, *334*, 629–634.
- [111] Nazeeruddin, M. K.; Kay, A.; Rodicio, I.; Humphry-Baker, R.; Mueller, E.; Liska, P.; Vlachopoulos, N.; Graetzel, M. *J. Am. Chem. Soc.* **1993**, *115*, 6382–6390.
- [112] Mahmood, A. *Solar Energy* **2016**, *123*, 127–144.
- [113] Venkateswararao, A.; Thomas, K. R. J.; Lee, C.-P.; Li, C.-T.; Ho, K.-C. *ACS Appl. Mater. Interfaces* **2014**, *6*, 2528–2539.
- [114] Seo, K. D.; Song, H. M.; Lee, M. J.; Pastore, M.; Anselmi, C.; De Angelis, F.; Nazeeruddin, M. K.; Grätzel, M.; Kim, H. K. *Dyes Pigm.* **2011**, *90*, 304–310.
- [115] Hu, Y.; Ivaturi, A.; Planells, M.; Boldrini, C. L.; Biroli, A. O.; Robertson, N. *J. Mater. Chem. C* **2016**, *4*, 2509–2516.
- [116] Feng, J.; Jiao, Y.; Ma, W.; Nazeeruddin, M. K.; Grätzel, M.; Meng, S. *J. Phys. Chem. C* **2013**, *117*, 3772–3778.
- [117] Zhang, Y.; Cheema, H.; McNamara, L.; Hunt, L. A.; Hammer, N. I.; Delcamp, J. H. *Chem. Eur. J.* **2018**, *24*, 5939–5949.
- [118] Qin, C.; Wong, W.-Y.; Han, L. *Chem. Asian J.* **2013**, *8*, 1706–1719.
- [119] Huang, Z.-S.; Meier, H.; Cao, D. *J. Mater. Chem. C* **2016**, *4*, 2404–2426.
- [120] Luo, J.-S.; Wan, Z.-Q.; Jia, C.-Y. *Chin. Chem. Lett.* **2016**, *27*, 1304–1318.
- [121] Bernthsen, A. *Ber. Dtsch. Chem. Ges.* **1883**, *16*, 2896–2904.
- [122] Taurand, G. *Ullmann's Encyclopedia of Industrial Chemistry*; 2000.
- [123] McDowell, J. *Acta Cryst.* **1976**, *32*, 5–10.
- [124] Aouine, Y.; Alami, A.; El Hallaoui, A.; Elachqar, A.; Zouihri, H. *Acta Cryst.* **2010**, *66*, 2830–2835.
- [125] Pan, D.; Phillips, D. L. *J. Phys. Chem. A* **1999**, *103*, 4737–4743.
- [126] Ding, X.; Chen, C.; Sun, L.; Li, H.; Chen, H.; Su, J.; Li, H.; Li, H.; Xu, L.; Cheng, M. *J. Mater. Chem. A* **2019**, *7*, 9510–9516.
- [127] Zhang, F.; Wang, S.; Zhu, H.; Liu, X.; Liu, H.; Li, X.; Xiao, Y.; Zakeeruddin, S. M.; Grätzel, M. *ACS Energy Lett.* **2018**, *3*, 1145–1152.
- [128] Unny, D.; Sivanadanam, J.; Mandal, S.; Aidhen, I. S.; Ramanujam, K. *J. Electrochem. Soc.* **2018**, *165*, H845–H860.
- [129] Cazzanti, S.; Caramori, S.; Argazzi, R.; Elliott, C. M.; Bignozzi, C. A. *J. Am. Chem. Soc.* **2006**, *128*, 9996–9997.
- [130] Argazzi, R.; Bignozzi, C. A.; Heimer, T. A.; Castellano, F. N.; Meyer, G. J. *J. Phys. Chem. B* **1997**, *101*, 2591–2597.

- [131] Tian, H.; Yang, X.; Chen, R.; Pan, Y.; Li, L.; Hagfeldt, A.; Sun, L. *Chem. Commun.* **2007**, 3741–3743.
- [132] Baheti, A.; Justin Thomas, K. R.; Li, C.-T.; Lee, C.-P.; Ho, K.-C. *ACS Appl. Mater. Interfaces* **2015**, *7*, 2249–2262.
- [133] Yao, L.; Sun, S.; Xue, S.; Zhang, S.; Wu, X.; Zhang, H.; Pan, Y.; Gu, C.; Li, F.; Ma, Y. *J. Phys. Chem. C* **2013**, *117*, 14189–14196.
- [134] Mao, X.; Jiang, X.; Hu, H.; Cheng, Y.; Zhu, C. *Synlett* **2013**, *24*, 1505–1508.
- [135] Harville, R.; Reed, S. F. *J. Org. Chem.* **1968**, *33*, 3976–3977.
- [136] Ci, Z.; Lin, C.; Fu, W.; Wang, Z.; Zhang, S.; Sun, C., Patent CN105693749A. 2016.
- [137] Fuse, S.; Sugiyama, S.; Maitani, M. M.; Wada, Y.; Ogomi, Y.; Hayase, S.; Katoh, R.; Kaiho, T.; Takahashi, T. *Chem. Eur. J.* **2014**, *20*, 10685–10694.
- [138] Sirohi, R.; Kim, D. H.; Yu, S.-C.; Lee, S. H. *Dyes Pigm.* **2012**, *92*, 1132–1137.
- [139] Wu, W.; Yang, J.; Hua, J.; Tang, J.; Zhang, L.; Long, Y.; Tian, H. *J. Mater. Chem.* **2010**, *20*, 1772–1779.
- [140] Yang, X.; Zhao, J.; Wang, L.; Tian, J.; Sun, L. *RSC Adv.* **2014**, *4*, 24377–24383.
- [141] Iqbal, Z.; Wu, W.-Q.; Kuang, D.-B.; Wang, L.; Meier, H.; Cao, D. *Dyes Pigm.* **2013**, *96*, 722–731.
- [142] Iqbal, Z.; Wu, W.-Q.; Huang, Z.-S.; Wang, L.; Kuang, D.-B.; Meier, H.; Cao, D. *Dyes Pigm.* **2016**, *124*, 63–71.
- [143] Yang, X.; Tian, H.; Chen, R. Patent CN101294004. 2008.
- [144] He, J.; Pei, H.; Li, H.; Zhang, S.; Zhang, S.; Tan, H.; Hu, Z. *Synth. Metals* **2019**, *247*, 228–232.
- [145] Cullinane, N. M.; Rees, W. T. *J. Chem. Soc. Faraday Trans.* **1940**, *35*, 507–514.
- [146] Villares, P.; Jiménez-Garay, R.; Conde, A.; Márquez, R. *Acta Cryst.* **1976**, *32*, 2293–2296.
- [147] Junk, T.; Irgolic, K. J.; Reibenspies, J. H.; Meyers, E. A. *Acta Cryst.* **1993**, *49*, 938–940.
- [148] Smith, N. L. *J. Org. Chem.* **1950**, *15*, 1125–1130.
- [149] Nodiff, E. A.; Hausman, M. *J. Org. Chem.* **1964**, *29*, 2453–2455.
- [150] Benati, L.; Montevecchi, P. C.; Spagnolo, P. *J.C.S. Chem. Comm.* **1980**, 715–717.
- [151] Ma, D.; Geng, Q.; Zhang, H.; Jiang, Y. *Angew. Chem.* **2010**, *122*, 1313–1316.
- [152] Dai, C.; Sun, X.; Tu, X.; Wu, L.; Zhan, D.; Zeng, Q. *Chem. Commun.* **2012**, *48*, 5367–5369.
- [153] Beresneva, T.; Abele, E. *Chem. Heterocycl. Compd.* **2012**, *48*, 1420–1422.
- [154] Liao, Y.; Jiang, P.; Chen, S.; Xiao, F.; Deng, G.-J. *RSC Adv.* **2013**, *3*, 18605–18608.
- [155] Marszalek, M.; Nagane, S.; Ichake, A.; Humphry-Baker, R.; Paul, V.; Zakeeruddin, S. M.; Grätzel, M. *J. Mater. Chem.* **2012**, *22*, 889–894.
- [156] Yang, Y. S.; Kim, H. D.; Ryu, J.-H.; Kim, K. K.; Park, S. S.; Ahn, K.-S.; Kim, J. H. *Synth. Met.* **2011**, *161*, 850–855.
- [157] Hart, A. S.; K. C. C. B.; Subbaiyan, N. K.; Karr, P. A.; D'Souza, F. *ACS Appl. Mater. Interfaces* **2012**, *4*, 5813–5820.
- [158] Kim, M.-J.; Yu, Y.-J.; Kim, J.-H.; Jung, Y.-S.; Kay, K.-Y.; Ko, S.-B.; Lee, C.-R.; Jang, I.-H.; Kwon, Y.-U.; Park, N.-G. *Dyes Pigm.* **2012**, *95*, 134–141.
- [159] Gao, H.-H.; Qian, X.; Chang, W.-Y.; Wang, S.-S.; Zhu, Y.-Z.; Zheng, J.-Y. *J. Power Sources* **2016**, *307*, 866–874.

- [160] Hua, Y.; Chang, S.; Huang, D. D.; Zhou, X.; Zhu, X. J.; Zhao, J. Z.; Chen, T.; Wong, W. Y.; Wong, W. K. *Chem. Mater.* **2013**, *25*, 2146–2153.
- [161] Manfredi, N.; Monai, M.; Montini, T.; Peri, F.; De Angelis, F.; Fornasiero, P.; Abboto, A. *ACS Energy Lett.* **2018**, *3*, 85–91.
- [162] Tian, H.; Yang, X.; Cong, J.; Chen, R.; Teng, C.; Liu, J.; Hao, Y.; Wang, L.; Sun, L. *Dyes Pigm.* **2010**, *84*, 62–68.
- [163] Mao, M.; Zhang, X.-L.; Fang, X.-Q.; Wu, G.-H.; Ding, Y.; Liu, X.-L.; Dai, S.-Y.; Song, Q.-H. *Organic Electronics* **2014**, *15*, 2079–2090.
- [164] Sun, X.; Wang, Y.; Li, X.; Agren, H.; Zhu, W.; Tian, H.; Xie, Y. *Chem. Commun.* **2014**, *50*, 15609–15612.
- [165] Bae, S. H.; Seo, K. D.; Choi, W. S.; Hong, J. Y.; Kim, H. K. *Dyes Pigm.* **2015**, *113*, 18–26.
- [166] Krishna, N. V.; Krishna, J. V. S.; Singh, S. P.; Giribabu, L.; Han, L.; Bedja, I.; Gupta, R. K.; Islam, A. *J. Phys. Chem. C* **2017**, *121*, 6464–6477.
- [167] Kim, S. H.; Kim, H. W.; Sakong, C.; Namgoong, J.; Park, S. W.; Ko, M. J.; Lee, C. H.; Lee, W. I.; Kim, J. P. *Org. Lett.* **2011**, *13*, 5784–5787.
- [168] Xie, Z.; Midya, A.; Loh, K. P.; Adams, S.; Blackwood, D. J.; Wang, J.; Zhang, X.; Chen, Z. *Prog. Photovolt. Res. Appl.* **2010**, *18*, 573–581.
- [169] Cao, D.; Peng, J.; Hong, Y.; Fang, X.; Wang, L.; Meier, H. *Org. Lett.* **2011**, *13*, 1610–1613.
- [170] Tsao, M.-H.; Wu, T.-Y.; Wang, H.-P.; Sun, I. W.; Su, S.-G.; Lin, Y.-C.; Chang, C.-W. *Materials Lett.* **2011**, *65*, 583–586.
- [171] Chen, C.; Liao, J.-Y.; Chi, Z.; Xu, B.; Zhang, X.; Kuang, D.-B.; Zhang, Y.; Liu, S.; Xu, J. *J. Mater. Chem.* **2012**, *22*, 8994–9005.
- [172] Chang, Y. J.; Chou, P.-T.; Lin, Y.-Z.; Watanabe, M.; Yang, C.-J.; Chin, T.-M.; Chow, T. J. *J. Mater. Chem.* **2012**, *22*, 21704–21712.
- [173] Yang, C.-J.; Chang, Y. J.; Watanabe, M.; Hon, Y.-S.; Chow, T. J. *J. Mater. Chem.* **2012**, *22*, 4040–4049.
- [174] Huang, Z.-S.; Feng, H.-L.; Zang, X.-F.; Iqbal, Z.; Zeng, H.; Kuang, D.-B.; Wang, L.; Meier, H.; Cao, D. *J. Mater. Chem. A* **2014**, *2*, 15365–15376.
- [175] Hung, W.-I.; Liao, Y.-Y.; Hsu, C.-Y.; Chou, H.-H.; Lee, T.-H.; Kao, W.-S.; Lin, J. T. *Chem. Asian J.* **2014**, *9*, 357–366.
- [176] Yang, X.; Zhao, J.; Wang, L.; Tian, J.; Sun, L. *RSC Adv.* **2014**, *4*, 24377–24383.
- [177] Zang, X.-F.; Huang, Z.-S.; Wu, H.-L.; Iqbal, Z.; Wang, L.; Meier, H.; Cao, D. *J. Power Sources* **2014**, *271*, 455–464.
- [178] Dai, X.-X.; Feng, H.-L.; Huang, Z.-S.; Wang, M.-J.; Wang, L.; Kuang, D.-B.; Meier, H.; Cao, D. *Dyes Pigm.* **2015**, *114*, 47–54.
- [179] Lin, R. Y.-Y.; Chuang, T.-M.; Wu, F.-L.; Chen, P.-Y.; Chu, T.-C.; Ni, J.-S.; Fan, M.-S.; Lo, Y.-H.; Ho, K.-C.; Lin, J. T. *ChemSusChem* **2015**, *8*, 105–113.
- [180] Hung, W.-I.; Liao, Y.-Y.; Lee, T.-H.; Ting, Y.-C.; Ni, J.-S.; Kao, W.-S.; Lin, J. T.; Wei, T.-C.; Yen, Y.-S. *Chem. Commun.* **2015**, *51*, 2152–2155.
- [181] Chen, S.-G.; Jia, H.-L.; Ju, X.-H.; Zheng, H.-G. *Dyes Pigm.* **2017**, *146*, 127–135.
- [182] Li, F.; Zhu, Y.-Z.; Zhang, S.-C.; Gao, H.-H.; Pan, B.; Zheng, J.-Y. *Dyes Pigm.* **2017**, *139*, 292–299.
- [183] Li, C.-T.; Wu, F.-L.; Liang, C.-J.; Ho, K.-C.; Lin, J. T. *J. Mater. Chem. A* **2017**, *5*, 7586–7594.



- [184] Velusamy, M.; Justin Thomas, K. R.; Lin, J. T.; Hsu, Y.-C.; Ho, K.-C. *Org. Lett.* **2005**, *7*, 1899–1902.
- [185] Hagberg, D. P.; Yum, J.-H.; Lee, H.; De Angelis, F.; Marinado, T.; Karlsson, K. M.; Humphry-Baker, R.; Sun, L.; Hagfeldt, A.; Grätzel, M.; Nazeeruddin, M. K. *J. Am. Chem. Soc.* **2008**, *130*, 6259–6266.
- [186] Jiang, X.; Marinado, T.; Gabrielsson, E.; Hagberg, D. P.; Sun, L.; Hagfeldt, A. *J. Phys. Chem. B* **2010**, *114*, 2799–2805.
- [187] Feldt, S. M.; Gibson, E. A.; Gabrielsson, E.; Sun, L.; Boschloo, G.; Hagfeldt, A. *J. Am. Chem. Soc.* **2010**, *132*, 16714–16724.
- [188] Hagberg, D. P.; Jiang, X.; Gabrielsson, E.; Linder, M.; Marinado, T.; Brinck, T.; Hagfeldt, A.; Sun, L. *J. Mater. Chem.* **2009**, *19*, 7232–7238.
- [189] Freitag, M.; Teuscher, J.; Saygili, Y.; Zhang, X.; Giordano, F.; Liska, P.; Hua, J.; Zakeeruddin, S. M.; Moser, J.-E.; Grätzel, M.; Hagfeldt, A. *Nat. Photonics* **2017**, *11*, 372–378.
- [190] Hagberg, D. P.; Edvinsson, T.; Marinado, T.; Boschloo, G.; Hagfeldt, A.; Sun, L. *Chem. Commun.* **2006**, 2245–2247.
- [191] Kim, S.; Lee, J. K.; Kang, S. O.; Ko, J.; Yum, J. H.; Fantacci, S.; De Angelis, F.; Di Censo, D.; Nazeeruddin, M. K.; Grätzel, M. *J. Am. Chem. Soc.* **2006**, *128*, 16701–16707.
- [192] Yella, A.; Humphry-Baker, R.; Curchod, B. F. E.; Ashari Astani, N.; Teuscher, J.; Polander, L. E.; Mathew, S.; Moser, J.-E.; Tavernelli, I.; Rothlisberger, U.; Grätzel, M.; Nazeeruddin, M. K.; Frey, J. *Chem. Mater.* **2013**, *25*, 2733–2739.
- [193] An, H.-C.; Jung, H.-J.; Bae, H.-G.; Park, C.-S.; Lee, C.-Y.; Grätzel, M.; Nazeeruddin, M. K.; Yi, C.; Delcamp, J. H. Patent WO2012102544A2. 2012.
- [194] Zhang, X.; Xu, Y.; Giordano, F.; Schreier, M.; Pellet, N.; Hu, Y.; Yi, C.; Robertson, N.; Hua, J.; Zakeeruddin, S. M.; Tian, H.; Grätzel, M. *J. Am. Chem. Soc.* **2016**, *138*, 10742–10745.
- [195] Phan, N.; Van Der Sluys, M.; Jones, C. *Adv. Synth. Catal.* **2006**, *348*, 609–679.
- [196] Hassan, J.; Sévignon, M.; Gozzi, C.; Schulz, E.; Lemaire, M. *Chem. Rev.* **2002**, *102*, 1359–1470.
- [197] Barder, T. E.; Walker, S. D.; Martinelli, J. R.; Buchwald, S. L. *J. Am. Chem. Soc.* **2005**, *127*, 4685–4696.
- [198] Miyaoura, N.; Yamada, K.; Suzuki, A. *Tetrahedron Lett.* **1979**, 3437–3440.
- [199] Suzuki, A. *Angew. Chem. Int. Ed.* **2011**, *50*, 6722–6737.
- [200] Miyaoura, N.; Suzuki, A. *J. Chem. Soc. Chem. Comm.* **1979**, 866–867.
- [201] Miyaoura, N.; Yanagi, T.; Suzuki, A. *Synth. Commun.* **1981**, *11*, 513–519.
- [202] Lennox, A. J. J.; Lloyd-Jones, G. C. *Chem. Soc. Rev.* **2014**, *43*, 412–443.
- [203] Zhang, N.; Hoffman, D. J.; Gutsche, N.; Gupta, J.; Percec, V. *J. Org. Chem.* **2012**, *77*, 5956–5964.
- [204] Martin, R.; Buchwald, S. L. *Acc. Chem. Res.* **2008**, *41*, 1461–1473.
- [205] Walker, S. D.; Barder, T. E.; Martinelli, J. R.; Buchwald, S. L. *Angew. Chem. Int. Ed.* **2004**, *43*, 1871–1876.
- [206] Polshettiwar, V.; Decottignies, A.; Len, C.; Fihri, A. *ChemSusChem* **2010**, *3*, 502–522.
- [207] Lennox, A. J. J.; Lloyd-Jones, G. C. *Angew. Chem. Int. Ed.* **2013**, *52*, 7362–7370.

- [208] Amatore, C.; Jutand, A.; Le Duc, G. *Chem. Eur. J.* **2011**, *17*, 2492–2503.
- [209] Amatore, C.; Carre, E.; Jutand, A.; M'Barki, M. A. *Organometallics* **1995**, *14*, 1818–1826.
- [210] Roy, A. H.; Hartwig, J. F. *Organometallics* **2004**, *23*, 1533–1541.
- [211] Roy, A. H.; Hartwig, J. F. *J. Am. Chem. Soc.* **2001**, *123*, 1232–1233.
- [212] Liang, L.-C.; Chien, P.-S.; Huang, M.-H. *Organometallics* **2005**, *24*, 353–357.
- [213] Weissman, H.; Milstein, D. *Chem. Commun.* **1999**, 1901–1902.
- [214] Carrow, B. P.; Hartwig, J. F. *J. Am. Chem. Soc.* **2011**, *133*, 2116–2119.
- [215] Thomas, A. A.; Denmark, S. E. *Science* **2016**, *352*, 329–332.
- [216] Miyaura, N.; Suzuki, A. *Chem. Rev.* **1995**, *95*, 2457–2483.
- [217] Lima, C. F. R. A. C.; Rodriguez-Borges, J. E.; Santos, L. M. N. B. F. *Tetrahedron* **2011**, *67*, 689–697.
- [218] Thomas, A. A.; Wang, H.; Zahrt, A. F.; Denmark, S. E. *J. Am. Chem. Soc.* **2017**, *139*, 3805–3821.
- [219] Zuidema, E.; van Leeuwen, P. W. N. M.; Bo, C. *Organometallics* **2005**, *24*, 3703–3710.
- [220] Hartwig, J. F. *Inorg. Chem.* **2007**, *46*, 1936–1947.
- [221] Rao, X.; Liu, C.; Zhang, Y.; Gao, Z.; Jin, Z. *Chin. J. Catal.* **2014**, *35*, 357–361.
- [222] Kitamura, Y.; Sakurai, A.; Udzu, T.; Maegawa, T.; Monguchi, Y.; Sajiki, H. *Tetrahedron* **2007**, *63*, 10596–10602.
- [223] Huang, Y.; Wei, Q.; Wang, Y.; Dai, L. *Carbon* **2018**, *136*, 150–159.
- [224] Billingsley, K. L.; Anderson, K. W.; Buchwald, S. L. *Angew. Chem. Int. Ed.* **2006**, *45*, 3484–3488.
- [225] Billingsley, K.; Buchwald, S. L. *J. Am. Chem. Soc.* **2007**, *129*, 3358–3366.
- [226] Kinzel, T.; Zhang, Y.; Buchwald, S. L. *J. Am. Chem. Soc.* **2010**, *132*, 14073–14075.
- [227] Molander, G. A.; Trice, S. L. J.; Kennedy, S. M. *J. Org. Chem.* **2012**, *77*, 8678–8688.
- [228] Molander, G. A.; Biolatto, B. *J. Org. Chem.* **2003**, *68*, 4302–4314.
- [229] Littke, A. F.; Dai, C.; Fu, G. C. *J. Am. Chem. Soc.* **2000**, *122*, 4020–4028.
- [230] Sicre, C.; Alonso-Gómez, J. L.; Cid, M. M. *Tetrahedron* **2006**, *62*, 11063–11072.
- [231] Kinzel, T.; Zhang, Y.; Buchwald, S. L. *J. Am. Chem. Soc.* **2010**, *132*, 14073–14075.
- [232] Dufert, M. A.; Billingsley, K. L.; Buchwald, S. L. *J. Am. Chem. Soc.* **2013**, *135*, 12877–12885.
- [233] Ragan, J. A.; Raggon, J. W.; Hill, P. D.; Jones, B. P.; McDermott, R. E.; Munchhof, M. J.; Marx, M. A.; Casavant, J. M.; Cooper, B. A.; Doty, J. L.; Lu, Y. *Org. Process Res. Dev.* **2003**, *7*, 676–683.
- [234] Holliday, S. et al. *Nat. Commun.* **2016**, *7*, 11585–11595.
- [235] Indolese, A. F. *Tetrahedron Lett.* **1997**, *38*, 3513–3516.
- [236] Han, F.-S. *Chem. Soc. Rev.* **2013**, *42*, 5270–5298.
- [237] Leonori, D.; Aggarwal, V. K. *Acc. Chem. Res.* **2014**, *47*, 3174–3183.
- [238] Brown, H. C.; Cole, T. E. *Organometallics* **1983**, *2*, 1316–1319.
- [239] Ishiyama, T.; Murata, M.; Miyaura, N. *J. Org. Chem.* **1995**, *60*, 7508–7510.
- [240] Billingsley, K. L.; Buchwald, S. L. *J. Org. Chem.* **2008**, *73*, 5589–5591.
- [241] Murata, M.; Oyama, T.; Watanabe, S.; Masuda, Y. *J. Org. Chem.* **2000**, *65*, 164–168.
- [242] Molander, G. A.; Trice, S. L. J.; Dreher, S. D. *J. Am. Chem. Soc.* **2010**, *132*, 17701–17703.
- [243] Molander, G. A.; Trice, S. L. J.; Kennedy, S. M.; Dreher, S. D.; Tudge, M. T. *J. Am. Chem.*

- Soc.* **2012**, *134*, 11667–11673.
- [244] Chen, H.; Hartwig, J. F. *Angew. Chem. Int. Ed.* **1999**, *38*, 3391–3393.
- [245] Ishiyama, T.; Takagi, J.; Ishida, K.; Miyaura, N.; Anastasi, N. R.; Hartwig, J. F. *J. Am. Chem. Soc.* **2002**, *124*, 390–391.
- [246] Ruiz-Castillo, P.; Buchwald, S. L. *Chem. Rev.* **2016**, *116*, 12564–12649.
- [247] Hartwig, J. F. *Nature* **2008**, *455*, 314–322.
- [248] Masanori, K.; Masayuki, K.; Toshihiko, M. *Chem. Lett.* **1983**, *12*, 927–928.
- [249] Louie, J.; Hartwig, J. F. *Tetrahedron Lett.* **1995**, *36*, 3609–3612.
- [250] Guram, A. S.; Rennels, R. A.; Buchwald, S. L. *Angew. Chem. Int. Ed.* **1995**, *34*, 1348–1350.
- [251] Yin, J.; Buchwald, S. L. *Org. Lett.* **2000**, *2*, 1101–1104.
- [252] Yin, J.; Buchwald, S. L. *J. Am. Chem. Soc.* **2002**, *124*, 6043–6048.
- [253] Anderson, K. W.; Tundel, R. E.; Ikawa, T.; Altman, R. A.; Buchwald, S. L. *Angew. Chem. Int. Ed.* **2006**, *45*, 6523–6527.
- [254] Xiang, S.; Huang, Z.; Sun, S.; Lv, X.; Fan, L.; Ye, S.; Chen, H.; Guo, R.; Wang, L. *J. Mater. Chem. C* **2018**, *6*, 11436–11443.
- [255] Yen, H.-J.; Liou, G.-S. *J. Mater. Chem.* **2010**, *20*, 9886–9894.
- [256] Louillat-Habermeyer, M.-L.; Jin, R.; Patureau, F. W. *Angew. Chem. Int. Ed.* **2015**, *54*, 4102–4104.
- [257] Muenmart, D.; Prachumrak, N.; Tarsang, R.; Namungruk, S.; Jungsuttiwong, S.; Sudyoasuk, T.; Pattanasattayavong, P.; Promarak, V. *RSC Adv.* **2016**, *6*, 38481–38493.
- [258] Grisorio, R.; Roose, B.; Colella, S.; Listorti, A.; Suranna, G. P.; Abate, A. *ACS Energy Lett.* **2017**, *2*, 1029–1034.
- [259] Ma, D.; Cai, Q.; Zhang, H. *Org. Lett.* **2003**, *5*, 2453–2455.
- [260] Huang, J.-H.; Lee, K.-C. *ACS Appl. Mater. Interfaces* **2014**, *6*, 7680–7685.
- [261] Jin, R.; Patureau, F. W. *Org. Lett.* **2016**, *18*, 4491–4493.
- [262] Driver, M. S.; Hartwig, J. F. *J. Am. Chem. Soc.* **1996**, *118*, 7217–7218.
- [263] Louie, J.; Driver, M. S.; Hamann, B. C.; Hartwig, J. F. *J. Org. Chem.* **1997**, *62*, 1268–1273.
- [264] Surry, D. S.; Buchwald, S. L. *Chem. Sci.* **2011**, *2*, 27–50.
- [265] Jones, G. *Organic Reactions*; John Wiley and Sons, Inc., 1967; pp 204–273.
- [266] Knoevenagel, E. *Ber. Dtsch. Chem. Ges.* **1898**, *31*, 2596–2619.
- [267] Tan, Q.; Yang, X.; Cheng, M.; Wang, H.; Wang, X.; Sun, L. *J. Phys. Chem. C* **2014**, *118*, 16851–16855.
- [268] Wild, M.; Griebel, J.; Hajduk, A.; Friedrich, D.; Stark, A.; Abel, B.; Siefertmann, K. R. *Sci. Rep.* **2016**, *6*, 26263–26270.
- [269] Cho, H.; Iwashita, T.; Hamaguchi, M.; Oyama, Y. *Chem. Pharm. Bull.* **1991**, *39*, 3341–3342.
- [270] Zhang, S.-J.; Hu, W.-X. *Synth. Commun.* **2010**, *40*, 3093–3100.
- [271] Maadi, A. E.; Matthiesen, C. L.; Ershadi, P.; Baker, J.; Herron, D. M.; Holt, E. M. *J. Chem. Crystallogr.* **2003**, *33*, 757–763.
- [272] Hong, J.; Lai, H.; Liu, Y.; Yuan, C.; Li, Y.; Liu, P.; Fang, Q. *RSC Adv.* **2013**, *3*, 1069–1072.
- [273] Zietz, B.; Gabrielsson, E.; Johansson, V.; El-Zohry, A. M.; Sun, L.; Kloos, L. *Phys. Chem.*

- Chem. Phys.* **2014**, *16*, 2251–2255.
- [274] Zhang, L.; Cole, J. M. *ACS Appl. Mater. Interfaces* **2014**, *6*, 3742–3749.
- [275] El-Zohry, A.; Orthaber, A.; Zietz, B. *J. Phys. Chem. C* **2012**, *116*, 26144–26153.
- [276] Kim, S.; Choi, H.; Kim, D.; Song, K.; Kang, S. O.; Ko, J. *Tetrahedron* **2007**, *63*, 9206–9212.
- [277] Bodedla, G. B.; Thomas, K. R. J.; Li, C.-T.; Ho, K.-C. *RSC Adv.* **2014**, *4*, 53588–53601.
- [278] Wang, S.; Guo, J.; He, L.; Wang, H.; Zhao, J.; Lu, C. *Synth. Met.* **2013**, *168*, 1–8.
- [279] Lin, Y.-D.; Chow, T. J. *J. Photochem. Photobiol. A Chem.* **2012**, *230*, 47–54.
- [280] Lee, M.-W.; Kim, J.-Y.; Son, H. J.; Kim, J. Y.; Kim, B.; Kim, H.; Lee, D.-K.; Kim, K.; Lee, D.-H.; Ko, M. *J. Sci. Rep.* **2015**, *5*, 7711–7718.
- [281] Buene, A. F.; Ose, E. E.; Zakariassen, A. G.; Hagfeldt, A.; Hoff, B. H. *J. Mater. Chem. A* **2019**, *7*, 7581–7590.
- [282] Chen, J.; Zhang, Y.; Yang, L.; Zhang, X.; Liu, J.; Li, L.; Zhang, H. *Tetrahedron* **2007**, *63*, 4266–4270.
- [283] Nagarajan, B.; Kushwaha, S.; Elumalai, R.; Mandal, S.; Ramanujam, K.; Raghavachari, D. *J. Mater. Chem. A* **2017**, *5*, 10289–10300.
- [284] Kelly, C. A.; Farzad, F.; Thompson, D. W.; Stipkala, J. M.; Meyer, G. J. *Langmuir* **1999**, *15*, 7047–7054.
- [285] Liu, Y.; Hagfeldt, A.; Xiao, X.-R.; Lindquist, S.-E. *Sol. Energy Mater. Sol. Cells* **1998**, *55*, 267–281.
- [286] Cao, F.; Oskam, G.; Meyer, G. J.; Searson, P. C. *J. Phys. Chem.* **1996**, *100*, 17021–17027.
- [287] Bisquert, J.; Vikhrenko, V. S. *J. Phys. Chem. B* **2004**, *108*, 2313–2322.
- [288] Kim, S. H.; Sakong, C.; Chang, J. B.; Kim, B.; Ko, M. J.; Kim, D. H.; Hong, K. S.; Kim, J. P. *Dyes Pigm.* **2013**, *97*, 262–271.
- [289] Lin, R. Y.-Y.; Wu, F.-L.; Li, C.-T.; Chen, P.-Y.; Ho, K.-C.; Lin, J. T. *ChemSusChem* **2015**, *8*, 2503–2513.
- [290] El-Shishtawy, R. M.; Decoppet, J.-D.; Al-Zahrani, F. A. M.; Cao, Y.; Khan, S. B.; Al-Ghamdi, M. S.; Alhogbi, B. G.; Asiri, A. M.; Zakeeruddin, S. M.; Grätzel, M. *New J. Chem.* **2018**, *42*, 9045–9050.
- [291] Zhang, C.; Wang, S.; Li, Y. *Solar Energy* **2017**, *157*, 94–102.
- [292] Lin, Y.-D.; Ke, B.-Y.; Chang, Y. J.; Chou, P.-T.; Liao, K.-L.; Liu, C.-Y.; Chow, T. J. *J. Mater. Chem. A* **2015**, *3*, 16831–16842.
- [293] Hauck, M.; Schönhaber, J.; Zuccherro, A. J.; Hardcastle, K. I.; Müller, T. J. J.; Bunz, U. H. F. *J. Org. Chem.* **2007**, *72*, 6714–6725.
- [294] Lai, R. Y.; Kong, X.; Jenekhe, S. A.; Bard, A. J. *J. Am. Chem. Soc.* **2003**, *125*, 12631–12639.
- [295] Jovanovic, M. V.; Biehl, E. R. *J. Org. Chem.* **1984**, *49*, 1905–1908.
- [296] Colombo, A.; Dragonetti, C.; Fagnani, F.; Roberto, D.; Melchiorre, F.; Biagini, P. *Dalton Trans.* **2019**, *48*, 9818–9823.
- [297] Nazeeruddin, M. K.; De Angelis, F.; Fantacci, S.; Selloni, A.; Viscardi, G.; Liska, P.; Ito, S.; Takeru, B.; Grätzel, M. *J. Am. Chem. Soc.* **2005**, *127*, 16835–16847.
- [298] Wu, K.-j.; Shen, K.; Yu, Y.; Wang, D.-l. *Chin. J. Chem. Phys.* **2012**, *25*, 733–738.
- [299] Tamao, K.; Sumitani, K.; Kumada, M. *J. Am. Chem. Soc.* **1972**, *94*, 4374–4376.
- [300] Kavan, L.; Saygili, Y.; Freitag, M.; Zakeeruddin, S. M.; Hagfeldt, A.; Grätzel, M. *Elec-*

- trochim. Acta* **2017**, *227*, 194–202.
- [301] Chiykowski, V. A.; Lam, B.; Du, C.; Berlinguette, C. P. *Chem. Commun.* **2017**, *53*, 2367–2370.
- [302] Bjørnholm, T.; Greve, D. R.; Reitzel, N.; Hassenkam, T.; Kjaer, K.; Howes, P. B.; Larsen, N. B.; Bøgelund, J.; Jayaraman, M.; Ewbank, P. C.; McCullough, R. D. *J. Am. Chem. Soc.* **1998**, *120*, 7643–7644.
- [303] Bumagin, N. A.; Veselov, I. S.; Belov, D. S. *Chem. Heterocycl. Compd.* **2014**, *50*, 19–25.
- [304] Joly, D.; Pellejà, L.; Narbey, S.; Oswald, F.; Chiron, J.; Clifford, J. N.; Palomares, E.; Demadrille, R. *Sci. Rep.* **2014**, *4*, 4033–4039.
- [305] Snaith, H. J. *Energy Environ. Sci.* **2012**, *5*, 6513–6520.
- [306] Dell’Orto, E.; Raimondo, L.; Sassella, A.; Abbotto, A. *J. Mater. Chem.* **2012**, *22*, 11364–11369.
- [307] Shahzad, N.; Pugliese, D.; Lamberti, A.; Sacco, A.; Virga, A.; Gazia, R.; Bianco, S.; Shahzad, M. I.; Tresso, E.; Pirri, C. F. *J. Phys. Conf. Ser.* **2013**, *439*, 12012–12023.

## APPENDED PAPERS

Paper I

Paper II

Paper III

Paper IV

Paper V

Paper VI





# PAPER I

## **Effect of $\pi$ -linkers on phenothiazine sensitizers for dye-sensitized solar cells**

Reprinted from *Dyes and Pigments*, Audun F. Buene, Nora Uggerud, Solon P. Economopoulos, Odd R. Gautun, Bård H. Hoff, Effect of  $\pi$ -linkers on phenothiazine sensitizers for dye-sensitized solar cells, 151, 263-271, **2018**, with permission from Elsevier.





Effect of  $\pi$ -linkers on phenothiazine sensitizers for dye-sensitized solar cells

Audun Formo Buene, Nora Uggerud, Solon P. Economopoulos, Odd R. Gautun, Bård Helge Hoff\*



Department of Chemistry, Norwegian University of Science and Technology, Høgskoleringen 5, NO-7491, Trondheim, Norway

## ARTICLE INFO

**Keywords:**  
Phenothiazine dyes  
Dye-sensitized solar cells  
 $\pi$ -spacer  
Auxiliary donor  
Furan

## ABSTRACT

Eleven new dyes have been synthesized in order to investigate the effect of five different  $\pi$ -spacers and two different auxiliary donors in phenothiazine-based sensitizers for dye-sensitized solar cells. The target molecules were synthesized in 5–7 steps from 10H-phenothiazine. Evaluation of the photovoltaic performance revealed that introducing a  $\pi$ -spacer does not necessarily increase the power conversion efficiency. Still, dyes with a furan  $\pi$ -spacer were found to be slightly more efficient compared to their thiophene counterparts, and more efficient than no spacer. Dyes with phenyl based  $\pi$ -spacers resulted in less efficient solar cells, and especially so when incorporating two fluorine atoms. Surprisingly, introducing an additional electron donating group in the auxiliary donor had no pronounced effect on the photovoltaic performance of the dyes.

## 1. Introduction

The need for increasing global power production has sparked the development of a number of new photovoltaic technologies. Dye-sensitized solar cells (DSSCs) are promising candidates allowing solar cells to be semi-transparent, flexible and of tunable color [1]. Under ambient light conditions, DSSCs have out-performed most other long established PV technologies [2]. Hot applications of DSSCs include building integration and powering an increasing number of devices in the Internet of Things (IoT) [3]. This development has, to a large extent, been supported by the introduction of new redox shuttles based on cobalt and copper complexes [4–8].

The dyes utilized in DSSCs have traditionally been metal-complexes, where N719, N3 and N749 also known as ‘black dye’ are the most famous examples [9]. Zinc porphyrins are also highly successful sensitizers with a metal-organic core [10]. In terms of efficiency, these metal-based complexes have achieved PCEs up to 13.0% [11]. Although the absorption properties of these dyes are excellent, the extinction coefficients are usually moderate and dye aggregation, synthesis and purification are common challenges. Thus, metal-free dyes have emerged as a viable alternative [12].

Improving the stability and efficiency of metal-free dyes is where the main efforts in this research area have been placed, and the current record for metal-free dyes is 14.7% [8]. Triarylamines, phenothiazines and polythiophenes are common dye scaffolds [13,14]. Phenothiazine, and its oxygen analog phenoxazine, were among the early metal-free dyes, and studies of  $\pi$ -spacers containing isomerizable double bonds have been conducted [15,16]. Furthermore, this class of sensitizers

have shown very promising results in DSSCs with aqueous electrolytes, as demonstrated by Lin et al. [17] The phenothiazine dye scaffold has been the subject of two recent reviews for the interested reader, and as with any other class of dyes the main challenge lies in improving the light harvesting properties of the molecules [18,19]. Pushing the absorption towards the infrared region of the spectrum is crucial, and the introduction of  $\pi$ -spacers and auxiliary donors can be efficient measures for achieving this.

While several studies have investigated the effect of different  $\pi$ -spacers [20–24], the lack of a larger data set is apparent. A study comparing five and six-membered  $\pi$ -spacers directly connecting the phenothiazine scaffold and anchoring group has to the best of our knowledge only been performed by Bodeda et al. comparing thiophene and phenyl [24]. They reported an insulating behavior of the phenyl spacer due to non-planarity, reducing the interactions between the donor and acceptor moieties. We prepared two complementary series of dyes with the same five  $\pi$ -spacers, to observe and verify any appearing trends. The two series of dyes only differ by the auxiliary donor group on the phenothiazine scaffold, and one of the series was extended with a reference dye without any  $\pi$ -spacer. The general layout of the sensitizers is illustrated by **AFB-10** in Fig. 1.

## 2. Experimental section

## 2.1. Materials and reagents

All reactions were carried out under nitrogen atmosphere, and all synthesis reagents were acquired from Sigma Aldrich.

\* Corresponding author.

E-mail address: [bard.helge.hoff@chem.ntnu.no](mailto:bard.helge.hoff@chem.ntnu.no) (B.H. Hoff).<https://doi.org/10.1016/j.dyepig.2018.01.011>

Received 24 November 2017; Received in revised form 6 January 2018; Accepted 7 January 2018

Available online 09 January 2018

0143-7208/© 2018 Elsevier Ltd. All rights reserved.

A.F. Buene et al.

Dyes and Pigments 151 (2018) 263–271

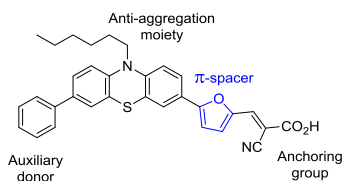


Fig. 1. General layout of the sensitizers in this study, illustrated by AFB-10.

## 2.2. Analytical instruments

<sup>1</sup>H and <sup>13</sup>C NMR spectra were recorded at 22 °C on either a Bruker 400 or 600 MHz spectrometer in DMSO-*d*<sub>6</sub>. All chemical shifts are reported in ppm, and the spectra were calibrated using the signal of DMSO at 2.50 ppm (<sup>1</sup>H) and 39.52 (<sup>13</sup>C), or that of TMS (0 ppm) in CDCl<sub>3</sub>. Infrared absorption (IR) spectra were recorded with a FTIR Thermo Nicolet Nexus FT-IR Spectrometer using a Smart Endurance reflection cell. Reported frequencies were in the range of 4000–400 cm<sup>-1</sup>. UV/Vis analyses were performed with a Hitachi U-1900 UV/Vis-spectrophotometer using quartz cuvettes (10 mm). Extinction coefficients were calculated from Lambert-Beer's law. UV/Vis measurements of sensitized TiO<sub>2</sub> films was performed in the same spectrophotometer with a non-stained electrode as the background. Melting points were determined with a Stuart SMP40 automatic melting point instrument. Accurate mass determination in positive and negative mode was performed on a "Synapt G2-S" Q-TOF instrument from Waters™. The samples were ionized by the use of ASAP probe (APCI) or by ESI. Spectra processing was done by Waters™ Software (Masslynx v4.1 SCN871). Fluorescence spectrophotometry was carried out on a Varian Cary Eclipse instrument. All emission spectra were measured in chloroform.

## 2.3. Fabrication of dye-sensitized solar cells

The cell fabrication is conducted based on the procedure from Hao et al. [25] TEC-8 FTO glass supplied by Dyesol was washed with Diconex 21 (2 g/L H<sub>2</sub>O) in an ultrasonic bath for 45 min, and then rinsed with deionized water and ethanol before air drying. Further cleaning was done in a UV-ozone cleaner for 15 min (Novascan PSD PRO-UV T6). A blocking layer was deposited by immersion of the FTO glass in an aq. solution of TiCl<sub>4</sub> (40 mM) for 30 min at 70 °C, rinsing with deionized water and ethanol followed by another immersion for 30 min in an aq. solution of TiCl<sub>4</sub> (40 mM) at 70 °C, then rinsing with deionized water and ethanol.

Five layers of transparent TiO<sub>2</sub> paste (18NR-T, Dyesol) were screen printed on the FTO glass (mesh count 250, active area 0.238 cm<sup>2</sup>). Between each layer, the electrodes were heated to 125 °C for 2–3 min. Finally, a scattering layer (WER2-O, Dyesol) was screen printed, and the electrodes were sintered at 500 °C for 30 min. The thickness of the sintered TiO<sub>2</sub> was measured to 17.5 μm (12.5 μm + 5 μm) with a profilometer (Veeco, Dektak 150). The electrodes were then post treated with TiCl<sub>4</sub> using the same conditions previously described for 30 min.

Counter electrodes were fabricated by drilling holes in the FTO glass with a diamond drill bit. The catalytic Pt layer was deposited by dropcasting a 10 mM solution of H<sub>2</sub>PtCl<sub>6</sub> in 2-propanol (5 μL/cm<sup>2</sup>), followed by firing at 400 °C for 15 min [6].

Before staining, the electrodes were annealed with a hot air gun at 480 °C for 25 min. The staining solution had 5 × 10<sup>-4</sup> M dye concentration, with a 10-fold amount of CDCA in a mixture of acetonitrile/THF (43:57, v/v). The dielectric constant for this solution is estimated to be around 20 Fm<sup>-1</sup>, which for Black dye is reported as the optimal dielectric constant [26]. N719 was stained from a 0.5 mM solution in

ethanol. The electrodes were stained for 20 h, then rinsed in acetonitrile for 2 min and dried under N<sub>2</sub> flow. The cells were sealed with a 25 μm Surlyn (Solaronix) gasket, melted with a 50 W PTC heat element for 3 × 20 s per cell.

The electrolyte was made following a procedure from Demadrille et al. [27], containing 0.5 M 1-butyl-3-methylimidazolium iodide, 0.1 M lithium iodide, 0.05 M I<sub>2</sub> and 0.5 M *tert*-butylpyridine in acetonitrile. This was injected by vacuum backfilling before the filling hole was sealed with Surlyn and a circular glass cover slip. The contacts for the anode and cathode were painted with a conductive silver paint (Electrolube, SCP) before characterization.

## 2.4. Device characterization

The device's I-V characteristics were measured with a Keithley 2450 under a Scientech SP300B solar simulator with an AM 1.5G filter, calibrated to 100 mW/cm<sup>2</sup> with a Newport Reference Solar Cell and Meter (91150 V). All cells were masked with a 0.1547 cm<sup>2</sup> black mask before characterization.

IPCE measurements were obtained from a device fabricated with a halogen lamp (Ocean Optics HL-2000), a monochromator (Spectral Products CM110), connected to the Keithley 2450. The light intensity was determined using a NIST traceable calibrated photodiode (Thorlabs, FDS100-CAL).

## 2.5. Synthesis

### 2.5.1. (E)-2-Cyano-3-(10-hexyl-7-(4-methoxyphenyl)-10H-phenothiazin-3-yl)acrylic acid (AFB-1)

Compound **5** (200 mg, 0.479 mmol) and cyanoacetic acid (815 mg, 9.58 mmol) were dissolved in degassed acetonitrile (55 mL) under N<sub>2</sub> atmosphere. Piperidine (569 μL, 489 mg, 5.75 mmol) was added and the reaction was heated at 80 °C for 40 min before cooling to 22 °C and quenched in aqueous HCl (2 M, 150 mL). EtOAc (50 mL) was added and the organic phase was washed with water (8 × 100 mL), then dried with brine (50 mL) and over anhydrous Na<sub>2</sub>SO<sub>4</sub>, filtered and the solvents were removed in vacuo. The crude product was purified by silica-gel column chromatography (gradient: 0–15% MeOH in CH<sub>2</sub>Cl<sub>2</sub>) to obtain AFB-1 as a dark solid (215 mg, 0.444 mmol, 93%), mp. 204–208 °C. <sup>1</sup>H NMR (600 MHz, DMSO-*d*<sub>6</sub>) δ: 13.72 (s, 1H), 8.15 (s, 1H), 7.91 (d, *J* = 8.8 Hz, 1H), 7.82 (s, 1H), 7.57 (d, *J* = 8.7 Hz, 2H), 7.45 (d, *J* = 8.6 Hz, 1H), 7.39 (s, 1H), 7.15 (d, *J* = 8.8 Hz, 1H), 7.09 (d, *J* = 8.6 Hz, 1H), 6.98 (d, *J* = 8.8 Hz, 2H), 3.94 (t, *J* = 7.0 Hz, 2H), 3.78 (s, 3H), 1.74–1.64 (m, 2H), 1.45–1.35 (m, 2H), 1.31–1.20 (m, 4H), 0.82 (t, *J* = 7.1 Hz, 3H); <sup>13</sup>C NMR (150 MHz, DMSO-*d*<sub>6</sub>) δ: 163.8, 158.8, 152.5, 148.6, 141.1, 135.3, 131.7, 130.9, 129.1, 127.2 (2C), 125.5, 125.4, 124.6, 122.7, 122.5, 116.8, 116.7, 115.5, 114.3 (2C), 99.4, 55.1, 47.0, 30.8, 26.0, 25.7, 22.1, 13.8; IR (neat, cm<sup>-1</sup>) ν: 2909 (w), 1683 (m), 1558 (m), 1470 (s), 1184 (s), 826 (m); HRMS (ASAP+, *m/z*): 484.1815 (calcd. C<sub>29</sub>H<sub>28</sub>N<sub>2</sub>O<sub>2</sub>S: 484.1821 [M]<sup>+</sup>); UV (CH<sub>2</sub>Cl<sub>2</sub>, 2 × 10<sup>-5</sup> M, 22 °C) λ<sub>max</sub> (nm): 305.5 (26200), 475.0 (14000).

### 2.5.2. (E)-2-Cyano-3-(4-(10-hexyl-7-phenyl-10H-phenothiazin-3-yl)phenyl)acrylic acid (AFB-2)

Dye AFB-2 was made as described in Section 2.5.1 but starting with compound **10** (294 mg, 0.634 mmol), cyanoacetic acid (1.08 g, 12.7 mmol) and piperidine (753 μL, 648.0 mg, 7.61 mmol). The crude product was purified by silica-gel column chromatography (gradient: 0–15% MeOH in CH<sub>2</sub>Cl<sub>2</sub>) to obtain AFB-2 as a dark brown solid (164 mg, 0.308 mmol, 49%), mp. 246 °C (dec.). <sup>1</sup>H NMR (400 MHz, DMSO-*d*<sub>6</sub>) δ: 8.05 (s, 1H), 7.95 (d, *J* = 8.4 Hz, 2H), 7.79 (d, *J* = 8.4 Hz, 2H), 7.65–7.61 (m, 2H), 7.59 (dd, *J* = 8.5 Hz, 2.1, 1H), 7.55 (d, *J* = 2.3 Hz, 1H), 7.50 (dd, *J* = 8.5, 2.3 Hz, 1H), 7.46 (d, *J* = 2.3 Hz, 1H), 7.44–7.40 (m, 2H), 7.32 (t, *J* = 7.3 Hz, 1H), 7.09 (dd, *J* = 8.7, 2.1 Hz, 2H), 3.92 (t, *J* = 6.9 Hz, 2H), 1.74–1.68 (m, 2H), 1.44–1.38 (m, 2H), 1.28–1.23 (m, 4H), 0.85–0.81 (m, 3H) (carboxylic acid proton not

visible);  $^{13}\text{C}$  NMR (100 MHz, DMSO- $d_6$ )  $\delta$ : 163.4, 147.9, 144.4, 143.5, 141.2, 138.8, 134.5, 132.9, 131.6, 130.2 (2C), 128.9 (2C), 127.1, 126.3 (2C), 126.1, 126.0 (2C), 125.9, 125.1, 125.0, 123.7, 123.5, 118.9, 116.1, 116.0, 111.4, 46.6, 30.8, 26.2, 25.8, 22.1, 13.8; IR (neat,  $\text{cm}^{-1}$ )  $\nu$ : 2961 (w), 2925 (w), 2852 (w), 2218 (w), 1600 (m), 1579 (m), 1464 (m), 1393 (m), 1247 (m), 1189 (m), 808 (m), 758 (s), 696 (m); HRMS (ASAP+,  $m/z$ ): 486.2127 (calcd.  $\text{C}_{33}\text{H}_{30}\text{N}_2\text{S}$ : 486.2130,  $[\text{M}-\text{CO}_2+\text{H}]^+$ ); UV ( $\text{CH}_2\text{Cl}_2$ ,  $2 \times 10^{-5}\text{M}$ , 22 °C)  $\lambda_{\text{max}}$  (nm): 425.0 (11350).

#### 2.5.3. (E)-2-Cyano-3-(4-(10-hexyl-7-(4-methoxyphenyl)-10H-phenothiazin-3-yl)phenyl)acrylic acid (AFB-3)

Dye AFB-3 was made as described in Section 2.5.1 but starting with compound 11 (190 mg, 0.385 mmol), cyanoacetic acid (655 mg, 7.70 mmol) and piperidine (457  $\mu\text{L}$ , 393 mg, 4.62 mmol). The crude product was purified by silica-gel column chromatography (gradient: 0–15% MeOH in  $\text{CH}_2\text{Cl}_2$ ) to obtain AFB-3 as a dark brown solid (186 mg, 0.331 mmol, 86%), mp. 237 °C (dec.).  $^1\text{H}$  NMR (400 MHz, DMSO- $d_6$ )  $\delta$ : 8.03 (s, 1H), 7.97–7.93 (m, 2H), 7.80–7.76 (m, 2H), 7.60–7.53 (m, 4H), 7.46–7.42 (m, 1H), 7.41–7.39 (m, 1H), 7.10–7.03 (m, 2H), 7.00–6.96 (m, 2H), 3.91 (t,  $J = 6.9$  Hz, 2H), 3.78 (s, 3H), 1.76–1.66 (m, 2H), 1.45–1.36 (m, 2H), 1.29–1.21 (m, 4H), 0.86–0.80 (m, 3H) (carboxylic acid proton not visible);  $^{13}\text{C}$  NMR (100 MHz, DMSO- $d_6$ )  $\delta$ : 163.2, 158.7, 147.9, 144.5, 142.8, 141.2, 134.3, 132.8, 131.6, 131.3, 130.2 (2C), 127.2 (2C), 126.3 (2C), 126.1, 125.3, 125.0, 124.5, 123.8, 123.5, 119.0, 116.1, 116.0, 114.3 (2C), 111.0, 55.2, 46.6, 30.9, 26.2, 25.8, 22.1, 13.8; IR (neat,  $\text{cm}^{-1}$ )  $\nu$ : 3033 (w, br), 2925 (w), 2847 (w), 2223 (w), 1719 (m), 1693 (m), 1574 (s, br), 1460 (s), 1242 (s), 1179 (s), 1023 (m), 805 (s); HRMS (ASAP+,  $m/z$ ): 516.2228 (calcd.  $\text{C}_{34}\text{H}_{32}\text{N}_2\text{O}_2\text{S}$ : 516.2235  $[\text{M}-\text{CO}_2]^+$ ); UV ( $\text{CH}_2\text{Cl}_2$ ,  $2 \times 10^{-5}\text{M}$ , 22 °C)  $\lambda_{\text{max}}$  (nm): 429.5 (12700).

#### 2.5.4. (E)-2-Cyano-3-(2-fluoro-4-(10-hexyl-7-phenyl-10H-phenothiazin-3-yl)phenyl)acrylic acid (AFB-4)

Dye AFB-4 was made as described in Section 2.5.1 but starting with compound 12 (205 mg, 0.425 mmol), cyanoacetic acid (722 mg, 8.49 mmol) and piperidine (504  $\mu\text{L}$ , 434 mg, 5.10 mmol). The crude product was purified by silica-gel column chromatography (gradient: 0–15% MeOH in  $\text{CH}_2\text{Cl}_2$ ) to obtain AFB-4 as a dark red solid (200 mg, 0.365 mmol, 86%), mp. 214 °C (dec.).  $^1\text{H}$  NMR (400 MHz, DMSO- $d_6$ )  $\delta$ : 8.19 (t,  $J = 8.2$  Hz, 1H), 8.14 (s, 1H), 7.70–7.57 (m, 6H), 7.53–7.48 (m, 1H), 7.47–7.39 (m, 3H), 7.35–7.29 (m, 1H), 7.12–7.05 (m, 2H), 3.92 (t,  $J = 6.9$  Hz, 2H), 1.76–1.66 (m, 2H), 1.45–1.36 (m, 2H), 1.29–1.21 (m, 4H), 0.86–0.80 (m, 3H) (carboxylic acid proton not visible);  $^{13}\text{C}$  NMR (100 MHz, DMSO- $d_6$ )  $\delta$ : 162.4, 160.9 (d,  $J = 251$  Hz), 144.9, 143.5 (d,  $J = 10.7$  Hz), 143.35, 138.8, 134.6, 131.8 (d,  $J = 3.8$  Hz), 131.7, 130.2, 128.9 (2C), 128.6 (d,  $J = 2.0$  Hz), 127.1, 126.2, 126.1 (2C), 125.9, 125.2, 125.0, 123.7, 123.4, 122.1 (d,  $J = 2.1$  Hz), 119.3 (d,  $J = 12.0$  Hz), 118.5, 116.0 (d,  $J = 21.3$  Hz), 113.0, 112.7, 46.6, 30.8, 26.1, 25.8, 22.1, 13.8; IR (neat,  $\text{cm}^{-1}$ )  $\nu$ : 2951 (w), 2935 (w), 2862 (w), 2218 (w), 1579 (m), 1465 (s), 1393 (m), 1257 (m), 808 (m), 758 (s), 696 (m); HRMS (ASAP+,  $m/z$ ): 504.2035 (calcd.  $\text{C}_{33}\text{H}_{29}\text{FN}_2\text{S}$ : 505.2035,  $[\text{M}-\text{CO}_2]^+$ ); UV ( $\text{CH}_2\text{Cl}_2$ ,  $2 \times 10^{-5}\text{M}$ , 22 °C)  $\lambda_{\text{max}}$  (nm): 431.5 (12950).

#### 2.5.5. (E)-2-Cyano-3-(2-fluoro-4-(10-hexyl-7-(4-methoxyphenyl)-10H-phenothiazin-3-yl)phenyl)acrylic acid (AFB-5)

Dye AFB-5 was made as described in Section 2.5.1 but starting with compound 13 (186 mg, 0.364 mmol), cyanoacetic acid (618 mg, 7.27 mmol) and piperidine (432  $\mu\text{L}$ , 371 mg, 4.36 mmol). The crude product was purified by silica-gel column chromatography (gradient: 0–15% MeOH in  $\text{CH}_2\text{Cl}_2$ ) to obtain AFB-5 as a dark red solid (121 mg, 0.209 mmol, 58%), mp. 220 °C (dec.).  $^1\text{H}$  NMR (400 MHz, DMSO- $d_6$ )  $\delta$ : 8.18 (t,  $J = 8.0$  Hz, 1H), 8.12 (s, 1H), 7.70–7.65 (m, 2H), 7.63 (dd,  $J = 8.5$  Hz, 2.2, 1H), 7.60–7.55 (m, 3H), 7.45 (dd,  $J = 8.5$ , 2.1 Hz, 1H), 7.40 (d,  $J = 2.2$  Hz, 1H), 7.07 (t,  $J = 8.4$  Hz, 2H), 6.98 (d,  $J = 8.8$  Hz,

2H), 3.91 (t,  $J = 6.9$  Hz, 2H), 3.78 (s, 3H), 1.75–1.67 (m, 2H), 1.45–1.36 (m, 2H), 1.30–1.21 (m, 4H), 0.86–0.81 (m, 3H) (carboxylic acid proton not visible);  $^{13}\text{C}$  NMR (100 MHz, DMSO- $d_6$ )  $\delta$ : 162.4, 160.8 (d,  $J = 251.1$  Hz), 158.7, 145.0, 143.4 (d,  $J = 9.6$  Hz), 142.7, 138.3, 134.4, 131.6, 131.2, 128.5, 127.2 (2C), 126.2, 125.4, 125.1, 124.5, 123.7, 123.4, 122.1 (d,  $J = 2.3$  Hz), 119.4 (d,  $J = 11.5$  Hz), 118.7, 116.1, 115.8, 114.3 (2C), 112.9, 112.8, 55.2, 46.6, 30.8, 26.2, 25.8, 22.1, 13.8; IR (neat,  $\text{cm}^{-1}$ )  $\nu$ : 3034 (w, br), 2925 (w), 2847 (w), 2223 (w), 1719 (m), 1693 (m), 1574 (s, br), 1460 (s), 1242 (s), 1179 (s), 1023 (m), 805 (s); HRMS (ASAP+,  $m/z$ ): 534.2139 (calcd.  $\text{C}_{34}\text{H}_{31}\text{N}_2\text{O}_2\text{FS}$ : 534.2141  $[\text{M}-\text{CO}_2]^+$ ); UV ( $\text{CH}_2\text{Cl}_2$ ,  $2 \times 10^{-5}\text{M}$ , 22 °C)  $\lambda_{\text{max}}$  (nm): 440.5 (12050).

#### 2.5.6. (E)-2-Cyano-3-(2,6-difluoro-4-(10-hexyl-7-phenyl-10H-phenothiazin-3-yl)phenyl)acrylic acid (AFB-6)

Dye AFB-6 was made as described in Section 2.5.1 but starting with compound 14 (228 mg, 0.457 mmol), cyanoacetic acid (777 mg, 9.13 mmol) and piperidine (542  $\mu\text{L}$ , 466 mg, 5.48 mmol). The crude product was purified by silica-gel column chromatography (gradient: 0–15% MeOH in  $\text{CH}_2\text{Cl}_2$ ) to obtain AFB-6 as a red solid (181 mg, 0.319 mmol, 70%), mp. 210 °C (dec.).  $^1\text{H}$  NMR (400 MHz, DMSO- $d_6$ )  $\delta$ : 7.85 (s, 1H), 7.68–7.56 (m, 6H), 7.51 (dd,  $J = 8.6$ , 2.1 Hz, 1H), 7.46 (d,  $J = 2.2$  Hz, 1H), 7.45–7.40 (m, 2H), 7.32 (t,  $J = 7.3$  Hz, 1H), 7.11–7.06 (m, 2H), 3.92 (t,  $J = 6.8$  Hz, 2H), 1.75–1.67 (m, 2H), 1.45–1.36 (m, 2H), 1.29–1.22 (m, 4H), 0.85–0.80 (m, 3H) (carboxylic acid proton not visible);  $^{13}\text{C}$  NMR (100 MHz, DMSO- $d_6$ )  $\delta$ : 161.7, 159.9 (dd,  $J = 251.6$ , 8.1 Hz, 2C), 145.1, 143.2, 143.0, 138.8, 135.5, 134.6, 130.8, 128.9 (2C), 127.1, 126.3, 126.0 (2C), 125.9, 125.2, 125.0, 123.7, 123.4, 121.5, 117.2, 116.1, 115.8, 109.7, 109.1 (d,  $J = 25.1$  Hz, 2C), 46.7, 30.8, 26.1, 25.8, 22.1, 13.8; IR (neat,  $\text{cm}^{-1}$ )  $\nu$ : 2956 (w), 2925 (w), 2847 (w), 2229 (w), 1627 (m), 1463 (m), 1392 (m), 1197 (m), 1024 (m), 808 (m), 758 (s), 696 (m); HRMS (ASAP+,  $m/z$ ): 522.1937 (calcd.  $\text{C}_{33}\text{H}_{28}\text{N}_2\text{F}_2\text{S}$ : 522.1941  $[\text{M}-\text{CO}_2]^+$ ); UV ( $\text{CH}_2\text{Cl}_2$ ,  $2 \times 10^{-5}\text{M}$ , 22 °C)  $\lambda_{\text{max}}$  (nm): 419.5 (10650).

#### 2.5.7. (E)-2-Cyano-3-(2,6-difluoro-4-(10-hexyl-7-(4-methoxyphenyl)-10H-phenothiazin-3-yl)phenyl)acrylate (20)

Compound 15 (410 mg, 0.80 mmol) and ammonium acetate (240 mg, 3.10 mmol) were mixed before acetic acid (4.5 mL) and tert-butyl 2-cyanoacetate (0.44 mL, 3.10 mmol) were added under  $\text{N}_2$  atmosphere. The reaction mixture was heated to 75 °C and left stirring for 1 h. Water (30 mL) was added to the solution and the aqueous phase was extracted with EtOAc ( $3 \times 20$  mL). The combined organic phases were dried over anhydrous  $\text{Na}_2\text{SO}_4$ , filtered and the solvents were removed in vacuo. Purification by silica-gel column chromatography (n-pentane:EtOAc, 14:1,  $R_f = 0.24$ ) gave compound 20 as a dark red oil (450 mg, 0.69 mmol, 89%).  $^1\text{H}$  NMR (400 MHz, DMSO- $d_6$ )  $\delta$ : 8.19 (s, 1H), 7.73–7.68 (m, 4H), 7.58–7.56 (m, 2H), 7.46–7.44 (m, 1H), 7.41–7.40 (m, 1H), 7.09–7.07 (m, 2H), 7.00–6.98 (m, 2H), 3.95–3.90 (m, 2H), 3.78 (s, 3H), 1.75–1.68 (m, 2H), 1.43 (s, 9H), 1.41–1.37 (m, 2H), 1.29–1.24 (m, 4H), 0.85–0.82 (m, 3H);  $^{13}\text{C}$  NMR (100 MHz, DMSO- $d_6$ )  $\delta$ : 163.3, 159.8 (2C), 158.7, 145.7, 145.3 (d,  $J = 2.0$  Hz), 142.42, 142.37, 134.5, 131.2, 130.3, 127.2 (2C), 125.4, 124.5, 123.8, 123.3, 116.4, 115.5 (d,  $J = 55.8$  Hz), 114.3 (2C), 111.5, 109.4 (d,  $J = 24.4$  Hz, 2C), 84.0, 82.7, 55.1, 46.7, 30.8, 27.5 (3C), 27.4, 26.1, 25.8, 22.0, 13.8 (2 shifts missing); IR (neat,  $\text{cm}^{-1}$ )  $\nu$ : 3065 (w), 2925 (w), 2852 (w), 1740 (s), 1719 (s), 1470 (s), 1273 (s), 1242 (s), 1148 (s), 1023 (s), 816 (s); HRMS (ASAP+,  $m/z$ ): 652.2566 (calcd.  $\text{C}_{39}\text{H}_{38}\text{F}_2\text{N}_2\text{O}_3$ : 652.2571,  $[\text{M}]^+$ ).

#### 2.5.8. (E)-2-Cyano-3-(2,6-difluoro-4-(10-hexyl-7-(4-methoxyphenyl)-10H-phenothiazin-3-yl)phenyl)acrylic acid (AFB-7)

Compound 20 (300 mg, 0.45 mmol) was stirred in TFA (28 mL) for 1 h, then the reaction mixture was poured into water (40 mL) and the precipitate that formed was filtered off. The crude product was purified by silica-gel column chromatography (gradient: 0–15% MeOH in

$\text{CH}_2\text{Cl}_2$ ) to obtain **AFB-7** as a dark red solid (190 mg, 0.30 mmol, 76%), mp. 115–120 °C (dec.).  $^1\text{H}$  NMR (400 MHz,  $\text{DMSO-d}_6$ )  $\delta$ : 7.86 (s, 1H), 7.65–7.55 (m, 6H), 7.44 (dd,  $J$  = 8.8, 1.9 Hz, 1H), 7.39 (d,  $J$  = 2.1 Hz, 1H), 7.05 (d,  $J$  = 8.6 Hz, 2H), 6.98 (d,  $J$  = 8.8 Hz, 2H), 3.90 (t,  $J$  = 6.9 Hz, 2H), 3.78 (s, 3H), 1.73–1.67 (m, 2H), 1.43–1.37 (m, 2H), 1.28–1.22 (m, 4H), 0.85–0.80 (m, 3H) (carboxylic acid proton not visible);  $^{13}\text{C}$  NMR (100 MHz,  $\text{DMSO-d}_6$ )  $\delta$ : 162.2, 160.1 (d,  $J$  = 268.3 Hz, 2C), 158.8, 147.5 (d,  $J$  = 3.1 Hz), 145.6, 142.5, 140.0, 134.5, 131.2, 130.1, 127.2 (2C), 126.4, 125.4, 125.3, 124.5, 123.8, 123.3, 117.4, 116.2, 116.0 (d,  $J$  = 41.6 Hz), 115.8, 114.3 (2C), 109.1 (d,  $J$  = 24.9 Hz, 2C), 98.0, 55.1, 46.6, 30.8, 26.1, 25.8, 22.1, 13.8; IR (neat,  $\text{cm}^{-1}$ )  $\nu$ : 2966 (w, br), 2925 (w), 2857 (w), 1703 (m, br), 1631 (s, br), 1465 (s), 1195 (s), 1018 (s), 805 (s); HRMS (ASAP+,  $m/z$ ): 552.2045 (calcd.  $\text{C}_{34}\text{H}_{30}\text{F}_2\text{N}_2\text{O}_5$ : 552.2047 [ $\text{M} - \text{CO}_2$ ] $^+$ ); UV ( $\text{CH}_2\text{Cl}_2$ ,  $2 \times 10^{-5}$  M, 22 °C)  $\lambda_{\text{max}}$  (nm): 424.0 (9650).

#### 2.5.9. (E)-2-Cyano-3-(5-(10-hexyl-7-phenyl-10H-phenothiazin-3-yl)thiophen-2-yl)acrylic acid (**AFB-8**)

Dye **AFB-8** was made as described in Section 2.5.1 but starting with compound **16** (222 mg, 0.472 mmol), cyanoacetic acid (803 mg, 9.44 mmol) and piperidine (561  $\mu\text{L}$ , 482 mg, 5.66 mmol). The crude product was purified by silica-gel column chromatography (gradient: 0–15% MeOH in  $\text{CH}_2\text{Cl}_2$ ) to obtain **AFB-8** as a dark solid (224 mg, 0.417 mmol, 88%), mp. 209 °C (dec.).  $^1\text{H}$  NMR (400 MHz,  $\text{DMSO-d}_6$ )  $\delta$ : 8.18 (s, 1H), 7.68 (d,  $J$  = 4.1 Hz, 1H), 7.63 (d,  $J$  = 7.5 Hz, 2H), 7.59 (d,  $J$  = 3.8 Hz, 1H), 7.54–7.49 (m, 3H), 7.46–7.40 (m, 3H), 7.32 (t,  $J$  = 7.3 Hz, 1H), 7.09 (d,  $J$  = 8.5 Hz, 1H), 7.06 (d,  $J$  = 8.5 Hz, 1H), 3.91 (t,  $J$  = 6.9 Hz, 2H), 1.73–1.67 (m, 2H), 1.43–1.37 (m, 2H), 1.28–1.22 (m, 4H), 0.84–0.80 (m, 3H) (carboxylic acid proton not visible);  $^{13}\text{C}$  NMR (100 MHz,  $\text{DMSO-d}_6$ )  $\delta$ : 163.6, 148.6, 144.9, 143.2, 141.9, 138.8, 137.5, 135.1, 134.7, 128.9 (2C), 127.2, 127.1, 126.1 (2C), 126.0, 125.5, 125.0, 124.1, 124.0, 123.9, 123.2, 118.6, 116.2, 116.1, 106.6, 46.7, 30.8, 26.1, 25.8, 22.1, 13.8; IR (neat,  $\text{cm}^{-1}$ )  $\nu$ : 2956 (w), 2909 (w), 2852 (w), 2213 (w), 1574 (m), 1470 (m), 1389 (s), 1247 (s), 1060 (m), 798 (s), 758 (s), 695 (m); HRMS (ASAP+,  $m/z$ ): 492.1690 (calcd.  $\text{C}_{31}\text{H}_{28}\text{N}_2\text{O}_5$ : 492.1694 [ $\text{M} - \text{CO}_2$ ] $^+$ ); UV ( $\text{CH}_2\text{Cl}_2$ ,  $2 \times 10^{-5}$  M, 22 °C)  $\lambda_{\text{max}}$  (nm): 356.5 (19000), 466.5 (18050).

#### 2.5.10. (E)-2-Cyano-3-(5-(10-hexyl-7-(4-methoxyphenyl)-10H-phenothiazin-3-yl)thiophen-2-yl)acrylic acid (**AFB-9**)

Dye **AFB-9** was made as described in Section 2.5.1 but starting with compound **17** (189 mg, 0.379 mmol), cyanoacetic acid (644 mg, 7.57 mmol) and piperidine (450  $\mu\text{L}$ , 387 mg, 4.54 mmol). The crude product was purified by silica-gel column chromatography (gradient: 0–15% MeOH in  $\text{CH}_2\text{Cl}_2$ ) to obtain **AFB-9** as a dark solid (165 mg, 0.290 mmol, 77%), mp. 233 °C (dec.).  $^1\text{H}$  NMR (400 MHz,  $\text{DMSO-d}_6$ )  $\delta$ : 8.16 (s, 1H), 7.73 (d,  $J$  = 3.9 Hz, 1H), 7.58 (d,  $J$  = 4.1 Hz, 1H), 7.57–7.54 (m, 2H), 7.52–7.49 (m, 2H), 7.44 (dd,  $J$  = 8.6, 2.1 Hz, 1H), 7.39 (d,  $J$  = 2.2 Hz, 1H), 7.07–7.03 (m, 2H), 6.98 (d,  $J$  = 8.6 Hz, 2H), 3.89 (t,  $J$  = 7.0 Hz, 2H), 3.78 (s, 3H), 1.72–1.66 (m, 2H), 1.42–1.36 (m, 2H), 1.28–1.22 (m, 4H), 0.85–0.80 (m, 3H) (carboxylic acid proton not visible);  $^{13}\text{C}$  NMR (100 MHz,  $\text{DMSO-d}_6$ )  $\delta$ : 163.7, 158.7, 148.2, 145.0, 142.5, 141.5, 137.1, 135.1, 134.5, 131.2, 127.2 (2C), 127.0, 125.5, 125.4, 124.5, 124.01, 123.98, 123.8, 123.2, 118.8, 116.2, 116.0, 114.3 (2C), 106.6, 55.2, 46.6, 30.8, 26.1, 25.8, 22.1, 13.8; IR (neat,  $\text{cm}^{-1}$ )  $\nu$ : 2950 (w, br), 2924 (w), 2852 (w), 1709 (m), 1688 (m, br), 1579 (s), 1444 (s), 1408 (s), 1236 (s), 1179 (s), 1060 (m), 800 (s); HRMS (ASAP+,  $m/z$ ): 566.1691 (calcd.  $\text{C}_{33}\text{H}_{30}\text{N}_2\text{O}_5\text{S}_2$ : 566.1698 [ $\text{M}]^+$ ); UV ( $\text{CH}_2\text{Cl}_2$ ,  $2 \times 10^{-5}$  M, 22 °C)  $\lambda_{\text{max}}$  (nm): 360 (16800), 471.0 (15200).

#### 2.5.11. (E)-2-Cyano-3-(5-(10-hexyl-7-phenyl-10H-phenothiazin-3-yl)furan-2-yl)acrylic acid (**AFB-10**)

Dye **AFB-10** was made as described in Section 2.5.1 but starting with compound **18** (264 mg, 0.583 mmol), cyanoacetic acid (992 mg, 11.7 mmol) and piperidine (693  $\mu\text{L}$ , 596 mg, 6.99 mmol). The crude product was purified by silica-gel column chromatography (gradient:

0–15% MeOH in  $\text{CH}_2\text{Cl}_2$ ) to obtain **AFB-10** as a dark solid (149 mg, 0.285 mmol, 49%), mp. 154 °C (dec.).  $^1\text{H}$  NMR (400 MHz,  $\text{DMSO-d}_6$ )  $\delta$ : 7.89 (s, 1H), 7.72 (dd,  $J$  = 8.7, 1.9 Hz, 1H), 7.68 (d,  $J$  = 2.1 Hz, 1H), 7.63 (d,  $J$  = 7.3 Hz, 2H), 7.51 (dd,  $J$  = 8.5, 2.1 Hz, 1H), 7.47 (d,  $J$  = 2.1 Hz, 1H), 7.43 (t,  $J$  = 7.7 Hz, 2H), 7.35 (d,  $J$  = 3.5 Hz, 1H), 7.32 (t,  $J$  = 7.3 Hz, 1H), 7.21 (d,  $J$  = 3.6 Hz, 1H), 7.14 (d,  $J$  = 8.7 Hz, 1H), 7.10 (d,  $J$  = 8.7 Hz, 1H), 3.94 (t,  $J$  = 6.9 Hz, 2H), 1.74–1.68 (m, 2H), 1.44–1.38 (m, 2H), 1.28–1.22 (m, 4H), 0.85–0.81 (m, 3H) (carboxylic acid proton not visible);  $^{13}\text{C}$  NMR (100 MHz,  $\text{DMSO-d}_6$ )  $\delta$ : 160.0, 156.8, 147.7, 145.2, 143.1, 138.7, 135.3, 134.8, 128.9 (2C), 127.2, 126.1 (2C), 126.0, 125.0, 124.4, 123.7, 123.2, 123.1 (2C), 118.0, 116.3, 116.1, 108.5, 102.0, 46.7, 30.8, 26.1, 25.7, 22.1, 13.8 (1 shift is missing); IR (neat,  $\text{cm}^{-1}$ )  $\nu$ : 2955 (w), 2917 (w), 2849 (w), 2215 (w), 1686 (w), 1580 (m), 1454 (s), 1390 (m), 1233 (m), 1023 (m), 791 (m), 759 (s), 695 (m); HRMS (ASAP+,  $m/z$ ): 476.1922 (calcd.  $\text{C}_{31}\text{H}_{28}\text{N}_2\text{O}_5$ : 476.1922 [ $\text{M} - \text{CO}_2$ ] $^+$ ); UV ( $\text{CH}_2\text{Cl}_2$ ,  $2 \times 10^{-5}$  M, 22 °C)  $\lambda_{\text{max}}$  (nm): 363.0 (14850), 479.5 (19150).

#### 2.5.12. (E)-2-Cyano-3-(5-(10-hexyl-7-(4-methoxyphenyl)-10H-phenothiazin-3-yl)furan-2-yl)acrylate (**21**)

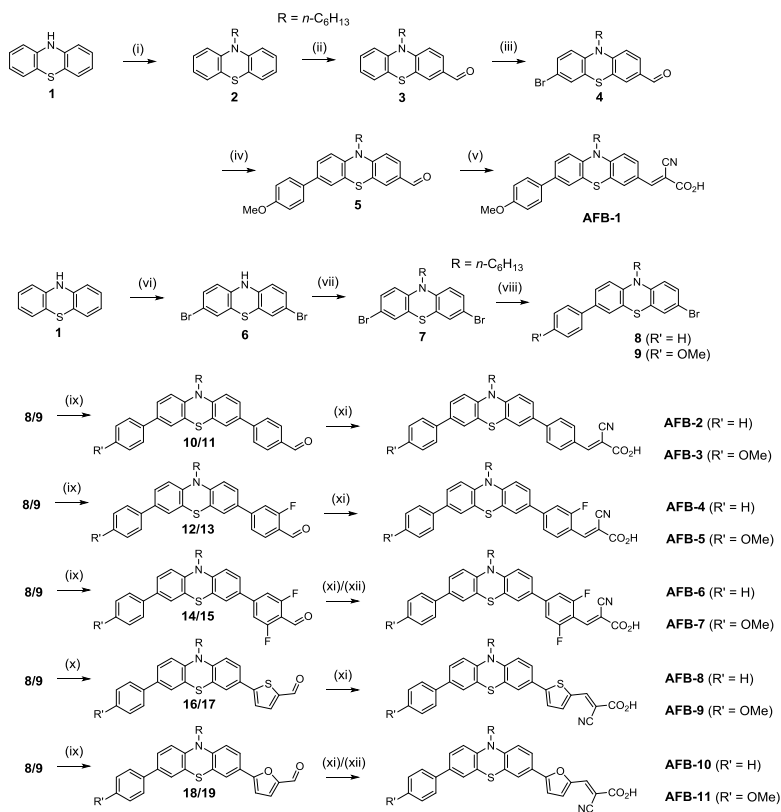
Compound **21** was made as described in Section 2.5.7 but starting with compound **19** (170 mg, 0.40 mmol), ammonium acetate (110 mg, 1.40 mmol), *tert*-butyl 2-cyanoacetate (0.20 mL, 1.40 mmol) in acetic acid (2.0 mL). The crude product was purified by silica-gel column chromatography (*n*-pentane: EtOAc, 19:1,  $R_f$  = 0.49) gave compound **21** as a dark red oil (120 mg, 0.198 mmol, 55%).  $^1\text{H}$  NMR (400 MHz,  $\text{DMSO-d}_6$ )  $\delta$ : 7.99 (s, 1H), 7.75–7.74 (m, 1H), 7.71–7.70 (m, 1H), 7.59–7.57 (m, 2H), 7.56–7.55 (m, 1H), 7.47–7.45 (m, 1H), 7.42–7.41 (m, 1H), 7.31–7.30 (m, 1H), 7.17–7.15 (m, 1H), 7.10–7.09 (m, 1H), 7.00–6.98 (m, 2H), 3.96–3.90 (m, 2H), 3.78 (s, 3H), 1.74–1.69 (m, 2H), 1.43 (s, 9H), 1.43–1.41 (m, 2H), 1.27–1.25 (m, 4H), 0.85–0.82 (m, 3H);  $^{13}\text{C}$  NMR (100 MHz,  $\text{DMSO-d}_6$ )  $\delta$ : 163.3, 158.6, 158.5, 147.1, 144.8, 143.2, 137.2, 134.0, 130.7, 127.4 (2C), 127.2, 125.1, 124.8, 124.6, 123.2, 123.0, 122.62, 122.61, 116.43, 116.42, 116.11, 116.11, 114.7 (2C), 109.4, 95.0, 83.6, 55.1, 46.6, 30.8, 27.6 (3C), 26.1, 25.7, 22.0, 13.8; IR (neat,  $\text{cm}^{-1}$ )  $\nu$ : 3138 (w), 2977 (w), 2930 (w), 2870 (w), 2262 (w), 2218 (w), 1740 (s), 1714 (s), 1610 (s), 1583 (s), 1456 (s), 1236 (s), 1152 (s), 1028 (s), 798 (s), 587 (m); HRMS (ASAP+,  $m/z$ ): 606.2548 (calcd.  $\text{C}_{37}\text{H}_{38}\text{N}_2\text{O}_4\text{S}$ : 606.2552, [ $\text{M}]^+$ ).

#### 2.5.13. (E)-2-Cyano-3-(5-(10-hexyl-7-(4-methoxyphenyl)-10H-phenothiazin-3-yl)furan-2-yl)acrylic acid (**AFB-11**)

Dye **AFB-11** was made as described in Section 2.5.8 but starting with compound **21** (120 mg, 0.19 mmol) in TFA (12 mL). The crude product was purified by silica-gel column chromatography (gradient: 0–15% MeOH in  $\text{CH}_2\text{Cl}_2$ ) to obtain **AFB-11** as a black solid (83 mg, 0.15 mmol, 79%), mp. 155–160 °C (dec.).  $^1\text{H}$  NMR (400 MHz,  $\text{DMSO-d}_6$ )  $\delta$ : 7.83 (s, 1H), 7.70 (dd,  $J$  = 8.5, 2.2 Hz, 1H), 7.66 (d,  $J$  = 2.1 Hz, 1H), 7.57 (d,  $J$  = 8.8 Hz, 2H), 7.45 (dd,  $J$  = 8.4, 2.1 Hz, 1H), 7.41 (d,  $J$  = 2.1 Hz, 1H), 7.27 (d,  $J$  = 3.6 Hz, 1H), 7.18 (d,  $J$  = 3.6 Hz, 1H), 7.12 (d,  $J$  = 8.8 Hz, 1H), 7.07 (d,  $J$  = 8.6 Hz, 1H), 6.98 (d,  $J$  = 8.8 Hz, 2H), 3.92 (t,  $J$  = 6.9 Hz, 2H), 3.78 (s, 3H), 1.75–1.66 (m, 2H), 1.45–1.36 (m, 2H), 1.29–1.21 (m, 4H), 0.85–0.80 (m, 3H) (carboxylic acid proton not visible);  $^{13}\text{C}$  NMR (100 MHz,  $\text{DMSO-d}_6$ )  $\delta$ : 164.0, 158.7, 156.1, 147.9, 145.1, 142.5, 134.6, 131.2, 127.2 (2C), 125.5, 125.4, 124.5, 124.2, 123.7, 123.3, 123.1, 122.9, 118.7, 116.3, 116.0, 114.3 (2C), 113.6, 108.2, 95.4, 55.2, 46.7, 30.8, 26.1, 25.7, 22.1, 13.8; IR (neat,  $\text{cm}^{-1}$ )  $\nu$ : 3132 (w, br), 2956 (w), 2919 (w), 2847 (w), 2213 (w), 1683 (s, br), 1579 (s), 1455 (s), 1418 (s), 1236 (s), 1034 (s), 935 (w), 790 (s); HRMS (ASAP+,  $m/z$ ): 506.2024 (calcd.  $\text{C}_{32}\text{H}_{30}\text{N}_2\text{O}_4\text{S}$ : 506.2028 [ $\text{M} - \text{CO}_2$ ] $^+$ ); UV ( $\text{CH}_2\text{Cl}_2$ ,  $2 \times 10^{-5}$  M, 22 °C)  $\lambda_{\text{max}}$  (nm): 362.5 (14200), 473.0 (14800).

### 3. Results and discussion

To investigate the realm of  $\pi$ -spacers for phenothiazine dyes, we planned for the synthesis of 10 new dyes having five different  $\pi$ -spacers.



**Scheme 1.** Synthesis of dyes **AFB-1** to **AFB-11**. i) NaH, 1-bromohexane, ii) DMF, POCl<sub>3</sub>, iii) NBS, iv) Pd(PPh<sub>3</sub>)<sub>4</sub>, 4-methoxyphenylboronic acid, K<sub>2</sub>CO<sub>3</sub>, v) cyanoacetic acid, piperidine, vi) Br<sub>2</sub>, vii) NaH, 1-bromohexane, viii) Pd(PPh<sub>3</sub>)<sub>4</sub>, phenylboronic acid/4-methoxyphenylboronic acid, K<sub>2</sub>CO<sub>3</sub>, ix) Pd(OAc)<sub>2</sub>, SPhos, arylboronic acid, K<sub>2</sub>CO<sub>3</sub>, x) PdCl<sub>2</sub>(CH<sub>3</sub>CN)<sub>2</sub>, Et<sub>3</sub>N, pinacol borane, then Pd(OAc)<sub>2</sub>, SPhos, K<sub>2</sub>CO<sub>3</sub>, 5-bromo-2-thiophenecarboxaldehyde xi) cyanoacetic acid, piperidine, xii) *tert*-butyl 2-cyanoacetate, ammonium acetate, then TFA hydrolysis.

In terms of  $\pi$ -spacers, thiophenes are the common choice, although dyes containing furans are not uncommon [28,29]. We also incorporated phenyl, *meta*-fluorophenyl and 3,5-difluorophenyl to investigate six-membered spacers and electron withdrawing fluorine substituents. All these variants were made using two different auxiliary donors (*para*-methoxyphenyl and phenyl). Additionally, as a reference dye **AFB-1** was prepared without a  $\pi$ -spacer. To prevent aggregation a hexyl chain was installed at the phenothiazine core, as this chain length previously has been found efficient for phenothiazine sensitizers [30].

### 3.1. Synthesis

Dye **AFB-1** without  $\pi$ -spacer was synthesized by *N*-alkylation of 10*H*-phenothiazine, followed by a Vilsmeier-Haack formylation and a subsequent bromination by NBS. Then, a Suzuki coupling introduced the 4-methoxyphenyl auxiliary donor before the Knoevenagel condensation assembled the cyanoacrylic acid anchoring group, as shown in Scheme 1.

To synthesize the other dyes the key building block 3,7-dibromo-10-hexyl-10*H*-phenothiazine (**7**) was needed. It was synthesized in two

steps from 10*H*-phenothiazine by bromination in acetic acid followed by *N*-alkylation with 1-bromohexane as shown in Scheme 1 [31,32]. Further, the different auxiliary donors were introduced by Suzuki cross-couplings with either 4-methoxyphenylboronic acid or phenylboronic acid, yielding the unsymmetrical building blocks **8** and **9**. This reaction displayed very low chemoselectivity, and a near statistical distribution of products was obtained. To maximize the amount of the desired coupling products **8** and **9**, only 1.1 equivalents of arylboronic acid was used, resulting in a 1:2:1 distribution of starting material, monocoupled and dicoupled product. Purification by silica-gel column chromatography was facile, also allowing for recovery of building block **7**.

The dyes with furan (**AFB-10** and **AFB-11**), phenyl (**AFB-2** and **AFB-3**), *meta*-fluorophenyl (**AFB-4** and **AFB-5**) and 3,5-difluorophenyl (**AFB-6** and **AFB-7**) as  $\pi$ -spacers were prepared in a subsequent Suzuki coupling of the building blocks **8** and **9**. This was followed by a Knoevenagel condensation with cyanoacetic acid as described by Iqbal et al. [33] However, finding a reliable procedure for coupling the building blocks **8** or **9** with 5-formyl-2-thienylboronic acid proved difficult, as these reactions were usually plagued by low conversion.

A.F. Buene et al.

Dyes and Pigments 151 (2018) 263–271

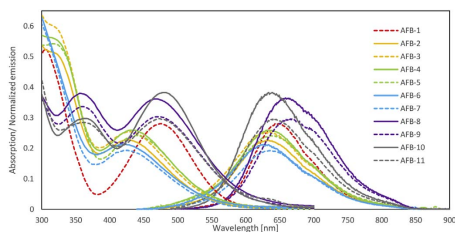


Fig. 2. Absorption spectra and normalized emission spectra for all dyes. The intersection of the absorption and normalized emission spectra gives  $E_{g,opt}$ . Each dye is excited at its ICT transition maximum absorption wavelength.

Instead, the building blocks **8** and **9** were first converted to their pinacol boronic esters in a palladium catalyzed coupling with  $\text{PdCl}_2(\text{CH}_3\text{CN})_2$ , SPhos and pinacol borane by the protocol developed by Billingsley and Buchwald [34]. Without further purification, these were then coupled with 5-bromo-2-thiophenecarboxaldehyde using  $\text{Pd}(\text{OAc})_2$ , SPhos and  $\text{K}_2\text{CO}_3$  in 1,4-dioxane and water. This gave the aldehydes **16** and **17** which were further converted in Knoevenagel condensations to **AFB-8** ( $R = \text{H}$ ) and **AFB-9** ( $R = \text{OMe}$ ). The dyes **AFB-7** and **AFB-11** were prepared via their *tert*-butyl cyanoacrylate analogs, with subsequent TFA hydrolysis to yield the final dyes. This was a more tedious route using harsher chemicals and two steps rather than one. As a result, this approach was abandoned in our further studies.

### 3.2. Photophysical properties

UV-Visible absorption spectrum of all dyes in solution ( $2 \times 10^{-5}$  M in  $\text{CH}_2\text{Cl}_2$ , Fig. 2) and on  $\text{TiO}_2$  (Fig. S3) shows a clear distinction between the five- and six-membered  $\pi$ -spacers, where the former dyes were considerably redshifted and had higher extinction coefficients than the latter. In order to obtain the values for the optical bandgaps, the emission spectra were normalized with respect to the internal charge transfer (ICT) transition peaks in the absorption spectra, and the intersect of these curves gives the bandgap energy [35]. All the photophysical properties are summarized in Table 1. Interestingly, **AFB-1** without any  $\pi$ -spacer showed similar  $\lambda_{max}$  to the dyes with five-membered spacers, albeit with a slightly lower extinction coefficient. These observations could indicate that a phenyl-based  $\pi$ -spacer is too large, twisting the aromatic system causing a weaker ICT process from the donor to the acceptor moieties, thus favoring the smaller five-membered  $\pi$ -spacers, and even no  $\pi$ -spacer.

Adsorption of the dyes onto  $\text{TiO}_2$  films resulted in blueshifts of the absorption maxima in the range of 50–60 nm (Supplementary information, Fig. S3). Deprotonation of the dye molecules in solution using triethylamine also led to blueshifts (Fig. S2), but not of the same magnitude as when adsorbed onto  $\text{TiO}_2$ . Fig. 3 compares the absorption of the four dyes with five-membered  $\pi$ -spacers in solution, deprotonated in solution and on  $\text{TiO}_2$ . This suggests there is an additional effect leading to further blueshifting of the absorption in addition to deprotonation, which is likely to be due to H-aggregation [13]. The deprotonated absorption spectra are generally in good accordance with the spectra from the  $\text{TiO}_2$  films, suggesting deprotonation of the dye molecules could be an easy way of simulating the UV/Vis-properties when adsorbed on the  $\text{TiO}_2$  photocathode.

### 3.3. Electrochemical properties

The energy levels of **AFB-1** to **AFB-11** were probed using electrochemistry to determine their position relative to the energy levels of the conduction band of  $\text{TiO}_2$  and the redox shuttle  $\text{I}^-/\text{I}_3^-$ . Due to poor film

forming properties, solution electrochemistry was employed. Cyclic voltammetry in solution for the “parent” phenothiazine building block **7** shows a very characteristic spectrum with one fully reversible process at  $E_{1/2} = 0.43$  V vs  $\text{Fc}/\text{Fc}^+$  and 3 quasi reversible processes at 1.01, 1.10 and 1.29 V (Fig. S5). The first process is attributed to the one electron process of the phenothiazine core and the formation of the radical cation. This characteristic electrochemical process is in good agreement with other phenothiazine-based molecules reported in the literature [36,37]. The processes observed at higher voltages are most likely the result of excimers or aggregates forming close to the electrode surface, similar to previous reports with related phenothiazine-containing molecules [38,39]. However, this will require additional electrochemical experimentation and lies beyond the scope of this study. Differential pulse voltammetry (DPV) was also employed to provide additional electrochemical information due to its virtue of removing the effect of electrode capacitive charging. This results in only faradaic processes and thus much higher signals than other conventional voltammetry methods can be achieved [40].

All the energy levels are reported vs. NHE in Table 1 and corresponding DPV spectra of all the dyes are shown in Supporting information (Fig. S6). The ionization potentials (HOMO level) for all the dyes were found to be between 0.67 and 0.88 V with **AFB-1** having the deepest ionization potential. In general, the electrochemical data show small differences of  $\pm 0.1$  V with regards to the HOMO levels of the dyes with different auxiliary donors. Exchanging the  $\pi$ -spacer, on the other hand, affects primarily the LUMO level of the dye, allowing for a  $\pm 0.3$  V tuning of this energy level. For the instances where the LUMO levels were extracted from the DPV measurements, the band gaps were in agreement with optical bandgaps. The electrochemical measurements confirm that the HOMO energy levels of the sensitizers are well below what is required for the dyes to be regenerated by the  $\text{I}^-/\text{I}_3^-$  electrolyte and the corresponding bandgaps ensure the LUMO levels are well above the conduction band edge of  $\text{TiO}_2$  to ensure efficient electron injection, as illustrated for the 4-methoxyphenyl series of dyes in Fig. 4.

### 3.4. Photovoltaic performance



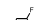


DSSC devices were fabricated from all 11 sensitizers, in order to investigate their current-voltage characteristics. Fig. 5 shows the I-V curves of the best cells from three parallels, while average values with standard deviation are given in Table 2. The photovoltaic performance of the five-membered  $\pi$ -spacer dyes was better than the dyes with phenyl-based spacers, as would be expected from the differences found in the UV/Vis measurements. In particular, the photocurrent from these cells was higher, resulting in elevated PCE values. The fill factors and open-circuit voltages were mostly unaffected by the nature of the  $\pi$ -spacer. This shows that the differences between the five- and six-membered  $\pi$ -spacers are equally apparent in devices as seen from their absorption behavior in solution.

The thiophene  $\pi$ -spacer is a very popular moiety in metal-free sensitizers for DSSCs, and these dyes were expected to perform well in this study. Furan is less commonly used, but has outperformed thiophene as a  $\pi$ -spacer in some previous studies [21,22]. This can be attributed to the smaller ring size of furan compared to thiophene, which result in a lower dihedral angle and better orbital overlap between phenothiazine and the  $\pi$ -spacer plane.

Another surprising finding was the poor performance of the 3,5-difluorophenyl containing dyes (**AFB-6** and **AFB-7**). This  $\pi$ -spacer has previously been reported to enhance the efficiency compared to a plain phenyl ring [20,41], while quite the opposite was observed in this study.

Alkoxy substituted phenyls are common auxiliary donors, providing extra electron donation and the long alkyl chains prevent aggregation. The methoxy group should be able to provide the additional electron donation without affecting aggregation. However, no clear effect from the methoxy substitution could be extracted from the dyes in this study.

**Table 1**  
Photophysical properties from spectroscopy and electrochemical measurements. The absorption spectra were measured in  $\text{CH}_2\text{Cl}_2$ , emission in  $\text{CHCl}_3$ .

Dye	Donor R gr.	$\pi$ -linker	Absorption [nm]			Emission $\lambda_{\text{max}}$ [nm]	$E_{\text{HOMO}}$ vs. NHE [V]	$E_{\text{LUMO}}$ vs. NHE [V]	$E_{\text{gchem}}$ [V]	$E_{\text{gopt}}$ [eV] <sup>a</sup>
			$\lambda_{\text{max, sol}}$	$\epsilon$ [ $\text{M}^{-1}\text{cm}^{-1}$ ]	$\lambda_{\text{max, TiO}_2}$					
<b>AFB-1</b>	OMe	None	475.0	14000	411.5	649	0.88	-1.30 <sup>c</sup>	n/a	2.18
<b>AFB-2</b>	H		425.0	11350	n/a <sup>b</sup>	631	0.75	-1.57	2.32	2.33
<b>AFB-3</b>	OMe		429.0	12700	n/a <sup>b</sup>	633	0.80	-1.40	2.20	2.33
<b>AFB-4</b>	H		431.5	12950	n/a <sup>b</sup>	632	0.73	-1.58	2.31	2.33
<b>AFB-5</b>	OMe		440.5	12050	n/a <sup>b</sup>	641	0.68	-1.66	2.34	2.34
<b>AFB-6</b>	H		419.5	10650	n/a <sup>b</sup>	626	0.76	-1.61 <sup>c</sup>	n/a	2.37
<b>AFB-7</b>	OMe		424.0	9650	n/a <sup>b</sup>	635	0.74	-1.64 <sup>c</sup>	n/a	2.38
<b>AFB-8</b>	H		466.5	18050	412.5	658	0.75	-1.35	2.10	2.12
<b>AFB-9</b>	OMe		471.0	15200	411.0	659	0.81	-1.31 <sup>c</sup>	n/a	2.12
<b>AFB-10</b>	H		479.5	19150	415.0	634	0.75	-1.50	2.25	2.18
<b>AFB-11</b>	OMe		473.0	14800	408.0	640	0.67	-1.61	2.28	2.19

<sup>a</sup>  $E_{\text{gopt}}$  was calculated from the intersection of the absorption and normalized emission spectra.

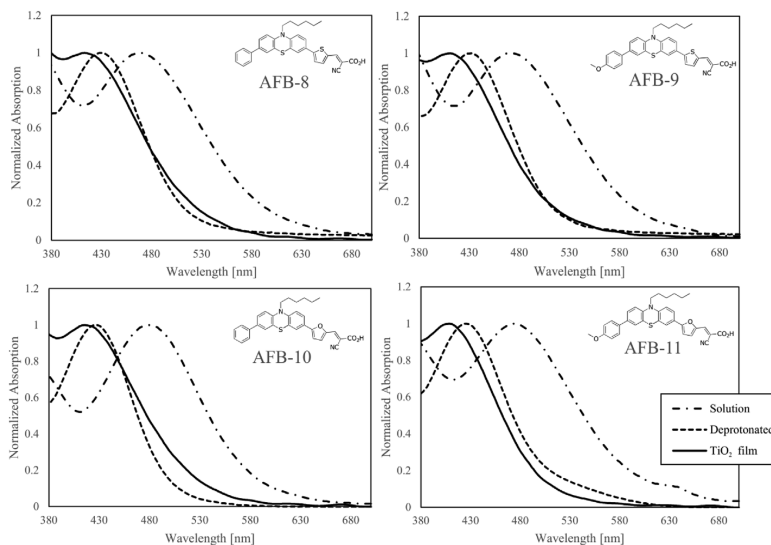
<sup>b</sup> No clear peak to assign.

<sup>c</sup> Calculated from the optical band gap ( $E_{\text{HOMO}} - E_{\text{gopt}}$ ).

The IPCE spectra were recorded for the best performing cell in each parallel of three, and the curves are plotted in Fig. 6, while the peak values and corresponding integrated short circuit current are given in Table 2. The calculated  $J_{\text{sc}}$  values from the IPCE spectra are 0.33–1.16  $\text{mA}/\text{cm}^2$  higher compared to those obtained under one sun illumination. This small difference could be due to different light intensities and the spectral mismatch from the Xenon solar simulator lamp.

The IPCE curves of the dyes with thiophene and furan  $\pi$ -spacers show the widest action spectra, compared to the narrower peaks of the six-membered dyes. The difluoro containing dyes **AFB-6** and **AFB-7** have the lowest and narrowest IPCE spectra of the series, while the furan based **AFB-10** has the highest plateau of all the dyes.

Although the efficiency of the reference dye **AFB-1** is the second highest in the series, its IPCE spectrum is significantly narrower compared to the dyes with five-membered  $\pi$ -spacers. Further efforts should



**Fig. 3.** Absorption spectra of **AFB-8**, **AFB-9**, **AFB-10** and **AFB-11** in solution, deprotonated in solution and on  $\text{TiO}_2$  films. The staining solution concentration was 0.5 mM in THF:acetonitrile (57:43, v:v) with 5 mM of CDCA. Deprotonation in solution was done with a drop of triethylamine into the UV cuvette.



A.F. Buene et al.

Dyes and Pigments 151 (2018) 263–271

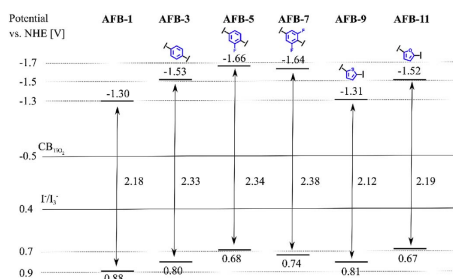


Fig. 4. HOMO and LUMO levels for the series of dyes with the 4-methoxyphenyl auxiliary donor. HOMO levels determined from DPV electrochemical measurements, and LUMO levels are derived from the optical band gaps.

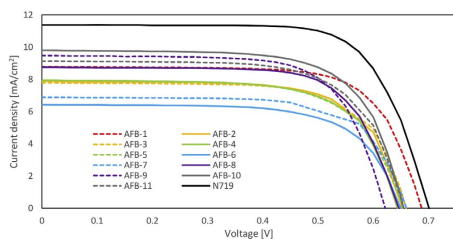


Fig. 5. J-V curves for all dyes under 1 sun AM1.5G illumination. The curve from the best cell from each parallel is included.

be focused on increasing the absorption of the sensitizers. From this study, it is clear that in order to improve the impact of  $\pi$ -spacers for the phenothiazine scaffold, it is necessary to extend the conjugation further than thiophene or furan. Meanwhile, not distorting the orbital overlap

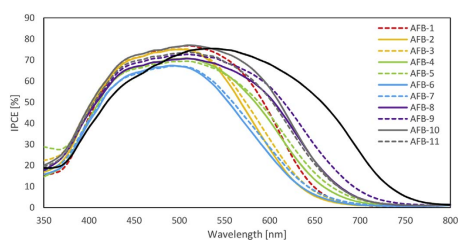


Fig. 6. IPCE spectra of all dyes.

between the phenothiazine core and the anchoring group is of high importance, and other challenges related to aggregation from  $\pi$ - $\pi$  stacking may occur when increasing the size of the  $\pi$ -spacers.

#### 4. Conclusion

We have delved into the realm of  $\pi$ -spacers for phenothiazine sensitizers in DSSCs, and eleven new dyes have been synthesized. The aim of this study was to compare the impact of five different  $\pi$ -spacers in two complementary series of dyes, including a dye with no  $\pi$ -spacer. The five membered  $\pi$ -spacers thiophene and furan were found to be superior to the six membered  $\pi$ -spacer dyes, with furan performing marginally better than thiophene. To our surprise, the general effect of introducing a  $\pi$ -spacer was not always positive, as demonstrated by the reference dye AFB-1, which outperformed all but the best furan dye, AFB-10.

To further improve this class of sensitizers, the use of  $\pi$ -spacers based on five membered heterocycles is a viable solution, but the conjugation should be increased beyond one thiophene or furan unit. Naturally, increasing the electron donating power of the phenothiazine donor could also improve the efficiency further, which can be achieved by altering and increasing the number of auxiliary donors.

Table 2

Photovoltaic properties from DSSCs fabricated with all 11 dyes. All values are averages from three cells. Standard deviation for all parameters can be found in Table S2.

Dye <sup>a</sup>	Donor R gr.	$\pi$ -linker	$J_{sc}$ [mA/cm <sup>2</sup> ]	$V_{oc}$ [V]	FF	PCE [%]	IPCE [%] at $\lambda_{max}$	IPCE $J_{sc}$ [mA/cm <sup>2</sup> ] <sup>c</sup>
AFB-1	OMe	None	8.64	0.68	0.71	4.15 $\pm$ 0.17	77 (510)	9.20
AFB-2	H		7.83	0.66	0.68	3.53 $\pm$ 0.04	75 (500)	8.16
AFB-3	OMe		7.83	0.66	0.67	3.46 $\pm$ 0.14	75 (500)	8.56
AFB-4	H		7.63	0.65	0.69	3.43 $\pm$ 0.07	71 (510)	8.74
AFB-5	OMe		7.87	0.65	0.67	3.41 $\pm$ 0.05	69 (510)	9.03
AFB-6	H		6.28	0.65	0.68	2.79 $\pm$ 0.02	67 (490)	7.27
AFB-7	OMe		6.77	0.66	0.67	2.96 $\pm$ 0.06	67 (490)	7.57
AFB-8	H		9.14	0.63	0.68	3.87 $\pm$ 0.08	71 (510)	9.68
AFB-9	OMe		9.56	0.62	0.68	4.03 $\pm$ 0.03	73 (510)	10.48
AFB-10	H		9.44	0.67	0.69	4.34 $\pm$ 0.05	77 (510)	10.44
AFB-11	OMe		9.15	0.65	0.67	3.97 $\pm$ 0.05	74 (510)	9.88
N719 <sup>b</sup>	–	–	11.32	0.69	0.72	5.64 $\pm$ 0.04	75 (540)	12.44

<sup>a</sup> Thickness of active TiO<sub>2</sub> was 12.5  $\mu$ m and scattering layer was 5  $\mu$ m. Electrolyte contained 0.5 M 1-butyl-3-methylimidazolium iodide, 0.1 M lithium iodide, 0.05 M I<sub>2</sub> and 0.5 M *tert*-butylpyridine in acetonitrile.

<sup>b</sup> Staining solution for N719 (from Solaronix) was ethanol.

<sup>c</sup> IPCE spectra integrated and normalized according to the ASTM G173 AM 1.5G solar spectrum available from NREL (<http://rredc.nrel.gov/solar/spectra/am1.5/>).

A.F. Buene et al.

Dyes and Pigments 151 (2018) 263–271

### Acknowledgements

The authors would like to thank the NV-faculty and the Department of Chemistry at NTNU for financial support, engineer Julie Asmussen and Dr. Susana Villa Gonzalez for HRMS analyses, Roger Aarvik for technical support and MSc Henrik Holthe Kringhaug for the synthesis of the precursors of AFB-1. The Research Council of Norway is acknowledged for the support to the Norwegian Micro- and Nano-Fabrication Facility, NorFab, project number 245963/F50.

### Appendix A. Supplementary data

Supplementary data related to this article can be found at <http://dx.doi.org/10.1016/j.dyepig.2018.01.011>.

### References

- O'Regan B, Grätzel M. A low-cost, high-efficiency solar cell based on dye-sensitized colloidal TiO<sub>2</sub> films. *Nature* 1991;353:737–40.
- Freitag M, Teuscher J, Saygili Y, Zhang X, Giordano F, Liska P, et al. Dye-sensitized solar cells for efficient power generation under ambient lighting. *Nat. Photonics* 2017;11:372–8.
- Jacoby M. The future of low-cost solar cells. *Chem. Eng News* 2016;94:30–5.
- Freitag M, Daniel Q, Pazoki M, Sveinbjörnsson K, Zhang J, Sun L, et al. High-efficiency dye-sensitized solar cells with molecular copper phenanthroline as solid hole conductor. *Energy Environ Sci* 2015;8:2634–7.
- Freitag M, Giordano F, Yang W, Pazoki M, Hao Y, Zietz B, et al. Copper phenanthroline as a fast and high-performance redox mediator for dye-sensitized solar cells. *J. Phys. Chem. C* 2016;120:9558–603.
- Hao Y, Yang W, Zhang L, Jiang R, Mijangos E, Hammarström L, et al. A small electron donor in cobalt complex electrolyte significantly improves efficiency in dye-sensitized solar cells. *Nat Commun* 2016;7:13934.
- Yum J-H, Baranoff E, Kessler F, Mochl T, Ahmad S, Bessho T, et al. A cobalt complex redox shuttle for dye-sensitized solar cells with high open-circuit potentials. *Nat Commun* 2012;3:631.
- Kakiage K, Aoyama Y, Yano T, Oya K, Fujisawa J-I, Hanaya M. Highly-efficient dye-sensitized solar cells with collaborative sensitization by silyl-anchor and carboxy-anchor dyes. *Chem Commun* 2015;51:15894–7.
- Robertson N. Optimizing dyes for dye-sensitized solar cells. *Angew Chem Int Ed* 2006;45:2338–45.
- Higashino T, Imahori H. Porphyrins as excellent dyes for dye-sensitized solar cells: recent developments and insights. *Dalton Trans* 2015;44:448–63.
- Mathew S, Yella A, Gao P, Humphry-Baker R, Curshed BFE, Ashari-Astani N, et al. Dye-sensitized solar cells with 13% efficiency achieved through the molecular engineering of porphyrin sensitizers. *Nat Chem* 2014;6:242–7.
- Ahmad S, Guillen E, Kavan L, Grätzel M, Nazeeruddin MK. Metal free sensitizer and catalyst for dye sensitized solar cells. *Energy Environ Sci* 2013;6:3439–66.
- Mishra A, Fischer MK, Bätierle P. Metal-free organic dyes for dye-sensitized solar cells: from structure: property relationships to design rules. *Angew Chem Int Ed* 2009;48:2474–99.
- Sheibani E, Zhang L, Liu P, Xu B, Mijangos E, Boschloo G, et al. A study of oligothiophene-acceptor dyes in p-type dye-sensitized solar cells. *RSC Adv* 2016;6:18165–77.
- Tian H, Yang X, Chen R, Pan Y, Li L, Hagfeldt A, et al. Phenothiazine derivatives for efficient organic dye-sensitized solar cells. *Chem Commun* 2007:3741–3.
- Tian H, Yang X, Cong J, Chen R, Liu J, Hao Y, et al. Tuning of phenoxazine chromophores for efficient organic dye-sensitized solar cells. *Chem Commun* 2009:6288–90.
- Lin R-Y, Wu F-L, Li C-T, Chen P-Y, Ho K-C, Lin J-T. High-performance aqueous/organic dye-sensitized solar cells based on sensitizers containing triethylene oxide methyl ether. *ChemSusChem*. 2015;8:2503–13.
- Luo J-S, Wan Z-Q, Jia C-Y. Recent advances in phenothiazine-based dyes for dye-sensitized solar cells. *Chin Chem Lett* 2016;27:1304–18.
- Huang Z-S, Meier H, Cao D. Phenothiazine-based dyes for efficient dye-sensitized solar cells. *J Mater Chem C* 2016;4:2404–26.
- Lee M-W, Kim J-Y, Son HJ, Kim JY, Kim B, Kim H, et al. Tailoring of energy levels in d- $\pi$ -a organic dyes via fluorination of acceptor units for efficient dye-sensitized solar cells. *Sci Rep* 2015;5:7711.
- Wan Z, Jia C, Duan Y, Zhou L, Lin Y, Shi Y. Phenothiazine-triphenylamine based organic dyes containing various conjugated linkers for efficient dye-sensitized solar cells. *J Mater Chem* 2012;22:25140–7.
- Kim SH, Kim HW, Sakong C, Namgoong J, Park SW, Ko MJ, et al. Effect of five-membered heteroaromatic linkers to the performance of phenothiazine-based dye-sensitized solar cells. *Org Lett* 2011;13:5784–7.
- Bhim Raju T, Vaghasiya JV, Afroz MA, Soni SS, Iyer PK. Design, synthesis and DSSC performance of o-fluorine substituted phenylene spacer sensitizers: effect of TiO<sub>2</sub> thickness variation. *Phys Chem Chem Phys* 2016;18:28485–91.
- Bodedla GB, Thomas KRJ, Li C-T, Ho K-C. Functional tuning of phenothiazine-based dyes by a benzimidazole auxiliary chromophore: an account of optical and photo-voltaic studies. *RSC Adv* 2014;4:53588–601.
- Hao Y, Gabriellsson E, Lohse PW, Yang W, Johansson EMJ, Hagfeldt A, et al. Peripheral hole acceptor moieties on an organic dye improve dye-sensitized solar cell performance. *Adv Sci* 2015;2:1500174.
- Ozawa H, Awa M, Ono T, Arakawa H. Effects of dye-adsorption solvent on the performances of the dye-sensitized solar cells based on black dye. *Chem Asian J* 2012;7:156–62.
- Joly D, Pellejà L, Narbey S, Oswald F, Chiron J, Clifford JN, et al. A robust organic dye for dye sensitized solar cells based on iodine/iodide electrolytes combining high efficiency and outstanding stability. *Sci Rep* 2014;4:4033.
- Hao Y, Saygili Y, Cong J, Eriksson A, Yang W, Zhang J, et al. Novel blue organic dye for dye-sensitized solar cells achieving high efficiency in cobalt-based electrolytes and by Co-Sensitization. *ACS Appl. Mater. Interfaces* 2016;8:32797–804.
- Liu P, Sharmoukh W, Xu B, Li YY, Boschloo G, Sun L, et al. Novel and stable D-A- $\pi$ -A dyes for efficient solid-state dye-sensitized solar cells. *ACS Omega* 2017;2:1812–9.
- Hua Y, Chang S, Huang DD, Zhou X, Zhu XJ, Zhao JZ, et al. Significant improvement of dye-sensitized solar cell performance using simple phenothiazine-based dyes. *Chem Mater* 2013;25:2146–53.
- Elkassih SA, Sista P, Magurudeniya HD, Papadimitratos A, Zakhidov AA, Biewer MC, et al. Phenothiazine semiconducting polymer for light-emitting diodes. *Macromol Chem Phys* 2013;214:572–7.
- Hurt CR, Lingappa V, Freeman B, Ategbu A, Kitaygorodskyy A. Phenothiazine derivatives as antiviral agents and their preparation, pharmaceutical compositions and use in the treatment of viral infections. 2014. Patent US 8759336B2.
- Iqbal Z, Wu W-Q, Huang Z-S, Wang L, Kuang D-B, Meier H, et al. Trilateral  $\pi$ -conjugation extensions of phenothiazine-based dyes enhance the photovoltaic performance of the dye-sensitized solar cells. *Dyes Pigments* 2016;124:63–71.
- Hilingsley KL, Buchwald SL. An improved system for the palladium-catalyzed borylation of aryl halides with pinacol borane. *J Org Chem* 2008;73:5589–91.
- Pazoki M, Cappel UB, Johansson EMJ, Hagfeldt A, Boschloo G. Characterization techniques for dye-sensitized solar cells. *Energy Environ Sci* 2017;10:672–709.
- Nagarajan B, Kushwaha S, Elumalai R, Mandal S, Ramanujam K, Raghavachari D. Novel ethynyl-pyrene substituted phenothiazine based metal free organic dyes in DSSC with 12% conversion efficiency. *J Mater Chem A* 2017;5:10289–300.
- Xie Z, Midya A, Loh KP, Adams S, Blackwood DJ, Wang J, et al. Highly efficient dye-sensitized solar cells using phenothiazine derivative organic dyes. *Prog Photovolt: Res Appl* 2010;18:573–81.
- Krämer CS, Zeiter K, Müller TJJ. First synthesis and electronic properties of (hetero)aryl bridged and directly linked redox active phenothiazinyl dyads and triads. *Tetrahedron Lett* 2001;42:8619–24.
- Zhao Y, Zhang Q, Chen K, Gao H, Qi H, Shi X, et al. Triphenothiazinyl triazacorones: donor-acceptor molecular graphene exhibiting multiple fluorescence and electrogenerated chemiluminescence emissions. *J Mater Chem C* 2017;5:4293–301.
- Bard AJ, Faulkner LR. *Electrochemical methods: fundamentals and applications*. second ed. New York: John Wiley and Sons; 2001.
- Lin Y-D, Chow TJ. Fluorine substituent effect on organic dyes for sensitized solar cells. *J Photochem Photobiol A Chem* 2012;230:47–54.

## Supplementary information

### Effect of $\pi$ -linkers on Phenothiazine Sensitizers for Dye-Sensitized Solar Cells

Audun Formo Buene, Nora Uggerud, Solon P. Economopoulos, Odd R. Gautun, Bård Helge Hoff\*

Department of Chemistry, Norwegian University of Science and Technology, Høgskoleringen 5, NO-7491 Trondheim, Norway

\* Corresponding author. Tel.: +47 73593973; E-mail address: [bard.helge.hoff@chem.ntnu.no](mailto:bard.helge.hoff@chem.ntnu.no) (B. H. Hoff).

<b>ABSORPTION AND EMISSION</b>	<b>2</b>
<b>DEVICES</b>	<b>4</b>
<b>ELECTROCHEMICAL MEASUREMENTS</b>	<b>5</b>
<b>EXPERIMENTAL INFORMATION</b>	<b>7</b>
<b>NMR</b>	<b>22</b>
<b>REFERENCES</b>	<b>33</b>

## Absorption and emission

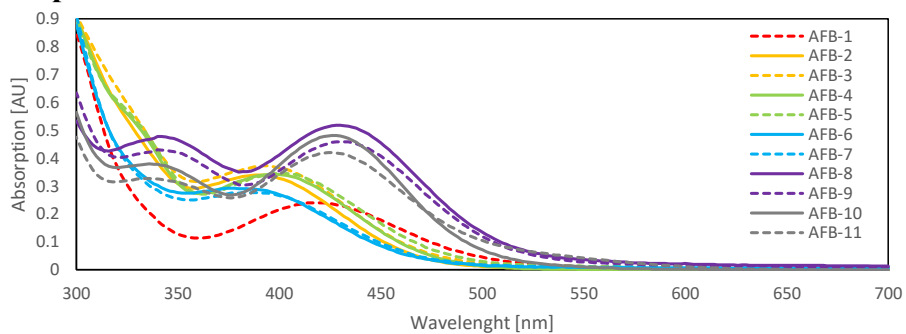


Fig. S1. UV/Visible absorption spectrum of all dyes when deprotonated with triethylamine.

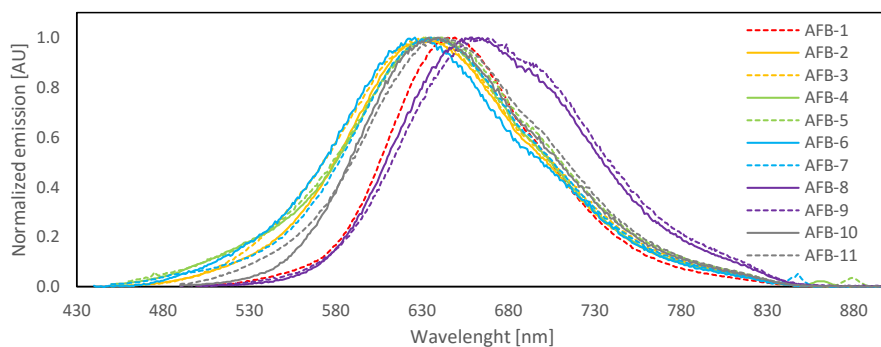


Fig. S2. Normalized emission spectrum of all dyes. Each dye is excited at its ICT transition maximum absorption wavelength.

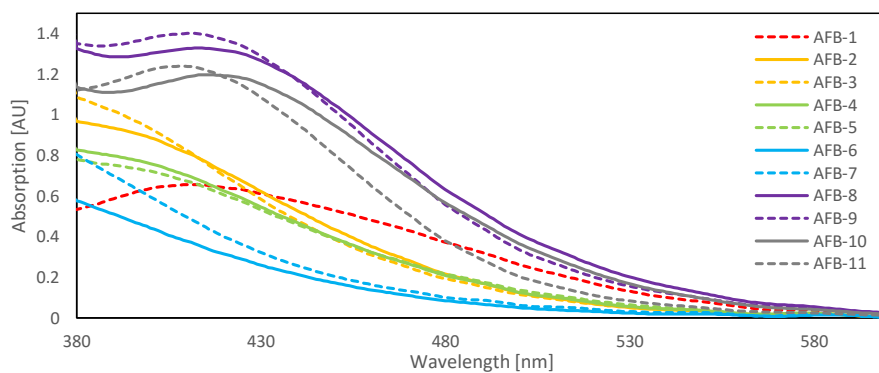


Fig. S3. UV/Visible absorption spectrum of all dyes on TiO<sub>2</sub> films (2.5  $\mu\text{m}$ , 18NR-T, Dyesol).

Tab. S1. Intersection between absorption and the normalized emission spectra in Figure 2, and corresponding band gaps in eV.

Dye	Intersection [nm]	Band gap [eV]
AFB-1	572	2.17
AFB-2	542	2.29
AFB-3	538	2.30
AFB-4	540	2.30
AFB-5	540	2.30
AFB-6	537	2.31
AFB-7	543	2.28
AFB-8	586	2.12
AFB-9	587	2.11
AFB-10	569	2.18
AFB-11	570	2.18

Tab. S1. Photovoltaic properties for all dyes including standard deviation.

Dye <sup>a</sup>	J <sub>sc</sub> [mA/cm <sup>2</sup> ]	V <sub>oc</sub> [V]	FF	PCE [%]
AFB-1	8.64 ± 0.27	0.68 ± 0.01	0.71 ± 0.01	4.15 ± 0.17
AFB-2	7.83 ± 0.25	0.66 ± 0.01	0.68 ± 0.02	3.53 ± 0.04
AFB-3	7.83 ± 0.04	0.66 ± 0.00	0.67 ± 0.03	3.46 ± 0.14
AFB-4	7.63 ± 0.28	0.65 ± 0.01	0.69 ± 0.01	3.43 ± 0.07
AFB-5	7.87 ± 0.05	0.65 ± 0.01	0.67 ± 0.00	3.41 ± 0.05
AFB-6	6.28 ± 0.12	0.65 ± 0.00	0.68 ± 0.01	2.79 ± 0.02
AFB-7	6.77 ± 0.11	0.66 ± 0.00	0.67 ± 0.00	2.96 ± 0.06
AFB-8	9.14 ± 0.45	0.63 ± 0.02	0.68 ± 0.03	3.87 ± 0.08
AFB-9	9.56 ± 0.15	0.62 ± 0.01	0.68 ± 0.01	4.03 ± 0.03
AFB-10	9.44 ± 0.31	0.67 ± 0.01	0.69 ± 0.01	4.34 ± 0.05
AFB-11	9.15 ± 0.07	0.65 ± 0.00	0.67 ± 0.01	3.97 ± 0.05
N719 <sup>b</sup>	11.32 ± 0.06	0.69 ± 0.01	0.72 ± 0.01	5.64 ± 0.04

## Devices

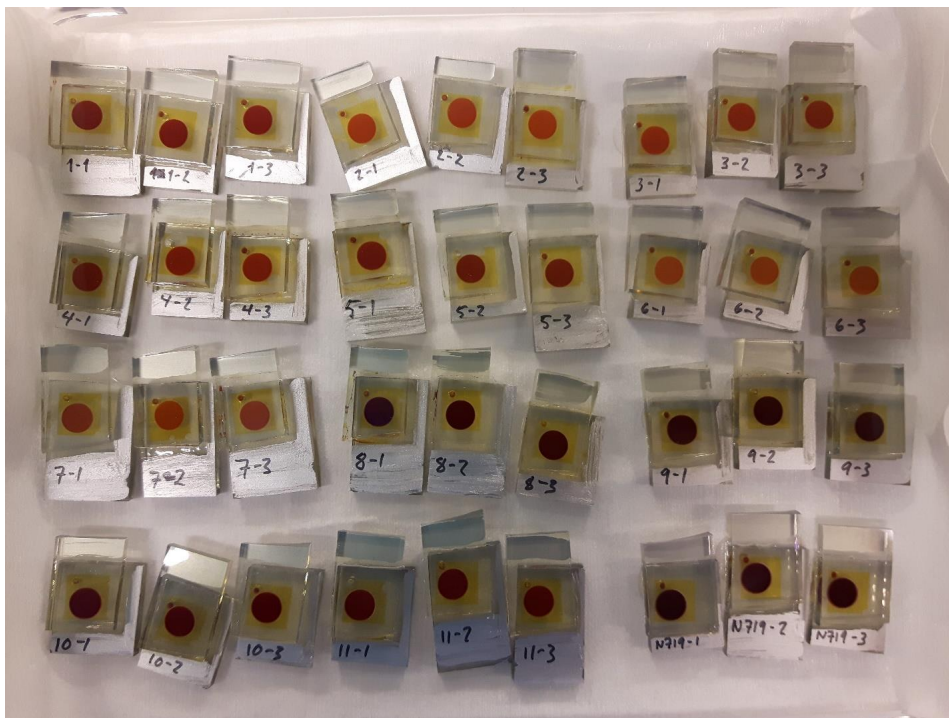


Fig. S4. The fabricated DSSC devices for this study.

## Electrochemical measurements

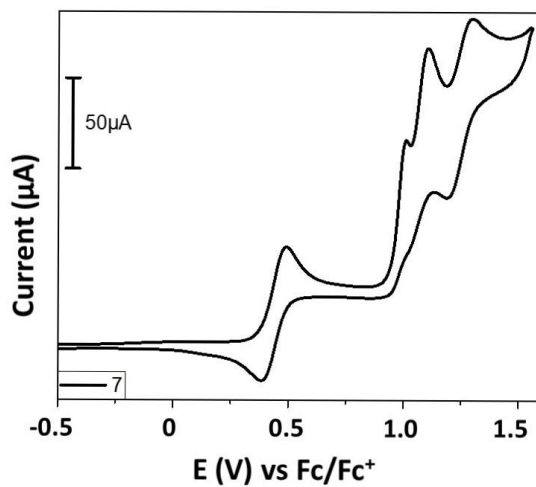


Fig. S5. Cyclic voltammogram of "parent" molecule 7. All measurements were run in solution with TBAPF<sub>6</sub> as supporting electrolyte (0.1 M in DMF). Scan rate 100 mV/s.

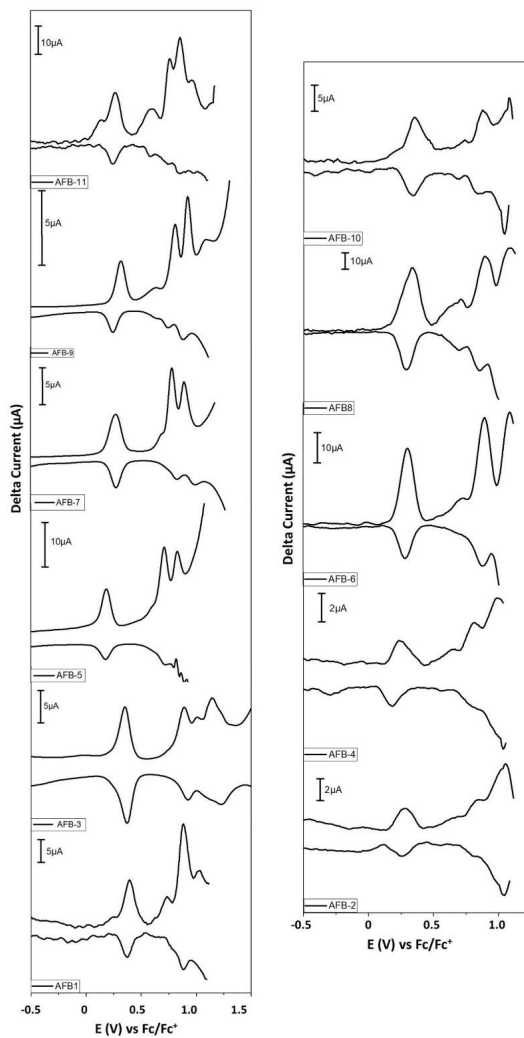


Fig. S6. Differential pulse voltammetry data for the synthesized dyes. The 4-methoxyphenyl series of dyes (left) and the phenyl series of dyes (right). All measurements were run in solution with TBAPF6 as supporting electrolyte (0.1 M in DMF). Experimental: Step height: 25 mV, Step Width: 5 mV, Pulse height: 50 ms, Pulse Width: 100 ms.



## Experimental information

### 2.1 Materials and reagents

All reactions were carried out under nitrogen atmosphere, and all synthesis reagents were acquired from Sigma Aldrich.

### 2.2 Analytical instruments

$^1\text{H}$  and  $^{13}\text{C}$  NMR spectra were recorded at 22 °C on either a Bruker 400 or 600 MHz spectrometer in  $\text{DMSO-}d_6$ . All chemical shifts are reported in ppm, and the spectra were calibrated using the signal of  $\text{DMSO}$  at 2.50 ppm ( $^1\text{H}$ ) and 39.52 ( $^{13}\text{C}$ ), or that of of TMS (0 ppm) in  $\text{CDCl}_3$ . Infrared absorption (IR) spectra were recorded with a FTIR Thermo Nicolet Nexus FT-IR Spectrometer using a Smart Endurance reflection cell. Reported frequencies were in the range of 4000–400  $\text{cm}^{-1}$ . UV/Vis analyses were performed with a Hitachi U-1900 UV/Vis-spectrophotometer using quartz cuvettes (10 mm) and scanning from 300–700 nm. Extinction coefficients were calculated from Lambert-Beer's law. UV/Vis measurements of sensitized  $\text{TiO}_2$  films was performed in the same spectrophotometer with a non-stained electrode as the background. Melting points were determined with a Stuart SMP40 automatic melting point instrument. Accurate mass determination in positive and negative mode was performed on a "Synapt G2-S" Q-TOF instrument from Waters<sup>TM</sup>. The samples were ionized by the use of ASAP probe (APCI) or by ESI. Spectra processing was done by Waters<sup>TM</sup> Software (Masslynx v4.1 SCN871). Fluorescence spectrophotometry was measured with a Varian Cary Eclipse instrument. All dyes were measured in chloroform.

Electrochemistry studies were performed using a standard three-electrode cell under argon atmosphere. All measurements were performed with Ar bubbling into the electrochemical cell for 15 min 10 s prior to the measurements; the Ar was turned to "blanket-mode". Platinum wires (99.99%) were used as working and pseudo-reference electrodes and platinum gauze (55 mesh, 99.9%) as counter electrode. Tetrabutylammonium hexafluorophosphate ( $\text{TBAPF}_6$ , 98%) was used as the electrolyte and was recrystallized three times from acetone and dried in vacuum at ca 100 °C before each experiment. Measurements were recorded using an EG&G Princeton Applied Research potentiostat/galvanostat Model Verstastat 3 connected to a personal computer running VersaStudio software. The scan rate was kept constant for all CV runs at 100 mV/s while for differential pulse voltammetry measurements, the following parameters were used Step height: 25 mV, Step Width: 5 mV, Pulse height: 50 ms, Pulse Width: 100 ms. All results were calibrated using commercially available ferrocene (purified by sublimation) as internal standard. All samples were studied in anhydrous DMF solution. To calculate HOMO/LUMO levels, using the potentials obtained the following equations from Cardona et al. were used [1]:

$$E_{\text{HOMO}} = 2 (E_{[\text{ox vs. Fe/Fc}^+]} + 5.1) \text{ (eV)}$$

$$E_{\text{LUMO}} = 2 (E_{[\text{red vs. Fe/Fc}^+]} + 5.1) \text{ (eV)}$$

For HOMO–LUMO estimations, the onset of the peak was considered. For conversions to NHE, a value of -4.5 eV was used as equivalent to 0.0 V vs. NHE. [2]

### *Device fabrication*

The cell fabrication is conducted based on the procedure from Hao et al. [3] TEC-8 FTO glass supplied by Dyesol was washed with Deconex 21 (2 g/L H<sub>2</sub>O) in an ultrasonic bath for 45 minutes, and then rinsed with deionized water and ethanol before air drying. Further cleaning was done in a UV-ozone cleaner for 15 minutes (Novascan PSD PRO-UV T6). A blocking layer was deposited by immersion of the FTO glass in an aq. solution of TiCl<sub>4</sub> (40 mM) for 30 minutes at 70 °C, rinsing with deionized water and ethanol followed by another immersion for 30 minutes in an aq. solution of TiCl<sub>4</sub> (40 mM) at 70 °C, then rinsing with deionized water and ethanol.

Five layers of transparent TiO<sub>2</sub> paste (18NR-T, Dyesol) were screen printed on the FTO glass (mesh count 250, active area 0.238 cm<sup>2</sup>). Between each layer, the electrodes were heated to 125 °C for 2-3 minutes. Finally, a scattering layer (WER2-O, Dyesol) was screen printed, and the electrodes were sintered at 500 °C for 30 minutes. The thickness of the sintered TiO<sub>2</sub> was measured to 17.5 μm (12.5 μm + 5 μm) with a profilometer (Veeco, Dektak 150). The electrodes were then post treated with TiCl<sub>4</sub> using the same conditions previously described for 30 minutes.

Counter electrodes were fabricated by drilling holes in the FTO glass with a diamond drill bit. The catalytic Pt layer was deposited by dropcasting a 10 mM solution of H<sub>2</sub>PtCl<sub>6</sub> in 2-propanol (5 μL/cm<sup>2</sup>), followed by firing at 400 °C for 15 minutes. [4]

Before staining, the electrodes were annealed with a hot air gun at 480 °C for 25 minutes. The staining solution had 5 × 10<sup>-4</sup> M dye concentration, with a 10-fold amount of CDCA in a mixture of acetonitrile/THF (43:57, v/v). The dielectric constant for this solution is estimated to be around 20 Fm<sup>-1</sup>, which for Black dye is reported as the optimal dielectric constant. [5] N719 was stained from a 0.5 mM solution in ethanol. The electrodes were stained for 20 hours, then rinsed in acetonitrile for 2 minutes and dried under N<sub>2</sub> flow. The cells were sealed with a 25 μm Surlyn (Solaronix) gasket, melted with a 50 W PTC heat element for 3 × 20 seconds per cell.

The electrolyte was made following a procedure from Demadrille et al. [6], containing 0.5 M 1-butyl-3-methylimidazolium iodide, 0.1 M lithium iodide, 0.05 M I<sub>2</sub> and 0.5 M *tert*-butylpyridine in acetonitrile. This was injected by vacuum backfilling before the filling hole was sealed with Surlyn and a circular glass cover slip. The contacts for the anode and cathode were painted with a conductive silver paint (Electrolube, SCP) before characterization.

### *Device characterization*

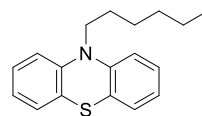
The device's J-V characteristics were measured with a Keithley 2450 under a Sciencetech SP300B solar simulator with an AM 1.5 G filter, calibrated to 100 mW/cm<sup>2</sup> with a Newport Reference Solar Cell and Meter (91150V). All cells were masked with a 0.1547 cm<sup>2</sup> black mask before characterization.

IPCE measurements were obtained from a device fabricated with a halogen lamp (Ocean Optics HL-2000), a monochromator (Spectral Products CM110), connected to the Keithley 2450. The light intensity was determined using a NIST traceable calibrated photodiode (Thorlabs, FDS100-CAL).

### 2.3 Synthesis

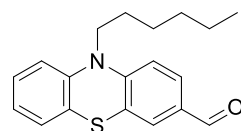
#### Synthesis of 10-hexyl-10*H*-phenothiazine (2) [7]

10*H*-Phenothiazine (5.00 g, 25.1 mmol) and NaH (904 mg, 37.7 mmol) were mixed before dry THF (85 mL) was added under N<sub>2</sub> atmosphere. The reaction was left stirring at 22 °C for 15 minutes. 1-Bromohexane (5.29 mL, 6.22 g, 37.7 mmol) was added dropwise over 30 minutes and the mixture was heated to reflux. After 24 hours the reaction was cooled to room temperature and quenched with an aqueous NH<sub>4</sub>Cl (50 mL, 5 wt%) solution, and the reaction mixture was extracted with EtOAc (3 × 50 mL). The combined organic phases were dried over anhydrous Na<sub>2</sub>SO<sub>4</sub>, filtered and the solvents were removed in vacuo. The crude product was purified by silica-gel column chromatography (*n*-pentane, R<sub>f</sub>= 0.17) to obtain compound **2** as a clear oil (5.12 g, 18.06 mmol, 72%). <sup>1</sup>H NMR (400 MHz, DMSO-*d*<sub>6</sub>) δ: 7.20-7.15 (m, 2H), 7.14-7.11 (m, 2H), 6.99-6.96 (m, 2H), 6.94-6.89 (m, 2H), 3.82 (t, *J* = 7.0 Hz, 2H), 1.69-1.609 (m, 2H), 1.39-1.30 (m, 2H), 1.23-1.17 (m, 4H), 0.82-0.77 (m, 3H). <sup>1</sup>H NMR recorded in CDCl<sub>3</sub> was in accordance with reported data. [8]



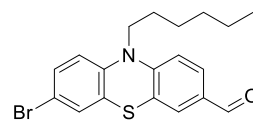
#### Synthesis of 10-hexyl-10*H*-phenothiazine-3-carbaldehyde (3) [8]

10-Hexyl-10*H*-phenothiazine (**2**) (10.0 g, 35.3 mmol) was dissolved in a mixture of dry 1,2-dichloroethane (300 mL) and DMF (12 mL) followed by cooling to 0 °C. POCl<sub>3</sub> (14 mL, 23.0 g, 150 mmol) was added slowly and the mixture heated to reflux and stirred for 12 hours. Water (500 mL) was added, and the aqueous phase was extracted with chloroform (3 × 300 mL). The combined organic phases were dried over anhydrous Na<sub>2</sub>SO<sub>4</sub>, then filtered and the solvents were removed in vacuo. The crude product was purified by silica-gel column chromatography (hexane:EtOAc, 9:1, R<sub>f</sub>= 0.32) to yield compound **3** as a yellow solid (8.24 g, 26.5 mmol, 75%). <sup>1</sup>H NMR (600 MHz, CDCl<sub>3</sub>) δ: 9.78 (s, 1H), 7.63 (d, *J* = 8.5 Hz, 1H), 7.58 (s, 1H), 7.18-7.13 (m, 1H), 7.10 (d, *J* = 7.6 Hz, 1H), 6.96 (t, *J* = 7.6 Hz, 1H), 6.88 (t, *J* = 8.5 Hz, 2H), 3.88 (t, *J* = 7.2 Hz, 2H), 1.84-1.77 (m, 2H), 1.47-1.41 (m, 2H), 1.34-1.27 (m, 4H), 0.87 (t, *J* = 7.1 Hz, 3H). <sup>1</sup>H NMR was in accordance with reported literature. [8]



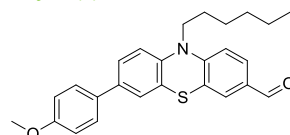
#### Synthesis of 7-bromo-10-hexyl-10*H*-phenothiazine-3-carbaldehyde (4) [8]

Compound **3** (8.40 g, 27.0 mmol) was dissolved in THF (300 mL) and cooled to 0 °C. NBS (5.50 g, 30.9 mmol) was added, the solution was heated to 22 °C, and stirred for 2 hours. Water (300 mL) was added, and the aqueous phase was extracted with dichloromethane (3 × 150 mL). The combined organic phases were dried over anhydrous Na<sub>2</sub>SO<sub>4</sub>, then filtered and the solvents were removed in vacuo. The crude product was purified by silica-gel column chromatography (CH<sub>2</sub>Cl<sub>2</sub>) to yield compound **4** as a yellow solid (8.20 g, 21.0 mmol, 68%). <sup>1</sup>H NMR (400 MHz, CDCl<sub>3</sub>) δ: 9.76 (s, 1H), 7.60 (dd, *J* = 8.5, 1.9 Hz, 1H), 7.50 (d, *J* = 1.9 Hz, 1H), 7.19 (dd, *J* = 8.6, 2.3 Hz, 1H), 7.13 (d, *J* = 2.3 Hz, 1H), 6.85 (d, *J* = 8.5 Hz, 1H), 6.66 (d, *J* = 8.7 Hz, 1H), 3.79 (t, *J* = 7.2 Hz, 2H), 1.79-1.70 (m, 2H), 1.45-1.36 (m, 2H), 1.33-1.22 (m, 4H), 0.86 (t, *J* = 6.9 Hz, 3H). <sup>1</sup>H NMR was in accordance with reported literature. [8]



#### Synthesis of 10-hexyl-7-(4-methoxyphenyl)-10*H*-phenothiazine-3-carbaldehyde (5)

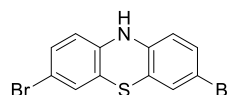
Compound **4** (3.50 g, 8.97 mmol), 4-methoxyphenylboronic acid (1.50 g, 9.86 mmol), Pd(PPh<sub>3</sub>)<sub>4</sub> (0.11 g, 0.10 mmol) and K<sub>2</sub>CO<sub>3</sub> (4.96 g, 35.9 mmol) were mixed. Degassed 1,4-Dioxane (100 mL) and water (100 mL) were added under N<sub>2</sub> atmosphere while stirring. The reaction mixture was heated to 80 °C and left stirring for 2 hours before cooling



to 22 °C. Water (200 mL) was added to the reaction mixture and CH<sub>2</sub>Cl<sub>2</sub> (3 × 150 mL) was used for extraction. The combined organic phases were washed with water and dried over anhydrous Na<sub>2</sub>SO<sub>4</sub>, filtered and the solvents were removed in vacuo. The crude product was purified by silica-gel column chromatography (*n*-pentane:EtOAc, 9:1, R<sub>f</sub>= 0.18) to obtain compound **5** as a brown oil (2.37 g, 5.74 mmol, 64%). <sup>1</sup>H NMR (600 MHz, CDCl<sub>3</sub>) δ: 9.78 (s, 1H), 7.63 (d, *J* = 8.4 Hz, 1H), 7.58 (s, 1H), 7.45 (d, *J* = 8.8 Hz, 2H), 7.32 (dd, *J* = 8.4, 2.0 Hz, 1H), 7.28 (d, *J* = 2.0 Hz, 1H), 6.95 (d, *J* = 8.8 Hz, 2H), 6.92-6.86 (m, 2H), 3.89 (t, *J* = 7.4 Hz, 2H), 1.83 (s, 3H), 1.87-1.80 (m, 2H), 1.49-1.42 (m, 2H), 1.45-1.39 (m, 4H), 0.88 (t, *J* = 7.0 Hz, 3H); <sup>13</sup>C NMR (150 MHz, CDCl<sub>3</sub>) δ: 190.0, 159.2, 150.6, 142.0, 136.4, 132.2, 131.0, 130.2, 128.4, 127.6 (2C), 125.7, 125.5, 124.6, 124.1, 116.1, 114.7, 114.3 (2C), 55.4, 48.1, 31.4, 26.7, 26.5, 22.6, 14.0; IR (neat, cm<sup>-1</sup>): 2925 (w), 1683 (m), 1579 (m), 1465 (s), 1236 (s), 1195 (s), 805 (m), 732 (m); HRMS (ASAP+, *m/z*): 417.1763 (calcd. C<sub>26</sub>H<sub>27</sub>NO<sub>2</sub>S: 417.1762 [M]<sup>+</sup>).

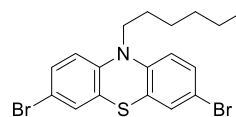
#### Synthesis of 3,7-dibromo-10*H*-phenothiazine (**6**) [9]

10*H*-Phenothiazine (25.0 g, 125.5 mmol) was suspended in glacial acetic acid (1000 mL) and stirred at 22 °C. Bromine (16.2 mL, 50.3 g, 314.5 mmol) dissolved in glacial acetic acid (400 mL) was added dropwise to the suspension over 90 minutes. After 2.5 hours the reaction mixture was cooled on an ice bath and Na<sub>2</sub>SO<sub>3</sub> (31.5 g) and water (15 mL) were added and the mixture was left stirring for 1 hour. By adding aqueous KOH (3 M, 1000 mL), a precipitate was formed and the mixture was left stirring for an additional hour. The precipitate was filtered off, washed with cold 2-propanol (100 mL), and dried to yield a green solid. The crude product was purified by recrystallization from toluene (940 mL) to obtain compound **6** as green crystals (35.89 g, 101.0 mmol, 80%), mp. 185-187 °C (lit. 195.6-196.8 °C [9]) <sup>1</sup>H NMR (400 MHz, DMSO-*d*<sub>6</sub>) δ: 8.84 (m, 1H), 7.16-7.12 (m, 4H), 6.59-6.57 (m, 2H). <sup>1</sup>H NMR was in accordance with reported data. [9]



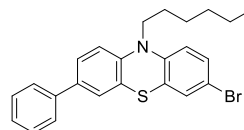
#### Synthesis of 3,7-dibromo-10-hexyl-10*H*-phenothiazine (**7**) [7]

Compound **6** (10.00 g, 28.0 mmol) and NaH (1.008 g, 42.0 mmol) were mixed before dry THF (112 mL) was added under N<sub>2</sub> atmosphere. The reaction was left stirring at 22 °C for 20 minutes. 1-Bromohexane (5.90 mL, 6.93 g, 42.0 mmol) was added dropwise over 40 minutes and the mixture was heated to reflux. After 20 hours the reaction was cooled to room temperature and quenched with an aqueous NH<sub>4</sub>Cl (50 mL, 5 wt%) solution, and the reaction mixture was extracted with EtOAc (3 × 50 mL). The combined organic phases were dried over anhydrous Na<sub>2</sub>SO<sub>4</sub>, filtered and the solvents were removed in vacuo. The crude product was purified by silica-gel column chromatography (*n*-pentane, R<sub>f</sub>= 0.24) to obtain compound **7** as a white solid (11.46 g, 26.0 mmol, 93%), mp. 53-54 °C (lit. 58 °C [10]) <sup>1</sup>H NMR (400 MHz, DMSO-*d*<sub>6</sub>) δ: 7.37-7.35 (m, 4H), 6.96-6.94 (m, 2H), 3.82-3.79 (m, 2H), 1.66-1.59 (m, 2H), 1.36-1.33 (m, 2H), 1.24-1.22 (m, 4H), 0.83-0.80 (m, 3H). <sup>1</sup>H NMR was in accordance with reported data. [7]



#### Synthesis of 3-bromo-10-hexyl-7-phenyl-10*H*-phenothiazine (**8**)

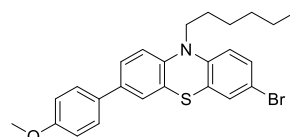
Compound **7** (2.00 g, 4.53 mmol), phenylboronic acid (608.0 mg, 4.99 mmol), Pd(PPh<sub>3</sub>)<sub>4</sub> (52.0 mg, 0.045 mmol) and K<sub>2</sub>CO<sub>3</sub> (2.506 g, 18.13 mmol) were mixed. Degassed 1,4-Dioxane (15 mL) and water (15 mL) were added under N<sub>2</sub> atmosphere while stirring. The reaction mixture was heated to 80 °C and left stirring for 7.5 hours before cooling to 22 °C. Water (25 mL) was added to the reaction mixture and EtOAc (3 × 30 mL) was used for extraction. The combined organic phases were dried with brine (30 mL) and over anhydrous Na<sub>2</sub>SO<sub>4</sub>, filtered and the solvents were removed in vacuo. The crude product was purified by silica-gel column chromatography (*n*-pentane:toluene, 19:1, R<sub>f</sub>= 0.22)



to obtain compound **8** as a white solid (921 mg, 2.10 mmol, 46%), mp. 79-80 °C. <sup>1</sup>H NMR (400 MHz, DMSO-*d*<sub>6</sub>) δ: 7.64-7.60 (m, 2H), 7.53-7.49 (m, 1H), 7.45-7.40 (m, 3H), 7.38-7.29 (m, 3H), 7.10-7.07 (m, 1H), 6.98-6.94 (m, 1H), 3.87 (t, *J* = 6.9 Hz, 2H), 1.72-1.63 (m, 2H), 1.43-1.34 (m, 2H), 1.29-1.21 (m, 4H), 0.85-0.80 (m, 3H); <sup>13</sup>C NMR (100 MHz, DMSO-*d*<sub>6</sub>) δ: 143.9, 143.6, 138.7, 134.6, 130.1, 128.94, 128.88 (2C), 127.1, 126.0 (3C), 125.8, 125.0, 123.4, 117.4, 116.2, 113.7, 46.6, 30.8, 26.0, 25.8, 22.0, 13.8; IR (neat, cm<sup>-1</sup>) v: 2956 (w), 2930 (w), 2847 (w), 1665 (m), 1453 (s), 1407 (m), 1249 (m), 1024 (m), 758 (s), 696 (m); HRMS (ASAP+, *m/z*): 437.0810 (calcd. C<sub>24</sub>H<sub>24</sub>NS<sup>79</sup>Br 437.0813, [M]<sup>+</sup>)

#### Synthesis of 3-bromo-10-hexyl-7-(4-methoxyphenyl)-10*H*-phenothiazine (**9**)

Compound **7** (2.01 g, 4.56 mmol), (4-methoxyphenyl)boronic acid (0.761 g, 5.01 mmol), Pd(PPh<sub>3</sub>)<sub>4</sub> (53.0 mg, 0.046 mmol) and K<sub>2</sub>CO<sub>3</sub> (2.52 g, 18.22 mmol) were mixed. Degassed 1,4-Dioxane (15 mL) and water (15 mL) were added under N<sub>2</sub> atmosphere while stirring. The reaction mixture was heated to 80 °C and left stirring for 19 hours before cooling to room temperature. Water (25 mL) was added to the reaction mixture and EtOAc (3 × 25 mL) was used for extraction. The combined organic phases were dried with brine (25 mL) and over anhydrous Na<sub>2</sub>SO<sub>4</sub>, filtered and the solvents were removed in vacuo. The crude product was purified by silica-gel column chromatography (*n*-pentane:toluene, 19:1, R<sub>f</sub> = 0.17) to obtain compound **9** as a yellow oil (1.09 g, 2.32 mmol, 51%). <sup>1</sup>H NMR (400 MHz, DMSO-*d*<sub>6</sub>) δ: 7.58-7.56 (m, 2H), 7.47-7.44 (m, 1H), 7.40-7.39 (m, 1H), 7.36-7.34 (m, 2H), 7.08-7.05 (m, 1H), 6.98-6.95 (m, 3H), 3.88-3.85 (m, 2H), 3.79 (s, 3H), 1.71-1.64 (m, 2H), 1.41-1.35 (m, 2H), 1.28-1.24 (m, 4H), 0.88-0.82 (m, 3H); <sup>13</sup>C NMR (100 MHz, DMSO-*d*<sub>6</sub>) δ: 158.7, 144.0, 143.0, 134.4, 131.2, 130.1, 128.9, 127.1 (2C), 125.8, 125.5, 124.5, 123.3, 117.3, 116.2, 114.3 (2C), 113.6, 55.1, 46.6, 30.8, 26.0, 25.8, 22.1, 13.8; IR (neat, cm<sup>-1</sup>) v: 2951 (m), 2929 (m), 2846 (m), 1610 (m), 1490 (m), 1464 (s), 1231 (m), 1179 (m), 873 (m), 800 (s); HRMS (ASAP+, *m/z*): 467.0919 (calcd. C<sub>25</sub>H<sub>27</sub>NS<sup>79</sup>Br 467.0918, [M+H]<sup>+</sup>).

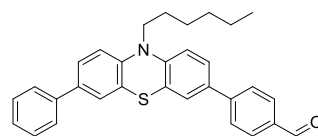


#### General procedure for Suzuki coupling of **7** or **8**

The phenothiazines **8** or **9** (1 eq.), arylboronic acid (1.5 eq.), Pd(OAc)<sub>2</sub> (0.02 eq.), SPhos (0.04 eq.) and K<sub>2</sub>CO<sub>3</sub> (4 eq.) were mixed. 1,4-Dioxane and water (1:1, v:v) were then degassed and added under N<sub>2</sub> atmosphere. The reactions were heated to 80 °C and stirred until full conversion (1-16 hours). Then the reaction mixture was cooled to room temperature before water was added and EtOAc was used for extraction. The combined organic phases were dried over anhydrous Na<sub>2</sub>SO<sub>4</sub>, filtered and the solvents were removed in vacuo. The crude products were purified by silica-gel column chromatography.

#### Synthesis of 4-(10-hexyl-7-phenyl-10*H*-phenothiazin-3-yl)benzaldehyde (**10**)

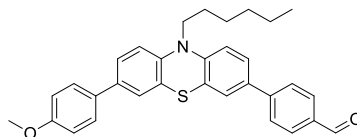
The synthesis was done in accordance with the general procedure starting with compound **8** (306 mg, 0.698 mmol), (4-formylphenyl)boronic acid (157 mg, 1.047 mmol), Pd(OAc)<sub>2</sub> (3.13 mg, 0.014 mmol), SPhos (11.5 mg, 0.028 mmol) and K<sub>2</sub>CO<sub>3</sub> (386 mg, 2.79 mmol). The reaction was left stirring at 80 °C for 4 hours before cooling and extraction of the reaction mixture with EtOAc (3 × 20 mL). The crude product was purified by silica-gel column chromatography (*n*-pentane:EtOAc, 7:1, R<sub>f</sub> = 0.39) to obtain compound **10** as a yellow solid (294 mg, 0.635 mmol, 91%), mp. 80-82 °C. <sup>1</sup>H NMR (400 MHz, DMSO-*d*<sub>6</sub>) δ: 10.02 (s, 1H), 7.97-7.87 (m, 4H), 7.66-7.57 (m, 4H), 7.53-7.49 (m, 1H), 7.47-7.40 (m, 3H), 7.35-7.30 (m, 1H), 7.15-7.08 (m, 2H), 3.93 (t, *J* = 6.9 Hz, 2H), 1.77-1.68 (m, 2H), 1.46-1.37 (m, 2H), 1.32-1.21 (m, 4H), 0.87-0.80 (m, 3H); <sup>13</sup>C NMR (100 MHz, DMSO-*d*<sub>6</sub>) δ: 192.6, 144.8, 144.5, 143.4, 138.8, 134.7, 134.6, 132.7, 130.1 (2C), 128.9 (2C), 127.1, 126.49 (2C), 126.47, 126.0 (2C), 125.9, 125.4, 125.0, 123.8, 123.5, 116.2, 116.1, 46.6, 30.8, 26.2, 25.8, 22.1, 13.8; IR (neat, cm<sup>-1</sup>) v: 2951 (w), 2919 (w), 2852



(w), 1690 (m), 1600 (m), 1462 (s), 1247 (m), 1212 (m), 1168 (m), 807 (s), 759 (s), 696 (s); HRMS (ASAP+,  $m/z$ ): 463.1964 (calcd.  $C_{31}H_{29}NOS$  463.1970,  $[M]^+$ ).

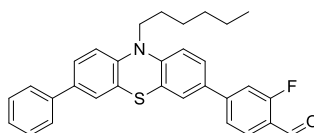
#### Synthesis of 4-(10-hexyl-7-(4-methoxyphenyl)-10H-phenothiazin-3-yl)benzaldehyde (**11**)

The synthesis was done in accordance with the general procedure starting with compound **9** (500 mg, 1.07 mmol), (4-formylphenyl)boronic acid (240 mg, 1.60 mmol),  $Pd(OAc)_2$  (4.79 mg, 0.021 mmol), SPhos (17.5 mg, 0.043 mmol) and  $K_2CO_3$  (590 mg, 4.27 mmol). The reaction was left stirring at 80 °C for 16 hours before cooling and extraction of the reaction mixture with EtOAc (3 × 30 mL). The crude product was purified by silica-gel column chromatography (*n*-pentane:EtOAc, 4:1,  $R_f$  = 0.35) to obtain compound **11** as an orange solid (431 mg, 0.873 mmol, 82%) mp. 71-73 °C;  $^1H$  NMR (400 MHz, DMSO- $d_6$ )  $\delta$ : 10.02 (s, 1H), 7.96-7.87 (m, 4H), 7.65-7.61 (m, 1H), 7.59-7.55 (m, 3H), 7.47-7.43 (m, 1H), 7.41-7.39 (m, 1H), 7.13-7.06 (m, 2H), 7.01-7.67 (m, 2H), 3.93 (t,  $J$  = 6.9 Hz, 2H), 3.78 (s, 3H), 1.77-1.68 (m, 2H), 1.46-1.37 (m, 2H), 1.31-1.22 (m, 4H), 0.87-0.81 (m, 3H);  $^{13}C$  NMR (100 MHz, DMSO- $d_6$ )  $\delta$ : 192.5, 158.7, 144.9, 144.5, 142.7, 134.7, 134.4, 132.5, 131.2, 130.1 (2C), 127.1 (2C), 126.46 (2C), 126.45, 126.42, 125.4, 124.5, 123.8, 123.4, 116.1, 116.0, 114.3 (2C), 55.1, 46.6, 30.8, 26.2, 25.8, 22.1, 13.8; IR (neat,  $cm^{-1}$ )  $\nu$ : 2956 (w), 2925 (w), 2842 (w), 1692 (m), 1600 (m), 1462 (s), 1239 (s), 1213 (m), 1168 (s), 805 (s), 790 (s); HRMS (ASAP+,  $m/z$ ): 493.2076 (calcd.  $C_{32}H_{31}NO_2S$  493.2075,  $[M]^+$ ).



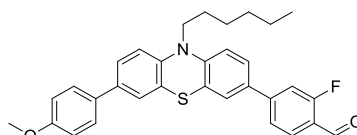
#### Synthesis of 2-fluoro-4-(10-hexyl-7-phenyl-10H-phenothiazin-3-yl)benzaldehyde (**12**)

The synthesis was done in accordance with the general procedure starting with compound **8** (350 mg, 0.798 mmol), (3-fluoro-4-formylphenyl)boronic acid (201 mg, 1.197 mmol),  $Pd(OAc)_2$  (3.58 mg, 0.016 mmol), SPhos (13.11 mg, 0.032 mmol) and  $K_2CO_3$  (441 mg, 3.19 mmol). The reaction was left stirring at 80 °C for 3 hours before cooling and extraction of the reaction mixture with EtOAc (3 × 25 mL). The crude product was purified by silica-gel column chromatography (*n*-pentane:EtOAc, 5:1,  $R_f$  = 0.48) to obtain compound **12** as a yellow solid (314.3 mg, 0.653 mmol, 82%), mp. 91-92 °C.  $^1H$  NMR (400 MHz, DMSO- $d_6$ )  $\delta$ : 10.21 (s, 1H), 7.88-7.83 (m, 1H), 7.76-7.60 (m, 6H), 7.53-7.48 (m, 1H), 7.46-7.40 (m, 3H), 7.34-7.29 (m, 1H), 7.12-7.07 (m, 2H), 3.92 (t,  $J$  = 6.9 Hz, 2H), 1.76-1.66 (m, 2H), 1.45-1.36 (m, 2H), 1.30-1.21 (m, 4H), 0.86-0.79 (m, 3H);  $^{13}C$  NMR (100 MHz, DMSO- $d_6$ )  $\delta$ : 187.2 (d,  $J$  = 4.7 Hz), 163.9 (d,  $J$  = 256.6 Hz), 147.0 (d,  $J$  = 9.2 Hz), 145.3, 143.2, 138.8, 134.7, 131.3, 129.8 (d,  $J$  = 2.2 Hz), 128.9 (2C), 127.1, 126.6, 126.0 (2C), 125.9, 125.5, 125.0, 123.8, 123.4, 122.2 (d,  $J$  = 2.5 Hz), 122.0 (d,  $J$  = 8.6 Hz), 116.1 (d,  $J$  = 26.2 Hz), 113.6, 113.4, 46.7, 30.8, 26.1, 25.8, 22.1, 13.8; IR (neat,  $cm^{-1}$ )  $\nu$ : 2949 (w), 2926 (w), 2848 (w), 1686 (m), 1614 (m), 1462 (m), 1252 (s), 820 (m), 763 (s), 690 (m); HRMS (ASAP+,  $m/z$ ): 481.1870 (calcd.  $C_{31}H_{28}NOFS$  481.1876,  $[M]^+$ ).



#### Synthesis of 2-fluoro-4-(10-hexyl-7-(4-methoxyphenyl)-10H-phenothiazin-3-yl)benzaldehyde (**13**)

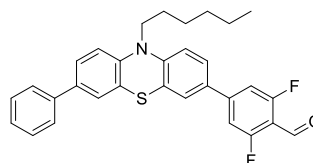
The synthesis was done in accordance with the general procedure starting with compound **9** (500 mg, 1.07 mmol), (3-fluoro-4-formylphenyl)boronic acid (269 mg, 1.60 mmol),  $Pd(OAc)_2$  (4.79 mg, 0.021 mmol), SPhos (17.5 mg, 0.043 mmol) and  $K_2CO_3$  (590 mg, 4.27 mmol). The reaction was left stirring at 80 °C for 16 hours before cooling and extraction of the reaction mixture with EtOAc (3 × 35 mL). The crude product was purified by silica-gel column chromatography (*n*-pentane:EtOAc, 4:1,  $R_f$  = 0.43) to obtain compound **13** as a red solid (422 mg, 0.865 mmol, 81%), mp. 71-73 °C.  $^1H$  NMR (400 MHz, DMSO- $d_6$ )  $\delta$ : 10.21 (s, 1H), 7.88-7.83 (m, 1H), 7.76-7.64



(m, 3H), 7.63-7.62 (m, 1H), 7.58-7.54 (m, 2H), 7.46-7.42 (m, 1H), 7.40-7.38 (m, 1H), 7.11-7.04 (m, 2H), 7.00-6.96 (m, 2H), 3.92 (t,  $J = 6.9$  Hz, 2H), 3.78 (s, 3H), 1.75-1.66 (m, 2H), 1.45-1.36 (m, 2H), 1.30-1.21 (m, 4H), 0.86-0.80 (m, 3H);  $^{13}\text{C}$  NMR (100 MHz,  $\text{DMSO-}d_6$ )  $\delta$ : 187.2 (d,  $J = 4.2$  Hz), 163.9 (d,  $J = 256.4$  Hz), 158.7, 147.0 (d,  $J = 9.0$  Hz), 145.4, 142.5, 134.5, 131.2 (d,  $J = 3.6$  Hz), 129.8 (d,  $J = 2.2$  Hz), 127.2 (2C), 126.6, 125.4 (d,  $J = 10.3$  Hz), 124.5, 123.8, 123.3, 122.2 (d,  $J = 3.0$  Hz), 122.0, 121.9, 116.2, 115.8, 114.3 (2C), 113.6, 113.3, 55.1, 46.6, 30.8, 26.1, 25.8, 22.1, 13.8; IR (neat,  $\text{cm}^{-1}$ ): 3029 (w), 2925 (m), 2847 (m), 2847 (m), 1688 (s), 1610 (s), 1465 (s), 1382 (m), 1242 (s), 1174 (s), 1117 (m), 1029 (m), 805 (s); HRMS (ASAP+,  $m/z$ ): 511.1982 (calcd.  $\text{C}_{32}\text{H}_{30}\text{NO}_2\text{FS}$  511.1981,  $[\text{M}]^+$ ).

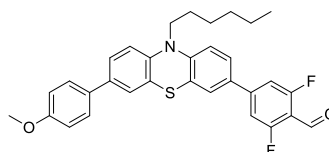
#### Synthesis of 2,6-difluoro-4-(10-hexyl-7-phenyl-10*H*-phenothiazin-3-yl)benzaldehyde (**14**)

The synthesis was done in accordance with the general procedure starting with compound **8** (350 mg, 0.798 mmol), (3,5-difluoro-4-formylphenyl)boronic acid (223 mg, 1.20 mmol),  $\text{Pd}(\text{OAc})_2$  (3.58 mg, 0.016 mmol), SPhos (13.11 mg, 0.032 mmol) and  $\text{K}_2\text{CO}_3$  (441 mg, 3.19 mmol). The reaction was left stirring at 80 °C for 2.5 hours before cooling and extraction of the reaction mixture with EtOAc ( $3 \times 25$  mL). The crude product was purified by silica-gel column chromatography (*n*-pentane:EtOAc, 5:1,  $R_f = 0.51$ ) to obtain compound **14** as a red solid (318 mg, 0.636 mmol, 80%), mp. 69-71 °C.  $^1\text{H}$  NMR (400 MHz,  $\text{DMSO-}d_6$ )  $\delta$ : 10.19 (s, 1H), 7.73-7.67 (m, 2H), 7.66-7.61 (m, 4H), 7.53-7.49 (m, 1H), 7.46-7.40 (m, 3H), 7.34-7.30 (m, 1H), 7.12-7.07 (m, 2H), 3.93 (t,  $J = 6.9$  Hz, 2H), 1.75-1.67 (m, 2H), 1.45-1.36 (m, 2H), 1.30-1.22 (m, 4H), 0.86-0.80 (m, 3H);  $^{13}\text{C}$  NMR (100 MHz,  $\text{DMSO-}d_6$ )  $\delta$ : 184.3, 162.7 (dd,  $J = 258.3$  Hz, 7.6 Hz, 2C), 147.2 (t,  $J = 11.5$  Hz), 145.8, 143.0, 138.7, 134.8, 130.1, 128.9 (2C), 127.1, 126.7, 126.0, 126.0 (2C), 125.6, 125.0, 123.8, 123.3, 116.3, 115.8, 111.7 (t,  $J = 11.6$  Hz), 109.5 (d,  $J = 24.5$  Hz, 2C), 46.7, 30.8, 26.1, 25.8, 22.1, 13.8; IR (neat,  $\text{cm}^{-1}$ ): 2956 (w), 2925 (w), 2857 (w), 1694 (m), 1624 (s), 1460 (s), 1245 (m), 1195 (s), 1037 (m), 809 (m), 759 (s), 696 (m); HRMS (ASAP+,  $m/z$ ): 499.1776 (calcd.  $\text{C}_{31}\text{H}_{27}\text{NOF}_2\text{S}$  499.1781,  $[\text{M}]^+$ ).



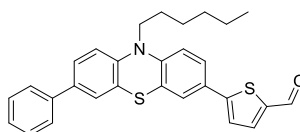
#### Synthesis of 2,6-difluoro-4-(10-hexyl-7-(4-methoxyphenyl)-10*H*-phenothiazin-3-yl)benzaldehyde (**15**)

The synthesis was done in accordance with the general procedure starting with compound **9** (500 mg, 1.10 mmol), (3,5-difluoro-4-formylphenyl)boronic acid (300 mg, 1.60 mmol),  $\text{Pd}(\text{OAc})_2$  (6 mg, 0.02 mmol), SPhos (19 mg, 0.05 mmol) and  $\text{K}_2\text{CO}_3$  (610 mg, 4.40 mmol). Full conversion was obtained after 1 hour. The crude product was purified by silica-gel column chromatography (*n*-pentane:EtOAc, 14:1,  $R_f = 0.27$ ) to obtain compound **15** as a red oil (440 mg, 0.84 mmol, 76%);  $^1\text{H}$  NMR (400 MHz,  $\text{DMSO-}d_6$ )  $\delta$ : 10.20 (s, 1H), 7.74-7.70 (m, 1H), 7.69-7.68 (m, 1H), 7.66-7.63 (m, 2H), 7.58-7.56 (m, 2H), 7.46-7.44 (m, 1H), 7.40-7.39 (m, 1H), 7.10-7.09 (m, 1H), 7.08-7.06 (m, 1H), 7.00-6.98 (m, 2H), 3.95-3.91 (m, 2H), 3.78 (s, 3H), 1.75-1.67 (m, 2H), 1.43-1.37 (m, 2H), 1.29-1.23 (m, 4H), 0.85-0.84 (m, 3H);  $^{13}\text{C}$  NMR (100 MHz,  $\text{DMSO-}d_6$ )  $\delta$ : 189.0, 184.3 (d,  $J = 4.1$  Hz), 163.0 (d,  $J = 278.0$  Hz), 158.7, 147.2 (d,  $J = 3.7$  Hz), 145.9, 142.4, 134.6, 131.4 (d,  $J = 1.5$  Hz), 131.2, 127.2 (2C), 126.7, 125.6, 125.4, 124.5, 123.8, 123.2, 116.3 (2C), 115.8 (d,  $J = 48.1$  Hz), 114.3 (2C), 109.5 (d,  $J = 23.6$  Hz, 2C), 55.1, 46.6, 30.8, 26.1, 25.8, 20.8, 13.8; IR (neat,  $\text{cm}^{-1}$ ): 2951 (w), 2879 (w), 2847 (w), 2774 (w), 1699 (s), 1625 (s), 1460 (s), 1242 (s), 1029 (s), 816 (s); HRMS (ASAP+,  $m/z$ ): 529.1888 (calcd.  $\text{C}_{32}\text{H}_{29}\text{F}_2\text{NO}_2\text{S}$ : 529.1887,  $[\text{M}]^+$ ).



### Synthesis of 5-(10-hexyl-7-phenyl-10*H*-phenothiazin-3-yl)thiophene-2-carbaldehyde (**16**)

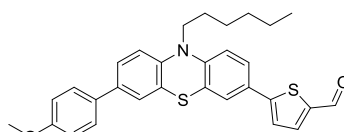
Compound **8** (390 mg, 0.890 mmol) was mixed with dichlorobis(acetonitrile)palladium (II) (4.62 mg, 0.018 mmol) and SPhos (29.2 mg, 0.071 mmol). Dry 1,4-dioxane (0.7 mL) and triethylamine (0.5 mL) were added under N<sub>2</sub> atmosphere and pinacol borane (170 mg, 193 μL, 1.335 mmol) was added to the mixture dropwise. The reaction mixture was stirred 80 °C for 1



hour before cooling, filtration through a Celite plug and removal of solvents in vacuo. This gave a light brown oil. To the crude product, Pd(OAc)<sub>2</sub> (3.70 mg, 0.016 mmol), SPhos (13.53 mg, 0.033 mmol) and K<sub>2</sub>CO<sub>3</sub> (455.0 mg, 3.30 mmol) was added. Under N<sub>2</sub> atmosphere, degassed 1,4-dioxane (3 mL) and water (3 mL) were added, followed by 5-bromothiophene-2-carbaldehyde (236 mg, 1.24 mmol). The reaction was stirred at 80 °C for 18 hours before cooling and extraction of the reaction mixture with EtOAc (3 × 30 mL). The crude product was purified by silica-gel column chromatography (*n*-pentane:EtOAc, 5:1, R<sub>f</sub> = 0.33) to obtain compound **16** as a red solid (228 mg, 0.486 mmol, 55%), mp. 66-68 °C. <sup>1</sup>H NMR (400 MHz, DMSO-*d*<sub>6</sub>) δ: 9.87 (s, 1H), 8.00 (d, *J* = 4.0 Hz, 1H), 7.67 (d, *J* = 4.0 Hz, 1H), 7.65-7.58 (m, 4H), 7.53-7.49 (m, 1H), 7.46-7.40 (m, 3H), 7.35-7.29 (m, 1H), 7.12-7.06 (m, 2H), 3.92 (t, *J* = 3.9 Hz, 2H), 1.75-1.66 (m, 2H), 1.445-1.36 (m, 2H), 1.29-1.21 (m, 4H), 0.86-0.80 (m, 3H); <sup>13</sup>C NMR (100 MHz, DMSO-*d*<sub>6</sub>) δ: 183.8, 151.9, 145.4, 143.1, 141.1, 139.4, 138.8, 134.8, 128.9 (2C), 127.2, 126.8, 126.1 (2C), 126.0, 125.9, 125.0, 124.43, 124.38, 124.0, 123.2, 116.3, 116.1, 46.7, 30.8, 26.1, 25.8, 22.1, 13.8; IR (neat, cm<sup>-1</sup>) v: 2956 (w), 2914 (w), 2847 (w), 1656 (s), 1433 (s), 1400 (m), 1223 (s), 1055 (m), 799 (m), 758 (s), 696 (m); HRMS (ASAP+, *m/z*): 469.1530 (calcd. C<sub>29</sub>H<sub>27</sub>NOS<sub>2</sub> 469.1534, [M]<sup>+</sup>).

### Synthesis of 5-(10-hexyl-7-(4-methoxyphenyl)-10*H*-phenothiazin-3-yl)thiophene-2-carbaldehyde (**17**)

Compound **9** (300 mg, 0.640 mmol) was mixed with dichlorobis(acetonitrile)palladium (II) (3.32 mg, 0.013 mmol) and SPhos (21.03 mg, 0.051 mmol). Dry 1,4-dioxane (0.4 mL) and triethylamine (0.3 mL) were added under N<sub>2</sub> atmosphere. Then pinacol borane (123 mg, 139 μL, 0.961 mmol) was added dropwise. The reaction mixture was stirred 80 °C for 1 hour

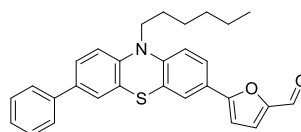


before cooling, filtration through a Celite plug and removal of solvents in vacuo. This gave a light brown oil. To the crude intermediate product, Pd(OAc)<sub>2</sub> (2.61 mg, 0.012 mmol), SPhos (9.56 mg, 0.023 mmol) and K<sub>2</sub>CO<sub>3</sub> (322 mg, 2.33 mmol) were added. Under N<sub>2</sub> atmosphere, degassed 1,4-dioxane (2 mL) and water (2 mL) were added, then 5-bromothiophene-2-carbaldehyde (167 mg, 0.873 mmol). The reaction was stirred at 80 °C for 18 hours before cooling and extraction of the reaction mixture with EtOAc (3 × 30 mL). The crude product was purified by silica-gel column chromatography (*n*-pentane:EtOAc, 5:1, R<sub>f</sub> = 0.31) to obtain compound **17** as a red solid (209 mg, 0.419 mmol, 72%), mp. 70-72 °C; <sup>1</sup>H NMR (400 MHz, DMSO-*d*<sub>6</sub>) δ: 9.87 (s, 1H), 7.99 (d, *J* = 3.9 Hz, 1H), 7.66 (d, *J* = 3.9 Hz, 1H), 7.61-7.53 (m, 4H), 7.46-7.42 (m, 1H), 7.40-7.38 (m, 1H), 7.08-7.02 (m, 2H), 7.00-6.95 (m, 2H), 3.89 (t, *J* = 6.9 Hz, 2H), 3.78 (s, 3H), 1.73-1.64 (m, 2H), 1.43-1.34 (m, 2H), 1.27-1.20 (m, 4H), 0.85-0.79 (m, 3H); <sup>13</sup>C NMR (100 MHz, DMSO-*d*<sub>6</sub>) δ: 183.7, 158.7, 152.0, 145.5, 142.4, 141.1, 139.4, 134.6, 131.2, 127.2 (2C), 126.6, 125.8, 125.4, 124.5, 124.4, 124.3, 123.9, 123.1, 116.2, 115.9, 114.3 (2C), 55.1, 46.7, 30.8, 26.1, 25.8, 22.1, 13.8; IR (neat, cm<sup>-1</sup>) v: 3033 (w), 2950 (m), 2924 (m), 2852 (m), 1657 (s), 1429 (s), 1226 (s), 1179 (s), 805 (s), 675 (s) HRMS (ASAP+, *m/z*): 499.1637 (calcd. C<sub>30</sub>H<sub>29</sub>NO<sub>2</sub>S<sub>2</sub> 499.1640, [M+H]<sup>+</sup>).



### Synthesis of 5-(10-hexyl-7-phenyl-10*H*-phenothiazin-3-yl)furan-2-carbaldehyde (**18**)

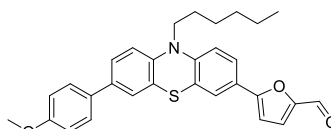
The synthesis was done in accordance with the general procedure starting with compound **8** (298 mg, 0.680 mmol), 5-formylfuran-2-yl)boronic acid (144 mg, 1.02 mmol), Pd(OAc)<sub>2</sub> (3.05 mg, 0.014 mmol), SPhos (11.17 mg, 0.027 mmol) and K<sub>2</sub>CO<sub>3</sub> (376.0 mg, 2.72 mmol). The reaction was left stirring at 80 °C for 2 hours before cooling and extraction of the reaction



mixture with EtOAc (3 × 30 mL). The crude product was purified by silica-gel column chromatography (*n*-pentane:EtOAc, 5:1, R<sub>f</sub> = 0.31) to obtain compound **18** as a brown solid (282 mg, 0.621 mmol, 91%), mp. 58–61 °C. <sup>1</sup>H NMR (400 MHz, DMSO-*d*<sub>6</sub>) δ: 9.56 (s, 1H), 7.70–7.66 (m, 1H), 7.65–7.61 (m, 4H), 7.53–7.49 (m, 1H), 7.46–7.40 (m, 3H), 7.35–7.30 (m, 1H), 7.20 (d, *J* = 3.8 Hz, 1H), 7.14–7.09 (m, 2H), 3.93 (t, *J* = 6.9 Hz, 2H), 1.75–1.67 (m, 2H), 1.45–1.36 (m, 2H), 1.29–1.21 (m, 4H), 0.85–0.80 (m, 3H); <sup>13</sup>C NMR (100 MHz, DMSO-*d*<sub>6</sub>) δ: 177.3, 157.7, 151.3, 145.6, 143.0, 138.7, 134.8, 128.9 (2C), 127.2, 126.1 (2C), 126.0, 125.8, 125.0, 124.7, 123.8, 123.5, 123.2, 122.9, 116.4, 116.0, 107.8, 46.7, 30.8, 26.1, 25.8, 22.1, 13.8; IR (neat, cm<sup>-1</sup>) v: 2945 (w), 2909 (w), 2847 (w), 1461 (s), 1251 (m), 1242 (m), 802 (m), 757 (s), 697 (s); HRMS (ASAP+, *m/z*): 453.1760 (calcd. C<sub>29</sub>H<sub>27</sub>NO<sub>2</sub>S 453.1762, [M]<sup>+</sup>).

### Synthesis of 5-(10-hexyl-7-(4-methoxyphenyl)-10*H*-phenothiazin-3-yl)furan-2-carbaldehyde (**19**)

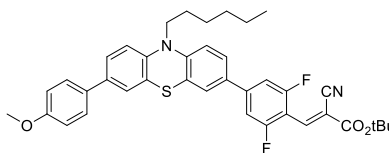
The synthesis was done in accordance with the general procedure starting with compound **9** (540 mg, 1.15 mmol), 5-formylfuran-2-boronic acid (240 mg, 1.73 mmol), Pd(OAc)<sub>2</sub> (5.8 mg, 0.02 mmol), SPhos (19.8 mg, 0.05 mmol) and K<sub>2</sub>CO<sub>3</sub> (640 mg, 4.60 mmol). Full conversion was obtained after 1 hour. The crude product was purified by silica-gel column chromatography



(gradient: 10–33% EtOAc in *n*-pentane) to obtain compound **19** as a red oil (300 mg, 0.62 mmol, 54%). <sup>1</sup>H NMR (400 MHz, DMSO-*d*<sub>6</sub>) δ: 9.56 (s, 1H), 7.69–7.68 (m, 1H), 7.65–7.64 (m, 1H), 7.63–7.62 (m, 1H), 7.58–7.57 (m, 2H), 7.47–7.45 (m, 1H), 7.41–7.40 (m, 1H), 7.21–7.20 (m, 1H), 7.14–7.12 (m, 1H), 7.10–7.08 (m, 1H), 7.00–6.98 (m, 2H), 4.03–4.02 (m, 2H), 3.78 (s, 3H), 1.74–1.69 (m, 2H), 1.44–1.39 (m, 2H), 1.28–1.26 (m, 4H), 0.85–0.84 (m, 3H); <sup>13</sup>C NMR (100 MHz, DMSO-*d*<sub>6</sub>) δ: 177.3, 158.7, 157.8, 151.3, 145.7, 142.4, 134.7, 131.1, 127.2 (2C), 125.5, 124.7, 124.5, 123.8, 123.5, 123.2, 122.8, 122.6, 116.3, 116.0, 114.3 (2C), 107.8, 55.1, 46.7, 30.8, 26.1, 25.7, 22.0, 13.8; IR (neat, cm<sup>-1</sup>) v: 3122 (w), 2925 (w), 2857 (w), 1662 (s), 1600 (m), 1460 (s), 1402 (s), 1237 (s), 1179 (m), 1018 (s), 790 (s); HRMS (ASAP+, *m/z*): 483.1862 (calcd. C<sub>30</sub>H<sub>29</sub>NO<sub>3</sub>S: 483.1868, [M]<sup>+</sup>).

### Synthesis of *tert*-butyl (*E*)-2-cyano-3-(2,6-difluoro-4-(10-hexyl-7-(4-methoxyphenyl)-10*H*-phenothiazin-3-yl)phenyl)acrylate (**20**)

Compound **15** (410 mg, 0.80 mmol) and ammonium acetate (240 mg, 3.10 mmol) were mixed before acetic acid (4.5 mL) and *tert*-butyl 2-cyanoacetate (0.44 mL, 3.10 mmol) were added under N<sub>2</sub> atmosphere. The reaction mixture was heated to 75 °C and left stirring for 1 hour. Water (30 mL) was added

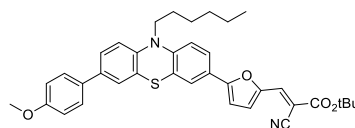


to the solution and the aqueous phase was extracted with EtOAc (3 × 20 mL). The combined organic phases were dried over anhydrous Na<sub>2</sub>SO<sub>4</sub>, filtered and the solvents were removed in vacuo. Purification by silica-gel column chromatography (*n*-pentane:EtOAc, 14:1, R<sub>f</sub> = 0.24) gave compound **20** as a dark red oil (450 mg, 0.69 mmol, 89%). <sup>1</sup>H NMR (400 MHz, DMSO-*d*<sub>6</sub>) δ: 8.19 (s, 1H), 7.73–7.68 (m, 4H), 7.58–7.56 (m, 2H), 7.46–7.44 (m, 1H), 7.41–7.40 (m, 1H), 7.09–7.07 (m, 2H), 7.00–6.98 (m, 2H), 3.95–3.90 (m, 2H), 3.78 (s, 3H), 1.75–1.68 (m, 2H), 1.43 (s, 9H), 1.41–1.37 (m, 2H), 1.29–1.24 (m, 4H), 0.85–0.82 (m, 3H); <sup>13</sup>C NMR (100 MHz, DMSO-*d*<sub>6</sub>) δ: 163.3, 159.8 (2C), 158.7, 145.7, 145.3 (d, *J* = 2.0 Hz), 142.42, 142.37, 134.5, 131.2, 130.3, 127.2 (2C), 125.4, 124.5, 123.8, 123.3, 116.4, 115.5 (d, *J* = 55.8 Hz), 114.3 (2C), 111.5, 109.4

(d,  $J = 24.4$  Hz, 2C), 84.0, 82.7, 55.1, 46.7, 30.8, 27.5 (3C), 27.4, 26.1, 25.8, 22.0, 13.8 (2 shifts missing); IR (neat,  $\text{cm}^{-1}$ ): 3065 (w), 2925 (w), 2852 (w), 1740 (s), 1719 (s), 1470 (s), 1273 (s), 1242 (s), 1148 (s), 1023 (s), 816 (s); HRMS (ASAP+,  $m/z$ ): 652.2566 (calcd.  $\text{C}_{39}\text{H}_{38}\text{F}_2\text{N}_2\text{O}_3\text{S}$ : 652.2571,  $[\text{M}]^+$ ).

#### Synthesis of compound *tert*-butyl (*E*)-2-cyano-3-(5-(10-hexyl-7-(4-methoxyphenyl)-10*H*-phenothiazin-3-yl)furan-2-yl)acrylate (**21**)

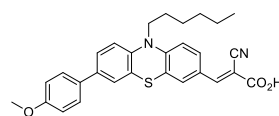
Compound **19** (170 mg, 0.40 mmol) and ammonium acetate (110 mg, 1.40 mmol) were mixed before acetic acid (2.0 mL) and *tert*-butyl 2-cyanoacetate (0.20 mL, 1.40 mmol) were added under  $\text{N}_2$  atmosphere. The reaction mixture was heated to 75 °C and left stirring for 1 hour. Water (30 mL) was added to the solution and the aqueous phase was extracted with EtOAc ( $3 \times 20$  mL). The



combined organic phases were dried over anhydrous  $\text{Na}_2\text{SO}_4$ , filtered and the solvents were removed in vacuo. Purification by silica-gel column chromatography (*n*-pentane: EtOAc, 19:1,  $R_f = 0.49$ ) gave compound **21** as a dark red oil (120 mg, 0.198 mmol, 55%).  $^1\text{H}$  NMR (400 MHz,  $\text{DMSO}-d_6$ )  $\delta$ : 7.99 (s, 1H), 7.75-7.74 (m, 1H), 7.71-7.70 (m, 1H), 7.59-7.57 (m, 2H), 7.56-7.55 (m, 1H), 7.47-7.45 (m, 1H), 7.42-7.41 (m, 1H), 7.31-7.30 (m, 1H), 7.17-7.15 (m, 1H), 7.10-7.09 (m, 1H), 7.00-6.98 (m, 2H), 3.96-3.90 (m, 2H), 3.78 (s, 3H), 1.74-1.69 (m, 2H), 1.43 (s, 9H), 1.43-1.41 (m, 2H), 1.27-1.25 (m, 4H), 0.85-0.82 (m, 3H);  $^{13}\text{C}$  NMR (100 MHz,  $\text{DMSO}-d_6$ )  $\delta$ : 163.3, 158.6, 158.5, 147.1, 144.8, 143.2, 137.2, 134.0, 130.7, 127.4 (2C), 127.2, 125.1, 124.8, 124.6, 123.2, 123.0, 122.62, 122.61, 116.43, 116.42, 116.1, 114.7 (2C), 109.4, 95.0, 83.6, 55.1, 46.6, 30.8, 27.6 (3C), 26.1, 25.7, 22.0, 13.8; IR (neat,  $\text{cm}^{-1}$ ): 3138 (w), 2977 (w), 2930 (w), 2870 (w), 2262 (w), 2218 (w), 1740 (s), 1714 (s), 1610 (s), 1583 (s), 1456 (s), 1236 (s), 1152 (s), 1028 (s), 798 (s), 587 (m); HRMS (ASAP+,  $m/z$ ): 606.2548 (calcd.  $\text{C}_{37}\text{H}_{38}\text{N}_2\text{O}_4\text{S}$ : 606.2552,  $[\text{M}]^+$ ).

#### Synthesis of (*E*)-2-cyano-3-(10-hexyl-7-(4-methoxyphenyl)-10*H*-phenothiazin-3-yl)acrylic acid (**AFB-1**)

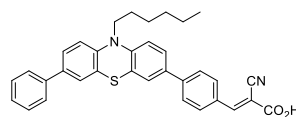
Compound **5** (200 mg, 0.479 mmol) and cyanoacetic acid (815 mg, 9.58 mmol) were dissolved in degassed acetonitrile (55 mL) under  $\text{N}_2$ -atmosphere. Piperidine (569  $\mu\text{L}$ , 489 mg, 5.75 mmol) was added and the reaction was heated to 80 °C for 40 minutes before cooling to 22 °C and quenched in aqueous HCl (2 M, 150 mL). EtOAc (50 mL) was added and the organic phase was washed with water ( $8 \times 100$  mL), then dried with brine (50 mL) and over anhydrous



$\text{Na}_2\text{SO}_4$ , filtered and the solvents were removed in vacuo. The crude product was purified by silica-gel column chromatography (gradient: 0-15% MeOH in  $\text{CH}_2\text{Cl}_2$ ) to obtain **AFB-1** as a dark solid (215 mg, 0.444 mmol, 93%), mp. 204-208 °C.  $^1\text{H}$  NMR (600 MHz,  $\text{DMSO}-d_6$ )  $\delta$ : 13.72 (s, 1H), 8.15 (s, 1H), 7.91 (d,  $J = 8.8$  Hz, 1H), 7.82 (s, 1H), 7.57 (d,  $J = 8.7$  Hz, 2H), 7.45 (d,  $J = 8.6$  Hz, 1H), 7.39 (s, 1H), 7.15 (d,  $J = 8.8$  Hz, 1H), 7.09 (d,  $J = 8.6$  Hz, 1H), 6.98 (d,  $J = 8.8$  Hz, 2H), 3.94 (t,  $J = 7.0$  Hz, 2H), 3.78 (s, 3H), 1.74-1.64 (m, 2H), 1.45-1.35 (m, 2H), 1.31-1.20 (m, 4H), 0.82 (t,  $J = 7.1$  Hz, 3H);  $^{13}\text{C}$  NMR (150 MHz,  $\text{DMSO}-d_6$ )  $\delta$ : 163.8, 158.8, 152.5, 148.6, 141.1, 135.3, 131.7, 130.9, 129.1, 127.2 (2C), 125.5, 125.4, 124.6, 122.7, 122.5, 116.8, 116.7, 115.5, 114.3 (2C), 99.4, 55.1, 47.0, 30.8, 26.0, 25.7, 22.1, 13.8; IR (neat,  $\text{cm}^{-1}$ ): 2909 (w), 1683 (m), 1558 (m), 1470 (s), 1184 (s), 826 (m); HRMS (ASAP+,  $m/z$ ): 484.1815 (calcd.  $\text{C}_{29}\text{H}_{28}\text{N}_2\text{O}_3\text{S}$ : 484.1821  $[\text{M}]^+$ ); UV ( $\text{CH}_2\text{Cl}_2$ ,  $2 \times 10^{-5}$  M, 22 °C)  $\lambda_{\text{max}}$  (nm): 305.5 (26200), 475.0 (14000)

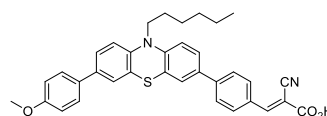
### Synthesis of (*E*)-2-cyano-3-(4-(10-hexyl-7-phenyl-10*H*-phenothiazin-3-yl)phenyl)acrylic acid (**AFB-2**)

Compound **10** (294 mg, 0.634 mmol) and cyanoacetic acid (1.079 g, 12.7 mmol) were dissolved in degassed acetonitrile (60 mL) under N<sub>2</sub> atmosphere. Piperidine (753 μL, 648.0 mg, 7.61 mmol) was added and the reaction was heated to 80 °C for 45 minutes before cooling 22 °C and quenched in aqueous HCl (2 M, 150 mL). EtOAc (50 mL) was added and the organic phase was washed with water (8 × 100 mL), then dried with brine (50 mL) and over anhydrous Na<sub>2</sub>SO<sub>4</sub>, filtered and the solvents were removed in vacuo. The crude product was purified by silica-gel column chromatography (gradient: 0-15% MeOH in CH<sub>2</sub>Cl<sub>2</sub>) to obtain **AFB-2** as a dark brown solid (164 mg, 0.308 mmol, 49%), mp. 246 °C (dec.). <sup>1</sup>H NMR (400 MHz, DMSO-*d*<sub>6</sub>) δ: 8.05 (s, 1H), 7.95 (d, *J* = 8.4 Hz, 2H), 7.79 (d, *J* = 8.4 Hz, 2H), 7.65-7.61 (m, 2H), 7.59 (dd, *J* = 8.5 Hz, 2.1, 1H), 7.55 (d, *J* = 2.3 Hz, 1H), 7.50 (dd, *J* = 8.5, 2.3 Hz, 1H), 7.46 (d, *J* = 2.3 Hz, 1H), 7.44-7.40 (m, 2H), 7.32 (t, *J* = 7.3 Hz, 1H), 7.09 (dd, *J* = 8.7, 2.1 Hz, 2H), 3.92 (t, *J* = 6.9 Hz, 2H), 1.74-1.68 (m, 2H), 1.44-1.38 (m, 2H), 1.28-1.23 (m, 4H), 0.85-0.81 (m, 3H) (carboxylic acid proton not visible); <sup>13</sup>C NMR (100 MHz, DMSO-*d*<sub>6</sub>) δ: 163.4, 147.9, 144.4, 143.5, 141.2, 138.8, 134.5, 132.9, 131.6, 130.2 (2C), 127.1, 126.3 (2C), 126.1, 126.0 (2C), 125.9, 125.1, 125.0, 123.7, 123.5, 118.9, 116.1, 116.0, 111.4, 46.6, 30.8, 26.2, 25.8, 22.1, 13.8; IR (neat, cm<sup>-1</sup>) v: 2961 (w), 2925 (w), 2852 (w), 2218 (w), 1600 (m), 1579 (m), 1464 (m), 1393 (m), 1247 (m), 1189 (m), 808 (m), 758 (s), 696 (m); HRMS (ASAP+, *m/z*): 486.2127 (calcd. C<sub>33</sub>H<sub>30</sub>N<sub>2</sub>S: 486.2130, [M-CO<sub>2</sub>+H]<sup>+</sup>); UV (CH<sub>2</sub>Cl<sub>2</sub>, 2 × 10<sup>-5</sup> M, 22 °C) λ<sub>max</sub> (nm): 425.0 (11350)



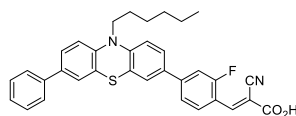
### Synthesis of (*E*)-2-cyano-3-(4-(10-hexyl-7-(4-methoxyphenyl)-10*H*-phenothiazin-3-yl)phenyl)acrylic acid (**AFB-3**)

Compound **11** (190 mg, 0.385 mmol) and cyanoacetic acid (655 mg, 7.70 mmol) were dissolved in degassed acetonitrile (46 mL) under N<sub>2</sub> atmosphere. Piperidine (457 μL, 393 mg, 4.62 mmol) was added and the reaction was heated to 80 °C for 15 minutes before cooling to 22 °C and quenched in aqueous HCl (2 M, 100 mL). EtOAc (50 mL) was added and the organic phase was washed with water (8 × 100 mL), then dried with brine (50 mL) and over anhydrous Na<sub>2</sub>SO<sub>4</sub>, filtered and the solvents were removed in vacuo. The crude product was purified by silica-gel column chromatography (gradient: 0-15% MeOH in CH<sub>2</sub>Cl<sub>2</sub>) to obtain **AFB-3** as a dark brown solid (186 mg, 0.331 mmol, 86%), mp. 237 °C (dec.). <sup>1</sup>H NMR (400 MHz, DMSO-*d*<sub>6</sub>) δ: 8.03 (s, 1H), 7.97-7.93 (m, 2H), 7.80-7.76 (m, 2H), 7.60-7.53 (m, 4H), 7.46-7.42 (m, 1H), 7.41-7.39 (m, 1H), 7.10-7.03 (m, 2H), 7.00-6.96 (m, 2H), 3.91 (t, *J* = 6.9 Hz, 2H), 3.78 (s, 3H), 1.76-1.66 (m, 2H), 1.45-1.36 (m, 2H), 1.29-1.21 (m, 4H), 0.86-0.80 (m, 3H) (carboxylic acid proton not visible); <sup>13</sup>C NMR (100 MHz, DMSO-*d*<sub>6</sub>) δ: 163.2, 158.7, 147.9, 144.5, 142.8, 141.2, 134.3, 132.8, 131.6, 131.3, 130.2 (2C), 127.2 (2C), 126.3 (2C), 126.1, 125.3, 125.0, 124.5, 123.8, 123.5, 119.0, 116.1, 116.0, 114.3 (2C), 111.0, 55.2, 46.6, 30.9, 26.2, 25.8, 22.1, 13.8; IR (neat, cm<sup>-1</sup>) v: 3033 (w, br), 2925 (w), 2847 (w), 2223 (w), 1719 (m), 1693 (m), 1574 (s, br), 1460 (s), 1242 (s), 1179 (s), 1242 (s), 1179 (s), 1023 (m), 805 (s); HRMS (ASAP+, *m/z*): 516.2228 (calcd. C<sub>34</sub>H<sub>32</sub>N<sub>2</sub>OS: 516.2235 [M-CO<sub>2</sub>]<sup>+</sup>); UV (CH<sub>2</sub>Cl<sub>2</sub>, 2 × 10<sup>-5</sup> M, 22 °C) λ<sub>max</sub> (nm): 429.5 (12700).



### Synthesis of (*E*)-2-cyano-3-(2-fluoro-4-(10-hexyl-7-phenyl-10*H*-phenothiazin-3-yl)phenyl)acrylic acid (**AFB-4**)

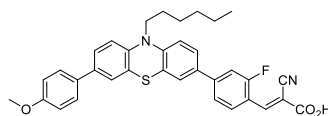
Compound **12** (205 mg, 0.425 mmol) and cyanoacetic acid (722 mg, 8.49 mmol) were dissolved in degassed acetonitrile (50 mL) under N<sub>2</sub> atmosphere. Piperidine (504 μL, 434 mg, 5.10 mmol) was added and the reaction was heated to 80 °C for 25 minutes before cooling to 22 °C and quenched in aqueous HCl (2 M, 100 mL). EtOAc (50 mL) was added and the organic phase was washed with water (6 × 100 mL), then dried with brine (50 mL) and over anhydrous Na<sub>2</sub>SO<sub>4</sub>, filtered and the solvents were removed in vacuo. The



crude product was purified by silica-gel column chromatography (gradient: 0-15% MeOH in CH<sub>2</sub>Cl<sub>2</sub>) to obtain **AFB-4** as a dark red solid (200 mg, 0.365 mmol, 86%), mp. 214 °C (dec.). <sup>1</sup>H NMR (400 MHz, DMSO-*d*<sub>6</sub>) δ: 8.19 (t, *J* = 8.2 Hz, 1H), 8.14 (s, 1H), 7.70-7.57 (m, 6H), 7.53-7.48 (m, 1H), 7.47-7.39 (m, 3H), 7.35-7.29 (m, 1H), 7.12-7.05 (m, 2H), 3.92 (t, *J* = 6.9 Hz, 2H), 1.76-1.66 (m, 2H), 1.45-1.36 (m, 2H), 1.29-1.21 (m, 4H), 0.86-0.80 (m, 3H) (carboxylic acid proton not visible); <sup>13</sup>C NMR (100 MHz, DMSO-*d*<sub>6</sub>) δ: 162.4, 160.9 (d, *J* = 251 Hz), 144.9, 143.5 (d, *J* = 10.7 Hz), 143.35, 138.8, 134.6, 131.8 (d, *J* = 3.8 Hz), 131.7, 130.2, 128.9 (2C), 128.6 (d, *J* = 2.0 Hz), 127.1, 126.2, 126.1 (2C), 125.9, 125.2, 125.0, 123.7, 123.4, 122.1 (d, *J* = 2.1 Hz), 119.3 (d, *J* = 12.0 Hz), 118.5, 116.0 (d, *J* = 21.3 Hz), 113.0, 112.7, 46.6, 30.8, 26.1, 25.8, 22.1, 13.8; IR (neat, cm<sup>-1</sup>) v: 2951 (w), 2935 (w), 2862 (w), 2218 (w), 1579 (m), 1465 (s), 1393 (m), 1257 (m), 808 (m), 758 (s), 696 (m); HRMS (ASAP+, *m/z*): 504.2035 (calcd. C<sub>33</sub>H<sub>29</sub>FN<sub>2</sub>S: 505.2035, [M-CO<sub>2</sub>]<sup>+</sup>); UV (CH<sub>2</sub>Cl<sub>2</sub>, 2 × 10<sup>-5</sup> M, 22 °C) λ<sub>max</sub> (nm): 431.5 (12950).

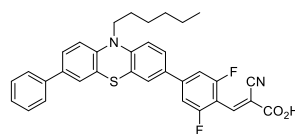
#### Synthesis of (*E*)-2-cyano-3-(2-fluoro-4-(10-hexyl-7-(4-methoxyphenyl)-10*H*-phenothiazin-3-yl)phenyl)acrylic acid (**AFB-5**)

Compound **13** (186 mg, 0.364 mmol) and cyanoacetic acid (618 mg, 7.27 mmol) were dissolved in degassed acetonitrile (44 mL) under N<sub>2</sub> atmosphere. Piperidine (432 μL, 371 mg, 4.36 mmol) was added and the reaction was heated to 80 °C for 20 minutes before cooling to 22 °C and quenched in aqueous HCl (2 M, 125 mL). EtOAc (50 mL) was added and the organic phase was washed with water (8 × 100 mL), then dried with brine (50 mL) and over anhydrous Na<sub>2</sub>SO<sub>4</sub>, filtered and the solvents were removed in vacuo. The crude product was purified by silica-gel column chromatography (gradient: 0-15% MeOH in CH<sub>2</sub>Cl<sub>2</sub>) to obtain **AFB-5** as a dark red solid (121 mg, 0.209 mmol, 58%), mp. 220 °C (dec.). <sup>1</sup>H NMR (400 MHz, DMSO-*d*<sub>6</sub>) δ: 8.18 (t, *J* = 8.0 Hz, 1H), 8.12 (s, 1H), 7.70-7.65 (m, 2H), 7.63 (dd, *J* = 8.5 Hz, 2.2, 1H), 7.60-7.55 (m, 3H), 7.45 (dd, *J* = 8.5, 2.1 Hz, 1H), 7.40 (d, *J* = 2.2 Hz, 1H), 7.07 (t, *J* = 8.4 Hz, 2H), 6.98 (d, *J* = 8.8 Hz, 2H), 3.91 (t, *J* = 6.9 Hz, 2H), 3.78 (s, 3H), 1.75-1.67 (m, 2H), 1.45-1.36 (m, 2H), 1.30-1.21 (m, 4H), 0.86-0.81 (m, 3H) (carboxylic acid proton not visible); <sup>13</sup>C NMR (100 MHz, DMSO-*d*<sub>6</sub>) δ: 162.4, 160.8 (d, *J* = 251.1 Hz), 158.7, 145.0, 143.4 (d, *J* = 9.6 Hz), 142.7, 138.3, 134.4, 131.6, 131.2, 128.5, 127.2 (2C), 126.2, 125.4, 125.1, 124.5, 123.7, 123.4, 122.1 (d, *J* = 2.3 Hz), 119.4 (d, *J* = 11.5 Hz), 118.7, 116.1, 115.8, 114.3 (2C), 112.9, 112.8, 55.2, 46.6, 30.8, 26.2, 25.8, 22.1, 13.8; IR (neat, cm<sup>-1</sup>) v: 3034 (w, br), 2925 (w), 2847 (w), 2223 (w), 1719 (m), 1693 (m), 1574 (s, br), 1460 (s), 1242 (s), 1179 (s), 1023 (m), 805 (s); HRMS (ASAP+, *m/z*): 534.2139 (calcd. C<sub>34</sub>H<sub>31</sub>N<sub>2</sub>OFS: 534.2141 [M-CO<sub>2</sub>]<sup>+</sup>); UV (CH<sub>2</sub>Cl<sub>2</sub>, 2 × 10<sup>-5</sup> M, 22 °C) λ<sub>max</sub> (nm): 440.5 (12050).



#### Synthesis of (*E*)-2-cyano-3-(2,6-difluoro-4-(10-hexyl-7-phenyl-10*H*-phenothiazin-3-yl)phenyl)acrylic acid (**AFB-6**)

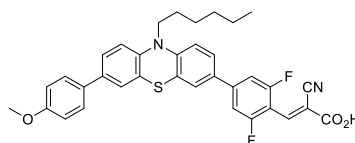
Compound **14** (228 mg, 0.457 mmol) and cyanoacetic acid (777 mg, 9.13 mmol) were dissolved in degassed acetonitrile (55 mL) under N<sub>2</sub> atmosphere. Piperidine (542 μL, 466 mg, 5.48 mmol) was added and the reaction was heated to 80 °C for 40 minutes before cooling to 22 °C and quenched in aqueous HCl (2 M, 150 mL). EtOAc (50 mL) was added and the organic phase was washed with water (8 × 100 mL), then dried with brine (50 mL) and over anhydrous Na<sub>2</sub>SO<sub>4</sub>, filtered and the solvents were removed in vacuo. The crude product was purified by silica-gel column chromatography (gradient: 0-15% MeOH in CH<sub>2</sub>Cl<sub>2</sub>) to obtain **AFB-6** as a red solid (181 mg, 0.319 mmol, 70%), mp. 210 °C (dec.). <sup>1</sup>H NMR (400 MHz, DMSO-*d*<sub>6</sub>) δ: 7.85 (s, 1H), 7.68-7.56 (m, 6H), 7.51 (dd, *J* = 8.6, 2.1 Hz, 1H), 7.46 (d, *J* = 2.2 Hz, 1H), 7.45-7.40 (m, 2H), 7.32 (t, *J* = 7.3 Hz, 1H), 7.11-7.06 (m, 2H), 3.92 (t, *J* = 6.8 Hz, 2H), 1.75-1.67 (m, 2H), 1.45-1.36 (m, 2H), 1.29-1.22 (m, 4H), 0.85-0.80 (m, 3H) (carboxylic acid proton not visible); <sup>13</sup>C NMR (100 MHz, DMSO-*d*<sub>6</sub>) δ: 161.7, 159.9 (dd, *J* = 251.6, 8.1 Hz, 2C), 145.1, 143.2, 143.0, 138.8, 135.5, 134.6, 130.8,



128.9 (2C), 127.1, 126.3, 126.0 (2C), 125.9, 125.2, 125.0, 123.7, 123.4, 121.5, 117.2, 116.1, 115.8, 109.7, 109.1 (d,  $J = 25.1$  Hz, 2C), 46.7, 30.8, 26.1, 25.8, 22.1, 13.8; IR (neat,  $\text{cm}^{-1}$ ): 2956 (w), 2925 (w), 2847 (w), 2229 (w), 1627 (m), 1463 (m), 1392 (m), 1197 (m), 1024 (m), 808 (m), 758 (s), 696 (m); HRMS (ASAP+,  $m/z$ ): 522.1937 (calcd.  $\text{C}_{33}\text{H}_{28}\text{N}_2\text{F}_2\text{S}$ : 522.1941  $[\text{M}-\text{CO}_2]^+$ ); UV ( $\text{CH}_2\text{Cl}_2$ ,  $2 \times 10^{-5}$  M, 22 °C)  $\lambda_{\text{max}}$  (nm): 419.5 (10650).

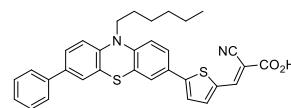
#### Synthesis of (*E*)-2-cyano-3-(2,6-difluoro-4-(10-hexyl-7-(4-methoxyphenyl)-10*H*-phenothiazin-3-yl)phenyl)acrylic acid (**AFB-7**)

Compound **20** (300 mg, 0.45 mmol) was stirred in TFA (28 mL) for 1 hour, then the reaction mixture was poured into water (40 mL) and the precipitate that formed was filtered off. The crude product was purified by silica-gel column chromatography (gradient: 0-15% MeOH in  $\text{CH}_2\text{Cl}_2$ ) to obtain **AFB-7** as a dark red solid (190 mg, 0.30 mmol, 76%), mp. 115-120 °C (dec.).  $^1\text{H}$  NMR (400 MHz,  $\text{DMSO}-d_6$ )  $\delta$ : 7.86 (s, 1H), 7.65-7.55 (m, 6H), 7.44 (dd,  $J = 8.8, 1.9$  Hz, 1H), 7.39 (d,  $J = 2.1$  Hz, 1H), 7.05 (d,  $J = 8.6$  Hz, 2H), 6.98 (d,  $J = 8.8$  Hz, 2H), 3.90 (t,  $J = 6.9$  Hz, 2H), 3.78 (s, 3H), 1.73-1.67 (m, 2H), 1.43-1.37 (m, 2H), 1.28-1.22 (m, 4H), 0.85-0.80 (m, 3H) (carboxylic acid proton not visible);  $^{13}\text{C}$  NMR (100 MHz,  $\text{DMSO}-d_6$ )  $\delta$ : 162.2, 160.1 (d,  $J = 268.3$  Hz, 2C), 158.8, 147.5 (d,  $J = 3.1$  Hz), 145.6, 142.5, 140.0, 134.5, 131.2, 130.1, 127.2 (2C), 126.4, 125.4, 125.3, 124.5, 123.8, 123.3, 117.4, 116.2, 116.0 (d,  $J = 41.6$  Hz), 115.8, 114.3 (2C), 109.1 (d,  $J = 24.9$  Hz, 2C), 98.0, 55.1, 46.6, 30.8, 26.1, 25.8, 22.1, 13.8; IR (neat,  $\text{cm}^{-1}$ ): 2966 (w, br), 2925 (w), 2857 (w), 1703 (m, br), 1631 (s, br), 1465 (s), 1195 (s), 1018 (s), 805 (s); HRMS (ASAP+,  $m/z$ ): 552.2045 (calcd.  $\text{C}_{34}\text{H}_{30}\text{F}_2\text{N}_2\text{O}\text{S}$ : 552.2047  $[\text{M}-\text{CO}_2]^+$ ); UV ( $\text{CH}_2\text{Cl}_2$ ,  $2 \times 10^{-5}$  M, 22 °C)  $\lambda_{\text{max}}$  (nm): 424.0 (9650).



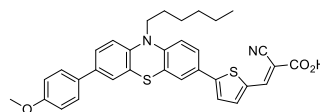
#### Synthesis of (*E*)-2-cyano-3-(5-(10-hexyl-7-phenyl-10*H*-phenothiazin-3-yl)thiophen-2-yl)acrylic acid (**AFB-8**)

Compound **16** (222 mg, 0.472 mmol) and cyanoacetic acid (803 mg, 9.44 mmol) were dissolved in degassed acetonitrile (55 mL) under  $\text{N}_2$  atmosphere. Piperidine (561  $\mu\text{L}$ , 482 mg, 5.66 mmol) was added and the reaction was heated to 80 °C for 30 minutes before cooling to 22 °C and quenched in aqueous HCl (2 M, 150 mL). EtOAc (50 mL) was added and the organic phase was washed with water ( $8 \times 100$  mL), then dried with brine (50 mL) and over anhydrous  $\text{Na}_2\text{SO}_4$ , filtered and the solvents were removed in vacuo. The crude product was purified by silica-gel column chromatography (gradient: 0-15% MeOH in  $\text{CH}_2\text{Cl}_2$ ) to obtain **AFB-8** as a dark solid (224 mg, 0.417 mmol, 88%), mp. 209 °C (dec.).  $^1\text{H}$  NMR (400 MHz,  $\text{DMSO}-d_6$ )  $\delta$ : 8.18 (s, 1H), 7.68 (d,  $J = 4.1$  Hz, 1H), 7.63 (d,  $J = 7.5$  Hz, 2H), 7.59 (d,  $J = 3.8$  Hz, 1H), 7.54-7.49 (m, 3H), 7.46-7.40 (m, 3H), 7.32 (t,  $J = 7.3$  Hz, 1H), 7.09 (d,  $J = 8.5$  Hz, 1H), 7.06 (d,  $J = 8.5$  Hz, 1H), 3.91 (t,  $J = 6.9$  Hz, 2H), 1.73-1.67 (m, 2H), 1.43-1.37 (m, 2H), 1.28-1.22 (m, 4H), 0.84-0.80 (m, 3H) (carboxylic acid proton not visible);  $^{13}\text{C}$  NMR (100 MHz,  $\text{DMSO}-d_6$ )  $\delta$ : 163.6, 148.6, 144.9, 143.2, 141.9, 138.8, 137.5, 135.1, 134.7, 128.9 (2C), 127.2, 127.1, 126.1 (2C), 126.0, 125.5, 125.0, 124.1, 124.0, 123.9, 123.2, 118.6, 116.2, 116.1, 106.6, 46.7, 30.8, 26.1, 25.8, 22.1, 13.8; IR (neat,  $\text{cm}^{-1}$ ): 2956 (w), 2909 (w), 2852 (w), 2213 (w), 1574 (m), 1470 (m), 1389 (s), 1247 (s), 1060 (m), 798 (s), 758 (s), 695 (m); HRMS (ASAP+,  $m/z$ ): 492.1690 (calcd.  $\text{C}_{31}\text{H}_{28}\text{N}_2\text{S}_2$ : 492.1694  $[\text{M}-\text{CO}_2]^+$ ); UV ( $\text{CH}_2\text{Cl}_2$ ,  $2 \times 10^{-5}$  M, 22 °C)  $\lambda_{\text{max}}$  (nm): 356.5 (19000), 466.5 (18050).



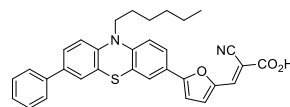
### Synthesis of (*E*)-2-cyano-3-(5-(10-hexyl-7-(4-methoxyphenyl)-10*H*-phenothiazin-3-yl)thiophen-2-yl)acrylic acid (**AFB-9**)

Compound **17** (189 mg, 0.379 mmol) and cyanoacetic acid (644 mg, 7.57 mmol) were dissolved in degassed acetonitrile (45 mL) under N<sub>2</sub> atmosphere. Piperidine (450 μL, 387 mg, 4.54 mmol) was added and the reaction was heated to 80 °C for 30 minutes before cooling to 22 °C and quenched in aqueous HCl (2 M, 150 mL). EtOAc (50 mL) was added and the organic phase was washed with water (8 × 100 mL), then dried with brine (50 mL) and over anhydrous Na<sub>2</sub>SO<sub>4</sub>, filtered and the solvents were removed in vacuo. The crude product was purified by silica-gel column chromatography (gradient: 0-15% MeOH in CH<sub>2</sub>Cl<sub>2</sub>) to obtain **AFB-9** as a dark solid (165 mg, 0.290 mmol, 77%), mp. 233 °C (dec.); <sup>1</sup>H NMR (400 MHz, DMSO-*d*<sub>6</sub>) δ: 8.16 (s, 1H), 7.73 (d, *J* = 3.9 Hz, 1H), 7.58 (d, *J* = 4.1 Hz, 1H), 7.57-7.54 (m, 2H), 7.52-7.49 (m, 2H), 7.44 (dd, *J* = 8.6, 2.1 Hz, 1H), 7.39 (d, *J* = 2.2 Hz, 1H), 7.07-7.03 (m, 2H), 6.98 (d, *J* = 8.6 Hz, 2H), 3.89 (t, *J* = 7.0 Hz, 2H), 3.78 (s, 3H), 1.72-1.66 (m, 2H), 1.42-1.36 (m, 2H), 1.28-1.22 (m, 4H), 0.85-0.80 (m, 3H) (carboxylic acid proton not visible); <sup>13</sup>C NMR (100 MHz, DMSO-*d*<sub>6</sub>) δ: 163.7, 158.7, 148.2, 145.0, 142.5, 141.5, 137.1, 135.1, 134.5, 131.2, 127.2 (2C), 127.0, 125.5, 125.4, 124.5, 124.01, 123.98, 123.8, 123.2, 118.8, 116.2, 116.0, 114.3 (2C), 106.6, 55.2, 46.6, 30.8, 26.1, 25.8, 22.1, 13.8; IR (neat, cm<sup>-1</sup>) v: 2950 (w, br), 2924 (w), 2852 (w), 1709 (m), 1688 (m, br), 1579 (s), 1444 (s), 1408 (s), 1236 (s), 1179 (s), 1060 (m), 800 (s); HRMS (ASAP+, *m/z*): 566.1691 (calcd. C<sub>33</sub>H<sub>30</sub>N<sub>2</sub>O<sub>3</sub>S<sub>2</sub>: 566.1698 [M]<sup>+</sup>); UV (CH<sub>2</sub>Cl<sub>2</sub>, 2 × 10<sup>-5</sup> M, 22 °C) λ<sub>max</sub> (nm): 360 (16800), 471.0 (15200).



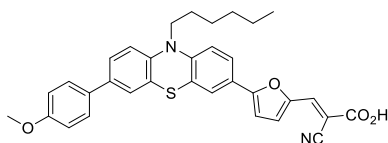
### Synthesis of (*E*)-2-cyano-3-(5-(10-hexyl-7-phenyl-10*H*-phenothiazin-3-yl)furan-2-yl)acrylic acid (**AFB-10**)

Compound **18** (264 mg, 0.583 mmol) and cyanoacetic acid (992 mg, 11.7 mmol) were dissolved in degassed acetonitrile (60 mL) under N<sub>2</sub> atmosphere. Piperidine (693 μL, 596 mg, 6.99 mmol) was added and the reaction was heated to 80 °C for 15 minutes before cooling to 22 °C and quenched in aqueous HCl (2 M, 150 mL). EtOAc (50 mL) was added and the organic phase was washed with water (8 × 100 mL), then dried with brine (50 mL) and over anhydrous Na<sub>2</sub>SO<sub>4</sub>, filtered and the solvents were removed in vacuo. The crude product was purified by silica-gel column chromatography (gradient: 0-15% MeOH in CH<sub>2</sub>Cl<sub>2</sub>) to obtain **AFB-10** as a dark solid (149 mg, 0.285 mmol, 49%), mp. 154 °C (dec.). <sup>1</sup>H NMR (400 MHz, DMSO-*d*<sub>6</sub>) δ: 7.89 (s, 1H), 7.72 (dd, *J* = 8.7, 1.9 Hz, 1H), 7.68 (d, *J* = 2.1 Hz, 1H), 7.63 (d, *J* = 7.3 Hz, 2H), 7.51 (dd, *J* = 8.5, 2.1 Hz, 1H), 7.47 (d, *J* = 2.1 Hz, 1H), 7.43 (t, *J* = 7.7 Hz, 2H), 7.35 (d, *J* = 3.5 Hz, 1H), 7.32 (t, *J* = 7.3 Hz, 1H), 7.21 (d, *J* = 3.6 Hz, 1H), 7.14 (d, *J* = 8.7 Hz, 1H), 7.10 (d, *J* = 8.7 Hz, 1H), 3.94 (t, *J* = 6.9 Hz, 2H), 1.74-1.68 (m, 2H), 1.44-1.38 (m, 2H), 1.28-1.22 (m, 4H), 0.85-0.81 (m, 3H) (carboxylic acid proton not visible); <sup>13</sup>C NMR (100 MHz, DMSO-*d*<sub>6</sub>) δ: 160.0, 156.8, 147.7, 145.2, 143.1, 138.7, 135.3, 134.8, 128.9 (2C), 127.2, 126.1 (2C), 126.0, 125.0, 124.4, 123.7, 123.2, 123.1 (2C), 118.0, 116.3, 116.1, 108.5, 102.0, 46.7, 30.8, 26.1, 25.7, 22.1, 13.8 (1 shift is missing); IR (neat, cm<sup>-1</sup>) v: 2955 (w), 2917 (w), 2849 (w), 2215 (w), 1686 (w), 1580 (m), 1454 (s), 1390 (m), 1233 (m), 1023 (m), 791 (m), 759 (s), 695 (m); HRMS (ASAP+, *m/z*): 476.1922 (calcd. C<sub>31</sub>H<sub>28</sub>N<sub>2</sub>O<sub>3</sub>S: 476.1922 [M-CO<sub>2</sub>]<sup>+</sup>); UV (CH<sub>2</sub>Cl<sub>2</sub>, 2 × 10<sup>-5</sup> M, 22 °C) λ<sub>max</sub> (nm): 363.0 (14850), 479.5 (19150).



Synthesis of (*E*)-2-cyano-3-(5-(10-hexyl-7-(4-methoxyphenyl)-10*H*-phenothiazin-3-yl)furan-2-yl)acrylic acid (**AFB-11**)

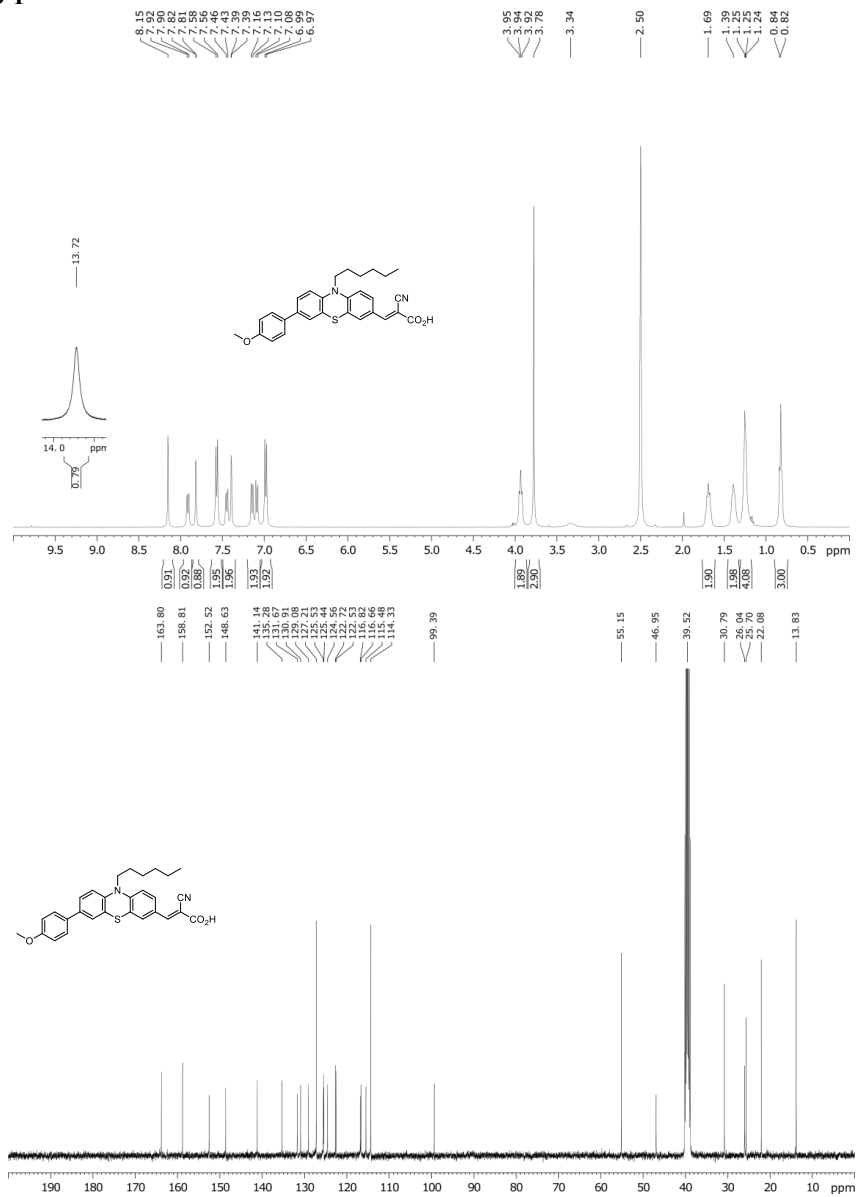
Compound **21** (120 mg, 0.19 mmol) was stirred in TFA (12 mL) for 10 minutes until full conversion was observed. The reaction mixture was poured into water (40 mL) and the precipitate that formed was filtered off. The crude product was purified by silica-gel column chromatography (gradient: 0-15% MeOH in CH<sub>2</sub>Cl<sub>2</sub>) to obtain **AFB-11** as a



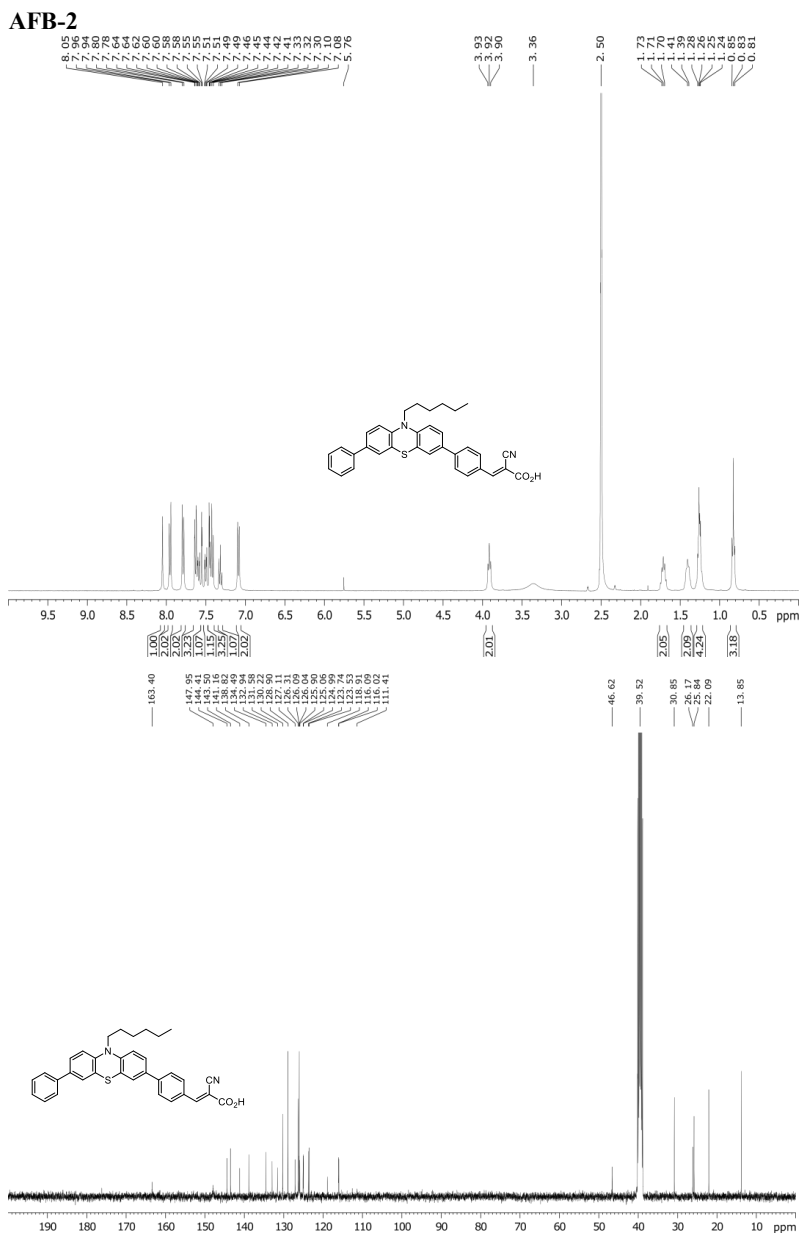
black solid (83 mg, 0.15 mmol, 79%), mp. 155-160 °C (dec.). <sup>1</sup>H NMR (400 MHz, DMSO-*d*<sub>6</sub>) δ: 7.83 (s, 1H), 7.70 (dd, *J* = 8.5, 2.2 Hz, 1H), 7.66 (d, *J* = 2.1 Hz, 1H), 7.57 (d, *J* = 8.8 Hz, 2H), 7.45 (dd, *J* = 8.4, 2.1 Hz, 1H), 7.41 (d, *J* = 2.1 Hz, 1H), 7.27 (d, *J* = 3.6 Hz, 1H), 7.18 (d, *J* = 3.6 Hz, 1H), 7.12 (d, *J* = 8.8 Hz, 1H), 7.07 (d, *J* = 8.6 Hz, 1H), 6.98 (d, *J* = 8.8 Hz, 2H), 3.92 (t, *J* = 6.9 Hz, 2H), 3.78 (s, 3H), 1.75-1.66 (m, 2H), 1.45-1.36 (m, 2H), 1.29-1.21 (m, 4H), 0.85-0.80 (m, 3H) (carboxylic acid proton not visible); <sup>13</sup>C NMR (100 MHz, DMSO-*d*<sub>6</sub>) δ: 164.0, 158.7, 156.1, 147.9, 145.1, 142.5, 134.6, 131.2, 127.2 (2C), 125.5, 125.4, 124.5, 124.2, 123.7, 123.3, 123.1, 122.9, 118.7, 116.3, 116.0, 114.3 (2C), 113.6, 108.2, 95.4, 55.2, 46.7, 30.8, 26.1, 25.7, 22.1, 13.8; IR (neat, cm<sup>-1</sup>) ν: 3132 (w, br), 2956 (w), 2919 (w), 2847 (w), 2213 (w), 1683 (s, br), 1579 (s), 1455 (s), 1418 (s), 1236 (s), 1034 (s), 935 (w), 790 (s); HRMS (ASAP+, *m/z*): 506.2024 (calcd. C<sub>32</sub>H<sub>30</sub>N<sub>2</sub>O<sub>4</sub>S: 506.2028 [M-CO<sub>2</sub>]<sup>+</sup>); UV (CH<sub>2</sub>Cl<sub>2</sub>, 2 × 10<sup>-5</sup> M, 22 °C): λ<sub>max</sub> (nm): 362.5 (14200), 473.0 (14800).

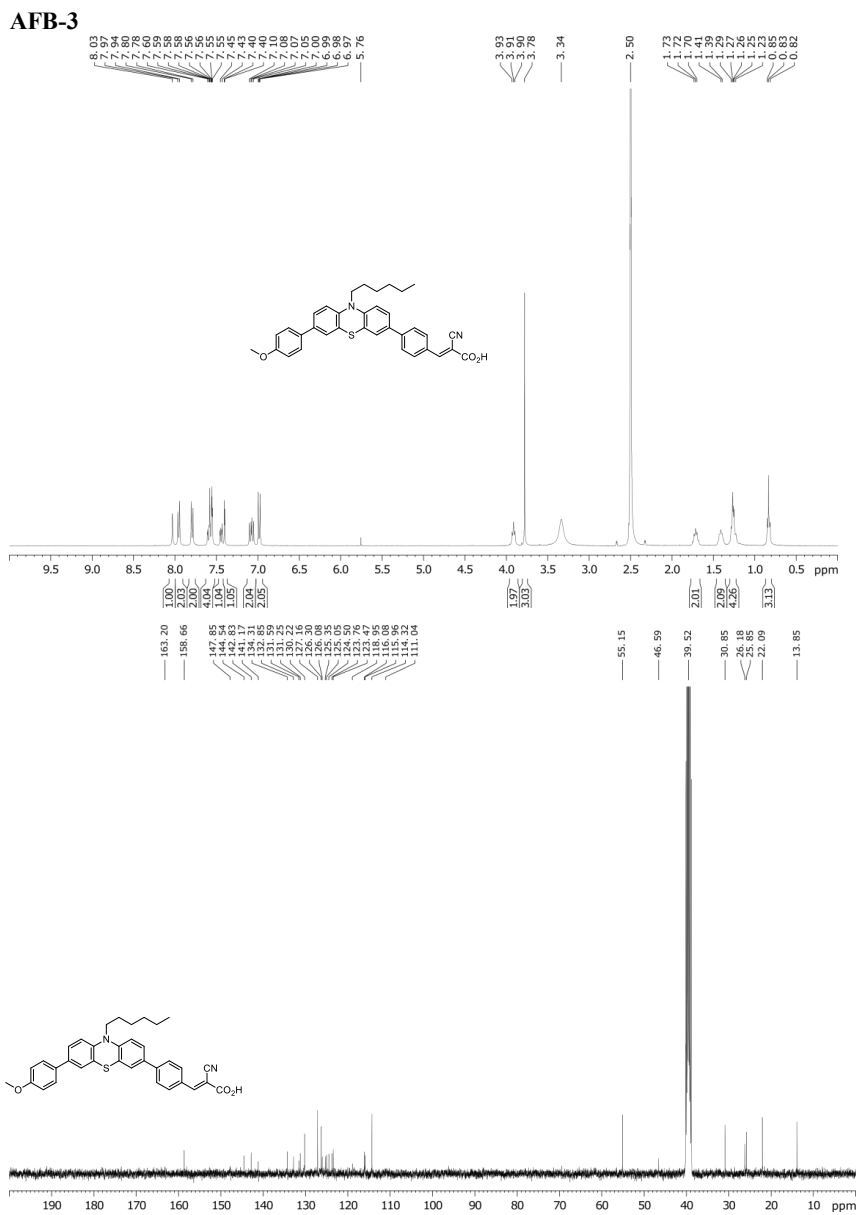
## NMR

## AFB-1

Fig. S7.  $^1\text{H}$  and  $^{13}\text{C}$  NMR spectra for AFB-1.



Fig. S8.  $^1\text{H}$  and  $^{13}\text{C}$  NMR spectra for AFB-2.

Fig. S9.  $^1\text{H}$  and  $^{13}\text{C}$  NMR spectra for AFB-3.

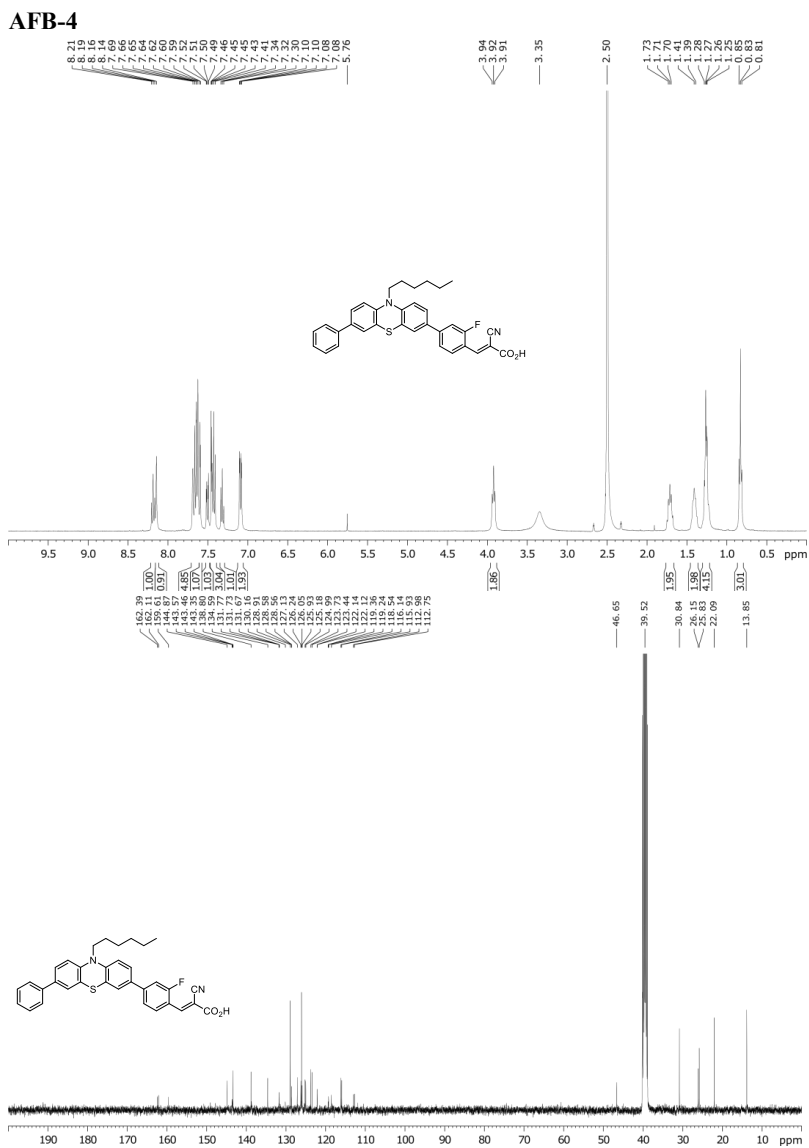


Fig. S10.  $^1\text{H}$  and  $^{13}\text{C}$  NMR spectra for AFB-4.

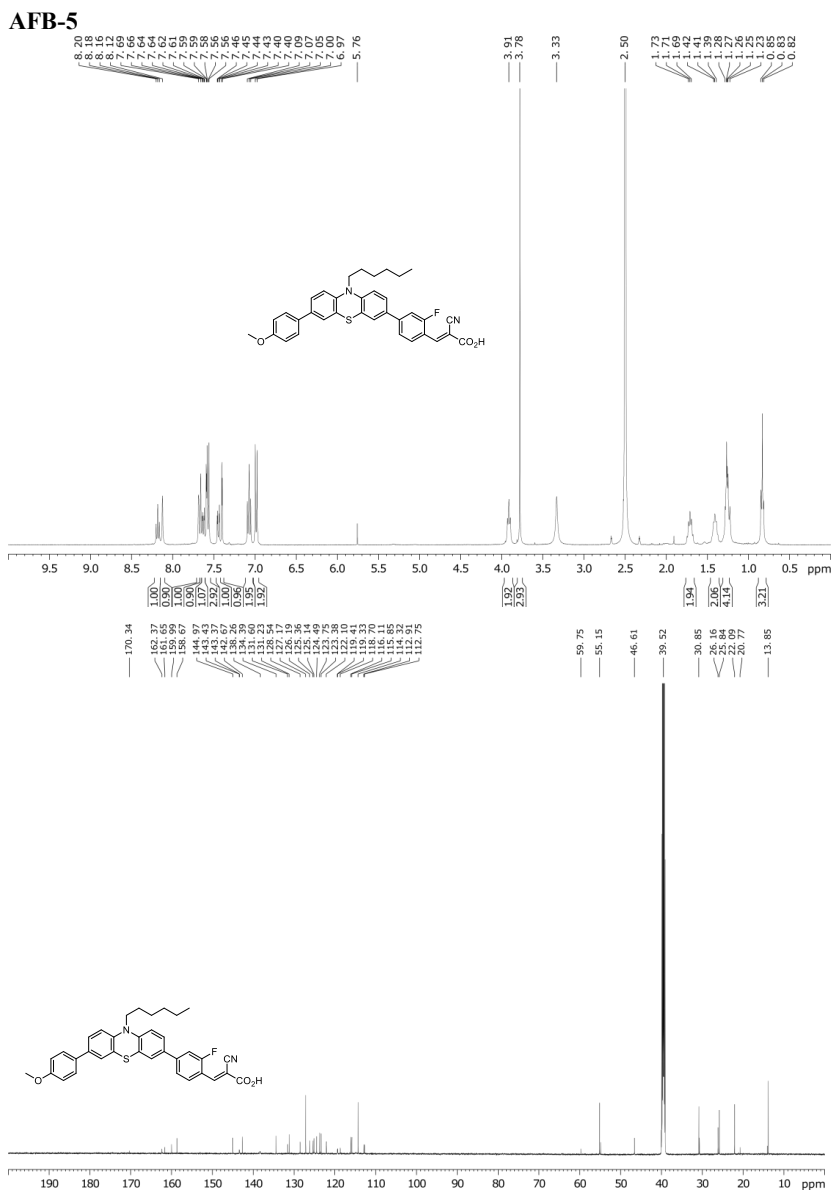
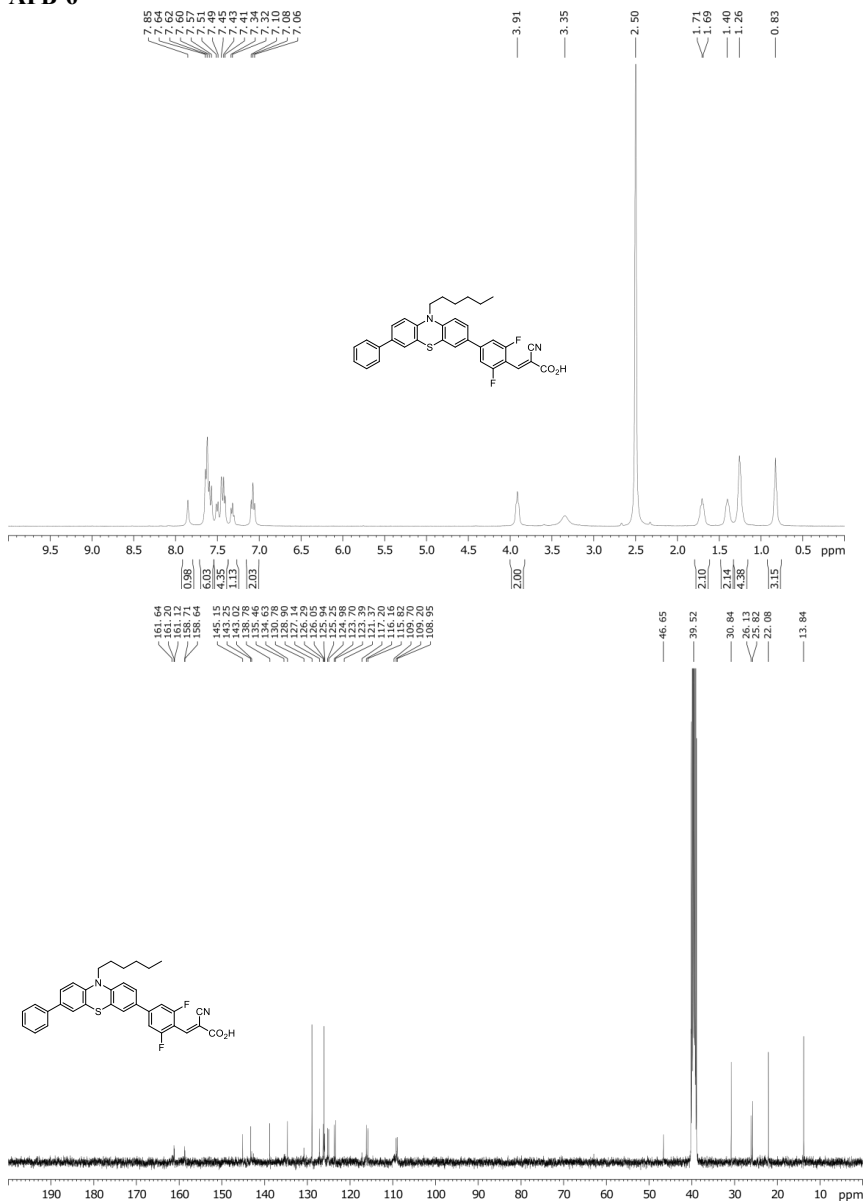
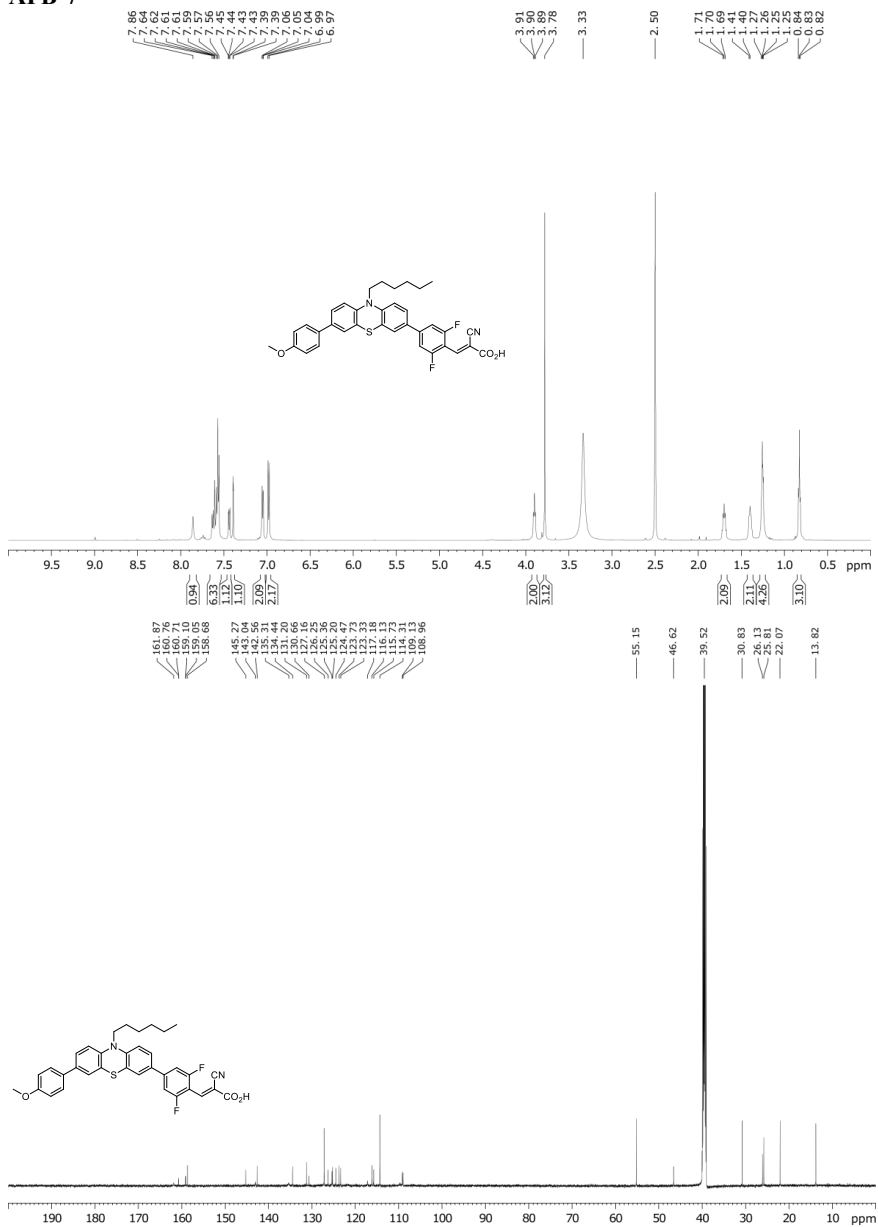


Fig. S11.  $^1\text{H}$  and  $^{13}\text{C}$  NMR spectra for AFB-5.

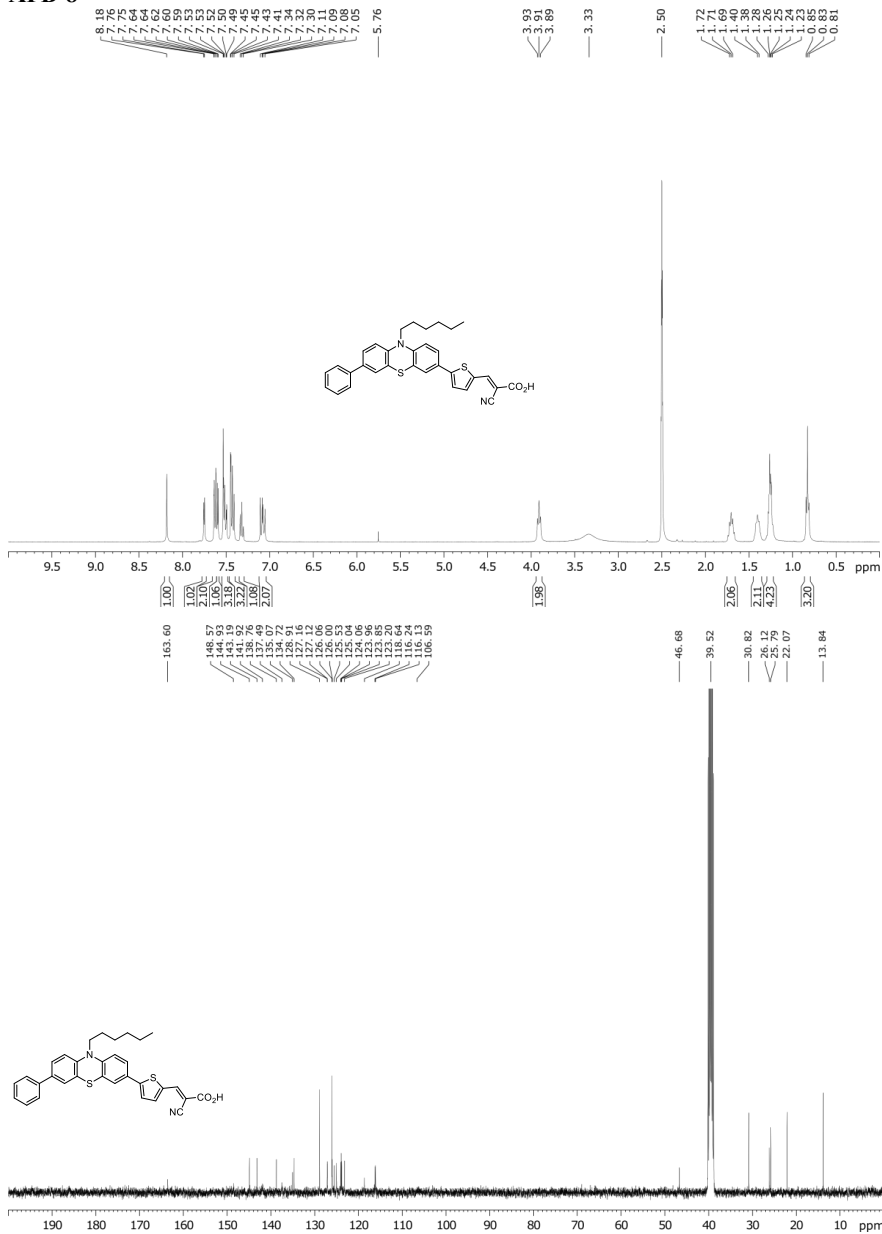
## AFB-6

Fig. S12.  $^1\text{H}$  and  $^{13}\text{C}$  NMR spectra for AFB-6.

## AFB-7

Fig. S13.  $^1\text{H}$  and  $^{13}\text{C}$  NMR spectra for AFB-7.

## AFB-8

Fig. S14.  $^1\text{H}$  and  $^{13}\text{C}$  NMR spectra for AFB-8.





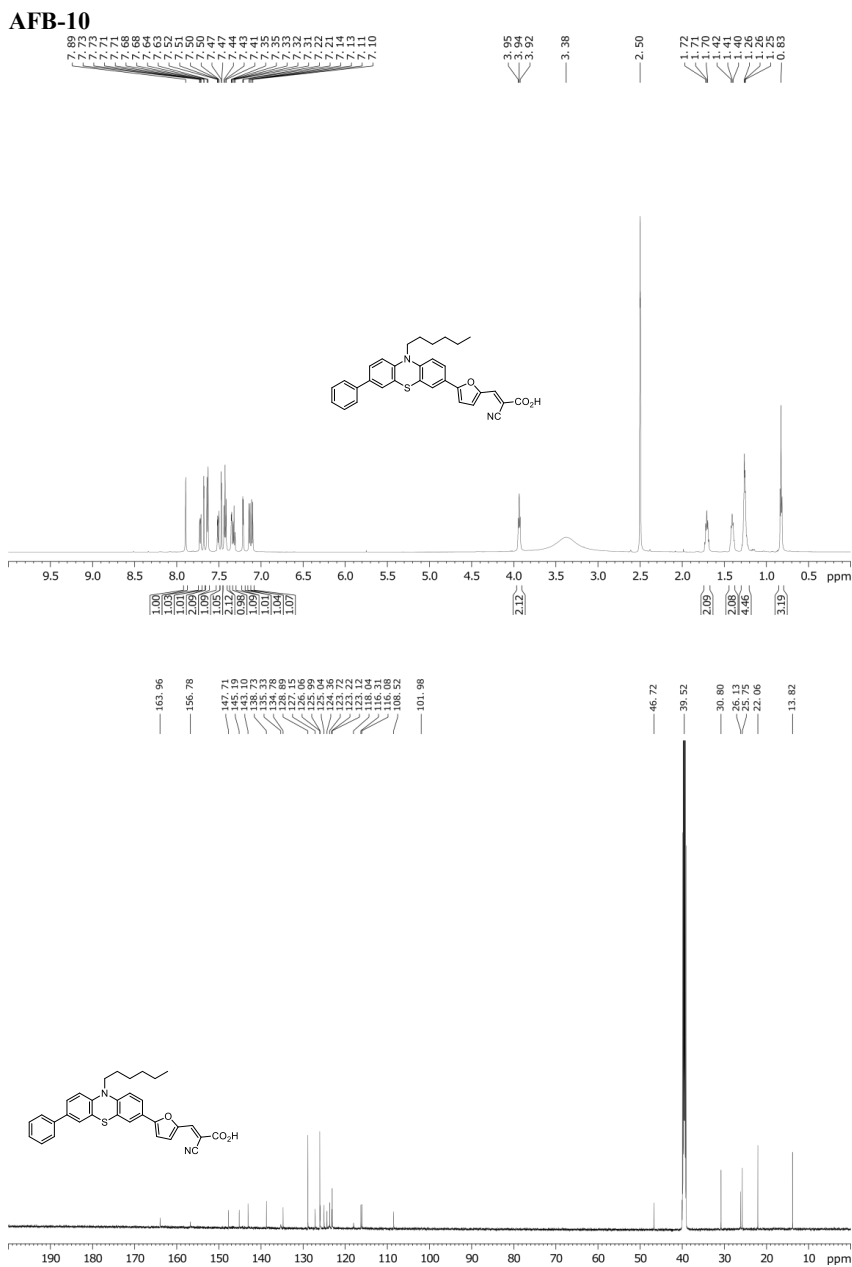
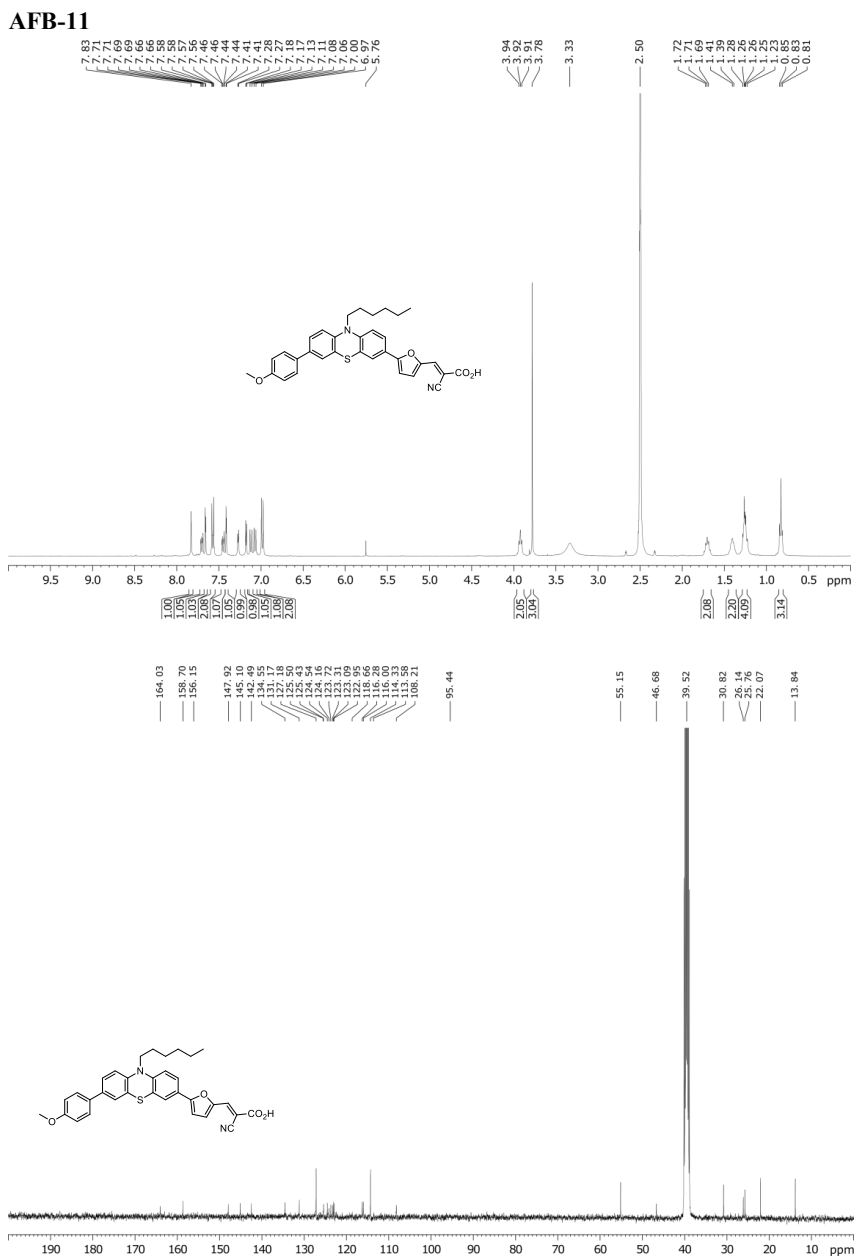


Fig. S16.  $^1\text{H}$  and  $^{13}\text{C}$  NMR spectra for AFB-10.

Fig. S17.  $^1\text{H}$  and  $^{13}\text{C}$  NMR spectra for AFB-11.



## PAPER II

**Auxiliary donors for phenothiazine sensitizers for dye-sensitized solar cells - How important are they really?**

Reprinted with permission from The Royal Society of Chemistry.







Cite this: *J. Mater. Chem. A*, 2019, 7, 7581

## Auxiliary donors for phenothiazine sensitizers for dye-sensitized solar cells – how important are they really?†

Audun Formo Buene,<sup>1b</sup> Eline Ekornhol Ose,<sup>a</sup> Ane Garborg Zakariassen,<sup>a</sup> Anders Hagfeldt<sup>1b</sup> and Bård Helge Hoff<sup>1b</sup>\*<sup>a</sup>

Auxiliary donors are common design motifs for phenothiazine sensitizers for dye-sensitized solar cells. Despite this, there are only a few reports on their overall contribution to the photon-to-electron conversion efficiency. Twelve sensitizers have been prepared and investigated, including ten different auxiliary donors in addition to a control with no auxiliary donor. The various auxiliary donors improved the PCE by a modest 4–11%, and pyrene (AFB-19) was determined to be the most efficient auxiliary donor, with the best cell delivering a PCE of 5.36%. Included in the dye series was also the champion dye within the phenothiazine class. With a reported PCE of 12.1%, it would be an excellent phenothiazine reference dye. The high  $V_{OC}$  of 0.83 V of this dye is worth further investigation, but the absorption and photovoltaic performance in this work does not correlate with the previously reported PCE of 12.1%.

Received 14th January 2019  
Accepted 21st February 2019

DOI: 10.1039/c9ta00472f

rsc.li/materials-a

### Introduction

Dye-sensitized solar cells based on mesoscopic oxide electrodes are a promising third generation photovoltaic technology first described by O'Regan and Grätzel in 1991.<sup>1</sup> Their major advantages over traditional solar cell technologies are their inherent tunability with regard to colour and flexibility. In addition, very low production costs and ease of production are encouraging aspects. Recently, DSSCs have also emerged as interesting components for low power devices for the Internet of Things (IoT).<sup>2</sup> Transparent solid state DSSCs are also a crucial component of a new technology for focus-induced photoresponse distance measurements, which is developed by the company trinamiX.<sup>3</sup>

Dye development has been an important driving force in the DSSC field. The earlier reported dyes were based on chlorophyll-like porphyrin structures<sup>4,5</sup> as well as ruthenium(II) bipyridine complexes such as N3, and later N719.<sup>6</sup> Recognizing the limitations of these dyes led to the development of metal-free dyes, allowing for higher extinction coefficients, tunability and easier purification in dye synthesis.<sup>7</sup> For a more complete description of the workings of a DSSC, dye development and device characterization, we refer the reader to a number of very good reviews on the topics.<sup>8–11</sup>

While metal-based dyes rely on a metal-to-ligand-charge-transfer (MLCT) process, metal-free dyes operate *via* an internal charge transfer excitation and often use a design concept following the donor- $\pi$ -acceptor/anchor (D- $\pi$ -A) layout.

Other design concepts without a traditional donor group have also been reported.<sup>12,13</sup> The most utilized anchoring group is cyanoacrylic acid which also provides a pulling effect.<sup>14</sup> Common  $\pi$ -spacers are usually based on phenyls,<sup>15</sup> five-membered heterocycles<sup>16</sup> or fused heterocycles,<sup>17</sup> while popular donor groups include triarylaminines,<sup>18</sup> phenothiazines,<sup>19,20</sup> and coumarins,<sup>21</sup> among others.

The role of the donor group is to provide an inductive pushing effect helping with charge injection upon excitation. Donor groups may also be able to carry the positive charge of the sensitizer, keeping them spatially separated from TiO<sub>2</sub> to suppress electron recombination and facilitate regeneration from the redox shuttle. Many metal-free dyes utilize a moiety called an auxiliary donor, making the dye layout a D-D- $\pi$ -A system, as illustrated in Fig. 1. These auxiliary donors are reported to increase the extinction coefficient of sensitizers when directly in conjugation with the main chromophore, leading to higher power conversion efficiencies of DSSCs.<sup>22</sup>

For the phenothiazine scaffold, some of the most common auxiliary donors are *para*-alkoxy phenyls,<sup>23,24</sup> *ortho*- and *para*-alkoxy phenyls,<sup>20,25</sup> triphenylaminines<sup>26,27</sup> and carbazoles.<sup>28</sup>

Although a number of auxiliary donors have been tested for the phenothiazine scaffold, only a few reports actually compared the auxiliary donors to the auxiliary donor-free dye.<sup>24,29,30</sup> In these cases the contribution from the auxiliary donors varies from a 16% decrease to a 14% increase in performance, thus highlighting the importance of understanding how different

<sup>a</sup>Department of Chemistry, Norwegian University of Science and Technology (NTNU), N-7491 Trondheim, Norway. E-mail: bard.h.hoff@ntnu.no

<sup>b</sup>Laboratory of Photomolecular Science, Institute of Chemical Sciences and Engineering, École Polytechnique Fédérale de Lausanne (EPFL), Chemin des Alambics, Station 6, CH-1015 Lausanne, Switzerland

† Electronic supplementary information (ESI) available. See DOI: 10.1039/c9ta00472f

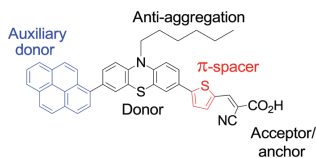


Fig. 1 D–D– $\pi$ –A structure of AFB-19.

auxiliary donors affect the phenothiazine dye performance. Because the aromatic system of 10H-phenothiazine in the ground state is bent, the conjugation is broken at the N and S bridges. This implies that the nature of the auxiliary donor is predominantly to provide an inductive push in the push–pull system of D–D– $\pi$ –A phenothiazine dyes.

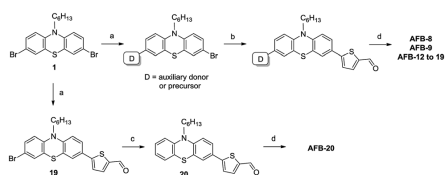
However, the auxiliary donor is also part of the sensitizer molecule that is most likely to interact with the redox shuttle in regeneration of the oxidized dye molecule. Therefore, the role of the auxiliary donor must be more complex than that of a simple electron donating substituent. Several auxiliary donors have been designed to increase its interactions with certain redox shuttles, in particular copper and cobalt complexes.<sup>31–33</sup>

In order to gain further understanding of the role and importance of the auxiliary donor in phenothiazine dyes, we have prepared ten dyes by varying only the auxiliary donor. The rest of the dye molecules remain the same with a thiophene  $\pi$ -spacer, *n*-hexyl anti-aggregation chain, 10H-phenothiazine core and cyanoacrylic acceptor and anchoring group. The auxiliary donors selected for this study include six different phenyl-based, three naphthyl-based and pyrene, as shown in Fig. 2. In addition we have included a dye without any auxiliary donor, which was previously reported by both Yang *et al.*<sup>34</sup> and Wei *et al.*<sup>35</sup>. Finally, a reference dye reported by Nagarajan *et al.*<sup>36</sup> was also synthesized in an attempt to verify their claim of over 12% efficiency, which was also used as a helpful yardstick for our own sensitizers.

## Results and discussion

### Dye synthesis

The synthesis of the building block 3,7-dibromo-10-hexyl-10H-phenothiazine (**1**) as well as dyes AFB-8 and AFB-9 has



Scheme 1 General synthesis route to dyes AFB-8, 9, and 12–19 as well as the dehalogenation route to AFB-20. (a) Suzuki coupling, (b) borylation-Suzuki two-step reaction, (c) Pd-catalyzed dehalogenation, and (d) Knoevenagel condensation. For details, see the ESI.†

previously been reported by the authors.<sup>37</sup> All detailed synthetic procedures are given in the ESI.† and a general synthesis scheme for dyes AFB-8, 9, and 12–19 is shown in Scheme 1. The various auxiliary donors were introduced using a Suzuki cross coupling from their respective aryl boronic acids. This reaction displays low chemoselectivity, leading to roughly a 1 : 2 : 1 distribution of starting material **1**, the desired monocoupled products and the dicoupled byproducts. The starting material is possible to recover, and the purifications are usually uncomplicated, so we have selected this approach rather than the fairly popular route of a monobromination followed by a Suzuki coupling and then another bromination.<sup>24,25</sup> If no  $\pi$ -spacer is required, then formylation followed by bromination is a common approach.<sup>23,38</sup> In the synthesis of dye **18**, the *tert*-butyldimethylsilyl ether (TBDMS) protecting group of the naphtholic boronic acid was cleaved during the Suzuki coupling, and rather conveniently the deprotected naphthol product **8** was obtained. Deprotection of TBDMS with mild carbonate bases or palladium(ii) is not unheard of,<sup>39,40</sup> but we were positively surprised by the efficiency of the deprotection, eliminating the need for a separate deprotection step.

In order to efficiently introduce the thiophene  $\pi$ -spacer, a borylation-Suzuki two-step approach was used. First the building blocks with the auxiliary donor moieties were borylated, following a protocol by Billingsley and Buchwald.<sup>41</sup> Without further purification, the crude phenothiazine pinacol boronic esters were coupled with 5-bromo-2-thiophenecarboxaldehyde using Pd(OAc)<sub>2</sub> and SPhos in a 1 : 1 (v/v) mixture of water and 1,4-dioxane at 80 °C. The resulting aldehydes were then converted into cyanoacrylic acid anchoring groups *via* the Knoevenagel condensation following the procedure of Iqbal *et al.*<sup>42</sup> using

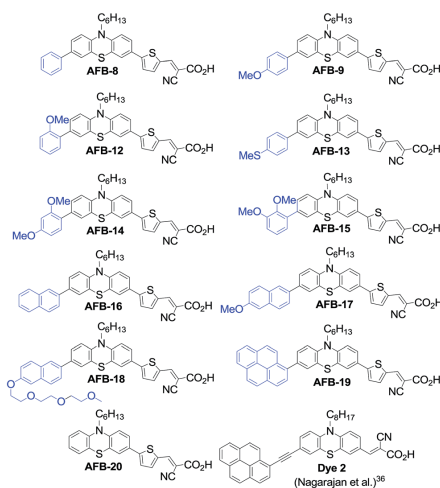
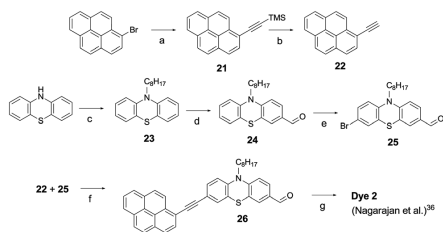


Fig. 2 Structures of the twelve dyes investigated.



Scheme 2 Synthetic route to Dye 2. (a) Ethynyltrimethylsilane,  $\text{PdCl}_2(\text{PPh}_3)_2$ , CuI,  $\text{Et}_3\text{N}$ , 80 °C; (b) NaOH, r.t.; (c) NaH, 1-bromooctane, 66 °C; (d) DMF,  $\text{POCl}_3$ , 1,2-dichloroethane, reflux; (e) NBS, r.t.; (f)  $\text{PdCl}_2(\text{PPh}_3)_2$ , CuI,  $\text{Et}_3\text{N}$ , 80 °C; (g) cyanoacetic acid, piperidine, 80 °C.

cyanoacetic acid and piperidine in acetonitrile. The workup and purification conditions were kept as similar as possible for all the target molecules, in case any residual reagents or solvents affected the molecular properties in any way.

Sensitizer AFB-20 has previously been prepared through monobromination approaches by Yang *et al.*<sup>34</sup> and Wei *et al.*<sup>35</sup> By using the precursors already at hand, we obtained AFB-20 through another route (Scheme 1). First, a Suzuki coupling catalyzed by the  $\text{Pd}(\text{OAc})_2/\text{SPhos}$  system introduced the thiophene carboxaldehyde in a non-selective manner. (5-Formylthiophen-2-yl)boronic acid proved to be less stable than

phenyl-based boronic acids; thus, a larger excess (1.5 eq.) was required to obtain comparable conversion.

The monocoupled product 19 obtained after purification was debrominated in a palladium catalyzed reaction as reported by Chen *et al.*,<sup>43</sup> using  $\text{Pd}(\text{OAc})_2$ , triphenylphosphine and  $\text{K}_2\text{CO}_3$  in *n*-butanol at 100 °C to yield compound 20. The Knoevenagel condensation produced sensitizer AFB-20, bearing no auxiliary donor.

Because the reference sensitizer Dye 2 has no  $\pi$ -spacer between the phenothiazine core and the anchoring group, a slightly different synthetic route had to be employed (see Scheme 2). First, 10H-phenothiazine was alkylated (see Scheme 2). First, 10H-phenothiazine was alkylated at the 10H nitrogen atom, followed by monoformylation by Vilsmeier-Haack reaction and a bromination with *N*-bromosuccinimide (NBS). The resulting building block 25 was then coupled with 1-ethynylpyrene (22) in a Sonogashira cross coupling before the final Knoevenagel reaction installed the anchoring group using the same conditions as for the other dyes.

### Photophysical properties

The UV/Vis absorption spectra of all dyes in THF and anchored on  $\text{TiO}_2$  films are shown in Fig. 3, and extinction coefficients and absorption maxima are given in Table 1. The absorption spectra of all dyes display two major peaks: one between 300 and 400 nm is attributed to the  $\pi$ - $\pi^*$  excitation of the aromatic system, while the other peak is found in the region between 400 and 500 nm, which is the internal charge transfer (ICT)

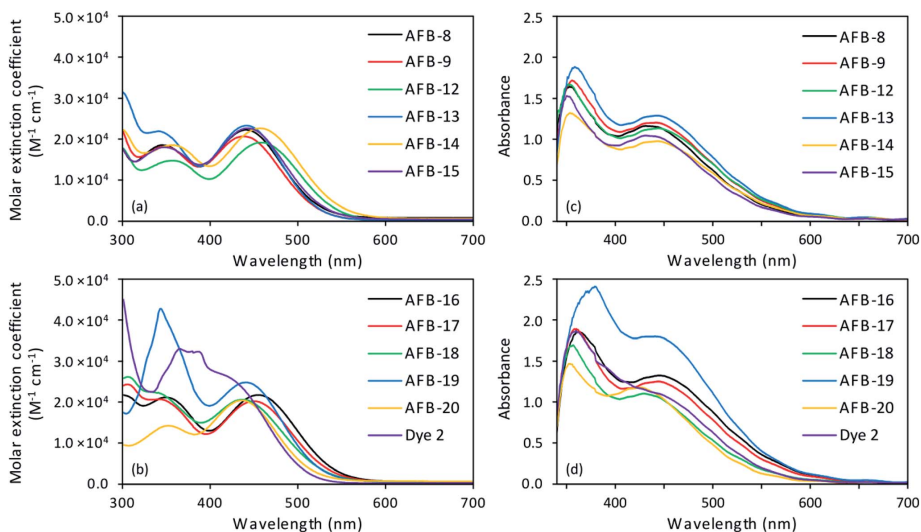


Fig. 3 (a and b) Absorption spectra of all dyes in THF solution ( $2 \times 10^{-5}$  M). (a) AFB-8, 9, and 12 to 15 have phenyl-based donors, (b) AFB-16 to 18 have naphthyl-based donors, and AFB-19 and Dye 2 have pyrene donors. Dye AFB-20 has no auxiliary donor. (c and d) Absorption spectra of all dyes on  $\text{TiO}_2$  films (2.5  $\mu\text{m}$ , 18NR-T, GreatcellSolar).



Table 1 Photophysical properties of all dyes

Dye	$\lambda_{\text{abs}}^a$ (nm)	$\epsilon$ ( $\text{M}^{-1} \text{cm}^{-1}$ )	$\text{Em}^b$ (nm)	$\lambda_{\text{abs}}^c$ on $\text{TiO}_2$ (nm)	$E_{0-0}^d$ (V)	$E_{\text{ox}}^e$ (V vs. SHE)	$E_{\text{LUMO}}^f$ (V vs. SHE)
AFB-8	441	22 200	626	432	2.32	0.94	-1.38
AFB-9	439	20 600	637	441	2.33	0.90	-1.43
AFB-12	459	19 050	601	444	2.36	0.91	-1.45
AFB-13	442	23 250	629	443	2.32	0.92	-1.40
AFB-14	457	22 600	618	444	2.32	0.87	-1.45
AFB-15	443	22 600	617	431	2.36	0.86	-1.50
AFB-16	455	21 350	618	445	2.34	0.93	-1.41
AFB-17	450	19 850	629	440	2.30	0.90	-1.40
AFB-18	437	20 200	594	430	2.32	0.90	-1.42
AFB-19	441	24 450	620	441	2.36	0.92	-1.44
AFB-20	436	20 050	624	426	2.36	1.01	-1.35
Dye 2	418	27 550	585	n/a <sup>g</sup>	2.42	1.06	-1.36

<sup>a</sup> Maximum of the most red-shifted peak. <sup>b</sup> Emission when the ICT band is excited, in THF solution. <sup>c</sup> Maximum of the most red-shifted peak on  $\text{TiO}_2$  (2.5  $\mu\text{m}$ , GreatCellSolar 18NR-1). <sup>d</sup> Calculated from the intersection of the absorption and normalized emission spectra. <sup>e</sup> Measured in DMF vs.  $\text{Fc}^+/ \text{Fc}$  and converted to V vs. SHE by a conversion factor of 0.624. <sup>f</sup> Calculated from  $E_{\text{ox}} - E_{0-0}$ . <sup>g</sup> No clear peak to assign.

transition process. The ICT peaks of dyes on  $\text{TiO}_2$  are blue-shifted by approximately 10 nm compared to the solution measurements. The absorption of the two pyrene-containing sensitizers displays irregular features in the spectra, likely to stem from separate absorptions within the pyrene moiety. The UV/Vis absorption spectra of 1-bromopyrene and 1-ethynylpyrene (ESI, Fig. S2†) display similar irregular absorption features in the same region.

All the sensitizers with phenyl-based auxiliary donors have very similar UV/Vis absorption properties. The absorption maxima of the two dyes with *ortho*-methoxy substituents on the phenyl donor are red-shifted by about 20 nm compared to the rest of the selection. However, the optical bandgaps are all in the range of 2.32–2.36 eV, and the differences in extinction coefficients are also very small. The naphthyl series displays largely the same properties as the phenyl dyes in terms of bandgaps, absorption maxima and extinction coefficients. For

this series, the triethylene oxide methyl ether containing dye **AFB-18** causes a blue-shift of the absorption maxima of about 15 nm; however, the bandgaps are virtually unchanged. The spectrum of **AFB-20** (no auxiliary donor) reveals an ICT band comparable in intensity and position to that of the dyes with auxiliary donors, but the  $\pi-\pi^*$  excitation is noticeably less pronounced. From UV/Vis absorption spectra it is therefore quite clear that the auxiliary donors in phenothiazine dyes do not significantly increase the ICT transition.

#### Electrochemical properties

Cyclic voltammetry was performed for all dyes to determine the oxidation potentials of the sensitizers, and they all displayed a single reversible oxidation peak. The dyes are sparingly soluble in acetonitrile, so DMF was selected to ensure that all dyes could be measured in the same solvent. Acetonitrile is the main component of the DSSC electrolyte, so when measuring

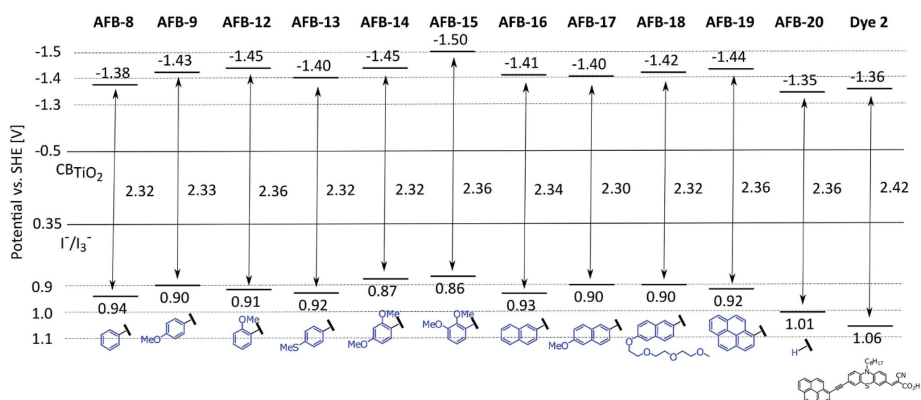


Fig. 4 HOMO and LUMO levels of all dyes. We calculated the HOMO levels from the oxidation potentials of the dyes measured with cyclic voltammetry, and the LUMO levels were calculated from the optical band gaps.

the sensitizers in DMF slightly shifted values may be obtained, but any difference is assumed to be comparable for all twelve sensitizers and not of significant magnitude.<sup>44</sup> Cyclic voltammograms are shown in the ESI (Fig. S3 and S4†), the extracted values for the oxidation potentials vs. SHE are shown in Table 1, and Fig. 4 gives a visual summary of the position of the HOMO and LUMO levels of the dyes. All the dyes apart from **AFB-20** and **Dye 2** display an  $E_{ox}$  value in the range of 0.86–0.94 V vs. SHE. For **AFB-20** and **Dye 2**, the  $E_{ox}$  values were found to be 1.01 and 1.06 V, respectively. Compared to **AFB-20**, the introduction of these auxiliary donors raises the HOMO levels by up to 0.15 eV. While using the  $I^-/I_3^-$  redox couple there is still sufficient driving force for regeneration, a higher HOMO could give rise to regeneration problems when working with cobalt or copper redox couples. The di-substituted auxiliary donor dyes (**AFB-14** and **15**) have, by a very small margin, the highest positioned HOMO levels. Only slightly below are the mono-substituted phenyl and naphthyl-substituted dyes, which are indistinguishable by cyclic voltammetry.

All the oxidation potentials should be sufficiently higher than the redox potential of the  $I^-/I_3^-$  electrolyte (0.35 V vs. NHE<sup>45</sup>) in order for efficient regeneration to take place. The calculated LUMO levels of the dyes ( $E_{ox} - E_{0-0}$ ) are all found from –1.35 to –1.50 V vs. SHE, giving all sensitizers sufficient driving force for the charge injection process into  $TiO_2$  (–0.5 V vs. SHE) to be favorable.

### Photovoltaic performance

Three DSSC devices were fabricated and characterized for each sensitizer. The  $J-V$  curves measured under 1 sun AM 1.5G illumination ( $100 \text{ mW cm}^{-2}$ ) and the incident-photon-to-current conversion efficiency (IPCE) spectra are shown in Fig. 5 and 6, respectively. When comparing **AFB-20** to the rest of the dyes, it is clear that the use of an auxiliary donor improves the PCE by 4–11%, with an average improvement of 7% (Table 2). The most efficient dyes, **Dye 2** and **AFB-19**, also display a higher dye loading compared to **AFB-20** (ESI, Table S1†). By grouping the efficiencies of the phenyl-based (**AFB-8, 9**, and **12–15**), naphthyl-

based (**AFB-16, 17**, and **18**) and pyrene (**AFB-19**) auxiliary donors, the average PCE values are 4.80, 4.86 and 5.00%, respectively. The series composed of **AFB-8**, **AFB-16** and **AFB-19** also displays the same trend. The efficiencies increase from 4.76% for phenyl to 4.90% for naphthyl and 5.00% for the pyrene auxiliary donor. We must however stress that the statistical basis for these claims is marginal, as the overall performance differences between the auxiliary donors are relatively small.

From the IPCE spectra in Fig. 6 it is clear that **Dye 2** is an efficient light harvesting molecule but has the narrowest IPCE

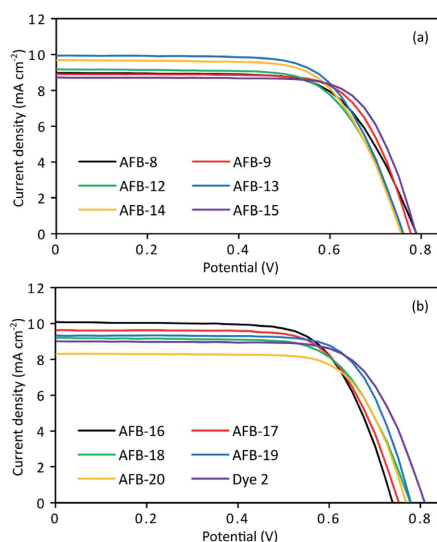


Fig. 5 Current–voltage plots for the best DSSC device fabricated for each sensitizer.

Table 2 Photovoltaic performance of all dyes under 1 sun AM 1.5G illumination and from IPCE measurements

Dye	IPCE $J_{sc}$ <sup>a</sup> ( $\text{mA cm}^{-2}$ )	$J_{sc}$ ( $\text{mA cm}^{-2}$ )	$V_{oc}$ (V)	FF	PCE (%)
<b>AFB-8</b>	8.76	$9.12 \pm 0.15$	$0.78 \pm 0.01$	$0.67 \pm 0.00$	$4.76 \pm 0.00$
<b>AFB-9</b>	8.73	$8.89 \pm 0.07$	$0.78 \pm 0.00$	$0.70 \pm 0.02$	$4.81 \pm 0.13$
<b>AFB-12<sup>b</sup></b>	8.84	$9.03 \pm 0.21$	$0.75 \pm 0.01$	$0.69 \pm 0.01$	$4.67 \pm 0.10$
<b>AFB-13</b>	9.28	$9.40 \pm 0.48$	$0.76 \pm 0.00$	$0.70 \pm 0.02$	$4.95 \pm 0.15$
<b>AFB-14</b>	9.49	$9.32 \pm 0.32$	$0.75 \pm 0.00$	$0.68 \pm 0.00$	$4.76 \pm 0.19$
<b>AFB-15</b>	8.62	$8.65 \pm 0.07$	$0.79 \pm 0.00$	$0.71 \pm 0.02$	$4.84 \pm 0.19$
<b>AFB-16</b>	10.02	$9.90 \pm 0.30$	$0.73 \pm 0.01$	$0.68 \pm 0.01$	$4.90 \pm 0.17$
<b>AFB-17</b>	9.47	$9.46 \pm 0.14$	$0.74 \pm 0.00$	$0.70 \pm 0.01$	$4.90 \pm 0.14$
<b>AFB-18</b>	8.91	$8.75 \pm 0.45$	$0.78 \pm 0.00$	$0.70 \pm 0.02$	$4.79 \pm 0.11$
<b>AFB-19</b>	9.16	$9.00 \pm 0.44$	$0.78 \pm 0.00$	$0.72 \pm 0.02$	$5.00 \pm 0.20$
<b>AFB-20</b>	7.97	$8.21 \pm 0.05$	$0.76 \pm 0.00$	$0.72 \pm 0.01$	$4.51 \pm 0.08$
<b>Dye 2</b>	8.55	$8.91 \pm 0.07$	$0.83 \pm 0.01$	$0.70 \pm 0.02$	$5.16 \pm 0.03$
<b>N719</b>	12.97	$13.20 \pm 0.13$	$0.76 \pm 0.01$	$0.70 \pm 0.01$	$6.98 \pm 0.10$

<sup>a</sup> Obtained by integration of the IPCE spectrum over the 1 sun AM 1.5 G spectrum. <sup>b</sup> Average values of two cells.

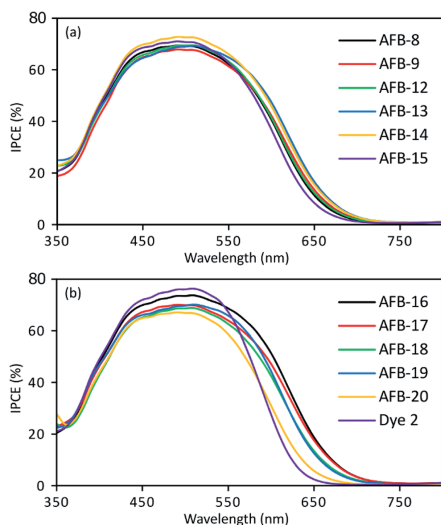


Fig. 6 IPCE spectra for the best DSSC device fabricated for each sensitizer.

spectrum of the dyes in this study. The no auxiliary donor dye **AFB-20** also suffers from lower absorption in the region above 500 nm, resulting in a lower overall performance. Not surprisingly, the rest of the sensitizers have very similar IPCE spectra.

The sensitizer **Dye 2** is previously characterized with an impressive  $J_{SC}$  of  $24.2 \text{ mA cm}^{-2}$  and  $V_{OC}$  of 846 mV.<sup>36</sup> By the addition of 50 eq. of chenodeoxycholic acid (CDCA) to the staining solutions, the authors reported a 6% decrease in dye loading from  $5.51 \times 10^{-7}$  to  $5.20 \times 10^{-7} \text{ mol cm}^{-2}$ ,  $J_{SC}$  increased by 77% and the PCE was improved by 62%. From Fig. 7, it is evident that a sensitizer delivering this impressive  $J_{SC}$  will need an absorption onset above 760 nm, corresponding to a bandgap smaller than 1.63 eV.<sup>46</sup> In addition, integration of the IPCE spectra published by Nagarajan *et al.*<sup>36</sup> yields a more modest  $7 \text{ mA cm}^{-2}$ , and an absorption onset of 605 nm estimated from the published absorption spectra on  $\text{TiO}_2$  supports a maximum short-circuit current of  $13 \text{ mA cm}^{-2}$ . The reported open-circuit voltage is also remarkably high, considering the reported electrolyte contains 0.5 M LiI. The presence of LiI in the electrolyte reduced the  $V_{OC}$  by lowering the Fermi level of  $\text{TiO}_2$ , and the  $V_{OC}$  obtained for the same sensitizer in this work was 830 mV without any addition of LiI. Based on the insufficient absorption properties, the lack of a reference sensitizer and the inconsistencies between the published IPCE and  $J-V$  data, it is the authors' opinion that a calibration error or similar is the cause of the 12.1% PCE reported by Nagarajan *et al.* As stated by Christians *et al.*<sup>47</sup> for the field of perovskite solar cells, any difference larger than 20% between  $J_{SC}$  values from  $J-V$  sweeps under 1 sun and  $J_{SC}$  from IPCE integration should call

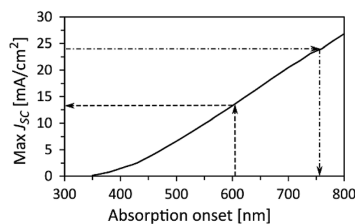


Fig. 7 By integration of the AM 1.5G solar spectrum the theoretical maximum  $J_{SC}$  attainable from a device can be calculated and plotted against the corresponding sensitizer absorption onset.<sup>46</sup> The arrows indicate the maximum  $J_{SC}$  for a dye with an absorption onset of 605 nm and the required onset to achieve a  $J_{SC}$  of  $24 \text{ mA cm}^{-2}$ .

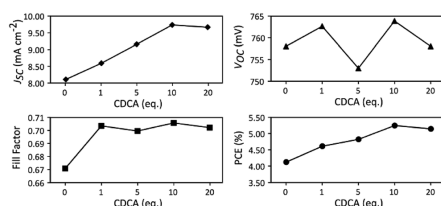
for further experimental support or explanation. There should be no reason for this not to be considered the best practice within the DSSC field as well.

The best sensitizer, **AFB-19**, was also tested with the copper electrolyte,  $\text{Cu}^{(II)}(\text{tmby})_2\text{TFSI}_{2/1}$ . The devices were fabricated using photoanodes with  $4 \mu\text{m}$  30NR-D  $\text{TiO}_2$  paste +  $4 \mu\text{m}$  scattering paste, and counter electrodes with a catalytic PEDOT layer deposited by electropolymerization.<sup>48</sup> A moderate PCE of 2.27% was obtained for the devices. The  $J-V$  spectra and data are given in the ESI (Fig. S5 and Table S2†). The performance was likely affected by the HOMO level position of **AFB-19**, only 50 mV below the redox potential of the  $\text{Cu}(\text{tmby})$  electrolyte reported at 0.87 V.<sup>49</sup> Photovoltages of up to 1.1 V are common for this electrolyte,<sup>50</sup> but our devices delivered a  $V_{OC}$  of only 910 mV, indicating that an insufficient driving force for the dye regeneration could be the issue. A solution could be to change to a redox couple with a more negative oxidation potential, as shown by El-Shishtawy *et al.* for similar compounds with a cobalt (ii/iii) electrolyte.<sup>51</sup>

The best dye from the preliminary screening with the iodide electrolyte was **AFB-19**. As pyrenes are prone to  $\pi$ -stacking<sup>52</sup> and as our best sensitizer had the pyrene auxiliary donor, we were eager to see how dependent the performance was on the presence of the anti-aggregation additive chenodeoxycholic acid (CDCA) in the staining solutions. Five new sets of devices were fabricated with zero, 1, 5, 10 and 20 molar equivalents of CDCA (relative to the sensitizer) in the staining solution, corresponding to 0, 0.5, 2.5, 5 and 10 mM CDCA. All other variables were unchanged from the initial efficiency screening, and the results are summarized in Table 3 and Fig. 8. As shown, no addition of CDCA yields the lowest  $J_{SC}$  and affects the fill factor negatively. We have no other explanation for this behavior than the undesirable intermolecular  $\pi$ - $\pi$  interactions between adjacent sensitizers. The  $V_{OC}$  varies by only 11 mV over the entire concentration range, meaning that the conduction band edge of  $\text{TiO}_2$  is not affected, nor the injected electron density. The  $J_{SC}$  is a crucial variable to the differences in PCE, and a slight drop in  $J_{SC}$  is observed with increasing the amount of CDCA from 10 to 20 equivalents, resulting in the peak PCE to be found at 10 equivalents. The peak PCE value for **AFB-19** in this

**Table 3** CDCA optimization study for sensitizer **AFB-19**. The concentrations of CDCA in the staining solutions were 0, 0.5, 2.5, 5.0 and 10.0 mM. The results are averages of three cells

CDCA (eq.)	CDCA conc. (mM)	$J_{sc}$ (mA cm <sup>-2</sup> )	$V_{oc}$ (mV)	FF	PCE (%)
0	0	8.11 ± 0.16	758 ± 6.9	0.67 ± 0.01	4.12 ± 0.07
1	0.5	8.59 ± 0.23	763 ± 9.4	0.70 ± 0.02	4.61 ± 0.21
5	2.5	9.16 ± 0.08	753 ± 4.5	0.70 ± 0.01	4.82 ± 0.11
10	5.0	9.73 ± 0.23	764 ± 6.0	0.71 ± 0.01	5.25 ± 0.11
20	10.0	9.66 ± 0.09	758 ± 7.8	0.70 ± 0.01	5.14 ± 0.04



**Fig. 8** DSSC characteristics for various CDCA concentrations ranging from zero to 20 equivalents for sensitizer **AFB-19**. Average values from three devices.

concentration screening was 5.25% with a smaller standard deviation compared to the same series in the preliminary screening, corresponding to a 27% increase in performance compared to 0 mM CDCA. As the other auxiliary donors are considered less prone to aggregation, lower concentrations of CDCA could be favorable, but further investigation would be needed for each sensitizer.

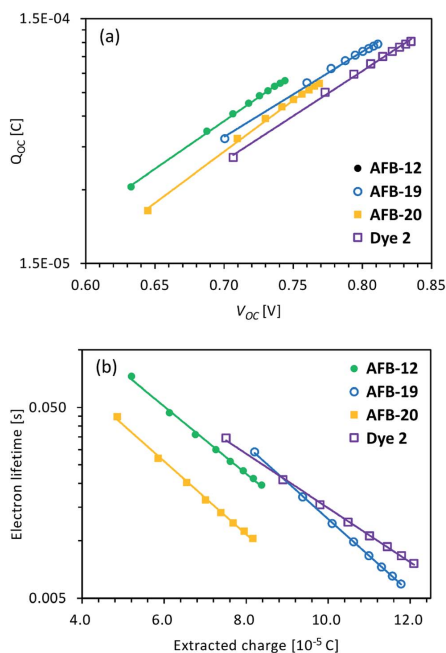
In order to explain the high  $V_{oc}$  observed for **Dye 2** we conducted electron lifetime and charge extraction experiments on a new set of devices. Also included were the most (**AFB-19**) and least (**AFB-12**) efficient dyes of the study in addition to the no auxiliary donor dye (**AFB-20**).

The  $V_{oc}$  of a device is normally dictated by the position of the  $TiO_2$  Fermi level and the redox potential of the redox couple. Further, the Fermi level position of the  $TiO_2$  is in turn dependent on both the conduction band edge and the electron concentration. From charge extraction measurements at different light intensities, one obtains a range of extracted charges with corresponding open circuit potentials. By comparing the lines from the sensitizers in Fig. 9a at the same charge density, it is possible to estimate the relative conduction band shift caused by each sensitizer from the horizontal shift of each line. Consequently, the conduction band edge of **Dye 2** is shifted upwards by 45 mV relative to that of **AFB-12**.

By correcting the  $V_{oc}$  values by the conduction band edge shift observed in Fig. 9a, a new set of lifetime curves can be obtained. By exponential regression, the lifetime values for the potentials of the charge extraction measurements can be calculated. Finally, by plotting the calculated lifetimes against the  $Q_{oc}$  values one is able to compare the lifetime

measurements of the sensitizers at the same electron density (see Fig. 9b).<sup>53</sup>

The effect of the auxiliary donor on the lifetime can be seen when comparing **AFB-20** to **AFB-12**. The presence of the 2-methoxyphenyl auxiliary donor in **AFB-12** doubles the lifetime compared to **AFB-20**, meaning that the recombination is slowed down by the introduction of the auxiliary donors. This could be highly useful if other redox couples more prone to recombination are of interest for similar sensitizers. Because the lifetime of **Dye 2** is similar to that of both **AFB-12** and **AFB-19**, we



**Fig. 9** (a) Charge extraction measurements at different light intensities and (b) electron lifetime measurements corrected for conduction band shift relative to **AFB-12** in (a) and then plotted against the extracted charge for the same potentials.

interpret the observed  $V_{OC}$  shift to be predominantly caused by the conduction band shift and not by longer electron lifetimes.

The overall assessment of auxiliary donors for phenothiazine sensitizers is that they do provide only a moderate performance enhancement, through a slight increase in absorption and increased electron lifetimes. Because they are not in conjugation with the anchoring group, their contribution is limited to an inductive nature. In turn, this could be why the observed effects are only moderate. On the other hand, auxiliary donors could be used for tuning the properties not directly related to absorption, such as interactions with the redox couple, adjacent sensitizers or other electrolyte additives. If the use of copper or cobalt redox couples is desired for phenothiazine sensitizers, the synthetic efforts should be placed on tailoring the HOMO level, lowering the LUMO level and increasing the molar extinction coefficients.

## Conclusions

In an attempt to understand the role of the auxiliary donor in phenothiazine sensitizers for DSSCs, we synthesized a series of dyes by varying only this moiety. Twelve sensitizers were evaluated, including ten different auxiliary donors, a reference sensitizer with no auxiliary donor and a "champion" phenothiazine dye (**Dye 2**).

The introduction of auxiliary donors marginally improved the absorption properties, raised the HOMO levels by up to 0.15 eV and improved the PCE by 4–11%, predominantly due to increased  $J_{SC}$  values. From electron lifetime and charge extraction measurements, it was also established that the addition of an auxiliary donor increased the electron lifetime by a factor of two. For the auxiliary donors, the efficiency followed the order phenyl < naphthyl < pyrene, with average PCEs of 4.76%, 4.90% and 5.00%. However, the overall performance differences between the auxiliary donors are within the limits of the standard deviations of the individual measurements. The effect of the chenodeoxycholic acid concentration in the staining solution for **AFB-19** revealed that a 10-fold molar excess was the most favorable concentration. The best device of the study was sensitized with **AFB-19**, delivering a photon-to-electron conversion efficiency of 5.36% with a  $J_{SC} = 9.99 \text{ mA cm}^{-2}$ ,  $V_{OC} = 765 \text{ mV}$  and  $FF = 0.70$ .

The phenothiazine sensitizer with the highest reported PCE of 12.1% with an  $I^-/I_3^-$  electrolyte was also evaluated.<sup>36</sup> Although the dye had a high  $V_{OC}$ , the performance in terms of PCE was not significantly different from that of the other phenothiazine dyes in this study. Furthermore, integration of the published IPCE spectra implies that the PCE values reported by Nagarajan *et al.* are twice as high as theoretically possible under 1 sun AM 1.5G illumination. We therefore strongly encourage the practice of integrating the IPCE spectra and the use of reference sensitizers in this field.

## Experimental section

### Materials and reagents

Unless specifically mentioned, all reactions were performed under an inert atmosphere with chemicals used as received

from Sigma Aldrich. The experimental procedure for the synthesis of the sensitizers can be found in the ESI.†

### Characterization

NMR analyses ( $^1\text{H}$  and  $^{13}\text{C}$ ) were performed on either a Bruker 400 or 600 MHz spectrometer. Infrared absorption (IR) spectra were recorded on a Bruker Alpha FTIR spectrometer in attenuated total reflection (ATR) mode. UV/Vis spectra were recorded on a Hitachi U-1900 UV/Vis-spectrophotometer in quartz cuvettes with 10 mm light path. Fluorescence spectrophotometry was carried out on a Varian Cary Eclipse in quartz cuvettes. HRMS analysis was performed on a Waters Synapt G2-S Q-TOF instrument using either ASAP or ESI ionization.

### Device fabrication

TEC-10 FTO glass sourced from Sigma Aldrich was washed with Deconex 21 solution ( $2 \text{ g L}^{-1} \text{ H}_2\text{O}$ ) in an ultrasonic bath for 45 minutes before being rinsed with deionized water and ethanol. UV/O<sub>3</sub> cleaning for 15 minutes (Novascan PSD PRO-UV T6) was performed to remove organic contaminants from the FTO glass. A TiO<sub>2</sub> blocking layer was deposited by two hydrothermal depositions in 40 mM aqueous TiCl<sub>4</sub> solution at 70 °C for 30 minutes.

Two active layers of TiO<sub>2</sub> (18NR-T, GreatcellSolar) and one scattering layer (WER2-0, GreatcellSolar) were screen printed (mesh 53T, active area  $0.238 \text{ cm}^2$ ) and then placed in a levelling chamber with ethanol for 3 minutes before drying on a hotplate for 6 minutes at 125 °C between each print. The electrodes were sintered in a programmable furnace (Nabertherm LT 9/12) with the ramping program of 125, 250, 325, 450, and 500 °C for 5, 5, 15 and 15 minutes with 10 minutes ramping between each step. The total TiO<sub>2</sub> thickness was measured to be  $16.5 \mu\text{m}$  ( $11 \mu\text{m} + 5.5 \mu\text{m}$ ) using a profilometer (Veeco, Dektak 150). Finally, a post treatment in 40 mM aqueous TiCl<sub>4</sub> solution at 70 °C for 30 minutes was performed, followed by rinsing with deionized water and ethanol.

Platinum counter electrodes were fabricated from TEC-8 FTO glass (GreatcellSolar). Holes were drilled with a diamond drill bit, and a 10 mM H<sub>2</sub>PtCl<sub>6</sub> platinum precursor solution in 2-propanol was drop-cast ( $5 \mu\text{L cm}^{-2}$ ) onto the FTO and heated at 400 °C for 15 minutes. Prior to assembly, the counter electrodes were dried by a hot air gun at 400 °C for 25 minutes.

Due to varying indoor temperatures in Arctic Norway, staining of the electrodes was performed overnight in a 30 °C cabinet. Prior to staining the electrodes were annealed by a hot air gun at 480 °C for 25 minutes, and upon cooling to 80 °C they were immersed in the staining solutions. A dye concentration of 0.5 mM was used along with 10 equivalents of CDCA unless specified otherwise. N719 was stained using absolute ethanol while the organic dyes were stained using a mixture of acetonitrile and stabilized THF (43 : 57, v/v), which equates to a dielectric constant of 20, previously reported as the optimal value for dye staining.<sup>34</sup> After a staining time of 18 hours, the electrodes were rinsed with acetonitrile for 2 minutes before being sealed with the counter electrodes using a Surlyn gasket

(60  $\mu\text{m}$ , Solaronix) in a drybox. Heating using a 50 W PTC heat element for  $2 \times 20$  seconds provided efficient sealing.

The A6141 electrolyte contained 0.60 M 1-butyl-3-methylimidazolium iodide, 0.03 M  $\text{I}_2$ , 0.10 M guanidinium thiocyanate and 0.50 M *tert*-butylpyridine in a mixture of acetonitrile and valeronitrile (85 : 15, v/v).<sup>6</sup> The electrolyte was injected by vacuum backfilling before the hole was sealed with Surlyn and a circular glass cover disc. The electrodes were painted with conductive silver paint (Electrolube, SCP) before characterization.

### Device characterization

*J*-*V* characteristics of the DSSCs were obtained under 1 sun AM 1.5G illumination from a Scientech SP300B solar simulator calibrated with a Newport Reference Cell (91150V), connected to a Keithley 2450 SourceMeter. The *J*-*V* scan rate was 12 mV s<sup>-1</sup>, scanning from short-circuit to open-circuit. A circular mask with an aperture of 0.238 cm<sup>2</sup> was used for all *J*-*V* measurements. IPCE measurements were recorded from a device assembled using a halogen lamp (Ocean Optics HL-2000) and a monochromator (Spectral Products CM110) connected to the Keithley 2450 and programmed in LabView. The DSSCs and the NIST traceable calibrated photodiode (Thorlabs, FDS100-CAL) were masked with an aperture of 0.049 cm<sup>2</sup>. Charge extraction and electron lifetime measurements were performed using a Dyanamo Toolbox. For the charge extraction measurements, the devices were illuminated using a white LED for 1 second at open circuit. When the light is switched off, the device is short-circuited and the extracted charge integrated. This is repeated for several light intensities by adjusting the LED bias from 50 to 450 mA in 50 mA increments. In the electron lifetime measurements, the LED light intensity was modulated, giving an AC response signal from the device from which the electron lifetimes were calculated.

### Conflicts of interest

There are no conflicts to declare.

### Acknowledgements

The authors would like to thank the Faculty of Natural Sciences and the Department of Chemistry at NTNU for financial support, Dr Susana Villa Gonzalez for HRMS analyses and Roger Aarvik for technical support. Associate professor Solon Economopoulos is thanked for helpful discussions on cyclic voltammetry, Sihai Luo for SEM imaging and Dr James Bannock for programming our IPCE setup. The Research Council of Norway is acknowledged for the support to the Norwegian Micro- and Nano-Fabrication Facility, NorFab (project number 245963/F50) and the Norwegian NMR Platform (project number 226244/F50).

### References

- 1 B. O'Regan and M. Grätzel, *Nature*, 1991, **353**, 737–740.

- 2 M. Freitag, J. Teuscher, Y. Saygili, X. Zhang, F. Giordano, P. Liska, J. Hua, S. M. Zakeeruddin, J.-E. Moser, M. Grätzel and A. Hagfeldt, *Nat. Photonics*, 2017, **11**, 372–378.
- 3 O. Pekkola, C. Lungenschmied, P. Fejes, A. Handreck, W. Hermes, S. Irle, C. Lennartz, C. Schildknecht, P. Schillen, P. Schindler, R. Send, S. Valouch, E. Thiel and I. Bruder, *Sci. Rep.*, 2018, **8**, 9208.
- 4 A. Kay and M. Grätzel, *J. Phys. Chem.*, 1993, **97**, 6272–6277.
- 5 S. Cherian and C. C. Wamser, *J. Phys. Chem. B*, 2000, **104**, 3624–3629.
- 6 M. K. Nazeeruddin, F. De Angelis, S. Fantacci, A. Selloni, G. Viscardi, P. Liska, S. Ito, B. Takeru and M. Grätzel, *J. Am. Chem. Soc.*, 2005, **127**, 16835–16847.
- 7 T. Horiuchi, H. Miura, K. Sumioka and S. Uchida, *J. Am. Chem. Soc.*, 2004, **126**, 12218–12219.
- 8 A. Hagfeldt, G. Boschloo, L. Sun, L. Kloo and H. Pettersson, *Chem. Rev.*, 2010, **110**, 6595–6663.
- 9 N. Robertson, *Angew. Chem., Int. Ed.*, 2006, **45**, 2338–2345.
- 10 A. Mishra, M. K. Fischer and P. Bäuerle, *Angew. Chem., Int. Ed.*, 2009, **48**, 2474–2499.
- 11 M. Pazoki, U. B. Cappel, E. M. J. Johansson, A. Hagfeldt and G. Boschloo, *Energy Environ. Sci.*, 2017, **10**, 672–709.
- 12 Y. Hu, A. Abate, Y. Cao, A. Ivaturi, S. M. Zakeeruddin, M. Grätzel and N. Robertson, *J. Phys. Chem. C*, 2016, **120**, 15027–15034.
- 13 Y. Hu, A. Ivaturi, M. Planells, C. L. Boldrini, A. O. Biroli and N. Robertson, *J. Mater. Chem. C*, 2016, **4**, 2509–2516.
- 14 L. Zhang and J. M. Cole, *ACS Appl. Mater. Interfaces*, 2015, **7**, 3427–3455.
- 15 D. Joly, L. Pellejà, S. Narbey, F. Oswald, J. Chiron, J. N. Clifford, E. Palomares and R. Demadrille, *Sci. Rep.*, 2014, **4**, 4033.
- 16 S. H. Kim, H. W. Kim, C. Sakong, J. Namgoong, S. W. Park, M. J. Ko, C. H. Lee, W. I. Lee and J. P. Kim, *Org. Lett.*, 2011, **13**, 5784–5787.
- 17 H. N. Tsao, C. Yi, T. Moehl, J.-H. Yum, S. M. Zakeeruddin, M. K. Nazeeruddin and M. Grätzel, *ChemSusChem*, 2011, **4**, 591–594.
- 18 A. Mahmood, *Sol. Energy*, 2016, **123**, 127–144.
- 19 Z.-S. Huang, H. Meier and D. Cao, *J. Mater. Chem. C*, 2016, **4**, 2404–2426.
- 20 R. Y.-Y. Lin, F.-L. Wu, C.-T. Li, P.-Y. Chen, K.-C. Ho and J. T. Lin, *ChemSusChem*, 2015, **8**, 2503–2513.
- 21 K. D. Seo, H. M. Song, M. J. Lee, M. Pastore, C. Anselmi, F. De Angelis, M. K. Nazeeruddin, M. Grätzel and H. K. Kim, *Dyes Pigm.*, 2011, **90**, 304–310.
- 22 A. Venkateswararao and K. R. J. Thomas, in *Solar Cell Nanotechnology*, 2013, pp. 41–96.
- 23 Y. Hua, S. Chang, D. D. Huang, X. Zhou, X. J. Zhu, J. Z. Zhao, T. Chen, W. Y. Wong and W. K. Wong, *Chem. Mater.*, 2013, **25**, 2146–2153.
- 24 H.-H. Gao, X. Qian, W.-Y. Chang, S.-S. Wang, Y.-Z. Zhu and J.-Y. Zheng, *J. Power Sources*, 2016, **307**, 866–874.
- 25 X. Yang, J. Zhao, L. Wang, J. Tian and L. Sun, *RSC Adv.*, 2014, **4**, 24377–24383.
- 26 W. Wu, J. Yang, J. Hua, J. Tang, L. Zhang, Y. Long and H. Tian, *J. Mater. Chem.*, 2010, **20**, 1772–1779.

- 27 J. Li, W. Wu, J. Yang, J. Tang, Y. Long and J. Hua, *Sci. China: Chem.*, 2011, **54**, 699–706.
- 28 D. Muenmart, N. Prachumrak, R. Tarsang, S. Namungruk, S. Jungstittiwong, T. Sudyoadsuk, P. Pattanasattayavong and V. Promarak, *RSC Adv.*, 2016, **6**, 38481–38493.
- 29 X. Zhang, F. Gou, J. Shi, H. Gao, C. Xu, Z. Zhu and H. Jing, *RSC Adv.*, 2016, **6**, 106380–106386.
- 30 S. Wang, H. Wang, J. Guo, H. Tang and J. Zhao, *Dyes Pigm.*, 2014, **109**, 96–104.
- 31 E. Mosconi, J.-H. Yum, F. Kessler, C. J. Gómez García, C. Zuccaccia, A. Cinti, M. K. Nazeeruddin, M. Grätzel and F. De Angelis, *J. Am. Chem. Soc.*, 2012, **134**, 19438–19453.
- 32 P. Gao, Y. J. Kim, J.-H. Yum, T. W. Holcombe, M. K. Nazeeruddin and M. Grätzel, *J. Mater. Chem. A*, 2013, **1**, 5535–5544.
- 33 S. M. Feldt, E. A. Gibson, E. Gabrielson, L. Sun, G. Boschloo and A. Hagfeldt, *J. Am. Chem. Soc.*, 2010, **132**, 16714–16724.
- 34 Y. S. Yang, H. D. Kim, J.-H. Ryu, K. K. Kim, S. S. Park, K.-S. Ahn and J. H. Kim, *Synth. Met.*, 2011, **161**, 850–855.
- 35 H. Wei, J. Shen, Y. Liu, T. Huang, Q. Zhang, J. Zhao and X. Zhao, *Dyes Pigm.*, 2018, **149**, 789–795.
- 36 B. Nagarajan, S. Kushwaha, R. Elumalai, S. Mandal, K. Ramanujam and D. Raghavachari, *J. Mater. Chem. A*, 2017, **5**, 10289–10300.
- 37 A. F. Buene, N. Uggerud, S. P. Economopoulos, O. R. Gautun and B. H. Hoff, *Dyes Pigm.*, 2018, **151**, 263–271.
- 38 R. Y.-Y. Lin, T.-M. Chuang, F.-L. Wu, P.-Y. Chen, T.-C. Chu, J.-S. Ni, M.-S. Fan, Y.-H. Lo, K.-C. Ho and J. T. Lin, *ChemSusChem*, 2015, **8**, 105–113.
- 39 N. S. Wilson and B. A. Keay, *Tetrahedron Lett.*, 1996, **37**, 153–156.
- 40 N. S. Wilson and B. A. Keay, *Tetrahedron Lett.*, 1997, **38**, 187–190.
- 41 K. L. Billingsley and S. L. Buchwald, *J. Org. Chem.*, 2008, **73**, 5589–5591.
- 42 Z. Iqbal, W.-Q. Wu, Z.-S. Huang, L. Wang, D.-B. Kuang, H. Meier and D. Cao, *Dyes Pigm.*, 2016, **124**, 63–71.
- 43 J. Chen, Y. Zhang, L. Yang, X. Zhang, J. Liu, L. Li and H. Zhang, *Tetrahedron*, 2007, **63**, 4266–4270.
- 44 H. Svith, H. Jensen, J. Almstedt, P. Andersson, T. Lundbäck, K. Daasbjerg and M. Jonsson, *J. Phys. Chem. A*, 2004, **108**, 4805–4811.
- 45 G. Boschloo and A. Hagfeldt, *Acc. Chem. Res.*, 2009, **42**, 1819–1826.
- 46 H. J. Snaith, *Adv. Funct. Mater.*, 2010, **20**, 13–19.
- 47 J. A. Christians, J. S. Manser and P. V. Kamat, *J. Phys. Chem. Lett.*, 2015, **6**, 852–857.
- 48 H. Ellis, N. Vlachopoulos, L. Häggman, C. Perruchot, M. Jouini, G. Boschloo and A. Hagfeldt, *Electrochim. Acta*, 2013, **107**, 45–51.
- 49 Y. Saygili, M. Söderberg, N. Pellet, F. Giordano, Y. Cao, A. B. Muñoz-García, S. M. Zakeeruddin, N. Vlachopoulos, M. Pavone, G. Boschloo, L. Kavan, J.-E. Moser, M. Grätzel, A. Hagfeldt and M. Freitag, *J. Am. Chem. Soc.*, 2016, **138**, 15087–15096.
- 50 P. Ferdowsi, Y. Saygili, S. M. Zakeeruddin, J. Mokhtari, M. Grätzel, A. Hagfeldt and L. Kavan, *Electrochim. Acta*, 2018, **265**, 194–201.
- 51 R. M. El-Shishtawy, J.-D. Decoppet, F. A. M. Al-Zahrani, Y. Cao, S. B. Khan, M. S. Al-Ghamdi, B. G. Alhogbi, A. M. Asiri, S. M. Zakeeruddin and M. Grätzel, *New J. Chem.*, 2018, **42**, 9045–9050.
- 52 R. Flamholz, D. Plažuk, J. Zakrzewski, R. Métivier, K. Nakatani, A. Makal and K. Woźniak, *RSC Adv.*, 2014, **4**, 31594–31601.
- 53 Y. Hao, H. Tian, J. Cong, W. Yang, I. Bora, L. Sun, G. Boschloo and A. Hagfeldt, *ChemPhysChem*, 2014, **15**, 3476–3483.
- 54 H. Ozawa, M. Awa, T. Ono and H. Arakawa, *Chem.-Asian J.*, 2012, **7**, 156–162.

**Electronic Supplementary Information****Auxiliary donors for phenothiazine sensitizers for dye-sensitized solar cells  
– How important are they really?**

Audun Formo Buene<sup>a</sup>, Eline Ekornhol Ose<sup>a</sup>, Ane Garborg Zakariassen<sup>a</sup>, Anders Hagfeldt<sup>b</sup>, Bård Helge Hoff<sup>\*,\*</sup>

*a*: Department of Chemistry, Norwegian University of Science and Technology (NTNU), N-7491 Trondheim, Norway

*b*: Laboratory of Photomolecular Science, Institute of Chemical Sciences and Engineering, École Polytechnique Fédérale de Lausanne (EPFL), Chemin des Alambics, Station 6, CH-1015 Lausanne, Switzerland

\* Corresponding author. Tel.: +47 73593973; E-mail address: bard.h.hoff@ntnu.no (B. H. Hoff).

**List of contents**

<b>Absorption, emission and dye loading</b>	<b>S2</b>
<b>Cyclic voltammetry</b>	<b>S4</b>
<b>Copper (II/I) electrolyte for AFB-19</b>	<b>S6</b>
<b>Experimental information</b>	<b>S7</b>
<b>NMR</b>	<b>S23</b>
<b>References</b>	<b>S33</b>



## Absorption, emission and dye loading

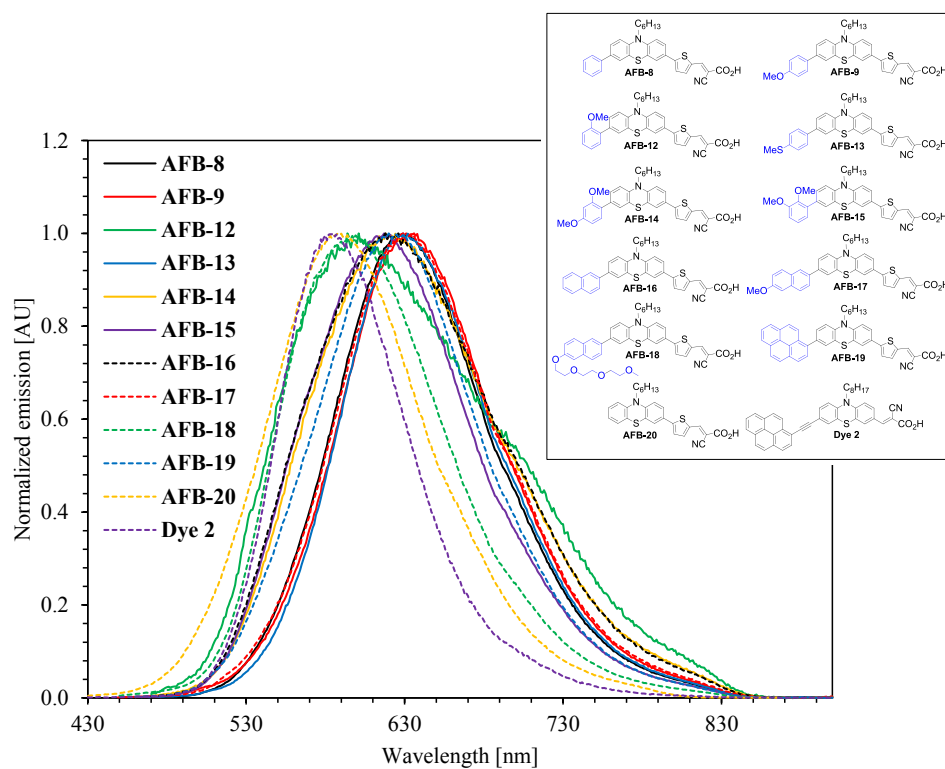


Figure S1. Normalized emission spectra of all dyes, recorded in THF.

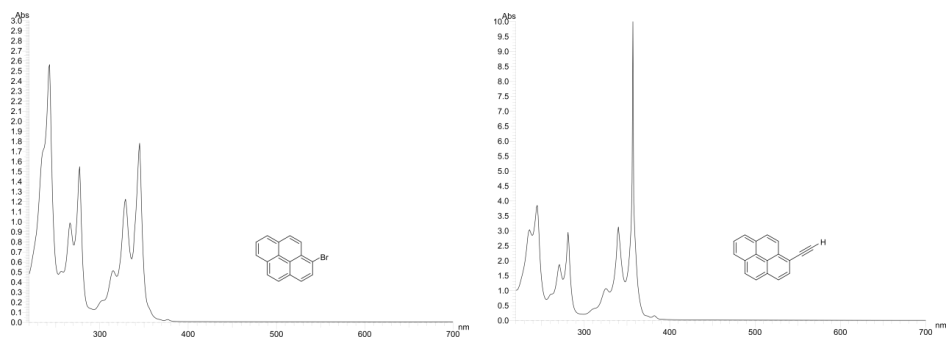


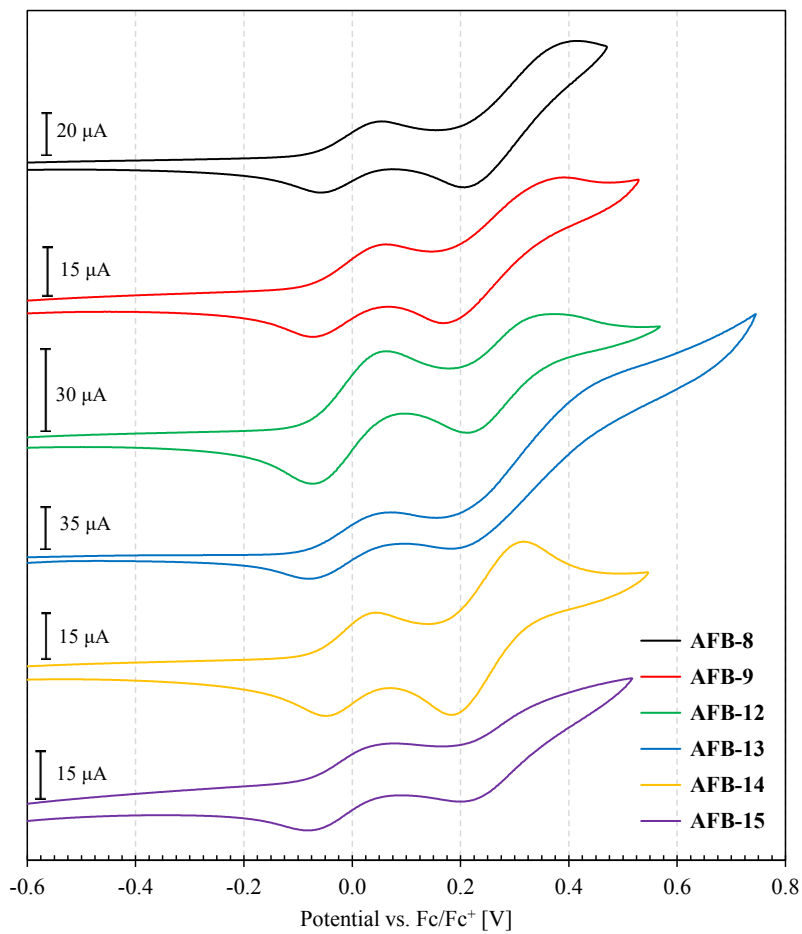
Figure S2. UV/Vis absorption spectra in THF of pyrene-containing 1-bromopyrene (left) and 1-ethynylpyrene (right).

**Table S1.** Dye loading data for **AFB-12**, **AFB-19**, **AFB-20** and **Dye 2**.

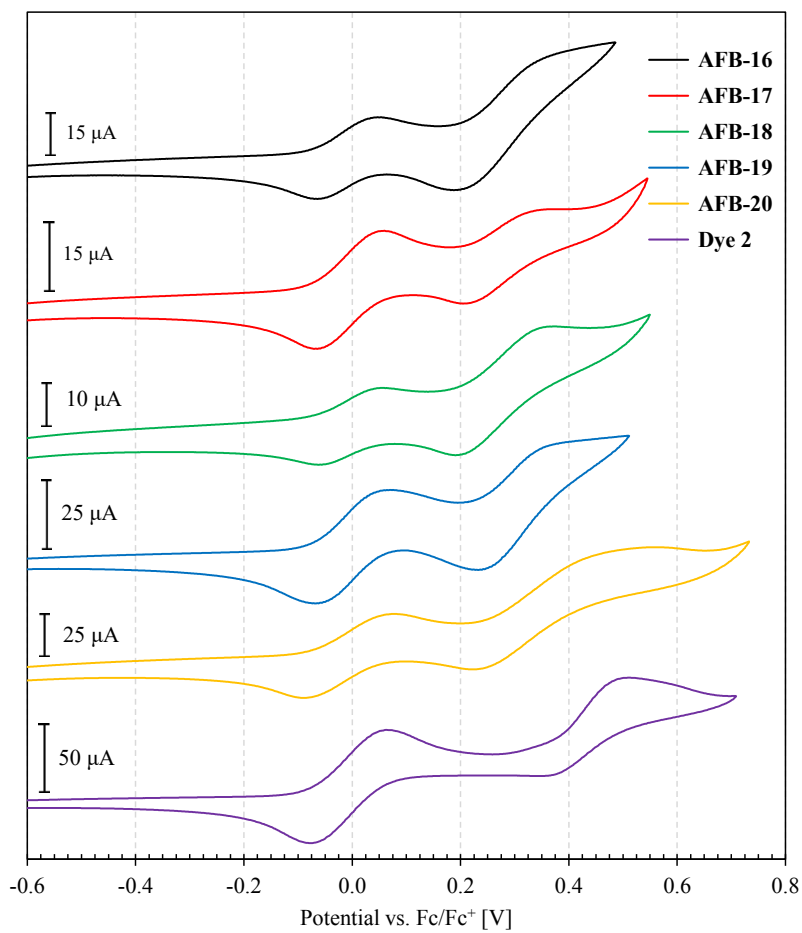
Dye	Dye loading ( $10^{-7}$ mol $\text{cm}^{-2}$ ) <sup>a</sup>
<b>AFB-12</b>	$2.63 \pm 0.22$
<b>AFB-19</b>	$4.89 \pm 0.61$
<b>AFB-20</b>	$2.99 \pm 0.15$
<b>Dye 2</b>	$3.51 \pm 0.20$

<sup>a</sup> Measured by UV/Vis from the staining solutions with 10-fold amount of CDCA. Averages of three separate staining baths.

## Cyclic voltammetry

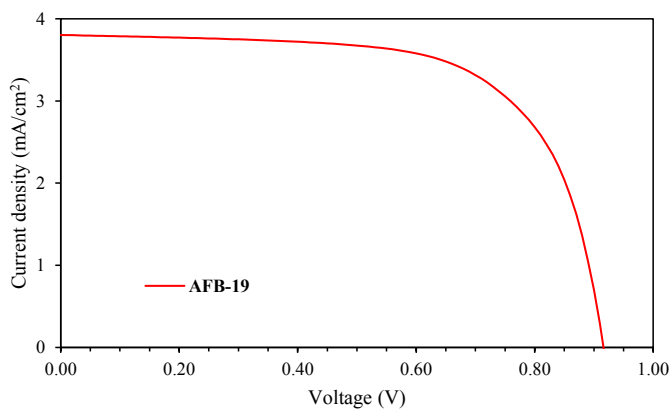


**Figure S3.** Cyclic voltammograms of dyes AFB-8, 9, 12-15 in DMF solution.



**Figure S4.** Cyclic voltammograms of dyes **AFB-16 to 20** and **Dye 2** in DMF solution.

### Copper (II/I) electrolyte for AFB-19



**Figure S5.** Current-voltage plot for **AFB-19** with  $\text{Cu}^{(II/I)}(\text{tmby})_2\text{TFSI}_{2/1}$  electrolyte (similar system as reported by Saygili et al.<sup>1</sup>) under 1 sun AM 1.5G illumination.

**Table S2.** Photovoltaic performance of **AFB-19** under 1 sun AM 1.5G illumination with the A6141 iodide electrolyte (same data set as in Table 2) and  $\text{Cu}^{(II/I)}(\text{tmby})_2\text{TFSI}_{2/1}$  electrolyte.

Electrolyte	$J_{sc}$ (mA cm <sup>-2</sup> )	$V_{oc}$ (V)	FF	PCE (%)
I <sup>-</sup> /I <sub>3</sub> <sup>-</sup> (A6141)	9.00 ± 0.44	0.78 ± 0.00	0.72 ± 0.02	5.00 ± 0.20
Cu(tmby)	3.82 ± 0.02	0.91 ± 0.01	0.65 ± 0.02	2.27 ± 0.08

## Experimental information

### Materials and reagents

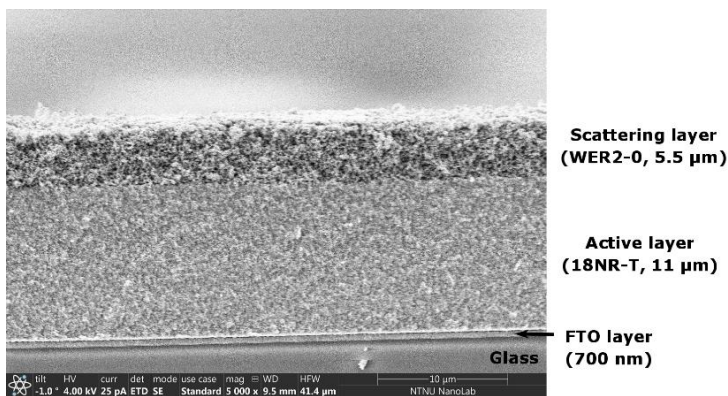
All reactions were carried out under nitrogen atmosphere, and all synthesis reagents were acquired from Sigma Aldrich. The synthesis of building block **1** was performed as previously reported by our research group.<sup>2</sup>

### Analytical instruments

<sup>1</sup>H and <sup>13</sup>C NMR spectra were recorded at 22 °C on either a Bruker 400 or 600 MHz spectrometer in DMSO-*d*<sub>6</sub> or CDCl<sub>3</sub>. All chemical shifts are reported in ppm, and the spectra were calibrated using the signal of DMSO at 2.50 ppm (<sup>1</sup>H) and 39.52 (<sup>13</sup>C), or that of TMS (0 ppm) in CDCl<sub>3</sub>. Infrared absorption (IR) spectra were recorded with a FTIR Thermo Nicolet Nexus FT-IR Spectrometer using a Smart Endurance reflection cell. Reported frequencies were in the range of 4000-400 cm<sup>-1</sup>. UV/Vis analyses were performed with a Hitachi U-1900 UV/Vis-spectrophotometer using quartz cuvettes (10 mm) and scanning from 300-700 nm. Extinction coefficients were calculated from Lambert-Beer's law. UV/Vis measurements of sensitized TiO<sub>2</sub> films were performed in the same spectrophotometer with a non-stained electrode as the background. Melting points were determined with a Stuart SMP40 automatic melting point instrument. Accurate mass determination in positive and negative mode was performed on a "Synapt G2-S" Q-TOF instrument from Waters<sup>TM</sup>. The samples were ionized by the use of ASAP probe (APCI) or by ESI. Spectra processing was done by Waters<sup>TM</sup> Software (Masslynx v4.1 SCN871). Fluorescence spectrophotometry was measured with a Varian Cary Eclipse instrument.

Cyclic voltammetry was performed in a three-electrode cell with platinum wire electrodes in DMF with 0.1 M tetrabutylammonium hexafluorophosphate (TBAPF<sub>6</sub>). A Princeton Applied Research Versastat 3 potentiostat was used along with the VersaStudio software. The scan rate was 100 mV/s for all measurements. Calculation of the E<sub>HOMO</sub> vs. SHE was done according to the following equation where a conversion constant of 624 mV of Fc<sup>+</sup>/Fc vs. SHE is used.<sup>3</sup>

$$E_{HOMO} = E_{1/2}(dye) - E_{1/2}(Fc) + 0.624$$



**Figure S6.** Cross-section scanning electron microscopy image of the screen-printed electrodes. The complete cross section is shown, with glass, FTO, active 18NR-T TiO<sub>2</sub> and scattering WER2-0 TiO<sub>2</sub>. A white compact layer on top of the FTO is most likely the TiO<sub>2</sub> blocking layer formed by hydrothermal deposition.

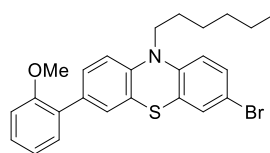
## Synthesis

### General procedure for Suzuki coupling

3,7-Dibromo-10-hexyl-10*H*-phenothiazine (**1**) (1 eq.), boronic acid containing the desired donor group (1.0-1.1 eq.), Pd(PPh<sub>3</sub>)<sub>4</sub> (0.01 eq.) and potassium carbonate (4 eq.) were mixed. The system was evacuated and backflushed with N<sub>2</sub>. 1,4-Dioxane and water (1:1, v:v, 6.6 mL/mmol) were degassed and added, and the reaction mixture was stirred at 80 °C until desired conversion. Water was added to the reaction mixture, and the aqueous phase extracted using ethyl acetate. The combined organic phases were dried over anhydrous Na<sub>2</sub>SO<sub>4</sub>, filtered and the solvents were removed *in vacuo*. The product was purified by silica gel column chromatography.

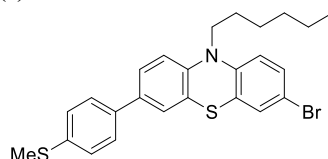
### 3-Bromo-10-hexyl-7-(2-methoxyphenyl)-10*H*-phenothiazine (**2**)

The synthesis was performed as described in the general procedure, starting with compound **1** (200 mg, 0.453 mmol), 2-methoxyphenylboronic acid (69 mg, 0.453 mmol), Pd(PPh<sub>3</sub>)<sub>4</sub> (5.2 mg, 4.5 μmol) and K<sub>2</sub>CO<sub>3</sub> (251 mg, 1.813 mmol). The reaction time was 16 hours. The crude product was purified by silica gel column chromatography (*n*-pentane/toluene, 5:1, *R<sub>f</sub>* = 0.17), to yield compound **2** as a yellow oil (80 mg, 0.171 mmol, 38%). <sup>1</sup>H NMR (600 MHz, DMSO-*d*<sub>6</sub>) δ: 7.37-7.34 (m, 2H), 7.33-7.29 (m, 2H), 7.26 (dd, *J* = 7.6, 1.7 Hz, 1H), 7.24 (d, *J* = 2.0 Hz, 1H), 7.09 (d, *J* = 8.2 Hz, 1H), 7.05 (d, *J* = 8.4 Hz, 1H), 7.00 (td, *J* = 7.5, 1.0 Hz, 1H), 6.98-6.95 (m, 1H), 3.86 (t, *J* = 7.0 Hz, 2H), 3.76 (s, 3H), 1.70-1.65 (m, 2H), 1.40-1.38 (m, 2H), 1.31-1.26 (m, 4H), 0.84-0.82 (m, 3H); <sup>13</sup>C NMR (150 MHz, DMSO-*d*<sub>6</sub>) δ: 156.0, 144.0, 143.2, 132.7, 130.1, 130.0, 129.0, 128.9, 128.7, 128.4, 127.7, 126.0, 122.1, 120.8, 117.4, 115.5, 113.6, 111.7, 55.5, 46.5, 30.8, 26.1, 25.8, 22.0, 13.8; IR (neat, cm<sup>-1</sup>) ν: 3065 (w, br), 2951 (m, br), 2914 (m, br), 2947 (m), 1595 (m), 1465 (s), 1247 (s), 1023 (m), 800 (m), 738 (s); HRMS (TOF MS ASAP+, *m/z*): found 467.0919 (calcd. C<sub>25</sub>H<sub>26</sub>NOS<sup>79</sup>Br: 467.0918, [M]<sup>+</sup>).



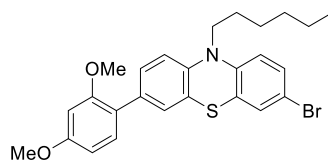
### 3-Bromo-10-hexyl-7-(4-(methylthio)phenyl)-10*H*-phenothiazine (**3**)

The synthesis was performed as described in the general procedure, starting with compound **1** (1.00 g, 2.266 mmol), (4-methylthio)phenylboronic acid (419 mg, 2.493 mmol), Pd(PPh<sub>3</sub>)<sub>4</sub> (26 mg, 0.022 mmol) and K<sub>2</sub>CO<sub>3</sub> (1.25 g, 9.07 mmol). The reaction time was 8 hours. The crude product was purified by silica gel column chromatography (*n*-pentane/toluene, 9:1, *R<sub>f</sub>* = 0.12), to yield compound **3** as an off-white solid (560 mg, 1.156 mmol, 51%), mp 69-70 °C. <sup>1</sup>H NMR (600 MHz, DMSO-*d*<sub>6</sub>) δ: 7.59-7.55 (m, 2H), 7.48 (dd, *J* = 8.5, 2.2 Hz, 1H), 7.42 (d, *J* = 2.2 Hz, 1H), 7.36-7.32 (m, 2H), 7.31-7.28 (m, 2H), 7.06 (d, *J* = 8.6 Hz, 1H), 6.96-6.93 (m, 1H), 3.85 (t, *J* = 6.9 Hz, 2H), 2.49 (s, 3H), 1.70-1.61 (m, 2H), 1.41-1.32 (m, 2H), 1.27-1.20 (m, 4H), 0.84-0.79 (m, 3H); <sup>13</sup>C NMR (150 MHz, DMSO-*d*<sub>6</sub>) δ: 143.9, 143.5, 137.1, 135.3, 134.0, 130.1, 128.9, 126.5 (2C), 126.4 (2C), 125.8, 125.7, 124.7, 123.4, 117.4, 116.2, 113.7, 46.6, 30.8, 26.0, 25.8, 22.1, 14.7, 13.8; IR (neat, cm<sup>-1</sup>) ν: 2952 (w), 2919 (w), 2852 (w), 1455 (s), 1248 (s), 1097 (m), 802 (s); HRMS (TOF MS ASAP+, *m/z*): found 484.0767 (calcd. C<sub>25</sub>H<sub>27</sub>NOS<sup>79</sup>Br: 484.0768, [M+H]<sup>+</sup>).

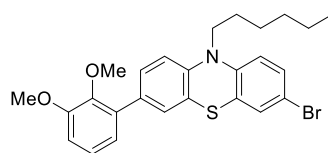


**3-Bromo-7-(2,4-dimethoxyphenyl)-10-hexyl-10H-phenothiazine (4)**

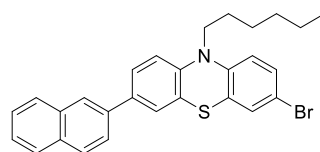
The synthesis was performed as described in the general procedure, starting with compound **1** (200 mg, 0.453 mmol), 2,4-dimethoxyphenylboronic acid (82 mg, 0.453 mmol), Pd(PPh<sub>3</sub>)<sub>4</sub> (5.2 mg, 4.5 μmol) and K<sub>2</sub>CO<sub>3</sub> (251 mg, 1.813 mmol). The reaction time was 1.5 hours. The crude product was purified by silica gel column chromatography (*n*-pentane/toluene, 4:1, *R<sub>f</sub>* = 0.14), to yield compound **4** as a yellow oil (110 mg, 0.221 mmol, 49%). <sup>1</sup>H NMR (600 MHz, DMSO-*d*<sub>6</sub>) δ: 7.36-7.34 (m, 2H), 7.26 (dd, *J* = 8.5, 2.0 Hz, 1H), 7.19 (s, 1H), 7.18 (d, *J* = 6.4 Hz, 1H), 7.02 (d, *J* = 8.5 Hz, 1H), 6.97-6.94 (m, 1H), 6.63 (d, *J* = 2.4 Hz, 1H), 6.58 (dd, *J* = 8.4, 2.5 Hz, 1H), 3.85 (t, *J* = 6.9 Hz, 2H), 3.79 (s, 3H), 3.75 (s, 3H), 1.70-1.65 (m, 2H), 1.41-1.37 (m, 2H), 1.26-1.17 (m, 4H), 0.84-0.82 (m, 3H); <sup>13</sup>C NMR (150 MHz, DMSO-*d*<sub>6</sub>) δ: 160.0, 157.0, 144.1, 142.7, 132.6, 130.4, 130.1, 128.9, 128.5, 127.5, 126.0, 122.1, 121.1, 117.3, 115.5, 113.5, 105.3, 98.9, 55.5, 55.3, 46.5, 30.8, 26.1, 25.8, 22.0, 13.8; IR (neat, cm<sup>-1</sup>) v: 2956 (m), 2925 (m), 2852 (m), 2369 (w), 1610 (m), 1455 (s), 1242 (s), 1205 (s), 1163 (s), 795 (s); HRMS (TOF MS ASAP+, *m/z*): found 497.1017 (calcd. C<sub>26</sub>H<sub>28</sub>NO<sub>2</sub>S<sup>79</sup>Br: 497.1024, [M]<sup>+</sup>).

**3-Bromo-7-(2,3-dimethoxyphenyl)-10-hexyl-10H-phenothiazine (5)**

The synthesis was performed as described in the general procedure, starting with compound **1** (200 mg, 0.453 mmol), 2,3-dimethoxyphenylboronic acid (82 mg, 0.453 mmol), Pd(PPh<sub>3</sub>)<sub>4</sub> (5.2 mg, 4.5 μmol) and K<sub>2</sub>CO<sub>3</sub> (251 mg, 1.813 mmol). The reaction time was 16 hours. The crude product was purified by silica gel column chromatography (*n*-pentane/toluene, 5:1, *R<sub>f</sub>* = 0.13), to yield compound **5** as a yellow oil (120 mg, 0.241 mmol, 53%). <sup>1</sup>H NMR (600 MHz, DMSO-*d*<sub>6</sub>) δ: 7.36-7.34 (m, 2H), 7.33-7.32 (m, 1H), 7.23 (d, *J* = 2.0 Hz, 1H), 7.11-7.06 (m, 2H), 7.02-7.02 (m, 1H), 6.98-6.95 (m, 1H), 6.89-6.87 (m, 1H), 3.87 (t, *J* = 7.0 Hz, 2H), 3.83 (s, 3H), 3.53 (s, 3H), 1.71-1.66 (m, 2H), 1.40-1.38 (m, 2H), 1.27-1.25 (m, 4H), 0.84-0.82 (m, 3H); <sup>13</sup>C NMR (150 MHz, DMSO-*d*<sub>6</sub>) δ: 152.8, 145.8, 143.9, 143.4, 133.6, 132.3, 130.1, 129.0, 128.5, 127.3, 125.9, 124.2, 122.3, 121.7, 117.4, 115.6, 113.7, 111.9, 60.1, 55.8, 46.6, 30.8, 26.1, 25.8, 22.0, 13.8. IR (neat, cm<sup>-1</sup>) v: 2945 (w, br), 2925 (m, br), 2852 (w, br), 1574 (m), 1444 (s), 1397 (m), 1252 (s), 1117 (s), 790 (s), 748 (s); HRMS (TOF MS ASAP+, *m/z*): found 497.1019 (calcd. C<sub>26</sub>H<sub>28</sub>NO<sub>2</sub>S<sup>79</sup>Br: 497.1024, [M]<sup>+</sup>).

**3-Bromo-10-hexyl-7-(naphthalen-2-yl)-10H-phenothiazine (6)**

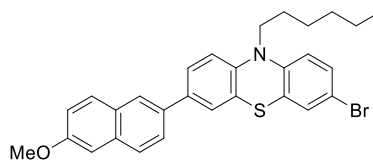
The synthesis was performed as described in the general procedure, starting with compound **1** (203 mg, 0.460 mmol), naphthalen-2-ylboronic acid (79 mg, 0.460 mmol), Pd(PPh<sub>3</sub>)<sub>4</sub> (5.3 mg, 4.60 μmol) and K<sub>2</sub>CO<sub>3</sub> (254 mg, 1.840 mmol). The reaction time was 19 hours. The crude product was purified by silica gel column chromatography (*n*-pentane/toluene, 20:1, *R<sub>f</sub>* = 0.13), to yield compound **6** as a yellow oil (94 mg, 0.192 mmol, 42%). <sup>1</sup>H NMR (400 MHz, DMSO-*d*<sub>6</sub>) δ: 8.18 (s, 1H), 7.98-7.94 (m, 2H), 7.91 (dd, *J* = 7.3, 1.4 Hz, 1H), 7.81 (dd, *J* = 8.6, 1.9 Hz, 1H), 7.66 (dd, *J* = 8.4, 2.2 Hz, 1H), 7.61 (d, *J* = 2.2 Hz, 1H), 7.55-7.47 (m, 2H), 7.37-7.34 (m, 2H), 7.12 (d, *J* = 8.6 Hz, 1H), 6.98-6.94 (m, 1H), 3.88 (t, *J* = 6.9 Hz, 2H), 1.73-1.64 (m, 2H), 1.43-1.34 (m, 2H), 1.27-1.21 (m, 4H), 0.85-0.79 (m, 3H); <sup>13</sup>C NMR (150 MHz, DMSO-*d*<sub>6</sub>) δ: 143.9, 143.7, 136.0, 134.4, 133.3, 132.1, 130.1, 128.9, 128.4, 128.1, 127.4, 126.4, 126.2, 125.9, 125.8, 125.3, 124.6, 124.4, 123.5, 117.4, 116.3, 113.7, 46.6, 30.8, 26.0, 25.7, 22.0, 13.8; IR (neat, cm<sup>-1</sup>) v: 3054 (br), 2924 (m), 2853 (m), 1600 (m), 1453 (s), 1264 (m), 805 (m); HRMS (TOF MS ASAP+, *m/z*): found 488.1043 (calcd. C<sub>28</sub>H<sub>27</sub>NS<sup>79</sup>Br: 488.1048, [M+H]<sup>+</sup>).





### 3-Bromo-10-hexyl-7-(6-methoxynaphthalen-2-yl)-10H-phenothiazine (7)

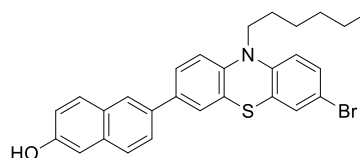
The synthesis was performed as described in the general procedure, starting with compound **1** (200 mg, 0.453 mmol), (6-methoxynaphthalen-2-yl)boronic acid (92 mg, 0.453 mmol), Pd(PPh<sub>3</sub>)<sub>4</sub> (5.2 mg, 4.5 μmol) and K<sub>2</sub>CO<sub>3</sub> (251 mg, 1.813 mmol). The reaction time was 16 hours. The crude product was purified by silica gel column chromatography (*n*-pentane/ethyl acetate, 77.5:2.5, *R<sub>f</sub>* = 0.11), to yield compound



**7** as a yellow oil (90 mg, 0.174 mmol, 38%). <sup>1</sup>H NMR (400 MHz, DMSO-*d*<sub>6</sub>) δ: 8.11 (d, *J* = 1.6 Hz, 1H), 7.89-7.84 (m, 2H), 7.79-7.75 (m, 1H), 7.63 (dd, *J* = 8.5, 2.2 Hz, 1H), 7.57 (d, *J* = 2.2 Hz, 1H), 7.38-7.34 (m, 2H), 7.33 (d, *J* = 2.5 Hz, 1H), 7.18 (dd, *J* = 9.0, 2.5 Hz, 1H), 7.12 (d, *J* = 8.6 Hz, 1H), 6.98 (d, *J* = 8.6 Hz, 1H), 3.91-3.86 (m, 5H), 1.73-1.65 (m, 2H), 1.42-1.36 (m, 2H), 1.26-1.24 (m, 4H), 0.85-0.81 (m, 3H); <sup>13</sup>C NMR (100 MHz, DMSO-*d*<sub>6</sub>) δ: 157.3, 143.9, 143.4, 134.5, 133.7, 133.3, 130.1, 129.6, 128.9, 128.7, 127.3, 126.0, 125.8, 125.0, 124.9, 123.4, 118.9, 117.4, 116.3, 113.7, 108.6, 105.7, 55.2, 46.6, 30.8, 26.1, 25.8, 22.1, 13.8; IR (neat, cm<sup>-1</sup>): 3065 (br), 2953 (m), 1628 (m), 1456 (s), 1391 (m), 1245 (s), 1029 (m), 799 (m); HRMS (TOF MS ASAP+, *m/z*): found 518.1148 (calcd. C<sub>29</sub>H<sub>29</sub>NOS<sup>79</sup>Br: 518.1141, [M+H]<sup>+</sup>).

### 6-(7-Bromo-10-hexyl-10H-phenothiazin-3-yl)naphthalen-2-ol (8)

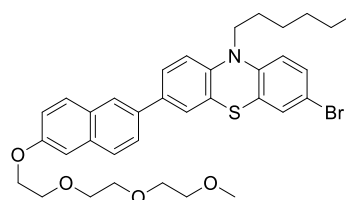
The synthesis was performed as described in the general procedure, starting with compound **1** (1.22 g, 2.77 mmol), ((tertbutyldimethylsilyloxy)naphthalen-2-yl)boronic acid (836 mg, 2.77 mmol), Pd(PPh<sub>3</sub>)<sub>4</sub> (32 mg, 0.028 mmol) and K<sub>2</sub>CO<sub>3</sub> (1.53 g, 11.07 mmol). The reaction time was 72 hours. The crude product was purified by silica gel column chromatography (*n*-pentane/toluene, 10:1, *R<sub>f</sub>* = 0.23), to yield



compound **8** as a green solid (710 mg, 1.407 mmol, 51%), mp 96-100 °C. <sup>1</sup>H NMR (400 MHz, DMSO-*d*<sub>6</sub>) δ: 9.77 (s, 1H), 8.04 (s, 1H), 7.80 (d, *J* = 8.8 Hz, 1H), 7.74-7.66 (m, 2H), 7.59 (dd, *J* = 8.5, 2.1 Hz, 1H), 7.54 (d, *J* = 2.1 Hz, 1H), 7.37-7.33 (m, 2H), 7.13-7.07 (m, 3H), 6.95 (d, *J* = 8.5 Hz, 1H), 3.86 (t, *J* = 7.0 Hz, 2H), 1.72-1.65 (m, 2H), 1.43-1.36 (m, 2H), 1.26-1.21 (m, 4H), 0.84-0.80 (m, 3H); <sup>13</sup>C NMR (150 MHz, DMSO-*d*<sub>6</sub>) δ: 155.4, 144.0, 143.3, 134.8, 133.7, 132.9, 130.1, 129.7, 128.9, 128.0, 126.6, 125.9, 125.9, 124.9, 124.7, 124.3, 123.4, 119.0, 117.3, 116.3, 113.6, 108.4, 46.6, 30.8, 26.0, 25.8, 22.0, 13.8; IR (neat, cm<sup>-1</sup>): 3326 (w, br), 2921 (m), 1697 (m), 1496 (m), 1455 (s), 1246 (m), 1145 (m), 797 (m); HRMS (TOF MS ASAP+, *m/z*): found 504.0996 (calcd. C<sub>28</sub>H<sub>27</sub>NOSBr: 504.0997, [M+H]<sup>+</sup>).

### 3-Bromo-10-hexyl-7-(6-(2-(2-(2-methoxyethoxy)ethoxy)ethoxy)naphthalen-2-yl)-10H-phenothiazine (9)

Compound **8** (401 mg, 0.794 mmol) and K<sub>2</sub>CO<sub>3</sub> (330 mg, 2.388 mmol) were mixed, under N<sub>2</sub>-atmosphere. DMF (32 mL) was added, and the mixture was stirred for 1 hour. 2-(2-(2-Methoxyethoxy)ethoxy)ethyl 4-methylbenzenesulfonate (504 mg, 1.583 mmol) was added, and the reaction was stirred at 130 °C for 20 hours. The reaction mixture was stirred with water (200 mL) for 30 minutes, followed by an extraction of the aqueous phase with ethyl acetate (2 × 100 mL) and the resulting organic phase was washed with water (4 × 100 mL). The

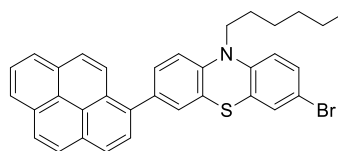


organic phase was dried over Na<sub>2</sub>SO<sub>4</sub>, filtered and solvents were removed *in vacuo*. The crude product was purified by silica gel column chromatography (ethyl acetate/*n*-pentane, 1:1, *R<sub>f</sub>* = 0.15), to yield compound **9** as a yellow oil (377 mg, 0.580 mmol, 73%). <sup>1</sup>H NMR (400 MHz, DMSO-*d*<sub>6</sub>) δ: 8.11 (s, 1H), 7.87 (d, *J* = 9.0 Hz, 1H), 7.85-7.83 (m, 1H), 7.77-7.75 (m, 1H), 7.63 (dd, *J* = 8.5, 1.7 Hz, 1H), 7.57 (d, *J* = 1.8 Hz, 1H),

7.37-7.33 (m, 3H), 7.19 (dd,  $J = 9.1, 2.0$  Hz, 1H), 7.11 (d,  $J = 8.6$ , 1H), 6.97 (d,  $J = 8.5$  Hz, 1H), 4.23-4.21 (m, 2H), 3.88 (t,  $J = 7.0$  Hz, 2H), 3.82-3.81 (m, 2H), 3.63-3.61 (m, 2H), 3.56-3.55 (m, 2H), 3.53-3.52 (m, 2H), 3.42-3.42 (m, 2H), 3.23 (s, 3H), 1.71-1.66 (m, 2H), 1.42-1.37 (m, 2H), 1.27-1.25 (m, 4H), 0.85-0.82 (m, 3H);  $^{13}\text{C}$  NMR (100 MHz, DMSO- $d_6$ )  $\delta$ : 156.5, 143.9, 143.4, 134.6, 133.8, 133.3, 130.1, 129.7, 128.9, 128.8, 127.3, 126.0, 125.8, 125.0, 124.9, 124.3, 123.5, 119.1, 117.4, 116.3, 113.6, 106.5, 71.2, 70.0, 69.8, 69.6, 69.9, 67.2, 54.9, 46.6, 30.8, 26.0, 25.7, 22.0, 13.8; IR (neat,  $\text{cm}^{-1}$ )  $\nu$ : 2923 (m), 2869 (m), 1604 (m), 1457 (s), 1391 (m), 1246 (s), 1105 (m), 803 (m); HRMS (TOF MS ASAP+,  $m/z$ ): found 649.1854 (calcd.  $\text{C}_{35}\text{H}_{40}\text{NO}_4\text{SBr}$ : 649.1861,  $[\text{M}]^+$ ).

### 3-Bromo-10-hexyl-7-(pyren-1-yl)-10H-phenothiazine (10)

The synthesis was performed as described in the general procedure, starting with compound **1** (800 mg, 1.813 mmol), pyren-1-ylboronic acid (491 mg, 1.994 mmol), Pd(PPh<sub>3</sub>)<sub>4</sub> (21 mg, 0.018 mmol) and K<sub>2</sub>CO<sub>3</sub> (1.00 g, 7.25 mmol). 1,4-Dioxane (6 mL) and water (6 mL) were added, and the reaction was stirred at 80 °C for 14 hours. The crude product was purified by silica gel column chromatography (*n*-pentane/Et<sub>2</sub>O, 20:1,  $R_f = 0.34$ ), to yield compound **10** as a yellow solid (409 mg, 0.726 mmol, 40%), mp 95-97 °C.  $^1\text{H}$  NMR (400 MHz, DMSO- $d_6$ )  $\delta$ : 8.35-8.31 (m, 2H), 8.28 (d,  $J = 7.3$  Hz, 1H), 8.22 (s, 2H), 8.18-8.15 (m, 1H), 8.13-8.07 (m, 2H), 8.00 (d,  $J = 7.9$  Hz, 1H), 7.47 (dd,  $J = 8.3, 2.0$  Hz, 1H), 7.42-7.39 (m, 3H), 7.25 (d,  $J = 8.4$  Hz, 1H), 7.05-7.02 (m, 1H), 3.95 (t,  $J = 6.9$  Hz, 2H), 1.79-1.73 (m, 2H), 1.48-1.42 (m, 2H), 1.33-1.26 (m, 4H), 0.88-0.84 (m, 3H);  $^{13}\text{C}$  NMR (100 MHz, DMSO- $d_6$ )  $\delta$ : 144.0, 143.8, 135.9, 134.8, 131.0, 130.4, 130.2, 130.1, 129.9, 129.1, 128.6, 127.7, 127.6, 127.5, 127.40, 127.36, 126.4, 125.9, 125.4, 124.98, 124.95, 124.5, 124.2, 124.0, 123.1, 117.6, 116.0, 113.8, 46.7, 30.8, 26.1, 25.8, 22.1, 13.8; IR (neat,  $\text{cm}^{-1}$ )  $\nu$ : 2945 (w), 2919 (w), 2849 (w), 1598 (w), 1454 (s), 1245 (m), 1103 (m), 842 (m); HRMS (TOF MS ASAP+,  $m/z$ ): found 562.1195 (calcd.  $\text{C}_{34}\text{H}_{29}\text{NSBr}$ : 562.1204,  $[\text{M}+\text{H}]^+$ ).



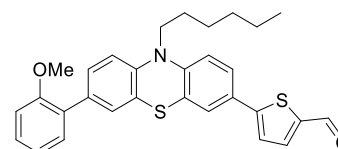
### General procedure for borylation and subsequent Suzuki coupling

The reaction procedure performed was based on a description by Billingsley and Buchwald.<sup>4</sup> The selected building block (**2-10**, 1 eq.) was mixed with dichlorobis(acetonitrile)palladium(II) (0.02 eq.) and SPhos (0.08 eq.). The system was sealed, evacuated and backflushed with N<sub>2</sub>. Dry and degassed 1,4-dioxane and triethylamine were added, followed by addition of 4,4,5,5-tetramethyl-1,3,2-dioxaborolane (1.5 eq.). The reaction was stirred at 80 °C until full conversion. The reaction solution was cooled, and filtered through a pad of Celite with ethyl acetate. The crude product was concentrated *in vacuo*.

Pd(OAc)<sub>2</sub> (0.02 eq.), SPhos (0.08 eq.) and K<sub>2</sub>CO<sub>3</sub> (4 eq.) were added to the crude borylation products (1 eq.), before the Schlenk tubes were sealed, evacuated and backflushed with N<sub>2</sub>. Water (194 eq.) and 1,4-dioxane (40 eq.) were degassed and added through the septum followed by 5-bromothiophene-2-carbaldehyde (1.5 eq.). The reaction was stirred at 80 °C until full conversion, followed by extraction by ethyl acetate (3 × 30 mL), drying of the combined organic phased with brine (30 mL) and drying over anhydrous Na<sub>2</sub>SO<sub>4</sub>. The solvents were removed *in vacuo* and the crude was purified by silica gel column chromatography.

### 5-(10-Hexyl-7-(2-methoxyphenyl)-10H-phenothiazin-3-yl)thiophene-2-carbaldehyde (11)

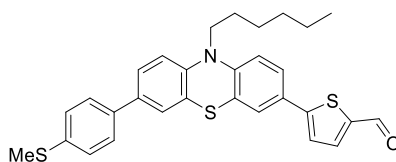
The reaction was performed as described in the general procedure for borylation and subsequent Suzuki cross-coupling, starting with compound **2** (400 mg, 0.854 mmol), SPhos (28 mg, 0.068 mmol), pinacol borane (164 mg, 1.281 mmol) and dichlorobis(acetonitrile)palladium(II) (4.4 mg, 0.017 mmol), achieving full conversion in 1.5 hours. The crude material (380



mg) was subjected to the above mentioned Suzuki reaction conditions with SPhos (12.1 mg, 0.029 mmol), Pd(OAc)<sub>2</sub> (3.3 mg, 0.015 mmol), K<sub>2</sub>CO<sub>3</sub> (408 mg, 2.95 mmol) and 5-bromothiophene-2-carbaldehyde (211 mg, 1.106 mmol) in water and 1,4-dioxane. The product was purified by silica gel column chromatography (*n*-pentane/ethyl acetate, 1:10, *R<sub>f</sub>* = 0.23), to yield compound **11** as a red solid (210 mg, 0.420 mmol, 57%), mp 81–84 °C. <sup>1</sup>H NMR (600 MHz, DMSO-*d*<sub>6</sub>) δ: 9.87 (s, 1H), 8.00 (d, *J* = 3.9 Hz, 1H), 7.68 (d, *J* = 4.0 Hz, 1H), 7.63–7.59 (m, 2H), 7.34–7.30 (m, 2H), 7.28 (dd, *J* = 7.5, 1.7 Hz, 1H), 7.26 (d, *J* = 2.0 Hz, 1H), 7.11–7.07 (m, 3H), 7.01 (td, *J* = 7.4, 1.0 Hz, 1H), 3.93 (t, *J* = 7.0 Hz, 2H), 3.76 (s, 3H), 1.73–1.71 (m, 2H), 1.43–1.41 (m, 2H), 1.28–1.27 (m, 4H), 0.85–0.83 (m, 3H); <sup>13</sup>C NMR (150 MHz, DMSO-*d*<sub>6</sub>) δ: 184.7, 156.0, 151.9, 145.5, 142.6, 141.1, 139.4, 132.8, 129.9, 128.7, 128.7, 128.4, 127.7, 126.7, 125.8, 124.4, 124.3, 124.1, 121.9, 120.8, 116.0, 115.5, 111.7, 55.5, 46.6, 30.8, 26.2, 25.8, 22.1, 13.8; IR (neat, cm<sup>-1</sup>) ν: 1951 (w, br), 2925 (m, br), 2847 (w), 1662 (s), 1584 (m), 1470 (m), 1429 (s), 1221 (s), 800 (s), 748 (s); HRMS (TOF MS ASAP+, *m/z*): found 499.1640 (calcd. C<sub>30</sub>H<sub>29</sub>NO<sub>2</sub>S<sub>2</sub>: 499.1640, [M]<sup>+</sup>).

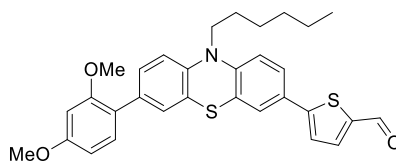
### 5-(10-Hexyl-7-(4-(methylthio)phenyl)-10H-phenothiazin-3-yl)thiophene-2-carbaldehyde (**12**)

The reaction was performed as described in the general procedure for borylation and subsequent Suzuki cross-coupling, starting with compound **3** (300 mg, 0.619 mmol), SPhos (20.3 mg, 0.05 mmol), pinacol borane (119 mg, 0.929 mmol) and dichlorobis(acetonitrile)palladium(II) (3.2 mg, 0.012 mmol), achieving full conversion in 2 hours. The crude material (329 mg) was subjected to the above mentioned Suzuki reaction conditions with SPhos (10.16 mg, 0.025 mmol), Pd(OAc)<sub>2</sub> (2.8 mg, 0.012 mmol), K<sub>2</sub>CO<sub>3</sub> (342 mg, 2.476 mmol) and 5-bromothiophene-2-carbaldehyde (177 mg, 0.928 mmol) in water and 1,4-dioxane. The product was purified by silica gel column chromatography (*n*-pentane/ethyl acetate, 6:1, *R<sub>f</sub>* = 0.14), to yield compound **12** as a red solid (167 mg, 0.323 mmol, 52%), mp 95–96 °C. <sup>1</sup>H NMR (600 MHz, DMSO-*d*<sub>6</sub>) δ: 9.87 (s, 1H), 8.00 (d, *J* = 4.0 Hz, 1H), 7.67 (d, *J* = 3.9 Hz, 1H), 7.62–7.57 (m, 4H), 7.49 (dd, *J* = 8.5, 2.1 Hz, 1H), 7.44 (d, *J* = 2.1 Hz, 1H), 7.33–7.28 (m, 2H), 7.10–7.05 (m, 2H), 3.91 (t, *J* = 7.0 Hz, 2H), 2.50 (s, 3H), 1.74–1.66 (m, 2H), 1.44–1.35 (m, 2H), 1.29–1.22 (m, 4H), 0.86–0.80 (m, 3H); <sup>13</sup>C NMR (150 MHz, DMSO-*d*<sub>6</sub>) δ: 183.8, 151.9, 145.4, 142.9, 141.1, 139.4, 137.1, 135.2, 134.1, 126.7, 126.5 (2C), 126.4 (2C), 125.9, 125.6, 124.7, 124.41, 124.36, 123.9, 123.1, 116.3, 116.0, 46.7, 30.8, 26.1, 25.8, 22.1, 14.7, 13.8; IR (neat, cm<sup>-1</sup>) ν: 2921 (w), 2851 (w), 1661 (s), 1472 (m), 1437 (s), 1226 (m), 804 (m); HRMS (TOF MS ASAP+, *m/z*): found 516.1489 (calcd. C<sub>30</sub>H<sub>30</sub>NOS<sub>3</sub>: 516.1490, [M+H]<sup>+</sup>).



### 5-(7-(2,4-Dimethoxyphenyl)-10-hexyl-10H-phenothiazin-3-yl)thiophene-2-carbaldehyde (**13**)

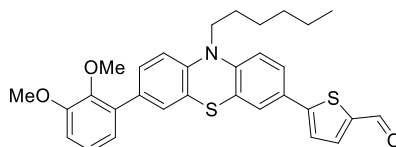
The reaction was performed as described in the general procedure for borylation and subsequent Suzuki cross-coupling, starting with compound **4** (280 mg, 0.562 mmol), SPhos (18.5 mg, 0.045 mmol), pinacol borane (108 mg, 0.843 mmol) and dichlorobis(acetonitrile)palladium(II) (2.9 mg, 0.011 mmol), achieving full conversion in 1.5 hours. The crude material (300 mg) was subjected to the above mentioned Suzuki reaction conditions with SPhos (10.9 mg, 0.027 mmol), Pd(OAc)<sub>2</sub> (3.8 mg, 0.017 mmol), K<sub>2</sub>CO<sub>3</sub> (313 mg, 2.265 mmol) and 5-bromothiophene-2-carbaldehyde (158 mg, 0.825 mmol) in water and 1,4-dioxane. The product was purified by silica gel column chromatography (*n*-pentane/ethyl acetate, 1:10, *R<sub>f</sub>* = 0.20), to yield compound **13** as a red solid (170 mg, 0.321 mmol, 58%). <sup>1</sup>H NMR (600 MHz, DMSO-*d*<sub>6</sub>) δ: 9.87 (s, 1H), 7.99 (d, *J* = 4.0 Hz, 1H), 7.67 (d, *J* = 4.0 Hz, 1H), 7.62–7.58 (m, 2H), 7.27 (dd, *J* = 8.4, 2.1 Hz, 1H), 7.21–7.18 (m, 2H), 7.07 (d, *J* = 8.6 Hz, 1H), 7.04 (d, *J* = 8.6 Hz, 1H), 6.64 (d, *J* = 2.5 Hz, 1H), 6.59 (dd, *J* = 8.5, 2.5 Hz, 1H), 3.91 (t, *J* = 7.0 Hz, 2H), 3.79 (s, 3H), 3.76 (s, 3H), 1.72–1.70 (m, 2H), 1.41–1.40 (m, 2H), 1.28–1.26 (m, 4H),



0.85-0.82 (m, 3H);  $^{13}\text{C}$  NMR (150 MHz, DMSO- $d_6$ )  $\delta$ : 183.7, 160.0, 157.0, 152.0, 145.6, 142.1, 141.0, 139.4, 132.8, 130.4, 128.5, 127.5, 126.6, 125.8, 124.4, 124.3, 124.1, 121.8, 121.1, 115.9, 114.5, 105.3, 98.9, 55.5, 55.3, 46.6, 30.8, 26.2, 25.8, 22.0, 13.8; IR (neat,  $\text{cm}^{-1}$ )  $\nu$ : 2951 (m, br), 2930 (m, br), 2852 (w, br), 1652 (s), 1605 (m), 1434 (s), 1226 (s), 1205 (s), 1060 (s), 795 (s); HRMS (TOF MS ASAP+,  $m/z$ ): found 529.1744 (calcd.  $\text{C}_{31}\text{H}_{31}\text{NO}_3\text{S}_2$ : 529.1745,  $[\text{M}]^+$ ).

#### 5-(7-(2,3-Dimethoxyphenyl)-10-hexyl-10H-phenothiazin-3-yl)thiophene-2-carbaldehyde (14)

The reaction was performed as described in the general procedure for borylation and subsequent Suzuki cross-coupling, starting with compound **5** (400 mg, 0.802 mmol), SPhos (26.4 mg, 0.064 mmol), pinacol borane (154 mg, 1.204 mmol) and dichlorobis(acetonitrile)palladium(II) (4.2 mg, 0.016 mmol), achieving full conversion in 4 hours.

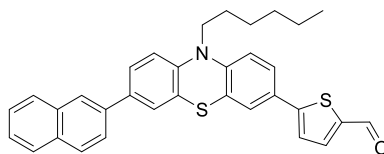


The crude material (438 mg) was subjected to the above

mentioned Suzuki reaction conditions with SPhos (13.2 mg, 0.032 mmol), Pd(OAc) $_2$  (3.6 mg, 16.0  $\mu\text{mol}$ ),  $\text{K}_2\text{CO}_3$  (444 mg, 3.21 mmol) and 5-bromothiophene-2-carbaldehyde (230 mg, 1.204 mmol) in water and 1,4-dioxane. The product was purified by silica gel column chromatography (*n*-pentane/ethyl acetate, 20:1,  $R_f$  = 0.10), to yield compound **14** as a red solid (106 mg, 0.200 mmol, 25%), mp 89-91  $^\circ\text{C}$ .  $^1\text{H}$  NMR (600 MHz, DMSO- $d_6$ )  $\delta$ : 9.87 (s, 1H), 8.00 (d,  $J$  = 4.1 Hz, 1H), 7.67 (d,  $J$  = 3.9 Hz, 1H), 7.63-7.59 (m, 2H), 7.34 (dd,  $J$  = 8.4, 1.8 Hz, 1H), 7.25 (d,  $J$  = 1.8 Hz, 1H), 7.12-7.07 (m, 3H), 7.05-7.02 (m, 1H), 6.90 (d,  $J$  = 7.6 Hz, 1H), 3.93 (t,  $J$  = 7.0 Hz, 2H), 3.83 (s, 3H), 3.54 (s, 3H), 1.74-1.70 (m, 2H), 1.44-1.39 (m, 2H), 1.28-1.24 (m, 4H), 0.85-0.82 (m, 3H);  $^{13}\text{C}$  NMR (150 MHz, DMSO- $d_6$ )  $\delta$ : 183.7, 152.8, 151.9, 145.8, 145.4, 142.8, 141.1, 139.4, 133.6, 132.5, 128.5, 127.3, 126.7, 125.8, 124.4, 124.3, 124.2, 124.0, 122.0, 121.7, 116.1, 115.6, 112.2, 60.1, 55.8, 46.7, 30.8, 26.1, 25.8, 22.1, 13.8; IR (neat,  $\text{cm}^{-1}$ )  $\nu$ : 2928 (m), 2854 (w), 1657 (s), 1580 (m), 1434 (s), 1258 (m), 1224 (m), 1120 (m), 802 (m), 735 (m); HRMS (TOF MS ASAP+,  $m/z$ ): found 530.1818 (calcd.  $\text{C}_{31}\text{H}_{32}\text{NO}_3\text{S}_2$ : 530.1824,  $[\text{M}+\text{H}]^+$ ).

#### 5-(10-Hexyl-7-(naphthalen-2-yl)-10H-phenothiazin-3-yl)thiophene-2-carbaldehyde (15)

The reaction was performed as described in the general procedure for borylation and subsequent Suzuki cross-coupling, starting with compound **6** (400 mg, 0.819 mmol), SPhos (26.9 mg, 0.066 mmol), pinacol borane (157 mg, 1.228 mmol) and dichlorobis(acetonitrile)palladium(II) (4.3 mg, 0.016 mmol), achieving full conversion in 4.5 hours.

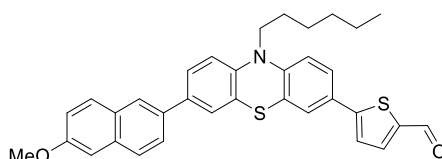


The crude material (439 mg) was subjected to the above

mentioned Suzuki reaction conditions with SPhos (13.5 mg, 0.033 mmol), Pd(OAc) $_2$  (3.7 mg, 0.016 mmol),  $\text{K}_2\text{CO}_3$  (453 mg, 3.28 mmol) and 5-bromothiophene-2-carbaldehyde (235 mg, 1.230 mmol) in water and 1,4-dioxane. The product was purified by silica gel column chromatography (*n*-pentane/ethyl acetate, 20:1,  $R_f$  = 0.11), to yield compound **15** as a red solid (183 mg, 0.352 mmol, 43%), mp 129-131  $^\circ\text{C}$ .  $^1\text{H}$  NMR (600 MHz, DMSO- $d_6$ )  $\delta$ : 9.88 (s, 1H), 8.20 (s, 1H), 8.01 (d,  $J$  = 4.0 Hz, 1H), 7.97 (d,  $J$  = 8.4 Hz, 2H), 7.92 (d,  $J$  = 7.9 Hz, 1H), 7.84 (dd,  $J$  = 8.6, 1.3 Hz, 1H), 7.70-7.67 (m, 2H), 7.64-7.61 (m, 3H), 7.55-7.48 (m, 2H), 7.16 (d,  $J$  = 8.6 Hz, 1H), 7.11 (d,  $J$  = 8.3 Hz, 1H), 3.96 (t,  $J$  = 7.0 Hz, 2H), 1.77-1.71 (m, 2H), 1.46-1.40 (m, 2H), 1.30-1.25 (m, 4H), 0.86-0.82 (m, 3H);  $^{13}\text{C}$  NMR (150 MHz, DMSO- $d_6$ )  $\delta$ : 183.8, 151.9, 145.4, 143.2, 141.1, 139.4, 136.0, 134.5, 133.3, 132.1, 128.4, 128.1, 127.4, 126.8, 126.4, 126.3, 126.0, 125.9, 125.3, 124.6, 124.43, 124.40 (2C), 123.9, 123.3, 116.4, 116.1, 46.7, 30.8, 26.1, 25.8, 22.1, 13.8; IR (neat,  $\text{cm}^{-1}$ )  $\nu$ : 2913 (w), 2851 (w), 1659 (s), 1580 (m), 1433 (s), 1229 (m), 1057 (m), 801 (s); HRMS (TOF MS ASAP+,  $m/z$ ): found 520.1761 (calcd.  $\text{C}_{33}\text{H}_{30}\text{NOS}_2$ : 520.1769,  $[\text{M}+\text{H}]^+$ ).

### 5-(10-Hexyl-7-(6-methoxynaphthalen-2-yl)-10H-phenothiazin-3-yl)thiophene-2-carbaldehyde (16)

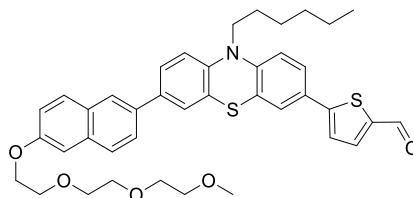
The reaction was performed as described in the general procedure for borylation and subsequent Suzuki cross-coupling, starting with compound **7** (350 mg, 0.675 mmol), SPhos (22.2 mg, 0.054 mmol), pinacol borane (130 mg, 1.013 mmol) and dichlorobis(acetonitrile)palladium(II) (3.5 mg, 0.014 mmol), achieving full conversion in 5 hours. The



crude material (382 mg) was subjected to the above mentioned Suzuki reaction conditions with SPhos (11.1 mg, 0.027 mmol), Pd(OAc)<sub>2</sub> (3.0 mg, 0.014 mmol), K<sub>2</sub>CO<sub>3</sub> (373 mg, 2.70 mmol) and 5-bromothiophene-2-carbaldehyde (194 mg, 1.013 mmol) in water and 1,4-dioxane. The product was purified by silica gel column chromatography (CH<sub>2</sub>Cl<sub>2</sub>/*n*-pentane, 4:1, *R<sub>f</sub>* = 0.18), to yield compound **16** as a red solid (226 mg, 0.411 mmol, 61%), mp 174-176 °C. <sup>1</sup>H NMR (600 MHz, DMSO-*d*<sub>6</sub>) δ: 9.88 (s, 1H), 8.12 (s, 1H), 8.00 (d, *J* = 3.9 Hz, 1H), 7.89-7.86 (m, 2H), 7.78 (dd, *J* = 6.9, 1.7 Hz, 1H), 7.68 (d, *J* = 3.9 Hz, 1H), 7.65-7.60 (m, 3H), 7.59 (d, *J* = 2.1 Hz, 1H), 7.33 (d, *J* = 2.3 Hz, 1H), 7.18 (dd, *J* = 9.0, 2.5 Hz, 1H), 7.14 (d, *J* = 8.6 Hz, 1H), 7.10 (d, *J* = 8.3 Hz, 1H), 3.95 (t, *J* = 7.0 Hz, 2H), 3.89 (s, 3H), 1.76-1.70 (m, 2H), 1.45-1.40 (m, 2H), 1.30-1.25 (m, 4H), 0.86-0.82 (m, 3H); <sup>13</sup>C NMR (150 MHz, DMSO-*d*<sub>6</sub>) δ: 183.8, 157.3, 151.9, 145.4, 142.9, 141.1, 139.4, 134.7, 133.7, 133.4, 129.6, 128.8, 127.3, 126.7, 126.0, 125.9, 125.0, 124.9, 124.42, 124.37, 124.3, 123.9, 123.2, 118.9, 116.3, 116.1, 105.7, 55.2, 46.7, 30.8, 26.1, 25.8, 22.1, 13.8; IR (neat, cm<sup>-1</sup>) ν: 2918 (w), 2852 (w), 1661 (s), 1600 (m), 1433 (s), 1372 (m), 1230 (m), 799 (s); HRMS (TOF MS ASAP+, *m/z*): found 550.1869 (calcd. C<sub>34</sub>H<sub>32</sub>NO<sub>2</sub>S<sub>2</sub>: 550.1874, [M+H]<sup>+</sup>).

### 5-(10-Hexyl-7-(6-(2-(2-(2-methoxyethoxy)ethoxy)ethoxy)naphthalen-2-yl)-10H-phenothiazin-3-yl)thiophene-2-carbaldehyde (17)

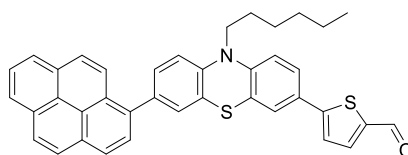
The reaction was performed as described in the general procedure for borylation and subsequent Suzuki cross-coupling, starting with compound **9** (378 mg, 0.581 mmol), SPhos (19.1 mg, 0.046 mmol), pinacol borane (112 mg, 0.871 mmol) and dichlorobis(acetonitrile)palladium(II) (3.0 mg, 0.012 mmol), achieving full conversion in 24 hours. The crude material (405 mg) was subjected to the above mentioned



Suzuki reaction conditions with SPhos (9.5 mg, 0.023 mmol), Pd(OAc)<sub>2</sub> (2.6 mg, 0.012 mmol), K<sub>2</sub>CO<sub>3</sub> (321 mg, 2.322 mmol) and 5-bromothiophene-2-carbaldehyde (166 mg, 0.871 mmol) in water and 1,4-dioxane. The product was purified by silica gel column chromatography (*n*-pentane/ethyl acetate, 3:2, *R<sub>f</sub>* = 0.07), to yield compound **17** as a red oil (216 mg, 0.316 mmol, 55%). <sup>1</sup>H NMR (600 MHz, DMSO-*d*<sub>6</sub>) δ: 9.87 (s, 1H), 8.12 (s, 1H), 8.00 (d, *J* = 4.0 Hz, 1H), 7.88 (d, *J* = 9.0 Hz, 1H), 7.86-7.83 (m, 1H), 7.78-7.76 (m, 1H), 7.68 (d, *J* = 4.0 Hz, 1H), 7.65-7.60 (m, 3H), 7.58 (d, *J* = 2.0 Hz, 1H), 7.34 (d, *J* = 2.0 Hz, 1H), 7.20 (dd, *J* = 8.9, 2.3 Hz, 1H), 7.14 (d, *J* = 8.7 Hz, 1H), 7.09 (d, *J* = 8.3 Hz, 1H), 4.24-4.21 (m, 2H), 3.94 (t, *J* = 7.0 Hz, 2H), 3.82-3.81 (m, 2H), 3.63-3.60 (m, 2H), 3.57-3.51 (m, 4H), 3.44-3.41 (m, 2H), 3.23 (s, 3H), 1.76-1.70 (m, 2H), 1.45-1.39 (m, 2H), 1.30-1.24 (m, 4H), 0.86-0.82 (m, 3H); <sup>13</sup>C NMR (150 MHz, DMSO-*d*<sub>6</sub>) δ: 183.7, 156.5, 151.9, 145.4, 142.9, 141.1, 139.4, 134.7, 133.8, 133.4, 129.7, 128.8, 127.3, 126.7, 126.0, 125.9, 125.0, 124.9, 124.41, 124.36, 124.3, 123.9, 123.2, 119.1, 116.3, 116.0, 106.5, 71.3, 70.0, 69.8, 69.6, 68.9, 67.2, 58.0, 46.7, 30.8, 26.1, 25.8, 22.1, 13.8; IR (neat, cm<sup>-1</sup>) ν: 2952 (m), 1725 (w), 1658 (s), 1602 (m), 1434 (s), 1269 (m), 1103 (m), 798 (m); HRMS (TOF MS ASAP+, *m/z*): found 682.2659 (calcd. C<sub>40</sub>H<sub>44</sub>NO<sub>5</sub>S<sub>2</sub>: 682.2661, [M+H]<sup>+</sup>).

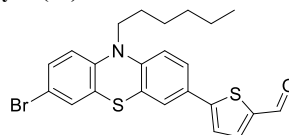
### 5-(10-Hexyl-7-(pyren-1-yl)-10H-phenothiazin-3-yl)thiophene-2-carbaldehyde (**18**)

The reaction was performed as described in the general procedure for borylation and subsequent Suzuki cross-coupling, starting with compound **10** (250 mg, 0.444 mmol), SPhos (14.6 mg, 0.036 mmol), pinacol borane (85 mg, 0.667 mmol) and dichlorobis(acetonitrile)palladium(II) (2.3 mg, 8.89  $\mu$ mol), achieving full conversion in 2 hours. The crude material (271 mg) was subjected to the above mentioned Suzuki reaction conditions with SPhos (7.3 mg, 0.018 mmol), Pd(OAc)<sub>2</sub> (2.0 mg, 8.89  $\mu$ mol), K<sub>2</sub>CO<sub>3</sub> (246 mg, 1.778 mmol) and 5-bromothiophene-2-carbaldehyde (127 mg, 0.667 mmol) in water and 1,4-dioxane. The product was purified by silica gel column chromatography (*n*-pentane/ethyl acetate, 3:1, *R<sub>f</sub>* = 0.32), to yield compound **18** as a red solid (153 mg, 0.257 mmol, 58%), mp 122-125 °C. <sup>1</sup>H NMR (600 MHz, DMSO-*d*<sub>6</sub>)  $\delta$ : 9.88 (s, 1H), 8.36-8.26 (m, 3H), 8.22 (s, 2H), 8.19-8.07 (m, 3H), 8.03-7.99 (m, 2H), 7.70 (d, *J* = 4.0 Hz, 1H), 7.67-7.63 (m, 2H), 7.47 (dd, *J* = 8.4, 2.0 Hz, 1H), 7.42 (d, *J* = 2.0 Hz, 1H), 7.27 (d, *J* = 8.4 Hz, 1H), 7.15 (d, *J* = 8.9 Hz, 1H), 4.01 (t, *J* = 6.9 Hz, 2H), 1.84-1.75 (m, 2H), 1.51-1.43 (m, 2H), 1.34-1.24 (m, 4H), 0.89-0.84 (m, 3H); <sup>13</sup>C NMR (150 MHz, DMSO-*d*<sub>6</sub>)  $\delta$ : 183.8, 151.9, 145.5, 143.2, 141.1, 139.4, 135.8, 134.9, 131.0, 130.4, 130.1, 129.9, 128.6, 127.7, 127.6, 127.5, 127.39, 127.35 (2C), 126.9, 126.4, 125.9, 125.3, 125.0, 124.9, 124.5, 124.4, 124.2, 124.0, 122.8, 116.2, 116.0, 54.9, 46.8, 30.8, 26.2, 25.8, 22.1, 13.8; IR (neat, cm<sup>-1</sup>)  $\nu$ : 2923 (w), 1658 (s), 1582 (m), 1433 (s), 1224 (m), 1056 (w), 845 (m); HRMS (TOF MS ASAP+, *m/z*): found 594.1921 (calcd. C<sub>39</sub>H<sub>32</sub>NOS<sub>2</sub>: 594.1925, [M+H]<sup>+</sup>).



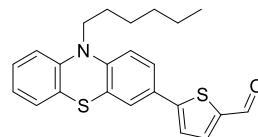
### 5-(7-Bromo-10-hexyl-10H-phenothiazin-3-yl)thiophene-2-carbaldehyde (**19**)<sup>5</sup>

Compound **1** (1.00 g, 2.266 mmol), (5-formylthiophen-2-yl)boronic acid (530 mg, 3.40 mmol), Pd(OAc)<sub>2</sub> (10.2 mg, 0.045 mmol), SPhos (37 mg, 0.091 mmol) and K<sub>2</sub>CO<sub>3</sub> (1.25 g, 9.07 mmol) were mixed in a Schlenk tube which was sealed with a septum, then evacuated and backflushed with N<sub>2</sub> three times. 1,4-Dioxane (6 mL) and water (6 mL) were degassed and added, and the reaction was stirred at 80 °C for 16 hours. The crude product was purified by silica gel column chromatography (*n*-pentane/EtOAc, 3:1, *R<sub>f</sub>* = 0.38), to yield compound **19** as a red solid (350 mg, 0.741 mmol, 33%), mp 77-78 °C. <sup>1</sup>H NMR (400 MHz, DMSO-*d*<sub>6</sub>)  $\delta$ : 9.87 (s, 1H), 7.99 (d, *J* = 4.0 Hz, 1H), 7.66 (d, *J* = 4.0 Hz, 1H), 7.62-7.57 (m, 2H), 7.37-7.33 (m, 2H), 7.07 (d, *J* = 8.5 Hz, 1H), 6.97 (d, *J* = 9.4 Hz, 1H), 3.86 (t, *J* = 6.9 Hz, 2H), 1.69-1.61 (m, 2H), 1.40-1.32 (m, 2H), 1.26-1.20 (m, 4H), 0.84-0.79 (m, 3H). <sup>1</sup>H NMR data are in accordance with that reported by Lin et al.<sup>5</sup>



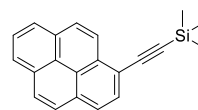
### 5-(10-Hexyl-10H-phenothiazin-3-yl)thiophene-2-carbaldehyde (**20**)<sup>6</sup>

Compound **19** (300 mg, 0.635 mmol), Pd(OAc)<sub>2</sub> (2.9 mg, 0.013 mmol), triphenylphosphine (13.3 mg, 0.051 mmol) and K<sub>2</sub>CO<sub>3</sub> (176 mg, 1.270 mmol) were mixed in a Schlenk tube which was sealed with a septum, then evacuated and backflushed with N<sub>2</sub> three times. *n*-Butanol (2 mL) was degassed and added, and the reaction was stirred at 100 °C for 2 hours. The crude product was purified by silica gel column chromatography (*n*-pentane/EtOAc, 9:1, *R<sub>f</sub>* = 0.21), to yield compound **20** as a red oil (151 mg, 0.384 mmol, 60%). <sup>1</sup>H NMR (400 MHz, DMSO-*d*<sub>6</sub>)  $\delta$ : 9.87 (s, 1H), 8.00 (d, *J* = 4.0 Hz, 1H), 7.66 (d, *J* = 4.0 Hz, 1H), 7.62-7.57 (m, 2H), 7.24-7.19 (m, 1H), 7.16 (dd, *J* = 7.6, 1.5 Hz, 1H), 7.09-7.03 (m, 2H), 6.99-6.94 (m, 1H), 3.90 (t, *J* = 6.9 Hz, 2H), 1.73-1.64 (m, 2H), 1.43-1.34 (m, 2H), 1.28-1.21 (m, 4H), 0.85-0.79 (m, 3H). <sup>1</sup>H NMR data are in accordance with that reported by Huang et al.<sup>6</sup>

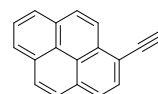


**Trimethyl(pyren-1-ylethynyl)silane (21)**<sup>7</sup>

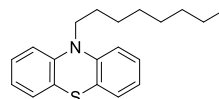
1-Bromopyrene (1.12 g, 4.00 mmol), ethynyltrimethylsilane (480 mg, 0.70 mL, 4.95 mmol), Pd(PPh<sub>3</sub>)<sub>2</sub>Cl<sub>2</sub> (347 mg, 0.494 mmol), CuI (42 mg, 0.221 mmol) were mixed with dry Et<sub>3</sub>N (60 mL) and stirred at 85 °C for 24 hours under nitrogen. The reaction mixture was quenched with distilled water (100 mL) and extracted with CH<sub>2</sub>Cl<sub>2</sub> (3 × 60 mL). The combined organic phase was dried with brine (50 mL) and over anhydrous Na<sub>2</sub>SO<sub>4</sub> and filtered. The solvent was removed and the crude product was purified using column chromatography (*n*-pentane, *R<sub>f</sub>* = 0.20). The product **21** was obtained as a yellow solid (851 mg, 2.850 mmol, 71%), mp 100-103 °C. <sup>1</sup>H NMR (400 MHz, DMSO-*d*<sub>6</sub>) δ: 8.32-8.28 (m, 1H), 8.22-8.17 (m, 3H), 8.12-8.07 (m, 2H), 8.05-7.97 (m, 3H), 0.37 (s, 9H). <sup>1</sup>H NMR analysis of **19** in CDCl<sub>3</sub> was in accordance with previously reported values.<sup>7</sup>

**1-Ethynylpyrene (22)**<sup>7</sup>

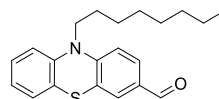
Compound **21** (1.00 g, 3.35 mmol), potassium carbonate (1.41 g, 10.2 mmol), MeOH (17 mL) and THF (40 mL) were mixed at room temperature for 1 hours. The reaction mixture was quenched with water (50 mL) and extracted with CH<sub>2</sub>Cl<sub>2</sub> (3 × 10 mL). The combined organic phase was washed with water (50 mL) before it was dried with brine (50 mL) and then over anhydrous Na<sub>2</sub>SO<sub>4</sub>. The solvent was removed after filtration and the crude product was purified using column chromatography (*n*-pentane, *R<sub>f</sub>* = 0.21). The product **22** was a brown solid (627 mg, 2.77 mmol, 82%), mp 112-113 °C. <sup>1</sup>H NMR (400 MHz, DMSO-*d*<sub>6</sub>) δ: 8.49 (d, *J* = 9.1 Hz, 1H), 8.40-8.34 (m, 3H), 8.29 (d, *J* = 9.3 Hz, 1H), 8.27 (d, *J* = 10.4 Hz, 1H), 8.24-8.19 (m, 2H), 8.14 (t, *J* = 7.6 Hz, 1H), 4.81 (s, 1H). <sup>1</sup>H NMR analysis of **22** in CDCl<sub>3</sub> was in accordance with previously reported values.<sup>7</sup>

**10-Octyl-10H-phenothiazine (23)**<sup>8</sup>

10H-Phenothiazine (5.08 g, 25.5 mmol) and sodium hydride (0.91 g, 37.9 mmol) were mixed and nitrogen atmosphere was established. Dry, degassed THF (85 mL) was added and the mixture was stirred at room temperature until the color changed from green to yellow. 1-Bromooctane (3.9 mL, 22.6 mmol) was added dropwise using a syringe pump over 20 minutes, after which the reaction mixture was heated at reflux for 5 hours. A 5% aqueous sol. of NH<sub>4</sub>Cl (50 mL) was added, and the reaction mixture was extracted with ethyl acetate (3 × 50 mL). The combined organic layer was dried with brine (50 mL) and over anhydrous Na<sub>2</sub>SO<sub>4</sub>. Solvents was removed under reduced pressure. The crude product was purified using column chromatography (*n*-pentane, *R<sub>f</sub>* = 0.21). The product **23** was a colourless liquid (6.47 g, 19.1 mmol, 84%). <sup>1</sup>H NMR (400 MHz, DMSO-*d*<sub>6</sub>) δ: 7.18-7.13 (m, 2H), 7.11 (dd, *J* = 7.6, 1.5 Hz, 2H), 6.94 (d, *J* = 8.1 Hz, 2H), 6.89 (td, *J* = 7.4, 0.9 Hz, 2H), 3.80 (t, *J* = 6.9 Hz, 2H), 1.68-1.59 (m, 2H), 1.36-1.28 (m, 2H), 1.22-1.10 (m, 8H), 0.81-0.76 (m, 3H). <sup>1</sup>H NMR analysis of **23** in CDCl<sub>3</sub> was in accordance with previously reported values.<sup>8</sup>

**10-Octyl-10H-phenothiazine-3-carbaldehyde (24)**<sup>9</sup>

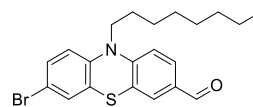
Compound **23** (6.14 g, 19.7 mmol) was dissolved in DMF (6.00 mL, 5.68 g, 77.8 mmol) and 1,2-dichloroethene (120 mL). The mixture was cooled using an ice bath. POC<sub>3</sub> (7.00 mL, 74.9 mmol) was added to the reaction mixture using a syringe pump over 45 minutes. The reaction was heated to reflux and left to stir over night. The reaction mixture was quenched with water and extracted with CHCl<sub>3</sub> (3 × 100 mL). The combined organic layer was washed with water (100 mL) and then dried with brine (100 mL) and over anhydrous Na<sub>2</sub>SO<sub>4</sub>. Solvents were removed *in vacuo* and the product purified using column chromatography (*n*-pentane/ethyl acetate 6:1, *R<sub>f</sub>* = 0.45). This gave **24** as a yellow liquid (4.84 g, 14.2 mmol, 72%). <sup>1</sup>H NMR (400 MHz, DMSO-*d*<sub>6</sub>) δ: 9.78 (s, 1H), 7.70 (dd, *J* = 6.4, 1.9 Hz, 1H), 7.58 (d, *J* =



2.0 Hz, 1H), 7.24-7.19 (m, 1H), 7.16-7.12 (m, 2H), 7.06 (d,  $J = 7.7$  Hz, 1H), 6.99 (td,  $J = 7.5, 0.9$  Hz, 1H), 3.92 (t,  $J = 6.9$  Hz, 2H), 1.70-1.62 (m, 2H), 1.40-1.31 (m, 2H), 1.24-1.14 (m, 8H), 0.82-0.77 (m, 3H).  $^1\text{H}$  NMR analysis of **24** in  $\text{CDCl}_3$  was in accordance with previously reported values.<sup>9</sup>

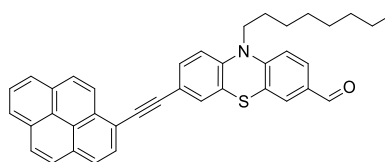
#### 7-Bromo-10-octyl-10H-phenothiazine-3-carbaldehyde (**25**)<sup>10</sup>

Compound **24** (1.01 g, 2.97 mmol) was dissolved in dry THF (100 mL) and cooled in an ice bath. NBS (0.84 g, 4.72 mmol) was added, and the reaction mixture was left to stir in room temperature for 2 days. The reaction mixture was quenched with water (100 mL) and extracted with  $\text{CH}_2\text{Cl}_2$  ( $3 \times 50$  mL). The combined organic layer was washed with water (100 mL) and then dried with brine (100 mL) and over anhydrous  $\text{Na}_2\text{SO}_4$ . The crude product was purified using column chromatography (ethyl acetate,  $R_f = 0.70$ ). The product **25** was obtained as a brown oil (1.17 g, 2.80 mmol, 94%).  $^1\text{H}$  NMR (400 MHz,  $\text{DMSO}-d_6$ )  $\delta$ : 9.79 (s, 1H), 7.72 (dd,  $J = 6.6, 2.1$  Hz, 1H), 7.59 (d,  $J = 2.0$  Hz, 1H), 7.38-7.34 (m, 2H), 7.16 (d,  $J = 8.4$  Hz, 1H), 7.02-6.98 (m, 1H), 3.90 (t,  $J = 6.8$  Hz, 2H), 1.69-1.60 (m, 2H), 1.39-1.31 (m, 2H), 1.25-1.15 (m, 8H), 0.83-0.77 (m, 3H); HRMS TOF MS ASAP+,  $m/z$ : found 418.0839 (calcd.  $\text{C}_{21}\text{H}_{25}\text{NOSBr}$ : 418.0840,  $[\text{M}+\text{H}]^+$ ).  $^1\text{H}$  NMR analysis of **25** in  $\text{CDCl}_3$  was in accordance with previously reported values.<sup>10</sup>



#### 10-Octyl-7-(pyren-1-ylethynyl)-10H-phenothiazine-3-carbaldehyde (**26**)<sup>11</sup>

Compound **25** (196 mg, 0.469 mmol), compound **20** (206 mg, 0.912 mmol),  $\text{Pd}(\text{PPh}_3)_2\text{Cl}_2$  (49 mg, 0.691 mmol), and  $\text{CuI}$  (10 mg, 0.050 mmol) were mixed with dry triethylamine (7.5 mL), and heated (80 °C) for 24 hours under nitrogen atmosphere. The reaction mixture was quenched with distilled water (15 mL) and extracted with  $\text{CH}_2\text{Cl}_2$  ( $3 \times 10$  mL). The combined organic layer was dried with brine (15 mL) and then over anhydrous  $\text{Na}_2\text{SO}_4$  and filtered. The solvent was removed and the crude product was purified using column chromatography (*n*-pentane/ethyl acetate 8:7,  $R_f = 0.41$ ). The product **26** was obtained as an orange solid (172 mg, 0.306 mmol, 65%).  $^1\text{H}$  NMR (400 MHz,  $\text{DMSO}-d_6$ )  $\delta$ : 9.82 (s, 1H), 8.63 (d,  $J = 9.2$  Hz, 1H), 8.42-8.21 (m, 7H), 8.14 (t,  $J = 7.7$  Hz, 1H), 7.76 (dd,  $J = 6.6, 1.9$  Hz, 1H), 7.67-7.58 (m, 3H), 7.24-7.17 (m, 2H), 4.01 (t,  $J = 6.9$  Hz, 2H), 1.77-1.69 (m, 2H), 1.46-1.37 (m, 2H), 1.30-1.20 (m, 8H), 0.86-0.80 (m, 3H); HRMS (TOF MS ASAP+,  $m/z$ ): found 564.2361 (calcd.  $\text{C}_{39}\text{H}_{34}\text{NOS}$ : 564.2350,  $[\text{M}+\text{H}]^+$ ).  $^1\text{H}$  NMR analysis of **26** was in accordance with previously reported values.<sup>11</sup>



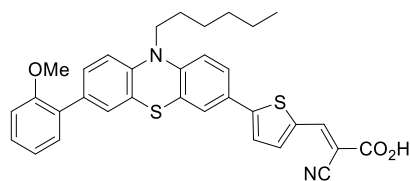
#### General procedure for Knoevenagel condensation

The aldehyde (1 eq.) was mixed with cyanoacetic acid (20 eq.) and dissolved in degassed acetonitrile under nitrogen atmosphere, then piperidine (12 eq.) was added, and the mixture was refluxed until full conversion. The reaction was quenched with HCl (2 M, 100-150 mL) before ethyl acetate was added, the phases separated and the aqueous phase was washed with water ( $5 \times 200$  mL). The organic phase was dried with brine (50 mL) and over anhydrous  $\text{Na}_2\text{SO}_4$ , filtered and concentrated *in vacuo*. The crude product was further purified by silica gel column chromatography.



**(E)-2-Cyano-3-(5-(10-hexyl-7-(2-methoxyphenyl)-10H-phenothiazin-3-yl)thiophen-2-yl)acrylic acid (AFB-12)**

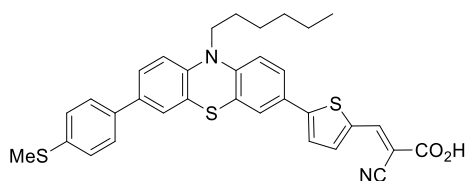
The synthesis was performed according to the general procedure, starting with compound **11** (200 mg, 0.400 mmol) and cyanoacetic acid (681 mg, 8.01 mmol) and piperidine (409 mg, 4.80 mmol) in acetonitrile (48 mL) for 2 hours. The crude product was purified by silica gel column chromatography (gradient: 0-15% MeOH in CH<sub>2</sub>Cl<sub>2</sub>) to yield compound **AFB-12** as a dark red solid (190 mg, 0.335 mmol, 84%), mp 160-163 °C. <sup>1</sup>H NMR



(600 MHz, DMSO-*d*<sub>6</sub>) δ: 13.66 (s, 1H), 8.42 (s, 1H), 7.95 (d, *J* = 3.9 Hz, 1H), 7.69 (d, *J* = 4.1 Hz, 1H), 7.60-7.57 (m, 2H), 7.34-7.30 (m, 2H), 7.28 (dd, *J* = 7.5, 1.6 Hz, 1H), 7.26 (d, *J* = 2.0 Hz, 1H), 7.11-7.07 (m, 3H), 7.00 (t, *J* = 7.3 Hz, 1H), 3.93 (t, *J* = 7.3 Hz, 2H), 3.77 (s, 3H), 1.75-1.70 (m, 2H), 1.45-1.40 (m, 2H), 1.30-1.25 (m, 4H), 0.86-0.83 (m, 3H); <sup>13</sup>C NMR (150 MHz, DMSO-*d*<sub>6</sub>) δ: 165.6, 163.6, 156.0, 145.6, 145.5, 142.5, 141.1, 134.0, 132.9, 129.9, 128.8, 128.7, 128.4, 127.7, 126.6, 125.8, 124.3, 124.2, 124.1, 121.8, 120.8, 116.1, 115.8, 115.5, 111.7, 55.5, 46.7, 30.8, 26.2, 25.8, 24.8, 22.1, 13.8; IR (neat, cm<sup>-1</sup>) v: 2951 (m), 2930 (m), 2841 (m), 2577 (w), 2499 (w), 2213 (w), 1730 (w), 1678 (m), 1553 (s), 1397 (s), 1242 (s), 1221 (s), 1060 (s), 805 (s); HRMS (TOF MS ASAP+, *m/z*): found 522.1798 (calcd. C<sub>32</sub>H<sub>30</sub>N<sub>2</sub>OS<sub>2</sub>: 522.1800, [M-CO<sub>2</sub>]<sup>+</sup>); UV (THF, 2 × 10<sup>-5</sup> M, 22 °C) λ<sub>max</sub> (nm): 459 (19050 M<sup>-1</sup> cm<sup>-1</sup>).

**(E)-2-Cyano-3-(5-(10-hexyl-7-(4-(methylthio)phenyl)-10H-phenothiazin-3-yl)thiophen-2-yl)acrylic acid (AFB-13)**

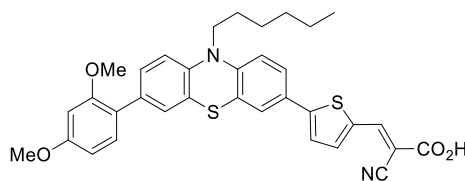
The synthesis was performed according to the general procedure, starting with compound **12** (150 mg, 0.291 mmol) and cyanoacetic acid (495 mg, 5.82 mmol) and piperidine (297 mg, 3.49 mmol) in acetonitrile (35 mL) for 3 hours. The crude product was purified by silica gel column chromatography (gradient: 0-15% MeOH in CH<sub>2</sub>Cl<sub>2</sub>) to yield compound **AFB-13** as a dark red solid (115 mg,



0.197 mmol, 68%), mp 253 °C (dec.). <sup>1</sup>H NMR (600 MHz, DMSO-*d*<sub>6</sub>) δ: 8.19 (s, 1H), 7.74 (d, *J* = 4.1 Hz, 1H), 7.59-7.55 (m, 3H), 7.52-7.45 (m, 3H), 7.42 (d, *J* = 2.2 Hz, 1H), 7.29 (d, *J* = 8.5 Hz, 2H), 7.04 (t, *J* = 8.5 Hz, 2H), 3.87 (t, *J* = 6.7 Hz, 2H), 2.49 (s, 3H), 1.72-1.63 (m, 2H), 1.42-1.33 (m, 2H), 1.27-1.20 (m, 4H), 0.84-0.79 (m, 3H) (COOH proton not visible); <sup>13</sup>C NMR (150 MHz, DMSO-*d*<sub>6</sub>) δ: 163.9, 148.3, 144.9, 143.0, 141.7, 137.2, 137.1, 135.2, 135.1, 134.0, 127.1, 126.45 (2C), 126.38 (2C), 125.6, 125.5, 124.7, 124.0, 123.9, 123.8, 123.2, 118.8, 116.2, 116.1, 106.7, 46.7, 30.8, 26.1, 25.8, 22.1, 14.7, 13.8; IR (neat, cm<sup>-1</sup>) v: 3395 (br), 2952 (w), 2920 (w), 2852 (w), 2215 (w), 1574 (m), 1470 (m), 1386 (s), 1248 (s), 800 (s); HRMS (TOF-ESI negative mode, *m/z*): found 581.1392 (calcd. C<sub>33</sub>H<sub>29</sub>N<sub>2</sub>O<sub>2</sub>S<sub>2</sub>: 581.1391, [M-H]<sup>-</sup>); UV (THF, 2 × 10<sup>-5</sup> M, 22 °C) λ<sub>max</sub> (nm): 442 (23250 M<sup>-1</sup> cm<sup>-1</sup>).

**(E)-2-Cyano-3-(5-(7-(2,4-dimethoxyphenyl)-10-hexyl-10H-phenothiazin-3-yl)thiophen-2-yl)acrylic acid (AFB-14)**

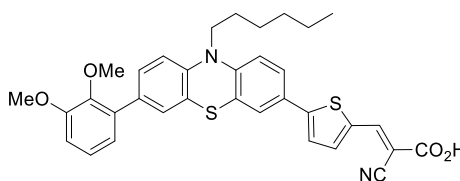
The synthesis was performed according to the general procedure, starting with compound **13** (170 mg, 0.321 mmol) and cyanoacetic acid (546 mg, 6.42 mmol) and piperidine (328 mg, 3.85 mmol) in acetonitrile (38 mL) for 1.5 hours. The crude product was purified by silica gel column chromatography (gradient: 0-15% MeOH in CH<sub>2</sub>Cl<sub>2</sub>) to yield compound **AFB-14** as a dark red



solid (121 mg, 0.202 mmol, 63%), mp 200 °C (dec.). <sup>1</sup>H NMR (600 MHz, DMSO-*d*<sub>6</sub>) δ: 13.83 (s, 1H), 8.38 (s, 1H), 7.91 (d, *J* = 3.8 Hz, 1H), 7.66 (d, *J* = 4.0 Hz, 1H), 7.59-7.55 (m, 2H), 7.27 (dd, *J* = 8.5, 1.9 Hz, 1H), 7.21-7.18 (m, 2H), 7.08 (d, *J* = 8.6 Hz, 1H), 7.05 (d, *J* = 8.5 Hz, 1H), 6.64 (d, *J* = 2.3 Hz, 1H), 6.59 (dd, *J* = 8.5, 2.3 Hz, 1H), 3.91 (t, *J* = 7.0 Hz, 2H), 3.79 (s, 3H), 3.76 (s, 3H), 1.74-1.69 (m, 2H), 1.43-1.39 (m, 2H), 1.28-1.23 (m, 4H), 0.85-0.83 (m, 3H); <sup>13</sup>C NMR (150 MHz, DMSO-*d*<sub>6</sub>) δ: 163.6, 160.0, 157.0, 151.1, 145.6, 145.1, 142.1, 140.4, 134.1, 132.8, 130.4, 128.5, 127.5, 126.6, 125.8, 124.3, 124.14, 124.10, 121.8, 121.1, 117.2, 116.0, 115.5, 105.3, 99.9, 98.9, 55.5, 55.3, 46.6, 30.8, 26.2, 25.8, 22.1, 13.8; IR (neat, cm<sup>-1</sup>) ν: 2956 (w), 2930 (m), 2842 (w), 2358 (m), 2213 (w), 1673 (m), 1610 (m), 1558 (s), 1397 (s), 1241 (s), 1205 (s), 1158 (s), 1070 (s), 800 (s); HRMS (TOF MS ASAP+, *m/z*): found 552.1904 (calcd. C<sub>33</sub>H<sub>32</sub>N<sub>2</sub>O<sub>2</sub>S<sub>2</sub>: 552.1905, [M-CO<sub>2</sub>]<sup>+</sup>); UV (THF, 2 × 10<sup>-5</sup> M, 22 °C) λ<sub>max</sub> (nm): 457 (22600 M<sup>-1</sup> cm<sup>-1</sup>).

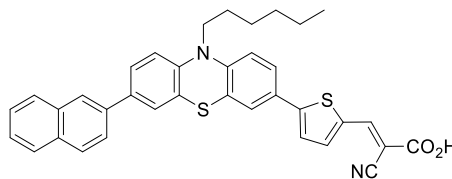
**(E)-2-Cyano-3-(5-(7-(2,3-dimethoxyphenyl)-10-hexyl-10H-phenothiazin-3-yl)thiophen-2-yl)acrylic acid (AFB-15)**

The synthesis was performed according to the general procedure, starting with compound **14** (140 mg, 0.264 mmol) and cyanoacetic acid (450 mg, 5.29 mmol) and piperidine (270 mg, 3.17 mmol) in acetonitrile (31 mL) for 1 hour. The crude product was purified by silica gel column chromatography (gradient: 0-15% MeOH in CH<sub>2</sub>Cl<sub>2</sub>) to yield compound **AFB-15** as a dark red solid (122 mg, 0.204 mmol, 77%), mp 183-186 °C. <sup>1</sup>H NMR (600 MHz, DMSO-*d*<sub>6</sub>) δ: 8.24 (s, 1H), 7.80 (d, *J* = 3.5 Hz, 1H), 7.61 (d, *J* = 3.8 Hz, 1H), 7.56-7.53 (m, 2H), 7.34 (dd, *J* = 8.5, 1.6 Hz, 1H), 7.25 (d, *J* = 1.8 Hz, 1H), 7.12-7.07 (m, 3H), 7.05-7.02 (m, 1H), 6.90 (d, *J* = 7.6 Hz, 1H), 3.92 (t, *J* = 7.0 Hz, 2H), 3.83 (s, 3H), 3.54 (s, 3H), 1.75-1.70 (m, 2H), 1.44-1.39 (m, 2H), 1.30-1.25 (m, 4H), 0.85-0.82 (m, 3H) (COOH proton not visible); <sup>13</sup>C NMR (150 MHz, DMSO-*d*<sub>6</sub>) δ: 163.5, 152.8, 149.3, 145.8, 145.1, 142.9, 138.4, 134.8, 133.6, 132.4, 128.4, 127.3, 127.0, 125.6, 124.2, 124.15, 124.06, 123.9, 122.1, 121.7, 118.2, 116.1, 115.6, 112.2, 60.1, 55.8, 54.9, 46.7, 30.8, 26.1, 25.8, 22.1, 13.8 (one <sup>13</sup>C shift missing); IR (neat, cm<sup>-1</sup>) ν: 2954 (w), 2214 (w), 1716 (w), 1574 (s), 1464 (m), 1391 (s), 1254 (s), 798 (m), 742 (m); HRMS (TOF MS ASAP+, *m/z*): 553.1984 (calcd. C<sub>33</sub>H<sub>33</sub>N<sub>2</sub>O<sub>2</sub>S<sub>2</sub>: found 553.1982, [M-CO<sub>2</sub>+H]<sup>+</sup>); UV (THF, 2 × 10<sup>-5</sup> M, 22 °C) λ<sub>max</sub> (nm): 443 (22600 M<sup>-1</sup> cm<sup>-1</sup>).



**(E)-2-Cyano-3-(5-(10-hexyl-7-(naphthalen-2-yl)-10H-phenothiazin-3-yl)thiophen-2-yl)acrylic acid (AFB-16)**

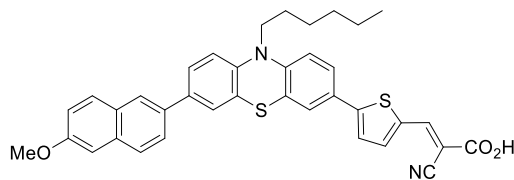
The synthesis was performed according to the general procedure, starting with compound **15** (135 mg, 0.260 mmol) and cyanoacetic acid (442 mg, 5.20 mmol) and piperidine (265 mg, 3.12 mmol) in acetonitrile (31 mL) for 1.5 hours. The crude product was purified by silica gel column chromatography (gradient: 0-15% MeOH in CH<sub>2</sub>Cl<sub>2</sub>) to yield compound **AFB-16** as a dark red solid (86 mg, 0.147 mmol, 56%), mp 211-213 °C. <sup>1</sup>H NMR (600 MHz, DMSO-*d*<sub>6</sub>) δ: 13.84 (s, 1H), 8.39 (s, 1H), 8.20 (s, 1H), 7.97 (d, *J* = 8.4 Hz, 2H), 7.94-7.90 (m, 2H), 7.83 (d, *J* = 8.7 Hz, 1H), 7.69-7.65 (m, 2H), 7.62 (s, 1H), 7.60-7.57 (m, 2H), 7.55-7.48 (m, 2H), 7.15 (d, *J* = 8.7 Hz, 1H), 7.10 (d, *J* = 8.9 Hz, 1H), 3.95 (t, *J* = 3.8 Hz, 2H), 1.76-1.70 (m, 2H), 1.45-1.40 (m, 2H), 1.30-1.24 (m, 4H), 0.86-0.82 (m, 3H); <sup>13</sup>C NMR (150 MHz, DMSO-*d*<sub>6</sub>) δ: 165.5, 163.6, 151.1, 145.3, 143.1, 140.5, 136.0, 134.5, 134.1, 133.3, 132.1, 128.4, 128.1, 127.4, 126.8, 126.4, 126.3, 125.9, 125.8, 125.3, 124.6, 124.4, 124.3, 124.2, 124.0, 123.2, 117.1, 116.4, 116.2, 116.0, 46.7, 30.8, 26.1, 25.8, 22.1, 13.8; IR (neat, cm<sup>-1</sup>) ν: 3051 (m), 2487 (w, br), 2216 (m), 1681 (m), 1557 (s), 1360 (s), 1212 (m), 1061 (m), 796 (m); HRMS (TOF



MS ASAP+,  $m/z$ ): found 543.1928 (calcd.  $C_{35}H_{31}N_2S_2$ : 543.1929,  $[M-CO_2+H]^+$ ); UV (THF,  $2 \times 10^{-5}$  M, 22 °C)  $\lambda_{max}$  (nm): 455 ( $21350 \text{ M}^{-1} \text{ cm}^{-1}$ ).

**(E)-2-Cyano-3-(5-(10-hexyl-7-(6-methoxynaphthalen-2-yl)-10H-phenothiazin-3-yl)thiophen-2-yl)acrylic acid (AFB-17)**

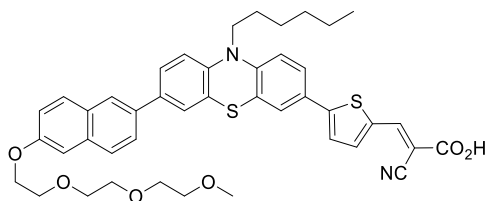
The synthesis was performed according to the general procedure, starting with compound **16** (150 mg, 0.273 mmol) and cyanoacetic acid (464 mg, 5.46 mmol) and piperidine (279 mg, 3.27 mmol) in acetonitrile (33 mL) for 1.5 hours. The crude product was purified by silica gel column chromatography (gradient: 0-15% MeOH in  $CH_2Cl_2$ ) to yield compound



**AFB-17** as a dark red solid (110 mg, 0.178 mmol, 65%), mp 218-224 °C.  $^1H$  NMR (600 MHz,  $DMSO-d_6$ )  $\delta$ : 13.89 (s, 1H), 8.28 (s, 1H), 8.12 (s, 1H), 7.90-7.86 (m, 2H), 7.84 (d,  $J = 3.5$  Hz, 1H), 7.77 (dd,  $J = 8.6$ , 1.6 Hz, 1H), 7.66-7.62 (m, 2H), 7.59-7.55 (m, 3H), 7.33 (d,  $J = 2.2$  Hz, 1H), 7.18 (dd,  $J = 9.0$ , 2.4 Hz, 1H), 7.14 (d,  $J = 8.6$  Hz, 1H), 7.11-7.09 (m, 1H), 3.94 (t,  $J = 6.9$  Hz, 2H), 3.89 (s, 3H), 1.76-1.71 (m, 2H), 1.45-1.40 (m, 2H), 1.30-1.24 (m, 4H), 0.86-0.82 (m, 3H);  $^{13}C$  NMR (150 MHz,  $DMSO-d_6$ )  $\delta$ : 163.5, 157.3, 149.8, 145.2, 143.7, 142.9, 139.0, 134.7, 134.6, 133.7, 133.4, 129.6, 128.8, 127.3, 126.9, 126.0, 125.7, 125.0, 124.9, 124.3, 124.2, 124.0, 123.9, 123.2, 122.8, 118.9, 117.9, 116.3, 116.1, 105.7, 55.2, 46.7, 30.8, 26.1, 25.8, 22.1, 13.8; IR (neat,  $cm^{-1}$ )  $\nu$ : 2921 (w, br), 2853 (w, br), 2216 (w), 1564 (s), 1392 (s), 1243 (s), 1064 (m), 797 (m); HRMS (TOF MS ASAP+,  $m/z$ ): found 573.2028 (calcd.  $C_{36}H_{33}N_2OS_2$ : 573.2034,  $[M-CO_2+H]^+$ ); UV (THF,  $2 \times 10^{-5}$  M, 22 °C)  $\lambda_{max}$  (nm): 450 ( $19850 \text{ M}^{-1} \text{ cm}^{-1}$ ).

**(E)-2-Cyano-3-(5-(10-hexyl-7-(6-(2-(2-methoxyethoxy)ethoxy)ethoxy)naphthalen-2-yl)-10H-phenothiazin-3-yl)thiophen-2-yl)acrylic acid (AFB-18)**

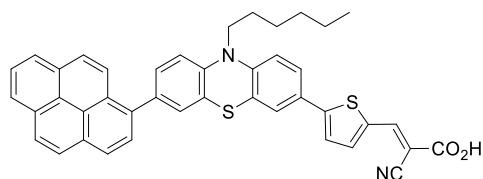
The synthesis was performed according to the general procedure, starting with compound **17** (160 mg, 0.235 mmol) and cyanoacetic acid (399 mg, 4.69 mmol) and piperidine (240 mg, 2.82 mmol) in acetonitrile (28 mL) for 1.5 hours. The crude product was purified by silica gel column chromatography (gradient: 0-15% MeOH in  $CH_2Cl_2$ ) to yield compound **AFB-18** as a dark red solid (136 mg, 0.182 mmol, 77%), mp 200-202



°C.  $^1H$  NMR (600 MHz,  $DMSO-d_6$ )  $\delta$ : 8.18 (s, 1H), 8.12 (s, 1H), 7.88 (d,  $J = 9.0$  Hz, 1H), 7.84 (d,  $J = 8.6$  Hz, 1H), 7.78-7.75 (m, 2H), 7.63 (dd,  $J = 8.5$ , 1.5 Hz, 1H), 7.61 (d,  $J = 3.9$  Hz, 1H), 7.59-7.57 (m, 1H), 7.56-7.53 (m, 2H), 7.34 (d,  $J = 1.6$  Hz, 1H), 7.19 (dd,  $J = 9.0$ , 2.1 Hz, 1H), 7.13 (d,  $J = 8.6$  Hz, 1H), 7.09 (d,  $J = 9.2$  Hz, 1H), 4.24-4.21 (m, 2H), 3.94 (t,  $J = 6.8$  Hz, 2H), 3.83-3.80 (m, 2H), 3.63-3.61 (m, 2H), 3.57-3.55 (m, 2H), 3.54-3.51 (m, 2H), 3.44-3.41 (m, 2H), 3.23 (s, 3H), 1.76-1.69 (m, 2H), 1.45-1.39 (m, 2H), 1.31-1.25 (m, 4H), 0.86-0.82 (m, 3H) (COOH proton not visible);  $^{13}C$  NMR (150 MHz,  $DMSO-d_6$ )  $\delta$ : 163.1, 156.6, 145.0, 142.9, 141.8, 137.5, 135.1, 134.7, 133.8, 133.4, 129.7, 128.8, 127.3, 127.1, 126.8, 126.0, 125.6, 125.0, 124.9, 124.3, 124.1, 124.0, 123.9, 123.3, 119.1, 118.6, 116.3, 116.1, 106.5, 71.3, 70.0, 69.8, 69.6, 68.9, 67.2, 58.0, 46.7, 30.8, 26.1, 25.8, 22.1, 13.8; IR (neat,  $cm^{-1}$ )  $\nu$ : 2914 (w), 2212 (w), 1713 (w), 1574 (s), 1435 (m), 1360 (s), 1243 (s), 1103 (m), 797 (s); HRMS (TOF MS ASAP+,  $m/z$ ): found 705.2813 (calcd.  $C_{42}H_{45}N_2O_4S_2$ : 705.2821,  $[M-CO_2+H]^+$ ); UV (THF,  $2 \times 10^{-5}$  M, 22 °C)  $\lambda_{max}$  (nm): 437 ( $20200 \text{ M}^{-1} \text{ cm}^{-1}$ ).

**(E)-2-Cyano-3-(5-(10-hexyl-7-(pyren-1-yl)-10H-phenothiazin-3-yl)thiophen-2-yl)acrylic acid (AFB-19)**

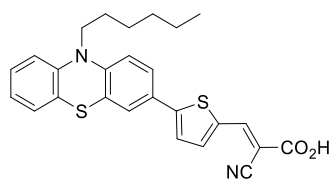
The synthesis was performed according to the general procedure, starting with compound **18** (120 mg, 0.202 mmol) and cyanoacetic acid (344 mg, 4.04 mmol) and piperidine (206 mg, 2.425 mmol) in acetonitrile (24 mL) for 2 hours. The crude product was purified by silica gel column chromatography (gradient: 0-15% MeOH in



$\text{CH}_2\text{Cl}_2$ ) to yield compound **AFB-19** as a dark red solid (101 mg, 0.154 mmol, 76%), mp 198-203 °C.  $^1\text{H}$  NMR (400 MHz,  $\text{DMSO}-d_6$ )  $\delta$ : 8.34-8.22 (m, 4H), 8.20 (s, 2H), 8.17-8.10 (m, 2H), 8.08 (t,  $J = 7.6$  Hz, 1H), 7.99 (d,  $J = 8.0$  Hz, 1H), 7.79 (d,  $J = 4.0$  Hz, 1H), 7.62 (d,  $J = 4.0$  Hz, 1H), 7.59-7.55 (m, 2H), 7.45 (dd,  $J = 8.1, 1.9$  Hz, 1H), 7.40 (d,  $J = 1.9$  Hz, 1H), 7.23 (d,  $J = 8.4$  Hz, 1H), 7.12 (d,  $J = 9.1$  Hz, 1H), 3.97 (t,  $J = 6.7$  Hz, 2H), 1.81-1.72 (m, 2H), 1.48-1.40 (m, 2H), 1.34-1.21 (m, 4H), 0.87-0.81 (m, 3H) (COOH proton not visible);  $^{13}\text{C}$  NMR (100 MHz,  $\text{DMSO}-d_6$ )  $\delta$ : 163.5, 149.2, 145.1, 143.3, 142.8, 138.2, 135.9, 134.9, 131.0, 130.4, 130.1, 129.9, 128.6, 127.7, 127.6, 127.5, 127.40, 127.39, 127.2, 126.4, 125.7, 125.4, 125.0 (2C), 124.6, 124.25, 124.19, 124.1 (2C), 124.0, 122.9, 118.4, 116.2, 115.9, 105.2, 46.8, 30.9, 26.2, 25.9, 22.1, 13.9; IR (neat,  $\text{cm}^{-1}$ )  $\nu$ : 2946 (w), 2855 (w), 2210 (w), 1715 (m), 1574 (s), 1404 (s), 1215 (s), 1131 (s), 1064 (s), 846 (m); HRMS (TOF MS ASAP+,  $m/z$ ): found 617.2076 (calcd.  $\text{C}_{41}\text{H}_{33}\text{N}_2\text{S}_2$ : 617.2085,  $[\text{M}-\text{CO}_2+\text{H}]^+$ ); UV (THF,  $2 \times 10^{-5}$  M, 22 °C)  $\lambda_{\text{max}}$  (nm): 441 (24450  $\text{M}^{-1} \text{cm}^{-1}$ ).

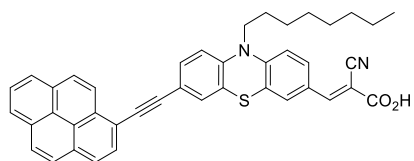
**(E)-2-Cyano-3-(5-(10-hexyl-10H-phenothiazin-3-yl)thiophen-2-yl)acrylic acid (AFB-20)<sup>12</sup>**

The synthesis was performed according to the general procedure, starting with compound **20** (115 mg, 0.292 mmol) and cyanoacetic acid (497 mg, 5.84 mmol) and piperidine (299 mg, 3.51 mmol) in acetonitrile (35 mL) for 30 min. The crude product was purified by silica gel column chromatography (gradient: 0-20% MeOH in  $\text{CH}_2\text{Cl}_2$ ) to yield compound **AFB-20** as a dark red solid (113 mg, 0.245 mmol, 84%), mp 190 °C (dec.).  $^1\text{H}$  NMR (400 MHz,  $\text{DMSO}-d_6$ )  $\delta$ : 8.21 (s, 1H), 7.76 (d,  $J = 3.9$  Hz, 1H), 7.59 (d,  $J = 3.9$  Hz, 1H), 7.54-7.49 (m, 2H), 7.24-7.18 (m, 1H), 7.17-7.13 (m, 1H), 7.07-7.01 (m, 2H), 6.99-6.93 (m, 1H), 3.88 (t,  $J = 6.8$  Hz, 2H), 1.72-1.63 (m, 2H), 1.42-1.33 (m, 2H), 1.27-1.20 (m, 4H), 0.85-0.78 (m, 3H) (COOH proton not visible); UV (THF,  $2 \times 10^{-5}$  M, 22 °C)  $\lambda_{\text{max}}$  (nm): 436 (20050  $\text{M}^{-1} \text{cm}^{-1}$ ).  $^1\text{H}$  NMR data are in accordance with that reported by Yang et al.<sup>12</sup>



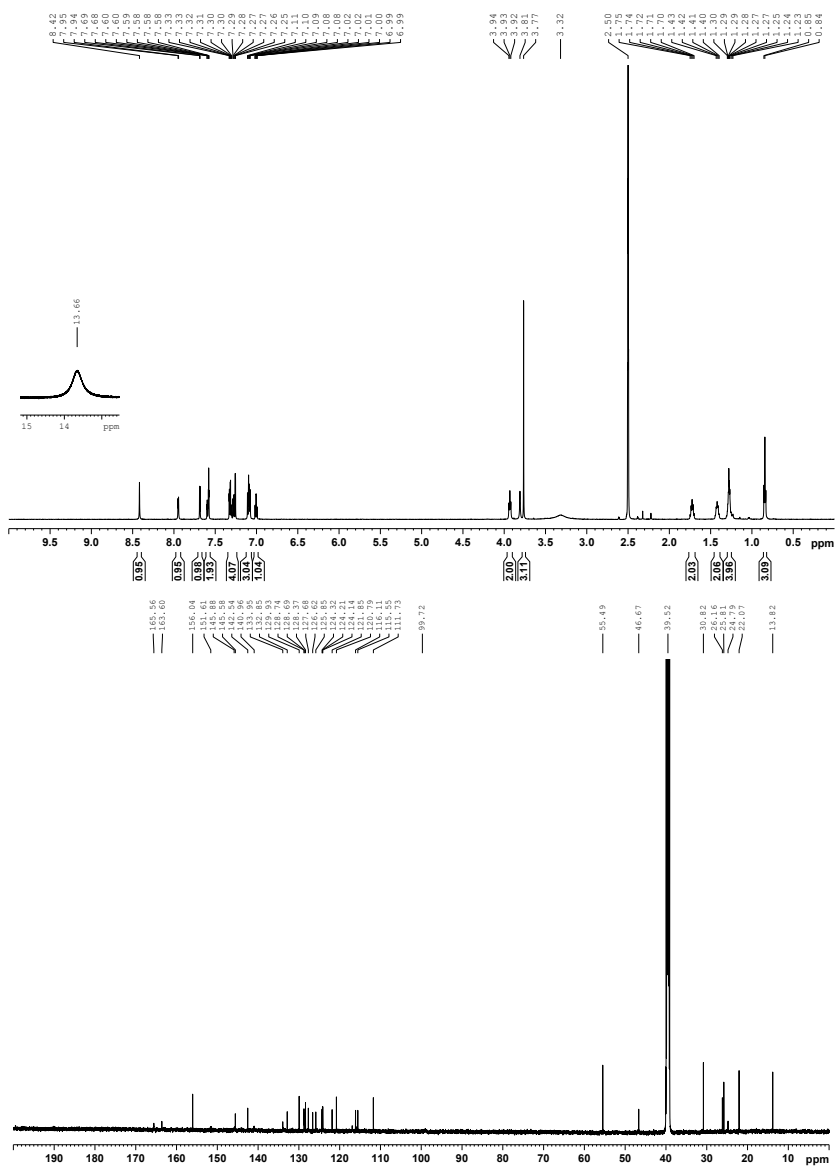
**2-Cyano-3-(10-octyl-7-(pyren-1-ylethynyl)-10H-phenothiazin-3-yl)acrylic acid (Dye 2)<sup>11</sup>**

The synthesis was performed according to the general procedure, starting with compound **26** (150 mg, 0.266 mmol) and cyanoacetic acid (453 mg, 5.32 mmol) and piperidine (272 mg, 3.19 mmol) in acetonitrile (32 mL) for 18 hours. The crude product was purified by silica gel column chromatography (gradient: 0-15% MeOH in  $\text{CH}_2\text{Cl}_2$ ) to yield sensitizer **Dye 2** as a dark red solid (109



mg, 0.172 mmol, 65%), mp 198 °C (dec.).  $^1\text{H}$  NMR (400 MHz,  $\text{DMSO}-d_6$ )  $\delta$ : 8.61 (d,  $J = 9.3$  Hz, 1H), 8.40-8.18 (m, 7H), 8.12 (t,  $J = 7.6$  Hz, 1H), 7.92 (s, 1H), 7.79 (dd,  $J = 7.0, 1.7$  Hz, 1H), 7.70 (d,  $J = 1.73$  Hz, 1H), 7.60-7.54 (m, 2H), 7.12 (t,  $J = 7.8$  Hz, 2H), 3.93 (t,  $J = 6.6$  Hz, 2H), 1.73-1.64 (m, 2H), 1.42-1.34 (m, 2H), 1.29-1.14 (m, 9H), 0.83-0.77 (m, 3H) (COOH proton not visible);  $^{13}\text{C}$  NMR (100 MHz,  $\text{DMSO}-d_6$ )  $\delta$ : 164.0, 147.7, 146.7, 144.3, 131.8, 131.4, 131.2, 131.2, 130.5, 130.2, 129.9, 129.2, 128.7, 128.4, 128.0, 127.7, 127.2, 126.4 (2C), 125.4 (2C), 124.1, 123.9, 123.4, 123.1, 119.5, 117.4 (2C), 116.6 (2C), 95.0, 89.0, 47.3, 31.6, 29.0, 28.9, 26.5, 26.4, 22.5, 14.1; IR (neat,  $\text{cm}^{-1}$ )  $\nu$ : 2915 (m), 2846 (m), 2212 (w), 1356 (s),

1272 (s), 806 (s), 714 (s); HRMS (TOF-ESI negative mode,  $m/z$ ): found 629.2263 (calcd.  $C_{42}H_{33}N_2O_2S$ : 629.2256, [M-H]).  $^1H$  and  $^{13}C$  NMR analysis of **Dye 2** is in accordance with previously reported values.<sup>11</sup>

NMR  
AFB-12Figure S7.  $^1\text{H}$  and  $^{13}\text{C}$  NMR spectra for AFB-12.



## AFB-14

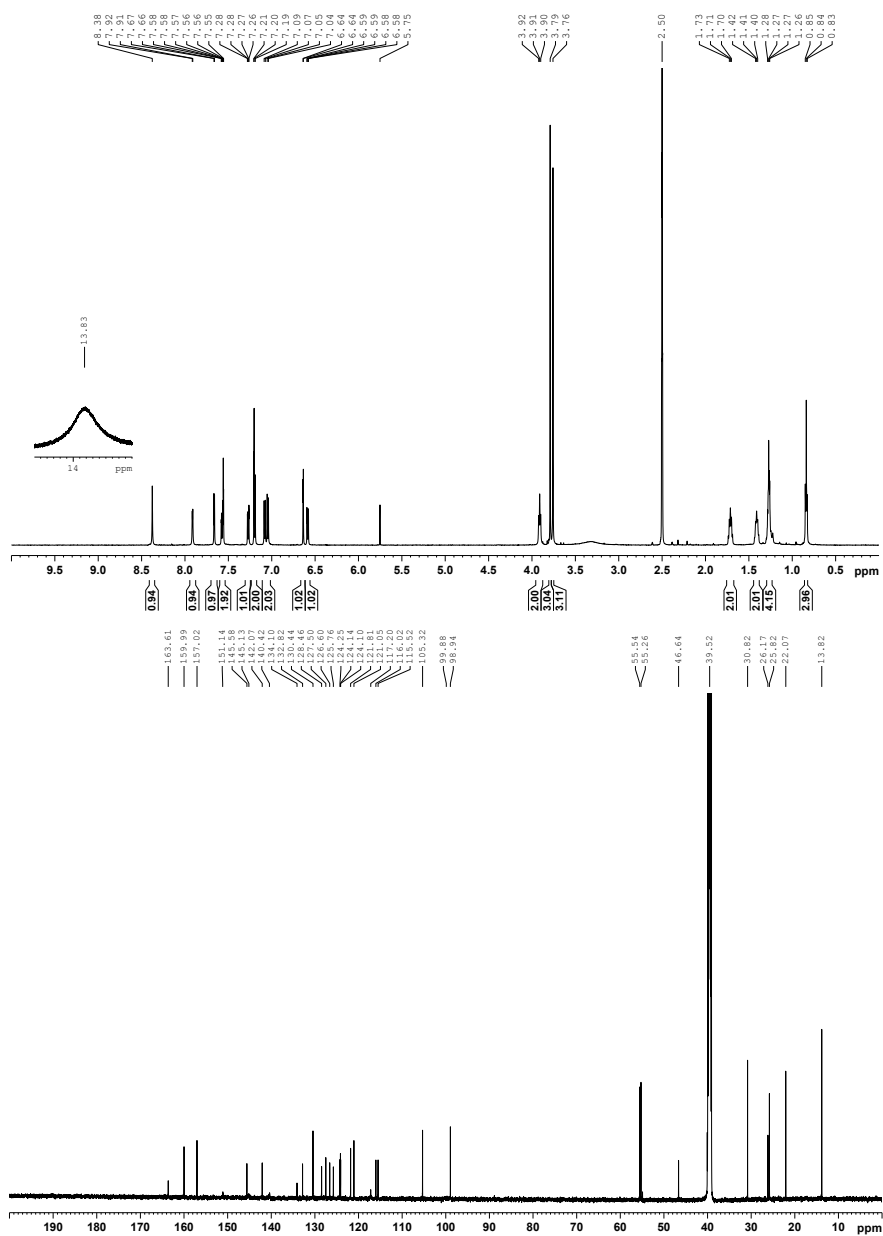


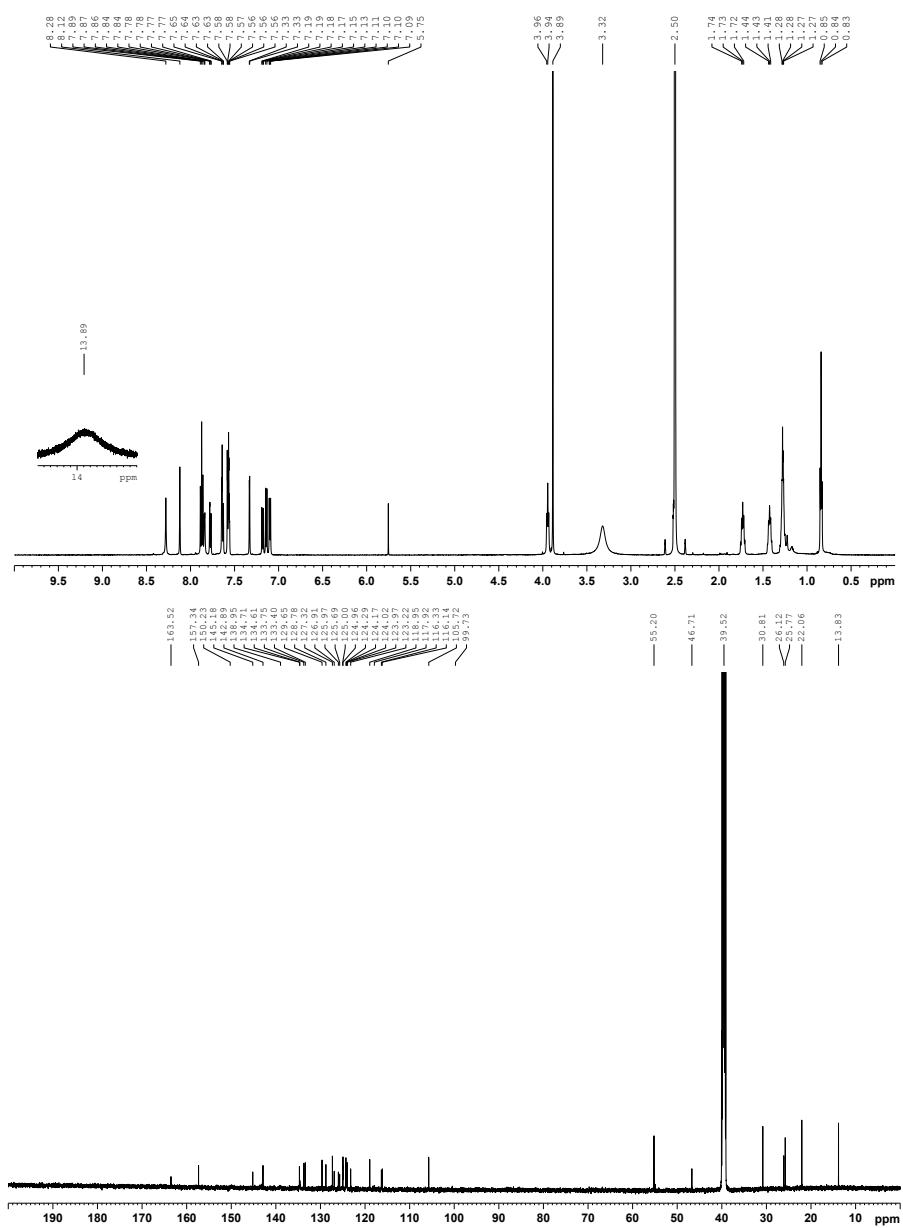
Figure S9. <sup>1</sup>H and <sup>13</sup>C NMR spectra for AFB-14.





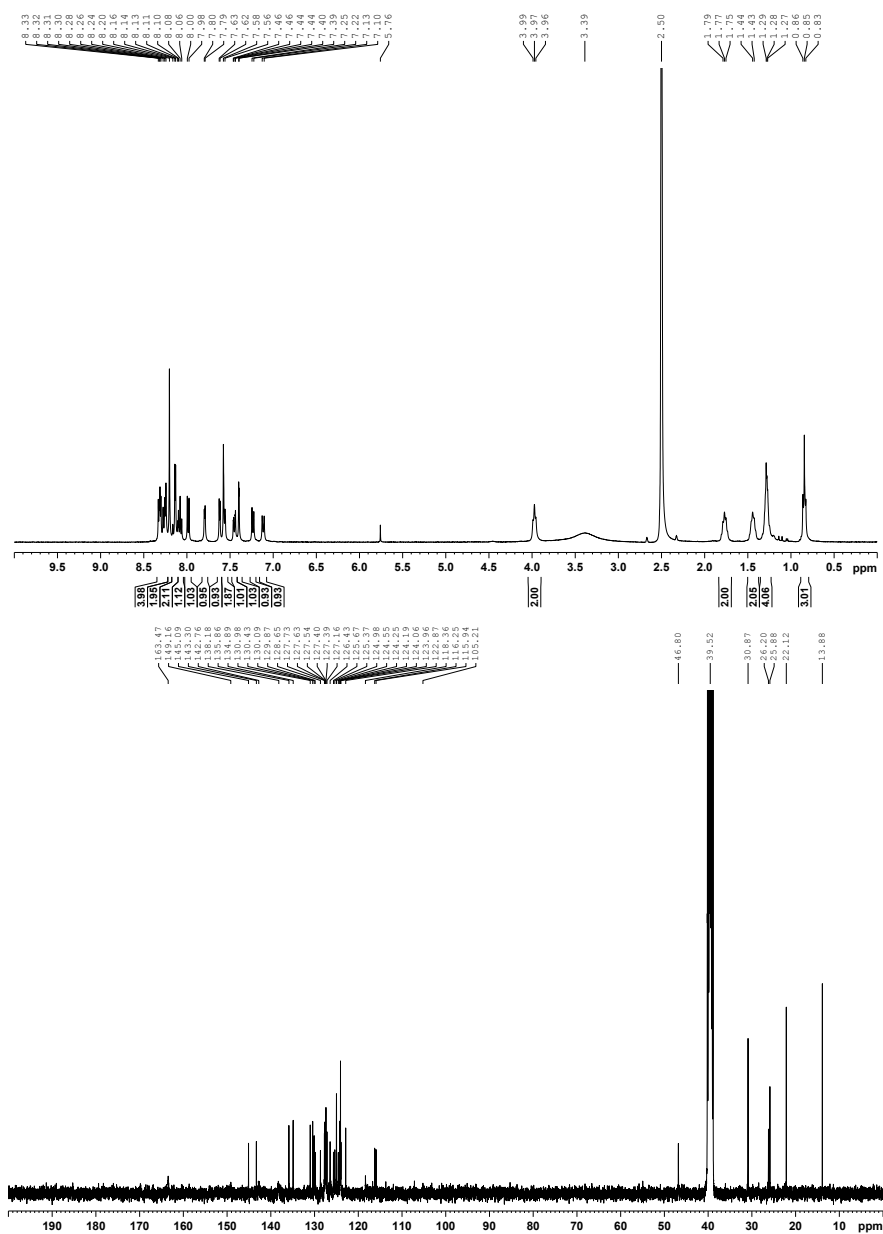


## AFB-17





## AFB-19

Figure S14. <sup>1</sup>H and <sup>13</sup>C NMR spectra for AFB-19.

## AFB-20

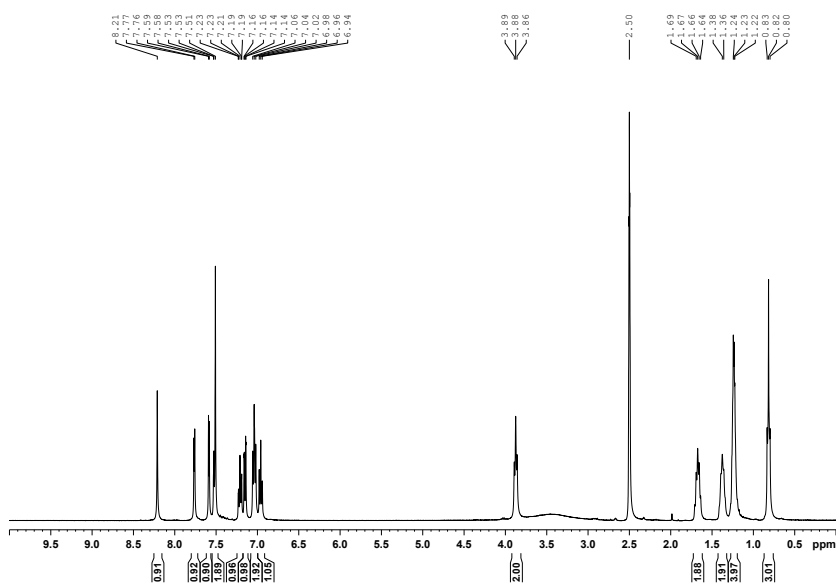


Figure S15.  $^1\text{H}$  NMR spectra for AFB-20.

## Dye 2

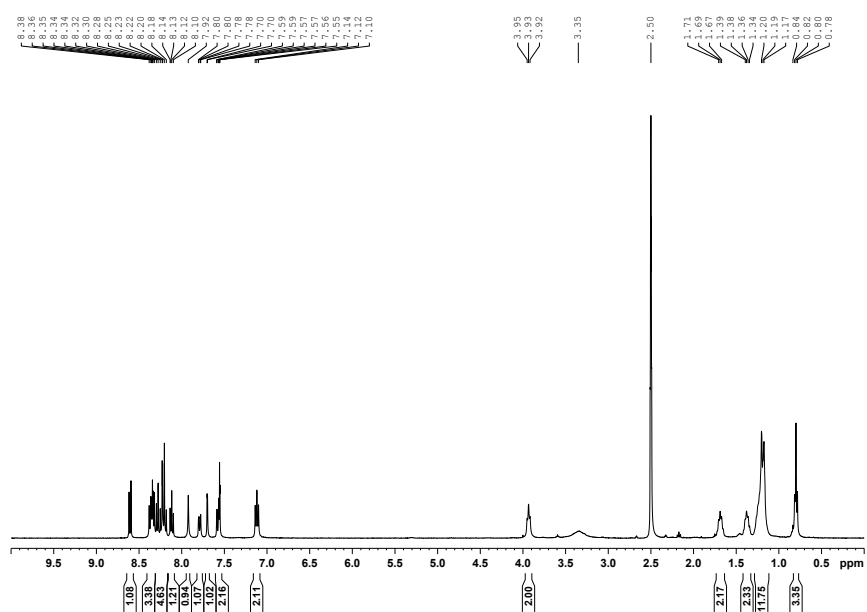


Figure S16.  $^1\text{H}$  NMR spectra for Dye 2.

## References

1. Y. Saygili, M. Söderberg, N. Pellet, F. Giordano, Y. Cao, A. B. Muñoz-García, S. M. Zakeeruddin, N. Vlachopoulos, M. Pavone, G. Boschloo, L. Kavan, J.-E. Moser, M. Grätzel, A. Hagfeldt and M. Freitag, *JACS*, 2016, **138**, 15087-15096.
2. A. F. Buene, N. Uggerud, S. P. Economopoulos, O. R. Gautun and B. H. Hoff, *Dyes Pigm.*, 2018, **151**, 263-271.
3. V. V. Pavlishchuk and A. W. Addison, *Inorganica Chim. Acta*, 2000, **298**, 97-102.
4. K. L. Billingsley and S. L. Buchwald, *J. Org. Chem.*, 2008, **73**, 5589-5591.
5. R. Y. Y. Lin, T. C. Chu, P. W. Chen, J. S. Ni, P. C. Shih, Y. C. Chen, K. C. Ho and J. T. Lin, *ChemSusChem*, 2014, **7**, 2221-2229.
6. J. H. Huang, P. H. Lin, W. M. Li, K. M. Lee and C. Y. Liu, *ChemSusChem*, 2017, **10**, 2284-2290.
7. Y.-Y. Chen, H. Wang, D.-W. Zhang, J.-L. Hou and Z.-T. Li, *Chem. Commun.*, 2015, **51**, 12088-12091.
8. Y. Zou, W. Wu, G. Sang, Y. Yang, Y. Liu and Y. Li, *Macromolecules*, 2007, **40**, 7231-7237.
9. X. Yang, R. Lu, H. Zhou, P. Xue, F. Wang, P. Chen and Y. Zhao, *J. Colloid Interface Sci.*, 2009, **339**, 527-532.
10. J. Zhang, B. Xu, J. Chen, L. Wang and W. Tian, *J. Phys. Chem. C*, 2013, **117**, 23117-23125.
11. B. Nagarajan, S. Kushwaha, R. Elumalai, S. Mandal, K. Ramanujam and D. Raghavachari, *J. Mater. Chem. A*, 2017, **5**, 10289-10300.
12. Y. S. Yang, H. D. Kim, J.-H. Ryu, K. K. Kim, S. S. Park, K.-S. Ahn and J. H. Kim, *Synth. Met.*, 2011, **161**, 850-855.



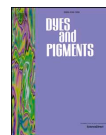


## PAPER III

**A comprehensive experimental study of five fundamental phenothiazine geometries increasing the diversity of the phenothiazine dye class for dye-sensitized solar cells**

Reprinted from *Dyes and Pigments*, Audun F. Buene, Anders Hagfeldt, Bård H. Hoff, A comprehensive experimental study of five fundamental phenothiazine geometries increasing the diversity of the phenothiazine dye class for dye-sensitized solar cells, 169, 66-72, **2019**, with permission from Elsevier.





## A comprehensive experimental study of five fundamental phenothiazine geometries increasing the diversity of the phenothiazine dye class for dye-sensitized solar cells



Audun Formo Buene<sup>a</sup>, Anders Hagfeldt<sup>b</sup>, Bård Helge Hoff<sup>a,\*</sup>

<sup>a</sup> Department of Chemistry, Norwegian University of Science and Technology, Høgskoleringen 5, NO-7491, Trondheim, Norway

<sup>b</sup> Laboratory of Photomolecular Science, Institute of Chemical Sciences and Engineering, École Polytechnique Fédérale de Lausanne (EPFL), Chemin des Atalambics, Station 6, CH-1015, Lausanne, Switzerland

### ARTICLE INFO

**Keywords:**  
Geometry study  
Phenothiazine  
Dye-sensitized solar cells  
Auxiliary donor position  
 $\pi$ -spacer

### ABSTRACT

Phenothiazine is a versatile scaffold frequently used in both pharmaceutical and photovoltaic applications. Still, the structural diversity within the class of phenothiazine sensitizers for dye-sensitized solar cells is minute. Substituents are found in 3, 7 and 10-positions, often all three. In this work, we report the synthesis and evaluation of sensitizers illuminating five geometries for the phenothiazine dye class, of which three are novel geometries. Eleven sensitizers were prepared, investigating auxiliary donor contributions, effect of  $\pi$ -spacer and also the position of the anchoring group. We have established that the  $\pi$ -spacer has to be connected *para* to the 10H nitrogen atom of phenothiazine, the 3-position. Also, thiophene is a far superior  $\pi$ -spacer than phenyl, but we were unable to find any significant photovoltaic performance differences between the 3,7 and 3,8 geometries. A higher dye loading for the 3,8 geometry indicates there is hidden potential in this geometry which could be harvested by further optimization. The best device of the study was fabricated with AFB-27 of the 3,8 geometry delivering a PCE of 5.88% ( $J_{SC} = 10.28 \text{ mA cm}^{-2}$ ,  $V_{OC} = 773 \text{ mV}$ ,  $FF = 0.75$ ) under 1 sun AM 1.5G illumination.

### 1. Introduction

The need for increasing global power production has sparked the development of a number of new photovoltaic technologies. Dye-sensitized solar cells (DSSCs) are promising candidates allowing solar cells to be semi-transparent, flexible and of tunable color [1]. Under ambient light conditions, DSSCs have out-performed most other long established PV technologies [2]. Hot applications of DSSCs include building integration [3] and the powering of an increasing amount of devices in the internet of things (IoT) [2,4]. This development has to a large extent been supported by the introduction of new redox shuttles based on cobalt and copper complexes [5–9].

The dyes utilized in DSSCs have traditionally been metal-complexes, where N719, N3 and N749 also known as ‘black dye’ are most well known. Zinc porphyrins are also highly successful sensitizers with a metal-organic core [10]. In terms of efficiency, these metal-based complexes have achieved PCEs up to 13.0% [11]. Although the absorption properties of these dyes are excellent, the extinction coefficients are usually moderate and dye aggregation, synthesis and purification are common challenges. Thus, metal-free dyes have emerged

as a viable alternative [12].

Improving the stability and efficiency of metal-free dyes is where the main efforts in this research area have been placed, and the current record for metal-free dyes is 14.3% [9]. Triarylaminers, phenothiazines and polythiophenes are common dye scaffolds [13,14]. Phenothiazine, and its oxygen analog phenoxazine, were among the early metal-free dyes, and studies of  $\pi$ -spacers containing isomerizable double bonds have been conducted [15,16]. Furthermore, this class of sensitizers have shown very promising results in DSSCs with aqueous electrolytes, as demonstrated by Lin et al. [17] The phenothiazine dye scaffold has been the subject of two recent reviews [18,19], and as with any other class of dyes, the main challenge is improving the light harvesting properties.

Despite its popularity, the phenothiazine class of dyes is not particularly diverse. Most dye molecules follow the same design principle. The  $\pi$ -spacer and/or anchoring group and the aromatic auxiliary donor is always in 3- and 7-position on the phenothiazine scaffold. On the phenothiazine nitrogen atom there is either an alkyl chain or an aromatic ring bearing an alkoxy group. Phenothiazine is also sometimes used as a symmetrical donor, which could be termed the 10H-geometry

\* Corresponding author.

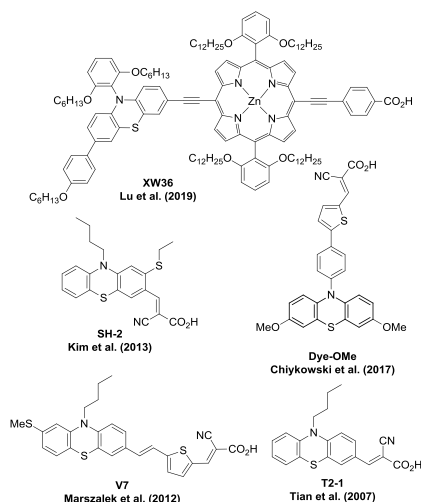
E-mail address: [bard.h.hoff@ntnu.no](mailto:bard.h.hoff@ntnu.no) (B.H. Hoff).

<https://doi.org/10.1016/j.dyepig.2019.05.007>

Received 29 March 2019; Received in revised form 26 April 2019; Accepted 3 May 2019

Available online 06 May 2019

0143-7208/ © 2019 Elsevier Ltd. All rights reserved.



**Fig. 1.** A selection of reported phenothiazine sensitizers. The auxiliary donor of XW36 [25] is an example of a 3,7-substituted phenothiazine, SH-2 [30] uses an ethylthio substituent in 2-position, Dye-OMe [24] has a 10*H*-geometry, dye V7 (and the simpler V5) [29] is the only example of a phenothiazine sensitizer with a 3,8-geometry, while T2-1<sup>15</sup> is the very first phenothiazine sensitizer for DSSCs and has the common 3-geometry.

where the anchoring group is connected to the phenothiazine through the 10*H* nitrogen atom [20–24]. In this geometry, the phenothiazine is used as a locked diphenylamine substituent, and has been compared to analogous triphenylamine sensitizers and found less efficient in DSSCs [23]. Phenothiazine has also been used as an auxiliary donor on other metal-based sensitizers, such as zinc porphyrins [25–28].

Of the 246 phenothiazine sensitizers published in the 113 publications (as of 20th February 2019 on SciFinder) containing the concepts *phenothiazine* and *dye-sensitized solar cell*, only two publications report structures with different geometries. These examples and other phenothiazine-based dyes are shown in Fig. 1. Marszalek et al. published two dyes with a methylthio substituent in the 8-position on the phenothiazine scaffold, with the  $\pi$ -spacer in the 3-position (using the numbering established in this work) [29]. However, neither the donating effect nor the position of the methylthio substituent were investigated. The other example is published by Kim et al. investigating the effect of ethylthio substitution in 2-position with the anchoring group in 3-position [30]. The ethylthio substituent increased the molar  $J_{SC}$  values (mA/mol dye), but lower dye loading values limited the efficiency and no improvement in PCE was reported.

We have synthesized and evaluated a selection of simple dyes (see Fig. 2) intending to extend the geometry landscape of the phenothiazine dye class. By doing so we hope to shed some light on how the substitution geometry affects the photophysical, electrochemical and photovoltaic performance of phenothiazine sensitizers.

## 2. Results and discussion

### 2.1. Dye synthesis

In order to achieve large variation in substitution patterns for phenothiazine dyes, a number of synthetic routes had to be used. To

improve the readability of this work we have constructed a new nomenclature system for the different geometries of phenothiazine sensitizers, naming the position of the  $\pi$ -spacer/anchoring group first with the lowest number, then the position of the auxiliary donor, separated by a comma, so AFB-27 has the 3,8-geometry. If there is no auxiliary donor, the name of the geometry is dictated by the position of the  $\pi$ -spacer/anchoring group only, which is the case for AFB-20, which has a 3-geometry.

Routes to the standard 3,7 sensitizer geometry are frequently utilized in the field, also by our group in previous publications [31,32]. Sensitizers AFB-20 and 22 were prepared along the same route, rather than through a monobromination approach. The excess bromine substituent was removed in a palladium catalyzed dehalogenation, based on a protocol reported by Chen et al. [33], as shown in Scheme 1 (ii). Sensitizer AFB-20 has previously been synthesized and characterized a number of times [32,34,35].

For the simple dyes AFB-23 and 24 with the  $\pi$ -spacer in 2-position, a very convenient route starting from 2-chloro-10*H*-phenothiazine was employed, see Scheme 1 (iii). Alkylation installed the hexyl chain and a Suzuki coupling introduced the aldehyde functionalized  $\pi$ -spacer precursor from commercial boronic acids. In our hands, the Suzuki coupling with 5-formyl-2-thienylboronic acid is sometimes a very poor reaction, especially when an aryl chloride is the coupling partner. Three equivalents of boronic acid were used, yet full conversion was still difficult to achieve, resulting in unimpressive yields for these reactions. The very reliable Knoevenagel condensation introducing the anchoring group was the last step for all the synthetic routes.

The dyes with 3,8 and 2,7 geometries were synthesized from the highly versatile building block 3. Preparation of 3 was achieved through a bromination of 2-chloro-10*H*-phenothiazine by molecular bromine followed by alkylation with NaH and 1-bromohexane, see Scheme 1 (i). The challenge in this route was the highly non-selective bromination step. The resulting crude mixture initially contained approximately 50% of the desired compound 2 measured by <sup>1</sup>H NMR, and reached a purity of over 97% following three to five recrystallizations from toluene. Although tedious, this was possible on a large scale, and a reliable alkylation of 2 gave adequate amounts of building block 3 for further reactions. By using the building blocks 1 and 3, in addition to 3,7-dibromo-10*H*-phenothiazine, all the sensitizers were synthesized successfully, and detailed procedures can be found in the ESI.

### 2.2. Photophysical properties

UV-Visible absorption spectra of all the sensitizers were recorded in THF and adsorbed on TiO<sub>2</sub> films. The solution spectra are shown in Fig. 3 and the TiO<sub>2</sub> film spectra in Fig. S4, while the extracted data are given in Table 1.

From such a diverse set of sensitizers, a number of different comparisons can be drawn from the UV/vis data, as highlighted in Fig. S5 (a-d). With regards to the position of the  $\pi$ -spacer, the ICT transition peak of the sensitizers with the  $\pi$ -spacer in 3-position are both hyper- and bathochromically shifted compared to the 2-position. In general, there is a clear difference between the thiophene and phenyl  $\pi$ -spacers, with the absorption of the thiophene-based compounds being redshifted by approximately 40 nm. In Fig. S5 (b) hardly any differences can be found between the two positions of the auxiliary donors, i.e. the 3,7 and 3,8 geometries have very similar absorption spectra. And lastly, the position of the anchoring group on a phenyl  $\pi$ -spacer is very important, as positioning of the cyanoacrylic anchoring group in the *meta*-position is totally detrimental to the ICT transition of the sensitizer.

### 2.3. Electrochemical properties

Cyclic voltammetry on stained FTO/TiO<sub>2</sub> electrodes was performed in acetonitrile with 0.1 M LiTFSI as a supporting electrolyte, a graphite carbon rod as counter electrode and a Ag/AgCl reference electrode. The

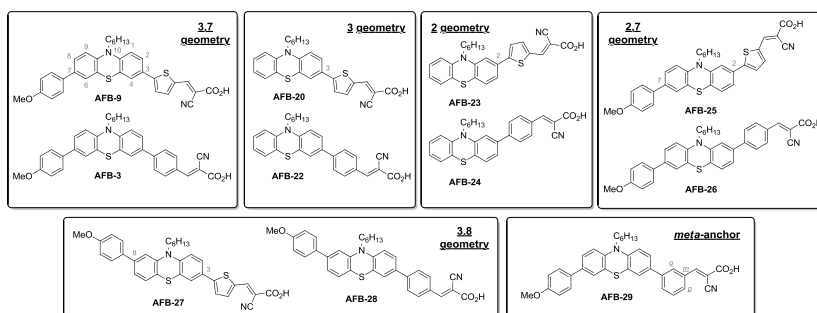
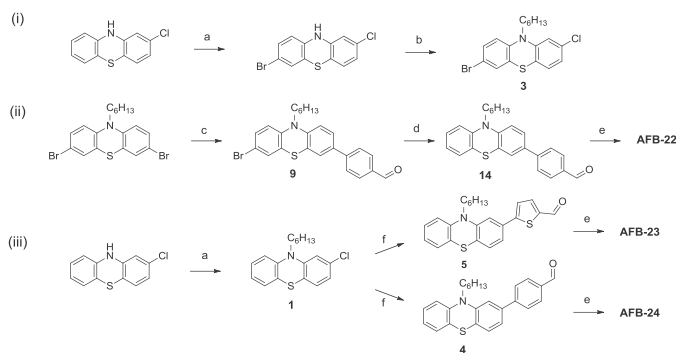


Fig. 2. Molecular structures of the sensitizers investigated in this study. The general numbering of the phthalocyanine scaffold is shown for AFB-9.



Scheme 1. Synthesis scheme to dyes AFB-23, 24 and 25. a) Br<sub>2</sub>, AcOH, b) NaH, 1-bromohexane, THF, c) boronic acid, Pd(PPh<sub>3</sub>)<sub>4</sub>, K<sub>2</sub>CO<sub>3</sub>, 1,4-dioxane/H<sub>2</sub>O (1:1), d) Pd(OAc)<sub>2</sub>, PPh<sub>3</sub>, K<sub>2</sub>CO<sub>3</sub>, *n*-butanol, e) cyanoacetic acid, piperidine, CH<sub>2</sub>CN, f) boronic acid, Pd(OAc)<sub>2</sub>, SPhos, K<sub>2</sub>CO<sub>3</sub>, 1,4-dioxane/H<sub>2</sub>O (1:1).

cyclic voltammograms are plotted in Fig. S6. All the sensitizers showed a single reversible oxidation in the range of 0.58–0.68 V vs. Ag/AgCl, while the E<sub>1/2</sub> value of ferrocene was found at 0.219 V vs. Ag/AgCl. Using the obtained sensitizer oxidation potentials and the optical bandgaps, the LUMO levels can be calculated, and the complete map of the HOMO-LUMO positions is given in Fig. 4. Sufficient potential differences are found for all dyes to have an efficient electron injection and be successfully regenerated from the I<sup>-</sup>/I<sub>3</sub><sup>-</sup> redox shuttle.

The HOMO levels are comparable for all the dyes, which is to be expected as they all share the same phthalocyanine scaffold. A slight shift of the HOMO levels of 20–70 mV towards more negative potentials is observed when introducing the auxiliary donor, and the oxidation potentials of the thiophene-linked dyes are on average found 30 mV below (more positive potentials) their phenyl analogs. For the LUMO level position, the largest differences can be seen when comparing the dyes with thiophene and phenyl  $\pi$ -spacers, where the LUMO levels of the thiophene-linked dyes are found shifted at least 200 mV towards more positive potentials compared to the phenyl analogs. The *meta*-position of the anchoring group in AFB-29 shifted the LUMO level up by almost 400 mV compared to the corresponding *para* derivative AFB-3, massively increasing the bandgap and lowering the light harvesting abilities considerably.

#### 2.4. Photovoltaic properties

The AFB dyes of different geometry were utilized in DSSCs, and Fig. 5 (a and b) shows the current density-voltage curves under 1 sun AM 1.5G illumination of the best device fabricated for each sensitizer (average data presented in Table 2). The solar cells were fabricated from photoanodes with 16.5  $\mu$ m TiO<sub>2</sub> (11  $\mu$ m 18NR-T and 5.5  $\mu$ m WER2-O scattering layer), platinum counter electrodes and an I<sup>-</sup>/I<sub>3</sub><sup>-</sup> electrolyte in a sandwich construction.

There are large differences in photovoltaic performance between the different geometries. The most efficient sensitizers were the thiophene containing AFB-9 (3,7) and AFB-27 (3,8) with incredibly similar average PCE values of 5.82% and 5.78%, respectively. For their phenyl analogs a small performance difference of 6% was found, in favor of the 3,8-geometry. Of the five different main geometries investigated in this work the order of photovoltaic performance was: 2 < 2,7 < 3 < 3,7  $\approx$  3,8. The sensitizer delivering the lowest efficiency was not surprisingly AFB-29, confirming that the anchoring group position on a phenyl  $\pi$ -spacer has to be in the *para*-position. Thiophene was the most efficient  $\pi$ -spacer across all geometries, outperforming phenyl by an average of 33%, despite lower average V<sub>OC</sub> values by 25 mV compared to the phenyl sensitizers. The 3,8-geometry was the least affected by the  $\pi$ -spacers with a performance difference of only 24% while the 2-geometry was most affected at 53% performance difference, also in favor of thiophene.

A.F. Buene, et al.

Dyes and Pigments 169 (2019) 66–72

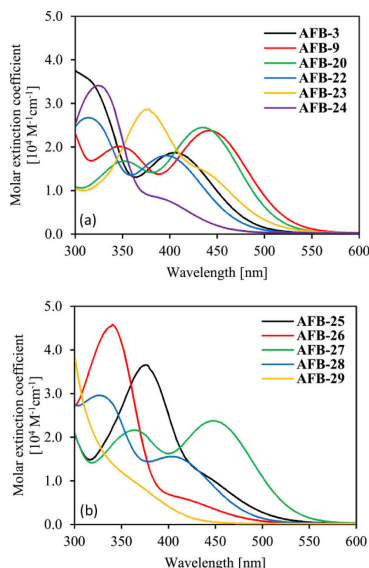


Fig. 3. UV-Visible spectra in THF solution ( $2 \times 10^{-5}$  M).

The introduction of the 4-methoxyphenyl auxiliary donor separating the 3 from the 3,7 and 3,8 geometries improved the photovoltaic performance by 8–15%, supporting our previous findings on auxiliary donors for phenothiazine sensitizers [32]. However, the effect was considerably larger between the 2 and 2,7 geometries where the auxiliary donor improved the PCE by 37% on average.

In the IPCE spectra shown in Fig. 5 (c and d), the absorption onsets are redshifted by over 100 nm compared to the UV/Vis solution spectra recorded in THF, indicating the molecular environment is quite different inside the devices compared to in THF solution. For further studies, choosing a different solvent for UV/Vis analyses could yield spectra more closely matching the absorption properties in devices. The

integrated short-circuit current densities from the IPCE spectra given in Table 2 are in reasonable agreement with the experimental  $J_{SC}$  values from the  $J$ - $V$  sweeps, underestimating the  $J_{SC}$  by a maximum of 8%, requiring no further explanation. The highest IPCE values from the devices were just exceeding 70%, meaning there is potential for further device optimization to reach the maximum theoretical value, dictated by the transmittance of the FTO glass (normally in the range of 80–85% depending on sheet resistance).

Charge extraction and electron lifetime measurements were conducted on the best device from each sensitizer, presented in Fig. 6. From the charge extraction measurements, a relative conduction band shift of up to 72 mV is observed as the horizontal distance between the parallel charge extraction curves in Fig. 6 (a and b). This shift is explained as a change in the conduction band edge ( $E_{CB}$ ) due to the protons released upon dye adsorption to  $TiO_2$  [36]. This means dye loading, but also the  $pK_a$  of the sensitizers could affect the conduction band position. Electron lifetime measurements (see Fig. 6c, uncorrected measurements in Fig. S7 in the ESI) were obtained and processed following the same procedure described by the authors previously [32]. A separated grouping of the thiophene and phenyl  $\pi$ -spacer series is found, with higher electron lifetime values obtained for the sensitizers with phenyl spacers. This corresponds well to the observations from the  $J$ - $V$  data, that these dyes have a 25 mV higher average  $V_{OC}$ , as the position of the Fermi level of  $TiO_2$  depends on the conduction band position, the electron density and the injected electron lifetime. The higher lifetime values of the phenyl sensitizers indicates electron recombination is slower, and similar results have been reported previously [37]. There are two possible recombination pathways for the injected electrons in the  $TiO_2$ : (i) back to the dye cation, or (ii) to the oxidized redox shuttle species (either  $I_3^-$  or  $I_2$ ). The recombination to the dye cation is usually reported to be a significantly slower process than (ii) [38], thus the effect observed here must be related to how the  $\pi$ -spacers restrict or promote access for the electrolyte through the dye monolayer to the  $TiO_2$  surface [36]. The complexation between thiophene units and iodide anions has been proposed, a mechanism which could bring these species closer to the  $TiO_2$  surface and hence accelerate this recombination pathway [39,40]. Despite the lower electron lifetimes, the thiophene  $\pi$ -spacers widen the absorption and improves the efficiency.

When comparing the phenyl sensitizers AFB-3 (3,7) to AFB-28 (3,8) and the thiophene derivatives AFB-9 (3,7) to AFB-27 (3,8), we observe closely grouped lifetime curves for both the 3,7 and 3,8 geometries, indicating that the position of the auxiliary donor does not affect the rate of recombination significantly.

From our investigations into the different geometries here reported,

Table 1  
Photophysical properties of dyes AFB-3, 9, 20, 22 to 29.

Dye	Geo-metry	$\pi$ -spacer	$\lambda_{abs}^a$ (nm)	$\epsilon$ ( $M^{-1}cm^{-1}$ )	Em. <sup>b</sup> (nm)	$\lambda_{abs}^c$ on $TiO_2$ (nm)	$E_{0,0}^d$ (eV)	$E_{ox}^e$ (V)	$E_{LUMO}^f$ (V)
AFB-3	3,7- <i>p</i>	Ph	406	18500	614	409	2.51	1.00	-1.51
AFB-9	3,7	Thio	442	23600	634	442	2.31	1.01	-1.30
AFB-20	3	Thio	435	24400	618	430	2.38	1.08	-1.30
AFB-22	3	Ph	396	17900	596	394	2.56	1.04	-1.52
AFB-23	2	Thio	433 <sup>g</sup>	14700	639	–	2.36	1.07	-1.29
AFB-24	2	Ph	393 <sup>g</sup>	7800	609	–	2.57	1.03	-1.54
AFB-25	2,7	Thio	442 <sup>g</sup>	10800	649	–	2.32	1.05	-1.27
AFB-26	2,7	Ph	419 <sup>g</sup>	5600	611	–	2.48	1.01	-1.47
AFB-27	3,8	Thio	449	23600	629	437	2.32	1.04	-1.28
AFB-28	3,8	Ph	404	15400	590	–	2.54	1.02	-1.52
AFB-29	3,7- <i>m</i>	Ph	358 <sup>g</sup>	13400	471	–	2.85	0.98	-1.87

<sup>a</sup> Maximum of most red-shifted peak.

<sup>b</sup> Emission when ICT band is excited, in THF solution.

<sup>c</sup> Maximum of most red-shifted peak on  $TiO_2$  (2.5  $\mu m$ , GreatcellSolar 18NR-T).

<sup>d</sup> Calculated from the intersection of the absorption and normalized emission spectra.

<sup>e</sup> Measured vs.  $F_c^+/F_c$  on stained  $TiO_2$  electrodes in acetonitrile with 0.1 M LiTFSI, converted to V vs. SHE by 0.624 V. Scan rate 20  $mV s^{-1}$ .

<sup>f</sup> Calculated from  $E_{ox}-E_{0,0}$ .

<sup>g</sup> Manual estimate due to no clear peak to assign.

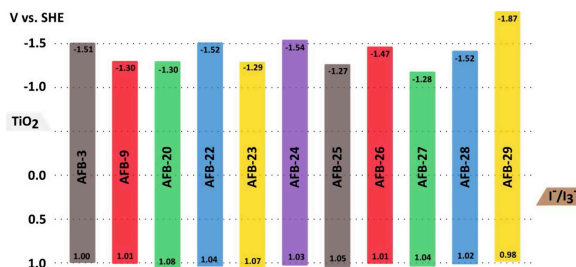
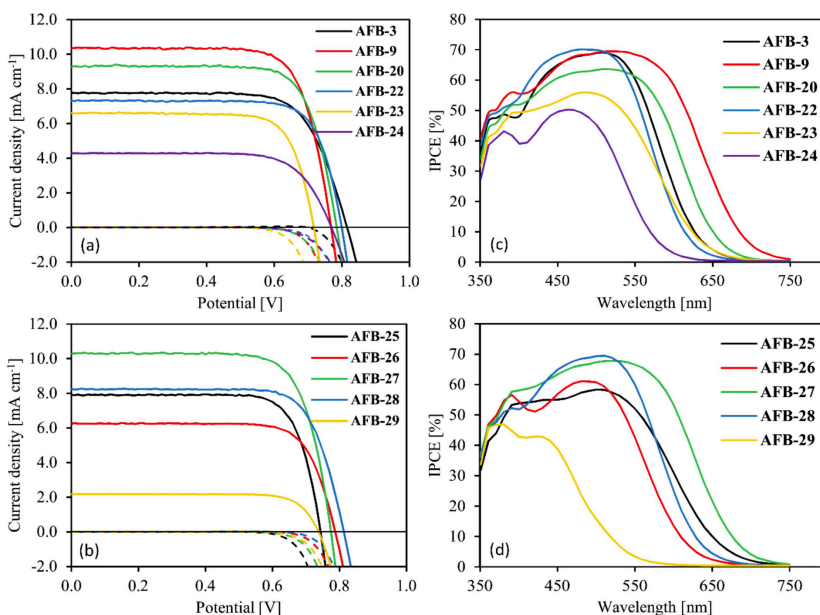


Fig. 4. Energy level diagram of the sensitizers.

Fig. 5. (a–b)  $J$ - $V$  curves for the best device for each sensitizer. Dashed lines are the dark current measurements. (c–d) IPCE spectra of the best device for each sensitizer.

we have a number of encouraging observations. Firstly, we were able to reproduce our previous findings of the modest positive effect from the auxiliary donors on phenothiazine sensitizers, improving the photovoltaic performance by around 10% [32]. Because the contribution from the auxiliary donor is only modest, we were unable to identify any effects from the position of this moiety. However, as we suspected the more linear 3,8 geometry to anchor on  $\text{TiO}_2$  in a more perpendicular fashion, we did dye loading measurements with the pure sensitizers having thiophene as  $\pi$ -spacer AFB-9 (3,7) and AFB-27 (3,8) without the additive CDCA, see Table 3. Indeed, the 3,8 geometry displayed 10% higher dye loading, indicating there could be a performance advantage to the 3,8 geometry. This can also be seen from the electron lifetime measurements, where AFB-27 has marginally higher electron lifetimes,

suggesting a denser dye monolayer compared to AFB-9. We think the key to fully exploit this potential lies in optimizing the CDCA concentration in the staining solutions. Also, by increasing the size of the auxiliary donor, we believe any differences will be more pronounced.

Further, attachment of the  $\pi$ -spacer in the 3-position is vastly superior to the 2-position, as would be expected from the elucidated  $^{13}\text{C}$  NMR shifts of the phenothiazine scaffold shown in Fig. 7. Generally, the  $^{13}\text{C}$  NMR shift of a carbon atom can be used to estimate the electron density at this atom, because high electron density produces a shielding effect shifting the  $^{13}\text{C}$  chemical shift upfield (to lower ppm values). Here the 2-position has a shift of 127.6 ppm, while the 3-position has 122.3 ppm, meaning the 3-position has the higher electron density.



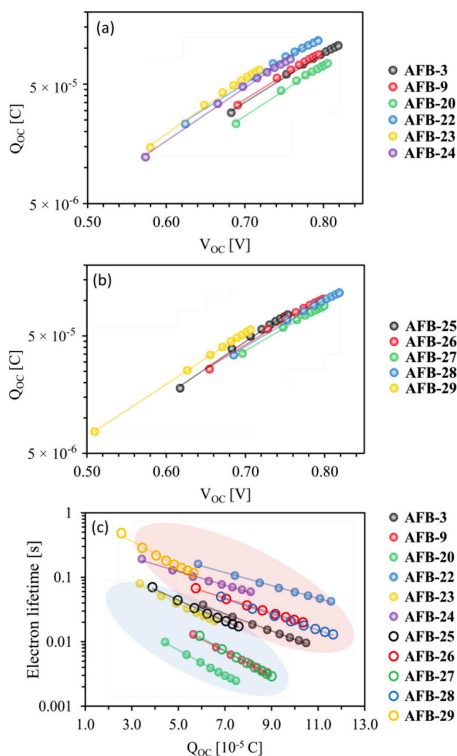
**Table 2**  
Photovoltaic performance of dyes AFB-3, 20, 22 to 29 under 1 sun AM 1.5G illumination, and from IPCE measurements. All devices were fabricated with 5 mM CDCA in the staining solution.

Dye	Geometry	$\pi$ -spacer	IPCE $J_{SC}$ (mA cm <sup>-2</sup> ) <sup>a</sup>	$J_{SC}$ (mA cm <sup>-2</sup> )	$V_{OC}$ (V)	FF	PCE (%)
AFB-3	3,7- <i>p</i>	Ph	7.83	7.65 ± 0.09	807 ± 7	0.71 ± 0.01	4.37 ± 0.10
AFB-9	3,7	Thio	10.43	10.20 ± 0.20	775 ± 8	0.75 ± 0.00	5.82 ± 0.06
AFB-20 <sup>b</sup>	3	Thio	8.40	9.13 ± 0.20	778 ± 7	0.76 ± 0.01	5.34 ± 0.11
AFB-22	3	Ph	7.50	7.11 ± 0.16	785 ± 15	0.74 ± 0.02	4.06 ± 0.26
AFB-23 <sup>b</sup>	2	Thio	6.34	6.57 ± 0.01	721 ± 8	0.75 ± 0.01	3.48 ± 0.01
AFB-24	2	Ph	4.21	4.17 ± 0.08	753 ± 19	0.74 ± 0.02	2.27 ± 0.03
AFB-25	2,7	Thio	7.48	8.10 ± 0.21	747 ± 4	0.72 ± 0.04	4.27 ± 0.09
AFB-26	2,7	Ph	6.36	6.08 ± 0.14	781 ± 5	0.74 ± 0.01	3.43 ± 0.16
AFB-27	3,8	Thio	9.85	10.11 ± 0.14	774 ± 3	0.75 ± 0.00	5.78 ± 0.09
AFB-28	3,8	Ph	7.89	8.01 ± 0.23	796 ± 16	0.75 ± 0.00	4.67 ± 0.18
AFB-29	3,7- <i>m</i>	Ph	2.45	1.95 ± 0.17	713 ± 18	0.78 ± 0.00	1.06 ± 0.10
N719 <sup>c</sup>	–	–	–	13.22	784	0.76	7.92

<sup>a</sup> Obtained by integration of the IPCE spectrum over the 1 sun AM 1.5 G spectrum.

<sup>b</sup> Average values of two cells.

<sup>c</sup> Best device. Staining solution of N719 utilized a solvent mixture of tert-butanol and acetonitrile (1:1, v/v), while staining time and concentration were the same as for the AFB dyes.



**Fig. 6.** (a–b) Charge extraction ( $Q_{OC}$ ) curves for all sensitizers measured at different light intensities, plotted against  $V_{OC}$ . (c) Electron lifetime measurements of all dyes, corrected for conduction band shift and plotted against charge extraction values for the same potentials. Sensitizers with thiophene  $\pi$ -spacers are circled in the blue oval while the phenyl  $\pi$ -spacer sensitizers are circled in red. (For interpretation of the references to color in this figure legend, the reader is referred to the Web version of this article.)

### 3. Conclusion

A total of eleven sensitizers from five phenothiazine geometries have been synthesized and evaluated in dye-sensitized solar cells, with three of the geometries (2, 2,7 and 3,8) being completely novel geometries. The photovoltaic performance of the five geometries for both the thiophene and phenyl  $\pi$ -spacers was in ascending order:  $2 < 2,7 < 3 < 3,7 \approx 3,8$ . We also established the position of the anchoring group should unquestionably be the 3-position, as is the case for all phenothiazine sensitizers published to date. The most efficient device was sensitized with AFB-27 from the 3,8 geometry with a *para*-methoxyphenyl auxiliary donor and thiophene  $\pi$ -spacer, delivering a PCE of 5.88% ( $J_{SC} = 10.28$  mA cm<sup>-2</sup>,  $V_{OC} = 773$  mV, FF = 0.75). The overall performances of the conventional 3,7 and novel 3,8 geometries were near identical, despite the 3,8 geometry displaying a 10% higher dye loading without additives. Consequently, the more linear 3,8 geometry upon optimization has the potential to outperform the bent 3,7 geometry by producing denser dye monolayers, yielding higher short-circuit currents. We hope this study will help the phenothiazine dye class to grow in new directions, yielding higher performing and more versatile phenothiazine sensitizers in the future.

### 4. Experimental

#### 4.1. Synthesis

A detailed description of the synthesis and characterization of dyes and intermediates is given in the ESI.

#### 4.2. Device fabrication

The photoanodes were fabricated starting from FTO glass (NSG10, Nippon Sheet Glass). It was cleaned in Deconex 21 solution in an ultrasonic bath for 45 min, and then rinsed with deionized water and ethanol. The FTO was further cleaned in a UV/O<sub>3</sub> cleaner for 15 min. A dense blocking layer of TiO<sub>2</sub> was deposited by immersion of the FTO glass slides twice in an aqueous TiCl<sub>4</sub> solution at 70 °C for 45 min

**Table 3**

Dye loading measurements of AFB-9 and AFB-27, without addition of CDCA. Desorption by immersion in a 40 mM solution of TBAOH in stabilized THF, averages of two electrodes.

Dye	Geometry	Dye loading (10 <sup>-7</sup> mol cm <sup>-2</sup> )
AFB-9	3,7	3.95 ± 0.04
AFB-27	3,8	4.34 ± 0.05

A.F. Buene, et al.

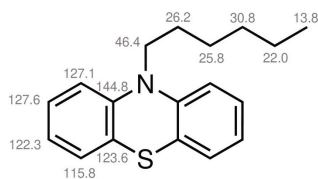


Fig. 7.  $^{13}\text{C}$  NMR shifts for 10-hexyl-10H-phenothiazine.

followed by rinsing with deionized water and ethanol. Screen printing deposited the mesoporous  $\text{TiO}_2$  pastes (54T mesh, 2 layers of 18NR-T and 1 layer of WER2-O) with heating to 125 °C for 5 min after each print. Sintering of the  $\text{TiO}_2$  was performed on a programmable hotplate following the temperature profile of 125, 250, 375, 450 and 500 °C for 5, 5, 15 and 15 min with ramping times of 5 min between each step. A final  $\text{TiCl}_4$  post treatment was performed under the same conditions as for the blocking layer, but only once and for 30 min. Sintering at 500 °C for 45 min on a hotplate was the last step in preparing the photoanodes.

The counter electrodes were prepared from TEC10 FTO glass, holes were drilled with a diamond drill bit under water before the glass slides were cleaned in Hellmanex solution, deionized water, ethanol and acetone, each for 15 min with sonication. The catalytic platinum layer was deposited by drop casting (5  $\mu\text{L}/\text{cm}^2$ ) a  $\text{H}_2\text{PtCl}_6$  solution (10 mM in 2-propanol) followed by heating from a hot air gun at 400 °C for 15 min.

Staining of the photoanodes was done in 0.5 mM solutions of the sensitizers with a 10-fold molar excess of chenodeoxycholic acid in a mixture of THF/acetonitrile (57:43, v/v) for 20 h. N719 was stained from a mixture of *tert*-butanol/acetonitrile (1:1, v/v). The stained electrodes were rinsed in acetonitrile for 2 min and air-dried. The solar cells were assembled in a sandwich construction by melting a 25  $\mu\text{m}$  Surlyn gasket between the photoanode and the counter electrode, and filling the cell with A6141 electrolyte by vacuum backfilling. The composition of the A6141 electrolyte was 0.60 M 1-butyl-3-methylimidazolium iodide, 0.03 M  $\text{I}_2$ , 0.10 M guanidinium thiocyanate and 0.50 M *tert*-butylpyridine in a mixture of acetonitrile and valeronitrile (85:15, v/v) [41]. Ultrasonic soldering was used to increase the conductivity of the contact points of the electrodes.

#### 4.3. Device characterization

*J-V* characteristics were measured with a Keithley 2400 under 100  $\text{mW}/\text{cm}^2$  illumination from a solar simulator (450 W, Oriol). The devices were masked with a 0.16  $\text{cm}^2$  circular black metal mask. Incident photon-to-current conversion efficiency measurements (IPCE) were recorded on an Arkeo-Ariadne (Cici Research s.r.l) with a 300 W Xenon lamp. A Dyanemo Toolbox was used for the electron lifetime and charge extraction measurements.

#### Acknowledgements

The support from the Research Council of Norway to the Norwegian Micro- and Nano-Fabrication Facility, NorFab (project number 245963/F50) and the Norwegian NMR Platform (project number 226244/F50) is highly appreciated.

#### Appendix A. Supplementary data

Supplementary data to this article can be found online at <https://doi.org/10.1016/j.dyepig.2019.05.007>.

Dyes and Pigments 169 (2019) 66–72

doi.org/10.1016/j.dyepig.2019.05.007.

#### References

- [1] O'Regan B, Grätzel M. *Nature* 1991;353:737–40.
- [2] Freitag M, Teuscher J, Saygılı Y, Zhang X, Giordano F, Liska P, Hua J, Zakeeruddin SM, Moser J-E, Grätzel M, Hagfeldt A. *Nat Photon* 2017;11:372–8.
- [3] Joly D, Pelleja L, Narbey S, Oswald F, Meyer T, Kervella Y, Maldivi F, Clifford JN, Palomares E, Demadrille R. *Energy Environ Sci* 2015;8:2010–8.
- [4] Raj A, Steingart D. *J Electrochem Soc* 2018;165:B3130–6.
- [5] Freitag M, Daniel Q, Pazoki M, Sveinbjörnsson K, Zhang J, Sun L, Hagfeldt A, Boschloo G. *Energy Environ Sci* 2015;8:2634–7.
- [6] Freitag M, Giordano F, Yang W, Pazoki M, Hao Y, Zietz B, Grätzel M, Hagfeldt A, Boschloo G. *J Phys Chem C* 2016;120:9595–603.
- [7] Hao Y, Yang W, Zhang L, Jiang R, Mijangos E, Saygılı Y, Hammarström L, Hagfeldt A, Boschloo G. *Nat Commun* 2016;7:13934.
- [8] Yum J-H, Baranoff E, Kessler F, Moehl T, Ahmad S, Bessho T, Marchioro A, Ghadiri E, Moser J-E, Yi C, Nazeeruddin MK, Grätzel M. *Nat Commun* 2012;3:631.
- [9] Kakiage K, Aoyama Y, Yano T, Oya K, Fujisawa J-i, Hanaya M. *Chem Commun* 2015;51:15894–7.
- [10] Higashino T, Imahori H. *Dalton Trans* 2015;44:448–63.
- [11] Mathew S, Yella A, Gao P, Humphry-Baker R, Curchod BFF, Ashari-Astani N, Tavanelli I, Rothlisberger U, Nazeeruddin K, Grätzel M. *Nat Chem* 2014;6:242–7.
- [12] Ahmad S, Guillen E, Kavan L, Grätzel M, Nazeeruddin MK. *Energy Environ Sci* 2013;6:3439–66.
- [13] Mishra A, Fischer MK, Bätjer P. *Angew Chem Int Ed* 2009;48:2474–99.
- [14] Sheibani E, Zhang L, Liu P, Xu B, Mijangos E, Boschloo G, Hagfeldt A, Hammarström L, Kloo L, Tian H. *RSC Adv* 2016;6:18165–77.
- [15] Tian H, Yang X, Chen R, Pan Y, Li L, Hagfeldt A, Sun L. *Chem Commun* 2007:3741–3.
- [16] Tian H, Yang X, Cong J, Chen R, Liu J, Hao Y, Hagfeldt A, Sun L. *Chem Commun* 2009:6288–90.
- [17] Lin RY-Y, Wu F-L, Li C-T, Chen P-Y, Ho K-C, Lin JT. *ChemSusChem* 2015;8:2503–13.
- [18] Liao J-S, Wan Z-Q, Jia C-Y. *Chin Chem Lett* 2016;27:1304–18.
- [19] Huang Z-S, Meier H, Cao D. *J Mater Chem C* 2016;4:2404–26.
- [20] Katsuhiko O, Tomoya Y, Masaaki T. *Chem Lett* 2010;39:864–6.
- [21] Hart AS, K.C.B, Subbaiyan NK, Karr PA, D'Souza F. *ACS Appl Mater Interfaces* 2012;4:5813–20.
- [22] Wan Z, Jia C, Duan Y, Zhou L, Lin Y, Shi Y. *J Mater Chem* 2012;22:25140–7.
- [23] Chiykowski VA, Lam B, Du C, Berlinguette CP. *Chem Commun* 2017;53:2367–70.
- [24] Chiykowski VA, Lam B, Du C, Berlinguette CP. *Chem Commun* 2017;53:2547–50.
- [25] Lu Y, Song H, Li X, Ågren H, Liu Q, Zhang J, Zhang X, Xie Y. *ACS Appl Mater Interfaces* 2019;11:5046–54.
- [26] Kumar R, Sudhakar V, Prakash K, Krishnamoorthy K, Sankar M. *ACS Appl Mater Interfaces* 2018;1:2793–801.
- [27] Yang G, Tang Y, Li X, Ågren H, Xie Y. *ACS Appl Mater Interfaces* 2017;9:36875–85.
- [28] Krishna NV, Krishna JVS, Singh SP, Giribabu L, Han L, Bedja I, Gupta RK, Islam A. *J Phys Chem C* 2017;121:6464–77.
- [29] Marszalek M, Nagane S, Ichake A, Humphry-Baker R, Paul V, Zakeeruddin SM, Grätzel M. *J Mater Chem* 2012;22:889–94.
- [30] Kim SH, Sakong C, Chang JB, Kim B, Ko MJ, Kim DH, Hong KS, Kim JP. *Dyes Pigments* 2013;97:262–71.
- [31] Buene AF, Uggerud N, Economopoulos SP, Gautun OR, Hoff BH. *Dyes Pigments* 2018;151:263–71.
- [32] Buene AF, Ose EE, Zakariassen AG, Hagfeldt A, Hoff BH. *J Mater Chem A* 2019;7:7581–90.
- [33] Chen J, Zhang Y, Yang L, Zhang X, Liu J, Li L, Zhang H. *Tetrahedron* 2007;63:4266–70.
- [34] Wei H, Shen J, Liu Y, Huang T, Zhang Q, Zhao J, Zhao X. *Dyes Pigments* 2018;149:789–95.
- [35] Yang YS, Kim HD, Ryu J-H, Kim KK, Park SS, Ahn K-S, Kim JH. *Synth Met* 2011;161:850–5.
- [36] Marinado T, Nonomura K, Nissfolk J, Karlsson MK, Hagberg DP, Sun L, Mori S, Hagfeldt A. *Langmuir* 2010;26:2592–8.
- [37] Wang S, Guo J, He L, Wang H, Zhao J, Lu C. *Synth Met* 2013;168:1–8.
- [38] Hagfeldt A, Grätzel M. *Chem Rev* 1995;95:49–68.
- [39] Teuscher J, Marchioro A, Andrés J, Roch LM, Xu M, Zakeeruddin SM, Wang P, Grätzel M, Moser J-E. *J Phys Chem C* 2014;118:17108–15.
- [40] Baumann A, Cheema H, Sabuj MA, McNamara LE, Zhang Y, Peddapuram A, Nguyen ST, Watkins DL, Hammer NI, Rai N, Delcamp JH. *J Phys Chem Chem Phys* 2018;20:17859–70.
- [41] Nazeeruddin MK, De Angelis F, Fantacci S, Selloni A, Viscardi G, Liska P, Ito S, Takeru B, Grätzel M. *JACS* 2005;127:16835–47.

**Electronic Supplementary Information****A comprehensive experimental study of five fundamental phenothiazine geometries increasing the diversity of the phenothiazine dye class for dye-sensitized solar cells**

Audun Formo Buene<sup>a</sup>, Anders Hagfeldt<sup>b</sup> and Bård Helge Hoff<sup>a\*</sup>

*a*: Department of Chemistry, Norwegian University of Science and Technology (NTNU), N-7491 Trondheim, Norway

*b*: Laboratory of Photomolecular Science, Institute of Chemical Sciences and Engineering, École Polytechnique Fédérale de Lausanne (EPFL), Chemin des Alambics, Station 6, CH-1015 Lausanne, Switzerland

\* Corresponding author. Tel.: +47 73593973; E-mail address: bard.h.hoff@ntnu.no (B. H. Hoff).

**List of contents**

<b>Absorption and emission</b>	<b>S2</b>
<b>Electrochemical measurements</b>	<b>S5</b>
<b>Electron lifetime measurements</b>	<b>S6</b>
<b>Synthesis</b>	<b>S7</b>
<b>NMR Spectra</b>	<b>S22</b>
<b>References</b>	<b>S30</b>

## Absorption and emission

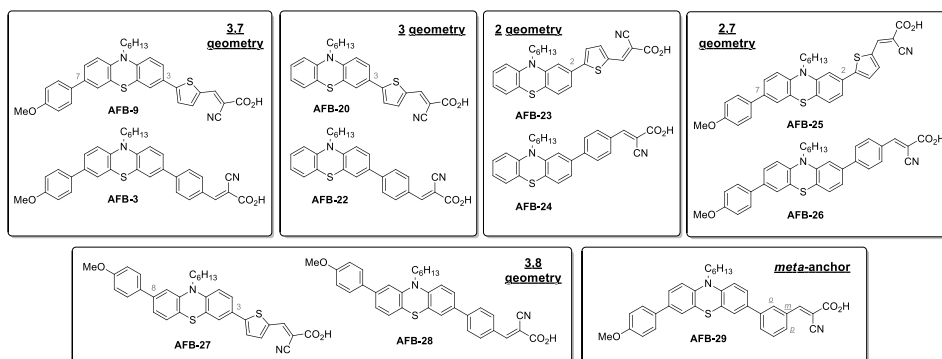


Figure S1. Structures of the sensitizers.

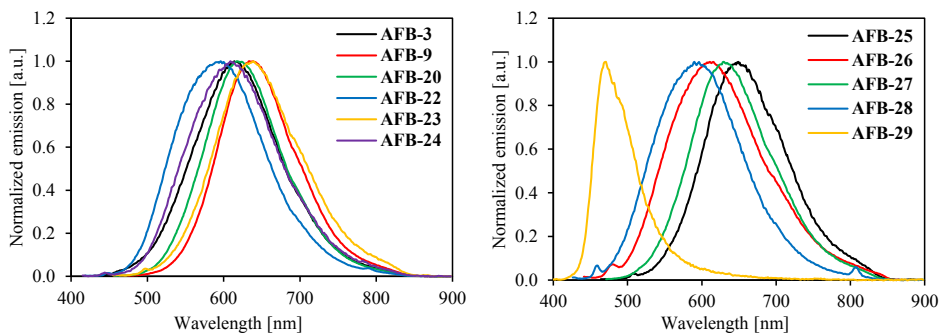
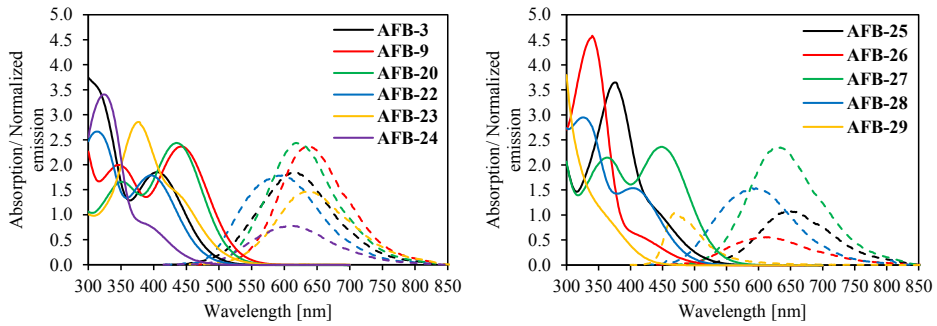
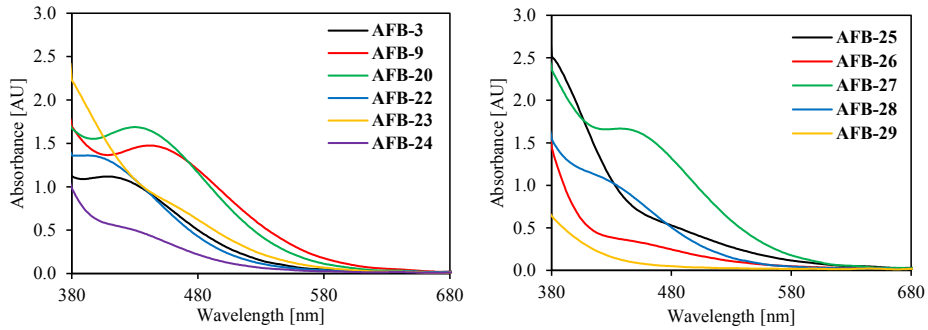


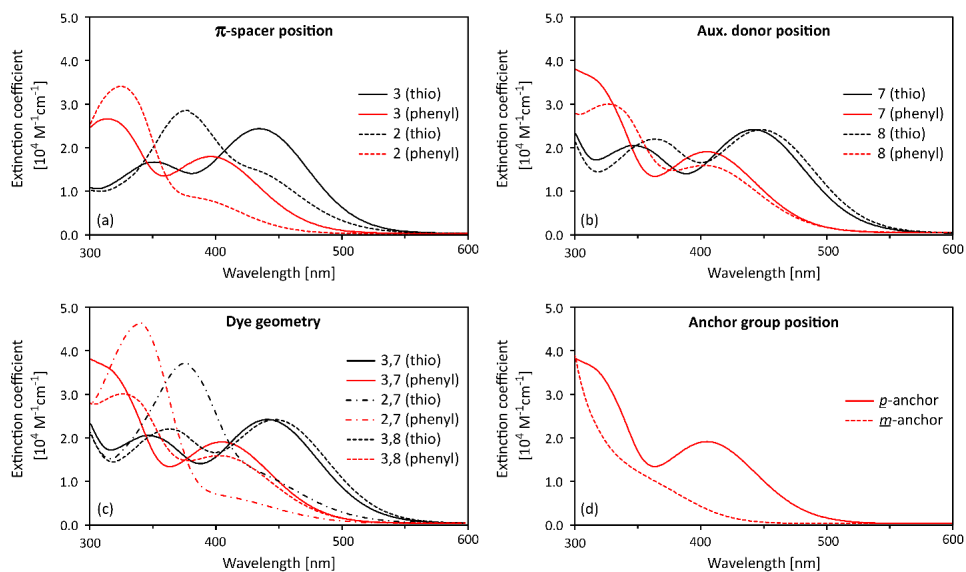
Figure S2. Normalized emission spectra of all dyes, recorded in THF. Excitation at the wavelength of the ICT peak from the UV/Vis absorption spectra in solution.



**Figure S3.** Absorption spectra in solution plotted with corresponding normalized emission spectra, with the intersections between the curves dictating the optical bandgaps. Intersecting wavelengths: *AFB-3* 495 nm, *AFB-9* 537 nm, *AFB-20* 522 nm, *AFB-22* 485 nm, *AFB-23* 525 nm, *AFB-24* 483 nm, *AFB-25* 535 nm, *AFB-26* 500 nm, *AFB-27* 535 nm, *AFB-28* 489 nm and *AFB-29* 435 nm.

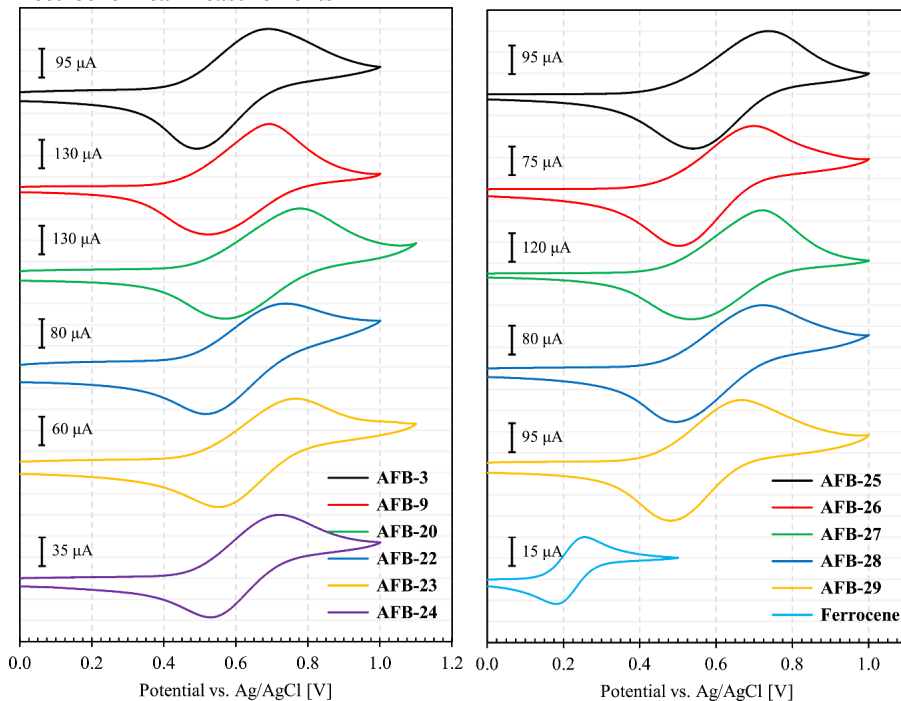


**Figure S4.** Absorption spectra on  $\text{TiO}_2$  films.

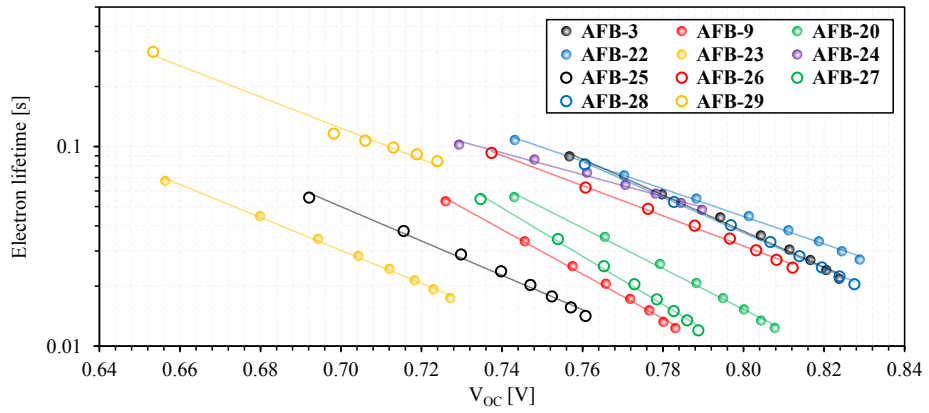


**Figure S5.** Comparison of UV/Vis spectra focusing on the differences in molecular structures. Dyes with phenyl  $\pi$ -spacers are plotted in red and thiophene  $\pi$ -spacers in black. a)  $\pi$ -spacer position, no auxiliary donors, b) auxiliary donor position with  $\pi$ -spacers in 3-position, c) complete dye geometry comparison of 3,7, 2,7 and 3,8 geometries, d) anchoring group in para vs. meta position on phenyl  $\pi$ -spacer.

## Electrochemical measurements



**Figure S6.** Cyclic voltammograms of all sensitizers on FTO/TiO<sub>2</sub> electrodes. For the measurement of ferrocene, the working electrode was a glassy carbon electrode.

**Electron lifetime measurements**

**Figure S7.** Original electron lifetime measurements, not corrected for conduction band shift.



## Synthesis

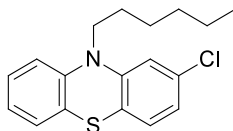
### Materials and reagents

All reactions were carried out under nitrogen atmosphere, and all synthesis reagents were acquired from Sigma Aldrich. 3,7-Dibromo-10-hexyl-10*H*-phenothiazine and 3-bromo-10-hexyl-7-(4-methoxyphenyl)-10*H*-phenothiazine were previously prepared and reported by the authors.<sup>1</sup> Sensitizers **AFB-3**, **9** and **20** are reported in previous studies by the authors, where the experimental procedures can be found.<sup>1,2</sup>

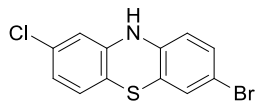
### Analytical instruments

NMR spectroscopy (<sup>1</sup>H and <sup>13</sup>C) was recorded on 400 and 600 MHz Bruker instruments, and all chemical shifts are reported relative to the respective solvent signals. Mass determination was performed on a Waters “Synapt G2-S” QTOF instrument in positive and negative modes. UV/Vis spectra were recorded on a Hitachi U-1900 instrument using quartz cuvettes for the solution samples, while fluorescence spectroscopy was recorded on a Cary Eclipse Fluorescence Spectrophotometer. Infrared spectroscopy was recorded on an FTIR Thermo Nicolet Nexus FT-IR spectrophotometer.

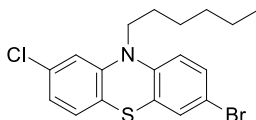
### Synthesis of 2-chloro-10-hexyl-10*H*-phenothiazine (**1**)



2-Chloro-10*H*-phenothiazine (1.00 g, 4.27 mmol) and NaH (0.154 g, 6.40 mmol) were mixed before dry THF (17 mL) was added under nitrogen atmosphere. The reaction stirred at room temperature for 30 min. 1-Bromohexane (1.056 g, 0.90 mL, 6.40 mmol) was added dropwise over 30 minutes and the mixture was heated to reflux. After 16 hours the reaction was cooled to room temperature and quenched with an aqueous NH<sub>4</sub>Cl solution (10 mL, 5 wt%), and then extracted with ethyl acetate (3 × 20 mL). The combined organic phases were dried with brine (20 mL) and over anhydrous Na<sub>2</sub>SO<sub>4</sub>, filtered and the solvents were removed *in vacuo*. The crude product was purified by silica gel column chromatography (*n*-pentane, *R<sub>f</sub>* = 0.29) to obtain compound **1** as a clear oil (1.29 g, 4.27 mmol, 95%). <sup>1</sup>H NMR (400 MHz, DMSO-*d*<sub>6</sub>) δ: 7.22-7.17 (m, 1H), 7.15-7.09 (m, 2H), 7.03-6.92 (m, 4H), 3.83 (t, *J* = 6.8 Hz, 2H), 1.67-1.58 (m, 2H), 1.38-1.29 (m, 2H), 1.24-1.15 (m, 4H), 0.83-0.75 (m, 3H); <sup>13</sup>C NMR (100 MHz, DMSO-*d*<sub>6</sub>) δ: 146.3, 144.0, 132.4, 128.0, 127.7, 127.2, 123.4, 122.9, 122.7, 122.0, 116.2, 115.7, 46.5, 30.7, 26.1, 25.7, 22.0, 13.8; IR (neat, cm<sup>-1</sup>): 2956 (w), 2919 (w), 2847 (w), 1566 (m), 1455 (s), 1406 (m), 1239 (m), 1126 (m), 1097 (m), 928 (m), 799 (m), 746 (s); HRMS (ASAP+, *m/z*): found 317.1008 (calcd. C<sub>18</sub>H<sub>20</sub>NS<sup>35</sup>Cl 317.1005, [M\*]<sup>+</sup>).

**Synthesis of 7-bromo-2-chloro-10H-phenothiazine (2)**

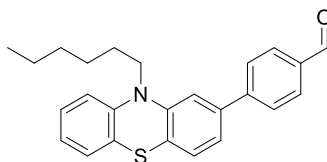
2-Chloro-10H-phenothiazine (13.0 g, 55.6 mmol) was suspended in glacial acetic acid (300 mL) and stirred at room temperature. Br<sub>2</sub> (3.0 mL, 58.37 mmol) dissolved in glacial acetic acid (300 mL) was added dropwise to the suspension over 90 minutes. After 22 hours, Na<sub>2</sub>SO<sub>3</sub> (11.0 g, 87.0 mmol) and water (10 mL) was added and the mixture was left stirring for 1 hour. By adding aqueous potassium hydroxide (0.4 M, 1500 mL), a precipitate formed and the mixture was left stirring for 1 hour. The precipitate was filtered off, washed with cold *iso*-propanol (100 mL), and then dried to yield a pink solid. The crude product was purified by three crystallizations from toluene to obtain compound **2** as offwhite crystals (5.44 g, 17.4 mmol, 31%), mp 183 °C (dec.). <sup>1</sup>H NMR (400 MHz, DMSO-*d*<sub>6</sub>) δ: 8.88 (s, 1H), 7.18-7.13 (m, 2H), 6.93 (d, *J* = 8.3 Hz, 1H), 6.80 (dd, *J* = 8.3, 2.3 Hz, 1H), 6.67 (d, *J* = 2.3 Hz, 1H), 6.58 (d, *J* = 8.3 Hz, 1H); <sup>13</sup>C NMR (100 MHz, DMSO-*d*<sub>6</sub>) δ: 142.9, 140.5, 132.0, 130.3, 128.2, 127.5, 121.5, 118.7, 116.1, 114.8, 113.9, 113.0; IR (neat, cm<sup>-1</sup>) ν: 3336 (w), 1587 (w), 1458 (w), 1387 (w), 1238 (w), 1092 (w), 920 (w), 877 (w), 850 (m), 811 (s), 803 (s), 742 (w), 675 (w), 631 (w), 582 (m), 537 (s), 483 (m), 438 (m); HRMS (ASAP+, *m/z*): found 310.9168 (calcd. C<sub>12</sub>H<sub>7</sub>NS<sup>35</sup>Cl<sup>79</sup>Br 310.9171, [M\*]<sup>+</sup>).

**Synthesis of 7-bromo-2-chloro-10-hexyl-10H-phenothiazine (3)**

Compound **2** (5.30 g, 16.96 mmol) and NaH (610 mg, 25.4 mmol) were mixed before dry THF (65 mL) was added under nitrogen atmosphere. The reaction stirred at room temperature for 30 min. 1-Bromohexane (3.96 g, 3.37 mL, 23.99 mmol) was added dropwise over 20 minutes and the mixture was heated to reflux. After 4.5 hours the reaction was cooled to room temperature and quenched with an aqueous NH<sub>4</sub>Cl solution (30 mL, 5 wt%). Water (300 mL) was added, and the reaction mixture was extracted with ethyl acetate (3 × 30 mL). The combined organic phases were dried with brine (30 mL) and over anhydrous Na<sub>2</sub>SO<sub>4</sub>, filtered and the solvents were removed *in vacuo*. The crude product was purified by silica gel column chromatography (*n*-pentane, *R<sub>f</sub>* = 0.40) to obtain compound **3** as a clear oil (6.27 g, 15.80 mmol, 93%). <sup>1</sup>H NMR (400 MHz, DMSO-*d*<sub>6</sub>) δ: 7.37-7.33 (m, 2H), 7.14 (d, *J* = 8.3 Hz, 1H), 7.05 (d, *J* = 2.3 Hz, 1H), 6.99 (dd, *J* = 8.3, 2.3 Hz, 1H), 6.96-6.93 (m, 1H), 3.83 (t, *J* = 6.9 Hz, 2H), 1.66-1.57 (m, 2H), 1.38-1.30 (m, 2H), 1.25-1.18 (m, 4H), 0.83-0.77 (m, 3H); <sup>13</sup>C NMR (100 MHz, DMSO-*d*<sub>6</sub>) δ: 146.0, 143.5, 132.7, 130.2, 129.1, 128.2, 126.0, 122.4, 121.9, 117.9, 116.0, 114.2, 46.6, 30.7, 25.9, 25.6, 22.0, 13.8; IR (neat, cm<sup>-1</sup>) ν: 2953 (w), 2925 (w), 2854 (w), 1587 (w), 1561 (w), 1453 (s), 1410 (m), 1264 (w), 1239 (w), 1193 (s), 1131 (m),

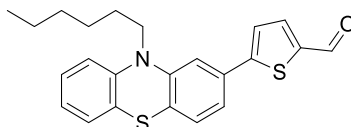
1104 (m), 927 (w), 867 (w), 848 (w), 797 (s), 738 (m), 701 (w), 584 (w), 543 (w), 463 (w), 444 (w); HRMS (ASAP+,  $m/z$ ): found 395.0107 (calcd.  $C_{18}H_{19}NS^{35}Cl^{79}Br$  395.0110,  $[M^*]^+$ ).

#### Synthesis of 4-(10-hexyl-10H-phenothiazin-2-yl)benzaldehyde (4)



Compound **1** (320.0 mg, 1.006 mmol), (4-formylphenyl)boronic acid (226.0 mg, 1.510 mmol),  $Pd(OAc)_2$  (4.0 mg, 0.018 mmol), SPhos (15.1 mg, 0.037 mmol) and  $K_2CO_3$  (562 mg, 4.06 mmol) were mixed. 1,4-Dioxane (4.5 mL) and water (4.5 mL) were degassed and added under nitrogen atmosphere. The reaction mixture was heated to 80 °C and left stirring for 2 hours before cooling to room temperature. The reaction mixture was extracted with ethyl acetate ( $3 \times 30$  mL). The combined organic phases were dried with brine (30 mL) and over anhydrous  $Na_2SO_4$ , filtered and the solvents were removed *in vacuo*. The crude product was purified by silica gel column chromatography (*n*-pentane/ethyl acetate, 6:1,  $R_f = 0.40$ ) to obtain compound **4** as a yellow resin (321.0 mg, 0.827 mmol, 82%).  $^1H$  NMR (400 MHz,  $DMSO-d_6$ )  $\delta$ : 10.05 (s, 1H), 8.01-7.96 (m, 2H), 7.93-7.88 (m, 2H), 7.34-7.24 (m, 3H), 7.24-7.19 (m, 1H), 7.19-7.15 (m, 1H), 7.07-7.02 (m, 1H), 6.98-6.93 (m, 1H), 3.99 (t,  $J = 6.9$  Hz, 2H), 1.75-1.66 (m, 2H), 1.45-1.36 (m, 2H), 1.28-1.20 (m, 4H), 0.84-0.76 (m, 3H);  $^{13}C$  NMR (100 MHz,  $DMSO-d_6$ )  $\delta$ : 192.7, 145.6, 145.5, 144.5, 138.3, 135.1, 130.1 (2C), 127.7, 127.6, 127.3 (2C), 127.1, 124.7, 123.4, 122.6, 121.2, 116.1, 114.3, 46.4, 30.8, 26.2, 25.8, 22.0, 13.8; IR (neat,  $cm^{-1}$ )  $\nu$ : 3065 (w), 2961 (w), 2925 (w), 2847 (w), 2722 (w), 1697 (s), 1602 (s), 1457 (s), 1211 (s), 1169 (m), 836 (m), 805 (s), 747 (s); HRMS (ASAP+,  $m/z$ ): found 388.1733 (calcd.  $C_{25}H_{26}NOS$  388.1735,  $[M+H]^+$ ).

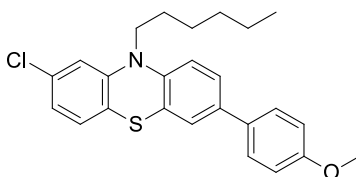
#### Synthesis of 5-(10-hexyl-10H-phenothiazin-2-yl)thiophene-2-carbaldehyde (5)



Compound **1** (400 mg, 1.258 mmol), (5-formylthiophen-2-yl)boronic acid (393 mg, 2.52 mmol),  $Pd(OAc)_2$  (5.65 mg, 0.025 mmol), SPhos (20.66 mg, 0.050 mmol) and  $K_2CO_3$  (696 mg, 5.03 mmol) were mixed. 1,4-Dioxane (4.5 mL) and water (4.5 mL) were degassed and added under nitrogen atmosphere. The reaction mixture was heated to 80 °C and left stirring for 24 hours before cooling to room temperature. The reaction mixture was extracted with ethyl acetate ( $3 \times 30$  mL). The combined organic phases were dried with brine (30 mL) and over anhydrous  $Na_2SO_4$ , filtered and the solvents were removed *in vacuo*. The crude product was purified by silica gel column chromatography (*n*-pentane/ethyl acetate, 9:1,  $R_f = 0.38$ ) to obtain

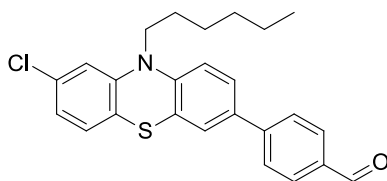
compound **5** as a red oil (206.4 mg, 0.524 mmol, 42%).  $^1\text{H}$  NMR (400 MHz,  $\text{DMSO-}d_6$ )  $\delta$ : 9.90 (s, 1H), 8.03 (d,  $J = 4.1$  Hz, 1H), 7.76 (d,  $J = 3.9$  Hz, 1H), 7.35 (dd,  $J = 7.9, 1.7$  Hz, 1H), 7.27 (d,  $J = 1.7$  Hz, 1H), 7.24-7.19 (m, 2H), 7.15 (dd,  $J = 7.6, 1.4$  Hz, 1H), 7.04 (d,  $J = 8.0$  Hz, 1H), 6.95 (td,  $J = 7.3, 0.6$  Hz, 1H), 3.95 (t,  $J = 7.0$  Hz, 2H), 1.73-1.65 (m, 2H), 1.44-1.36 (m, 2H), 1.27-1.21 (m, 4H), 0.84-0.79 (m, 3H);  $^{13}\text{C}$  NMR (100 MHz,  $\text{DMSO-}d_6$ )  $\delta$ : 184.0, 152.3, 145.5, 144.2, 141.8, 139.1, 131.9, 127.8, 127.7, 127.1, 125.7, 125.4, 123.0, 122.7, 120.3, 116.2, 113.0, 46.5, 30.8, 26.1, 25.8, 22.0, 13.8; IR (neat,  $\text{cm}^{-1}$ )  $\nu$ : 2952 (w), 2924 (w), 2852 (w), 1657 (s), 1592 (w), 1555 (w), 1437 (s), 1413 (m), 1217 (s), 1132 (w), 1106 (w), 1051 (m), 799 (m), 745 (m), 666 (m), 496 (w); HRMS (ASAP+,  $m/z$ ): found 394.1292 (calcd.  $\text{C}_{23}\text{H}_{24}\text{NOS}_2$  394.1299,  $[\text{M}+\text{H}]^+$ ).

#### Synthesis of 2-chloro-10-hexyl-7-(4-methoxyphenyl)-10H-phenothiazine (**6**)



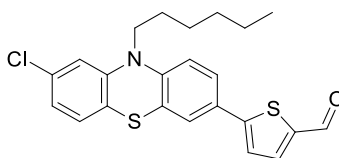
Compound **3** (410 mg, 1.033 mmol), (4-methoxyphenyl)boronic acid (236 mg, 1.55 mmol),  $\text{Pd}(\text{PPh}_3)_4$  (11.9 mg, 0.010 mmol) and  $\text{K}_2\text{CO}_3$  (571 mg, 4.13 mmol) were mixed. 1,4-Dioxane (3.5 mL) and water (3.5 mL) were added under nitrogen atmosphere while stirring. The reaction mixture was heated to 80 °C and left stirring for 16 hours before cooling to room temperature. Water (25 mL) was added to the reaction mixture and ethyl acetate ( $3 \times 25$  mL) was used for extraction. The combined organic phases were dried with brine (25 mL) and over anhydrous  $\text{Na}_2\text{SO}_4$ , filtered and the solvents were removed *in vacuo*. The crude product was purified by silica gel column chromatography (*n*-pentane/ethyl acetate, 19:1,  $R_f = 0.39$ ) to obtain compound **6** as a clear oil (381 mg, 0.898 mmol, 87%).  $^1\text{H}$  NMR (400 MHz,  $\text{DMSO-}d_6$ )  $\delta$ : 7.58-7.54 (m, 2H), 7.45 (dd,  $J = 8.4, 2.2$  Hz, 1H), 7.39 (d,  $J = 2.2$  Hz, 1H), 7.16 (d,  $J = 8.1$  Hz, 1H), 7.07 (d,  $J = 7.4$  Hz, 1H), 7.06 (s, 1H), 7.01-6.96 (m, 3H), 3.89 (t,  $J = 6.9$  Hz, 2H), 3.78 (s, 3H), 1.72-1.63 (m, 2H), 1.43-1.35 (m, 2H), 1.29-1.20 (m, 4H), 0.85-0.80 (m, 3H);  $^{13}\text{C}$  NMR (100 MHz,  $\text{DMSO-}d_6$ )  $\delta$ : 158.7, 146.2, 142.6, 134.7, 132.4, 131.2, 128.1, 127.2 (2C), 125.4, 124.6, 123.9, 122.3, 122.0, 116.5, 115.6, 114.3 (2C), 55.1, 46.5, 30.8, 26.1, 25.7, 22.0, 13.8; IR (neat,  $\text{cm}^{-1}$ )  $\nu$ : 2951 (w), 2923 (w), 2854 (w), 1605 (m), 1573 (m), 1489 (m), 1453 (s), 1409 (m), 1321 (m), 1283 (m), 1265 (m), 1239 (s), 1180 (s), 1107 (m), 1093 (m), 1043 (m), 1025 (m), 923 (m), 892 (w), 867 (m), 811 (s), 591 (w), 533 (w), 445 (w); HRMS (ASAP+,  $m/z$ ): found 423.1420 (calcd.  $\text{C}_{25}\text{H}_{26}\text{NOS}^{35}\text{Cl}$  423.1424,  $[\text{M}^*]^+$ ).

### Synthesis of 4-(10-hexyl-8-methyl-10H-phenothiazin-3-yl)benzaldehyde (7)



Compound **3** (449 mg, 1.132 mmol), (4-formylphenyl)boronic acid (255 mg, 1.697 mmol), Pd(PPh<sub>3</sub>)<sub>4</sub> (13.1 mg, 0.011 mmol) and K<sub>2</sub>CO<sub>3</sub> (626 mg, 4.53 mmol) were mixed. 1,4-Dioxane (4 mL) and water (4 mL) were added under nitrogen atmosphere while stirring. The reaction mixture was heated to 80 °C and left stirring for 19 hours before cooling to room temperature. Water (25 mL) was added to the reaction mixture and ethyl acetate (3 × 25 mL) was used for extraction. The combined organic phases were dried with brine (25 mL) and over anhydrous Na<sub>2</sub>SO<sub>4</sub>, filtered and the solvents were removed *in vacuo*. The crude product was purified by silica gel column chromatography (*n*-pentane/ethyl acetate, 9:1, *R<sub>f</sub>* = 0.22) to obtain compound **7** as a yellow solid (340.3 mg, 0.803 mmol, 71%), mp 100-101 °C. <sup>1</sup>H NMR (400 MHz, DMSO-*d*<sub>6</sub>) δ: 10.02 (s, 1H), 7.96-7.86 (m, 4H), 7.64 (dd, *J* = 8.5, 2.3 Hz, 1H), 7.58 (d, *J* = 2.2 Hz, 1H), 7.17 (d, *J* = 8.2 Hz, 1H), 7.13 (d, *J* = 8.6 Hz, 1H), 7.08 (d, *J* = 2.1 Hz, 1H), 7.01 (dd, *J* = 8.2, 2.1 Hz, 1H), 3.92 (t, *J* = 6.9 Hz, 2H), 1.72-1.63 (m, 2H), 1.43-1.35 (m, 2H), 1.29-1.20 (m, 4H), 0.85-0.80 (m, 3H); <sup>13</sup>C NMR (100 MHz, DMSO-*d*<sub>6</sub>) δ: 192.6, 145.9, 145.8, 144.4, 134.8, 133.2, 132.5, 130.1 (2C), 128.2, 126.59 (2C), 126.57, 125.5, 124.1, 122.3, 122.1, 116.6, 115.9, 46.6, 30.7, 26.1, 25.7, 22.0. IR (neat, cm<sup>-1</sup>) ν: 2924 (w), 2851 (w), 1689 (m), 1592 (m), 1567 (m), 1456 (s), 1407 (m), 1329 (w), 1278 (w), 1240 (s), 1218 (m), 1174 (m), 1133 (m), 1093 (m), 925 (m), 847 (m), 805 (s), 583 (w), 444 (m); HRMS (ASAP+, *m/z*): found 422.1338 (calcd. C<sub>25</sub>H<sub>25</sub>NOS<sup>35</sup>Cl 422.1345, [M+H]<sup>+</sup>).

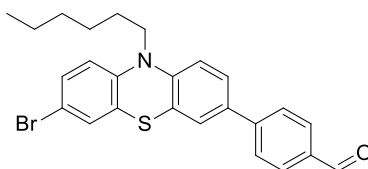
### Synthesis of 5-(8-chloro-10-hexyl-10H-phenothiazin-3-yl)thiophene-2-carbaldehyde (8)



Compound **3** (400 mg, 1.01 mmol), (5-formylthiophen-2-yl)boronic acid (241 mg, 1.55 mmol) SPhos (21 mg, 0.05 mmol), Pd(OAc)<sub>2</sub> (6 mg, 0.25 mmol) and potassium carbonate (565.0 mg, 4.09 mmol) were mixed under nitrogen atmosphere. 1,4-Dioxane (3.4 mL) and water (3.4 mL) were added, and the reaction was stirred at 80 °C for 20 hours, then cooled to room temperature. Water (5 mL) was added to the reaction mixture, and the aqueous phase was extracted with ethyl acetate (3 × 50 mL). The combined organic phases were dried over anhydrous Na<sub>2</sub>SO<sub>4</sub>, filtered and the solvent removed *in vacuo*. The crude product was purified by silica gel column chromatography (*n*-pentane/ethyl acetate, 10:1, *R<sub>f</sub>* = 0.17), to yield compound **8** as an orange oil (339 mg, 0.79 mmol, 78%). <sup>1</sup>H NMR (600 MHz, DMSO-*d*<sub>6</sub>) δ: 9.87 (s, 1H), 7.99-7.99

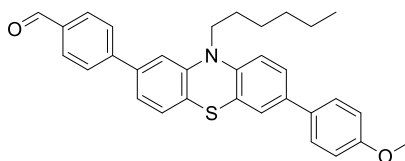
(m, 1H), 7.66-7.65 (m, 1H), 7.61-7.59 (m, 1H), 7.58-7.58 (m, 1H), 7.16-7.15 (m, 1H), 7.08-7.07 (m, 2H), 7.02-7.00 (m, 1H), 3.90-3.88 (t,  $J = 6.9$  Hz, 2H), 1.67-1.63 (t,  $J = 7.2$  Hz, 2H), 1.39-1.34 (m, 2H), 1.25-1.22 (m, 4H), 0.82-0.80 (m, 3H).  $^{13}\text{C}$  NMR (150 MHz, DMSO- $d_6$ )  $\delta$ : 183.8, 151.7, 145.4, 145.0, 141.2, 139.3, 132.6, 128.2, 127.2, 125.9, 124.5, 124.5, 124.3, 122.5, 121.7, 116.6, 115.9, 46.7, 30.7, 26.0, 25.6, 22.0, 13.8. IR (neat,  $\text{cm}^{-1}$ )  $\nu$ : 2921.6 (w), 2849.2 (w), 1664.4 (s), 1566.1 (m), 1435.3 (s), 1226.3 (m), 1131.6 (m), 797.4 (s). HRMS (TOF MS ASAP+,  $m/z$ ): found 428.0910 (calcd.  $\text{C}_{23}\text{H}_{23}\text{NOS}_2^{35}\text{Cl}$ : 428.0910,  $[\text{M}+\text{H}]^+$ ).

#### Synthesis of 4-(7-bromo-10-hexyl-10H-phenothiazin-3-yl)benzaldehyde (9)



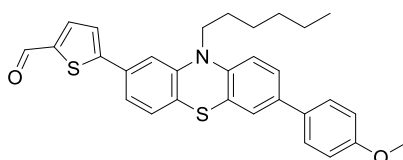
3,7-Dibromo-10-hexyl-10H-phenothiazine (1.00 g, 2.266 mmol), (4-formylphenyl)boronic acid (0.374 g, 2.493 mmol),  $\text{Pd}(\text{PPh}_3)_4$  (26.0 mg, 0.023 mmol) and  $\text{K}_2\text{CO}_3$  (1.253 g, 9.07 mmol) were mixed. 1,4-Dioxane (7.5 mL) and water (7.5 mL) were degassed and added under nitrogen atmosphere. The reaction mixture was heated to 80 °C and left stirring for 7 hours before cooling to room temperature. The reaction mixture was extracted with ethyl acetate ( $2 \times 50$  mL). The combined organic phases were dried with brine (50 mL) and over anhydrous  $\text{Na}_2\text{SO}_4$ , filtered and the solvents were removed *in vacuo*. The crude product was purified by silica gel column chromatography (*n*-pentane/ethyl acetate, 4:1,  $R_f = 0.49$ ) to obtain compound **9** as a yellow solid (452.0 mg, 0.974 mmol, 43%), mp 88-89 °C.  $^1\text{H}$  NMR (400 MHz, DMSO- $d_6$ )  $\delta$ : 10.02 (s, 1H), 7.97-7.92 (m, 2H), 7.90-7.86 (m, 2H), 7.65-7.61 (m, 1H), 7.58-7.56 (m, 1H), 7.38-7.33 (m, 2H), 7.14-7.09 (m, 1H), 6.99-6.95 (m, 1H), 3.88 (t,  $J = 6.9$  Hz, 2H), 1.72-1.63 (m, 2H), 1.43-1.34 (m, 2H), 1.29-1.20 (m, 4H), 0.86-0.79 (m, 3H);  $^{13}\text{C}$  NMR (100 MHz, DMSO- $d_6$ )  $\delta$ : 192.5, 144.7, 144.4, 143.6, 134.7, 133.0, 130.2, 130.1 (2C), 129.0, 126.6, 126.5 (2C), 125.6, 125.5, 123.5, 117.5, 116.3, 113.9, 46.7, 30.8, 26.0, 25.7, 22.0, 13.8; IR (neat,  $\text{cm}^{-1}$ )  $\nu$ : 2951 (w), 2919 (w), 2852 (w), 2722 (w), 1698 (m), 1598 (m), 1461 (s), 1390 (m), 1242 (m), 1170 (m), 808 (s), 794 (s); HRMS (ASAP+,  $m/z$ ): found 465.0758 (calcd.  $\text{C}_{25}\text{H}_{24}\text{NOS}^{79}\text{Br}$  465.0762,  $[\text{M}^*]^+$ ).

#### Synthesis of 4-(10-hexyl-7-(4-methoxyphenyl)-10H-phenothiazin-2-yl)benzaldehyde (10)

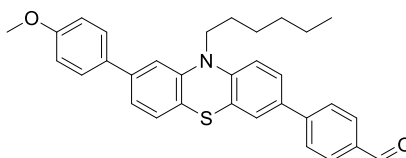


Compound **6** (230 mg, 0.542 mmol), (4-formylphenyl)boronic acid (122 mg, 0.814 mmol), Pd(OAc)<sub>2</sub> (2.436 mg, 0.0109 mmol), SPhos (8.91 mg, 0.022 mmol) and K<sub>2</sub>CO<sub>3</sub> (300 mg, 2.170 mmol) were mixed. 1,4-Dioxane (2 mL) and water (2 mL) were added under nitrogen atmosphere while stirring. The reaction mixture was heated to 80 °C and left stirring for 3 hours before cooling to room temperature. Water (25 mL) was added to the reaction mixture and ethyl acetate (3 × 20 mL) was used for extraction. The combined organic phases were dried with brine (20 mL) and over anhydrous Na<sub>2</sub>SO<sub>4</sub>, filtered and the solvents were removed *in vacuo*. The crude product was purified by silica gel column chromatography (*n*-pentane/ethyl acetate, 4:1, *R<sub>f</sub>* = 0.42) to obtain compound **10** as an orange solid (250.4 mg, 0.507 mmol, 94%), mp 61-63 °C. <sup>1</sup>H NMR (400 MHz, DMSO-*d*<sub>6</sub>) δ: 10.06 (s, 1H), 8.01-7.97 (m, 2H), 7.94-7.91 (m, 2H), 7.60-7.55 (m, 2H), 7.46 (dd, *J* = 8.3, 2.3 Hz, 1H), 7.41 (d, *J* = 2.3 Hz, 1H), 7.34-7.27 (m, 3H), 7.08 (d, *J* = 8.6 Hz, 1H), 7.01-6.96 (m, 2H), 4.02 (t, *J* = 6.9 Hz, 2H), 3.78 (s, 3H), 1.78-1.69 (m, 2H), 1.47-1.39 (m, 2H), 1.30-1.21 (m, 4H), 0.85-0.80 (m, 3H); <sup>13</sup>C NMR (100 MHz, DMSO-*d*<sub>6</sub>) δ: 192.7, 158.7, 145.5, 145.4, 143.1, 138.4, 135.2, 134.3, 131.3, 130.1 (2C), 127.7, 127.3 (2C), 127.2 (2C), 125.4, 124.5, 124.3, 123.9, 121.2, 116.4, 114.32 (2C), 114.26, 55.1, 46.5, 30.8, 26.2, 25.8, 22.1, 13.8; IR (neat, cm<sup>-1</sup>) ν: 2952 (w), 2926 (w), 2851 (w), 1697 (m), 1601 (m), 1462 (s), 1426 (m), 1403 (m), 1241 (s), 1210 (m), 1173 (m), 1108 (m), 1025 (m), 831 (m), 801 (s), 446 (m); HRMS (ASAP+, *m/z*): found 493.2069 (calcd. C<sub>32</sub>H<sub>31</sub>NO<sub>2</sub>S 493.2075, [M\*]<sup>+</sup>).

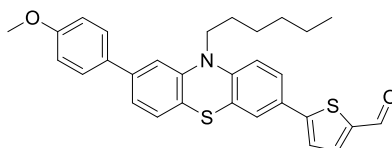
#### Synthesis of 5-(10-hexyl-7-(4-methoxyphenyl)-10H-phenothiazin-2-yl)thiophene-2-carbaldehyde (**11**)



Compound **6** (115 mg, 0.271 mmol), (5-formylthiophen-2-yl)boronic acid (127 mg, 0.814 mmol), Pd(OAc)<sub>2</sub> (1.2 mg, 0.005 mmol), SPhos (4.5 mg, 0.011 mmol) and K<sub>2</sub>CO<sub>3</sub> (150 mg, 1.09 mmol) were mixed. Degassed 1,4-dioxane (1 mL) and water (1 mL) were added under nitrogen atmosphere while stirring. The reaction mixture was heated to 80 °C and left stirring for 5 hours before cooling to room temperature. Water (25 mL) was added to the reaction mixture and ethyl acetate (3 × 20 mL) was used for extraction. The combined organic phases were dried with brine (20 mL) and over anhydrous Na<sub>2</sub>SO<sub>4</sub>, filtered and the solvents were removed *in vacuo*. The crude product was purified by silica gel column chromatography (*n*-pentane/ethyl acetate, 4:1, *R<sub>f</sub>* = 0.23) to obtain compound **11** as an orange oil (39 mg, 0.078 mmol, 29%). <sup>1</sup>H NMR (600 MHz, DMSO-*d*<sub>6</sub>) δ: 9.91 (s, 1H), 8.04 (d, *J* = 4.0 Hz, 1H), 7.78 (d, *J* = 3.9 Hz, 1H), 7.58-7.55 (m, 2H), 7.46 (dd, *J* = 8.4, 2.3 Hz, 1H), 7.40 (d, *J* = 2.1 Hz, 1H), 7.36 (dd, *J* = 7.9, 1.8 Hz, 1H), 7.29 (d, *J* = 1.7 Hz, 1H), 7.24 (d, *J* = 8.0 Hz, 1H), 7.08 (d, *J* = 8.5 Hz, 1H), 7.00-6.97 (m, 2H), 3.99 (t, *J* = 7.0 Hz, 2H), 3.78 (s, 3H), 1.75-1.69 (m, 2H), 1.46-1.40 (m, 2H), 1.30-1.24 (m, 4H), 0.83 (t, *J* = 7.1 Hz, 3H); <sup>13</sup>C NMR (150 MHz, DMSO-*d*<sub>6</sub>) δ: 184.0, 158.7, 152.3, 145.3, 142.8, 141.8, 139.2, 134.5, 131.9, 131.2, 127.8, 127.2 (2C), 125.5, 125.4, 125.3, 124.5, 123.5, 120.3, 116.4, 114.3 (2C), 112.9, 55.1, 46.6, 30.8, 26.1, 25.8, 22.0, 13.8; IR (neat, cm<sup>-1</sup>) ν: 2952 (w), 2924 (w), 2852 (w), 1659 (s), 1438 (s), 1240 (m), 1220 (m), 1178 (m), 1049 (m), 1025 (m), 798 (s), 663 (w), 531 (w); HRMS (ASAP+, *m/z*): found 500.1711 (calcd. C<sub>30</sub>H<sub>30</sub>NO<sub>2</sub>S<sub>2</sub> 500.1718, [M+H]<sup>+</sup>).

**Synthesis of 4-(10-hexyl-8-(4-methoxyphenyl)-10H-phenothiazin-3-yl)benzaldehyde (12)**

Compound **7** (250 mg, 0.593 mmol), (4-methoxyphenyl)boronic acid (135 mg, 0.890 mmol), Pd(OAc)<sub>2</sub> (2.66 mg, 0.012 mmol), SPhos (9.74 mg, 0.024 mmol) and K<sub>2</sub>CO<sub>3</sub> (328 mg, 2.373 mmol) were mixed. 1,4-Dioxane (2 mL) and water (2 mL) were added under nitrogen atmosphere while stirring. The reaction mixture was heated to 80 °C and left stirring for 2 hours before cooling to room temperature. Water (25 mL) was added to the reaction mixture and ethyl acetate (3 × 20 mL) was used for extraction. The combined organic phases were dried with brine (20 mL) and over anhydrous Na<sub>2</sub>SO<sub>4</sub>, filtered and the solvents were removed *in vacuo*. The crude product was purified by silica gel column chromatography (*n*-pentane/ethyl acetate, 4:1, *R<sub>f</sub>* = 0.36) to obtain compound **12** as an orange solid (226 mg, 0.458 mmol, 77%), mp 129-130 °C. <sup>1</sup>H NMR (400 MHz, DMSO-*d*<sub>6</sub>) δ: 10.02 (s, 1H), 7.97-7.93 (m, 2H), 7.92-7.87 (m, 2H), 7.66-7.58 (m, 4H), 7.21-7.17 (m, 3H), 7.14 (d, *J* = 8.6 Hz, 1H), 7.04-7.00 (m, 2H), 7.02 (t, *J* = 6.9 Hz, 2H), 4.02 (t, *J* = 6.9 Hz, 2H), 3.80 (s, 3H), 1.78-1.69 (m, 2H), 1.47-1.39 (m, 2H), 1.30-1.21 (m, 4H), 0.85-0.80 (m, 3H); <sup>13</sup>C NMR (100 MHz, DMSO-*d*<sub>6</sub>) δ: 192.6, 159.0, 145.1, 144.7, 144.5, 139.6, 134.7, 132.6, 132.1, 130.2 (2C), 127.7 (2C), 127.5, 126.5 (2C), 126.4, 125.4, 124.4, 121.5, 120.7, 116.3, 114.3 (2C), 113.8, 55.2, 46.6, 30.8, 26.2, 25.8, 22.0, 13.8; IR (neat, cm<sup>-1</sup>) ν: 2957 (w), 2915 (w), 2848 (w), 1694 (m), 1600 (m), 1466 (s), 1250 (s), 1167 (s), 1023 (w), 829 (m), 798 (s), 744 (w), 660 (w), 521 (w); HRMS (ASAP+, *m/z*): found 493.2068 (calcd. C<sub>32</sub>H<sub>31</sub>NO<sub>2</sub>S 493.2075, [M\*]<sup>+</sup>).

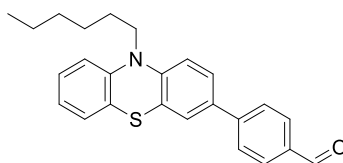
**Synthesis of 5-(10-hexyl-8-(4-methoxyphenyl)-10H-phenothiazin-3-yl)thiophene-2-carbaldehyde (13)**

Compound **8** (204 mg, 0.478 mmol), (4-methoxyphenyl)boronic acid (109 mg, 0.716 mmol), Pd(OAc)<sub>2</sub> (2.1 mg, 0.009 mmol), SPhos (7.8 mg, 0.019 mmol) and K<sub>2</sub>CO<sub>3</sub> (264 mg, 1.91 mmol) were mixed. Degassed 1,4-dioxane (2 mL) and water (2 mL) were added under nitrogen atmosphere while stirring. The reaction mixture was heated to 80 °C and left stirring for 20 hours before cooling to room temperature. Water (25 mL) was added to the reaction mixture and ethyl acetate (3 × 20 mL) was used for extraction. The combined organic phases were dried with brine (20 mL) and over anhydrous Na<sub>2</sub>SO<sub>4</sub>, filtered and the solvents were removed *in vacuo*. The crude product was purified by silica gel column chromatography (*n*-



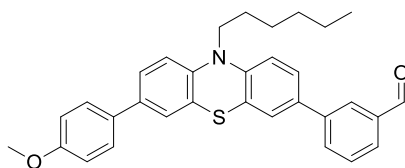
pentane/ethyl acetate, 4:1,  $R_f = 0.26$ ) to obtain compound **13** as an orange solid (172 mg, 0.344 mmol, 72%), mp 91-94 °C.  $^1\text{H NMR}$  (400 MHz,  $\text{DMSO-}d_6$ )  $\delta$ : 8.87 (s, 1H), 7.99 (d,  $J = 4.0$  Hz, 1H), 7.66 (d,  $J = 4.0$  Hz, 1H), 7.62-7.58 (m, 4H), 7.20-7.17 (m, 3H), 7.07 (d,  $J = 8.3$  Hz, 1H), 7.03-6.99 (m, 2H), 3.99 (t,  $J = 6.8$  Hz, 2H), 3.76 (s, 3H), 1.75-1.67 (m, 2H), 1.44-1.36 (m, 2H), 1.27-1.22 (m, 4H), 0.83-0.79 (m, 3H);  $^{13}\text{C NMR}$  (100 MHz,  $\text{DMSO-}d_6$ )  $\delta$ : 183.7, 159.0, 151.9, 145.7, 144.4, 141.1, 139.7, 139.4, 132.0, 127.7 (2C), 127.5, 126.7, 125.8, 124.5, 124.4, 124.3, 121.1, 120.8, 116.3, 114.3 (2C), 113.9, 55.2, 46.6, 30.8, 26.2, 25.8, 22.0, 13.8; IR (neat,  $\text{cm}^{-1}$ )  $\nu$ : 2924 (w), 2852 (w), 2798 (w), 1662 (s), 1435 (m), 1248 (m), 1220 (s), 1179 (m), 802 (s), 670 (w), 499 (w); HRMS (ASAP+,  $m/z$ ): found 500.1715 (calcd.  $\text{C}_{30}\text{H}_{30}\text{NO}_2\text{S}_2$  500.1718,  $[\text{M}+\text{H}]^+$ ).

#### Synthesis of 4-(10-hexyl-10H-phenothiazin-3-yl)benzaldehyde (**14**)



Compound **9** (208 mg, 0.446 mmol),  $\text{Pd}(\text{OAc})_2$  (2.3 mg, 0.01 mmol),  $\text{PPh}_3$  (9.2 mg, 0.035 mmol) and  $\text{K}_2\text{CO}_3$  (119.0 mg, 0.858 mmol) were mixed. Degassed *n*-butanol (2 mL) was added under nitrogen atmosphere. The reaction mixture was heated to 80 °C and left stirring for 5 hours before cooling to room temperature. The reaction mixture was extracted with ethyl acetate ( $3 \times 20$  mL). The combined organic phases were dried with brine (20 mL) and over anhydrous  $\text{Na}_2\text{SO}_4$ , filtered and the solvents were removed *in vacuo*. The crude product was purified by silica gel column chromatography (*n*-pentane/ethyl acetate, 9:1,  $R_f = 0.25$ ) to obtain compound **14** as a yellow resin (65.0 mg, 0.168 mmol, 38%).  $^1\text{H NMR}$  (400 MHz,  $\text{DMSO-}d_6$ )  $\delta$ : 10.02 (s, 1H), 7.98-7.92 (m, 2H), 7.92-7.87 (m, 2H), 7.66-7.61 (m, 1H), 7.59-7.56 (m, 1H), 7.25-7.10 (m, 3H), 7.08-7.02 (m, 1H), 6.99-6.93 (m, 1H), 3.91 (t,  $J = 6.9$  Hz, 2H), 1.75-1.66 (m, 2H), 1.45-1.36 (m, 2H), 1.29-1.21 (m, 4H), 0.85-0.81 (m, 3H); HRMS (ASAP+,  $m/z$ ): found 387.1651 (calcd.  $\text{C}_{25}\text{H}_{25}\text{NOS}$  387.1657,  $[\text{M}^*]^+$ ). The spectroscopic data were in accordance with data previously reported.<sup>3</sup>

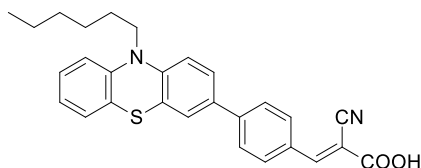
#### Synthesis of 3-(10-hexyl-7-(4-methoxyphenyl)-10H-phenothiazin-3-yl)benzaldehyde (**15**)



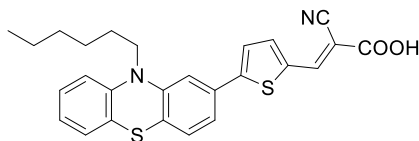
3-Bromo-10-hexyl-7-(4-methoxyphenyl)-10H-phenothiazine (300 mg, 0.640 mmol), (3-formylphenyl)boronic acid (144 mg, 0.961 mmol),  $\text{Pd}(\text{OAc})_2$  (2.9 mg, 0.013 mmol), SPhos (10.5 mg, 0.026 mmol) and  $\text{K}_2\text{CO}_3$  (354 mg, 2.56 mmol) were mixed in a Schlenk flask. Degassed 1,4-dioxane (7.5 mL)

and water (7.5 mL) were added under nitrogen atmosphere. The reaction mixture was heated to 80 °C and left stirring for 5 hours before cooling to room temperature, before extractation with ethyl acetate (3 × 30 mL). The combined organic phases were dried with brine (50 mL) and over anhydrous Na<sub>2</sub>SO<sub>4</sub>, filtered and the solvents were removed *in vacuo*. The crude product was purified by silica gel column chromatography (*n*-pentane/ethyl acetate, 4:1, *R<sub>f</sub>* = 0.31) to obtain compound **15** as a yellow solid (238 mg, 0.48 mmol, 75%) mp 51-53 °C. <sup>1</sup>H NMR (400 MHz, DMSO-*d*<sub>6</sub>) δ: 10.08 (s, 1H), 8.19 (s, 1H), 8.00 (d, *J* = 8.0 Hz, 1H), 7.84 (d, *J* = 7.8 Hz, 1H), 7.66 (t, *J* = 7.6 Hz, 1H), 7.62-7.55 (m, 4H), 7.46 (dd, *J* = 8.5, 2.3 Hz, 1H), 7.41 (d, *J* = 2.1 Hz, 1H), 7.13 (d, *J* = 8.7 Hz, 1H), 7.08 (d, *J* = 8.7 Hz, 1H), 7.01-6.97 (m, 2H), 3.93 (t, *J* = 6.9 Hz, 2H), 3.78 (s, 3H), 1.77-1.69 (m, 2H), 1.47-1.38 (m, 2H), 1.31-1.24 (m, 4H), 0.87-0.82 (m, 3H); <sup>13</sup>C NMR (100 MHz, DMSO-*d*<sub>6</sub>) δ: 193.3, 158.7, 144.5, 142.9, 139.7, 136.8, 134.3, 132.8, 131.9, 131.3, 129.8, 127.6, 127.3, 127.2 (2C), 126.1, 125.4, 125.1, 124.5, 123.9, 123.5, 116.1, 116.0, 114.3 (2C), 55.2, 46.6, 30.8, 26.2, 25.8, 22.1, 13.8; IR (neat, cm<sup>-1</sup>) ν: 2953 (w), 2926 (w), 2852 (w), 1695 (s), 1605 (m), 1583 (m), 1462 (s), 1238 (s), 1178 (m), 788 (s), 685 (m); HRMS (ASAP+, *m/z*): found 493.2073 (calcd. C<sub>32</sub>H<sub>31</sub>NO<sub>2</sub>S 493.2075, [M\*]<sup>+</sup>).

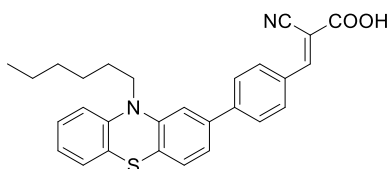
#### Synthesis of (*E*)-2-cyano-3-(4-(10-hexyl-10*H*-phenothiazin-3-yl)phenyl)acrylic acid (AFB-22)



Compound **14** (59.4 mg, 0.153 mmol) and cyanoacetic acid (263 mg, 3.10 mmol) were dissolved in degassed acetonitrile (15 mL) under nitrogen atmosphere. Piperidine (184 μL, 1.86 mmol) was added and the reaction was heated to 80 °C for 45 min before cooling to room temperature and quenched in HCl (2 M, 100 mL). Ethyl acetate (50 mL) was added and the organic phase was washed with water (5 × 200 mL), then dried with brine (50 mL) and over anhydrous Na<sub>2</sub>SO<sub>4</sub>, filtered and the solvents were removed *in vacuo*. The crude product was purified by silica gel column chromatography (gradient: 0-15% MeOH in CH<sub>2</sub>Cl<sub>2</sub>) to obtain sensitizer **AFB-22** as a black solid (51.0 mg, 0.112 mmol, 72%), mp 149 °C (dec.). <sup>1</sup>H NMR (600 MHz, DMSO-*d*<sub>6</sub>) δ: 8.12 (s, 1H), 7.99 (d, *J* = 8.5 Hz, 2H), 7.80 (d, *J* = 8.3 Hz, 2H), 7.60 (dd, *J* = 8.6, 2.1 Hz, 1H), 7.54 (d, *J* = 2.2 Hz, 1H), 7.21 (td, *J* = 7.4, 1.5 Hz, 1H), 7.15 (dd, *J* = 7.6, 1.5 Hz, 1H), 7.08 (d, *J* = 8.7 Hz, 1H), 7.03 (d, *J* = 8.24 Hz, 1H), 6.95 (td, *J* = 7.5, 0.9 Hz, 1H), 3.89 (t, *J* = 6.9 Hz, 2H), 1.72-1.66 (m, 2H), 1.42-1.36 (m, 2H), 1.27-1.21 (m, 4H), 0.84-0.80 (m, 3H) (CO<sub>2</sub>H proton not visible); <sup>13</sup>C NMR (150 MHz, DMSO-*d*<sub>6</sub>) δ: 163.5, 149.4, 144.9, 144.2, 141.7, 132.8, 131.2, 130.5 (2C), 127.7, 127.2, 126.3 (2C), 126.1, 125.1, 124.2, 123.0, 122.7, 118.3, 116.1, 115.9, 109.2, 46.5, 30.8, 26.2, 25.8, 22.1, 13.8; IR (neat, cm<sup>-1</sup>) ν: 2945 (w), 2919 (w), 2852 (w), 2218 (w), 1589 (m), 1573 (m), 1461 (m), 1392 (m), 1249 (m), 1188 (s), 809 (m), 746 (s); HRMS (ASAP+, *m/z*): found 454.1711 (calcd. C<sub>28</sub>H<sub>26</sub>N<sub>2</sub>O<sub>2</sub>S 454.1713, [M\*]<sup>+</sup>).

**Synthesis of (*E*)-2-cyano-3-(5-(10-hexyl-10*H*-phenothiazin-2-yl)thiophen-2-yl)acrylic acid (AFB-23)**

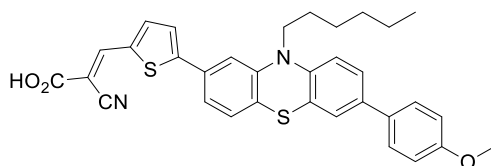
Compound **5** (124 mg, 0.314 mmol) and cyanoacetic acid (535 mg, 6.29 mmol) were dissolved in degassed acetonitrile (38 mL) under nitrogen atmosphere. Piperidine (373  $\mu$ L, 321 mg, 3.77 mmol) was added and the reaction was heated to 80  $^{\circ}$ C for 1 hour before cooling to room temperature, then quenched with HCl (2 M, 150 mL). Ethyl acetate (50 mL) was added and the organic phase was washed with water ( $5 \times 100$  mL), then dried with brine (50 mL) and over anhydrous  $\text{Na}_2\text{SO}_4$ , filtered and the solvents were removed *in vacuo*. The crude product was purified by silica gel column chromatography ( $\text{CH}_2\text{Cl}_2/\text{MeOH}$ , 4:1,  $R_f = 0.16$ ) to obtain sensitizer **AFB-23** as a red solid (128 mg, 0.276 mmol, 88%), mp 160  $^{\circ}$ C (dec.).  $^1\text{H}$  NMR (600 MHz,  $\text{DMSO}-d_6$ )  $\delta$ : 8.36 (s, 1H), 7.91 (d,  $J = 3.9$  Hz, 1H), 7.74 (d,  $J = 3.9$  Hz, 1H), 7.31 (dd,  $J = 8.0$ , 1.7 Hz, 1H), 7.25-7.20 (m, 3H), 7.15 (dd,  $J = 7.6$ , 1.6 Hz, 1H), 7.05 (d,  $J = 8.1$  Hz, 1H), 6.96 (td,  $J = 7.4$ , 1.0 Hz, 1H), 3.94 (t,  $J = 7.0$  Hz, 2H), 1.73-1.67 (m, 2H), 1.43-1.37 (m, 2H), 1.28-1.21 (m, 4H), 0.81 (t,  $J = 7.1$  Hz, 3H) ( $\text{CO}_2\text{H}$  proton not visible);  $^{13}\text{C}$  NMR (150 MHz,  $\text{DMSO}-d_6$ )  $\delta$ : 163.5, 150.8, 145.5, 144.4, 144.1, 139.5, 135.1, 131.9, 127.80, 127.78, 127.1, 125.5, 125.1, 123.0, 122.8, 120.2, 117.4, 116.2, 112.8, 102.3, 46.6, 30.8, 26.1, 25.8, 22.0, 13.8; IR (neat,  $\text{cm}^{-1}$ )  $\nu$ : 2922 (w), 2851 (w), 2216 (w), 1682 (w), 1571 (s), 1410 (m), 1243 (s), 1213 (s), 1184 (s), 1055 (m), 796 (s), 743 (s); HRMS (ASAP+,  $m/z$ ): found 417.1452 (calcd.  $\text{C}_{25}\text{H}_{25}\text{N}_2\text{S}_2$  417.1459,  $[\text{M}-\text{CO}_2+\text{H}]^+$ ).

**Synthesis of (*E*)-2-cyano-3-(4-(10-hexyl-10*H*-phenothiazin-2-yl)phenyl)acrylic acid (AFB-24)**

Compound **4** (196.0 mg, 0.506 mmol) and cyanoacetic acid (874 mg, 10.3 mmol) were dissolved in degassed acetonitrile (60 mL) under nitrogen atmosphere. Piperidine (597  $\mu$ L, 514.0 mg, 6.03 mmol) was added and the reaction was heated to 80  $^{\circ}$ C for 1 hour before cooling to room temperature and quenched in HCl (2 M, 150 mL). Ethyl acetate (50 mL) was added and the organic phase was washed with water ( $8 \times 100$  mL), then dried with brine (50 mL) and over anhydrous  $\text{Na}_2\text{SO}_4$ , filtered and the solvents were removed *in vacuo*. The crude product was purified by silica gel column chromatography ( $\text{CH}_2\text{Cl}_2/\text{MeOH}$ , 4:1,  $R_f = 0.19$ ) to obtain sensitizer **AFB-24** as a red solid (153.0 mg, 0.338 mmol, 67%), mp 238  $^{\circ}$ C (dec.).  $^1\text{H}$  NMR (400 MHz,  $\text{DMSO}-d_6$ )  $\delta$ : 8.06 (s, 1H), 8.00-7.96 (m, 2H), 7.84-7.79 (m, 2H), 7.32-7.26 (m, 2H), 7.24-7.18 (m, 2H), 7.18-7.14 (m, 1H), 7.06-7.01 (m, 1H), 6.98-6.92 (m, 1H), 3.98 (t,  $J = 6.8$  Hz, 2H), 1.75-1.66 (m,

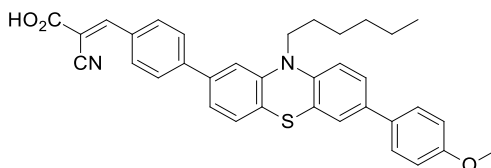
2H), 1.44-1.35 (m, 2H), 1.28-1.19 (m, 4H), 0.84-0.77 (m, 3H) (CO<sub>2</sub>H proton not visible); <sup>13</sup>C NMR (100 MHz, DMSO-*d*<sub>6</sub>) δ: 163.3, 147.7, 145.5, 144.5, 142.0, 138.5, 132.2, 130.1 (2C), 127.6, 127.5, 127.1, 127.0 (2C), 124.1, 123.4, 122.6, 120.9, 118.9, 116.1, 114.1, 112.0, 46.4, 30.8, 26.2, 25.8, 22.0, 13.8; IR (neat, cm<sup>-1</sup>) ν: 2951 (w), 2930 (w), 2847 (w), 2223 (w), 1593 (m), 1460 (m), 1397 (s), 1191 (m), 807 (s), 746 (s); HRMS (ASAP+, *m/z*): found 410.1811 (calcd. C<sub>27</sub>H<sub>26</sub>N<sub>2</sub>S 410.1817, [M-CO<sub>2</sub>]<sup>+</sup>).

#### Synthesis of (*E*)-2-cyano-3-(5-(10-hexyl-7-(4-methoxyphenyl)-10*H*-phenothiazin-2-yl)thiophen-2-yl)acrylic acid (AFB-25)



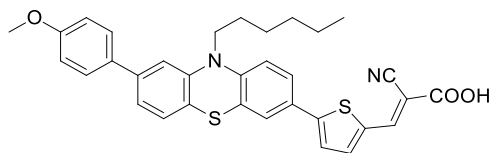
Compound **11** (39 mg, 0.078 mmol) and cyanoacetic acid (133 mg, 1.561 mmol) were dissolved in degassed acetonitrile (10 mL) under nitrogen atmosphere. Piperidine (93 μL, 80.0 mg, 0.937 mmol) was added and the reaction was heated to 80 °C for 2 hours before cooling to room temperature and quenched in HCl (2 M, 50 mL). Ethyl acetate (30 mL) was added and the organic phase was washed with water (3 × 200 mL), then dried with brine (30 mL) and over anhydrous Na<sub>2</sub>SO<sub>4</sub>, filtered and the solvents were removed *in vacuo*. The crude product was purified by silica gel column chromatography (gradient: 0-10% MeOH in CH<sub>2</sub>Cl<sub>2</sub>) to obtain sensitizer **AFB-25** as a brown solid (35 mg, 0.062 mmol, 79%), mp 222 °C (dec.). <sup>1</sup>H NMR (600 MHz, DMSO-*d*<sub>6</sub>) δ: 8.23 (s, 1H), 7.80 (d, *J* = 4.0 Hz, 1H), 7.70 (d, *J* = 4.0 Hz, 1H), 7.58-7.54 (m, 2H), 7.45 (dd, *J* = 8.6, 2.0 Hz, 1H), 7.39 (d, *J* = 2.2 Hz, 1H), 7.29 (dd, *J* = 7.9, 1.6 Hz, 1H), 7.24-7.20 (m, 2H), 7.07 (d, *J* = 8.6 Hz, 1H), 7.00-6.96 (m, 2H), 3.96 (t, *J* = 7.0 Hz, 2H), 3.78 (s, 3H), 1.75-1.69 (m, 2H), 1.45-1.39 (m, 2H), 1.29-1.23 (m, 4H), 0.84-0.80 (m, 3H) (CO<sub>2</sub>H proton not visible); <sup>13</sup>C NMR (150 MHz, DMSO-*d*<sub>6</sub>) δ: 163.6, 158.7, 149.2, 145.3, 142.7, 142.2, 137.6, 135.7, 134.4, 132.2, 131.2, 127.8, 127.2 (2C), 125.4, 124.9, 124.6, 124.5, 123.5, 120.0, 118.3, 116.4, 114.3 (2C), 112.5, 106.2, 55.1, 46.7, 30.8, 26.1, 25.8, 22.0, 13.8; IR (neat, cm<sup>-1</sup>) ν: 2924 (w), 2851 (s), 2215 (w), 1577 (m), 1376 (s), 1240 (s), 1177 (m), 1047 (w), 1025 (w), 797 (s), 530 (w), 509 (w); HRMS (ASAP+, *m/z*): found 523.1874 (calcd. C<sub>32</sub>H<sub>31</sub>N<sub>2</sub>OS<sub>2</sub> 523.1878, [M-CO<sub>2</sub>+H]<sup>+</sup>).

#### Synthesis of (*E*)-2-cyano-3-(4-(10-hexyl-7-(4-methoxyphenyl)-10*H*-phenothiazin-2-yl)phenyl)acrylic acid (AFB-26)

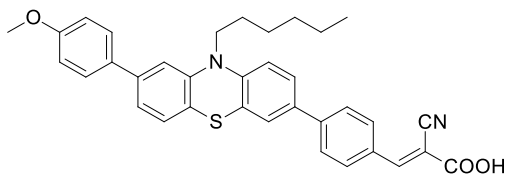


Compound **10** (175.0 mg, 0.354 mmol) and cyanoacetic acid (603 mg, 7.09 mmol) were dissolved in degassed acetonitrile (40 mL) under nitrogen atmosphere. Piperidine (421  $\mu$ L, 362.0 mg, 4.25 mmol) was added and the reaction was heated to 80 °C for 25 min before cooling to room temperature and quenched in HCl (2 M, 100 mL). Ethyl acetate (30 mL) was added and the organic phase was washed with water (3  $\times$  200 mL), then dried with brine (30 mL) and over anhydrous Na<sub>2</sub>SO<sub>4</sub>, filtered and the solvents were removed *in vacuo*. The crude product was purified by silica gel column chromatography (gradient: 0-4% MeOH in CH<sub>2</sub>Cl<sub>2</sub>) to obtain sensitizer **AFB-26** as a brown solid (163.0 mg, 0.291 mmol, 82%), mp 190 °C (dec.). <sup>1</sup>H NMR (400 MHz, DMSO-*d*<sub>6</sub>)  $\delta$ : 8.28 (s, 1H), 8.10 (d, *J* = 8.6 Hz, 2H), 7.90 (d, *J* = 8.6 Hz, 2H), 7.57 (d, *J* = 8.9 Hz, 2H), 7.45 (dd, *J* = 8.5, 2.2 Hz, 1H), 7.40 (d, *J* = 2.2 Hz, 1H), 7.36-7.30 (m, 2H), 7.26 (d, *J* = 7.9 Hz, 1H), 7.07 (d, *J* = 8.6 Hz, 1H), 6.98 (d, *J* = 8.9 Hz, 2H), 4.01 (t, *J* = 6.7 Hz, 2H), 3.78 (s, 3H), 1.78-1.68 (m, 2H), 1.47-1.37 (m, 2H), 1.31-1.21 (m, 4H), 0.85-0.79 (m, 3H) (CO<sub>2</sub>H proton not visible); <sup>13</sup>C NMR (100 MHz, DMSO-*d*<sub>6</sub>)  $\delta$ : 163.3, 158.6, 151.8, 145.3, 143.4, 143.1, 138.3, 134.3, 131.3, 131.1, 131.0 (2C), 127.63, 127.61, 127.20 (2C), 127.16 (2C), 125.3, 124.5, 124.1, 123.9, 121.0, 116.3, 114.3 (2C), 114.0, 106.0, 55.1, 46.5, 30.8, 26.2, 25.8, 22.1, 13.8; IR (neat, cm<sup>-1</sup>)  $\nu$ : 2952 (w), 2924 (w), 2848 (w), 1700 (m), 1588 (s), 1462 (s), 1403 (m), 1273 (m), 1242 (s), 1219 (s), 1191 (s), 805 (s), 443 (w); HRMS (ASAP+, *m/z*): found 517.2305 (calcd. C<sub>34</sub>H<sub>33</sub>N<sub>2</sub>OS 517.2314, [M-CO<sub>2</sub>+H]<sup>+</sup>).

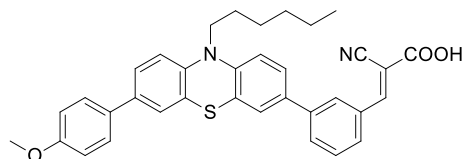
#### Synthesis of (*E*)-2-cyano-3-(5-(10-hexyl-8-(4-methoxyphenyl)-10*H*-phenothiazin-3-yl)thiophen-2-yl)acrylic acid (AFB-27)



Compound **13** (150 mg, 0.30 mmol) and cyanoacetic acid (511 mg, 6.00 mmol) were dissolved in degassed acetonitrile (36 mL) under nitrogen atmosphere. Piperidine (357  $\mu$ L, 307 mg, 3.60 mmol) was added and the reaction was heated to 80 °C for 1 hour before cooling to room temperature and quenched in HCl (2 M, 100 mL). Ethyl acetate (30 mL) was added and the organic phase was washed with water (3  $\times$  200 mL), then dried with brine (30 mL) and over anhydrous Na<sub>2</sub>SO<sub>4</sub>, filtered and the solvents were removed *in vacuo*. The crude product was purified by silica gel column chromatography (gradient: 0-2% MeOH in CH<sub>2</sub>Cl<sub>2</sub>) to obtain sensitizer **AFB-27** as a dark solid (166 mg, 0.294 mmol, 98%), mp 213 °C (dec.). <sup>1</sup>H NMR (600 MHz, DMSO-*d*<sub>6</sub>)  $\delta$ : 8.35 (s, 1H), 7.89 (d, *J* = 4.1 Hz, 1H), 7.65 (d, *J* = 3.9 Hz, 1H), 7.60 (d, *J* = 8.8 Hz, 2H), 7.57-7.54 (m, 2H), 7.20-7.17 (m, 3H), 7.08 (d, *J* = 8.7 Hz, 1H), 7.01 (d, *J* = 8.8 Hz, 2H), 3.99 (t, *J* = 6.8 Hz, 2H), 3.79 (s, 3H), 1.74-1.69 (m, 2H), 1.43-1.38 (m, 2H), 1.27-1.22 (m, 4H), 0.83-0.79 (m, 3H) (CO<sub>2</sub>H proton not visible); <sup>13</sup>C NMR (150 MHz, DMSO-*d*<sub>6</sub>)  $\delta$ : 163.7, 159.0, 150.7, 145.6, 144.7, 144.4, 140.0, 139.7, 134.3, 132.0, 127.7 (2C), 127.5, 126.8, 125.7, 124.5, 124.2, 124.1, 121.1, 120.8, 117.4, 116.4, 114.3 (2C), 113.9, 100.9, 55.2, 46.6, 30.8, 26.2, 25.8, 22.0, 13.8; IR (neat, cm<sup>-1</sup>)  $\nu$ : 2953 (w), 2911 (w), 2851 (w), 2218 (w), 1681 (m), 1569 (s), 1397 (s), 1247 (s), 1213 (s), 1167 (s), 1061 (m), 793 (s), 731 (m), 452 (w); HRMS (TOF ESI-, *m/z*): found 521.1718 (calcd. C<sub>32</sub>H<sub>29</sub>N<sub>2</sub>OS<sub>2</sub> 521.1721, [M-CO<sub>2</sub>-H]<sup>-</sup>).

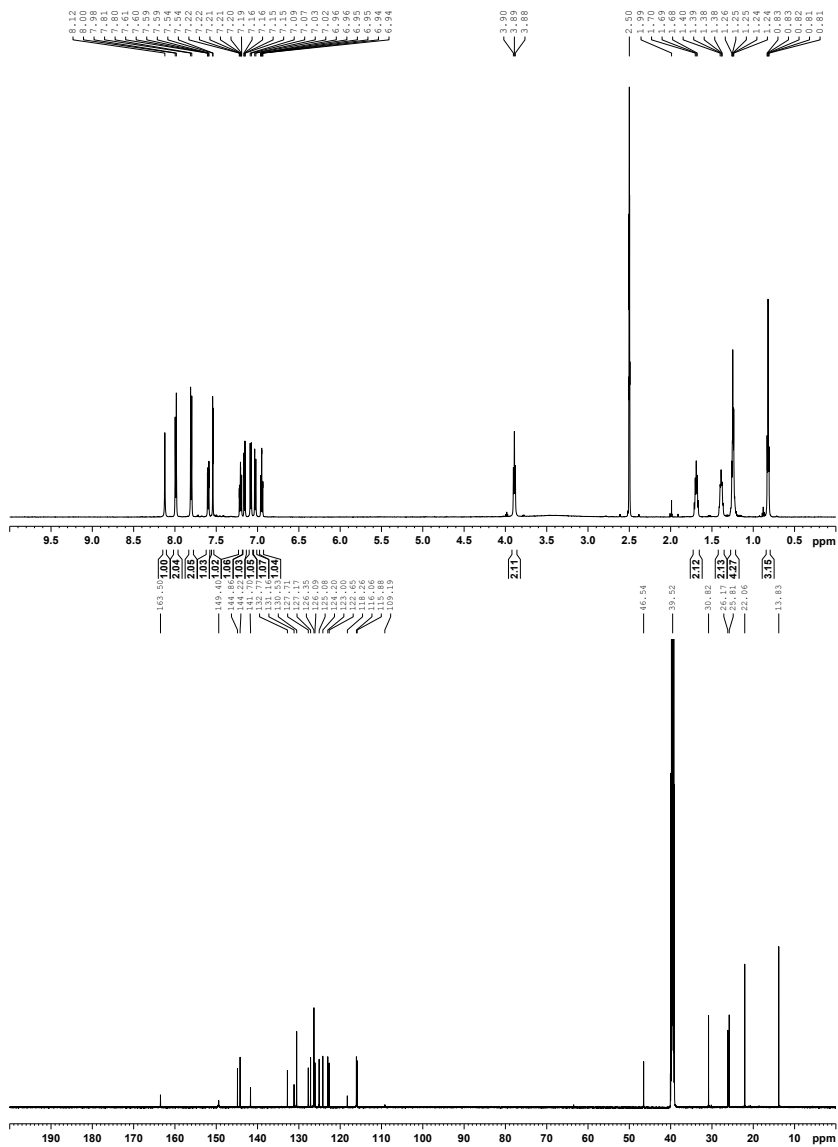
**Synthesis of (*E*)-2-cyano-3-(4-(10-hexyl-8-(4-methoxyphenyl)-10*H*-phenothiazin-3-yl)phenyl)acrylic acid (AFB-28)**

Compound **12** (175 mg, 0.354 mmol) and cyanoacetic acid (603 mg, 7.09 mmol) were dissolved in degassed acetonitrile (40 mL) under nitrogen atmosphere. Piperidine (421  $\mu$ L, 362 mg, 4.25 mmol) was added and the reaction was heated to 80  $^{\circ}$ C for 25 min before cooling to room temperature and quenched in HCl (2 M, 100 mL). Ethyl acetate (30 mL) was added and the organic phase was washed with water ( $3 \times 200$  mL), then dried with brine (30 mL) and over anhydrous  $\text{Na}_2\text{SO}_4$ , filtered and the solvents were removed *in vacuo*. The crude product was purified by silica gel column chromatography (gradient: 0-2% MeOH in  $\text{CH}_2\text{Cl}_2$ ) to obtain sensitizer **AFB-28** as a dark solid (180 mg, 0.322 mmol, 91%), mp 189  $^{\circ}$ C (dec.).  $^1\text{H}$  NMR (400 MHz,  $\text{DMSO}-d_6$ )  $\delta$ : 8.18 (s, 1H), 8.03 (d,  $J = 8.6$  Hz, 2H), 7.84 (d,  $J = 8.6$  Hz, 2H), 7.65-7.56 (m, 4H), 7.20-7.16 (m, 3H), 7.11 (d,  $J = 8.6$  Hz, 1H), 7.02 (d,  $J = 9.0$  Hz, 2H), 4.01 (t,  $J = 6.7$  Hz, 2H), 3.80 (s, 3H), 1.78-1.69 (m, 2H), 1.47-1.37 (m, 2H), 1.31-1.21 (m, 4H), 0.85-0.79 (m, 3H) ( $\text{CO}_2\text{H}$  proton not visible);  $^{13}\text{C}$  NMR (100 MHz,  $\text{DMSO}-d_6$ )  $\delta$ : 163.3, 159.0, 150.8, 144.9, 144.8, 142.1, 139.6, 132.7, 132.1, 130.85, 130.79 (2C), 127.7 (2C), 127.5, 126.4 (2C), 126.11, 126.09, 125.1, 124.3, 121.5, 120.6, 117.7, 116.3, 114.3 (2C), 113.8, 55.2, 46.6, 30.8, 26.2, 25.8, 22.0, 13.8; IR (neat,  $\text{cm}^{-1}$ )  $\nu$ : 2951 (w), 2924 (w), 2852 (w), 2221 (w), 1692 (w), 1579 (s), 1463 (s), 1246 (s), 1177 (s), 1027 (w), 803 (s), 518 (w); HRMS (ASAP+,  $m/z$ ): found 560.2127 (calcd.  $\text{C}_{35}\text{H}_{32}\text{N}_2\text{O}_3\text{S}$  560.2134,  $[\text{M}^*]^+$ ).

**Synthesis of (*E*)-2-cyano-3-(3-(10-hexyl-7-(4-methoxyphenyl)-10*H*-phenothiazin-3-yl)phenyl)acrylic acid (AFB-29)**

Compound **15** (210 mg, 0.425 mmol) and cyanoacetic acid (724 mg, 8.50 mmol) were dissolved in degassed acetonitrile (51 mL) under nitrogen atmosphere. Piperidine (505  $\mu$ L, 435 mg, 5.10 mmol) was added and the reaction was heated to 80  $^{\circ}$ C for 30 min before cooling to room temperature and quenched in HCl (2 M, 150 mL). Ethyl acetate (50 mL) was added and the organic phase was washed with water ( $8 \times 100$  mL), then dried with brine (50 mL) and over anhydrous  $\text{Na}_2\text{SO}_4$ , filtered and the solvents were removed *in vacuo*.

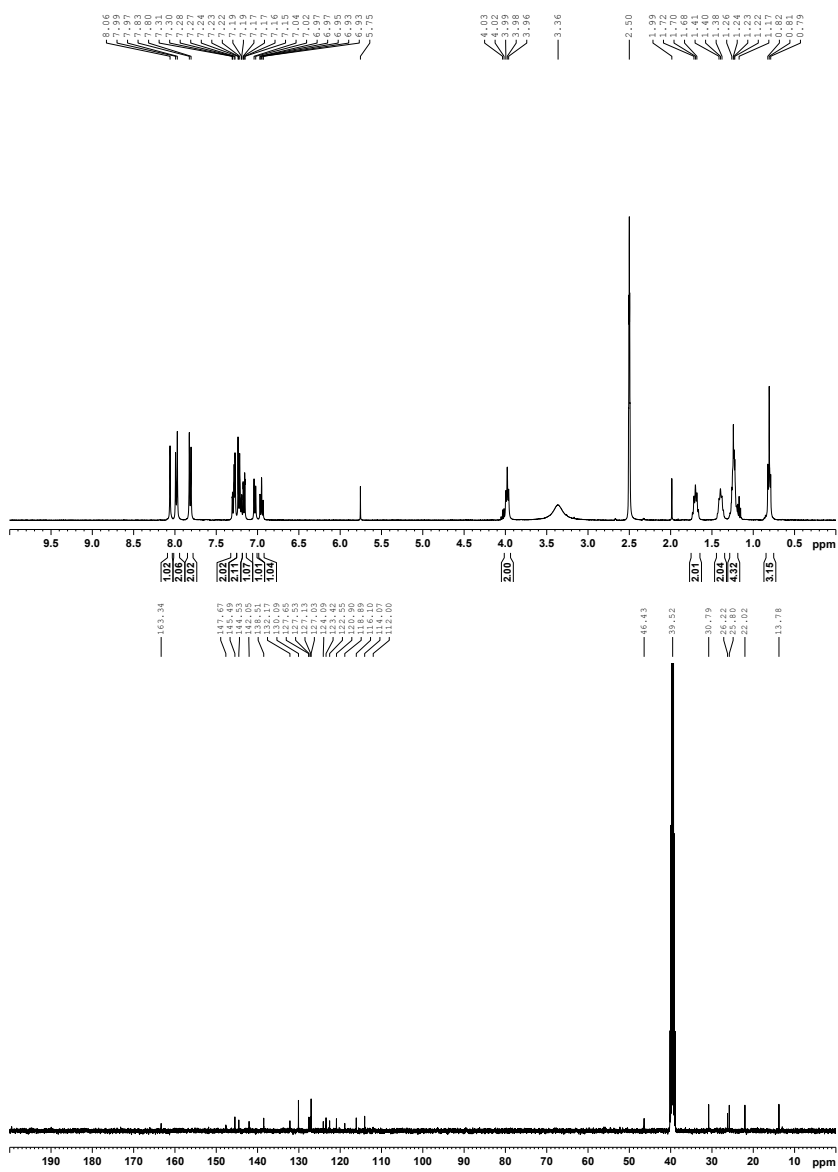
The crude product was purified by silica gel column chromatography (gradient: 0-15% MeOH in CH<sub>2</sub>Cl<sub>2</sub>) to obtain sensitizer **AFB-29** as a dark brown solid (202 mg, 0.361 mmol, 85%), mp 145 °C (dec.). <sup>1</sup>H NMR (600 MHz, DMSO-*d*<sub>6</sub>) δ: 8.24 (s, 1H), 8.21 (s, 1H), 7.90 (d, *J* = 7.7 Hz, 1H), 7.80 (d, *J* = 7.7 Hz, 1H), 7.60-7.53 (m, 4H), 7.51 (d, *J* = 2.0 Hz, 1H), 7.44 (dd, *J* = 8.5, 2.1 Hz, 1H), 7.40 (d, *J* = 2.1 Hz, 1H), 7.10 (d, *J* = 8.5 Hz, 1H), 7.05 (d, *J* = 8.6 Hz, 1H), 6.98 (d, *J* = 8.7, 2H), 3.90 (t, *J* = 6.9 Hz, 2H), 3.78 (s, 3H), 1.74-1.68 (m, 2H), 1.44-1.38 (m, 2H), 1.28-1.22 (m, 4H), 0.85-0.81 (m, 3H) (CO<sub>2</sub>H proton not visible); <sup>13</sup>C NMR (150 MHz, DMSO-*d*<sub>6</sub>) δ: 163.2, 158.6, 150.7, 144.3, 142.9, 139.5, 134.3, 133.1 (2C), 131.3, 129.7, 129.2, 128.0, 127.6, 127.1 (2C), 125.9, 125.3, 125.0, 124.5, 123.8, 123.5, 117.9, 116.03, 115.99, 114.3 (2C), 109.7, 55.1, 46.6, 30.8, 26.2, 25.8, 22.1, 13.8; IR (neat, cm<sup>-1</sup>) ν: 2925 (w), 2852 (w), 2220 (w), 1604 (m), 1463 (s), 1389 (m), 1239 (s), 1177 (m), 1025 (w), 796 (s), 683 (m), 526 (w); HRMS (ASAP+, *m/z*): found 516.2232 (calcd. C<sub>34</sub>H<sub>32</sub>N<sub>2</sub>OS 516.2235, [M-CO<sub>2</sub>]<sup>+</sup>).

NMR Spectra  
AFB-22Figure S8.  $^1\text{H}$  and  $^{13}\text{C}$  NMR spectra for AFB-22.





## AFB-24

Figure S10.  $^1\text{H}$  and  $^{13}\text{C}$  NMR spectra for AFB-24.











## References

1. A. F. Buene, N. Uggerud, S. P. Economopoulos, O. R. Gautun and B. H. Hoff, *Dyes Pigm.*, 2018, **151**, 263-271.
2. A. F. Buene, E. E. Ose, A. G. Zakariassen, A. Hagfeldt and B. H. Hoff, *J. Mater. Chem. A*, 2019, **7**, 7581-7590.
3. A. W. Franz, Z. Zhou, R. Turdean, A. Wagener, B. Sarkar, M. Hartmann, S. Ernst, W. R. Thiel and T. J. J. Müller, *European Journal of Organic Chemistry*, 2009, **2009**, 3895-3905.





## PAPER IV

**Effect of furan  $\pi$ -spacer and triethylene oxide methyl ether substituents on performance of phenothiazine sensitizers in dye-sensitized solar cells**

Reprinted with permission from the Centre National de la Recherche Scientifique (CNRS) and The Royal Society of Chemistry.



NJC



PAPER

View Article Online

View Journal | View Issue



Cite this: *New J. Chem.*, 2019, 43, 9403

## Effect of furan $\pi$ -spacer and triethylene oxide methyl ether substituents on performance of phenothiazine sensitizers in dye-sensitized solar cells†

Audun Formo Buene,<sup>a</sup> Nanna Boholm,<sup>b</sup> Anders Hagfeldt<sup>c</sup> and Bård Helge Hoff<sup>b,\*</sup>

Conjugated  $\pi$ -spacers are used to improve the light harvesting properties of sensitizers for dye-sensitized solar cells. In several recent works, furan has outperformed other popular  $\pi$ -spacers such as thiophene and phenyl. One of the best performing phenothiazine dyes in the literature has no  $\pi$ -spacer, and two polar triethylene oxide methyl ether (TEOME) chains. Herein we report the synthesis and evaluation of three novel sensitizers based on **EO3**, investigating the effect of introducing a furan linker and stepwise removal of the TEOME chains. The furan linker redshifted the onsets in the IPCE spectra by 50 nm and improved the PCE by up to 29% compared to **EO3**, despite lowering the  $V_{OC}$  by more than 60 mV. The best sensitizer of the study was **AFB-30**, with an average PCE of 5.86% ( $J_{SC} = 10.41 \text{ mA cm}^{-2}$ ,  $V_{OC} = 783 \text{ mV}$ , FF = 0.73) under 1 sun AM 1.5G illumination.

Received 3rd April 2019,  
Accepted 15th May 2019

DOI: 10.1039/c9nj01720h

rsc.li/njc

### Introduction

The introduction of dye-sensitized solar cells made quite a stir in 1991, when Michael Grätzel and Brian O'Regan published the remarkably efficient photoelectrochemical cell using light harvesting sensitizers anchored on mesoporous titania nanoparticles.<sup>1</sup> Since then, a number of great advancements have been made within the field of dye-sensitized solar cells (DSSCs). Although still popular, focus has largely moved from rare earth metal complex sensitizers to fully organic sensitizers.<sup>2</sup> Advantages such as higher extinction coefficients and a larger available toolbox of reliable organic reactions favour the organic sensitizers.<sup>3</sup>

Increasing the efficiency and stability is always a high priority in solar cell research. For the field of DSSCs, dye development strives to increase the light harvesting properties and the development of new semiconducting oxides and redox shuttles are improving the photovoltages of the devices.<sup>4,5</sup> Fully organic sensitizers are commonly based a donor- $\pi$ -acceptor design, where the donor is an electron rich conjugated system such as triarylamine,<sup>6</sup> coumarins,<sup>7,8</sup> carbazole<sup>9,10</sup> or phenothiazine<sup>11</sup>

among many others. The acceptor is electron deficient, often also acting as the anchoring group, resulting in a push-pull system which is transferring charge upon excitation. Because the photon flux in the solar spectrum is finite, increasing the absorption of the sensitizers is crucial in improving the photocurrents. A common design strategy to accomplish this is the introduction of  $\pi$ -spacers.<sup>12</sup> A range of spacers have been reported in the dye literature, ranging from the very simple, such as a single double bond,<sup>13</sup> various aromatic and heteroaromatic spacers,<sup>14-16</sup> to the more complex electron withdrawing units such as diketopyrrolo-pyrrole<sup>17</sup> or benzothiadiazole.<sup>18</sup>

Much effort has also been devoted to developing solid-state DSSCs,<sup>19</sup> and one of the most recent advancements is the discovery of the so-called 'Zombie cells' improving on the already efficient cells based on solid hole conducting materials such as spiro-OMeTAD.<sup>20</sup> Another direction for the DSSC field is the development of aqueous electrolytes.<sup>21</sup> Water has a higher boiling point than most organic solvents commonly used in DSSC electrolytes and most salts are excellently soluble in it. There are a number of aqueous iodide electrolytes reported in the literature,<sup>21,22</sup> and fully organic redox couple aqueous electrolytes have also successfully been developed.<sup>23</sup> The first aqueous cobalt electrolyte was reported by Spiccia *et al.* in 2013.<sup>24</sup> Later, cobalt complexes have been reengineered for increased water solubility avoiding the use of surfactants, producing very efficient aqueous DSSCs with 5.5% PCE.<sup>25</sup>

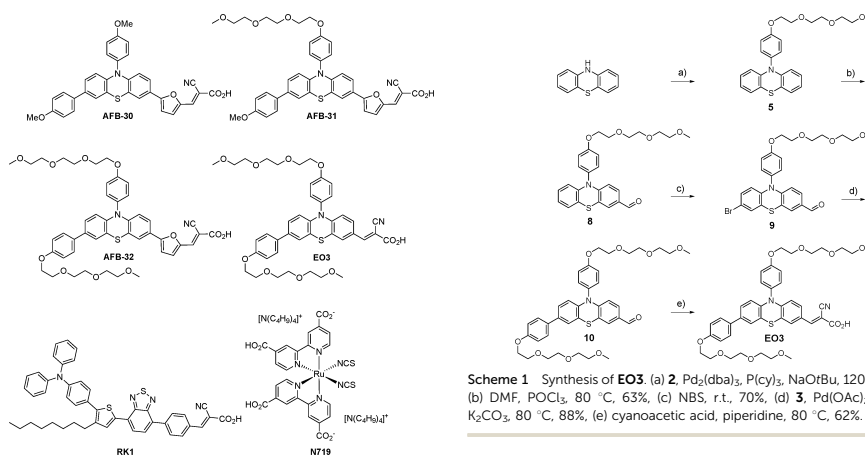
Despite the alluring advantages of aqueous electrolytes, the best power conversion efficiency of an aqueous DSSC reported

<sup>a</sup> Department of Chemistry, Norwegian University of Science and Technology, Høgskoleringen 5, NO-7491 Trondheim, Norway. E-mail: bard.h.hoff@ntnu.no; Tel: +47 73593973

<sup>b</sup> Department of Chemistry, Aarhus University, DK-8000 Aarhus, Denmark

<sup>c</sup> Laboratory of Photomolecular Science, Institute of Chemical Sciences and Engineering, École Polytechnique Fédérale de Lausanne (EPFL), Chemin des Alambics, Station 6, CH-1015 Lausanne, Switzerland

† Electronic supplementary information (ESI) available. See DOI: 10.1039/c9nj01720h



**Scheme 1** Synthesis of **EO3**. (a) **2**, Pd<sub>2</sub>(dba)<sub>3</sub>, P(cy)<sub>3</sub>, NaOtBu, 120 °C, 66%, (b) DMF, POCl<sub>3</sub>, 80 °C, 63%, (c) NBS, r.t., 70%, (d) **3**, Pd(OAc)<sub>2</sub>, SPhos, K<sub>2</sub>CO<sub>3</sub>, 80 °C, 88%, (e) cyanoacetic acid, piperidine, 80 °C, 62%.

**Fig. 1** Structures of sensitizers **AFB-30** to **32**, **EO3**, **RK1** and **N719**.

to date is a modest 5.97%, achieved by Lin and coworkers with the phenothiazine sensitizer **EO3**.<sup>26</sup> This sensitizer incorporates two hydrophilic TEOME chains, which increases the wetting of the TiO<sub>2</sub>, chelates Li<sup>+</sup> ions, while also repressing sensitizer aggregation.<sup>27–29</sup> A remarkable efficiency of 9.98% PCE under 1 sun AM 1.5G illumination for **EO3** with an organic solvent-based electrolyte was also achieved, despite the very limited absorption onset of 551 nm.<sup>26</sup>

This study is focusing on improving the photophysical properties of **EO3** by introducing a  $\pi$ -spacer between the phenothiazine donor and the cyanoacrylic acid anchoring group. In a few recent publications, furan has been reported to outperform thiophene as a  $\pi$ -spacer.<sup>12,30–32</sup> Thus, we chose furan for extending the conjugation of **EO3**. We also wanted to investigate the effect of the TEOME chains, so in addition to **EO3**, three furan  $\pi$ -spacer dyes with zero, one and two TEOM-groups were synthesized, shown in Fig. 1.

## Results and discussion

### Synthesis

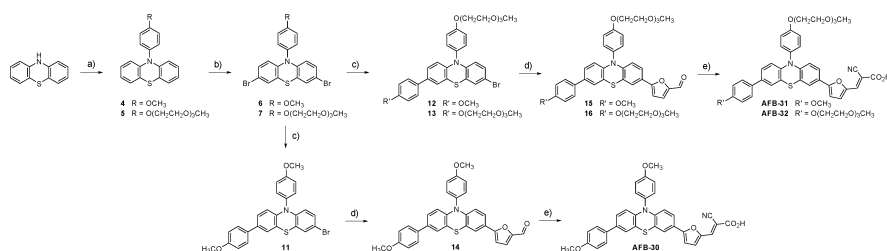
The synthesis of the literature dye **EO3** followed a synthetic route much the same as the one reported by Lin and coworkers.<sup>26</sup> An overview of the total reaction sequence is found in Scheme 1. All synthesis details can be found in the ESI.†

Compound **5** was prepared through a Buchwald–Hartwig cross coupling in over 10 g scale. Despite being a highly reliable reaction, the purification and removal of palladium are the challenges in this step. Further, a Vilsmeier–Haack formylation on **5** gave compound **8** in 63% yield, and brominations with *N*-bromosuccinimide (NBS) gave compound **9** in 70% yield. In the penultimate step, a Suzuki coupling was employed to

introduce the auxiliary donor in 80% yield using an aryl boronic ester prepared inhouse (**3**) before employing the Knoevenagel condensation for converting the aldehyde into the cyanoacrylic acid anchoring group present in all these sensitizers.

A route previously used by Iqbal and coworkers lay the foundations for the synthesis towards the AFB dyes, see Scheme 2.<sup>33</sup> A Buchwald coupling introduced the *N*-aryl substituents, while a dibromination with NBS separates this route from the previous method used for **EO3**. The brominations are efficient reactions and the products were obtained as convenient solid materials. Further, two sequential Suzuki cross couplings are performed. The first introduces the auxiliary donors in a non-selective manner also leading to the formation of the dicoupled byproducts, lowering the yields considerably. The second Suzuki coupling introduces the furan  $\pi$ -bridge from 5-formyl-2-furanylboronic acid, while the Knoevenagel condensation is used for the anchor group installation.

The melting points of the two dyes with two TEOME chains (**EO3** and **AFB-32**) were observed around 125 °C, while no melting point was observed for **AFB-30** and **31**. This suggests the TEOME chains decrease the crystallinity of the sensitizers. Upon further heating, visible decompositions were observed at the following temperatures: 145 °C (**AFB-31**) < 150 °C (**AFB-32**) < 170 °C (**EO3**) < 264 °C (**AFB-30**). We assume the observed decomposition is a decarboxylation because of visible gas formation. The high decomposition temperature of **AFB-30** was intriguing, and we suspected this to have one of two possible explanations. Either the presence of TEOME chains lowers the thermal stability, or the first decarboxylation step was not detected in the manual melting point analyses of **AFB-30**. We suspected the latter to be the case, because the molecular landscape around the anchoring cyanoacrylic acid is identical for all the AFB dyes, thus similar decarboxylation behaviours were expected. In order to conclude, we performed thermogravimetric analyses on all four dyes under air to investigate the decomposition as a function of temperature, and the results are plotted in Fig. 2.

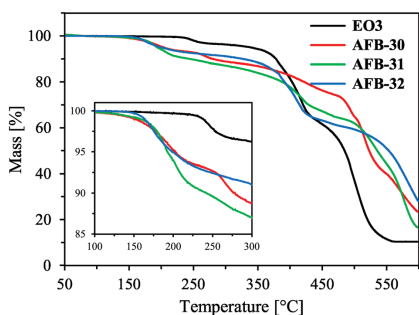


**Scheme 2** Synthesis route to AFB dyes. (a) **2** or 4-bromoanisole,  $\text{Pd}_2(\text{dba})_3$ ,  $\text{P}(\text{cy})_3$ ,  $\text{NaOtBu}$ ,  $120\text{ }^\circ\text{C}$ . (b) NBS, r.t., (c) for prod. **11/12**:  $\text{Pd}(\text{PPh}_3)_2$ ,  $\text{K}_2\text{CO}_3$ ,  $80\text{ }^\circ\text{C}$ , **13**:  $\text{Pd}(\text{OAc})_2$ , SPhos,  $\text{K}_2\text{CO}_3$ ,  $80\text{ }^\circ\text{C}$ . (d) (5-formyl-2-furanyl)boronic acid,  $\text{Pd}(\text{OAc})_2$ , SPhos,  $\text{K}_2\text{CO}_3$ ,  $80\text{ }^\circ\text{C}$ . (e) cyanoacetic acid, piperidine,  $80\text{ }^\circ\text{C}$ .

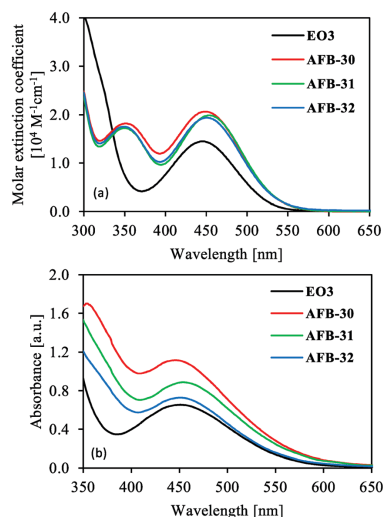
A number of decomposition steps are observed for the four sensitizers in Fig. 2. The weight losses in the first steps are proportional in size to be attributed to decarboxylation processes. The decarboxylations are observed around  $150\text{ }^\circ\text{C}$  for all the AFB sensitizers while **EO3** does not decompose until  $225\text{ }^\circ\text{C}$ . This indicates the introduction of the furan  $\pi$ -spacer does affect the thermal stability negatively compared to **EO3**. Fortunately, despite the lowered thermal stability, under no part of the fabrication process or device operation will the sensitizers be subjected to temperatures in this range. However, it must be stressed that the chemical environment in devices cannot be compared to TGA analysis under air, so any device stability claims would have to be investigated by other means.

#### Photophysical properties

The solution and  $\text{TiO}_2$  film UV/Vis absorption spectra of the three sensitizers and **EO3** are shown in Fig. 3, with the extracted data in Table 1. In solution, both hyper- and bathochromic shifts of the ICT band are observed upon the introduction of the furan  $\pi$ -spacer. In the region 350–400 nm a significant improvement in absorption can be seen for the AFB dyes as compared to **EO3** (Fig. 3a). This can only be attributed to the increase in conjugation from the furan unit. On  $\text{TiO}_2$  films the



**Fig. 2** Thermogravimetric curves for the four sensitizers measured under air atmosphere. Inset shows the decarboxylation region.



**Fig. 3** UV/Vis absorption properties of sensitizers **AFB-30** to **32** compared to the literature dye **EO3**. (a) Measured in THF solution (0.02 mM), (b) measured on screen printed  $\text{TiO}_2$  films ( $2.5\text{ }\mu\text{m}$  18NR-T on TEC10 FTO glass).

differences are most prominent in the intensities of the ICT bands, and the relative extinction coefficients increased in the order  $\text{EO3} < \text{AFB-32} < \text{AFB-31} < \text{AFB-30}$ . The order mirrors the extinction coefficients from solution, but the differences are larger. This could be caused by minute variances in thickness of the  $\text{TiO}_2$  films, but dye loading could also certainly play a role. The ICT peak position did not change when the dyes were anchored on  $\text{TiO}_2$  compared to in solution, suggesting no aggregation issues with any of the dyes. However, a considerable broadening of the absorption was observed, shifting the absorption onset towards the red by about 50 nm.

From the emission spectra (Fig. S2, ESI<sup>†</sup>), a peak shift of 16–21 nm is observed when introducing the furan moiety.

Table 1 Photophysical properties of dyes **AFB-30** to **32** and **EO3**

Dye	$\lambda_{\text{abs}}^a$ (nm)	$\epsilon$ ( $\text{M}^{-1} \text{cm}^{-1}$ )	Em. <sup>b</sup> (nm)	$\lambda_{\text{abs}}^c$ on $\text{TiO}_2$ (nm)	Rel. $\epsilon$ on $\text{TiO}_2$	$E_{0-0}^d$ (eV)	$E_{0-0}^e$ (eV)	$E_{\text{ox}}^f$ (V)	$E_{\text{LUMO}}^g$ (V)
<b>EO3</b>	446	14 448	584	451	1.00	2.38	2.36	1.07	-1.31
<b>AFB-30</b>	449	20 634	603	446	1.70	2.38	2.32	0.96	-1.42
<b>AFB-31</b>	454	19 844	605	454	1.36	2.39	2.32	0.93	-1.46
<b>AFB-32</b>	451	19 385	600	451	1.11	2.39	2.32	0.93	-1.46

<sup>a</sup> Maximum of most red-shifted peak. <sup>b</sup> Emission when ICT band is excited, in THF solution. <sup>c</sup> Maximum of most red-shifted peak on  $\text{TiO}_2$  (2.5  $\mu\text{m}$ , 18NR-T). <sup>d</sup> Calculated from the intersection of the absorption and normalized emission spectra in solution. <sup>e</sup> Calculated from the absorption onset in solution. <sup>f</sup> Measured vs.  $\text{Fc}^+/\text{Fc}$  on stained  $\text{TiO}_2$  electrodes in acetonitrile with 0.1 M LiTFSI, converted to V vs. SHE by 0.624 V. Scan rate 20  $\text{mV s}^{-1}$ . <sup>g</sup> Calculated from  $E_{\text{ox}} - E_{0-0}$ .

Despite the shifted peak positions, when the emission spectra are normalized to the absorption spectra, virtually identical optical bandgaps are obtained for all the four sensitizers from the absorption-emission intersection. We expected the increased conjugation from the furan moieties to lower the bandgaps. Optical bandgaps can alternatively be obtained by the absorption onset estimated from where the tangent to the ICT peak crosses the baseline. When using this method an optical bandgap of 2.36 eV is obtained for **EO3**, and 2.32 eV for all three AFB dyes, see Table 1.

### Electrochemical properties

Cyclic voltammetry of the sensitizers adsorbed on  $\text{TiO}_2$  was measured in acetonitrile with 0.1 M LiTFSI supporting electrolyte with a scan rate of 20  $\text{mV s}^{-1}$ . The electrodes had no blocking layer, a 6  $\mu\text{m}$  screen printed layer of 18 NR-T  $\text{TiO}_2$  paste on FTO glass, no scattering layer and no CDCA in the staining solutions. The cyclic voltammograms can be found in the ESI† (Fig. S4). The  $E_{1/2}$  value of  $\text{Fc}^+/\text{Fc}$  vs.  $\text{Ag}/\text{AgCl}$  was found at 0.2216 V. The subsequent measurements are given in Table 1 vs. SHE by the conversion constant of 624 mV.<sup>34</sup> We find the described method to be a highly efficient way of measuring the oxidation potentials of sensitizers, with the added benefit of the methodology being more closely related to actual device operating conditions. Reversible oxidation peaks were recorded for all the sensitizers. However, as the stability of the oxidized sensitizers usually is very limited, a fading of the signal is observed upon multiple cycles especially at low scan rates.

The oxidation potential of the literature dye **EO3** was found at 1.07 V vs. SHE, only 30 mV away from the reported value of 1.04 V vs. NHE in solution. Li and coworkers further developed **EO3** by closing one of the triethylene oxide methyl ether chains into a 12-crown-4 ether (**DCE1**).<sup>35</sup> The reported photophysical properties of **DCE1** are very similar to the values obtained for **EO3** in this work.

As the oxidation potential of **EO3** is 1.07 V vs. SHE, it is clear that the introduction of the furan  $\pi$ -spacer lifts the HOMO levels significantly, as presented visually in Fig. 4. The extracted oxidation potentials of **AFB-31** and **AFB-32** are indistinguishable by cyclic voltammetry at 0.93 V vs. SHE, while the value for **AFB-30** is slightly lower at 0.96 V vs. SHE. **AFB-30** is the only sensitizer without any TEOME chains, and the difference in oxidation potential could arise from the interactions of these moieties with the lithium cations present in the supporting electrolyte, marginally raising the oxidation potentials of **AFB-31** and **AFB-32**. For the  $\Gamma^-/\text{I}_3^-$  electrolyte, the HOMO and LUMO

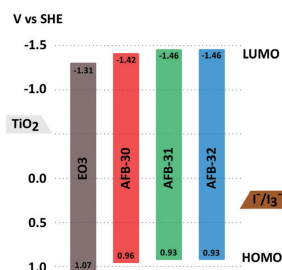


Fig. 4 Energy level diagram displaying the bandgap size and position of HOMO and LUMO of **EO3** and the AFB sensitizers.

positions are suitable for efficient electron injection and dye regeneration to take place.

### Photovoltaic performance

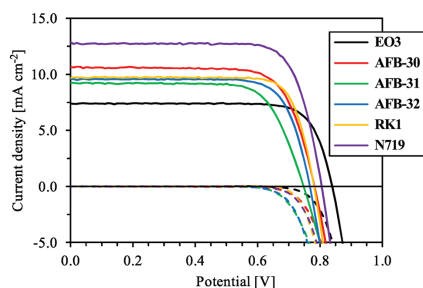
The photovoltaic performance of the devices fabricated with the novel sensitizers, **EO3** and the references **N719** and **RK1**<sup>36</sup> was evaluated. Data from  $J$ - $V$  sweeps under 1 sun AM 1.5G illumination and from incident photon-to-current conversion efficiency (IPCE) measurements are given in Table 2.

The photovoltaic measurements using the  $\Gamma^-/\text{I}_3^-$  electrolyte A6141<sup>37</sup> show that the introduction of the furan  $\pi$ -spacer increases the current, but at a considerable cost in the voltage, see Fig. 5. Similar behaviour in photovoltage has been observed previously in studies on phenothiazine dyes with and without  $\pi$ -spacers.<sup>31,38</sup> A direct comparison between **AFB-32** and **EO3**, only differing in the furan  $\pi$ -spacer, shows an increased performance by 16%. Among the AFB dyes, **AFB-30** is the most efficient at 5.86% PCE, comparable in performance to the literature dye **RK1** previously delivering over 10% PCE.<sup>36</sup> In the dark current measurements, no leaking could be observed from any of the devices, which confirms the recombination pathway from the  $\text{TiO}_2$  to  $\text{I}_3^-$  is a slow process. From the IPCE measurements (Fig. 6) significant differences can be seen between **EO3** and the AFB dyes. The effect of the furan  $\pi$ -spacer can be seen clearly as increased power conversion in the region around 400 nm and an extension of the IPCE curves of about 60 nm towards longer wavelengths. A clear difference is observed in the absorption onsets between **EO3** and the AFB dyes in the IPCE spectra, suggesting the difference in optical bandgaps should be larger than those

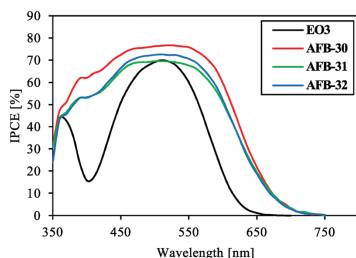
**Table 2** Photovoltaic performance under 1 sun AM 1.5G illumination of dyes **AFB-30**, **31** and **32**, compared to **EO3**, **RK1** and **N719**. Averages of three devices with corresponding standard deviations

Dye	Dye loading ( $10^{-7}$ mol $\text{cm}^{-2}$ )	IPCE $J_{\text{SC}}^a$ (mA $\text{cm}^{-2}$ )	$J_{\text{SC}}$ (mA $\text{cm}^{-2}$ )	$V_{\text{OC}}$ (mV)	FF	PCE <sup>b</sup> (%)
<b>EO3</b>	0.86	6.68	$7.17 \pm 0.19$	$829 \pm 9.17$	$0.78 \pm 0.01$	$4.53 \pm 0.23$
<b>AFB-30</b>	2.83	10.91	$10.41 \pm 0.34$	$783 \pm 6.56$	$0.73 \pm 0.01$	$5.86 \pm 0.11$
<b>AFB-31</b>	2.07	9.71	$8.95 \pm 0.24$	$764 \pm 19.31$	$0.73 \pm 0.01$	$4.91 \pm 0.06$
<b>AFB-32</b>	1.64	9.92	$9.30 \pm 0.26$	$763 \pm 4.51$	$0.75 \pm 0.02$	$5.25 \pm 0.21$
<b>RK1</b>	—	—	$9.48 \pm 0.26$	$778 \pm 2.39$	$0.79 \pm 0.01$	$5.81 \pm 0.19$
<b>N719</b>	—	—	$12.82 \pm 0.04$	$808 \pm 4.40$	$0.74 \pm 0.03$	$7.54 \pm 0.32$

<sup>a</sup> Obtained by integration of the IPCE spectrum over the 1 sun AM 1.5G spectrum. <sup>b</sup> Electrolyte composition 0.03 M  $\text{I}_2$ , 0.6 M 1-butyl-3-methylimidazolium iodide (BMII), 0.1 M guanidinium thiocyanate (GuSCN) and 0.5 M *tert*-butylpyridine in acetonitrile/valeronitrile (85:15, v/v).



**Fig. 5**  $J$ - $V$  curves of the best device in each parallel. Corresponding dark current measurements included as dashed lines.



**Fig. 6** IPCE spectra of dyes **EO3**, **AFB-30** to **32** with A6141  $\Gamma/\Gamma_3^-$  electrolyte.

obtained from the UV/Vis-emission intersection method. The photocurrent response of the devices is redshifted compared to the photophysical measurements of the dyes. Part of this shift can be explained by the broadening of the absorption peak observed when the sensitizers were anchored on  $\text{TiO}_2$ , while the remaining difference must arise from interactions with the device electrolyte. Upon integration of the IPCE spectra, short-circuit current density estimates were obtained, which were within 8% of the  $J_{\text{SC}}$  values from the  $J$ - $V$  sweeps under 1 sun illumination.

Dye loading measurements by desorption was performed in 40 mM tetrabutylammonium hydroxide in stabilized THF. For **AFB-30**, the dye loading is nearly identical to the reported value for the thiophene analogue **RD-SC**, recently reported by Liao

*et al.*<sup>39</sup> Looking at dye **AFB-30** compared to **AFB-31** and **32**, it appears the presence of the TEOME chains reduces dye loading by up to 40%. While similar dye loading values for the two dyes with two TEOME chains (**EO3** and **AFB-32**) were expected, higher values were measured for **AFB-32**. A possible explanation could be the staining conditions favouring the dyes with furan  $\pi$ -spacer over **EO3**. The variance in dye loading in-part explain the efficiency differences. Likely, a more careful optimisation of CDCA concentration could increase the dye loading and efficiency of the devices based on TEOME containing dyes.

Inspired by the high performance of **EO3** in aqueous DSSC, we tested the four sensitizers in devices with the aqueous cobalt electrolyte  $[\text{Co}(\text{bpy-pz})_2]^{2+/3+}$  reported by Ellis *et al.*<sup>23</sup> The electrolyte composition was 0.13 M  $[\text{Co}(\text{bpy-pz})_2]\text{Cl}_2$ , 0.06 M  $[\text{Co}(\text{bpy-pz})_2]\text{Cl}_3$  and 0.8 M 1-methylbenzimidazole (MBI) in deionized water.  $J$ - $V$  curves and photovoltaic parameters are reported in the ESI† (Fig. S5 and Table S1). The average efficiencies were, in ascending order: **EO3** (0.17%) < **AFB-32** (0.18%) < **AFB-31** (0.40%) < **AFB-30** (0.57%). The open-circuit voltages were considerably lower than the ones previously reported for the  $[\text{Co}(\text{bpy-pz})_2]^{2+/3+}$  electrolyte, and **AFB-30** was again the most efficient sensitizer. The low efficiency could be a result of mismatched energy levels or unfavourable dye-electrolyte interactions, but the phenomenon has not been further investigated.

Attempting to further unnest the behaviour of these dyes, charge extraction and electron lifetime measurements were performed on the devices, see Fig. 7. The electron densities obtained from the charge extraction measurements (Fig. 7a) were comparable for all four dyes, with the highest values found for **AFB-32**. Also from these measurements, it is clear that dye **EO3** delivers a much higher  $V_{\text{OC}}$  than the AFB dyes. This could be the result of a conduction band shift, higher electron concentration or longer electron lifetimes. The charge extraction values ( $Q_{\text{OC}}$ ) are direct measurements of the electron concentration in the  $\text{TiO}_2$ , and any conduction band shift may be found from the charge extraction measurements as a horizontal shift of one curve relative to another for the same  $Q_{\text{OC}}$  value. However, in order to determine the contribution of electron lifetime to the photovoltage, one has to correct for the conduction band shift and compare the electron lifetime measurements for the same charge densities, *i.e.*  $Q_{\text{OC}}$  values, as described previously<sup>40</sup> and shown in Fig. 7b.

Very little difference is found for the  $Q_{\text{OC}}$  values for the four sensitizers, but a large relative conduction band shift of



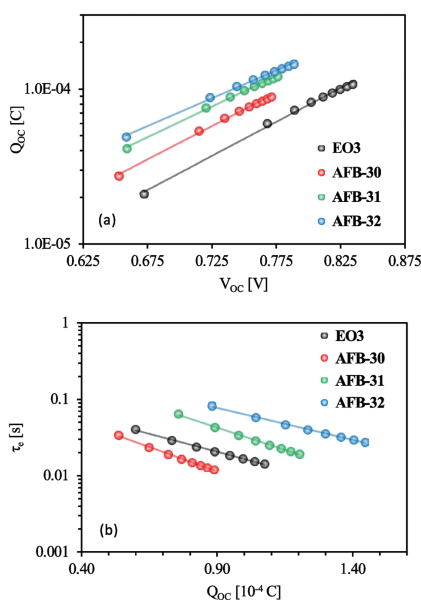


Fig. 7 (a) Charge extraction values measured at different light intensities. (b) electron lifetime measurements corrected for the observed conduction band shifts from (a) and then plotted versus the extracted charges at the same potentials. Devices fabricated with A6141 organic electrolyte.

approximately 80 mV is observed between **AFB-32** and **EO3**. From Fig. 7b we observe only small differences in electron lifetimes following the order of **AFB-30** < **EO3** < **AFB-31** < **AFB-32**. Considering the lower charge densities and electron lifetime values of **EO3** we would expect the actual difference in photovoltage to be lower than 80 mV. From the  $J$ - $V$  sweeps, a shift of 66 mV is found, thus confirming the conduction band shift is the main contributor to the high  $V_{oc}$  for this dye.

## Experimental

### Synthesis

All details on the synthesis and characterization of the sensitizers in this work can be found in the ESI.†

### Device fabrication

FTO glass (NSG10, Nippon Sheet Glass) was cut to size and cleaned with Deconex 21 ( $2 \text{ g L}^{-1}$  in  $\text{H}_2\text{O}$ ) in an ultrasonic bath for 45 minutes before being further cleaned in a UV/ $\text{O}_3$  cleaner for 15 minutes. A  $\text{TiO}_2$  blocking layer was deposited with hydrothermal deposition by immersion in an aqueous 40 mM  $\text{TiCl}_4$  solution for 45 minutes at  $70^\circ\text{C}$  then rinsed with deionized water and ethanol, repeated once. The mesoporous titania nanoparticle

paste (18NR-T, GreatCellSolar) was screenprinted onto the FTO glass with a 54T mesh then dried at  $125^\circ\text{C}$  for 5 minutes. Two layers of 18NR-T was deposited, followed by a scattering layer (WER2-O, GreatCellSolar) printed with the same screen. The total thickness of the active layer was measured to be  $10 \mu\text{m}$  by profilometer. The titania electrodes were then sintered on a programmable hotplate with the ramping profile of 125, 250, 375, 450 and  $500^\circ\text{C}$  for 5, 5, 5, 15 and 15 minutes with 5 minutes ramping time between each temperature step.  $\text{TiCl}_4$  post treatment was performed on the electrodes by immersion in aqueous 40 mM  $\text{TiCl}_4$  solution for 30 minutes at  $70^\circ\text{C}$ , followed by rinsing with deionized water and ethanol. The photoanodes were completed by sintering on a hotplate at  $500^\circ\text{C}$  for 45 minutes.

Counter electrodes were fashioned from TEC15 FTO glass, cut to size and holes for electrolyte filling were drilled with a diamond drill bit. The FTO slides were then cleaned with ultrasonication in Hellmanex solution, deionized water, ethanol and finally in acetone, each for 15 minutes. A solution of  $\text{H}_2\text{PtCl}_6$  (10 mM in iso-propanol,  $5 \mu\text{L cm}^{-2}$ ) was dropcast on the individual electrodes and then they were fired at  $400^\circ\text{C}$  for 15 minutes to leave only the catalytic layer of platinum.

Staining solutions had a concentration of 0.5 mM of dye and 5 mM of chenodeoxycholic acid. For the AFB dyes, a mixture of THF and acetonitrile (57:43, v/v) was used, while absolute ethanol was used for RK1 and a mixture of *tert*-butanol and acetonitrile (1:1, v/v) for N719. The electrodes were stained for 20 hours at room temperature before being rinsed in acetonitrile for 2 minutes, dried under air and sealed with the counter electrodes in a drybox using  $25 \mu\text{m}$  thick Surlyn gaskets.

The A6141 electrolyte contained 0.03 M  $\text{I}_2$ , 0.6 M 1-butyl-3-methylimidazolium iodide (BMII), 0.1 M guanidinium thiocyanate (GuSCN) and 0.5 M *tert*-butylpyridine in acetonitrile/valeronitrile (85:15, v/v), and was injected by vacuum backfilling. The filling hole was sealed with Surlyn and a glass disk, and the protruding edges of the working and counter electrodes were covered in soldering tin from an ultrasonic soldering iron for lowered sheet resistance.

### Device characterization

Current–voltage characteristics were measured under 1 sun AM 1.5G illumination from a solar simulator (Oriel, USA, 450 W) connected to a Keithley 2400. A black metal mask with an aperture of  $0.16 \text{ cm}^2$  was used for all the measurements. Incident photon-to-current conversion efficiency measurements (IPCE) were measured on an Arkeo-Ariadne (Cicci Research s.r.l.) with a 300 W xenon lamp, from 350 to 750 nm. Electron lifetime and charge extraction measurements were performed with the Dyenamo Toolbox (Dyemamo, Sweden).

## Conclusion

Three new sensitizers based on the efficient literature dye **EO3** were synthesized and evaluated with an  $\text{I}^-/\text{I}_3^-$  electrolyte. The photophysical and photovoltaic properties were improved and the best sensitizer, **AFB-30**, achieved an average PCE of 5.86%,

an improvement of 29% compared to EO3. The introduction of furan also shifted the HOMO levels towards more negative potentials, which could affect regeneration efficiency negatively when using cobalt or copper electrolytes with more positive  $E_{\text{redox}}$  than the  $\text{I}^-/\text{I}_3^-$  shuttle. Finally, the  $V_{\text{OC}}$  values obtained for the sensitizers were significantly reduced by the insertion of the furan moiety and a drop in  $V_{\text{OC}}$  of 46–66 mV compared to EO3 was attributed to a relative conduction band shift. We also established through TGA measurements that the introduction of the furan  $\pi$ -spacer lowered the decomposition temperature compared to no  $\pi$ -spacer, but the decomposition temperatures are still sufficiently high for successful device fabrication and operation. These results indicate that there still is potential to improve even the best sensitizers. Lastly, we find that working on the phenothiazine scaffold is a careful balancing act, because you may improve the absorption properties, but at a considerable cost in photovoltage.

## Conflicts of interest

There are no conflicts to declare.

## Acknowledgements

Dr Nick Vlachopoulos is acknowledged for very helpful instructions on the cyclic voltammetry measurements, and Nikolai Helth Gaukås for the TGA analyses. The support from the Research Council of Norway to the Norwegian Micro- and Nano-Fabrication Facility, NorFab (project number 245963/F50) and the Norwegian NMR Platform (project number 226244/F50) is highly appreciated.

## References

- B. O'Regan and M. Grätzel, *Nature*, 1991, **353**, 737–740.
- C.-P. Lee, R. Y.-Y. Lin, L.-Y. Lin, C.-T. Li, T.-C. Chu, S.-S. Sun, J. T. Lin and K.-C. Ho, *RSC Adv.*, 2015, **5**, 23810–23825.
- Y. Hong, Z. Iqbal, X. Yin and D. Cao, *Tetrahedron*, 2014, **70**, 6296–6302.
- A. Hagfeldt, G. Boschloo, L. Sun, L. Kloo and H. Pettersson, *Chem. Rev.*, 2010, **110**, 6595–6663.
- Y. Saygili, M. Stojanovic, N. Flores-Diaz, S. M. Zakeeruddin, N. Vlachopoulos, M. Grätzel and A. Hagfeldt, *Inorganics*, 2019, **7**, 30.
- A. Mahmood, *Sol. Energy*, 2016, **123**, 127–144.
- K. D. Seo, H. M. Song, M. J. Lee, M. Pastore, C. Anselmi, F. De Angelis, M. K. Nazeeruddin, M. Grätzel and H. K. Kim, *Dyes Pigm.*, 2011, **90**, 304–310.
- K. Hara, Z.-S. Wang, T. Sato, A. Furube, R. Katoh, H. Sugihara, Y. Dan-oh, C. Kasada, A. Shinpo and S. Suga, *J. Phys. Chem. B*, 2005, **109**, 15476–15482.
- N. Koumura, Z.-S. Wang, M. Miyashita, Y. Uemura, H. Sekiguchi, Y. Cui, A. Mori, S. Mori and K. Hara, *J. Mater. Chem.*, 2009, **19**, 4829–4836.
- K. Kakiage, Y. Aoyama, T. Yano, T. Otsuka, T. Kiyomen, M. Unno and M. Hanaya, *Chem. Commun.*, 2014, **50**, 6379–6381.
- R. M. El-Shishtawy, J.-D. Decoppet, F. A. M. Al-Zahrani, Y. Cao, S. B. Khan, M. S. Al-Ghamdi, B. G. Alhogbi, A. M. Asiri, S. M. Zakeeruddin and M. Grätzel, *New J. Chem.*, 2018, **42**, 9045–9050.
- S. H. Kim, H. W. Kim, C. Sakong, J. Namgoong, S. W. Park, M. J. Ko, C. H. Lee, W. I. Lee and J. P. Kim, *Org. Lett.*, 2011, **13**, 5784–5787.
- H. Tian, X. Yang, R. Chen, Y. Pan, L. Li, A. Hagfeldt and L. Sun, *Chem. Commun.*, 2007, 3741–3743.
- N. V. Krishna, J. V. S. Krishna, S. P. Singh, L. Giribabu, L. Han, I. Bedja, R. K. Gupta and A. Islam, *J. Phys. Chem. C*, 2017, **121**, 6464–6477.
- R. Li, X. Lv, D. Shi, D. Zhou, Y. Cheng, G. Zhang and P. Wang, *J. Phys. Chem. C*, 2009, **113**, 7469–7479.
- B.-S. Chen, D.-Y. Chen, C.-L. Chen, C.-W. Hsu, H.-C. Hsu, K.-L. Wu, S.-H. Liu, P.-T. Chou and Y. Chi, *J. Mater. Chem.*, 2011, **21**, 1937–1945.
- X. Sun, Y. Wang, X. Li, H. Agren, W. Zhu, H. Tian and Y. Xie, *Chem. Commun.*, 2014, **50**, 15609–15612.
- S. Haid, M. Marszalek, A. Mishra, M. Wielopolski, J. Teuscher, J.-E. Moser, R. Humphry-Baker, S. M. Zakeeruddin, M. Grätzel and P. Bäuerle, *Adv. Funct. Mater.*, 2012, **22**, 1291–1302.
- I. Benesperi, H. Michaels and M. Freitag, *J. Mater. Chem. C*, 2018, **6**, 11903–11942.
- M. Freitag, Q. Daniel, M. Pazoki, K. Sveinbjörnsson, J. Zhang, L. Sun, A. Hagfeldt and G. Boschloo, *Energy Environ. Sci.*, 2015, **8**, 2634–2637.
- F. Bella, C. Gerbaldi, C. Barolo and M. Grätzel, *Chem. Soc. Rev.*, 2015, **44**, 3431–3473.
- F. Bella, S. Galliano, M. Falco, G. Viscardi, C. Barolo, M. Grätzel and C. Gerbaldi, *Chem. Sci.*, 2016, **7**, 4880–4890.
- H. Tian, E. Gabriësson, P. W. Lohse, N. Vlachopoulos, L. Kloo, A. Hagfeldt and L. Sun, *Energy Environ. Sci.*, 2012, **5**, 9752–9755.
- W. Xiang, F. Huang, Y.-B. Cheng, U. Bach and L. Spiccia, *Energy Environ. Sci.*, 2013, **6**, 121–127.
- H. Ellis, R. Jiang, S. Ye, A. Hagfeldt and G. Boschloo, *Phys. Chem. Chem. Phys.*, 2016, **18**, 8419–8427.
- R. Y.-Y. Lin, F.-L. Wu, C.-T. Li, P.-Y. Chen, K.-C. Ho and J. T. Lin, *ChemSusChem*, 2015, **8**, 2503–2513.
- J.-H. Yum, S.-J. Moon, C. S. Karthikeyan, H. Wietasch, M. Thelakkat, S. M. Zakeeruddin, M. K. Nazeeruddin and M. Grätzel, *Nano Energy*, 2012, **1**, 6–12.
- S. Panagiotakis, E. Giannoudis, A. Charisiadis, R. Paravatou, M.-E. Lazaridi, M. Kandyli, K. Ladomenou, P. A. Angaridis, H. C. Bertrand, G. D. Sharma and A. G. Coutsolelos, *Eur. J. Inorg. Chem.*, 2018, 2369–2379.
- D. Kuang, C. Klein, H. J. Snaith, J.-E. Moser, R. Humphry-Baker, P. Comte, S. M. Zakeeruddin and M. Grätzel, *Nano Lett.*, 2006, **6**, 769–773.
- Z. Wan, C. Jia, Y. Duan, L. Zhou, Y. Lin and Y. Shi, *J. Mater. Chem.*, 2012, **22**, 25140–25147.
- A. F. Buene, N. Uggerud, S. P. Economopoulos, O. R. Gautun and B. H. Hoff, *Dyes Pigm.*, 2018, **151**, 263–271.
- M. Cariello, S. M. Abdalhadhi, P. Yadav, J.-D. Decoppet, S. M. Zakeeruddin, M. Grätzel, A. Hagfeldt and G. Cooke, *Dalton Trans.*, 2018, **47**, 6549–6556.

[View Article Online](#)

Paper

NJC

- 33 Z. Iqbal, W.-Q. Wu, Z.-S. Huang, L. Wang, D.-B. Kuang, H. Meier and D. Cao, *Dyes Pigm.*, 2016, **124**, 63–71.
- 34 V. V. Pavlishchuk and A. W. Addison, *Inorg. Chim. Acta*, 2000, **298**, 97–102.
- 35 C.-T. Li, F.-L. Wu, C.-J. Liang, K.-C. Ho and J. T. Lin, *J. Mater. Chem. A*, 2017, **5**, 7586–7594.
- 36 D. Joly, L. Pellejà, S. Narbey, F. Oswald, J. Chiron, J. N. Clifford, E. Palomares and R. Demadrille, *Sci. Rep.*, 2014, **4**, 4033.
- 37 M. K. Nazeeruddin, F. De Angelis, S. Fantacci, A. Selloni, G. Viscardi, P. Liska, S. Ito, B. Takeru and M. Grätzel, *J. Am. Chem. Soc.*, 2005, **127**, 16835–16847.
- 38 H. Tian, X. Yang, J. Cong, R. Chen, J. Liu, Y. Hao, A. Hagfeldt and L. Sun, *Chem. Commun.*, 2009, 6288–6290.
- 39 X. Liao, H. Zhang, J. Huang, G. Wu, X. Yin and Y. Hong, *Dyes Pigm.*, 2018, **158**, 240–248.
- 40 A. F. Buene, E. E. Ose, A. G. Zakariassen, A. Hagfeldt and B. H. Hoff, *J. Mater. Chem. A*, 2019, **7**, 7581–7590.

## Electronic Supplementary Information

**Effect of furan  $\pi$ -spacer and triethylene oxide methyl ether substituents on performance of phenothiazine sensitizers in dye-sensitized solar cells**

Audun Formo Buene<sup>a</sup>, Nanna Boholm<sup>b</sup>, Anders Hagfeldt<sup>c</sup>, Bård Helge Hoff<sup>\*</sup>

*a*: Department of Chemistry, Norwegian University of Science and Technology (NTNU), N-7491 Trondheim, Norway

*b*: Department of Chemistry, Aarhus University, DK-8000 Aarhus, Denmark

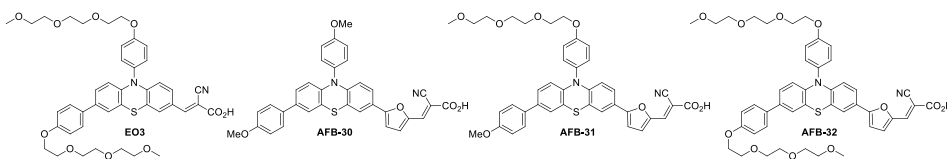
*c*: Laboratory of Photomolecular Science, Institute of Chemical Sciences and Engineering, École Polytechnique Fédérale de Lausanne (EPFL), Chemin des Alambics, Station 6, CH-1015 Lausanne, Switzerland

\* Corresponding author. Tel.: +47 73593973; E-mail address: bard.h.hoff@ntnu.no (B. H. Hoff).

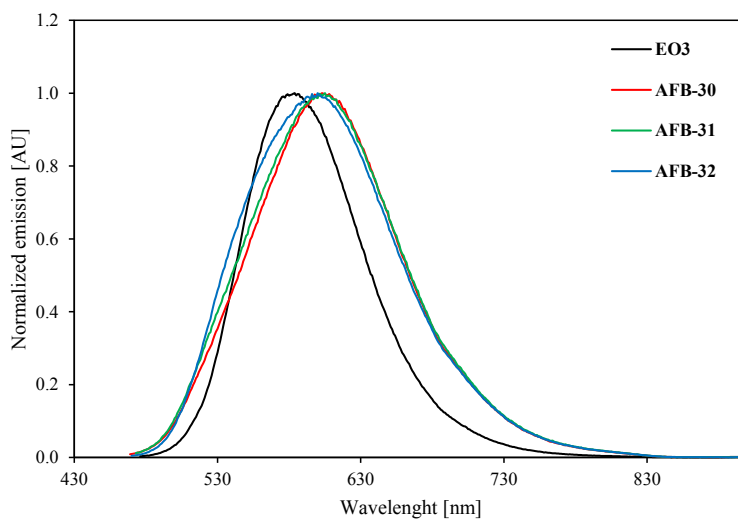
**List of contents**

<b>Absorption and emission</b>	<b>S2</b>
<b>Cyclic voltammetry</b>	<b>S4</b>
<b>Photovoltaic performance with aqueous [Co(bpy-pz)<sub>2</sub>]<sup>2+/3+</sup> electrolyte</b>	<b>S5</b>
<b>Synthesis and characterization</b>	<b>S6</b>
<b>NMR Spectra</b>	<b>S20</b>
<b>References</b>	<b>S24</b>

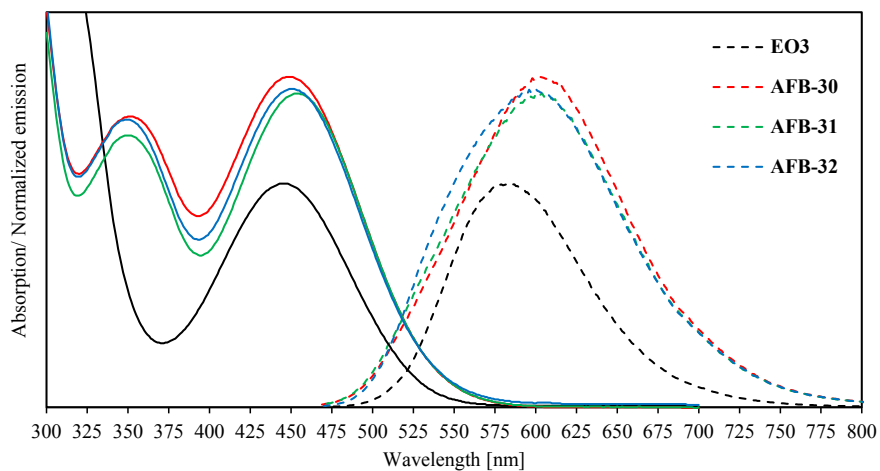
## Absorption and emission



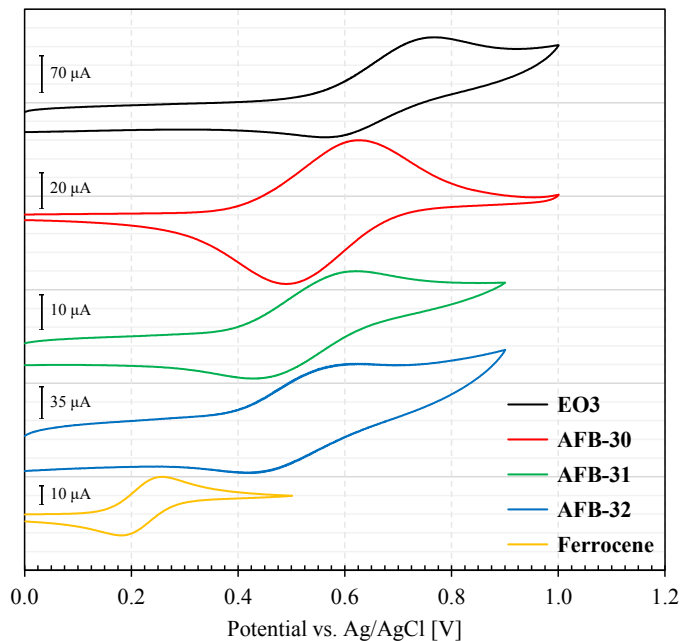
**Fig. S1** Structures of the four sensitizers **EO3**, **AFB-30**, **AFB-31** and **AFB-32**.



**Fig. S2** Normalized emission spectra of all dyes, recorded in THF. Emission at the wavelength of the ICT peak from the UV/vis absorption.

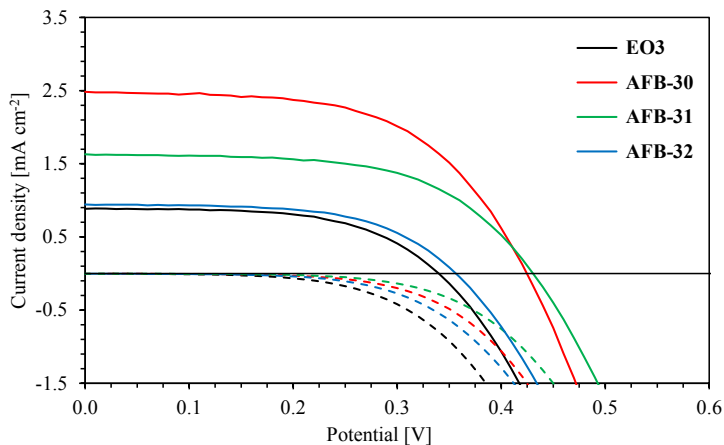


**Fig. S3** Absorption spectra in solution plotted with corresponding normalized emission spectra (dashed lines). The intersects dictates the optical bandgaps. Intersecting wavelengths: **EO3** 521 nm, **AFB-30** 520 nm, **AFB-31** 518 nm and **AFB-32** 518 nm.

**Cyclic voltammetry**

**Fig. S4** Cyclic voltammograms of all dyes on TiO<sub>2</sub> measured in acetonitrile with 0.1 M LiTFSI, with a carbon counter electrode and Ag/AgCl reference electrode. For the measurement of ferrocene, the working electrode was a glassy carbon electrode.

### Photovoltaic performance with aqueous $[\text{Co}(\text{bpy-pz})_2]^{2+/3+}$ electrolyte



**Fig. S5** *J-V characteristics of devices sensitized with EO3 and AFB-30 to 32 using the aqueous  $[\text{Co}(\text{bpy-pz})_2]^{2+/3+}$  electrolyte.*

**Table S1** *Photovoltaic performance of dyes AFB-30, 31 and 32 with aqueous  $[\text{Co}(\text{bpy-pz})_2]^{2+/3+}$  electrolyte under 1 sun AM 1.5G illumination. Averages of two devices.*

Dye	$J_{SC}$ ( $\text{mA cm}^{-2}$ )	$V_{OC}$ (mV)	FF	PCE (%)
<b>EO3</b>	$0.83 \pm 0.08$	$347 \pm 11$	$0.57 \pm 0.01$	$0.17 \pm 0.01$
<b>AFB-30</b>	$2.36 \pm 0.18$	$430 \pm 7$	$0.58 \pm 0.00$	$0.57 \pm 0.03$
<b>AFB-31</b>	$1.66 \pm 0.04$	$426 \pm 7$	$0.59 \pm 0.00$	$0.40 \pm 0.00$
<b>AFB-32</b>	$0.91 \pm 0.05$	$354 \pm 3$	$0.58 \pm 0.00$	$0.18 \pm 0.01$

*Electrolyte composition 0.13 M  $[\text{Co}(\text{bpy-pz})_2]\text{Cl}_2$ , 0.06 M  $[\text{Co}(\text{bpy-pz})_2]\text{Cl}_3$  and 0.8 M 1-methylbenzimidazole (MBI) in deionized  $\text{H}_2\text{O}$ .*



## Synthesis and characterization

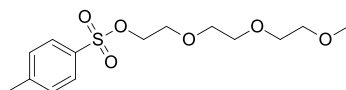
### Materials

All reagents were acquired from Sigma Aldrich unless otherwise stated.

### Characterization

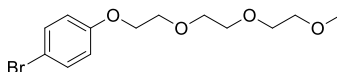
<sup>1</sup>H NMR and <sup>13</sup>C NMR spectra were recorded at room temperature on either a Bruker 400 MHz or 600 MHz spectrometer, and all chemical shifts were reported in ppm relative to respective solvent peaks. Accurate mass determination in positive and negative mode was performed on a "Synapt G2-S" Q-TOF instrument from Waters™. UV/Vis spectrometry was measured on a Hitachi U-1900 instrument using quartz cuvettes for the solution measurements, fluorescence measurements on a Cary Eclipse Fluorescence Spectrophotometer and infrared spectra were recorded on an FTIR Thermo Nicolet Nexus FT-IR spectrophotometer with a Smart Endurance reflection cell. Thermogravimetric analyses were performed on a Netzsch STA 449 F3 Jupiter instrument, ramping from 20-275 °C with a rate of 5 °C/min and from 275-600 °C with 10 °C/min. The airflow was 50 mL/min.

### Synthesis of 2-(2-(2-methoxyethoxy)ethoxy)ethyl 4-methylbenzenesulfonate (**1**)<sup>1</sup>



*p*-Toluenesulfonyl chloride (10.0 g, 52.5 mmol), dichloromethane (125 mL) and triethylene glycol monomethyl ether (10 mL, 62 mmol) were mixed in a flask. Finely powdered potassium hydroxide (5.97 g, 106 mmol) was added in portions and the reaction mixture was stirred for 2 hours at room temperature before it was quenched with deionized water (100 mL). The aqueous phase was extracted with dichloromethane (100 mL) and the organic phase was washed with deionized water (3 × 150 mL) and brine (150 mL) and dried over anhydrous Na<sub>2</sub>SO<sub>4</sub>. The solvent was removed *in vacuo*, and compound **1** was obtained as a colorless oil (15.7 g, 49.4 mmol, 94%), *R*<sub>f</sub> (ethyl acetate/pentane, 3:1) = 0.30. <sup>1</sup>H NMR (400 MHz, DMSO-*d*<sub>6</sub>) δ: 7.79 (d, *J* = 8.3 Hz, 2H), 7.48 (d, *J* = 8.0 Hz, 2H), 4.14-4.08 (m, 2H), 3.59-3.54 (m, 2H), 3.51-3.39 (m, 8H), 3.23 (s, 3H), 2.42 (s, 3H); HRMS (ASCI/ASAP, *m/z*): found 319.1214 (calcd. C<sub>14</sub>H<sub>22</sub>O<sub>6</sub>S, 319.1215, [M+H]<sup>+</sup>).

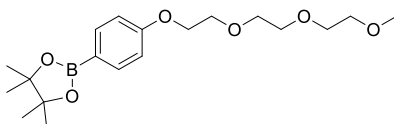
### Synthesis of 1-bromo-4-(2-(2-(2-methoxyethoxy)ethoxy)ethoxy)benzene (**2**)<sup>2</sup>



A flask was charged with 4-bromophenol (1.55 g, 8.96 mmol) and K<sub>2</sub>CO<sub>3</sub> (4.43 g, 32.1 mmol) and a nitrogen atmosphere was established. Dimethylformamide (30 mL) was added and the mixture was stirred for 15 minutes. 2-(2-(2-Methoxyethoxy)ethoxy)ethyl 4-methylbenzenesulfonate (2 mL, 8 mmol) was added and the reaction was stirred at 90 °C for 19 hours before the mixture was diluted with deionized water (50 mL) and dichloromethane (50 mL). The phases were separated and the aqueous phase was extracted with

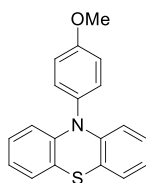
dichloromethane ( $2 \times 50$  mL) and the combined organic phases were washed with deionized water ( $3 \times 100$  mL) and brine ( $3 \times 100$  mL) before it was dried over anhydrous  $\text{Na}_2\text{SO}_4$ . The solvent was removed *in vacuo*, and silica gel column chromatography (gradient: 25-50% ethyl acetate in pentane) afforded compound **2** as a colorless oil (2.46 g, 7.71 mmol, 96%).  $^1\text{H NMR}$  (400 MHz,  $\text{DMSO}-d_6$ )  $\delta$ : 7.43 (d,  $J = 9.1$  Hz, 2H), 6.92 (d,  $J = 9.0$  Hz, 2H), 4.10-4.06 (m, 2H), 3.74-3.71 (m, 2H), 3.59-3.56 (m, 2H), 3.54-3.49 (m, 4H), 3.44-3.40 (m, 2H), 3.23 (s, 3H); HRMS (ASCI/ASAP,  $m/z$ ): found 319.0544 (calcd.  $\text{C}_{13}\text{H}_{19}^{79}\text{BrO}_4$ , 319.0545,  $[\text{M}+\text{H}]^+$ ).

### Synthesis of 2-(4-(2-(2-(2-methoxyethoxy)ethoxy)ethoxy)phenyl)-4,4,5,5-tetramethyl-1,3,2-dioxaborolane (**3**)<sup>3</sup>



To a dry Schlenk flask was added  $\text{PdCl}_2(\text{CH}_3\text{CN})_2$  (68 mg, 0.26 mmol) and SPhos (202 mg, 0.493 mmol). Under nitrogen atmosphere, dry 1,4-dioxane (20 mL) was added through the septum followed by compound **2** (1.95 g, 6.11 mmol), dry  $\text{NEt}_3$  (2.6 mL, 19 mmol) and pinacol borane (1.1 mL, 7.6 mmol). The reaction mixture was stirred at  $80^\circ\text{C}$  for 2.5 hours before it was cooled to room temperature and filtered through a pad of Celite with ethyl acetate as eluent. Upon removal of the solvent *in vacuo*, compound **3** was obtained as a dark red oil (2.19 g, 5.98 mmol, 98%). The material was used without further purification,  $R_f$  (ethyl acetate/pentane, 3:1) = 0.38.  $^1\text{H NMR}$  (400 MHz,  $\text{DMSO}-d_6$ )  $\delta$ : 7.59 (d,  $J = 8.7$  Hz, 2H), 6.93 (d,  $J = 8.7$  Hz, 2H), 4.13-4.09 (m, 2H), 3.76-3.72 (m, 2H), 3.60-3.57 (m, 2H), 3.54-3.49 (m, 4H), 3.44-3.40 (m, 2H), 3.23 (s, 3H), 1.27 (s, 12H); HRMS (ASCI/ASAP,  $m/z$ ): found 365.2245 (calcd.  $\text{C}_{19}\text{H}_{31}\text{BO}_6$ , 365.2250,  $[\text{M}]^+$ ).

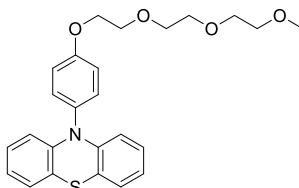
### Synthesis of 10-(4-methoxyphenyl)-10H-phenothiazine (**4**)<sup>4</sup>



10H-Phenothiazine (11.0 g, 55.3 mmol),  $\text{P}(\text{Cy})_3$  (0.63 g, 2.3 mmol), sodium *tert*-butoxide (13.0 g, 135 mmol) and  $\text{Pd}_2(\text{dba})_3$  (2.54 g, 2.8 mmol) were placed in a flask under nitrogen atmosphere. Degassed toluene (200 mL) was then added followed by 4-bromoanisole (9 mL, 71.8 mmol). The reaction mixture was stirred at reflux for 4 hours before it was cooled to room temperature and the solvent was removed *in vacuo*. The reaction mixture was dissolved in dichloromethane (200 mL) and washed with deionized water ( $3 \times 200$  mL) and brine (50 mL), then dried over anhydrous  $\text{Na}_2\text{SO}_4$ . The solvent was removed *in vacuo*. The crude product was purified by recrystallization from ethyl acetate, which afforded compound **4** as pale yellow crystals (12.2 g, 39.9 mmol, 72%).  $R_f$  (ethyl acetate/pentane, 1:20) = 0.32, mp  $174\text{--}176^\circ\text{C}$  (lit.<sup>5</sup>  $171\text{--}$

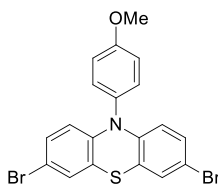
172 °C). <sup>1</sup>H NMR (400 MHz, DMSO-*d*<sub>6</sub>) δ: 7.34 (d, *J* = 8.7 Hz, 2H), 7.20 (d, *J* = 8.7 Hz, 2H), 7.03 (d, *J* = 7.4 Hz, 2H), 6.91 (t, *J* = 7.3 Hz, 2H), 6.82 (t, *J* = 7.4 Hz, 2H), 6.14 (d, *J* = 8.1 Hz, 2H), 3.85 (s, 3H); HRMS (ASAP+, *m/z*): found 305.0875 (calcd. C<sub>19</sub>H<sub>15</sub>NOS, 305.0874, [M]<sup>+</sup>).

#### Synthesis of 10-(4-(2-(2-(2-methoxyethoxy)ethoxy)ethoxy)phenyl)-10*H*-phenothiazine (**5**)<sup>6</sup>



To a dry flask was added Pd(OAc)<sub>2</sub> (79 mg, 0.35 mmol), XPhos (418 mg, 0.88 mmol), 10*H*-phenothiazine (6.99 g, 35.1 mmol), compound **2** (7.00 g, 21.9 mmol) and Cs<sub>2</sub>CO<sub>3</sub> (8.93 g, 27.4 mmol), an atmosphere of nitrogen was made followed by injection of toluene (35 mL) and *tert*-butanol (7 mL) through the septum. The reaction mixture was stirred at reflux for 22 hours. The solvent was removed *in vacuo* and the crude material was dissolved in dichloromethane (200 mL) and washed with deionized water (3 × 200 mL) and brine (200 mL), then dried over anhydrous Na<sub>2</sub>SO<sub>4</sub>. The solvent was removed *in vacuo*. Silica gel column chromatography (ethyl acetate/pentane, 1:1, *R<sub>f</sub>* = 0.26) afforded compound **5** as an off-white solid (9.12 g, 20.8 mmol, 95%), mp 67-70 °C (lit.<sup>6</sup> oil). <sup>1</sup>H NMR (400 MHz, DMSO-*d*<sub>6</sub>) δ: 7.30 (d, *J* = 8.9 Hz, 2H), 7.20 (d, *J* = 8.9 Hz, 2H), 7.02 (dd, *J* = 7.5, 1.6 Hz, 2H), 6.88 (td, *J* = 7.4, 1.6 Hz, 2H), 6.81 (td, *J* = 7.4, 1.3 Hz, 2H), 6.14 (dd, *J* = 8.2, 1.1 Hz, 2H), 4.19-4.15 (m, 2H), 3.81-3.77 (m, 2H), 3.63-3.59 (m, 2H), 3.57-3.50 (m, 4H), 3.45-3.40 (m, 2H), 3.24 (s, 3H); HRMS (ASCI/ASAP, *m/z*): found 437.1660 (calcd. C<sub>25</sub>H<sub>27</sub>NO<sub>4</sub>S, 437.1661, [M]<sup>+</sup>).

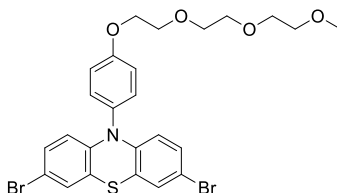
#### Synthesis of 3,7-dibromo-10-(4-methoxyphenyl)-10*H*-phenothiazine (**6**)<sup>7</sup>



Compound **1** (8.95 g, 29.3 mmol) was dissolved in chloroform (250 mL) and acetic acid (250 mL). The solution was degassed for 15 minutes. *N*-Bromosuccinimide (10.5 g, 59.2 mmol) was added in portions giving a purple solution. The reaction mixture was stirred for 1 hour before it was quenched with deionized water (250 mL). The aqueous phase was extracted with dichloromethane (2 × 150 mL) and the combined organic phases were washed with deionized water (2 × 150 mL) and brine (150 mL), then dried over anhydrous Na<sub>2</sub>SO<sub>4</sub>. The solvent was removed *in vacuo*. Purification by silica gel column chromatography (pentane/ethyl acetate, 25:1) afforded compound **6** as a yellow solid (9.15 g, 19.75 mmol, 67%). *R<sub>f</sub>* (ethyl

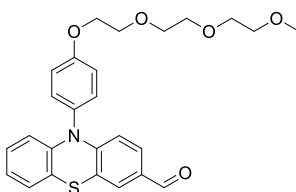
acetate/pentane, 1:3) = 0.63, mp 155-156 °C (lit.<sup>7</sup> 157-158 °C). <sup>1</sup>H NMR (400 MHz, DMSO-*d*<sub>6</sub>) δ: 7.34 (d, *J* = 8.8 Hz, 2H), 7.25 (d, *J* = 2.1 Hz, 2H), 7.21 (d, *J* = 8.7 Hz, 2H), 7.08 (dd, *J* = 8.8, 2.2 Hz, 2H), 6.00 (d, *J* = 8.8 Hz, 2H), 3.85 (s, 3H); HRMS (ASAP+, *m/z*): found 460.9087 (calcd. C<sub>19</sub>H<sub>13</sub><sup>79</sup>Br<sub>2</sub>NOS, 460.9085, [M]<sup>+</sup>).

#### Synthesis of 3,7-dibromo-10-(4-(2-(2-(2-methoxyethoxy)ethoxy)ethoxy)phenyl)-10*H*-phenothiazine (7)



Compound **3** (3.00 g, 6.86 mmol) was dissolved in chloroform (45 mL) and acetic acid (45 mL). The solution was degassed for 15 minutes before *N*-bromosuccinimide (2.56 g, 14.4 mmol) was added. The reaction mixture was stirred at room temperature for 5 hours before it was quenched with deionized water (100 mL). The aqueous phase was extracted with dichloromethane (50 mL) and the organic phase was washed with deionized water (2 × 100 mL) and brine (100 mL) and dried over anhydrous Na<sub>2</sub>SO<sub>4</sub>. The solvent was removed *in vacuo*, and silica gel column chromatography (ethyl acetate/pentane, 1:1, *R<sub>f</sub>* = 0.31) afforded compound **7** as a light brown solid (4.08 g, 6.03 mmol, 88%), mp 74-75 °C. <sup>1</sup>H NMR (400 MHz, DMSO-*d*<sub>6</sub>) δ: 7.33 (d, *J* = 8.9 Hz, 2H), 7.25 (d, *J* = 2.3 Hz, 2H), 7.21 (d, *J* = 9.0 Hz, 2H), 7.07 (dd, *J* = 8.8, 2.3 Hz, 2H), 6.00 (d, *J* = 8.8 Hz, 2H), 4.20-4.16 (m, 2H), 3.81- 3.76 (m, 2H), 3.63-3.59 (m, 2H), 3.57-3.51 (m, 4H), 3.45-3.41 (m, 2H), 3.24 (s, 3H); HRMS (ASCI/ASAP, *m/z*): found 592.9865 (calcd. C<sub>25</sub>H<sub>25</sub><sup>79</sup>Br<sub>2</sub>NO<sub>4</sub>S, 592.9871, [M]<sup>+</sup>).

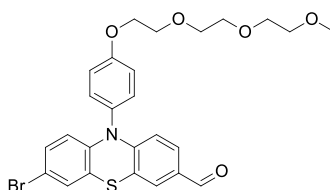
#### Synthesis of 10-(4-(2-(2-(2-methoxyethoxy)ethoxy)ethoxy)phenyl)-10*H*-phenothiazine-3-carbaldehyde (8)<sup>6</sup>



Compound **5** (2.19 g, 5.01 mmol) was dissolved in a mixture of anhydrous dimethylformamide (1.5 mL) and 1,2-dichloroethane (25 mL) followed by cooling in a water-ice bath. Slowly, POCl<sub>3</sub> (1.75 mL) was added to the reaction mixture over 30 minutes using a syringe. The mixture was heated to 80 °C and left stirring overnight. The reaction was quenched by addition of deionized water (100 mL) followed by extraction with chloroform (3 × 100 mL). The combined organic phases were washed with deionized water

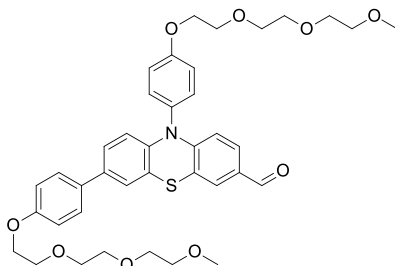
(100 mL), then dried with brine (100 mL) and over anhydrous  $\text{Na}_2\text{SO}_4$ . The solvents were removed *in vacuo* and the crude product was purified using silica gel column chromatography (*n*-pentane/ethyl acetate, 1:1,  $R_f = 0.14$ ). Compound **8** was obtained as a yellow solid (1.46 g, 3.14 mmol, 63%), mp 77-78 °C.  $^1\text{H NMR}$  (400 MHz,  $\text{DMSO}-d_6$ )  $\delta$ : 9.69 (s, 1H), 7.50 (d,  $J = 1.9$  Hz, 1H), 7.42 (dd,  $J = 8.6, 1.9$  Hz, 1H), 7.37 (d,  $J = 8.8$  Hz, 2H), 7.24 (d,  $J = 8.8$  Hz, 2H), 7.06 (dd,  $J = 7.2, 1.9$  Hz, 1H), 6.95-6.86 (m, 2H), 6.20 (d,  $J = 8.6$  Hz, 1H), 6.11 (dd,  $J = 7.9, 1.5$  Hz, 1H), 4.20 (t,  $J = 4.5$  Hz, 2H), 3.80 (t,  $J = 4.5$  Hz, 2H), 3.64-3.60 (m, 2H), 3.57-3.52 (m, 4H), 3.46-3.42 (m, 2H), 3.24 (s, 3H); HRMS (ASAP+,  $m/z$ ): found 466.1688 (calcd.  $\text{C}_{26}\text{H}_{28}\text{NO}_5\text{S}$ , 466.1696,  $[\text{M}+\text{H}]^+$ ).

#### Synthesis of 7-bromo-10-(4-(2-(2-(2-methoxyethoxy)ethoxy)ethoxy)phenyl)-10H-phenothiazine-3-carbaldehyde (**9**)<sup>6</sup>



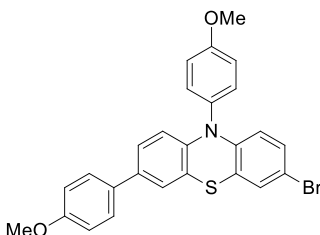
Compound **8** (1.18 g, 2.53 mmol) was dissolved in acetic acid (10 mL). *N*-Bromosuccinimide (457 mg, 2.57 mmol) was added and the reaction mixture was stirred at room temperature for 30 minutes. The reaction was quenched by addition of deionized water (100 mL) followed by extraction with diethyl ether ( $3 \times 100$  mL). The organic phases were collected and washed with deionized water (100 mL), then dried with brine (100 mL) and over anhydrous  $\text{Na}_2\text{SO}_4$ . The solvents were removed *in vacuo* and the crude product was purified using silica gel column chromatography (*n*-pentane/ethyl acetate, 1:2,  $R_f = 0.31$ ). Compound **9** was obtained as a yellow solid (982 mg, 1.80 mmol, 70%), mp 75-77 °C.  $^1\text{H NMR}$  (400 MHz,  $\text{DMSO}-d_6$ )  $\delta$ : 9.70 (s, 1H), 7.50 (d,  $J = 1.9$  Hz, 1H), 7.42 (dd,  $J = 8.5, 1.9$  Hz, 1H), 7.37 (d,  $J = 9.0$  Hz, 2H), 7.29 (d,  $J = 2.3$  Hz, 1H), 7.24 (d,  $J = 9.0$  Hz, 2H), 7.09 (dd,  $J = 8.7, 2.3$  Hz, 1H), 6.19 (d,  $J = 8.5$  Hz, 1H), 6.01 (d,  $J = 8.5$  Hz, 1H), 4.20 (t,  $J = 4.4$  Hz, 2H), 3.79 (t,  $J = 4.4$  Hz, 2H), 3.64-3.60 (m, 2H), 3.57-3.52 (m, 4H), 3.45-3.42 (m, 2H), 3.24 (s, 3H); HRMS (ASAP+,  $m/z$ ): found 544.0793 (calcd.  $\text{C}_{26}\text{H}_{27}^{79}\text{BrNO}_5\text{S}$ , 544.0786,  $[\text{M}+\text{H}]^+$ ).

### Synthesis of 7,10-bis(4-(2-(2-(2-methoxyethoxy)ethoxy)ethoxy)phenyl)-10*H*-phenothiazine-3-carbaldehyde (**10**)<sup>6</sup>



Compound **9** (420 mg, 0.771 mmol), compound **3** (583 mg, 1.59 mmol), Pd(OAc)<sub>2</sub> (12 mg, 0.053 mmol), SPhos (35 mg, 0.085 mmol), K<sub>2</sub>CO<sub>3</sub> (431 mg, 3.12 mmol) were added to a round-bottom flask. 1,4-Dioxane (6 mL), followed by deionized water (6 mL), were added to the flask, and the mixture was stirred at 80 °C for 1 hour. The reaction was quenched with deionized water (100 mL) followed by extraction with ethyl acetate (3 × 100 mL). The combined organic phases were washed with deionized water (100 mL), and then dried with brine (100 mL) and over anhydrous Na<sub>2</sub>SO<sub>4</sub>. Excess solvent was removed under reduced pressure. The crude product was purified using silica gel column chromatography (3% methanol in dichloromethane, *R<sub>f</sub>* = 0.35). Compound **10** was obtained as a yellow oil (476 mg, 0.676 mmol, 88%). <sup>1</sup>H NMR (400 MHz, DMSO-*d*<sub>6</sub>) δ: 9.70 (s, 1H), 7.50 (d, *J* = 8.8 Hz, 1H), 7.42 (dd, *J* = 8.8, 2.0 Hz, 1H), 7.39 (d, *J* = 8.8 Hz, 2H), 7.31 (d, *J* = 2.2 Hz, 1H), 7.26 (d, *J* = 8.8 Hz, 2H), 7.18 (dd, *J* = 8.7, 2.2 Hz, 1H), 7.00–6.90 (m, 4H), 6.19 (d, *J* = 8.6 Hz, 1H), 6.13 (d, *J* = 8.6 Hz, 1H), 4.21 (t, *J* = 4.4 Hz, 2H), 4.11 (t, *J* = 4.4 Hz, 2H), 3.81 (t, *J* = 4.4 Hz, 2H), 3.77–3.72 (m, 2H), 3.64–3.49 (m, 12H), 3.46–3.40 (m, 4H), 3.24 (s, 3H), 3.23 (s, 3H); HRMS (ASAP+, *m/z*): found 704.2893 (calcd. C<sub>39</sub>H<sub>46</sub>NO<sub>9</sub>S, 704.2888, [M+H]<sup>+</sup>).

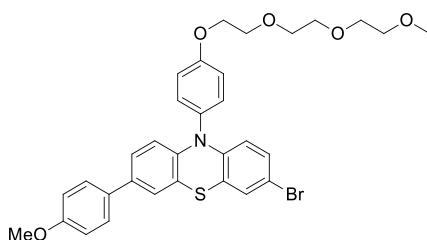
### Synthesis of 3-bromo-7,10-bis(4-methoxyphenyl)-10*H*-phenothiazine (**11**)<sup>7</sup>



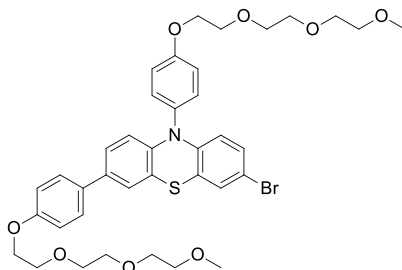
Compound **2** (1.51 g, 3.3 mmol), Pd(PPh<sub>3</sub>)<sub>4</sub> (0.34 g, 0.3 mmol) and K<sub>2</sub>CO<sub>3</sub> (1.82 g, 13.2 mmol) were added to a flask and a nitrogen atmosphere was established. 1,4-Dioxane (30 mL) and deionized water (30 mL) were added and the mixture was stirred at 40 °C for 30 minutes. Then (4-methoxyphenyl)boronic acid (0.53 g, 3.5 mmol) dissolved in 1,4-dioxane (5 mL) was added dropwise to the reaction mixture which was then stirred at 80 °C for 24 hours before it was quenched with deionized water (50 mL) and dichloromethane (50

mL), and the phases separated. The aqueous phase was extracted with dichloromethane (50 mL) and the combined organic phases were washed with deionized water (50 mL) and brine (30 mL). The solvent was removed *in vacuo*, and the crude product was filtered through a silica plug (dichloromethane/pentane, 2:3) and afterwards purified by silica gel column chromatography (gradient: 2.5-5% acetone in pentane) which afforded compound **11** as a fluffy yellow powder (0.51 g, 1.040 mmol, 32%),  $R_f$  (pentane/ethyl acetate, 3:1) = 0.51, mp 130-133 °C (lit.<sup>7</sup> 126-127 °C). <sup>1</sup>H NMR (600 MHz, DMSO-*d*<sub>6</sub>)  $\delta$ : 7.50 (d,  $J$  = 8.2 Hz, 2H), 7.36 (d,  $J$  = 8.1 Hz, 2H), 7.29 (s, 1H), 7.26 (s, 1H), 7.22 (d,  $J$  = 8.5 Hz, 2H), 7.17 (d,  $J$  = 8.7 Hz, 1H), 7.08 (d,  $J$  = 9.1 Hz, 1H), 6.96 (d,  $J$  = 9.0 Hz, 2H), 6.13 (d,  $J$  = 8.5 Hz, 1H), 6.02 (d,  $J$  = 10.4 Hz, 1H), 3.86 (s, 3H), 3.76 (s, 3H); <sup>13</sup>C NMR (150 MHz, DMSO-*d*<sub>6</sub>)  $\delta$ : 159.1, 158.7, 143.2, 142.1, 134.4, 132.1, 131.8 (2C), 131.0, 129.7, 128.2, 127.0 (2C), 125.1, 123.9, 121.0, 118.4, 116.9, 116.4 (2C), 116.0, 114.3 (2C), 113.5, 55.5, 55.2; HRMS (ASAP+, *m/z*): found 489.0393 (calcd. C<sub>26</sub>H<sub>20</sub><sup>79</sup>BrNO<sub>2</sub>S, 489.0398, [M]<sup>+</sup>).

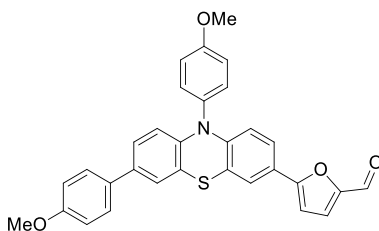
### Synthesis of 3-bromo-10-(4-(2-(2-(2-methoxyethoxy)ethoxy)ethoxy)phenyl)-7-(4-methoxyphenyl)-10*H*-phenothiazine (**12**)



To a Schlenk flask compound **4** (2.07 g, 3.48 mmol), Pd(PPh<sub>3</sub>)<sub>4</sub> (356 mg, 0.308 mmol), and K<sub>2</sub>CO<sub>3</sub> (1.70 g, 13.9 mmol) were added, and a nitrogen atmosphere established. Degassed 1,4-dioxane (20 mL) and deionized water (20 mL) were added through the septum. The mixture was stirred at 40 °C for 30 minutes before (4-methoxyphenyl)boronic acid (519 mg, 3.42 mmol) dissolved in 1,4-dioxane (0.5 mL) was added dropwise through the septum. The reaction mixture was stirred at 80 °C for 22 hours before deionized water (80 mL) and dichloromethane (80 mL) were added and the phases separated. The aqueous phase was extracted with dichloromethane (80 mL). The combined organic phases were washed with deionized water (2 × 100 mL) and brine (100 mL), then dried over anhydrous Na<sub>2</sub>SO<sub>4</sub>. The solvents were removed *in vacuo*, and silica gel column chromatography (15% acetone in pentane) afforded compound **12** as a yellow oil (0.730 g, 1.173 mmol, 34%),  $R_f$  (pentane/acetone, 3:1) = 0.24. <sup>1</sup>H NMR (400 MHz, DMSO-*d*<sub>6</sub>)  $\delta$ : 7.48 (d,  $J$  = 8.8 Hz, 2H), 7.32 (d,  $J$  = 8.9 Hz, 2H), 7.28 (d,  $J$  = 2.1 Hz, 1H), 7.24 (d,  $J$  = 2.3 Hz, 1H), 7.21 (d,  $J$  = 9.0 Hz, 2H), 7.15 (dd,  $J$  = 8.7, 2.2 Hz, 1H), 7.05 (dd,  $J$  = 8.9, 2.4 Hz, 1H), 6.95 (d,  $J$  = 8.9 Hz, 2H), 6.13 (d,  $J$  = 8.7 Hz, 1H), 6.01 (d,  $J$  = 8.8 Hz, 1H), 4.21-4.16 (m, 2H), 3.82-3.77 (m, 2H), 3.76 (s, 3H), 3.64-3.59 (m, 2H), 3.57-3.51 (m, 4H), 3.46-3.41 (m, 2H), 3.24 (s, 3H); <sup>13</sup>C NMR (100 MHz, DMSO-*d*<sub>6</sub>)  $\delta$ : 158.7, 158.4, 143.2, 142.1, 134.4, 132.1, 131.7 (2C), 130.9, 129.7, 128.2, 127.0 (2C), 125.0, 123.8, 120.9, 118.4, 116.9, 116.8 (2C), 116.0, 114.3 (2C), 113.5, 71.3, 69.9, 69.8, 69.6, 68.9, 67.5, 58.0, 55.1; HRMS (ASCI/ASAP, *m/z*): found 621.1180 (calcd. C<sub>32</sub>H<sub>32</sub><sup>79</sup>BrNO<sub>5</sub>S, 621.1185, [M]<sup>+</sup>).

**Synthesis of 3-bromo-7,10-bis(4-(2-(2-(2-methoxyethoxy)ethoxy)ethoxy)phenyl)-10H-phenothiazine (13)**

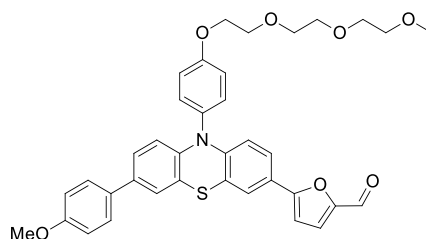
Compound **4** (1.00 g, 1.68 mmol), Pd(PPh<sub>3</sub>)<sub>4</sub> (0.184 g, 159 μmol) and K<sub>2</sub>CO<sub>3</sub> (0.894 g, 6.47 mmol) were added to a flask and a nitrogen atmosphere established. Degassed toluene (6 mL) and degassed deionized water (6 mL) were added, and the mixture was stirred at 40 °C for 30 minutes before compound **5** (604 mg, 1.65 mmol) was added through the septum. The reaction mixture was stirred at 80 °C for 21 hours before it was diluted with deionized water (40 mL) and dichloromethane (40 mL). The phases were separated and the aqueous phase was extracted with more dichloromethane (40 mL). The combined organic phase was washed with deionized water (80 mL) and brine (80 mL), then dried over Na<sub>2</sub>SO<sub>4</sub>. The solvent was removed *in vacuo*, and silica gel column chromatography (gradient: 25-50% acetone in pentane) afforded compound **13** as a yellow oil (0.568 g, 0.753 mmol, 45%), *R<sub>f</sub>* (acetone/pentane, 1:1) = 0.67. <sup>1</sup>H NMR (400 MHz, DMSO-*d*<sub>6</sub>) δ: 7.48 (d, *J* = 8.8 Hz, 2H), 7.33 (d, *J* = 8.9 Hz, 2H), 7.28 (d, *J* = 1.9 Hz, 1H), 7.24 (d, *J* = 2.3 Hz, 1H), 7.22 (d, *J* = 8.9 Hz, 2H), 7.16 (dd, *J* = 8.7, 2.2 Hz, 1H), 7.06 (dd, *J* = 8.8, 2.4 Hz, 1H), 6.96 (d, *J* = 8.8 Hz, 2H), 6.13 (d, *J* = 8.6 Hz, 1H), 6.01 (d, *J* = 8.8 Hz, 1H), 4.21-4.16 (m, 2H), 4.11-4.07 (m, 2H), 3.82-3.77 (m, 2H), 3.75-3.71 (m, 2H), 3.64-3.39 (m, 16H), 3.24 (s, 3H), 3.23 (s, 3H); <sup>13</sup>C NMR (100 MHz, DMSO-*d*<sub>6</sub>) δ: 158.4, 157.9, 143.2, 142.1, 134.4, 132.1, 131.7 (2C), 131.0, 129.7, 128.2, 127.0 (2C), 125.1, 123.9, 120.9, 118.4, 116.9, 116.8 (2C), 116.0, 114.8 (2C), 113.5, 71.3, 71.3, 69.9, 69.9, 69.8, 69.8, 69.6, 69.6, 68.9, 68.9, 67.5, 67.2, 58.0, 58.0; HRMS (ASCI/ASAP, *m/z*): found 753.1961 (calcd. C<sub>38</sub>H<sub>44</sub><sup>79</sup>BrNO<sub>8</sub>S, 753.1971, [M]<sup>+</sup>).

**Synthesis of 5-(7,10-bis(4-methoxyphenyl)-10H-phenothiazin-3-yl)furan-2-carbaldehyde (14)**



Compound **3** (376 mg, 0.77 mmol), SPhos (19.6 mg, 0.048 mmol), (5-formyl-2-furanyl)boronic acid (299 mg, 2.1 mmol), Pd(OAc)<sub>2</sub> (8.5 mg, 0.038 mmol) and K<sub>2</sub>CO<sub>3</sub> (416 mg, 3.0 mmol) were added to a flask which was then evacuated and flushed with N<sub>2</sub> to obtain an inert atmosphere. Degassed 1,4-dioxane (12 mL) and deionized water (12 mL) were added and the reaction mixture was stirred at 80 °C for 2 hours before it was diluted with dichloromethane (50 mL) and deionized water (50 mL). The aqueous phase was extracted with dichloromethane (50 mL) and the combined organic phases were washed with deionized water (30 mL) and brine (30 mL), then dried over anhydrous Na<sub>2</sub>SO<sub>4</sub> before the solvent was removed *in vacuo*. The crude product was purified by silica gel column chromatography (gradient: 15-25% ethyl acetate in pentane) and compound **14** was obtained as an orange foam (327 mg, 0.647 mmol, 84%), *R<sub>f</sub>* (ethyl acetate/pentane, 1:4) = 0.16. <sup>1</sup>H NMR (400 MHz, DMSO-*d*<sub>6</sub>) δ: 9.52 (s, 1H), 7.56 (d, *J* = 3.8 Hz, 1H), 7.50 (d, *J* = 2.0 Hz, 1H), 7.48 (d, *J* = 8.8 Hz, 2H), 7.38-7.32 (m, 3H), 7.27 (d, *J* = 2.2 Hz, 1H), 7.22 (d, *J* = 8.9 Hz, 2H), 7.13 (dd, *J* = 8.7, 2.2 Hz, 1H), 7.08 (d, *J* = 3.8 Hz, 1H), 6.94 (d, *J* = 8.9 Hz, 2H), 6.16 (d, *J* = 8.7 Hz, 1H), 6.11 (d, *J* = 8.9 Hz, 1H) 3.86 (s, 3H), 3.75 (s, 3H); <sup>13</sup>C NMR (100 MHz, DMSO-*d*<sub>6</sub>) δ: 177.1, 159.1, 158.7, 157.6, 151.3, 144.6, 141.6, 134.6, 131.9, 131.7 (2C), 130.9, 127.0 (2C), 124.9, 124.2, 123.8, 122.9, 122.8, 119.3, 118.5, 116.3 (2C), 116.2, 115.5, 114.2 (2C), 112.1, 107.6, 55.4, 55.1. HRMS (ASAP+, *m/z*): found 505.1344 (calcd. C<sub>31</sub>H<sub>23</sub>NO<sub>4</sub>S, 505.1348, [M]<sup>+</sup>).

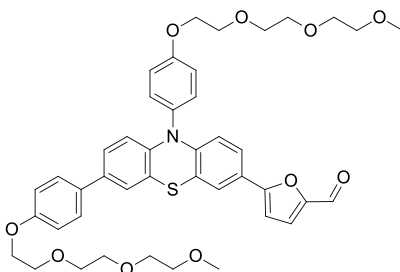
**Synthesis of 5-(10-(4-(2-(2-(2-methoxyethoxy)ethoxy)ethoxy)phenyl)-7-(4-methoxyphenyl)-10H-phenothiazin-3-yl)furan-2-carbaldehyde (15)**



SPhos (50.1 mg, 0.122 mmol), Pd(OAc)<sub>2</sub> (18.3 mg, 0.0815 mmol), K<sub>2</sub>CO<sub>3</sub> (650 mg, 4.70 mmol) and 5-formyl-2-furanylboronic acid (260 mg, 1.86 mmol) were added to a flask which then was evacuated and flushed with nitrogen. 1,4-Dioxane (25 mL) and deionized water (25 mL) were added through the septum followed by compound **10** (700 mg, 1.12 mmol) dissolved in 1,4-dioxane (1 mL). The reaction mixture was stirred at 80 °C for 3 hours before it was diluted with dichloromethane (30 mL) and deionized water (20 mL). The phases were separated and the aqueous phase was further extracted with dichloromethane (50 mL) and the combined organic phases were washed with deionized water (2 × 100 mL) and brine (100 mL). Silica gel column chromatography (gradient: 25-50% acetone in pentane) afforded compound **15** as a yellow foam (475 mg, 0.745 mmol, 66%). *R<sub>f</sub>* (acetone/pentane, 3:5) = 0.21. <sup>1</sup>H NMR (400 MHz, DMSO-*d*<sub>6</sub>) δ: 9.53 (s, 1H), 7.60 (d, *J* = 3.8 Hz, 1H), 7.54 (d, *J* = 2.0 Hz, 1H), 7.51 (d, *J* = 8.7 Hz, 2H), 7.41-7.35 (m, 3H), 7.31 (d, *J* = 2.1 Hz, 1H), 7.25 (d, *J* = 8.9 Hz, 2H), 7.16 (dd, *J* = 8.6, 2.2 Hz, 1H), 7.13 (d, *J* = 3.8 Hz, 1H), 6.96 (d, *J* = 8.8 Hz, 2H), 6.18 (d, *J* = 8.6 Hz, 1H), 6.12 (d, *J* = 8.6 Hz, 1H), 4.23-4.18 (m, 2H), 3.82-3.78 (m, 2H), 3.77 (s, 3H), 3.65-3.61 (m, 2H), 3.58-3.52 (m, 4H), 3.46-3.42 (m, 2H), 3.24 (s, 3H); <sup>13</sup>C NMR (100 MHz, DMSO-*d*<sub>6</sub>) δ: 177.3, 158.7, 158.5, 157.6, 151.3, 144.6, 141.7, 134.7, 132.0, 131.7 (2C),

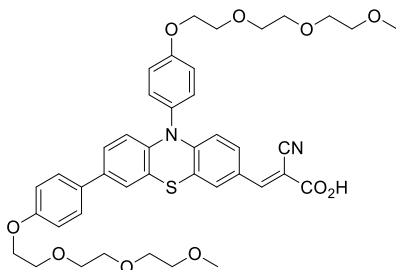
130.9, 127.1 (2C), 125.8, 125.0, 124.2, 123.9, 122.9, 122.8, 119.2, 118.5, 116.9 (2C), 116.2, 115.6, 114.3 (2C), 107.7, 71.3, 70.0, 69.8, 69.6, 68.9, 67.5, 58.1, 55.2; HRMS (ASCI/ASAP, m/z): found 638.2205 (calcd. C<sub>37</sub>H<sub>36</sub>NO<sub>7</sub>S, 638.2212, [M+H]<sup>+</sup>).

**Synthesis of 5-(7,10-bis(4-(2-(2-(2-methoxyethoxy)ethoxy)ethoxy)phenyl)-10H-phenothiazin-3-yl)furan-2- carbaldehyde (16)**



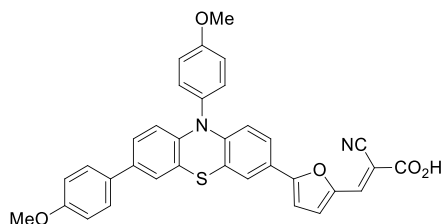
SPhos (15.3 mg, 0.0373 mmol), Pd(OAc)<sub>2</sub> (10.6 mg, 0.0472 mmol), K<sub>2</sub>CO<sub>3</sub> (220 mg, 1.59 mmol) and 5-formyl-2-furanylboronic acid (70.8 mg, 0.506 mmol) were added to a flask which then was evacuated and flushed with nitrogen. 1,4-Dioxane (8 mL) and deionized water (8 mL) were added through the septum followed by compound **6** (240 mg, 0.318 mmol) dissolved in 1,4-dioxane (1 mL). The reaction mixture was stirred at 80 °C for 3.5 hours before it was diluted with dichloromethane (30 mL) and deionized water (30 mL). The phases were separated and the aqueous phase was extracted with dichloromethane (20 mL) and the combined organic phases were washed with deionized water (2 × 30 mL) then brine (30 mL). Silica gel column chromatography (gradient: 25-50% acetone in pentane) afforded compound **16** as a yellow oil (147 mg, 0.191 mmol, 60%), *R<sub>f</sub>* (pentane/acetone, 1:1) = 0.20. <sup>1</sup>H NMR (400 MHz, DMSO-*d*<sub>6</sub>) δ: 9.52 (s, 1H), 7.58 (d, *J* = 3.7 Hz, 1H), 7.52 (d, *J* = 2.1 Hz, 1H), 7.48 (d, *J* = 8.8 Hz, 2H), 7.38-7.31 (m, 3H), 7.29 (d, *J* = 2.2 Hz, 1H), 7.22 (d, *J* = 8.9 Hz, 2H), 7.14 (dd, *J* = 8.7, 2.2 Hz, 1H), 7.11 (d, *J* = 3.7 Hz; 1H), 6.95 (d, *J* = 8.8 Hz, 2H), 6.16 (d, *J* = 8.7 Hz, 1H), 6.11 (d, *J* = 8.5 Hz, 1H), 4.21-4.16 (m, 2H), 4.11-4.06 (m, 2H), 3.81-3.77 (m, 2H), 3.75-3.71 (m, 2H), 3.64-3.39 (m, 16H), 3.24 (s, 3H), 3.22 (s, 3H); <sup>13</sup>C NMR (100 MHz, DMSO-*d*<sub>6</sub>) δ: 177.2, 158.4, 157.9, 157.6, 151.3, 144.6, 141.6, 134.6, 132.0, 131.7 (2C), 131.0, 127.0 (2C), 125.7, 124.9, 124.2, 123.8, 122.9, 122.8, 119.2, 118.5, 116.8 (2C), 116.2, 115.5, 114.8 (2C), 107.7, 71.3, 71.3, 70.0, 69.9, 69.8, 69.8, 69.6, 69.6, 68.9, 68.9, 67.5, 67.2, 58.0, 58.0; HRMS (ASCI/ASAP, m/z): found 770.2989 (calcd. C<sub>43</sub>H<sub>48</sub>NO<sub>10</sub>S, 770.2999, [M+H]<sup>+</sup>).

**Synthesis of (*E*)-3-(7,10-bis(4-(2-(2-(2-methoxyethoxy)ethoxy)ethoxy)phenyl)-10*H*-phenothiazin-3-yl)-2-cyanoacrylic acid (**EO3**)<sup>6</sup>**



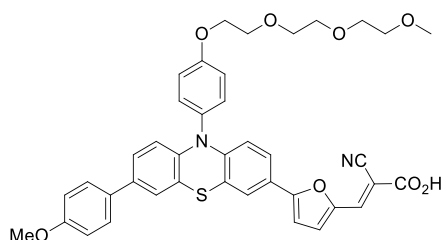
Compound **10** (62 mg, 0.088 mmol) was dissolved in acetonitrile (17 mL). Cyanoacetic acid (198 mg, 2.33 mmol) and piperidine (0.14 mL, 1.38 mmol) were added to the reaction mixture, followed by stirring at 80 °C for 2 hours. The reaction was quenched with HCl (1 M, 50 mL) followed by extraction with ethyl acetate (2 × 50 mL). The organic phases were collected and washed with deionized water (6 × 100 mL), then dried with brine (100 mL) and over anhydrous Na<sub>2</sub>SO<sub>4</sub>. The solvents were removed *in vacuo* and the crude product was purified using silica gel column chromatography (gradient: 0-15% methanol in dichloromethane), *R<sub>f</sub>* (methanol/dichloromethane, 1:9) = 0.27). The product was dissolved in dichloromethane, filtered and the solvent was removed *in vacuo* to yield sensitizer **EO3** as a red solid (42 mg, 0.054 mmol, 62%), mp 125-127 °C, 170 °C (dec.). <sup>1</sup>H NMR (600 MHz, DMSO-*d*<sub>6</sub>) δ: 7.78 (s, 1H), 7.61 (d, *J* = 1.5 Hz, 1H), 7.50 (d, *J* = 8.7 Hz, 2H), 7.39 (dd, *J* = 8.7, 1.5 Hz, 1H), 7.35 (d, *J* = 8.7 Hz, 2H), 7.30 (d, *J* = 2.0 Hz, 1H), 7.23 (d, *J* = 8.7 Hz, 2H), 7.17 (dd, *J* = 8.7, 2.0 Hz, 1H), 6.96 (d, *J* = 8.7 Hz, 2H), 6.12 (d, *J* = 2.5 Hz, 1H), 6.11 (d, *J* = 2.9 Hz, 1H), 4.19 (t, *J* = 3.7 Hz, 2H), 4.09 (t, *J* = 4.4 Hz, 2H), 3.79 (t, *J* = 4.4 Hz, 2H), 3.73 (t, *J* = 4.5 Hz, 2H), 3.63-3.61 (m, 2H), 3.59-3.49 (m, 10H), 3.45-3.41 (m, 4H), 3.24 (s, 3H), 3.23 (s, 3H) (COOH proton not visible); <sup>13</sup>C NMR (150 MHz, DMSO-*d*<sub>6</sub>) δ: 164.0, 158.5, 158.0, 146.5, 145.6, 141.3, 134.8, 131.8, 131.6 (2C), 130.9, 129.8, 127.1, 127.0 (2C), 126.8, 125.0, 123.8, 119.2, 118.5 (2C), 116.9 (2C), 116.3, 115.1, 114.8 (2C), 109.4, 71.3, 69.95, 69.93, 69.83, 69.78, 69.62, 69.59, 68.92, 68.87, 67.5, 67.2, 58.1, 58.0. (1C missing due to overlapping peaks); UV (THF, 2 × 10<sup>-5</sup> M, 20 °C) λ<sub>max</sub> (nm): 451 (14448 M<sup>-1</sup> cm<sup>-1</sup>); HRMS (ESI-, *m/z*): found 769.2795 (calcd. C<sub>42</sub>H<sub>45</sub>N<sub>2</sub>O<sub>10</sub>S, 769.2786, [M-H]).

**Synthesis of (*E*)-3-(5-(7,10-bis(4-methoxyphenyl)-10*H*-phenothiazin-3-yl)furan-2-yl)-2-cyanoacrylic acid (AFB-30)**



Compound **14** (224 mg, 0.443 mmol) and cyanoacetic acid (754 mg, 8.87 mmol) were added to a flask and dissolved in acetonitrile (59 mL) under a nitrogen atmosphere. Piperidine (0.53 mL, 5.4 mmol) was added and the reaction mixture was stirred at 70 °C for 30 minutes before it was cooled to room temperature and poured into an HCl solution (2 M, 100 mL). After stirring for 15 minutes, ethyl acetate (200 mL) was added. The phases were separated and the organic phase was washed with deionized water (5 × 150 mL) and brine (150 mL), then dried over anhydrous Na<sub>2</sub>SO<sub>4</sub>. Silica gel column chromatography (gradient: 0-20% methanol in ethyl acetate) afforded the sensitizer **AFB-30** as a dark purple solid (99.1 mg, 39%). *R<sub>f</sub>* (ethyl acetate/methanol, 3:1) = 0.15, mp 264 °C (dec.). <sup>1</sup>H NMR (400 MHz, DMSO-*d*<sub>6</sub>) δ: 7.79 (s, 1H), 7.56 (d, *J* = 2.0 Hz, 1H), 7.51 (d, *J* = 8.8 Hz, 2H), 7.42-7.38 (m, 3H), 7.33 (d, *J* = 2.2 Hz, 1H), 7.26-7.22 (m, 3H), 7.18 (dd, *J* = 8.7, 2.2 Hz, 1H), 7.09 (d, *J* = 3.7 Hz, 1H), 6.96 (d, *J* = 8.9 Hz, 2H), 6.15 (d, *J* = 6.9 Hz, 1H), 6.14 (d, *J* = 6.7 Hz, 1H), 3.87 (s, 3H), 3.77 (s, 3H) (COOH proton not visible); <sup>13</sup>C NMR (100 MHz, DMSO-*d*<sub>6</sub>) δ: 163.7, 159.2, 158.7, 155.7, 147.9, 144.1, 141.8, 134.0, 133.9, 132.0, 131.7 (2C), 131.0, 127.5, 127.0 (2C), 125.0, 123.9, 123.7, 123.3, 122.3, 119.1, 118.7, 118.5, 116.4 (2C), 116.1, 115.5, 114.5, 114.3 (2C), 108.0, 55.5, 55.2; UV (THF, 2 × 10<sup>-5</sup> M, 20 °C) λ<sub>max</sub> (nm): 446 (20634 M<sup>-1</sup> cm<sup>-1</sup>); IR (neat, cm<sup>-1</sup>) ν: 3474 (w, br), 3041 (w), 2956 (w), 2836 (w), 2357 (w), 2214 (w), 1606 (m), 1448 (s), 1382 (s), 1247 (w), 1026 (m), 791 (m); HRMS (TOF MS ASAP+, *m/z*): found 528.1502 (calcd. C<sub>33</sub>H<sub>24</sub>N<sub>2</sub>O<sub>3</sub>S, 528.1508, [M-CO<sub>2</sub>]<sup>+</sup>).

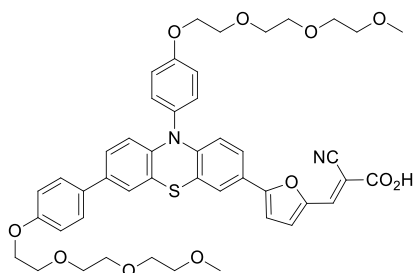
**Synthesis of (*E*)-2-cyano-3-(5-(10-(4-(2-(2-(2-methoxyethoxy)ethoxy)ethoxy)phenyl)-7-(4-methoxyphenyl)-10*H*-phenothiazin-3-yl)furan-2-yl)acrylic acid (AFB-31)**



Compound **15** (404 mg, 0.633 mmol) and cyanoacetic acid (518 mg, 6.09 mmol) were added to a flask and dissolved in acetonitrile (37 mL) under nitrogen atmosphere. Piperidine (0.36 mL, 3.6 mmol) was added

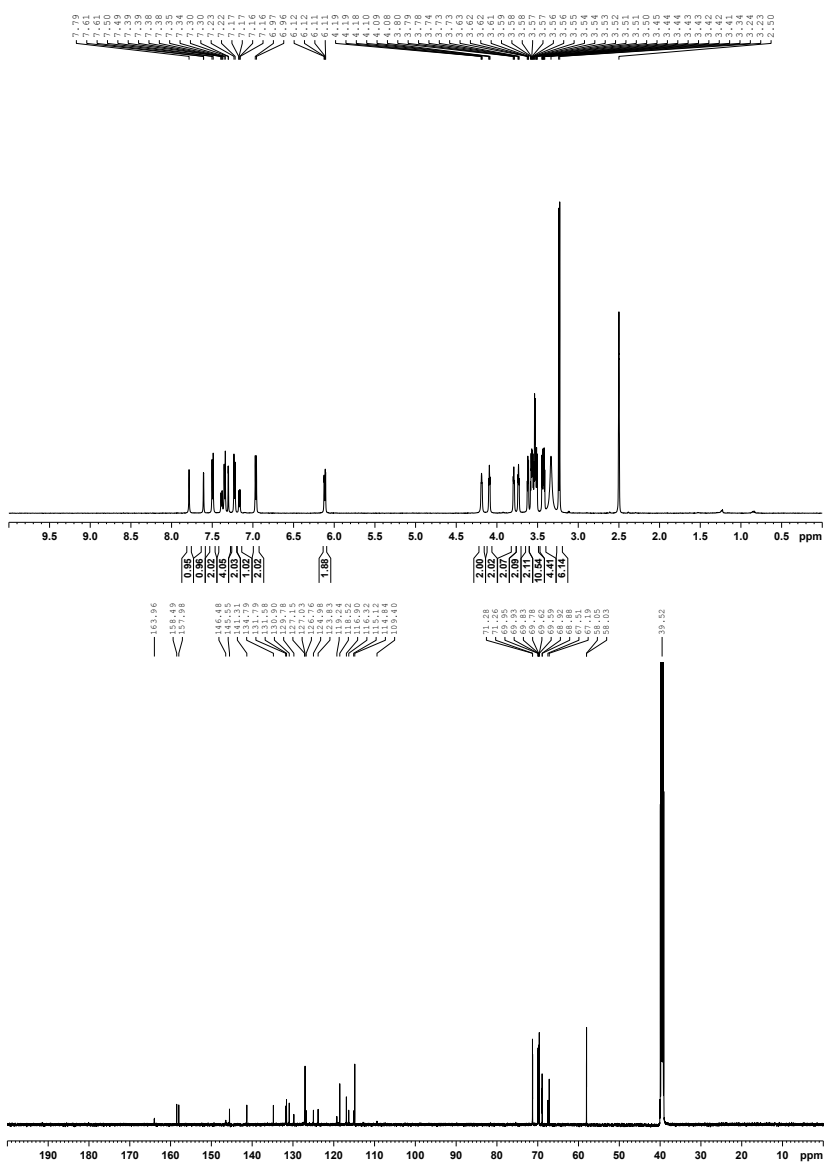
and the reaction mixture was stirred at 70 °C for 40 minutes before it was cooled to room temperature and poured into an HCl solution (2 M, 100 mL). After stirring for 15 minutes, ethyl acetate (150 mL) was added. The phases were separated and the organic phase was washed with deionized water (2 × 150 mL) and brine (150 mL) and dried over anhydrous Na<sub>2</sub>SO<sub>4</sub>. Silica gel column chromatography (gradient: 0-25% methanol in ethyl acetate) afforded the sensitizer **AFB-31** as dark purple crystals (377 mg, 0.535 mmol, 84%), *R<sub>f</sub>* (ethyl acetate/methanol, 5:3) = 0.40, mp 145 °C (dec.). <sup>1</sup>H NMR (600 MHz, DMSO-*d*<sub>6</sub>) δ: 7.80 (s, 1H), 7.56 (d, *J* = 2.1 Hz, 1H), 7.51 (d, *J* = 8.8 Hz, 2H), 7.40-7.37 (m, 3H), 7.33 (d, *J* = 2.2 Hz, 1H), 7.26-7.23 (m, 3H), 7.17 (dd, *J* = 8.6, 2.2 Hz, 1H), 7.09 (d, *J* = 3.6 Hz, 1H), 6.96 (d, *J* = 8.9 Hz, 2H), 6.15 (d, *J* = 6.8 Hz, 1H), 6.14 (d, *J* = 6.7 Hz, 1H), 4.23-4.19 (m, 2H), 3.82-3.79 (m, 2H), 3.77 (s, 3H), 3.64-3.43 (m, 8H), 3.25 (s, 3H) (COOH proton not visible); <sup>13</sup>C NMR (150 MHz, DMSO-*d*<sub>6</sub>) δ: 164.9, 158.7, 158.4, 155.6, 147.9, 144.0, 141.7, 134.6, 132.0, 131.7 (2C), 131.0, 127.1, 127.0 (2C), 125.0, 123.9, 123.6, 123.4, 122.3, 121.6, 119.1, 118.5, 118.0, 116.9 (2C), 116.2, 115.5, 114.3 (2C), 108.1, 106.8, 71.3, 70.0, 69.8, 69.6, 68.9, 67.5, 58.1, 55.2; IR (neat, cm<sup>-1</sup>) v: 3416 (w, br), 3049 (w), 2932 (w), 2214 (w), 1606 (m), 1459 (s), 1382 (s), 1235 (s), 1023 (m), 798 (m), 721 (m); UV (THF, 2 × 10<sup>-5</sup> M, 20 °C) λ<sub>max</sub> (nm): 454 (19844 M<sup>-1</sup> cm<sup>-1</sup>); HRMS (TOF MS ASAP+, *m/z*): found 660.2289 (calcd. C<sub>39</sub>H<sub>36</sub>N<sub>2</sub>O<sub>6</sub>S, 660.2294, [M-CO<sub>2</sub>]<sup>+</sup>).

**Synthesis of (*E*)-3-(5-(7,10-bis(4-(2-(2-methoxyethoxy)ethoxy)ethoxy)phenyl)-10*H*-phenothiazin-3-yl)furan-2-yl)- 2-cyanoacrylic acid (**AFB-32**)**

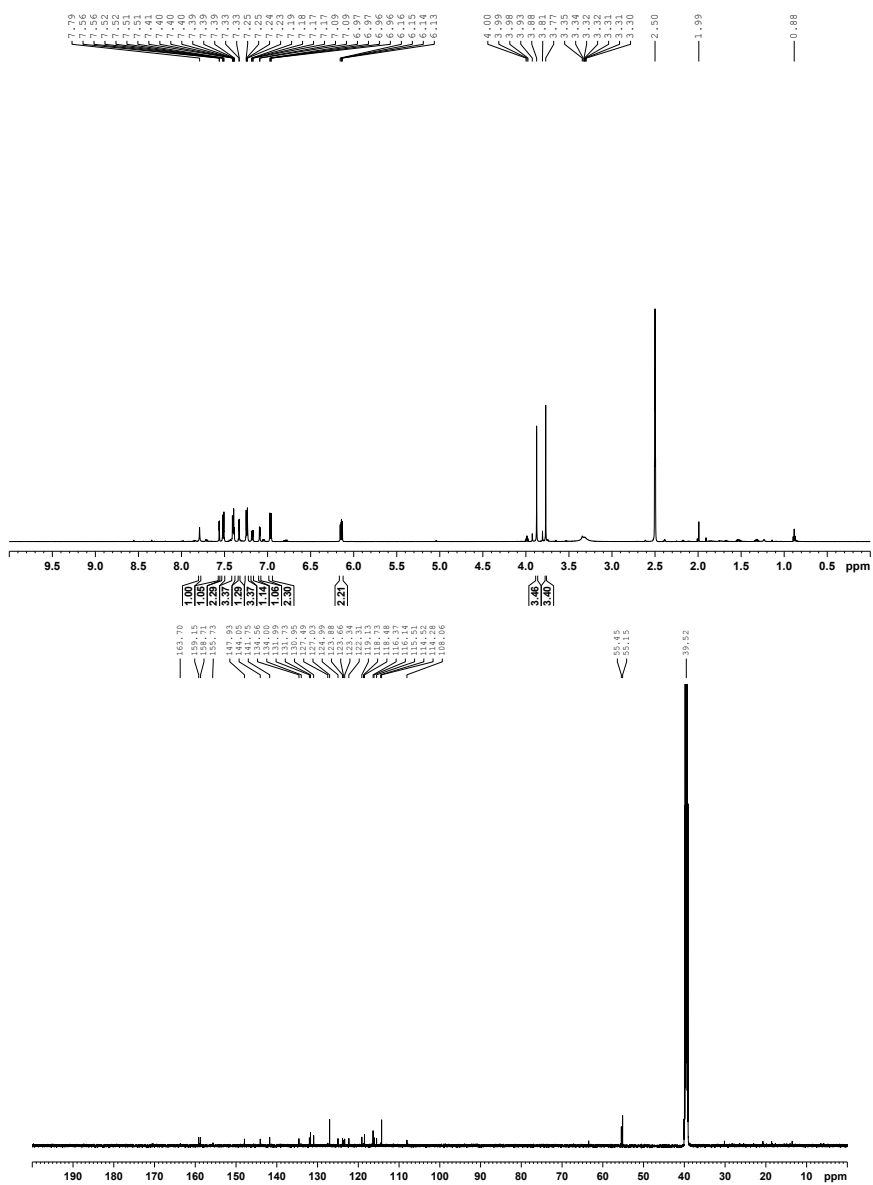


Compound **8** (194 mg, 0.252 mmol) and cyanoacetic acid (480 mg, 5.64 mmol) were added to a flask and dissolved in acetonitrile (30 mL) under nitrogen atmosphere. Piperidine (0.3 mL, 3 mmol) was added and the reaction mixture was stirred at 70 °C for 50 minutes before it was cooled to room temperature and poured into an HCl solution (2 M, 100 mL) where it was stirred for 15 minutes before ethyl acetate (150 mL) was added. The phases were separated and the organic phase was washed with deionized water (2 × 150 mL) and brine (150 mL), then dried over anhydrous Na<sub>2</sub>SO<sub>4</sub>. Silica gel column chromatography (gradient: 2-25% methanol in ethyl acetate) afforded the sensitizer **AFB-32** as a dark purple solid (148 mg, 0.177 mmol, 70%), *R<sub>f</sub>* (ethyl acetate/methanol, 3:1) = 0.11, mp 123-125 °C, 150 °C (dec.). <sup>1</sup>H NMR (600 MHz, DMSO-*d*<sub>6</sub>) δ: 7.75 (s, 1H), 7.56 (d, *J* = 2.1 Hz, 1H), 7.51 (d, *J* = 8.8 Hz, 2H), 7.41-7.37 (m, 3H), 7.33 (d, *J* = 2.2 Hz, 1H), 7.25 (d, *J* = 8.9 Hz, 2H), 7.21-7.15 (m, 2H), 7.07 (d, *J* = 3.6 Hz, 1H), 6.97 (d, *J* = 8.9 Hz, 2H), 6.15 (d, *J* = 6.5 Hz, 1H), 6.14 (d, *J* = 6.5 Hz, 1H), 4.25-4.18 (m, 2H), 4.13-4.08 (m, 2H), 3.84-3.78 (m, 2H), 3.76-3.72 (m, 2H), 3.65-3.40 (m, 16H), 3.25 (s, 3H), 3.23 (s, 3H) (COOH proton not visible); <sup>13</sup>C NMR (150 MHz, DMSO-*d*<sub>6</sub>) δ: 163.9, 158.4, 157.9, 155.5, 148.0, 144.0, 141.8, 134.5, 133.9, 132.1, 131.7 (2C), 131.0, 127.0 (2C), 125.0, 123.9, 123.6, 123.4, 122.3, 121.6, 119.1, 118.5, 118.1, 116.9 (2C),

116.2, 115.5, 114.8 (2C), 108.0, 105.9, 71.3, 71.3, 70.0, 69.9, 69.8, 69.8, 69.6, 69.6, 68.9, 68.9, 67.5, 67.2, 58.1, 58.0; IR (neat,  $\text{cm}^{-1}$ ): 3041 (w), 2871 (m, br), 2353 (w), 2209 (w), 1606 (m), 1579 (m), 1452 (s), 1250 (s), 1100 (s), 794 (s); UV (THF,  $2 \times 10^{-5}$  M, 20 °C)  $\lambda_{\text{max}}$  (nm): 451 ( $19385 \text{ M}^{-1} \text{ cm}^{-1}$ ); HRMS (TOF MS ASAP+, m/z): found 792.3080 (calcd.  $\text{C}_{45}\text{H}_{48}\text{N}_2\text{O}_9\text{S}$ , 792.3081,  $[\text{M}-\text{CO}_2]^+$ ).

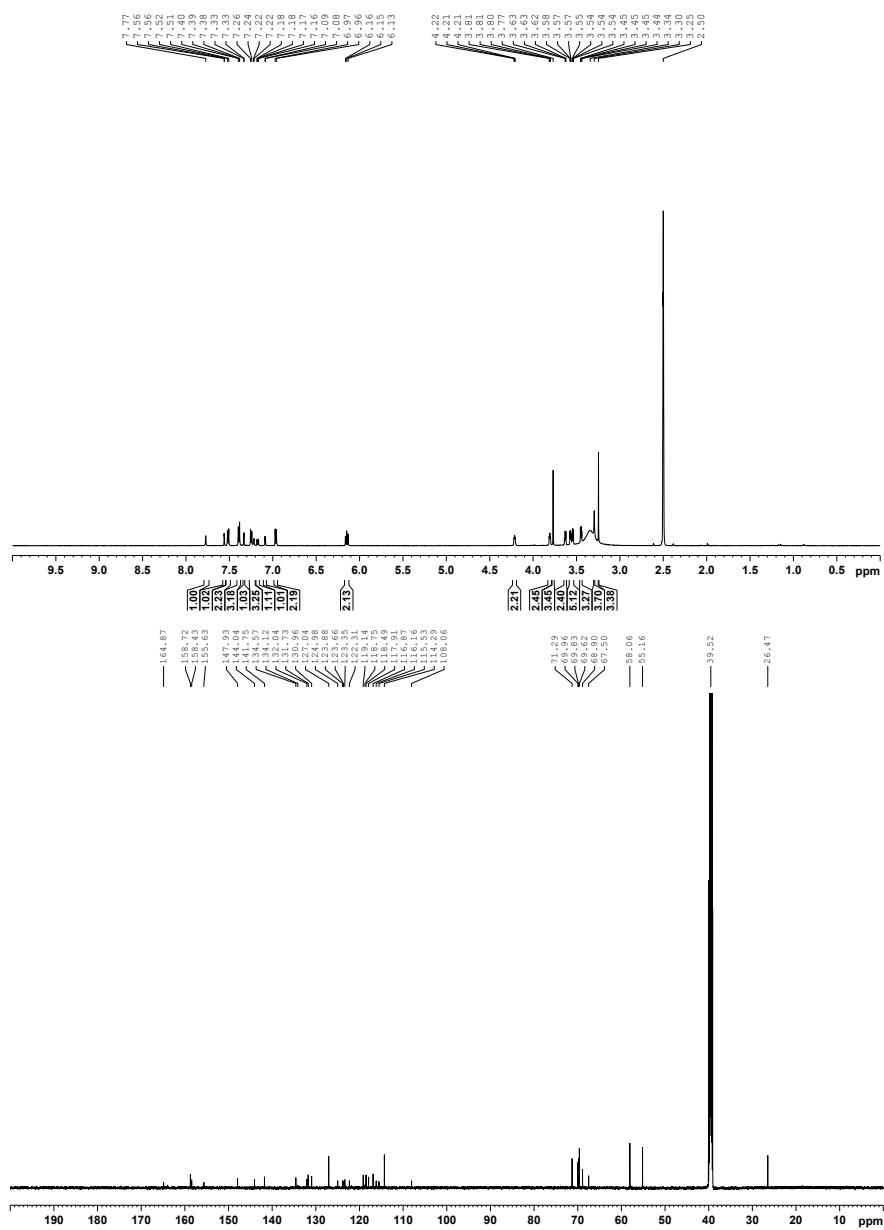
**NMR Spectra  
EO3**Fig. S6  $^1\text{H}$  and  $^{13}\text{C}$  NMR spectra for EO3.

## AFB-30

Fig. S7  $^1\text{H}$  and  $^{13}\text{C}$  NMR spectra for AFB-30.



## AFB-31

Fig. S8  $^1\text{H}$  and  $^{13}\text{C}$  NMR spectra for AFB-31.



## References

1. S. H. Jung, J.-W. Lee and H.-J. Kim, *Supramol. Chem.*, 2016, **28**, 634-639.
2. Y. Lu, T. Suzuki, W. Zhang, J. S. Moore and B. J. Mariñas, *Chem. Mater.*, 2007, **19**, 3194-3204.
3. A. T. Bui, A. Grichine, A. Duperray, P. Lidon, F. Riobé, C. Andraud and O. Maury, *JACS*, 2017, **139**, 7693-7696.
4. Y.-H. Seo, W.-H. Lee, J.-H. Park, C. Bae, Y. Hong, J.-W. Park and I.-N. Kang, *J. Polym. Sci. A*, 2012, **50**, 649-658.
5. T. Liu, Y.-G. Wei, Y.-Q. Yuan and Q.-X. Guo, *Chin. J. Chem.*, 2005, **23**, 1430-1436.
6. R. Y.-Y. Lin, F.-L. Wu, C.-T. Li, P.-Y. Chen, K.-C. Ho and J. T. Lin, *ChemSusChem*, 2015, **8**, 2503-2513.
7. W. Yang, D. Cao, H. Zhang, X. Yin, X. Liao, J. Huang, G. Wu, L. Li and Y. Hong, *Electrochim. Acta*, 2018, **283**, 1732-1741.

## **PAPER V**

**Experimental study comparing the 3,7 and 3,8 substitution geometry of phenothiazine sensitizers for DSSC**





## Experimental study comparing the 3,7 and 3,8 substitution geometries of phenothiazine sensitizers for dye-sensitized solar cells

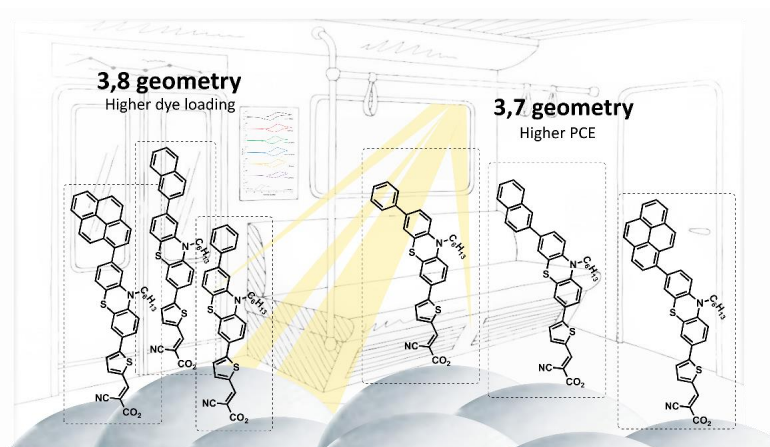
Audun Formo Buene, Mats Christensen and Bård Helge Hoff\*

Department of Chemistry, Norwegian University of Science and Technology, Høgskoleringen 5, NO-7491 Trondheim, Norway

\* Corresponding author. Tel.: +47 73593973; E-mail address: [bard.h.hoff@ntnu.no](mailto:bard.h.hoff@ntnu.no) (B. H. Hoff).

### Abstract

The 3,7 substitution geometry is by far the most common for phenothiazine sensitizers for dye-sensitized solar cells. Recently, we reported several new sensitizer geometries, and found the 3,8 geometry to be as efficient as the widely used 3,7 geometry. In this study we compare three pairs of sensitizers differing only in the geometry and auxiliary donors, in an attempt to identify any performance differences between the 3,7 and 3,8 geometries. Comprehensive photophysical, electrochemical and photovoltaic experiments were employed to differentiate the two geometries. Varying between the phenyl, naphthyl and pyrenyl auxiliary donors had no pronounced effect on performance. Generally, the 3,7 geometry was found to narrowly outperform the 3,8 geometry in terms of power-conversion efficiency, despite lower dye loading. The best device of the study was sensitized with 3,7-naphthyl delivering a PCE of 6.25% (10 eq. CDCA,  $J_{SC} = 11.09 \text{ mA cm}^{-2}$ ,  $V_{OC} = 761 \text{ mV}$  and  $FF = 0.734$ ).



*Keywords: Geometry study, phenothiazine, dye-sensitized solar cells, donor position*

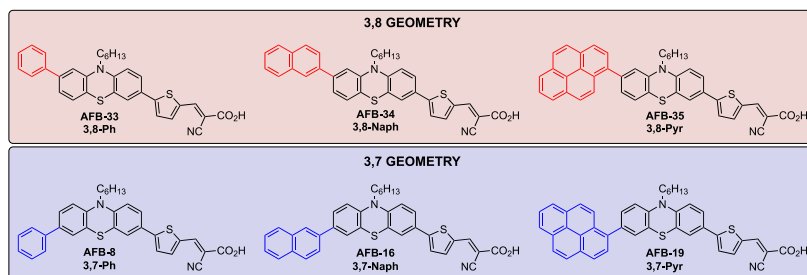
## 1. Introduction

The dye molecule is the heart and soul of a dye-sensitized solar cell. It has the all-important task of harvesting sunlight and transferring the photon energy to an electron by exciting it to a molecular state of higher energy.[1] The task of the rest of the solar cell architecture is to convert as much of the potential energy of the electron to kinetic energy, i.e. electricity.

When first reported in 1991 by O'Regan and Grätzel, the DSSCs relied on metal complex sensitizers.[2] Upon photoexcitation, these dyes injected electrons into a mesoporous TiO<sub>2</sub> layer on a fluorine-doped tin oxide coated glass substrate comprising the photoanode. An electrolyte containing a redox couple, such as I<sup>-</sup>/I<sub>3</sub><sup>-</sup>, would regenerate the oxidized sensitizers with electrons from the counter electrode. This device architecture is still in frequent use, but new developments such as p-type DSSCs[1], novel metal coordination redox complexes[3] and metal-free organic sensitizers[4] have added a greater variety to the DSSC field.

As the primary component, dye molecules have been the focus of numerous studies.[5-7] For the metal-free sensitizers, researchers have a massive toolbox of available organic reactions for synthesis and dye development.[4] These sensitizers also offer higher molar extinction coefficients and often less complicated purifications are required during synthesis. The structural diversity within the metal-free sensitizers is enormous, with triarylamine,[5, 8, 9] carbazole,[10, 11] squaraine,[12] phenanthroline[13] and phenothiazine[14, 15] being just a few examples of common dye scaffolds.

The phenothiazine dye class has since the first publication in 2007 by Tian et al.[16], developed to over 250 sensitizers reported in at least 115 publications.[14, 17, 18] In a previous study on novel fundamental phenothiazine geometries, we found the new 3,8 geometry and the conventional 3,7 geometries equally efficient in dye-sensitized solar cells.[14] The 3,8 dyes have a more linear structure, and are thus expected to produce dye monolayers with higher dye loading than the corresponding 3,7 sensitizers.



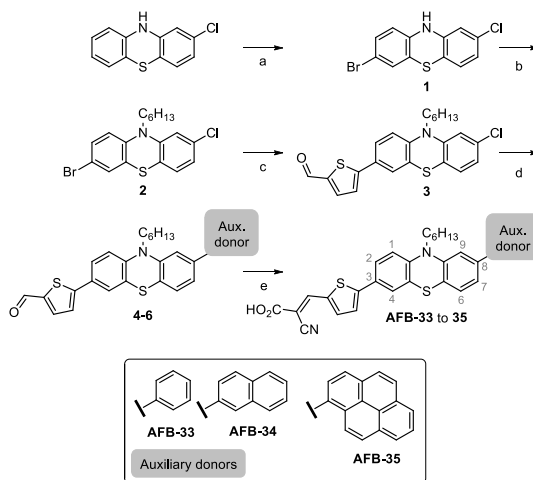
**Figure 1.** The dyes investigated in this study from the 3,7 and 3,8 geometries.

In this study we have prepared a larger data set investigating the 3,7 and 3,8 geometries for three pairs of phenothiazine sensitizers, see structures in Figure 1. Auxiliary donors of increasing size were selected (phenyl, naphthyl and pyrenyl), in case effects due to the geometry is more pronounced for larger substituents.

## 2. Results and Discussion

### 2.1. Dye synthesis

The synthesis for the novel dyes **AFB-33** to **35** was performed following a route previously reported by the authors[14], see Scheme 1. The 3,7 dyes **AFB-8**, **16** and **19** are previously described by the authors.[15, 19] All details on the synthesis and characterization of the sensitizers can be found in the ESI. For improved clarity, the sensitizers will be referred to by their geometry and auxiliary donor, i.e. **AFB-33** is simply referred to as 3,8-Ph. The numbering of the positions on the 10*H*-phenothiazine scaffold are given in Scheme 1.



**Scheme 1.** Synthesis route for the three novel 3,8 sensitizers with phenyl, naphthyl and pyrenyl auxiliary donors. a)  $\text{Br}_2$ ,  $\text{AcOH}$ , b) 1-bromohexane,  $\text{NaH}$ ,  $\text{THF}$ , c/d) 5-formyl-2-thienylboronic acid/auxiliary donor boronic acid,  $\text{Pd}(\text{OAc})_2$ ,  $\text{SPhos}$ , 1,4-dioxane,  $\text{H}_2\text{O}$ , e) cyanoacetic acid, piperidine, acetonitrile.



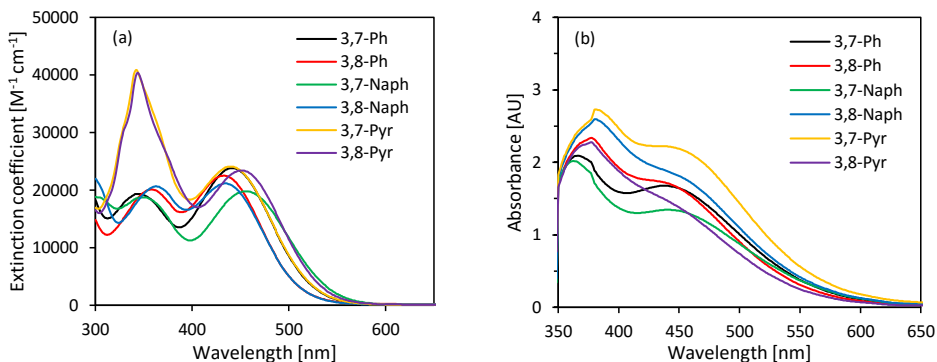
## 2.2. Photophysical properties

The recorded UV/Vis spectra from dye solutions in THF are given in Figure 2, while the extracted data are found in Table 1. The absorption properties of all the six sensitizers are very similar both in terms of the position of the internal charge transfer (ICT) peak around 440 nm and the molar extinction coefficients in the range of 20000-24000 M<sup>-1</sup> cm<sup>-1</sup>. Emission spectra in Figure S1 also indicates the six different sensitizers have very comparable photophysical behaviour. On TiO<sub>2</sub> films without CDCA co-adsorbent, the position of the ICT peak does not change compared to in solution, but the shoulders of the absorption peak are wider, resulting in an estimated onset red-shift of approximately 50 nm. As no considerable shift in absorption on TiO<sub>2</sub> films is observed, we assume the dyes are not particularly prone to aggregation affecting the photophysical properties. The dye pair with the largest absorption difference has the naphthyl auxiliary donor, with the ICT peak of the 3,7 dye redshifted by 20 nm compared to the 3,8 dye. However, on TiO<sub>2</sub> the absorbance peak position of the same two sensitizers is within 5 nm. As the extinction coefficients are similar, the difference in the absorbance of the dyes on the TiO<sub>2</sub> films is attributed to different dye loading values, reported in Table 3.

**Table 1.** Photophysical properties of the dyes.

Dye	Geometry	$\lambda_{\text{abs}}^a$ (nm)	$\epsilon$ (M <sup>-1</sup> cm <sup>-1</sup> )	Em. <sup>b</sup> (nm)	$\lambda_{\text{abs}}^c$ on TiO <sub>2</sub> (nm)	E <sub>0-0</sub> <sup>d</sup> (eV)	E <sub>ox</sub> <sup>e</sup> (V)	E <sub>LUMO</sub> <sup>f</sup> (V)
<b>AFB-8</b>	3,7-Ph	441	23800	623	438	2.34	1.01	-1.33
<b>AFB-33</b>	3,8-Ph	433	22500	621	433 <sup>g</sup>	2.37	1.05	-1.32
<b>AFB-16</b>	3,7-Naph	456	19800	610	442	2.35	0.99	-1.36
<b>AFB-34</b>	3,8-Naph	434	21100	615	440 <sup>g</sup>	2.37	1.04	-1.33
<b>AFB-19</b>	3,7-Pyr	440	24100	622	441 <sup>g</sup>	2.34	1.03	-1.31
<b>AFB-35</b>	3,8-Pyr	451	23400	634	439 <sup>g</sup>	2.32	1.07	-1.25

<sup>a</sup> Maximum of most red-shifted peak. <sup>b</sup> Emission when ICT band is excited, in THF solution. <sup>c</sup> Maximum of most red-shifted peak on TiO<sub>2</sub> (2.5  $\mu\text{m}$ , GreatcellSolar 18NR-T). <sup>d</sup> Calculated from the intersection of the absorption and normalized emission spectra. <sup>e</sup> Measured vs. F<sub>c</sub><sup>+/</sup>F<sub>c</sub> on stained TiO<sub>2</sub> electrodes in acetonitrile with 0.1 M LiTFSI, converted to V vs. SHE by 0.624 V. Scan rate 20 mV s<sup>-1</sup>. <sup>f</sup> Calculated from E<sub>ox</sub>-E<sub>0-0</sub>. <sup>g</sup> Manual estimate due to no clear peak to assign.



**Figure 2.** a) UV/Vis absorption spectra of all dyes in THF solution. b) UV/Vis absorbance spectra of all dyes on TiO<sub>2</sub> films without CDCA co-adsorbent (2.5  $\mu$ m, 18NR-T).

### 2.3. Electrochemical properties

Cyclic voltammetry on stained FTO/TiO<sub>2</sub> electrodes was performed in acetonitrile with 0.1 M LiTFSI as a supporting electrolyte, a graphite rod as counter electrode and a Ag/AgCl reference (Figure S2). For the measurement of ferrocene, the working electrode was replaced by a glassy carbon disc, and the half-wave potential ( $E_{1/2}$ ) of ferrocene was found to be 0.358 V vs. Ag/AgCl. Fully reversible oxidations were found for all the sensitizers, and the extracted oxidation potentials are comparable with earlier measurements on similar sensitizers with the same technique.[14] Hence, the HOMO level potentials are well below the redox potential of the I<sup>-</sup>/I<sub>3</sub><sup>-</sup> redox couple, and dye regeneration should thus be efficient. Paired with the optical bandgaps, the elucidated LUMO level energies of the sensitizers are sufficiently above the conduction band of TiO<sub>2</sub>, thus efficient electron injection is expected. The oxidation potentials of the 3,8 sensitizers are all found shifted by 40-50 mV towards more positive potentials vs. SHE compared to their 3,7 counterparts, but the reason for this is not immediately apparent.

### 2.4. Photovoltaic properties

The two series of dyes with the 3,7 and 3,8 geometries were tested in DSSCs, and Figure 3 shows the  $J-V$  curves under 1 sun AM1.5 G illumination (data summarized in Table 2). The solar cells were fabricated from photoanodes with 16.5  $\mu$ m TiO<sub>2</sub> (11  $\mu$ m 18NR-T and 5.5  $\mu$ m WER2-O scattering layer), platinum coated FTO counter electrodes and an I<sup>-</sup>/I<sub>3</sub><sup>-</sup> electrolyte in a sandwich construction.

Chenodeoxycholic acid (CDCA) is a co-adsorbent added to the staining solution to inhibit dye aggregation, and is a very common additive in DSSCs.[20, 21] In the absence of CDCA, the photovoltaic performance depended on the auxiliary donor following the trend Ph > Naph > Pyr for the 3,7-series. In the 3,8-series, the order was Ph > Pyr ~ Naph. For both geometries, the smallest auxiliary donor yields the highest PCE

values, without any anti-aggregation additive. This could suggest the bigger aromatic systems of the naphthyl and pyrenyl dyes are susceptible to unwanted aggregation.

**Table 2.** Photovoltaic performance of the dyes under 1 sun AM 1.5G illumination, and from IPCE measurements.

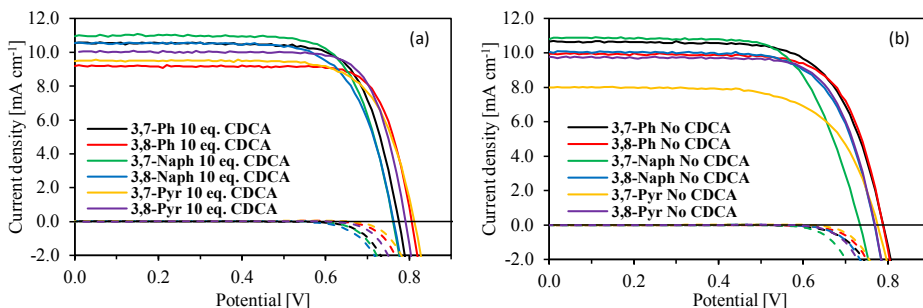
Dye	CDCA (eq.)	IPCE $J_{SC}$ (mA cm <sup>-2</sup> ) <sup>a</sup>	$J_{SC}$ (mA cm <sup>-2</sup> )	$V_{OC}$ (mV)	FF	PCE (%)
<b>3,7-Ph</b>	0	10.35	11.01 ± 0.34	781 ± 7	0.66 ± 0.03	5.75 ± 0.11
	10	9.91	10.31 ± 0.16	781 ± 7	0.74 ± 0.01	5.99 ± 0.12
<b>3,8-Ph</b>	0	9.80	9.95 ± 0.19	779 ± 13	0.73 ± 0.01	5.70 ± 0.15
	10	8.64	9.67 ± 0.29	790 ± 14	0.75 ± 0.04	5.77 ± 0.20
<b>3,7-Naph</b>	0	10.68	11.09 ± 0.17	726 ± 12	0.65 ± 0.03	5.33 ± 0.28
	10	10.75	11.27 ± 0.20	754 ± 10	0.71 ± 0.03	6.08 ± 0.21
<b>3,8-Naph</b>	0	10.22	10.25 ± 0.08	768 ± 1	0.69 ± 0.02	5.46 ± 0.12
	10	9.87	10.55 ± 0.17	770 ± 8	0.70 ± 0.01	5.72 ± 0.08
<b>3,7-Pyr</b>	0	8.31	7.93 ± 0.28	784 ± 8	0.65 ± 0.02	4.07 ± 0.16 <sup>b</sup>
	10	9.54	9.43 ± 0.25	810 ± 3	0.74 ± 0.01	5.68 ± 0.13
<b>3,8-Pyr</b>	0	8.63	9.90 ± 0.01	771 ± 3	0.71 ± 0.02	5.51 ± 0.14
	10	9.67	10.10 ± 0.39	771 ± 18	0.75 ± 0.01	5.88 ± 0.24
<b>N719</b>	10	-	12.85	805	0.76	7.77

<sup>a</sup> Obtained by integration of the IPCE spectrum over the 1 sun AM 1.5 G spectrum.

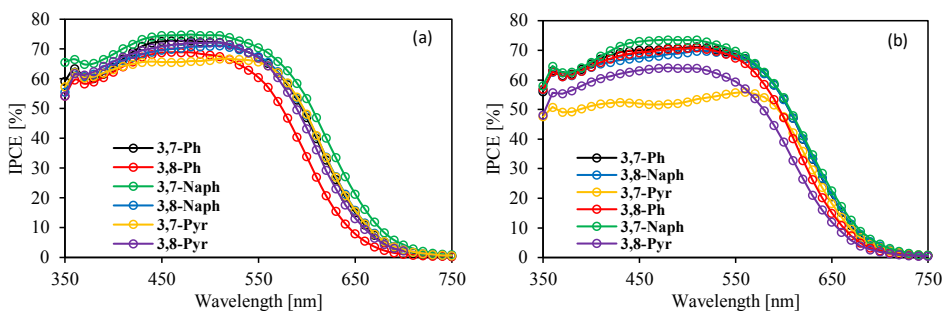
<sup>b</sup> Visible aggregation of dye on the FTO glass.

With the addition of 10 molar equivalents of CDCA in the staining solutions, smaller differences are found between the auxiliary donors. For the 3,7-dyes, the performance order is Naph > Ph > Pyr, while the 3,8-dyes follow the exact opposite order of Pyr > Ph > Naph, bearing in mind the relative differences are quite moderate. Interestingly, sensitizer **3,7-Pyr** seems to be strongly aggregating without CDCA, evident from the large performance difference between 0 and 10 equivalents of CDCA. For the rest of the selection, adding CDCA to the staining solutions improved the PCE by only 6%. This suggests the dyes are not excessively prone to aggregation, a trait commonly claimed for the phenothiazine scaffold in general, due to its inherently bent aggregation inhibiting backbone.[18, 22, 23] Another explanation could be the dyes are prone to aggregate even in the presence of co-adsorbents, and more control of the distribution of co-adsorbents in the dye monolayer is needed to provide sufficient aggregation inhibition. We expected the more linear 3,8 geometry dyes to aggregate more readily compared to the 3,7 dyes. However, although the differences are small, the 3,7 dyes show a larger efficiency improvement than the 3,8 dyes in response to

CDCA addition, suggesting the opposite could be the case. The effect of CDCA is most prominent as higher fill factors, while the open-circuit voltage appears to be unaffected, see Table 2 and Figure 3.

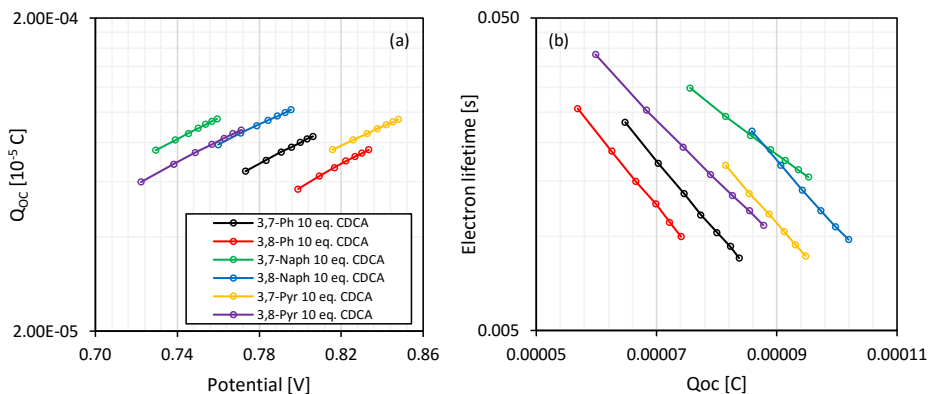


**Figure 3.** Current-density-voltage curves for devices built with the six sensitizers with 10 eq. CDCA in the staining solutions. a) with 10 eq. CDCA, b) without CDCA.



**Figure 4.** Incident photon-to-current conversion efficiency (IPCE) spectra of the six sensitizers with 10 eq. CDCA in the staining solutions. a) with 10 eq. CDCA, b) without CDCA.

The IPCE spectra in Figure 4 display the same trends as observed from the  $J$ - $V$  data, especially the lower performance of the sensitizers with pyrene auxiliary donors without CDCA co-adsorbent. The onsets from the IPCE curves are redshifted by over 50 nm compared to the absorbance measurements on TiO<sub>2</sub> films. This is attributed to the solvent of the electrolyte, predominantly acetonitrile, which is known for red-shifting the absorption of organic sensitizers.[24]



**Figure 5.** a) Charge extraction measurements. b) Electron lifetime measurements corrected for conduction band shift and plotted for the corresponding charge extraction value.

Charge extraction and injected electron lifetimes were measured for the best devices fabricated with each sensitizer, see Figure 5. Very comparable charge extraction values were found for all six sensitizers, albeit spread over a large  $V_{OC}$  range. Correcting the electron lifetime curves for the observed conduction band shift from the  $Q_{oc}$  curves and plotting the electron lifetime vs.  $Q_{oc}$ , we obtain Figure 5b. We find the sensitizer pairs with the same auxiliary donors grouped with the ascending order: phenyl < pyrenyl < naphthyl, with marginally higher electron lifetime values found for the dyes with 3,7 geometry.

**Table 3.** Dye loading measurements. Average values of three simultaneously stained and separately desorbed electrodes with corresponding standard deviation.

Dye	Dye loading ( $10^{-7}$ mol $\text{cm}^{-2}$ )	Standard deviation
<b>3,7-Ph</b>	5.07	$\pm$ 0.46
<b>3,8-Ph</b>	5.82	$\pm$ 0.42
<b>3,7-Naph</b>	4.18	$\pm$ 0.08
<b>3,8-Naph</b>	7.66	$\pm$ 0.21
<b>3,7-Pyr</b>	9.04	$\pm$ 0.09
<b>3,8-Pyr</b>	6.30	$\pm$ 0.76

The dye loading values in Table 3 confirm, to a large extent, our hypothesis that the more linear 3,8 geometry is able to yield higher density monolayers. For the pyrene-substituted dyes, the dye-loading order is reversed, a fact likely attributed to aggregation or precipitation of **3,7-Pyr**. Following staining, dye

particles were observed on the FTO glass substrate. These were not soluble in acetonitrile, thus the regular washing procedure after the staining was not able to remove sensitizer molecules adsorbed only through aggregation to the TiO<sub>2</sub> photoanode.

Although the 3,8-dyes currently are not surpassing the conventional 3,7-dyes in terms of power conversion efficiency, we believe they may still hold untapped potential. The HOMO level positions are more favorable and they require a smaller area for anchoring compared to the 3,7-dyes. Both properties could make the 3,8 phenothiazine dyes potentially valuable co-sensitizers in future studies.

### 3. Conclusion

Attempting to differentiate between the 3,7 and 3,8 geometries for phenothiazine sensitizers, we synthesized a selection of three pairs of dyes from both geometries. No major differences were found for the photophysical properties of the dyes, while for the electrochemical performance a weak trend was observed. The HOMO levels of the novel 3,8 dyes were shifted towards more positive potentials by 40-50 mV compared to the 3,7 sensitizers. In terms of dye loading, the 3,8 dyes displayed higher dye loading than the 3,7 dyes, although for the pyrene auxiliary donor the order was reversed. In DSSC devices, despite largely very similar performance from all six dyes, a performance advantage was found for the 3,7 dyes, by the slightest of margins. The effect of the co-adsorbent CDCA was only modest, resulting in average efficiency improvements of 6%, not including 3,7-pyrene, which was prone to significant aggregation without CDCA. The highest performing sensitizer of the series was 3,7-naphthyl delivering a PCE of 6.25% in the best device.

Overall, the position of the auxiliary donor is of little importance to the photovoltaic performance. The auxiliary donors, regardless of position, are not fully in conjugation with the anchoring group, due to the inherent butterfly shape of the phenothiazine scaffold reducing the orbital overlap. Consequently, any positive contributions from the auxiliary donors will be limited. However, the promising dye loading and slightly lower HOMO levels could make the 3,8 phenothiazine dyes more suited as co-sensitizers, compared to the conventional 3,7-dyes.

## 4. Experimental

### 4.1. Synthesis

Detailed descriptions of synthesis and characterization of dyes and intermediates is given in the electronic supporting information (ESI). All chemicals for dye synthesis and device fabrication were sourced from Sigma Aldrich, unless another supplier is specified.

#### 4.2. DSSC fabrication

The photoanodes were fabricated from FTO glass (NSG10, Nippon Sheet Glass), washed with Deconex 21 in an ultrasonic bath for 45 minutes, then cleaned in a UV/Ozone cleaner for 15 minutes. A dense TiO<sub>2</sub> blocking layer was deposited by hydrothermal deposition of aqueous TiCl<sub>4</sub> (40 mM in deionized water) at 70 °C for 2 × 30 minutes, followed by rinsing with deionized water and ethanol before heating on a hotplate for 1 hour at 250 °C. The active (18NR-D, Greatcell Solar) and scattering TiO<sub>2</sub> (WER2-O, GreatCell Solar) layers were screenprinted (54T mesh, 0.283 cm<sup>2</sup> active area) onto the FTO glass slides. Thickness measurements by profilometer determined a thickness of 11 + 6.5 μm of the active and scattering layers. The photoanodes were sintered on a programmable hotplate at 125, 250, 375, 450 and 500 °C for 5, 5, 5, 15 and 30 minutes, with a ramp time of 5 minutes between each step. Afterwards, a TiCl<sub>4</sub> post-treatment was performed following the same procedure as for the blocking layer, followed by sintering at 500 °C for 1 hour (25 minutes ramping from room temperature). Before immersion in the dye staining solutions, the photoanodes were annealed by heatgun at 450 °C for 30 minutes and allowed to reach approximately 80 °C before immersion.

Counter electrodes were fabricated with TEC8 FTO glass. Electrolyte filling holes were drilled with a diamond drill bit, and the electrodes rinsed in Hellmanex 2% solution, deionized water, ethanol and acetone, each for 15 minutes under sonication. A thin catalytic layer of Pt was deposited by dropcasting a solution of H<sub>2</sub>PtCl<sub>6</sub> (10 mM in isopropanol, 5 μL/cm<sup>2</sup>), followed by heating at 400 °C for 15 minutes.

The solvent mixture for the staining solutions was tetrahydrofuran/acetonitrile (57:43, v/v), dye concentration was 0.5 mM and concentrations of CDCA was either 0 or 5 mM. The photoanodes were stained for 22 hours at room temperature and rinsed with acetonitrile before assembly. A Surlyn gasket (35 μm) was melted between the photoanode and counter electrodes, and the A6141 electrolyte was injected by vacuum backfilling and the hole sealed with Surlyn and a glass cover. The A6141 electrolyte consisted of 0.60 M 1-butyl-3-methylimidazolium iodide, 0.03 M I<sub>2</sub>, 0.10 M guanidinium thiocyanate and 0.50 M *tert*-butylpyridine in a mixture of acetonitrile and valeronitrile (85:15, v/v).[25] The conductive edges of the working and counter electrodes protruding from the device were covered by ultrasonic soldering tin for improved contact.

#### 4.3. Device characterization

Current-density-voltage characteristics of the devices were measured under 1 sun AM1.5G illumination by a solar simulator with a Xenon lamp (300W, Oriol) with a Keithley 2400. The potential scan direction was from open-circuit to short-circuit, and the devices were masked off by a 0.158 cm<sup>2</sup> black metal mask. Incident photon-to-current conversion efficiency (IPCE) measurements were recorded on a commercial

setup from Arkeo-Ariadne (Cicci research s.r.l.) with a 300 W Xenon lamp. Charge extraction and electron lifetime measurements were recorded with a Dyenamo Toolbox instrument.

### Acknowledgements

The support from the Research Council of Norway to the Norwegian Micro- and Nano-Fabrication Facility, NorFab (project number 245963/F50) and the Norwegian NMR Platform (project number 226244/F50) is highly appreciated. So is the help from the Mass Spectrometry Lab at the NV Faculty, and all help from the LPI/LSPM research groups at EPFL.

### References

- [1] Hagfeldt A., Boschloo G., Sun L., Kloo L., Pettersson H. Dye-Sensitized Solar Cells. *Chem. Rev.* 2010;110:6595-6663.
- [2] O'Regan B., Grätzel M. A low-cost, high-efficiency solar cell based on dye-sensitized colloidal TiO<sub>2</sub> films. *Nature.* 1991;353:737-740.
- [3] Saygili Y., Stojanovic M., Flores-Diaz N., Zakeeruddin S. M., Vlachopoulos N., Grätzel M., et al. Metal Coordination Complexes as Redox Mediators in Regenerative Dye-Sensitized Solar Cells. *Inorganics.* 2019;7:30-98.
- [4] Mishra A., Fischer M. K., Bäuerle P. Metal-free organic dyes for dye-sensitized solar cells: from structure: property relationships to design rules. *Angew. Chem. Int. Ed.* 2009;48:2474-2499.
- [5] Mahmood A. Triphenylamine based dyes for dye sensitized solar cells: A review. *Solar Energy.* 2016;123:127-144.
- [6] Zhang L., Cole J. M. Dye aggregation in dye-sensitized solar cells. *J. Mater. Chem. A.* 2017;5:19541-19559.
- [7] Robertson N. Optimizing dyes for dye-sensitized solar cells. *Angew. Chem. Int. Ed.* 2006;45:2338-2345.
- [8] Yu Q.-Y., Liao J.-Y., Zhou S.-M., Shen Y., Liu J.-M., Kuang D.-B., et al. Effect of Hydrocarbon Chain Length of Disubstituted Triphenyl-amine-Based Organic Dyes on Dye-Sensitized Solar Cells. *J. Phys. Chem. C.* 2011;115:22002-22008.
- [9] Gabrielsson E., Ellis H., Feldt S., Tian H., Boschloo G., Hagfeldt A., et al. Convergent/Divergent Synthesis of a Linker-Variied Series of Dyes for Dye-Sensitized Solar Cells Based on the D35 Donor. *Adv. Energy Mater.* 2013;3:1647-1656.



- [10] Venkateswararao A., Thomas K. R. J., Lee C.-P., Li C.-T., Ho K.-C. Organic Dyes Containing Carbazole as Donor and  $\pi$ -Linker: Optical, Electrochemical, and Photovoltaic Properties. *ACS Appl. Mater. Interfaces*. 2014;6:2528-2539.
- [11] Kakiage K., Aoyama Y., Yano T., Otsuka T., Kyomen T., Unno M., et al. An achievement of over 12 percent efficiency in an organic dye-sensitized solar cell. *Chem. Commun.* 2014;50:6379-6381.
- [12] Bae S. H., Seo K. D., Choi W. S., Hong J. Y., Kim H. K. Near-IR organic sensitizers containing squaraine and phenothiazine units for dye-sensitized solar cells. *Dyes Pigm.* 2015;113:18-26.
- [13] Ren Y., Sun D., Cao Y., Tsao H. N., Yuan Y., Zakeeruddin S. M., et al. A Stable Blue Photosensitizer for Color Palette of Dye-Sensitized Solar Cells Reaching 12.6% Efficiency. *J. Am. Chem. Soc.* 2018;140:2405-2408.
- [14] Buene A. F., Hagfeldt A., Hoff B. H. A comprehensive experimental study of five fundamental phenothiazine geometries increasing the diversity of the phenothiazine dye class for dye-sensitized solar cells. *Dyes Pigm.* 2019;169:66-72.
- [15] Buene A. F., Ose E. E., Zakariassen A. G., Hagfeldt A., Hoff B. H. Auxiliary donors for phenothiazine sensitizers for dye-sensitized solar cells – how important are they really? *J. Mater. Chem. A*. 2019;7:7581-7590.
- [16] Tian H., Yang X., Chen R., Pan Y., Li L., Hagfeldt A., et al. Phenothiazine derivatives for efficient organic dye-sensitized solar cells. *Chem. Commun.* 2007:3741-3743.
- [17] Luo J.-S., Wan Z.-Q., Jia C.-Y. Recent advances in phenothiazine-based dyes for dye-sensitized solar cells. *Chin. Chem. Lett.* 2016;27:1304-1318.
- [18] Huang Z.-S., Meier H., Cao D. Phenothiazine-based dyes for efficient dye-sensitized solar cells. *J. Mater. Chem. C*. 2016;4:2404-2426.
- [19] Buene A. F., Uggerud N., Economopoulos S. P., Gautun O. R., Hoff B. H. Effect of  $\pi$ -linkers on phenothiazine sensitizers for dye-sensitized solar cells. *Dyes Pigm.* 2018;151:263-271.
- [20] Li J., Wu W., Yang J., Tang J., Long Y., Hua J. Effect of chenodeoxycholic acid (CDCA) additive on phenothiazine dyes sensitized photovoltaic performance. *Sci. China Chem.* 2011;54:699-706.
- [21] Dryza V., Bieske E. J. Does the triphenylamine-based D35 dye sensitizer form aggregates on metal-oxide surfaces? *J. Photochem. Photobiol. A*. 2015;302:35-41.
- [22] Agrawal S., Pastore M., Marotta G., Reddy M. A., Chandrasekharam M., De Angelis F. Optical Properties and Aggregation of Phenothiazine-Based Dye-Sensitizers for Solar Cells Applications: A Combined Experimental and Computational Investigation. *J. Phys. Chem. C*. 2013;117:9613-9622.
- [23] Hua Y., Chang S., Huang D. D., Zhou X., Zhu X. J., Zhao J. Z., et al. Significant Improvement of Dye-Sensitized Solar Cell Performance Using Simple Phenothiazine-Based Dyes. *Chem. Mater.* 2013;25:2146-2153.

[24] Deshpande S. S., Kumbhar H. S., Shankarling G. S. Solvatochromic fluorescence properties of phenothiazine-based dyes involving thiazolo[4,5-b]quinoxaline and benzo[e]indole as strong acceptors. *Spectrochim. Acta A*. 2017;174:154-163.

[25] Nazeeruddin M. K., De Angelis F., Fantacci S., Selloni A., Viscardi G., Liska P., et al. Combined Experimental and DFT-TDDFT Computational Study of Photoelectrochemical Cell Ruthenium Sensitizers. *J. Am. Chem. Soc.* 2005;127:16835-16847.

**Electronic Supplementary Information****Experimental study comparing the 3,7 and 3,8 substitution geometry of phenothiazine sensitizers for dye-sensitized solar cells**

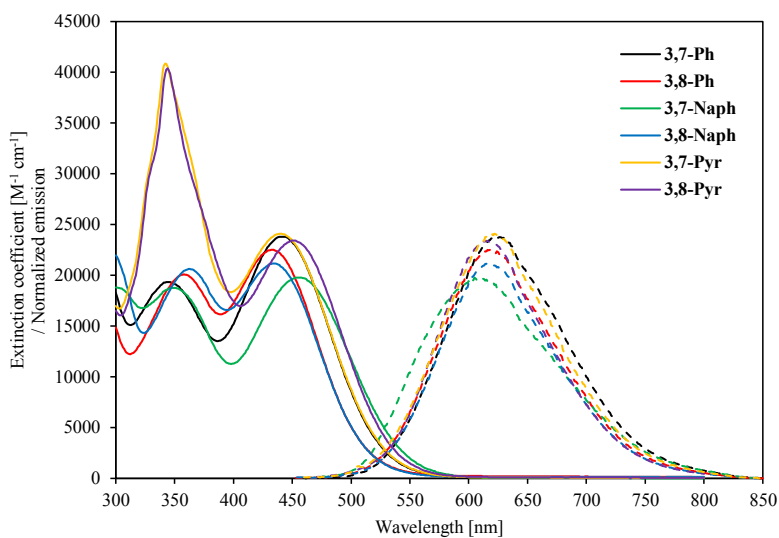
Audun Formo Buene, Mats Christensen and Bård Helge Hoff\*

*Department of Chemistry, Norwegian University of Science and Technology (NTNU), N-7491 Trondheim, Norway*

*\* Corresponding author. Tel.: +47 73593973; E-mail address: bard.h.hoff@ntnu.no (B. H. Hoff).*

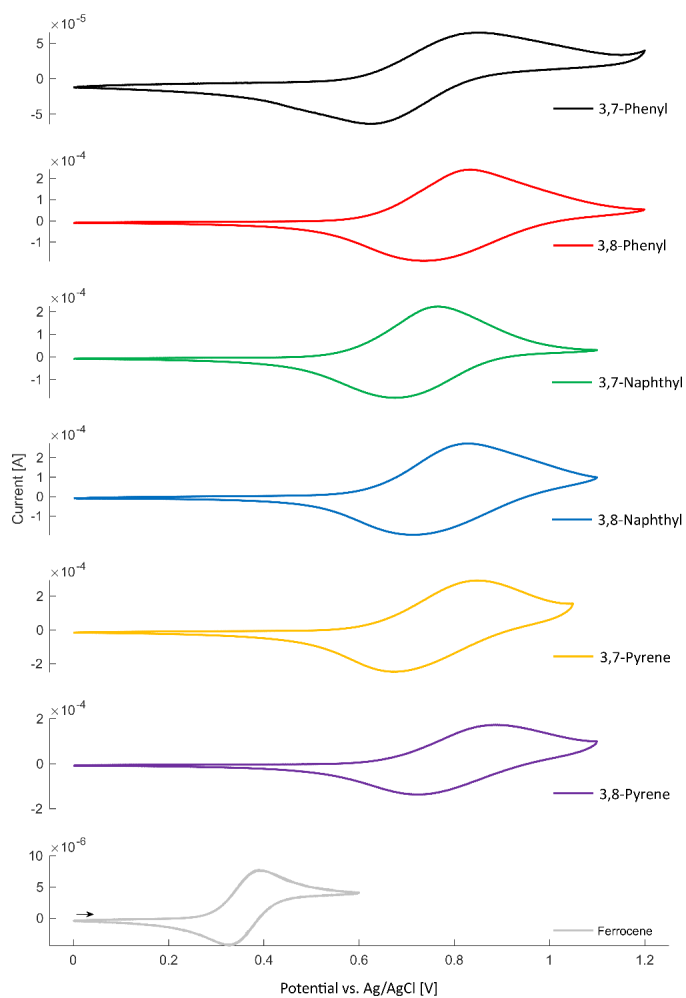
**List of contents**

<b>Photophysical data</b>	<b>S2</b>
<b>Cyclic voltammetry</b>	<b>S3</b>
<b>Experimental information</b>	<b>S4</b>
<b>NMR</b>	<b>S8</b>

**Photophysical data**

**Figure S1.** Dashed curves show the emission spectra of all dyes, recorded in THF. The spectra are normalized to the absorption spectra of the same dyes in THF solution.

### Cyclic voltammetry



**Figure S2.** Cyclic voltammograms of all sensitizers adsorbed on  $2.5 \mu\text{m}$   $\text{TiO}_2$  films on FTO glass. CV measured in  $0.1 \text{ M LiTFSI}$  in acetonitrile with a graphite counter electrode and a  $\text{Ag}/\text{AgCl}$  reference electrode.

## Experimental information

### Materials and reagents

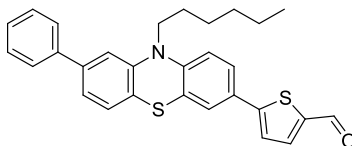
Unless specifically mentioned, all reagents and solvents used were sourced from Sigma Aldrich. Sensitizers **AFB-8**, **AFB-16** and **AFB-19** are previously synthesized and reported by the authors.<sup>1,2</sup>

### Analytical instruments

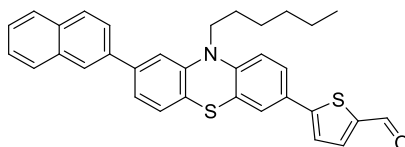
NMR analysis were recorded on Bruker 400 or 600 MHz spectrometers, with chemical shifts reported relative to the solvent peak of DMSO, 2.50 ppm in <sup>1</sup>H and 39.53 ppm in <sup>13</sup>C NMR. Accurate mass determination was performed by the MS laboratory at the NV Faculty at NTNU with a "Synapt G2-S" Q-TOF instrument from Waters™ with an *atmospheric solids analysis probe* (ASAP) in positive mode. UV/Vis spectrometry was measured on a Hitachi U-1900 spectrophotometer using quartz cuvettes for the solution measurements. Fluorescence spectra were recorded with an FS5 Spectrofluorometer from Edinburgh instruments, and infrared spectra were recorded on a Bruker Alpha FT-IR spectrometer with an ATR module.

### Synthesis

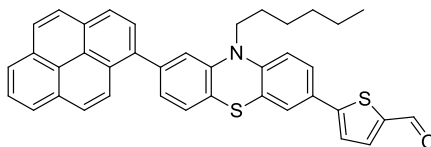
#### 5-(10-Hexyl-8-phenyl-10*H*-phenothiazin-3-yl)thiophene-2-carbaldehyde (**4**) MC1-066



Compound **3**<sup>3</sup> (71.2 mg, 166  $\mu$ mol), phenylboronic acid (24.1 mg, 198  $\mu$ mol), SPhos (3.5 mg, 8.5  $\mu$ mol), Pd(OAc)<sub>2</sub> (0.8 mg, 4  $\mu$ mol) and K<sub>2</sub>CO<sub>3</sub> (92 mg, 0.67 mmol) were mixed under nitrogen atmosphere. Degassed 1,4-dioxane/water (1:1, 2 mL) was added, and the reaction was stirred at 80 °C for 23 hours. The reaction mixture was quenched with water (5 mL), and extracted with ethyl acetate (3  $\times$  5 mL). The combined organic phases were washed with water, and dried with brine and over anhydrous Na<sub>2</sub>SO<sub>4</sub>, and the solvents removed in vacuo to give the crude product as a dark oil. Purification by silica-gel column chromatography (*n*-pentane/ethyl acetate, 6:1, *R<sub>f</sub>* = 0:21) gave compound **4** as an orange solid (64.1 mg, 82%), mp 108-109 °C. <sup>1</sup>H NMR (600 MHz, DMSO-*d*<sub>6</sub>)  $\delta$ : 9.87 (s, 1H), 8.00 (d, *J* = 4.0 Hz, 1H), 7.68-7.66 (m, 3H), 7.62 (dd, *J* = 8.4, 2.3 Hz, 1H), 7.40 (d, *J* = 2.1, 1H), 7.46 (m, 2H), 7.38 (tt, *J* = 7.4, 1.2 Hz, 1H), 7.27-7.23 (m, 3H), 7.10 (d, *J* = 8.5 Hz, 1H), 4.02 (t, *J* = 7.0 Hz, 2H), 1.73 (quint., *J* = 7.2 Hz, 2H), 1.42 (quint., *J* = 7.3 Hz, 2H), 1.29-1.21 (m, 4H), 0.82 (t, *J* = 7.1 Hz, 3H); <sup>13</sup>C NMR (150 MHz, DMSO-*d*<sub>6</sub>)  $\delta$ : 183.7, 151.9, 145.6, 144.5, 141.1, 140.0, 139.7, 139.4, 128.9 (2C), 127.62, 127.57, 127.49, 126.8, 126.6 (2C), 125.8, 124.40, 124.37, 124.36, 122.0, 121.3, 116.3, 114.4, 46.6, 30.8, 26.1, 25.7, 22.0, 13.8; IR (neat, cm<sup>-1</sup>)  $\nu$ : 2952 (m), 2919 (m), 2848 (m), 1662 (s), 1466 (m), 1442 (s), 1225 (s), 864 (m), 808 (s), 787 (s), 695 (s). HRMS (TOF MS ASAP+, *m/z*): found 470.1608 (calcd. C<sub>29</sub>H<sub>28</sub>NOS<sub>2</sub>: 470.1612 [M + H]<sup>+</sup>).

**5-(10-Hexyl-8-(naphthalen-2-yl)-10H-phenothiazin-3-yl)thiophene-2-carbaldehyde (5)**


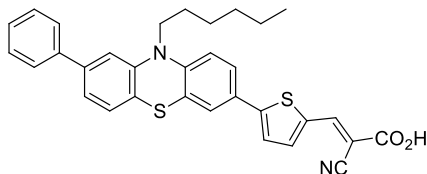
Compound **3** (201 mg, 0.47 mmol), naphthalen-2-ylboronic acid (140 mg, 0.81 mmol), SPhos (16 mg, 0.038 mmol), Pd(OAc)<sub>2</sub> (8 mg, 0.036 mmol) and potassium carbonate (260 g, 1.88 mmol) were mixed. Degassed 1,4-dioxane (1.6 mL) and water (1.6 mL) were added, and the reaction was stirred at 80 °C for 9.5 h, then cooled to room temperature. Water (5 mL) was added to the reaction mixture, and the aqueous phase was extracted with ethyl acetate (3 × 5 mL). The organic phase was dried over anhydrous Na<sub>2</sub>SO<sub>4</sub>, filtered and the solvent removed in vacuo. The crude product was purified by silica-gel column chromatography (*n*-pentane/ethyl acetate, 20:1, *R<sub>f</sub>* = 0.10), to yield compound **5** as a red oil (225 mg, 0.43 mmol, 92%). <sup>1</sup>H NMR (600 MHz, DMSO-*d*<sub>6</sub>) δ: 9.87 (s, 1H), 8.22 (s, 1H), 8.00-7.98 (m, 3H), 7.95-7.93 (m, 1H), 7.85-7.83 (m, 1H), 7.67-7.66 (m, 1H), 7.63-7.61 (m, 2H), 7.56-7.51 (m, 2H), 7.41-7.38 (m, 2H), 7.28-7.27 (m, 1H), 7.11-7.09 (m, 1H), 4.06-4.04 (m, 2H), 1.77-1.72 (m, 2H), 1.45-1.40 (m, 2H), 1.28-1.22 (m, 4H), 0.82-0.80 (m, 3H). <sup>13</sup>C NMR (150 MHz, DMSO-*d*<sub>6</sub>) δ: 183.7, 151.9, 145.6, 144.6, 141.1, 139.8, 139.3, 137.0, 133.2, 132.3, 128.4, 128.1, 127.6, 127.5, 126.8, 126.4, 126.2, 125.8, 125.2, 125.0, 124.42, 124.41, 124.36, 122.2, 121.6, 116.4, 114.6, 46.7, 30.8, 26.2, 25.8, 22.0, 13.8; IR (neat, cm<sup>-1</sup>) ν: 2921.3 (w), 2849.6 (w), 1738.0 (s), 1651.3 (s), 1432.5 (s), 1276.2 (m), 1216.9 (s), 1052.2 (m), 793.2 (m). HRMS (TOF MS ASAP+, *m/z*): found 520.1767 (calcd. C<sub>33</sub>H<sub>30</sub>NOS<sub>2</sub>: 520.1769, [M+H]<sup>+</sup>).

**5-(10-Hexyl-8-(pyren-1-yl)-10H-phenothiazin-3-yl)thiophene-2-carbaldehyde (6)**


Compound **3** (151 mg, 0.35 mmol), pyren-1-ylboronic acid (104 mg, 0.423 mmol), SPhos (5.7 mg, 14 μmol), Pd(OAc)<sub>2</sub> (1.5 mg, 6.7 μmol), and K<sub>2</sub>CO<sub>3</sub> (198 mg, 1.44 mmol) were added to degassed 1,4-dioxane (2 mL) and deionized water (2 mL) under nitrogen atmosphere. The reaction mixture was stirred for 3 hours at 80 °C. The reaction was quenched with water (10 mL) and extracted with ethyl acetate (3 × 20 mL). The combined organic phases were washed with brine (50 mL) and dried over anhydrous Na<sub>2</sub>SO<sub>4</sub>, and the solvent removed *in vacuo*. The crude product was purified using silica-gel column chromatography (*n*-pentane/ethyl acetate, 10:1) to give compound **6** as orange crystals (160 mg, 0.27 mmol, 76%), mp 108-111 °C. <sup>1</sup>H NMR (600 MHz, DMSO-*d*<sub>6</sub>) δ: 9.88 (s, 1H), 8.34 (d, *J* = 7.9 Hz, 1H), 8.31 (d, *J* = 7.6 Hz, 1H), 8.27 (d, *J* = 7.5 Hz, 1H), 8.21 (s, 2H), 8.12 (q, *J* = 8.2 Hz, 2H), 8.08 (t, *J* = 7.6 Hz, 1H), 8.01 (d, *J* = 7.9 Hz, 1H), 7.99 (d, *J* = 3.9 Hz, 1H), 7.67 (d, *J* = 3.9 Hz, 1H), 7.63 (d, *J* = 2.2 Hz, 1H), 7.60 (dd, *J* = 8.4, 2.2 Hz, 1H), 7.36 (d, *J* = 7.7 Hz, 1H), 7.20 (dd, *J* = 7.8, 1.2 Hz, 1H) 7.18 (s, 1H), 7.06 (d, *J* = 8.6 Hz, 1H), 3.90 (t, *J* = 7.0 Hz, 2H), 1.73 (quint., *J* = 7.2 Hz, 2H), 1.34 (quint., *J* = 7.4 Hz, 2H), 1.24-1.14 (m, 4H), 0.74 (t, *J* = 7.1 Hz, 3H); <sup>13</sup>C NMR (150 MHz, DMSO-*d*<sub>6</sub>) δ: 183.7, 151.9, 145.6, 143.8, 141.1, 140.0, 139.3, 136.5, 130.9, 130.4, 130.2, 127.70, 127.66, 127.5, 127.3, 127.2, 126.9, 126.4, 125.9, 125.4, 125.0, 124.9, 124.8, 124.5, 124.45 (2C), 124.36, 124.2, 124.1, 124.0, 122.0, 117.9, 116.3, 46.7, 30.8, 26.1, 25.7, 22.0,

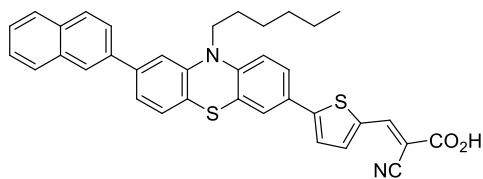
13.7; IR (neat,  $\text{cm}^{-1}$ ): 2920.0 (m), 2849.2 (m), 1655.4 (s), 1432.0 (s), 1221.9 (s), 1054.6 (m), 844.8 (s). HRMS (TOF MS ASAP+,  $m/z$ ): found 594.1916 (calcd.  $\text{C}_{39}\text{H}_{32}\text{NOS}_2$ : 594.1925  $[\text{M} + \text{H}]^+$ ).

**(E)-2-Cyano-3-(5-(10-hexyl-8-phenyl-10H-phenothiazin-3-yl)thiophen-2-yl)acrylic acid (AFB-33)**



Compound **4** (73 mg, 155  $\mu\text{mol}$ ) and 2-cyanoacetic acid (270 mg, 3.17 mmol) were dissolved in degassed acetonitrile (20 mL) under nitrogen atmosphere. Piperidine (0.19 mL, 1.9 mmol) was added, and the reaction was heated to 80  $^{\circ}\text{C}$  and left stirring for 1 hour. The mixture was cooled to room temperature and quenched with aqueous HCl (25 mL, 4 M). The mixture was extracted with ethyl acetate ( $3 \times 15$  mL) and the combined organic phases were washed with water ( $6 \times 100$  mL), then with brine (50 mL) and dried over anhydrous  $\text{Na}_2\text{SO}_4$ , filtered, and the solvents removed *in vacuo*, to give the crude product as a dark oil. Purification by silica-gel column chromatography (gradient: 0-15% methanol in dichloromethane) gave sensitizer **AFB-33** as a dark solid (72.3 mg, 87%), mp 225  $^{\circ}\text{C}$  (dec.).  $^1\text{H}$  NMR (600 MHz,  $\text{DMSO}-d_6$ )  $\delta$ : 12.02 (s), 8.12 (s, 1H), 7.71 (d,  $J = 3.7$  Hz, 1H), 7.66 (d,  $J = 7.7$  Hz, 2H), 7.56 (d,  $J = 3.8$  Hz, 1H), 7.54-7.53 (m, 2H), 7.46 (t,  $J = 7.7$  Hz, 2H), 7.37 (t,  $J = 7.3$  Hz, 1H), 7.25-7.22 (m, 3H), 7.09 (d,  $J = 9.2$  Hz, 1H), 4.00 (t,  $J = 6.8$  Hz, 2H), 1.73 (quint.,  $J = 7.7$  Hz, 2H), 1.42 (quint.,  $J = 7.2$  Hz, 2H), 1.29-1.22 (m, 4H), 0.82 (t,  $J = 7.0$  Hz, 3H).  $^{13}\text{C}$  NMR (150 MHz,  $\text{DMSO}-d_6$ )  $\delta$ : 163.3, 147.9, 145.0, 144.6, 141.1, 140.0, 139.7, 136.8, 135.4, 128.9 (2C), 127.63, 127.57, 127.2, 126.6 (2C), 125.4, 124.4, 124.0, 123.8, 122.1, 121.3, 119.0, 116.4, 114.3, 107.9, 46.6, 30.8, 26.2, 25.8, 22.0, 13.8. IR (neat,  $\text{cm}^{-1}$ ): 2924 (w), 2850 (w), 2213 (w), 1575 (m), 1558 (m), 1387 (s), 1237 (m), 1061 (w), 797 (m), 756 (m). HRMS (TOF MS ASAP+,  $m/z$ ): found 493.1767 (calcd.  $\text{C}_{31}\text{H}_{29}\text{N}_2\text{S}_2$ : 493.1772  $[\text{M}-\text{CO}_2+\text{H}]^+$ ).

**(E)-2-Cyano-3-(5-(10-hexyl-8-(naphthalen-2-yl)-10H-phenothiazin-3-yl)thiophen-2-yl)acrylic acid (AFB-34)**

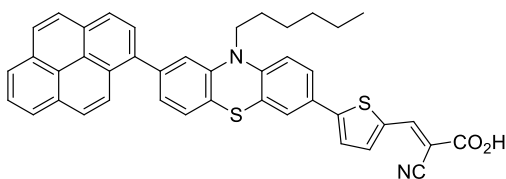


Compound **2** (150 mg, 0.29 mmol) and cyanoacetic acid (492 mg, 5.78 mmol) were dissolved in degassed acetonitrile (40 mL) under nitrogen atmosphere. Piperidine (340  $\mu\text{L}$ , 292 mg, 3.4 mmol) was added and the reaction was heated to 80  $^{\circ}\text{C}$  for 25 minutes before cooling to room temperature and quenched in HCl (2 M, 150 mL). The reaction was extracted with ethyl acetate ( $2 \times 50$  mL) and the organic phase was washed with water ( $5 \times 200$  mL), then dried with brine (50 mL) and over anhydrous  $\text{Na}_2\text{SO}_4$ , filtered and the solvents were removed *in vacuo*. The crude product was purified by silica gel column chromatography (gradient: 0-10% MeOH in  $\text{CH}_2\text{Cl}_2$ ) to obtain sensitizer **AFB-34** as a dark solid (121 mg, 0.210 mmol,



71%), mp 286 °C (dec.). <sup>1</sup>H NMR (600 MHz, DMSO-*d*<sub>6</sub>) δ: 8.23 (s, 1H), 8.12 (s, 1H), 8.01-7.99 (m, 2H), 7.96-7.94 (m, 1H), 7.86-7.85 (m, 1H), 7.71 (m, 1H), 7.59 (m, 1H), 7.55-7.52 (m, 4H), 7.42-7.39 (m, 2H), 7.29-7.28 (m, 1H), 7.13-7.11 (m, 1H), 4.07-4.05 (m, 2H), 1.79-1.74 (m, 2H), 1.47-1.42 (m, 2H), 1.30-1.25 (m, 4H), 0.83-0.81 (m, 3H) (CO<sub>2</sub>H proton missing); <sup>13</sup>C NMR (150 MHz, DMSO-*d*<sub>6</sub>) δ: 163.4, 152.2, 147.9, 144.8, 139.8, 139.8, 137.0, 136.5, 133.3, 132.2, 128.4, 128.2, 127.7, 127.7, 127.5, 126.5, 125.4, 125.2, 125.2, 125.0, 125.0, 124.4, 124.0, 123.8, 123.8, 121.6, 121.3, 119.0, 116.5, 114.6, 46.7, 30.8, 26.2, 25.8, 22.0, 13.8. IR (neat, cm<sup>-1</sup>) ν: 3391.3 (w, br), 2924.6 (w), 2214.8 (w), 1710.9 (w), 1574.9 (s), 1391.7 (s), 1063.2 (w), 801.7 (m). HRMS (TOF MS ASAP+, *m/z*): found 543.1920 (calcd. C<sub>35</sub>H<sub>31</sub>N<sub>2</sub>S<sub>2</sub>: 543.1929, [M-CO<sub>2</sub>+H]<sup>+</sup>).

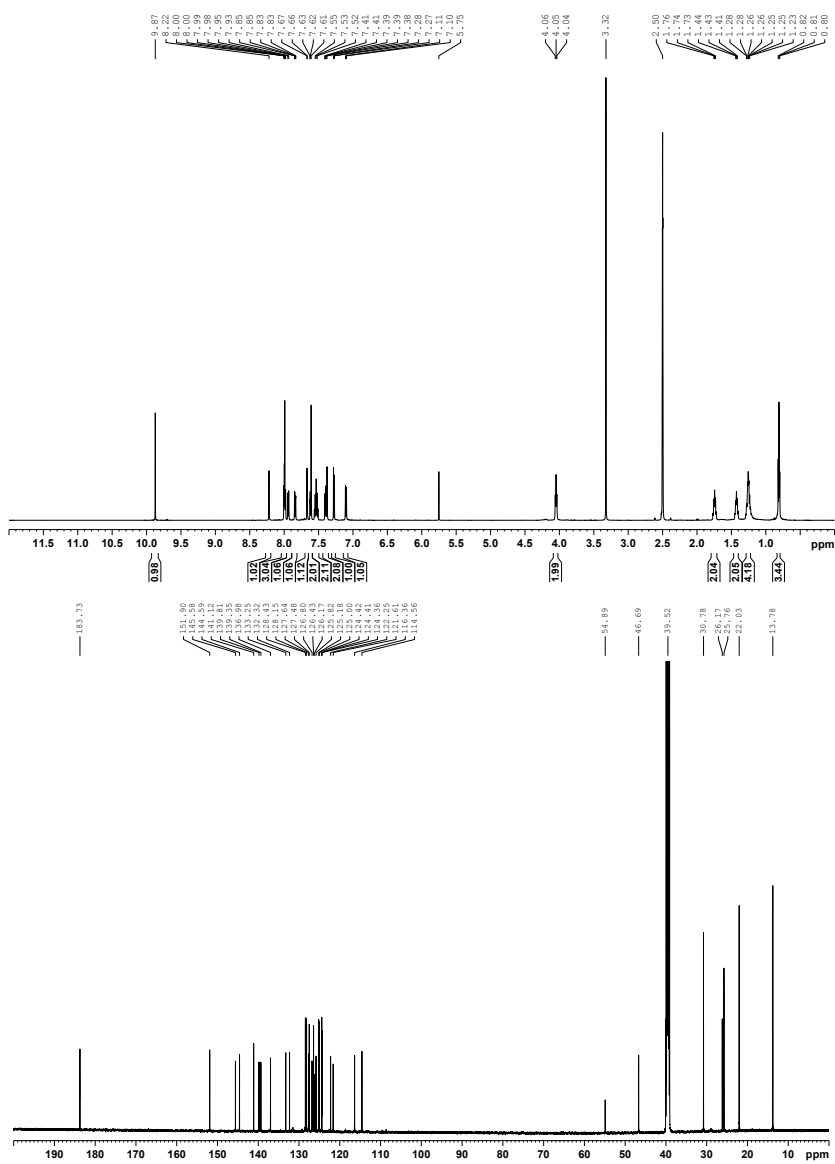
**(*E*)-2-Cyano-3-(5-(10-hexyl-8-(pyren-1-yl)-10*H*-phenothiazin-3-yl)thiophen-2-yl)acrylic acid (AFB-35)**



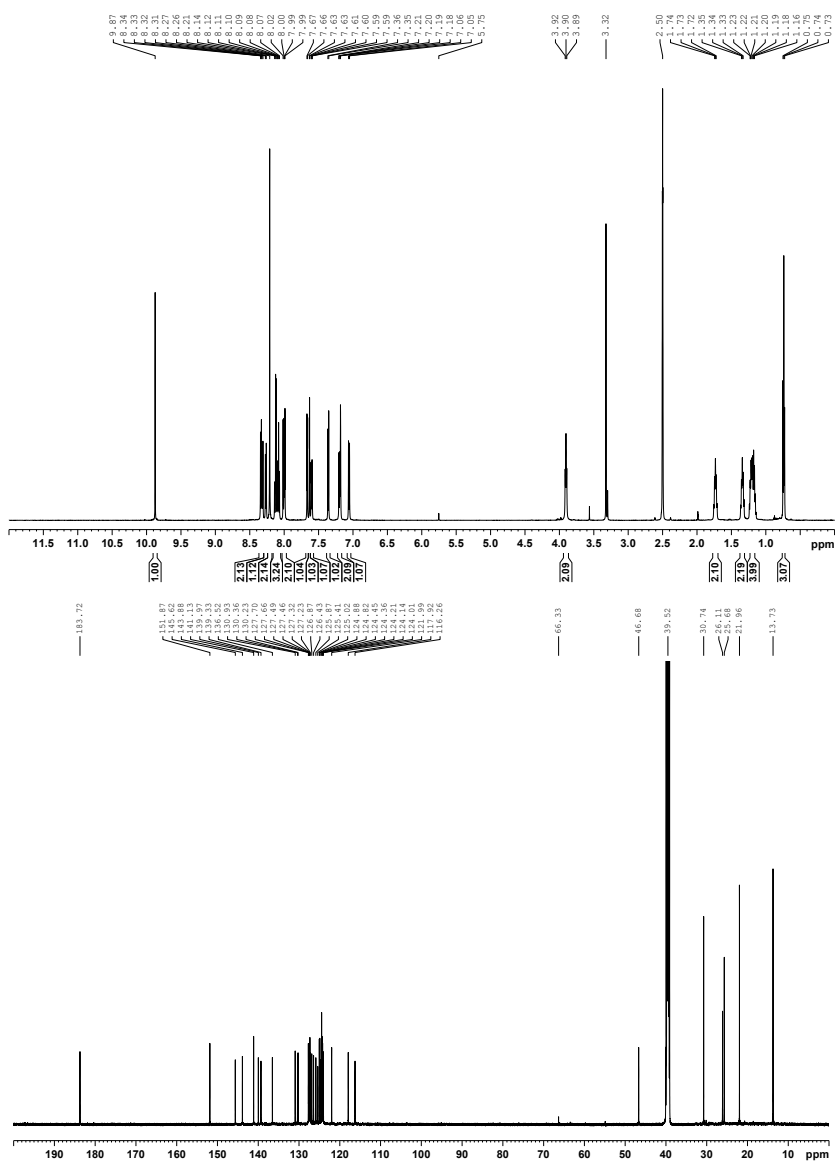
Compound **3** (120 mg, 0.20 mmol) and cyanoacetic acid (415 mg, 4.88 mmol) were dissolved in degassed acetonitrile (25 mL) under nitrogen atmosphere, and piperidine (240 μL, 206 mg, 2.4 mmol) was added. The reaction mixture was stirred for 2 hours at 80 °C. The reaction was quenched with HCl (50 mL, 2 M), and extracted with ethyl acetate (3 × 30 mL). The combined organic phases were washed with water (5 × 200 mL), and dried with brine (50 mL) and over anhydrous Na<sub>2</sub>SO<sub>4</sub>, and the solvent was removed *in vacuo*. The crude product was purified using silica-gel column chromatography (gradient: 0-15% MeOH in CH<sub>2</sub>Cl<sub>2</sub>) to give **AFB-35** as dark red crystals (67.2 mg, 0.102 mmol, 50%), mp 171 °C (dec.). <sup>1</sup>H NMR (600 MHz, DMSO-*d*<sub>6</sub>) δ: 13.69 (s, 1H), 8.64 (s, 1H), 8.32 (dd, *J* = 12.7, 7.8 Hz, 2H), 8.26 (d, *J* = 7.6 Hz, 1H), 8.21 (s, 2H), 8.12 (q, *J* = 7.6 Hz, 2H), 8.08 (t, *J* = 7.6 Hz, 1H), 8.01 (d, *J* = 7.7 Hz, 1H), 7.97 (d, *J* = 4.0 Hz, 1H), 7.69 (d, *J* = 3.9 Hz, 1H), 7.61 (d, *J* = 1.7 Hz, 1H), 7.57 (dd, *J* = 8.4, 1.6 Hz, 1H), 7.35 (d, *J* = 7.6 Hz, 1H), 7.20 (d, *J* = 7.9 Hz, 1H), 7.18 (s, 1H), 7.06 (d, *J* = 8.6 Hz, 1H), 3.90 (t, *J* = 6.6 Hz, 2H), 1.73 (quint., *J* = 7.2 Hz, 2H), 1.34 (quint., *J* = 7.1 Hz, 2H), 1.26-1.14 (m, 4H), 0.74 (t, *J* = 7.0 Hz, 3H). <sup>13</sup>C NMR (150 MHz, DMSO-*d*<sub>6</sub>) δ: 163.7, 152.1, 146.6, 145.7, 143.8, 141.6, 140.0, 136.5, 133.8, 130.9, 130.4, 130.2, 127.70, 127.66, 127.49, 127.46, 127.3, 127.2, 126.7, 126.4, 125.9, 125.4, 125.0, 124.9 (2C), 124.5, 124.4, 124.3, 124.2, 124.1, 124.0, 121.9, 118.0, 116.6, 116.3, 97.5, 46.7, 30.7, 26.1, 25.7, 22.0, 13.7. IR (neat, cm<sup>-1</sup>) ν: 2046.0 (br), 2216.2 (w), 1680.7 (m), 1559.2 (s), 1405.0 (s), 1216.0, 1066.0, 797.7. HRMS (TOF MS ASAP+, *m/z*): found 617.2075 (calcd. C<sub>41</sub>H<sub>33</sub>N<sub>2</sub>S<sub>2</sub>: 617.2085 [M-CO<sub>2</sub>+H]<sup>+</sup>).



## Compound 5

Figure S5.  $^1\text{H}$  and  $^{13}\text{C}$  NMR spectra for compound 5.

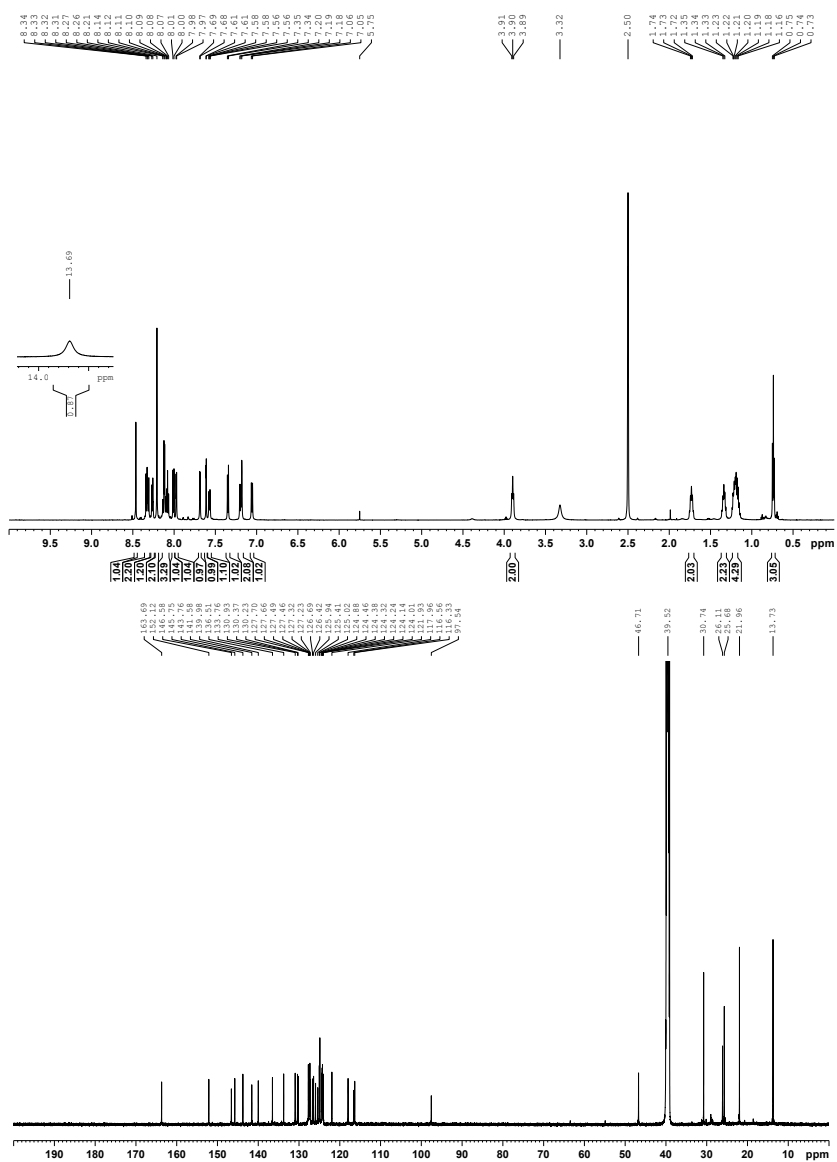
## Compound 6

Figure S6.  $^1\text{H}$  and  $^{13}\text{C}$  NMR spectra for compound 6.





## Compound AFB-35

Figure S9. <sup>1</sup>H and <sup>13</sup>C NMR spectra for sensitizer AFB-35.

## References

1. A. F. Buene, E. E. Ose, A. G. Zakariassen, A. Hagfeldt and B. H. Hoff, *J. Mater. Chem. A*, 2019, **7**, 7581-7590.
2. A. F. Buene, N. Uggerud, S. P. Economopoulos, O. R. Gautun and B. H. Hoff, *Dyes Pigm.*, 2018, **151**, 263-271.
3. A. F. Buene, A. Hagfeldt and B. H. Hoff, *Dyes Pigm.*, 2019, **169**, 66-72.





# PAPER VI

## **First Report of CDCA-Substituted Dyes for DSSC Improving Efficiency through Reduced Aggregation**

---

\*At the time of submitting this thesis, the characterization work of the compounds reported in this paper is not yet completed. Most compounds are confirmed by high-resolution mass spectrometry.



## First Report of CDCA-Substituted Dyes for Dye-Sensitized Solar Cells Improving Efficiency through Reduced Aggregation

Audun Formo Buene<sup>a</sup>, David Moe Almenningen<sup>a</sup>, Anders Hagfeldt<sup>b</sup>, Odd Reidar Gautun<sup>a</sup>, Bård Helge Hoff<sup>†\*</sup>

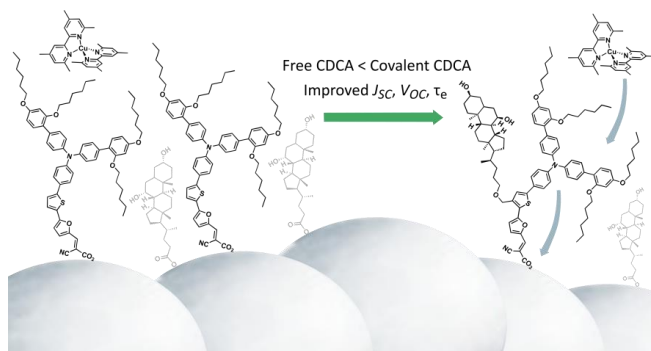
<sup>a</sup>: Department of Chemistry, Norwegian University of Science and Technology, Høgskoleringen 5, NO-7491 Trondheim, Norway

<sup>b</sup>: Laboratory of Photomolecular Science, Institute of Chemical Sciences and Engineering, École Polytechnique Fédérale de Lausanne (EPFL), Chemin des Alambics, Station 6, CH-1015 Lausanne, Switzerland

\* Corresponding author. Tel.: +47 73593973; E-mail address: [bard.h.hoff@ntnu.no](mailto:bard.h.hoff@ntnu.no) (B. H. Hoff).

### Abstract

Chenodeoxycholic acid (CDCA) has been the most used anti-aggregation additive in dye-sensitized solar cells since its introduction to the field in 1993. Herein we report the first example of CDCA covalently attached to sensitizers, directly compared to reference dyes synthesized without CDCA substituents. Four novel triarylamine dyes were prepared and evaluated in devices with  $[\text{Cu}^{+2+}(\text{tmby})_2](\text{TFSI})_{1/2}$  electrolyte. The CDCA substituents attached to the  $\pi$ -spacer did not affect the photophysical or electrochemical properties of the sensitizers, but had a positive effect on the photovoltaic performance. The best device was fabricated with the dye **C<sub>6</sub>-CDCA** delivering a PCE of 6.84% (8  $\mu\text{m}$   $\text{TiO}_2$ , 1 mM CDCA,  $J_{\text{SC}} = 8.64 \text{ mA cm}^{-2}$ ,  $V_{\text{OC}} = 1007 \text{ mV}$ , FF = 0.77). This study indicates that the CDCA substituent is considerably improving the quality of the monomolecular dye layer, resulting in increased power-conversion efficiency.



**Keywords:** triphenylamine dyes, chenodeoxycholic acid, covalent CDCA, copper electrolyte, sensitizer quantum efficiency, anti-aggregation.

## 1. Introduction

Dye-sensitized solar cells (DSSCs) is a photovoltaic technology based on sensitized mesoscopic nanoparticles of a wide bandgap semiconductor such as TiO<sub>2</sub>.<sup>1,2</sup> Coupled with a counter electrode and an electrolyte the complete photoelectrochemical cell is remarkably efficient. Flexible, semi-transparent and aesthetically decorative devices can be manufactured from low-cost materials.<sup>3</sup> The task of the sensitizer is to harvest as much of the incident light as possible, while the rest of the device is designed to efficiently convert as much of the harvested energy into electricity.

As the most important component of a DSSC, dyes have been the subject of extensive development and optimization throughout the history of the field.<sup>4</sup> Improvements in device architecture or electrolyte composition often spark the development of new dyes, which are more compatible with the new components.<sup>5, 6</sup> Improving the efficiency of DSSC's through dye development is largely focussed on enhancing the absorption properties, i.e. harvest more of the available sunlight. Increasing the size of the conjugated system is a popular measure. Also strengthening the push-pull characteristics of the sensitizers can lead to wider absorption. Alas, there is a drawback to all the wonderful conjugation, namely  $\pi$ - $\pi$  interactions. The resulting unfavourable intermolecular aggregation will increase charge recombination and can be detrimental to the device performance.<sup>7</sup>

One solution was presented as early as in 1993, by Kay and Grätzel.<sup>8</sup> Bile acids are compounds based on a steroid scaffold with one to three hydroxyl groups in addition to a flexible chain with a carboxylic acid. Consequently, they are amphiphilic and chiral compounds. In biology they are well known to facilitate fat absorption and are signalling molecules affecting both nuclear and membrane receptors,<sup>9</sup> and are useful in various applications due to their tendency to form micelles.<sup>10</sup> Bile acids were expected to anchor onto TiO<sub>2</sub> through the carboxylic acid group and were introduced into the dye monolayer as insulator molecules, effectively breaking up the undesirable dye-dye interactions. Since then, chenodeoxycholic acid has become the most widely used additive in dye-sensitized solar cells. It was early found that quite large concentrations of CDCA was necessary to compete with dye molecules for adsorption onto the TiO<sub>2</sub> surface.<sup>8</sup> The exact dye:CDCA ratio will vary between dyes and solvents, but concentrations 10-20 times higher than of the dye are frequently reported in the literature.<sup>11-13</sup>

Another, extremely common anti-aggregation measure for both metal-complex dyes and organic sensitizers are the use of alkyl or alkoxy chains, present in just about all of the highest performing sensitizers.<sup>6, 14-19</sup> Some sensitizers have been fitted with polyether chains for anti-aggregation while increasing hydrophilicity and chelating small cations, especially desirable for aqueous DSSCs.<sup>20-22</sup> One of the more exciting examples of a novel anti-aggregation unit was the use of a glucose derivative attached by click chemistry to a dianchoring phenothiazine sensitizer, reported by Manfredi et al. for dye-sensitized photocatalytic

hydrogen production.<sup>23</sup> Some dyes are claimed to be aggregation-free, simply because they show no performance enhancement with co-adsorbents. However, staining of a dye with an inert co-adsorbent is a very complex and poorly understood process. Consequently, a proclaimed aggregation-free sensitizer may in fact be significantly aggregating, and sub-optimal distribution of co-adsorbent is the reason why no performance enhancement is found.

Recently, a number of triarylamine-based sensitizers have been used with great results in DSSC using novel cobalt and copper electrolytes.<sup>6, 24-29</sup> The HOMO level energies of these sensitizers are suitable for efficient dye regeneration from the novel electrolytes, while different  $\pi$ -spacers are used to tune the light absorption properties. Because of the slower diffusion properties of the large redox shuttle complexes, thin TiO<sub>2</sub> films are required and high dye extinction coefficients is therefore an advantage.<sup>30</sup> While aggregation is not an issue commonly raised for triarylamine dyes, one report of small domains of J-aggregate formation of dye **D35** has been found.<sup>31</sup>

Herein we report the first two examples of sensitizers with chenodeoxycholic substituents. The dyes differ only by the length of the alkoxy chains on the donor moiety (C<sub>3</sub>H<sub>7</sub> vs. C<sub>6</sub>H<sub>13</sub>). With this approach, we hope to improve the distribution of CDCA moieties in the self-assembled monolayer (SAM). Simultaneously, we envision this will reduce the total number of carboxylate anchoring groups on the TiO<sub>2</sub>, leading to increased  $V_{OC}$ . Two reference sensitizers without CDCA substituents, but otherwise identical, have also been prepared in order for the effects of the CDCA substituents to be measured. The four novel sensitizers will thus allow the study of the CDCA substituent effects, but also the effect of alkoxy chain length in triarylamine sensitizers. The choice of triarylamine was made so that novel copper electrolytes can be used in the DSSC devices to conduct the study. With copper electrolytes, the energy loss in the dye regeneration can be significantly reduced compared to conventional I<sup>-</sup>/I<sub>3</sub><sup>-</sup> electrolytes.<sup>25, 30</sup> The  $\pi$ -spacer chosen for the study was the thiophene-furan unit, recently used with success in a number of DSSC studies.<sup>32-36</sup> More importantly, this  $\pi$ -spacer proved suitable as a point of attachment for the very large CDCA substituent without inducing excessive ring twisting. Additionally, this  $\pi$ -spacer allows the CDCA substituent to be situated in a position comparable to that of pure CDCA when anchored on the TiO<sub>2</sub> surface as a co-adsorbent.

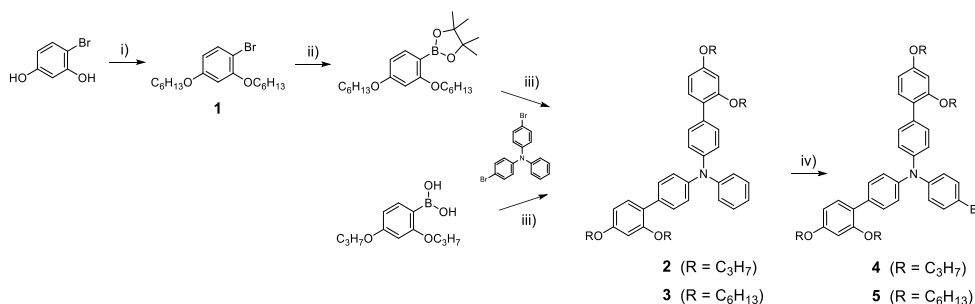
## 2. Results and Discussion

The aim for this work was to synthesize and evaluate sensitizers with CDCA substituents for dye-sensitized solar cells. We wanted the dyes' energy levels to be compatible with novel copper electrolytes, so triarylamine became the basis for the study. It was essential that the large CDCA substituent did not induce any ring twisting of the conjugated system, negatively affecting the optical properties of the sensitizers. To

minimize the likelihood for induced ring twist, we decided to attach the CDCA substituent in the bay region of two linked five-membered heterocycles. This makes up the rationale behind the dye design, and succeeding in the preparation and evaluation of the sensitizers was of a much higher priority than the actual photovoltaic performance.

## 2.1 Dye synthesis

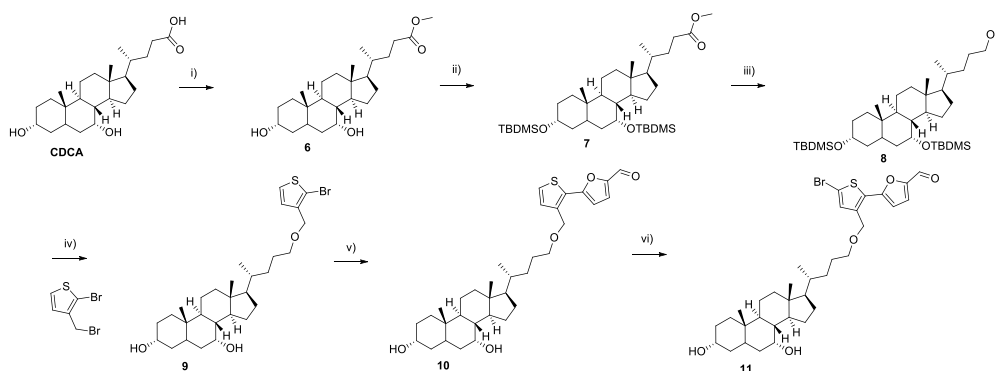
The complexity of the target sensitizers meant the preparation resemble more of a total synthesis than the preparation of a simple dye. Preparation of the donor fragment however was fairly straight forward, as shown in Scheme 1. Synthesis routes based on those reported by Gabrielsson et al. and Zhang et al. were used to prepare the triarylamine donor fragments.<sup>14, 37</sup> While (2,4-dipropoxyphenyl)boronic acid was commercially available, 2-(2,4-bis(hexyloxy)phenyl)-pinacol boronic ester had to be prepared inhouse, using the convenient palladium-catalysed borylation reaction developed by Billingsley and Buchwald.<sup>38</sup> The crude pinacol boronic ester was directly coupled to yield triarylamine **3** without intermediate purification. The last bromination step by *N*-bromosuccinimide (NBS) proved stereospecific with high yields of the advanced intermediates **4** and **5**.



**Scheme 1.** Synthesis route of triphenylamine donor fragment **3**. i) KOH, DMSO, 1-bromohexane, *r.t.*, ii) HBpin, PdCl<sub>2</sub>(CH<sub>3</sub>CN)<sub>2</sub>, SPhos, Et<sub>3</sub>N/1,4-dioxane, 110 °C, iii) Pd(OAc)<sub>2</sub>, SPhos, K<sub>2</sub>CO<sub>3</sub>, H<sub>2</sub>O/1,4-dioxane, iv) NBS, CH<sub>2</sub>Cl<sub>2</sub>, *r.t.*

Our strategy to arrive at the CDCA-functionalized  $\pi$ -spacer involved a number of different reactions, from the old textbook chemistry to more modern coupling reactions, see Scheme 2. Firstly, chenodeoxycholic acid was converted to its methyl ester analogue **6**, in a Fischer esterification. Secondly, the hydroxyl groups of **6** were protected as *tert*-butyldimethylsilane ethers (TBDMS), and compound **7** was further reduced by LiAlH<sub>4</sub> to yield the primary alcohol **8**. To install the CDCA moiety onto the  $\pi$ -spacer, a Williamson ether synthesis between compound **8** and 2-bromo-3-(bromomethyl)thiophene based on the procedure reported by Bjørnholm et al. was performed.<sup>39</sup> Subsequently, removal of the TBDMS protection groups by HCl gave compound **9**. The first four steps were all quantitative in terms of yields (97-99%). Initially, a Kumada

coupling was intended to merge the CDCA and thiophene moieties. Despite a lot of work, this was not successful and the ether linkage strategy reported in this work was settled upon. Introduction of the furan moiety proved to be a challenging step, but a Suzuki coupling catalyzed by PdCl<sub>2</sub>(dppf) using 3 eq. of (5-formylfuran-2-yl)boronic acid was eventually developed, giving compound **10** in a satisfactory yield of 68%. The last step in the synthesis of the CDCA  $\pi$ -spacer building block was a bromination by NBS, which proved to be highly challenging, and should be further optimized. Despite the low yield of 25%, enough material was prepared for the target sensitizers to be synthesized in sufficient amounts.

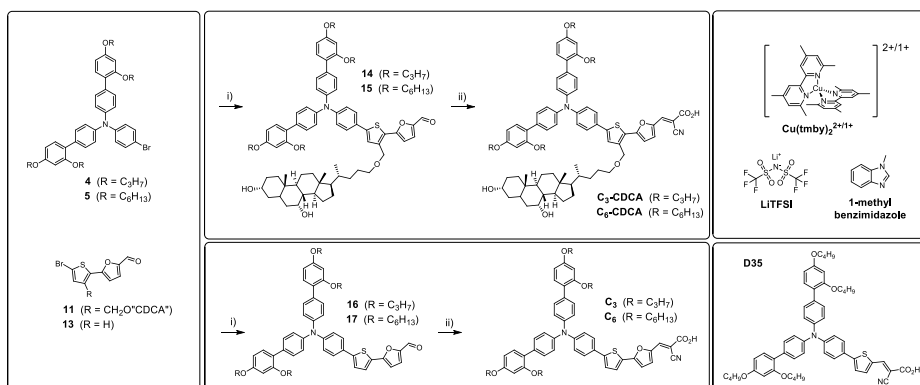


**Scheme 2.** Synthesis route for CDCA-functionalized  $\pi$ -spacer **12**. i) MeOH, H<sub>2</sub>SO<sub>4</sub>, r.t., ii) TBDMS triflate, 2,6-lutidine, DCM, r.t., iii) LiAlH<sub>4</sub>, THF, r.t., iv) NaH, THF, 60 °C followed by deprotection by HCl, v) (5-formylfuran-2-yl)boronic acid, PdCl<sub>2</sub>(dppf), K<sub>2</sub>CO<sub>3</sub>, H<sub>2</sub>O/1,4-dioxane, 80 °C, vi) NBS, CHCl<sub>3</sub>/AcOH, 0 °C.

Preparation of the  $\pi$ -spacer without the CDCA substituent required two steps. Firstly, a Suzuki coupling between 2-bromothiophene and 5-formylfuran-2-yl boronic acid gave compound **12** in 48% yield, confirming it is not the steric bulk of the CDCA substituent that caused the low yield in the same reaction to compound **10**. Lastly, a bromination by NBS in 59% yield completed the reference  $\pi$ -spacer building block **13**.

The triarylamine donor fragments **4** and **5** were converted to boronic esters by the procedure from Billingsley and Buchwald,<sup>38</sup> see Scheme 3. Subsequently, they were coupled to the  $\pi$ -spacer building blocks **11** and **13**, giving the carboxaldehydes **14-17**, as seen in Scheme 3. The Knoevenagel condensation installed the cyanoacrylic acid anchoring group in mostly good yields from 54-95%, successfully concluding the synthesis of the first two sensitizers bearing CDCA-substituents and their two corresponding reference dyes.





**Scheme 3.** Fusion of triphenylamine donor **5** and CDCA-functionalized  $\pi$ -spacer **10**. i) Pd(OAc)<sub>2</sub>, SPhos, 1,4-dioxane/H<sub>2</sub>O, 80 °C, ii) cyanoacetic acid, piperidine, ACN/THF, 65 °C. Included are also the electrolyte components and reference sensitizer **D35**.

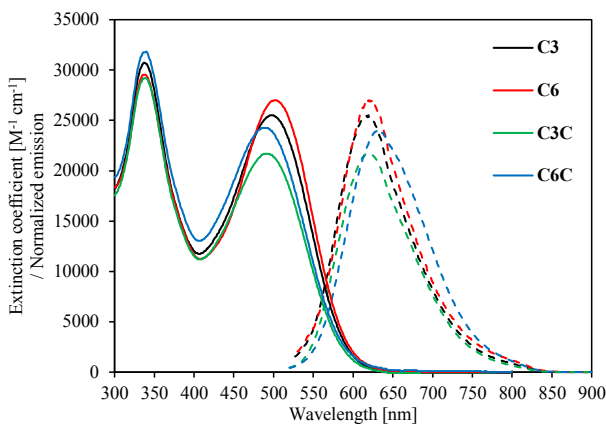
## 2.2 Photophysical properties

One aim with the design of the sensitizers is for the CDCA substituent not to affect the photophysical and electrochemical properties. The CDCA moiety should simply be an inert substituent affecting only the aggregation properties of the dyes. From the UV/Vis absorption spectra in solution shown in Figure 1, there are only minor differences between the four sensitizers. The reference dyes, **C<sub>3</sub>** and **C<sub>6</sub>**, have slightly higher molar extinction coefficients and the ICT transition peaks are redshifted by about 10 nm. These changes can only be explained by the large CDCA substituent introducing a slight ring twist between the thiophene and furan rings. Of the four dyes, the two with C<sub>6</sub>-chains have 6-12% higher molar extinction coefficients compared to the C<sub>3</sub> analogues. Although difficult to explain, the phenomena of higher molar extinction coefficients for longer alkyl chains has been previously observed for triarylamines<sup>40</sup>, phenothiazine<sup>41</sup> and ruthenium complex dyes.<sup>42</sup>

When anchored on TiO<sub>2</sub> without additional co-adsorbents (Figure S1, ESI), the ICT transition peaks of the reference sensitizers are blueshifted by 53-59 nm, indicating they could be prone to H-aggregation.<sup>7</sup> Sensitizers **C<sub>3</sub>-CDCA** and **C<sub>6</sub>-CDCA** are also affected, but by 35-44 nm, suggesting the CDCA substituents prevent aggregation to a certain extent and that additional CDCA added to the staining solution may be required when fabricating devices.

Normalized emission spectra are also plotted in Figure 1, and very similar emission behaviours are found for all the sensitizers. Optical bandgaps extracted from the intersections of the absorption and emission curves are in the range of 2.18-2.20 eV for all four sensitizers, further indicating the CDCA substituents do not affect the photophysical properties noticeably. Another useful calculation is the integration of the 1 sun AM1.5 G solar spectrum to obtain the maximum short-circuit current obtainable from a sensitizer with a

specific absorption onset or bandgap. For the sensitizers in this work, with bandgap around 2.20 eV, a maximum  $J_{SC}$  value of 10.4 mA cm<sup>-2</sup> can be expected. All the photophysical and electrochemical properties are summarized in Table 1.



**Figure 1.** UV/vis measurements and normalized emission spectra of all dyes in dichloromethane solution.

**Table 1.** Photophysical properties of the triarylamine dyes **C<sub>3</sub>**, **C<sub>6</sub>**, **C<sub>3</sub>-CDCA** and **C<sub>6</sub>-CDCA**.

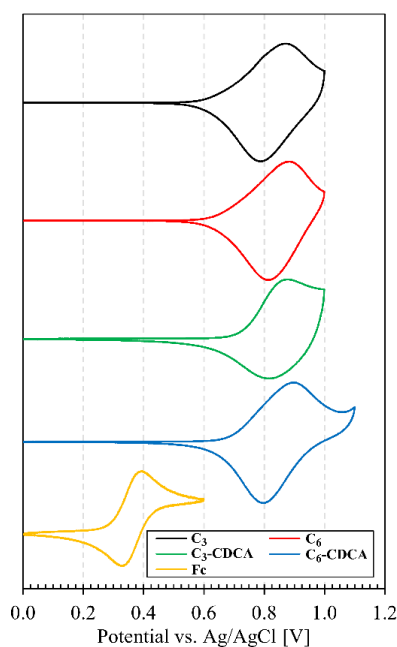
Dye	$\lambda_{\text{abs}}^a$ (nm)	$\epsilon$ (M <sup>-1</sup> cm <sup>-1</sup> )	Em. <sup>b</sup> (nm)	$\lambda_{\text{abs}}^c$ on TiO <sub>2</sub> (nm)	Rel. $\epsilon$ on TiO <sub>2</sub>	E <sub>0-0</sub> <sup>d</sup> (eV)	E <sub>ox</sub> <sup>e</sup> (V vs SHE)	E <sub>LUMO</sub> <sup>f</sup> (V)
<b>C<sub>3</sub></b>	498	25500	617	442	1.43	2.20	1.09	-1.11
<b>C<sub>6</sub></b>	502	27000	621	445	1.29	2.19	1.12	-1.07
<b>C<sub>3</sub>-CDCA</b>	492	21700	619	448	1.00	2.20	1.11	-1.09
<b>C<sub>6</sub>-CDCA</b>	489	24300	632	451	1.01	2.18	1.11	-1.07

<sup>a</sup> Maximum of most red-shifted peak. <sup>b</sup> Emission when ICT band is excited, in DCM solution. <sup>c</sup> Maximum of most red-shifted peak on TiO<sub>2</sub> (2.5  $\mu\text{m}$ , GreatcellSolar 18NR-T). <sup>d</sup> Calculated from the intersection of the absorption and normalized emission spectra. <sup>e</sup> Measured vs. F<sub>c</sub><sup>+</sup>/F<sub>c</sub> on stained TiO<sub>2</sub> electrodes in acetonitrile with 0.1 M LiTFSI, converted to V vs. SHE by 0.624 V. Scan rate 20 mV s<sup>-1</sup>. <sup>f</sup> Calculated from E<sub>ox</sub>-E<sub>0-0</sub>.

### 2.3 Electrochemical properties

The four dyes adsorbed onto TiO<sub>2</sub> films were investigated by cyclic voltammetry to determine the oxidation potentials. The films were 2.5  $\mu\text{m}$  thick prepared by 30NR-D TiO<sub>2</sub> screen-printed on FTO glass. The stained photoanodes were attached to the working electrode of the potentiostat, a carbon graphite rod was used as a counter electrode, Ag/AgCl reference electrode and the supporting electrolyte was 0.1 M LiTFSI in dry acetonitrile. The cyclic voltammograms are shown in Figure 2, and the extracted electrochemical

information is found in Table 1. All the dyes display a single reversible oxidation, and very similar electrochemical behaviour. This indicates that neither the presence of CDCA substituent, nor the length of the alkoxy chains affect the electrochemical properties of the sensitizers. When the ferrocene standard was measured, the working electrode was replaced by a glassy carbon electrode, and the  $E_{1/2}$  of Fc was found at 0.36 V vs. Ag/AgCl. The calculated values for the oxidation potentials of the four sensitizers were all found in the range of 1.09-1.12 V vs. SHE, suggesting they should be compatible with the redox potential of the  $[\text{Cu}^{+2+}(\text{tmby})_2](\text{TFSI})_{1/2}$  electrolyte, reported at 0.87 V vs. SHE.<sup>25</sup> Excited state energies calculated from the  $E_{0,0}$  values and  $E_{\text{ox}}$ , are found between -1.07 and -1.11 V vs. SHE, giving all sensitizers sufficient driving force for efficient electron injection into the conduction band of  $\text{TiO}_2$ , commonly reported around -0.5 V vs. SHE.

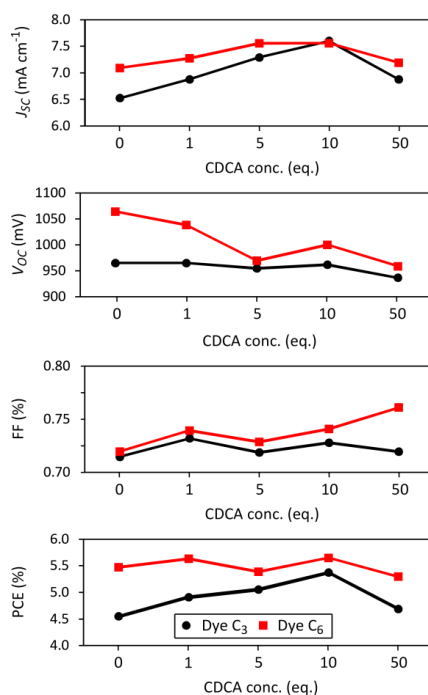


**Figure 2.** Cyclic voltammograms of the four sensitizers and ferrocene. Sensitizers measured on  $\text{TiO}_2$  films (2.5  $\mu\text{m}$  on FTO glass), carbon counter electrode, Ag/AgCl reference, 0.1 M LiTFSI supporting electrolyte. Ferrocene (Fc) was measured with a glassy carbon working electrode and used for calibration with a value of 0.624 V vs. SHE.<sup>43</sup>

## 2.4 Photovoltaic properties

The four sensitizers were evaluated in dye-sensitized solar cells alongside the structurally related reference dye, **D35** reported by Hagberg et al.<sup>44</sup> The fabrication procedure for the DSSCs is described in the Experimental section. The complete set of photovoltaic data is reported in Table 2 while a selection of  $J-V$  curves are shown in Figure 4 (a-b).

Firstly, the effect of CDCA as a co-adsorbent for the reference sensitizers  $C_3$  and  $C_6$  had to be established. Therefore, a range of CDCA concentrations were tested (0, 1, 5, 10 and 50 equivalents relative to the sensitizers). The results of this screening is shown in Figure 3, and the top part of Table 2. The full set of  $J-V$  curves and IPCE spectra of all CDCA concentrations are shown in the Supporting information. (Figure S2)



**Figure 3.** Screening of CDCA concentration for dyes  $C_3$  and  $C_6$ . Each data point is the average of three devices.

On a general note,  $C_6$  outperforms  $C_3$  in all performance characteristics in the CDCA concentration screening, and  $C_3$  is also affected to a greater extent by the CDCA concentration than  $C_6$  is. The most

noticeable difference between the two dyes, differing only by the alkoxy chain length, is the open-circuit voltage. When no CDCA co-adsorbent is used, the difference in  $V_{OC}$  is exactly 100 mV in favour of dye  $C_6$ . As the CDCA concentration is increased the  $V_{OC}$  of both dyes decreases, something which can be explained by a lowered conduction band edge due to protonation of the  $TiO_2$  by the carboxylic acid of CDCA. For both dyes, the maximum short circuit current is found for 5-10 equivalents of CDCA, leading to the highest power-conversion efficiencies being obtained for 10 eq. of CDCA.

With the co-adsorbent dependence of the reference sensitizers determined, the dyes with CDCA substituents were tested in identical devices, with no additional CDCA additive. Compared to the optimized  $C_3$  and  $C_6$  devices, the relative efficiencies were 75% and 95% for  $C_3$ -CDCA and  $C_6$ -CDCA. Interestingly, the increase in  $V_{OC}$  from  $C_3$  to  $C_3$ -CDCA was a monumental 60 mV. In other studies, the use of longer alkoxy chains has produced the same  $V_{OC}$  enhancing behaviour,<sup>45</sup> and thus we conclude the CDCA substituent is blocking the electron recombination from the  $TiO_2$  to the electrolyte and thereby improving the photovoltage. This is supported by a slight improvement in electron lifetimes, see Figure 5c. Following the same arguments, for the  $C_6$  dyes no change in  $V_{OC}$  was observed nor expected, as the longer alkoxy chains are already sufficiently blocking the electron recombination. From charge extraction measurements, see Figure 5, we also note that there is no significant shift in conduction band position between the dyes with or without CDCA groups.

We then tested the optimized CDCA co-adsorbent concentrations (10 eq.) with the dyes  $C_3$ -CDCA and  $C_6$ -CDCA, and to our surprise, this further improved the efficiencies significantly. In the case of  $C_3$ -CDCA with 10 eq. CDCA, near identical PCE as for the optimized  $C_3$  was achieved. For  $C_6$ -CDCA, an improvement in PCE of 10% was achieved when 10 eq. of CDCA was used. This indicates that more than one unit of CDCA per dye molecule is required for the sensitizer to operate efficiently. Furthermore, because  $C_6$ -CDCA is more efficient than  $C_6$  with the same amount of CDCA in the staining solution, this could indicate a more optimal distribution of covalent and non-covalent CDCA, so that a higher short-circuit current can be obtained despite lowered dye loading values, see Table 3.

Lastly, for dyes  $C_3$ -CDCA and  $C_6$ -CDCA we attempted to double the thickness of the  $TiO_2$  layers, from  $4 + 2 \mu m$  to  $8 + 4 \mu m$ , see Table 2. This resulted in an average reduction in  $V_{OC}$  of 39 mV, but a larger increase in  $J_{SC}$  resulted in overall increased average power conversion efficiency by 9%. This suggests that the optimal thickness of active  $TiO_2$  can be found between 4 and 8  $\mu m$ . The reduction in the open circuit voltage can be explained by more restricted diffusion for the redox shuttle in the  $TiO_2$  network, increasing recombination, thus lowering the electron lifetime and  $V_{OC}$ . Interestingly, also the fill factors of the devices increased significantly with thicker  $TiO_2$  films, something that is not expected under full illumination if there are diffusion issues.

**Table 2.** Photovoltaic performance of all dyes under 1 sun AM 1.5G illumination, and from IPCE measurements. Electrolyte composition 0.09 M [Cu(tmby)<sub>2</sub>]TFSI<sub>2</sub>, 0.20 M [Cu(tmby)<sub>2</sub>]TFSI, 0.1 M LiTFSI and 0.6 M 1-methylbenzimidazole in dry acetonitrile.

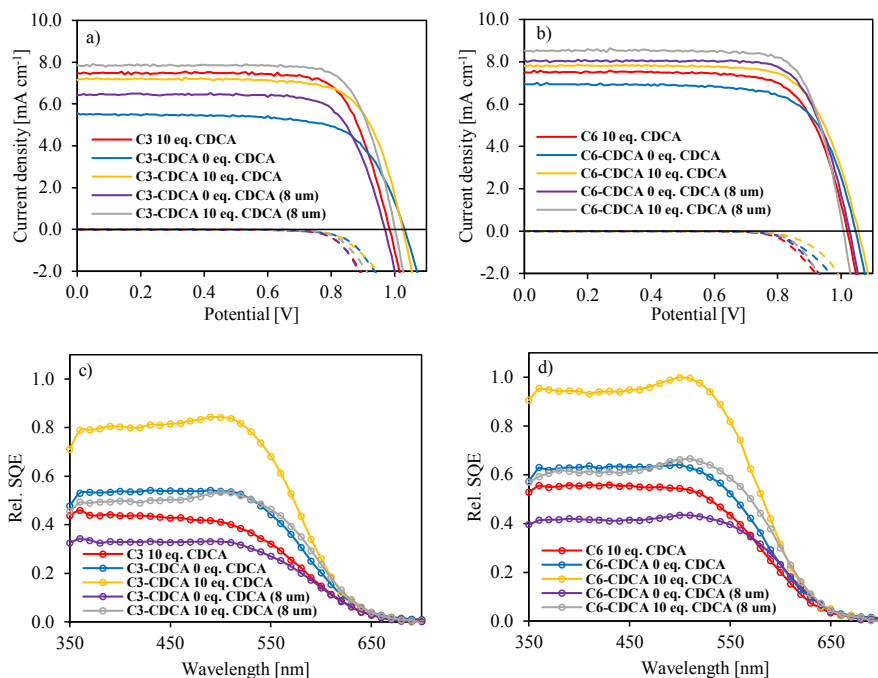
Dye	CDCA (eq.)	TiO <sub>2</sub> (μm)	IPCE $J_{SC}$ (mA cm <sup>-2</sup> ) <sup>a</sup>	$J_{SC}$ (mA cm <sup>-2</sup> )	$V_{OC}$ (mV)	FF (%)	PCE (%)
<b>C<sub>3</sub></b>	0	4 + 2	6.31	6.53 ± 0.13	965 ± 3	0.72 ± 0.01	4.55 ± 0.12
	1	4 + 2	6.91	6.88 ± 0.43	965 ± 10	0.73 ± 0.01	4.91 ± 0.42
	5	4 + 2	7.04	7.29 ± 0.27	955 ± 14	0.72 ± 0.01	5.05 ± 0.28
	10	4 + 2	6.88	7.60 ± 0.14	962 ± 20	0.73 ± 0.02	5.37 ± 0.23
	50	4 + 2	6.32	6.88 ± 0.40	937 ± 8	0.72 ± 0.04	4.69 ± 0.50
<b>C<sub>6</sub></b>	0	4 + 2	7.68	7.09 ± 0.14	1064 ± 5	0.72 ± 0.01	5.48 ± 0.14
	1	4 + 2	7.96	7.27 ± 0.32	1038 ± 28	0.74 ± 0.02	5.64 ± 0.26
	5	4 + 2	6.96	7.56 ± 0.08	970 ± 21	0.73 ± 0.02	5.39 ± 0.20
	10	4 + 2	7.26	7.56 ± 0.18	1000 ± 22	0.74 ± 0.01	5.65 ± 0.14
	50	4 + 2	6.18	7.19 ± 0.09	959 ± 13	0.76 ± 0.01	5.29 ± 0.15
<b>C<sub>3</sub>-CDCA</b>	0	4 + 2	6.49	5.55 ± 0.09	1025 ± 5	0.70 ± 0.01	4.03 ± 0.04
	0	8 + 4	6.98	6.21 ± 0.43	961 ± 11	0.74 ± 0.02	4.49 ± 0.46
	10	4 + 2	7.27	7.12 ± 0.17	1013 ± 15	0.73 ± 0.01	5.34 ± 0.24
	10	8 + 4	8.05	7.50 ± 0.39	1000 ± 2	0.76 ± 0.01	5.81 ± 0.32
<b>C<sub>6</sub>-CDCA</b>	0	4 + 2	6.77	7.07 ± 0.08	1044 ± 3	0.72 ± 0.02	5.39 ± 0.07
	0	8 + 4	8.54	7.84 ± 0.47	1008 ± 25	0.76 ± 0.01	6.11 ± 0.44
	10	4 + 2	7.81	8.00 ± 0.09	1035 ± 15	0.74 ± 0.00	6.20 ± 0.02
	10	8 + 4	8.54	8.30 ± 0.30	992 ± 14	0.77 ± 0.02	6.44 ± 0.35
<b>D35</b>	0	4 + 2	7.40	7.51 ± 0.22	1016 ± 23	0.73 ± 0.00	5.60 ± 0.31

<sup>a</sup> Obtained by integration of the IPCE spectrum over the 1 sun AM 1.5 G spectrum.

The IPCE spectra in Figure S3 (Supporting material) show that light harvest is less than optimal for all devices fabricated with these sensitizers, as the maximum IPCE value is only 70%. This is a consequence of modest molar extinction coefficients, paired with thin TiO<sub>2</sub> layers required for the slow diffusing copper complex redox couple in the electrolyte. However, for the purpose of testing the CDCA substituents, it is of little significance. The IPCE spectra resemble the UV/Vis absorption spectra, but the onset is redshifted by up to 50 nm compared to the absorption spectra, likely an effect of different solvents in device operation and the photophysical measurements. From Table 2, the values for the integrated short-circuit current from the IPCE spectra are in good agreement with the values obtained from the  $J$ - $V$  sweeps.

While the original IPCE spectra show only minor differences, a different picture is available when adjusting the IPCE spectra for the respective dye loading values, as has been done in Figure 4 (c-d). This way, the photovoltaic contribution per sensitizer can be displayed and compared, and the plot would resemble an absorbed photon-to-current conversion efficiency spectra, as  $IPCE = APCE \cdot LHE$ . The light harvesting efficiency is defined by IUPAC as  $(1-10^{-A})$  where A is absorbance, which again is a product of extinction coefficient and dye loading of the sensitizer on the TiO<sub>2</sub> surface. However, for thicker films the LHE is close to 1 in most cases regardless of the sensitizer, making dye loading values the more sensible choice for scaling the IPCE spectra. Additionally, when comparing dyes of similar extinction coefficients, any differences in absorbance comes from the respective dye loading values. To the best of our knowledge, this approach has not been used to investigate the individual efficiency contributions of sensitizers, and thus we suggest the term sensitizer quantum efficiency (SQE) for the technique.

High SQE values in these plots indicate high efficiency of the individual sensitizer molecules, and low values can be an indication of recombination, diffusion issues or poor absorption properties. Here, the performance advantage of the CDCA-substituted dyes is very clear for both the C<sub>3</sub> and C<sub>6</sub> dyes. Firstly, with the same concentration of CDCA in the staining solutions, the C<sub>3</sub>/C<sub>6</sub>-CDCA dyes are remarkably more efficient than their non-CDCA analogues. This suggests a more optimized molecular environment for the CDCA-dyes in the self-assembled monolayer. Secondly, by increasing the thickness of the TiO<sub>2</sub> the individual sensitizer performance is lowered. The mechanism behind this behaviour must be related to either the increased redox shuttle diffusion resistance, electron transport resistance or complete light attenuation leaving a portion of the active layer without any illumination.



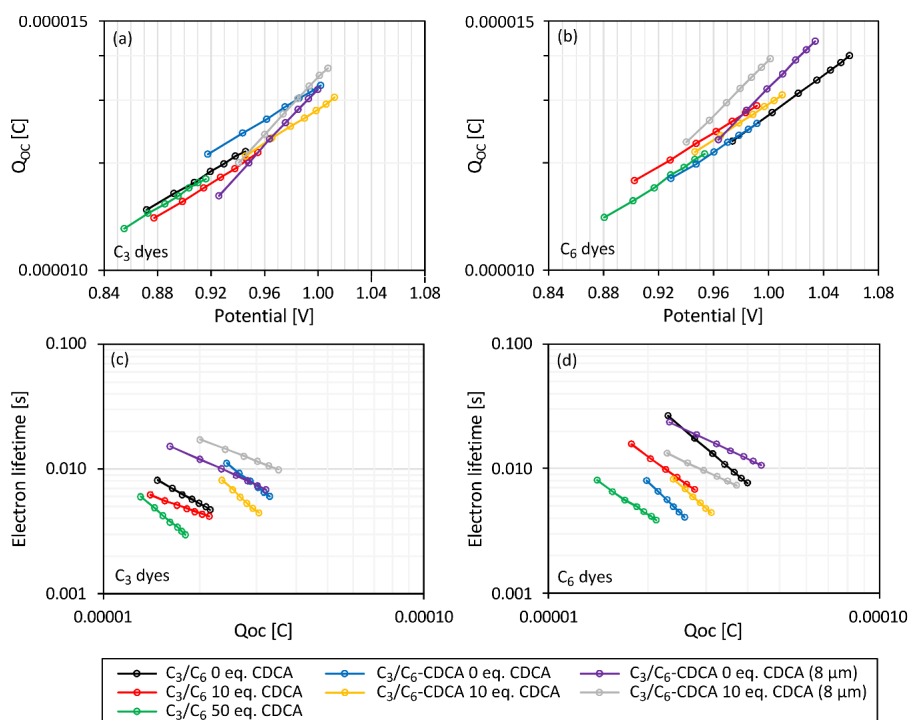
**Figure 4.** (a-b) Current density vs. applied potential plots under 1 sun AM1.5 G illumination (lines) and under darkness (dashed lines). (c-d) Sensitizer quantum efficiency (SQE) spectra, essentially dye loading-adjusted incident photon-to-current conversion efficiency curves. Curves are scaled relative to the highest performing device. Comment of 8 um means 8+4  $\mu\text{m}$   $\text{TiO}_2$  was used, while no specification implies 4+2  $\mu\text{m}$   $\text{TiO}_2$  electrodes. Original IPCE measurements available in the Supporting material.

Charge extraction and electron lifetime measurements were used to further investigate the properties of the dye monolayers in the devices. In the charge extraction measurements of the C<sub>3</sub> dyes, the same  $V_{OC}$  trend observed from the  $J-V$  sweeps can be seen. The CDCA substituent shifts the curves towards higher  $V_{OC}$  values, and also towards higher  $Q_{OC}$  values. For the C<sub>6</sub> dyes (Figure 5 b), the trend is not as clear, as would be expected from the very similar photovoltaic performance. However, the devices with 8  $\mu\text{m}$  thick active  $\text{TiO}_2$  layer deliver slightly higher  $Q_{OC}$  values compared to the 4  $\mu\text{m}$  devices.

The effect of different CDCA concentrations (0, 10 and 50 eq.) has the same effect on the electron lifetime behaviour for both C<sub>3</sub> and C<sub>6</sub>. An increased amount of CDCA causes a drop in electron lifetime, despite the fact that the relative conduction band shift associated with the protonation from the carboxylic acid of CDCA is accounted for. The same separated grouping of C<sub>3</sub> and C<sub>3</sub>-CDCA dyes is observed, suggesting the CDCA substituent is contributing to an overall denser dye/CDCA monolayer, restricting the access to the  $\text{TiO}_2$  for the  $\text{Cu}^{2+}$  species. However, C<sub>6</sub> and C<sub>6</sub>-CDCA do not display the same trend. An explanation



could be superior anti-aggregation properties of the hexyl chains over the propyl chains. Somewhat surprisingly, the thicker TiO<sub>2</sub> electrodes display the highest electron lifetimes in both C<sub>3</sub> and C<sub>6</sub> dyes series. We expected the hindered diffusion of the copper redox species in and out of the TiO<sub>2</sub> layer to facilitate recombination of injected electrons to the electrolyte, but it appears the quality of the monolayer is sufficiently high to block this recombination pathway.



**Figure 5.** (a-b) Charge extraction measurements at different light intensities. C<sub>3</sub> dyes in (a) and C<sub>6</sub> dyes in (b). (c-d) Lifetime measurements at different light intensities, plotted against collected charge for the same devices at the same potentials. C<sub>3</sub> dyes in (c) and C<sub>6</sub> dyes in (d). Measured with the Dyenamo Toolbox instrument.

Knowing the exact dye loading of a given system can be extremely informative, and for this work the measurements were made by desorption of stained electrodes in 40 mM tetrabutylammonium hydroxide (TBAOH) in THF. The reported dye loading values in Table 3 are averages of two separately desorbed electrodes, producing standard deviations within 6%. The extinction coefficients are averages of two separate solutions for increased accuracy. Some observations from the data set in Table 3 are:

- The longer alkyl chains of  $C_6$  reduces dye loading by 19% compared to  $C_3$ . For  $C_6$ -CDCA vs.  $C_3$ -CDCA the average is a reduction of 12%.
- The CDCA substituent lowers dye loading by 39-45%.
- Doubling the  $TiO_2$  thickness led to a 67% increase in dye loading.

By doubling the  $TiO_2$  thickness an increase in dye loading of 100% would be expected. However, the slightly lower value obtained here could be caused by a number of factors. While screen-printing is a very useful technique for preparing electrodes, an inherent uncertainty in layer thickness has to be accepted. Lastly, as the staining process is diffusion dependent, longer staining times may be required to achieve the same dye loading for thicker electrodes.

**Table 3.** Dye loading experiments for a selection of staining solutions and film  $TiO_2$  film thicknesses.

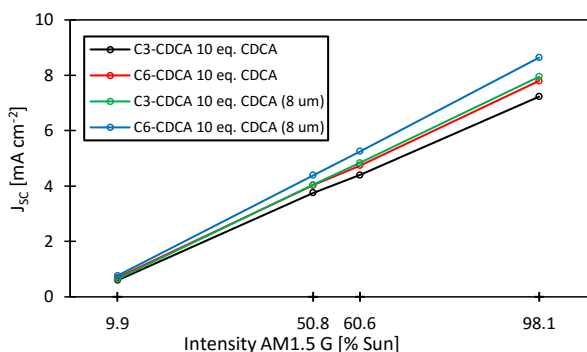
Dye	$\epsilon$ ( $M^{-1} cm^{-1}$ ) <sup>a</sup>	CDCA (eq.)	$TiO_2$ ( $\mu m$ )	Dye loading <sup>b</sup> ( $10^{-8} mol/cm^2$ )
$C_3$	34700	10	4 + 2	$8.52 \pm 0.33$
$C_6$	36300	10	4 + 2	$6.86 \pm 0.03$
$C_3$ -CDCA	31200	0	4 + 2	$6.17 \pm 0.07$
		0	8 + 4	$10.65 \pm 0.12$
		10	4 + 2	$4.66 \pm 0.19$
		10	8 + 4	$7.70 \pm 0.49$
$C_6$ -CDCA	33500	0	4 + 2	$5.48 \pm 0.11$
		0	8 + 4	$9.51 \pm 0.20$
		10	4 + 2	$4.21 \pm 0.21$
		10	8 + 4	$6.54 \pm 0.19$

<sup>a</sup> Average extinction coefficient from two solutions of dye in 40 mM TBAOH in stabilized THF.

<sup>b</sup> Average of two stained electrodes separately desorbed.

The photovoltaic performance of the highest performing devices in this study was measured under a range of light intensities to investigate the linearity of the devices, see Figure 6. A non-linear short-circuit current, as a function of light intensity would indicate diffusion limitations in the device. We suspected the thickest devices with 8  $\mu m$  active  $TiO_2$  layer to suffer from diffusion problems, but all the devices were perfectly linear from 0.1 to 1 sun AM1.5 G illumination, see Figure 6. This indicates that diffusion issues are not the culprits for the non-linear performance observed in the SQE measurements for the 8 + 4  $\mu m$  devices. It should be noted that the thicker scattering layer of the 8  $\mu m$  devices can play a role in enhancing the short-circuit current, and fully or partially mask any diffusion issues.

Furthermore, we believe light attenuation in the thicker devices could be the factor limiting the performance enhancement over the devices with  $4\ \mu\text{m}$  active titania. If at some depth in the  $\text{TiO}_2$  layer, all the light of of the absorbed wavelengths has been absorbed, the dye molecules adsorbed below this depth may not contribute to the  $J_{SC}$ . This can explain the marginal performance enhancement, but not the lack of signs of diffusion issues. To circumvent this, a sensitizer with a wider absorption spectrum or several dyes with complementary spectra will have to be used to increase the overall efficiency.



**Figure 6.** Short-circuit current measurements for four devices at light intensities from 0.1 to 1 sun. Comment of 8 um means 8+4  $\mu\text{m}$   $\text{TiO}_2$  was used, while no specification implies 4+2  $\mu\text{m}$   $\text{TiO}_2$  electrodes.

### 3. Conclusion

We report on the first successful synthesis and evaluation of sensitizers for dye-sensitized solar cells with a covalently attached CDCA substituent. The two triarylamine dyes were prepared in a convergent synthesis involving 10-12 steps, and two reference sensitizers without CDCA-substituent were also prepared along a similar route. The four dyes investigated varied only in alkoxy chain lengths (C3 vs. C6) and in the presence of the covalent CDCA substituent. The CDCA substituents did not affect the photophysical or electrochemical properties of the dyes, providing a solid basis for investigating the effects of the CDCA substituents.

The longer alkoxy chains reduced dye loading by 12-19%, while the large CDCA substituent reduced it by 39-45%. The dyes were paired with a recently reported  $[\text{Cu}^{+2}(\text{tmb}y)_2](\text{TFSI})_{1/2}$  electrolyte in DSSCs. The effect of the different alkoxy chain lengths in the reference dyes was significant, with C3 delivering a  $V_{OC}$  100 mV below that of C6. However, with the CDCA substituents, the difference was much smaller, and the addition of free CDCA co-adsorbent to the staining solutions reduced  $V_{OC}$  and electron lifetimes. Ten equivalents of CDCA in the staining solutions produced the most efficient devices for C3, but the effect was very small for the C6 reference. With 10 equivalents of additional CDCA co-adsorbent, the PCE of C6-

CDCA improved by 10%, most likely due to an overall better distribution of the covalent and non-covalent CDCA in the monomolecular sensitizer layer on the TiO<sub>2</sub>. From the SQE spectra (IPCE spectra corrected with the dye loading), the combination of 10 eq. of free CDCA and the CDCA substituent was determined to be vastly superior. Our suggestion is that this combination provides the correct amount and distribution of total CDCA in the self-assembled monolayer, providing the optimal molecular environment for the sensitizer.

By doubling the TiO<sub>2</sub> thickness, marginally higher PCE values were obtained due to increased  $J_{SC}$ , but the  $V_{OC}$  was reduced slightly. The most efficient device was sensitized with C<sub>6</sub>-CDCA delivering a PCE of 6.84% (8 μm TiO<sub>2</sub>, 1 mM CDCA,  $J_{SC}$  = 8.64 mA cm<sup>-2</sup>,  $V_{OC}$  = 1007 mV, FF = 0.77).

Although the synthetic protocol for the introduction of the CDCA substituents certainly should be optimized further, the effects of the CDCA substituents on the photovoltaic performance are very promising. The authors are of the perception that any large non-chromophore dye substituent with hydrogen bonding abilities will increase the quality of the monomolecular layer, as shown for CDCA in this work. This work has revealed a dye/CDCA ratio greater than 1 is required, so perhaps introduction of several anti-aggregation units may produce a truly non-aggregating sensitizer, capable of producing a high quality monolayer without additives. In conclusion, we believe this work has uncovered a new design strategy for DSSC sensitizers or other applications where controlling aggregation is of high importance.

## 4. Experimental

### 4.1 Materials

All chemicals and reagents used for the synthesis and device fabrication of the sensitizers were sourced from Sigma Aldrich. TiO<sub>2</sub> pastes were bought from GreatCell Solar and the D35 reference dye, [Cu(tmby)<sub>2</sub>]TFSI and [Cu(tmby)<sub>2</sub>]TFSI<sub>2</sub> were bought from Dyenamo.

### 4.2 Solar cell assembly

The working electrodes of the devices were fabricated from FTO glass (NSG10, Nippon Sheet Glass), cut to size and washed with Deconex 21 (2 g/L) in an ultrasonic bath for 45 minutes. Following UV/O<sub>3</sub> cleaning for 15 minutes (Novascan PSD-UV), a dense blocking layer of TiO<sub>2</sub> was deposited by immersion in aqueous TiCl<sub>4</sub> solution (40 mM) for 30 minutes at 70 °C. The glass slides were rinsed with deionized water and ethanol before the procedure was repeated and before heating the glass slides on a hotplate at 250 °C for 1 hour. The titania pastes were screenprinted onto the FTO glass with a 120T mesh (Seritec Services S.A.), giving each electrode an active area of 0.283 cm<sup>2</sup>. For the 4 + 2 μm electrodes, two layers of 30NR-D and one layer of scattering paste were printed, and for the electrodes with 8 + 4 μm, four layers of 30NR-D and two layers of scattering paste. Between each layer, the FTO glass slides were heated at 125 °C for 5 minutes,

then cooled back to room temperature before printing the next layer. The working electrodes were finished by sintering on a programmable hotplate at 125, 250, 375, 450 and 500 °C for 5, 5, 5, 15 and 30 minutes with 5 minutes ramping between each step.

Counter electrodes were made from TEC15 FTO glass. Holes were drilled with a diamond drill bit, and the glass slides were washed in an ultrasonic bath for 15 minutes in each of the following solutions: Hellmanex 2% detergent solution, deionized water, ethanol and acetone. A layer of PEDOT was electrochemically deposited on the FTO glass from an aqueous solution of EDOT, as described by Ellis et al.<sup>46</sup>

The solvent mixture used for the dye staining solutions was acetonitrile/*tert*-butanol/tetrahydrofuran (1:1:1, v/v), with a dye concentration of 0.1 mM, and various amounts of the co-adsorbent chenodeoxycholic acid (CDCA) as specified in the Results and Discussion part. The staining time for all experiments was 20 hours, and the electrodes were rinsed in acetonitrile and air dried in a drybox before assembly. Surlyn gaskets (35 μm) were melted between the working and counter electrodes (50 W heating element, 2 × 9 seconds for sufficient sealing).

The electrolyte contained 0.09 M [Cu(tmby)<sub>2</sub>]TFSI<sub>2</sub>, 0.20 M [Cu(tmby)<sub>2</sub>]TFSI, 0.1 M LiTFSI and 0.6 M 1-methylbenzimidazole in dry acetonitrile, and the DSSCs was filled with electrolyte by vacuum backfilling. The filling hole was sealed by Surlyn and a glass cover slip, before the protruding edges of the electrodes were covered with soldering tin for increased conductivity.

### 4.3 Component and device characterization

The UV/Vis absorption measurements were recorded on a Hitachi U-1900 spectrophotometer, emission spectra recorded with a FS5 Spectrofluorometer from Edinburgh Instruments and electrochemical experiments recorded with a Versastat 3 potentiostat from Princeton Applied Research. Dye loading experiments were performed by desorption of stained photoanodes in a solution of 40 mM TBAOH in stabilized THF. Separate molar extinction coefficients of the dyes in the basic media were measured for increased accuracy. The *J-V* characteristics of the devices under 1 sun AM 1.5G illumination were recorded with an Oriel xenon lamp solar simulator (300 W), connected to a Keithley 2400, scanned from open-circuit to short-circuit with a settling time of 100 ms at each voltage step of 10 mV. IPCE measurements were recorded on a commercial Arkeo-Ariadne setup (Cicci Research s.r.l., 300 W xenon light source) with 50% sun bias light. For the *J-V* sweeps and IPCE measurements, the devices were masked with a 0.158 cm<sup>2</sup> aperture black metal mask. Charge extraction and electron lifetime measurements were measured using the Dyenamo Toolbox (Dyenko, Sweden).

### Associated content

Supporting information: All synthesis details of intermediates and sensitizers and absorption properties on TiO<sub>2</sub> films.

### Acknowledgements

The authors want to thank MSc Ingunn Schröder for embarking on the Kumada coupling of CDCA as a preliminary investigation for this work. Staff engineer Roger Aarvik and PhD Susana Villa Gonzalez are acknowledged for their technical and mass spectrometry contributions. The support from the Research Council of Norway to the Norwegian NMR Platform (project number 226244/F50) is much appreciated.

### References

1. B. O'Regan and M. Grätzel, *Nature*, 1991, **353**, 737-740.
2. A. Hagfeldt, G. Boschloo, L. Sun, L. Kloo and H. Pettersson, *Chem. Rev.*, 2010, **110**, 6595-6663.
3. D. Joly, L. Pelleja, S. Narbey, F. Oswald, T. Meyer, Y. Kervella, P. Maldivi, J. N. Clifford, E. Palomares and R. Demadrille, *Energy Environ. Sci.*, 2015, **8**, 2010-2018.
4. N. Robertson, *Angew. Chem. Int. Ed.*, 2006, **45**, 2338-2345.
5. E. Mosconi, J.-H. Yum, F. Kessler, C. J. Gómez García, C. Zuccaccia, A. Cinti, M. K. Nazeeruddin, M. Grätzel and F. De Angelis, *J. Am. Chem. Soc.*, 2012, **134**, 19438-19453.
6. S. M. Feldt, E. A. Gibson, E. Gabrielsson, L. Sun, G. Boschloo and A. Hagfeldt, *J. Am. Chem. Soc.*, 2010, **132**, 16714-16724.
7. L. Zhang and J. M. Cole, *J. Mater. Chem. A*, 2017, **5**, 19541-19559.
8. A. Kay and M. Grätzel, *J. Phys. Chem.*, 1993, **97**, 6272-6277.
9. J. M. Donkers, R. L. P. Roscam Abbing and S. F. J. van de Graaf, *Biochem. Pharmacol.*, 2019, **161**, 1-13.
10. N. A. Malik, *Appl. Biochem. Biotechnol.*, 2016, **179**, 179-201.
11. R. Cisneros, M. Beley and F. Lapique, *Phys. Chem. Chem. Phys.*, 2016, **18**, 9645-9651.
12. A. F. Buene, E. E. Ose, A. G. Zakariassen, A. Hagfeldt and B. H. Hoff, *J. Mater. Chem. A*, 2019, **7**, 7581-7590.
13. Y. Hong, Z. Iqbal, X. Yin and D. Cao, *Tetrahedron*, 2014, **70**, 6296-6302.
14. X. Zhang, Y. Xu, F. Giordano, M. Schreier, N. Pellet, Y. Hu, C. Yi, N. Robertson, J. Hua, S. M. Zakeeruddin, H. Tian and M. Grätzel, *J. Am. Chem. Soc.*, 2016, **138**, 10742-10745.
15. K. Kakiage, Y. Aoyama, T. Yano, K. Oya, J.-i. Fujisawa and M. Hanaya, *Chem. Commun.*, 2015, **51**, 15894-15897.

16. A. Yella, R. Humphry-Baker, B. F. E. Curchod, N. Ashari Astani, J. Teuscher, L. E. Polander, S. Mathew, J.-E. Moser, I. Tavernelli, U. Rothlisberger, M. Grätzel, M. K. Nazeeruddin and J. Frey, *Chem. Mater.*, 2013, **25**, 2733-2739.
17. M. Xu, R. Li, N. Postrakulchote, D. Shi, J. Guo, Z. Yi, S. M. Zakeeruddin, M. Grätzel and P. Wang, *J. Phys. Chem. C*, 2008, **112**, 19770-19776.
18. J.-H. Yum, D. P. Hagberg, S.-J. Moon, K. M. Karlsson, T. Marinado, L. Sun, A. Hagfeldt, M. K. Nazeeruddin and M. Grätzel, *Angew. Chem. Int. Ed.*, 2009, **48**, 1576-1580.
19. S. Mathew, A. Yella, P. Gao, R. Humphry-Baker, B. F. E. Curchod, N. Ashari-Astani, I. Tavernelli, U. Rothlisberger, K. Nazeeruddin and M. Grätzel, *Nat. Chem.*, 2014, **6**, 242-247.
20. R. Y.-Y. Lin, F.-L. Wu, C.-T. Li, P.-Y. Chen, K.-C. Ho and J. T. Lin, *ChemSusChem*, 2015, **8**, 2503-2513.
21. J.-H. Yum, S.-J. Moon, C. S. Karthikeyan, H. Wietasch, M. Thelakkat, S. M. Zakeeruddin, M. K. Nazeeruddin and M. Grätzel, *Nano Energy*, 2012, **1**, 6-12.
22. D. Kuang, C. Klein, H. J. Snaith, J.-E. Moser, R. Humphry-Baker, P. Comte, S. M. Zakeeruddin and M. Grätzel, *Nano Lett.*, 2006, **6**, 769-773.
23. N. Manfredi, M. Monai, T. Montini, F. Peri, F. De Angelis, P. Fornasiero and A. Abboto, *ACS Energy Lett.*, 2018, **3**, 85-91.
24. Y. Cao, Y. Liu, S. M. Zakeeruddin, A. Hagfeldt and M. Grätzel, *Joule*, 2018, **2**, 1108-1117.
25. Y. Saygili, M. Söderberg, N. Pellet, F. Giordano, Y. Cao, A. B. Muñoz-García, S. M. Zakeeruddin, N. Vlachopoulos, M. Pavone, G. Boschloo, L. Kavan, J.-E. Moser, M. Grätzel, A. Hagfeldt and M. Freitag, *J. Am. Chem. Soc.*, 2016, **138**, 15087-15096.
26. Y. Hao, Y. Saygili, J. Cong, A. Eriksson, W. Yang, J. Zhang, E. Polanski, K. Nonomura, S. M. Zakeeruddin, M. Grätzel, A. Hagfeldt and G. Boschloo, *ACS Appl. Mater. Interfaces*, 2016, **8**, 32797-32804.
27. M. Freitag, F. Giordano, W. Yang, M. Pazoki, Y. Hao, B. Zietz, M. Grätzel, A. Hagfeldt and G. Boschloo, *J. Phys. Chem. C*, 2016, **120**, 9595-9603.
28. J.-H. Yum, E. Baranoff, F. Kessler, T. Moehl, S. Ahmad, T. Bessho, A. Marchioro, E. Ghadiri, J.-E. Moser, C. Yi, M. K. Nazeeruddin and M. Grätzel, *Nat. Commun.*, 2012, **3**, 631-639.
29. M. Freitag, Q. Daniel, M. Pazoki, K. Sveinbjörnsson, J. Zhang, L. Sun, A. Hagfeldt and G. Boschloo, *Energy Environ. Sci.*, 2015, **8**, 2634-2637.
30. Y. Saygili, M. Stojanovic, N. Flores-Diaz, S. M. Zakeeruddin, N. Vlachopoulos, M. Grätzel and A. Hagfeldt, *Inorganics*, 2019, **7**, 30-98.
31. V. Dryza and E. J. Bieske, *J. Photochem. Photobiol. A*, 2015, **302**, 35-41.

32. J. T. Lin, P.-C. Chen, Y.-S. Yen, Y.-C. Hsu, H.-H. Chou and M.-C. P. Yeh, *Org. Lett.*, 2009, **11**, 97-100.
33. J. Zhao, T. Jin, A. Islam, E. Kwon, M. Akhtaruzzaman, N. Asao, L. Han, K. A. Alamry, S. A. Kosa, A. M. Asiri and Y. Yamamoto, *Tetrahedron*, 2014, **70**, 6211-6216.
34. H. Zhu, Y. Wu, J. Liu, W. Zhang, W. Wu and W.-H. Zhu, *J. Mater. Chem. A*, 2015, **3**, 10603-10609.
35. K.-M. Lu, W.-M. Li, P.-Y. Lin, K.-T. Liu and C.-Y. Liu, *Adv. Synth. Catal.*, 2017, **359**, 3805-3817.
36. A. Baumann, H. Cheema, M. A. Sabuj, L. E. McNamara, Y. Zhang, A. Peddapuram, S. T. Nguyen, D. L. Watkins, N. I. Hammer, N. Rai and J. H. Delcamp, *Phys. Chem. Chem. Phys.*, 2018, **20**, 17859-17870.
37. E. Gabrielson, H. Ellis, S. Feldt, H. Tian, G. Boschloo, A. Hagfeldt and L. Sun, *Adv. Energy Mater.*, 2013, **3**, 1647-1656.
38. K. L. Billingsley and S. L. Buchwald, *J. Org. Chem.*, 2008, **73**, 5589-5591.
39. T. Bjørnholm, D. R. Greve, N. Reitzel, T. Hassenkam, K. Kjaer, P. B. Howes, N. B. Larsen, J. Bøgelund, M. Jayaraman, P. C. Ewbank and R. D. McCullough, *J. Am. Chem. Soc.*, 1998, **120**, 7643-7644.
40. Q.-Y. Yu, J.-Y. Liao, S.-M. Zhou, Y. Shen, J.-M. Liu, D.-B. Kuang and C.-Y. Su, *J. Phys. Chem. C*, 2011, **115**, 22002-22008.
41. Y. Hua, S. Chang, D. D. Huang, X. Zhou, X. J. Zhu, J. Z. Zhao, T. Chen, W. Y. Wong and W. K. Wong, *Chem. Mater.*, 2013, **25**, 2146-2153.
42. L. Schmidt-Mende, J. E. Kroeze, J. R. Durrant, M. K. Nazeeruddin and M. Grätzel, *Nano Lett.*, 2005, **5**, 1315-1320.
43. V. V. Pavlishchuk and A. W. Addison, *Inorganica Chim. Acta*, 2000, **298**, 97-102.
44. D. P. Hagberg, X. Jiang, E. Gabrielson, M. Linder, T. Marinado, T. Brinck, A. Hagfeldt and L. Sun, *J. Mater. Chem.*, 2009, **19**, 7232-7238.
45. Y. Saygili, M. Stojanovic, H. Michaels, J. Tjepelt, J. Teuscher, A. Massaro, M. Pavone, F. Giordano, S. M. Zakeeruddin, G. Boschloo, J.-E. Moser, M. Grätzel, A. B. Muñoz-García, A. Hagfeldt and M. Freitag, *ACS Appl. Energy Mater.*, 2018, **1**, 4950-4962.
46. H. Ellis, R. Jiang, S. Ye, A. Hagfeldt and G. Boschloo, *Phys. Chem. Chem. Phys.*, 2016, **18**, 8419-8427.



**Electronic Supplementary Information****First Report of CDCA-Substituted Dyes for Dye-Sensitized Solar Cells  
Improving Efficiency through Reduced Aggregation**

Audun Formo Buene<sup>a</sup>, David Moe Almenningen<sup>a</sup>, Anders Hagfeldt<sup>b</sup>, Odd Reidar Gautun<sup>a</sup>, Bård Helge Hoff<sup>a\*</sup>

*a: Department of Chemistry, Norwegian University of Science and Technology, Høgskoleringen 5, NO-7491 Trondheim, Norway*

*b: Laboratory of Photomolecular Science, Institute of Chemical Sciences and Engineering, École Polytechnique Fédérale de Lausanne (EPFL), Chemin des Alambics, Station 6, CH-1015 Lausanne, Switzerland*

\* Corresponding author. Tel.: +47 73593973; E-mail address: [bard.h.hoff@ntnu.no](mailto:bard.h.hoff@ntnu.no) (B. H. Hoff).

**List of contents**

<b>Absorption and emission</b>	<b>S2</b>
<b>Photovoltaic performance</b>	<b>S2</b>
<b>Experimental</b>	<b>S3</b>
<b>NMR</b>	<b>S21</b>

### Absorption and emission

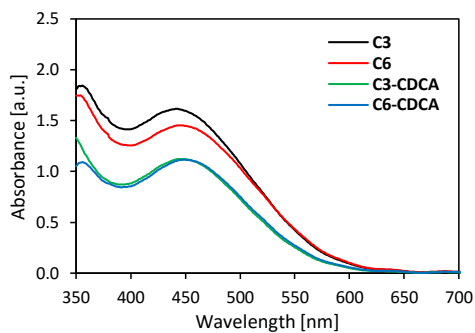


Figure S1. Absorption spectra of the four dyes on  $\text{TiO}_2$  films ( $2.5 \mu\text{m}$  thickness).

### Photovoltaic performance

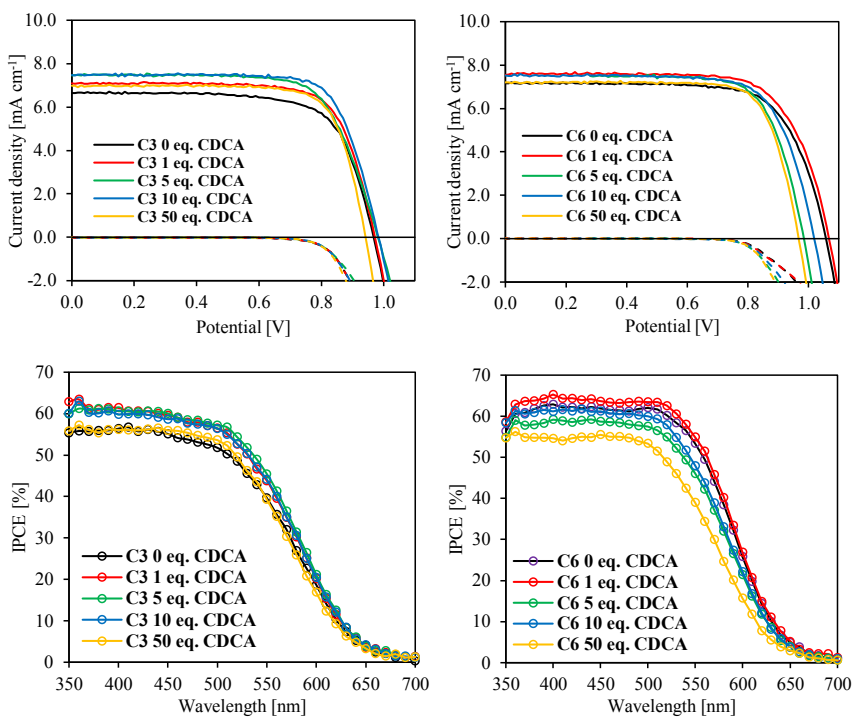
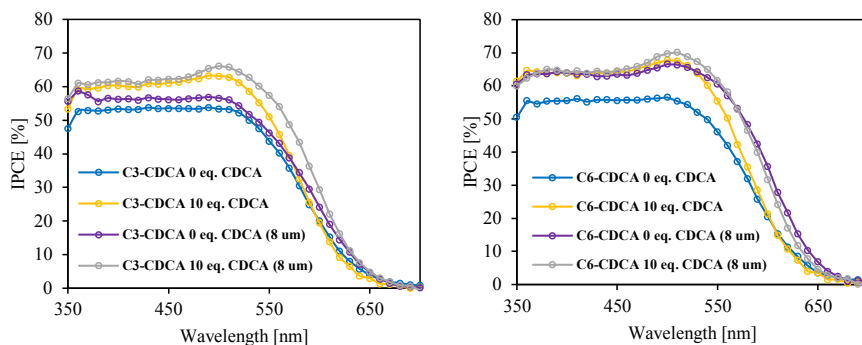


Figure S2. Photovoltaic performance of optimization process of dyes **C3** and **C6** with different amounts of chenodeoxycholic acid (0, 1, 5, 10 and 50 eq. of CDCA).



*Figure S3. Photocurrent action spectra of the dyes with CDCA substituents, with different additional CDCA concentrations and thickness of TiO<sub>2</sub>.*

## Experimental

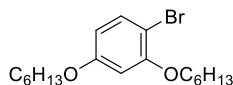
### Materials and reagents

All reactions were carried out under nitrogen atmosphere, and all synthesis reagents were acquired from Sigma Aldrich.

### Analytical instruments

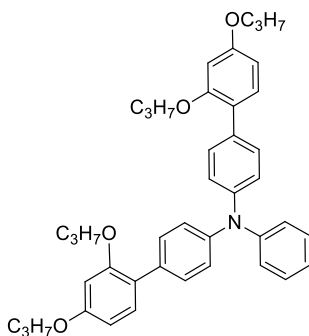
NMR spectroscopy (<sup>1</sup>H and <sup>13</sup>C) was recorded on 400 and 600 MHz Bruker instruments, and all chemical shifts are reported relative to the respective solvent signals. Mass determination was performed on a Waters “Synapt G2-S” QTOF instrument in positive and negative modes. UV/Vis spectra were recorded on a Hitachi U-1900 instrument using quartz cuvettes for the solution samples, while fluorescence spectroscopy was recorded on an Edinburgh instruments FS5 Spectrofluorometer. Infrared spectra were recorded on a Bruker Alpha FT-IR spectrometer with an ATR module.

### Synthesis of 1-bromo-2,4-bis(hexyloxy)benzene (**1**)<sup>1</sup>



4-Bromoresorcinol (3.00 g, 15.9 mmol) and KOH (2.42 g, 43.1 mmol) were dissolved in DMSO (20 mL), before 1-bromohexane (6.7 mL, 47.7 mmol) was added. The resulting mixture was stirred at room temperature overnight. The product was extracted from DMSO using pentane (4 × 40 mL), the combined pentane phases were washed with water (4 × 40 mL), before drying with brine solution (40 mL) and ultimately dried over anhydrous Na<sub>2</sub>SO<sub>4</sub>. The pentane phase was then filtered and the solvents were removed *in vacuo*. The crude product was purified by silica gel column chromatography (dichloromethane/*n*-pentane, 1:4, *R<sub>f</sub>* = 0.27). Compound **1** was isolated as a clear oil (5.29 g, 14.8 mmol, 93%). <sup>1</sup>H NMR (400 MHz, DMSO-*d*<sub>6</sub>) δ: 7.39 (d, *J* = 8.7 Hz, 1H), 6.62 (d, *J* = 2.6 Hz, 1H), 6.46 (dd, *J* = 8.7, 2.7 Hz, 1H), 4.01 (t, *J* = 6.4 Hz, 2H), 3.94 (t, *J* = 6.5 Hz, 2H), 1.74-1.64 (m, 4H), 1.47-1.35 (m, 4H), 1.34-1.26 (m, 8H), 0.89-0.85 (m, 6H).

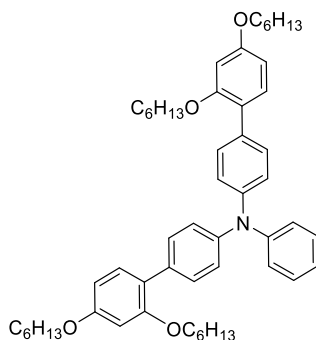
### Synthesis of *N*-(2',4'-dipropoxy-[1,1'-biphenyl]-4-yl)-*N*-phenyl-2',4'-dipropoxy-[1,1'-biphenyl]-4-amine (**2**)



4-Bromo-*N*-(4-bromophenyl)-*N*-phenylaniline (1.00 g, 0.992 mmol), (2,4-dipropoxyphenyl)boronic acid (1.48 g, 5.55 mmol), Pd(OAc)<sub>2</sub> (22 mg, 0.098 mmol), SPhos (81 mg, 0.197 mmol) and K<sub>2</sub>CO<sub>3</sub> (1.37 g, 22.9 mmol) were mixed. 1,4-Dioxane (8 mL) and water (8 mL) were degassed and added under nitrogen. The reaction mixture was heated to 80 °C and left stirring for 20 hours before cooling to room temperature. Water (40 mL) was added and the aqueous phase extracted by ethyl acetate (3 × 40 mL). The combined organic phases were dried with brine (40 mL) and over anhydrous Na<sub>2</sub>SO<sub>4</sub>, filtered and the solvents were removed *in vacuo*. The crude product was purified by silica gel column chromatography (CH<sub>2</sub>Cl<sub>2</sub>, *R<sub>f</sub>* = 0.67) to obtain compound **2** as a clear oil (1.45 g, 2.12 mmol, 85%). <sup>1</sup>H NMR (400 MHz, CHCl<sub>3</sub>) δ: 7.51-7.45 (m, 4H), 7.33-7.26 (m, 4H), 7.24-7.20 (m, 2H), 7.19-7.15 (m, 4H), 7.04 (t, *J* = 6.6 Hz, 1H), 6.60-6.55 (m, 4H), 4.02-3.93 (m, 8H), 1.91-1.77 (m, 8H), 1.09 (t, *J* = 7.3 Hz, 6H), 1.02 (t, *J* = 7.3 Hz, 6H); <sup>13</sup>C NMR (100 MHz, CHCl<sub>3</sub>) δ: 159.5 (2C), 157.0 (2C), 148.0, 146.0 (2C), 132.7 (2C), 130.8 (2C), 130.1 (4C), 129.1

(2C), 124.2 (2C), 123.5 (2C), 123.1 (2C), 122.4, 105.4 (2C), 100.5 (2C), 70.0 (2C), 69.6 (2C), 22.7 (2C), 22.6 (2C), 10.8 (2C), 10.6 (2C); IR (neat,  $\text{cm}^{-1}$ ): 2963 (w), 2935 (w), 2875 (w), 1602 (m), 1491 (s), 1468 (m), 1243 (s), 1180 (s), 1132 (m), 908 (w), 731 (w); HRMS (ASAP+,  $m/z$ ): HRMS (ASAP+,  $m/z$ ): found 630.3574 (calcd.  $\text{C}_{42}\text{H}_{48}\text{NO}_4$  630.3583,  $[\text{M}+\text{H}]^+$ ).

**Synthesis of *N*-(2',4'-bis(hexyloxy)-[1,1'-biphenyl]-4-yl)-2',4'-bis(hexyloxy)-*N*-phenyl-[1,1'-biphenyl]-4-amine (3)**

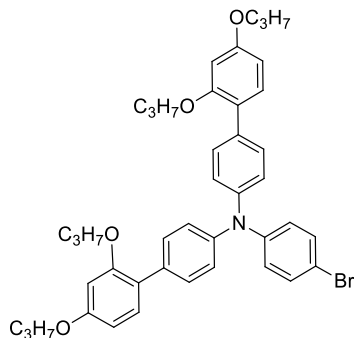


Compound **1** (1.98 g, 5.54 mmol),  $\text{PdCl}_2(\text{CH}_3\text{CN})_2$  (43 mg, 0.17 mmol) and SPhos (136 mg, 0.33 mmol) were added to a two-neck round-bottom flask before it was evacuated, and  $\text{N}_2$ -atmosphere established. Dry 1,4-dioxane (15 mL) was used to dissolve the compounds and the reaction mixture was stirred at rt. before 4,4,5,5-tetramethyl-1,3,2-dioxaborolane (1.7 mL, 11.7 mmol) and dry triethyl amine (2.4 mL, 17.2 mmol) were added. The reaction mixture was heated to 110 °C and left stirring for 90 minutes before cooling to room temperature. The reaction mixture was filtered through Celite using ethyl acetate as eluent, the solvents were removed *in vacuo*. The crude mixture obtained was a yellow oil and was used without further purification.

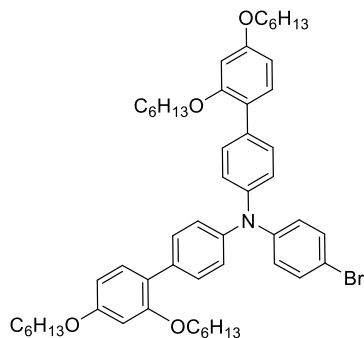
The aforementioned crude product was added to a single neck round-bottom flask along with 4-bromo-*N*-(4-bromophenyl)-*N*-phenylaniline (0.90 g, 2.23 mmol),  $\text{Pd}(\text{OAc})_2$  (24 mg, 0.11 mmol), SPhos (81 mg, 0.20 mmol) and  $\text{K}_2\text{CO}_3$  (1.23 g, 8.90 mmol). 1,4-Dioxane (8 mL) and water (8 mL) were degassed and added under nitrogen. The reaction mixture was heated to 80 °C and stirred for 24 hours before cooling to room temperature. Water (50 mL) was added and the aqueous phase extracted by dichloromethane ( $3 \times 50$  mL). The combined organic phases were dried over anhydrous  $\text{Na}_2\text{SO}_4$ , filtered and the solvents were removed *in vacuo*. The crude product was purified by silica gel column chromatography (dichloromethane/*n*-pentane, 1:4,  $R_f = 0.19$ ) and recrystallized from acetonitrile to yield compound **3** as a white solid (1.11 g, 1.38 mmol, 62%).  $^1\text{H}$  NMR (400 MHz,  $\text{CHCl}_3$ )  $\delta$ : 7.45-7.40 (m, 4H), 7.28-7.22 (m, 4H), 7.20-7.16 (m, 2H), 7.15-7.10 (m, 4H), 7.00 (t,  $J = 6.8$  Hz, 1H), 6.56-6.51 (m, 4H), 4.00-3.92 (m, 8H), 1.84-1.69 (m, 8H), 1.52-1.44 (m, 4H), 1.44-1.23 (m, 20H), 0.91 (t,  $J = 7.1$  Hz, 6H), 0.86 (t,  $J = 6.9$  Hz, 6H);  $^{13}\text{C}$  NMR (100 MHz,  $\text{CHCl}_3$ )  $\delta$ : 159.5 (2C), 157.0 (2C), 148.0, 146.0 (2C), 132.7 (2C), 130.8 (2C), 130.1 (4C), 129.1 (2C), 124.2 (2C), 123.5 (4C), 123.1 (2C), 122.4, 105.3 (2C), 100.4 (2C), 68.4 (2C), 68.1 (2C), 31.6 (2C), 31.5 (2C), 29.3 (2C), 29.1 (2C), 25.78 (2C), 25.76 (2C), 22.63 (2C), 22.57 (2C), 14.1 (2C), 14.0 (2C). IR (neat,  $\text{cm}^{-1}$ )

v: 2927 (m), 2857 (m), 1603 (m), 1491 (s), 1467 (m), 1271 (s), 1178 (s), 1134 (m), 1045 (m), 835 (m). HRMS (ASAP+,  $m/z$ ): HRMS (ASAP+,  $m/z$ ): found 798.5456 (calcd.  $C_{54}H_{72}NO_4$  798.5461,  $[M+H]^+$ ).

**Synthesis of *N*-(4-bromophenyl)-*N*-(2',4'-dipropoxy-[1,1'-biphenyl]-4-yl)-2',4'-dipropoxy-[1,1'-biphenyl]-4-amine (4)**

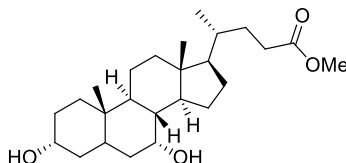


Compound **2** (0.65 g, 1.03 mmol) and NBS (0.19 g, 1.08 mmol) were added to a round-bottom flask under dark conditions. Dichloromethane (20 mL) was degassed and added under nitrogen at 0 °C. The reaction mixture was then allowed to warm to rt. while stirring for 5 hours. Water (40 mL) was added and the aqueous phase was extracted using dichloromethane (3 × 20 mL). The combined organic phases were dried over anhydrous  $Na_2SO_4$ , filtered and the solvents were removed *in vacuo*. The crude product was purified by silica gel column chromatography (dichloromethane,  $R_f$  = 0.74). Compound **4** was isolated as a clear oil (0.60 g, 0.85 mmol, 82%).  $^1H$  NMR (400 MHz,  $CHCl_3$ )  $\delta$ : 7.45-7.41 (m, 4H), 7.36-7.31 (m, 2H), 7.27-7.23 (m, 2H), 7.14-7.09 (m, 4H), 7.07-7.02 (m, 2H), 6.56-6.51 (m, 4H), 3.97-3.89 (m, 8H), 1.88-1.73 (m, 8H), 1.05 (t,  $J$  = 7.0 Hz, 6H), 0.99 (t,  $J$  = 7.0 Hz, 6H);  $^{13}C$  NMR (100 MHz,  $CHCl_3$ )  $\delta$ : 159.6 (2C), 157.0 (2C), 147.2 (2C), 145.5 (2C), 133.3 (2C), 132.0 (2C), 130.9 (2C), 130.3 (4C), 125.2 (2C), 123.7 (4C), 122.9 (2C), 114.4, 105.4 (2C), 100.4 (2C), 70.0 (2C), 69.6 (2C), 22.7 (2C), 22.6 (2C), 10.7 (2C), 10.6 (2C); IR (neat,  $cm^{-1}$ ) v: 2962 (w), 2934 (w), 2874 (w), 1605 (m), 1580 (m), 1485 (s), 1269 (s), 1180 (s), 1133 (m), 1002 (m), 795 (m), 731 (m); HRMS (ASAP+,  $m/z$ ): HRMS (ASAP+,  $m/z$ ): found 708.2681 (calcd.  $C_{42}H_{47}NO_4Br$  708.2688,  $[M+H]^+$ ).

**Synthesis of *N*-(2',4'-bis(hexyloxy)-[1,1'-biphenyl]-4-yl)-*N*-(4-bromophenyl)-2',4'-bis(hexyloxy)-[1,1'-biphenyl]-4-amine (5)<sup>2</sup>**

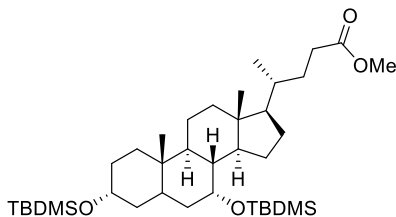
Compound **3** (1.00 g, 1.25 mmol) and NBS (0.22 g, 1.25 mmol) were added to a round-bottom flask under dark conditions. Dichloromethane (25 mL) was degassed and added under nitrogen at 0 °C. The reaction mixture was then allowed to warm to room temperature while stirring for 15 hours. Water (40 mL) was added and the aqueous phase was extracted using dichloromethane (3 × 30 mL). The combined organic phases were dried over anhydrous Na<sub>2</sub>SO<sub>4</sub>, filtered and the solvents were removed *in vacuo*. The crude product was purified by silica gel column chromatography (dichloromethane, *R<sub>f</sub>* = 0.8). Compound **5** was isolated as a clear oil (0.99 g, 1.12 mmol, 90%). <sup>1</sup>H NMR (400 MHz, CHCl<sub>3</sub>) δ: 7.46-7.41 (m, 4H), 7.35-7.30 (m, 2H), 7.27-7.23 (m, 2H), 7.14-7.08 (m, 4H), 7.06-7.02 (m, 2H), 6.56-6.51 (m, 4H), 4.00-3.92 (m, 8H), 1.84-1.70 (m, 8H), 1.52-1.44 (m, 4H), 1.44-1.25 (m, 20H), 0.91 (t, *J* = 6.5 Hz, 6H), 0.87 (t, *J* = 6.5 Hz, 6H); <sup>13</sup>C NMR (100 MHz, CHCl<sub>3</sub>) δ: 159.6 (2C), 157.0 (2C), 147.2, 145.5 (2C), 133.3 (2C), 132.0 (2C), 130.8 (2C), 130.3 (4C), 125.1 (2C), 123.7 (4C), 122.9 (2C), 114.4, 105.3 (2C), 100.3 (2C), 68.4 (2C), 68.1 (2C), 31.6 (2C), 31.5 (2C), 29.3 (2C), 29.1 (2C), 25.78 (2C), 25.76 (2C), 22.64 (2C), 22.58 (2C), 14.1 (2C), 14.0 (2C); IR (neat, cm<sup>-1</sup>) ν: 2928 (m), 2858 (m), 1606 (m), 1581 (m), 1487 (s), 1468 (m), 1281 (m), 1180 (m), 1135 (w); HRMS (ASAP+, *m/z*): HRMS (ASAP+, *m/z*): found 876.4559 (calcd. C<sub>54</sub>H<sub>71</sub>NO<sub>4</sub>Br 876.4566, [M+H]<sup>+</sup>).

Synthesis of methyl (4S)-4-((3S,7S,8S,9R,10R,13S,14R,17S)-3,7-dihydroxy-10,13-dimethylhexadecahydro-1H-cyclopenta[a]phenanthren-17-yl)pentanoate (**6**)<sup>3</sup>



Chenodeoxycholic acid (10.0 g, 25.5 mmol) was dissolved in methanol (300 mL), and while stirring, conc. H<sub>2</sub>SO<sub>4</sub> (1.5 mL) was added slowly. Then, the reaction mixture was stirred at room temperature for 1 hour. The reaction mixture was poured into aqueous NaHCO<sub>3</sub> solution (0.5 M, 150 mL) and extracted with ethyl acetate (3 × 150 mL). Upon removal of the solvents *in vacuo*, compound **6** was obtained as white solid (10.1 g, 24.7 mmol, 97%), mp 69-73 °C (lit.<sup>3</sup> 85.2-86.0 °C). <sup>1</sup>H NMR (400 MHz, DMSO-*d*<sub>6</sub>) δ: 4.31 (d, *J* = 4.7 Hz, 1H), 4.11 (d, *J* = 3.7 Hz, 1H), 3.62 (pent, *J* = 2.8 Hz, 1H), 3.57 (s, 3H), 3.23-3.13 (m, 1H), 2.37-2.27 (m, 1H), 2.25-2.13 (m, 2H), 1.93-1.87 (m, 1H), 1.84-1.61 (m, 6H), 1.50-1.30 (m, 7H), 1.28-0.95 (m, 9H), 0.88 (d, *J* = 6.5 Hz, 3H), 0.83 (s, 3H), 0.60 (s, 3H); HRMS (ESI+, *m/z*): found 371.2946 (calcd. C<sub>25</sub>H<sub>42</sub>O<sub>4</sub>Na 429.2981, [M+Na]<sup>+</sup>).

Synthesis of methyl (4S)-4-((3S,7S,8S,9R,10R,13S,14R,17S)-3,7-bis((tert-butyl dimethylsilyl)oxy)-10,13-dimethylhexadecahydro-1H-cyclopenta[a]phenanthren-17-yl)pentanoate (**7**)

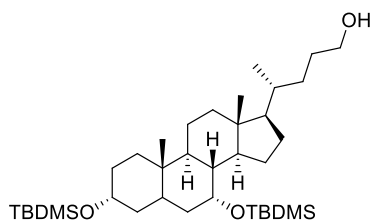


Compound **6** (6.00 g, 14.8 mmol), 2,6-lutidine (17.2 mL, 148 mmol) and dichloromethane (216 mL) were added to a flask at 0 °C under nitrogen atmosphere. *tert*-Butyl dimethylsilyltrifluoromethanesulphonate (10.2 mL, 44.3 mmol) was added and the reaction was stirred for 22 hours. The reaction mixture was quenched in aqueous NaHSO<sub>4</sub> solution (1 M, 150 mL) and the water phase was extracted with CH<sub>2</sub>Cl<sub>2</sub> (3 × 150 mL). The combined organic phases were washed with aqueous NaHSO<sub>4</sub> solution (1 M, 3 × 100 mL) and brine (100 mL), then dried over anhydrous Na<sub>2</sub>SO<sub>4</sub>. Compound **7** was obtained as a clear oil (9.30 g, 14.6 mmol, 99%) upon the removal of the solvents *in vacuo*. <sup>1</sup>H NMR (400 MHz, acetone-*d*<sub>6</sub>) δ: 3.89-3.89 (m, 1H), 3.60 (s, 3H), 3.53-3.45 (m, 1H), 2.39-2.29 (m, 2H), 2.26-2.18 (m, 1H), 2.03-1.01 (m, 25H), 0.99-0.93 (m, 16H), 0.90-0.89 (m, 12H), 0.69 (s, 3H), 0.15 (s, 3H), 0.10 (s, 3H), 0.06-0.05 (m, 9H); <sup>13</sup>C NMR (100 MHz, acetone-*d*<sub>6</sub>) δ: 174.5, 73.3, 70.6, 56.9, 51.5, 51.0, 43.2, 42.7, 41.6, 41.4, 40.6, 36.3, 36.2, 35.8,

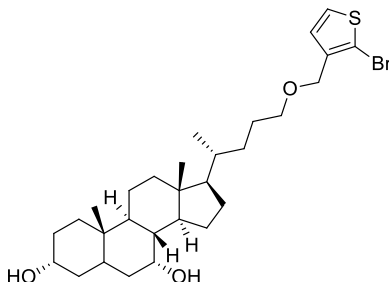


35.3, 33.3, 31.89, 31.86, 31.5, 28.7, 26.6 (2C), 26.2 (2C), 26.1, 24.6, 23.3, 21.3, 19.0, 18.7, 18.6, 12.3, -1.9, -2.7, -4.37, -4.40, -5.4. IR (neat,  $\text{cm}^{-1}$ )  $\nu$ : 2952 (m), 2929 (m), 2855 (m), 1739 (m), 1462 (m), 1436 (m), 1373 (m), 1263 (s), 1252 (s), 1088 (s), 1026 (s), 834 (s), 770 (s), 736 (s), 701 (s); HRMS (ASAP+,  $m/z$ ): found 657.4713 (calcd.  $\text{C}_{37}\text{H}_{70}\text{O}_4\text{NaSi}_2$  657.4710,  $[\text{M}+\text{Na}]^+$ ).

**Synthesis of (4*S*)-4-((3*S*,7*S*,8*S*,9*R*,10*R*,13*S*,14*R*,17*S*)-3,7-bis((*tert*-butyldimethylsilyloxy)-10,13-dimethylhexadecahydro-1*H*-cyclopenta[*a*]phenanthren-17-yl)pentan-1-ol (8)<sup>4</sup>**

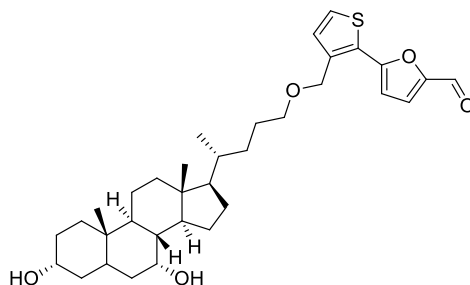


Compound 7 (9.00 g, 14.2 mmol) was dissolved in THF (210 mL) under nitrogen atmosphere at 0 °C. Lithium aluminium hydride in THF solution (2 M, 21.2 mL, 42.5 mmol) was added, and the reaction was stirred for 19 hours while reaching room temperature, before work-up by a modified Fieser work-up procedure. Addition of water (1.6 mL) causing vigorous bubbling, then aqueous NaOH (4 M, 1.6 mL) was added which formed a white granulate. Water (5 mL) was added and the reaction mixture was stirred for 10 minutes, before addition of anhydrous  $\text{Na}_2\text{SO}_4$  and 10 minutes stirring before removal of solids by filtration. The solvents were removed *in vacuo* to yield compound 8 as a white solid (8.43 g, 13.9 mmol, 98%), mp 116-117 °C (lit. not reported).  $^1\text{H}$  NMR (400 MHz, acetone- $d_6$ )  $\delta$ : 3.89-3.88 (m, 1H), 3.52-3.46 (m, 3H), 3.36 (t,  $J = 5.4$  Hz, 0.5H), 2.39-2.29 (m, 1H), 2.01-1.01 (m, 28H), 0.96-0.93 (m, 15H), 0.88 (s, 10H), 0.69 (s, 3H), 0.15 (s, 3H), 0.10 (s, 3H), 0.052 (s, 3H), 0.045 (s, 3H);  $^{13}\text{C}$  NMR (100 MHz, acetone- $d_6$ )  $\delta$ : 72.3, 69.6, 62.0, 61.9, 56.3, 50.0, 42.1, 41.7, 40.6, 40.4, 39.7, 35.7, 35.2, 34.8, 34.3, 32.4, 32.0, 30.9, 27.8, 25.6 (3C), 25.2 (3C), 23.6, 22.3, 20.3, 18.2, 18.0, 17.6, 11.3, -2.9, -5.38, -5.42, -6.4; IR (neat,  $\text{cm}^{-1}$ )  $\nu$ : 3324 (w (br), OH), 2928 (s), 2855 (s), 1462 (m), 1373 (m), 1251 (s), 1091 (s), 1026 (s), 930 (s), 834 (s), 770 (s); HRMS (ESI+,  $m/z$ ): found 629.4751 (calcd.  $\text{C}_{36}\text{H}_{70}\text{O}_3\text{NaSi}_2$  629.4761,  $[\text{M}+\text{Na}]^+$ ).

**Synthesis of (3*S*,7*S*,8*S*,9*R*,10*R*,13*S*,14*R*,17*S*)-17-((*S*)-5-((2-bromothiophen-3-yl)methoxy)pentan-2-yl)-10,13-dimethylhexadecahydro-1*H*-cyclopenta[*a*]phenanthrene-3,7-diol (9)**

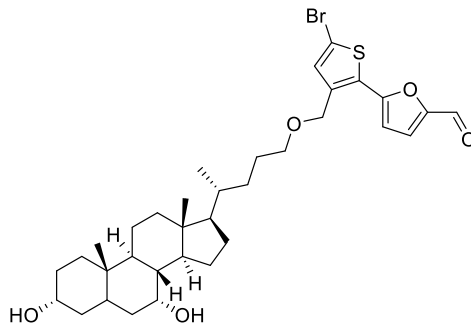
Compound **8** (3.01 g, 4.96 mmol), NaH (357 mg, 14.9 mmol) and THF (14 mL) were placed in a flask under nitrogen atmosphere and stirred for 1 hour at 0 °C. 2-Bromo-3-bromomethylthiophene (1.90 g, 7.44 mmol) was added dropwise over 5 minutes before the reaction was heated to 60 °C and stirred for 19 hours. The reaction mixture was cooled to room temperature, and was quenched by addition of aqueous NH<sub>4</sub>Cl (5 wt%, 15 mL). The aqueous phase was extracted ethyl acetate (3 × 50 mL), washed with brine (50 mL) and dried over anhydrous Na<sub>2</sub>SO<sub>4</sub> before the solvents were removed *in vacuo*. The crude product (light yellow oil) was then suspended in methanol (200 mL) and heated to 60 °C. HCl (37%, 10 mL) was added and the reaction stirred over night. All solids dissolved during the course of the reaction and TLC confirmed full conversion after 17 hours. Aqueous NaHCO<sub>3</sub> solution (10 wt%, 150 mL) was added, and the aqueous phase was extracted by ethyl acetate (3 × 100 mL). The combined organic phases were washed with brine and dried over anhydrous Na<sub>2</sub>SO<sub>4</sub> before concentrated in *vacuo*. The crude product was purified by silica gel column chromatography (ethyl acetate, *R<sub>f</sub>* = 0.38) to yield compound **9** as a white solid (2.73 g, 4.93 mmol, 99%), mp 80-82 °C. <sup>1</sup>H NMR (600 MHz, acetone-*d*<sub>6</sub>) δ: 7.50 (d, *J* = 5.6 Hz, 1H), 7.04 (d, *J* = 5.6 Hz, 1H), 4.42 (s, 2H), 3.82-3.79 (m, 1H), 3.44 (t, *J* = 6.2 Hz, 2H), 3.36-3.30 (m, 1H), 2.38-2.31 (m, 1H), 2.02-1.15 (m, 25H), 1.13-1.05 (m, 2H), 0.95 (d, *J* = 6.3 Hz, 3H), 0.92 (s, 3H), 0.69 (s, 3H); <sup>13</sup>C NMR (150 MHz, acetone-*d*<sub>6</sub>) δ: 140.3, 129.5, 127.4, 110.8, 72.1, 71.6, 68.1, 67.3, 57.2, 51.4, 43.3, 43.0, 40.86, 40.85, 40.6, 36.5, 36.02, 36.01, 33.8, 33.2, 31.7, 30.6, 29.2, 27.1, 24.4, 23.5, 21.6, 19.2, 12.3; HRMS (ESI+, *m/z*): found 575.2177 (calcd. C<sub>29</sub>H<sub>45</sub><sup>79</sup>BrO<sub>3</sub>S 575.2170, [M+Na]<sup>+</sup>).

Synthesis of 5-(3-((((4S)-4-((3S,7S,8S,9R,10R,13S,14R,17S)-3,7-dihydroxy-10,13-dimethylhexadecahydro-1H-cyclopenta[a]phenanthren-17-yl)pentyl)oxy)methyl)thiophen-2-yl)furan-2-carbaldehyde (**10**)



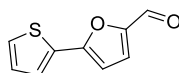
Compound **9** (500 mg, 0.903 mmol), (5-formylfuran-2-yl)boronic acid (379 mg, 2.71 mmol), PdCl<sub>2</sub>(dppf) (33 mg, 0.045 mmol), and K<sub>2</sub>CO<sub>3</sub> (499 mg, 3.61 mmol) were mixed. 1,4-Dioxane (6 mL) and water (6 mL) were degassed and added under nitrogen atmosphere. The reaction mixture was heated to 80 °C and left stirring for 25 minutes before cooling to room temperature. Water (10 mL) was added and the aqueous phase extracted by ethyl acetate (3 × 50 mL). The combined organic phases were washed with brine (30 mL) and over anhydrous Na<sub>2</sub>SO<sub>4</sub>, filtered and the solvents were removed *in vacuo*. The crude product was purified by silica gel column chromatography (ethyl acetate, *R<sub>f</sub>* = 0.32) to obtain compound **10** as a light brown solid (350 mg, 0.615 mmol, 68%), mp 70-72 °C. <sup>1</sup>H NMR (600 MHz, acetone-*d*<sub>6</sub>) δ: 9.65 (s, 1H), 7.61 (d, *J* = 5.0 Hz, 1H), 7.54 (d, *J* = 3.6 Hz, 1H), 7.24 (d, *J* = 5.0 Hz, 1H), 6.92 (d, *J* = 3.8 Hz, 1H), 4.69 (s, 2H), 3.80 (s, 1H), 3.52 (t, *J* = 6.3 Hz, 2H), 3.37-3.30 (m, 1H), 3.38-3.31 (m, 1H), 2.00-1.87 (m, 3H), 1.85-1.77 (m, 2H), 1.75-1.65 (m, 2H), 1.62-1.37 (m, 10H), 1.36-1.00 (m, 10H), 0.99-0.95 (m, 1H), 0.94 (d, *J* = 6.6 Hz, 3H), 0.91 (s, 3H), 0.67 (s, 3H); <sup>13</sup>C NMR (150 MHz, acetone-*d*<sub>6</sub>) δ: 177.6, 154.4, 152.8, 140.3, 131.4, 128.6, 127.6, 124.8, 110.7, 72.1, 71.6, 68.1, 67.2, 57.1, 51.2, 43.2, 42.9, 40.8, 40.7, 40.5, 36.4, 35.92, 35.90, 33.7, 33.2, 31.7, 30.3, 29.0, 27.1, 24.3, 23.4, 21.4, 19.1, 12.2; HRMS (ESI+, *m/z*): found 591.3120 (calcd. C<sub>34</sub>H<sub>48</sub>O<sub>5</sub>S 591.3120, [M+Na]<sup>+</sup>).

**Synthesis of 5-(5-bromo-3-(((4S)-4-((3S,7S,8S,9R,10R,13S,14R,17S)-3,7-dihydroxy-10,13-dimethylhexadecahydro-1H-cyclopenta[a]phenanthren-17-yl)pentyl)oxy)methyl)thiophen-2-yl)furan-2-carbaldehyde (11)**



Compound **10** (230 mg, 0.404 mmol) was dissolved in a mixture of chloroform (3 mL) and glacial acetic acid (3 mL) under nitrogen atmosphere at 0 °C. *N*-Bromosuccinimide (NBS) (120 mg, 0.667 mmol) was added and the reaction was stirred in the dark, at 0 °C for 17 hours slowly reaching room temperature, before water (20 mL) was added and the aqueous phase was extracted by chloroform (3 × 30 mL). The combined organic phases were washed with brine (30 mL), dried over anhydrous Na<sub>2</sub>SO<sub>4</sub>, filtered and concentrated *in vacuo*. Purification by silica gel column chromatography (ethyl acetate, *R<sub>f</sub>* = 0.33) gave compound **11** as a brown solid (76 mg, 0.117 mmol, 29%), mp 83–85 °C. <sup>1</sup>H NMR (600 MHz, acetone-*d*<sub>6</sub>) δ: 9.66 (s, 1H), 7.54 (d, *J* = 3.7 Hz, 1H), 7.29 (s, 1H), 6.93 (d, *J* = 3.8 Hz, 1H), 4.66 (s, 2H), 3.80 (s, 1H), 3.52 (t, *J* = 6.3 Hz, 2H), 3.36–3.30 (m, 1H), 2.39–2.31 (m, 1H), 2.02–1.05 (m, 25H), 1.13–1.05 (m, 2H), 0.94 (d, *J* = 6.5 Hz, 3H), 0.92 (s, 3H), 0.68 (s, 3H); <sup>13</sup>C NMR (150 MHz, acetone-*d*<sub>6</sub>) δ: 176.8, 152.0, 151.7, 139.9, 133.2, 129.1, 123.6, 112.9, 110.3, 70.7, 65.9, 56.1, 50.3, 42.2, 41.9, 39.8, 39.5, 35.44, 35.42, 34.94, 34.90, 32.7, 32.1, 30.7, 29.34, 29.27, 28.3, 28.0, 26.0, 23.3, 22.4, 20.4, 18.1, 11.2; HRMS (ASAP+, *m/z*): found 611.2189 (calcd. C<sub>34</sub>H<sub>44</sub>O<sub>3</sub>S<sup>79</sup>Br 611.2195, [M-2H<sub>2</sub>O+H]<sup>+</sup>).

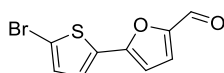
**Synthesis of 5-(thiophen-2-yl)furan-2-carbaldehyde (12)<sup>5</sup>**



2-Bromothiophene (842 mg, 5.16 mmol), (5-formylfuran-2-yl)boronic acid (1.08 g, 7.75 mmol), PdCl<sub>2</sub>(dppf) (113 mg, 0.155 mmol) and K<sub>2</sub>CO<sub>3</sub> (2.86 g, 20.7 mmol) were mixed, and degassed water (18 mL) and degassed 1,4-dioxane (18 mL) were added under nitrogen atmosphere. The reaction was heated to 80 °C and stirred for 24 hours. Upon cooling to room temperature, the solvents were removed from the reaction mixture *in vacuo*, then deionized water (30 mL) and ethyl acetate (30 mL) were added and the phases separated. The aqueous phase was extracted with ethyl acetate (3 × 50 mL) before the combined organic phases were washed with brine (50 mL), dried over anhydrous Na<sub>2</sub>SO<sub>4</sub>, filtered and the solvents were removed *in vacuo*. The crude product was purified by silica gel column chromatography (*n*-pentane/ethyl acetate 1:1, *R<sub>f</sub>* = 0.60) to yield compound **12** as a yellow oil (445 mg, 2.502 mmol, 48%). <sup>1</sup>H

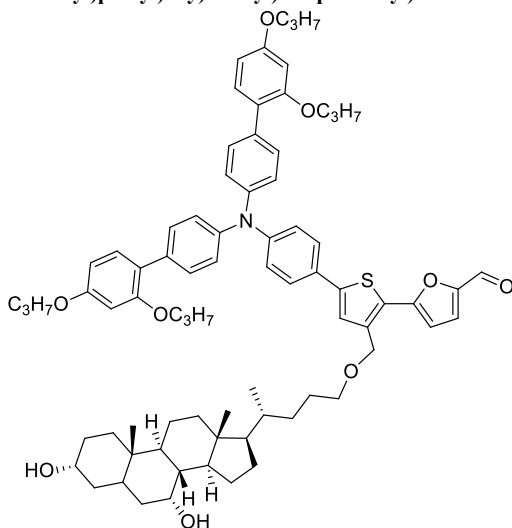
NMR (400 MHz, acetone- $d_6$ )  $\delta$ : 9.63 (s, 1H), 7.67 (dd,  $J = 5.0, 1.1$  Hz, 1H), 7.64 (dd,  $J = 3.7, 1.0$  Hz, 1H), 7.52 (d,  $J = 3.7$  Hz, 1H), 7.20 (dd,  $J = 5.0, 3.7$  Hz, 1H), 6.98 (d,  $J = 3.7$  Hz, 1H); HRMS (ASAP+,  $m/z$ ): found 179.0164 (calcd.  $C_9H_7O_2S$  179.0167,  $[M+H]^+$ ).

### Synthesis of 5-(5-bromothiophen-2-yl)furan-2-carbaldehyde (**13**)<sup>6</sup>



Compound **12** (203 mg, 1.139 mmol) was dissolved in a mixture of chloroform (6 mL) and glacial acetic acid (6 mL) under nitrogen atmosphere at 0 °C. *N*-Bromosuccinimide (NBS) (250 mg, 1.405 mmol) was added and the reaction was stirred under darkness, at 0 °C for 17 hours. Due to incomplete conversion, another portion of NBS (71 mg, 0.399 mmol) was added and the reaction stirred for another 2 hours before water (10 mL) was added and the aqueous phase was extracted by chloroform (3  $\times$  30 mL). The combined organic phases were washed with brine (30 mL), dried over anhydrous  $Na_2SO_4$ , filtered and concentrated *in vacuo*. Purification by silica gel column chromatography (*n*-pentane/ethyl acetate 1:1,  $R_f = 0.57$ ) gave compound **13** as a light brown solid (173 mg, 0.673 mmol, 59%), mp 90-91 °C (lit.<sup>6</sup> 91-92 °C).  $^1H$  NMR (400 MHz, acetone- $d_6$ )  $\delta$ : 9.64 (s, 1H), 7.52 (d,  $J = 3.8$  Hz, 1H), 7.46 (d,  $J = 4.0$  Hz, 1H), 7.27 (d,  $J = 4.0$  Hz, 1H), 7.01 (d,  $J = 3.8$  Hz, 1H); HRMS (ASAP+,  $m/z$ ): found 256.9269 (calcd.  $C_9H_6O_2S^{79}Br$  256.9272,  $[M+H]^+$ ).

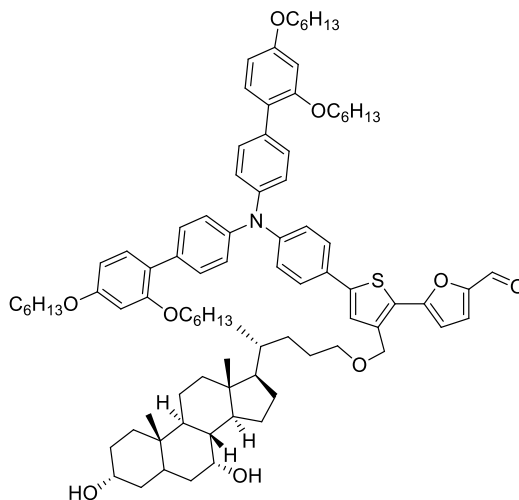
### Synthesis of 5-(5-(4-(bis(2',4'-dipropoxy-[1,1'-biphenyl]-4-yl)amino)phenyl)-3-(((4*S*)-4-((3*S*,7*S*,8*S*,9*R*,10*R*,13*S*,14*R*,17*S*)-3,7-dihydroxy-10,13-dimethylhexadecahydro-1*H*-cyclopenta[*a*]phenanthren-17-yl)pentyl)oxy)methyl)thiophen-2-yl)furan-2-carbaldehyde (**14**)



Compound **4** (72 mg, 0.10 mmol), PdCl<sub>2</sub>(CH<sub>3</sub>CN)<sub>2</sub> (0.53 mg, 2.04 μmol) and SPhos (3.4 mg, 8.2 μmol) were added to a Schlenk-tube before it was evacuated, and N<sub>2</sub>-atmosphere established. Dry 1,4-dioxane (0.2 mL) was used to dissolve the compounds and the reaction mixture was stirred at rt. before 4,4,5,5-tetramethyl-1,3,2-dioxaborolane (20 μL, 0.165 mmol) and dry triethylamine (130 μL) were added. The reaction mixture was heated to 80 °C and left stirring for 1 hour before cooling to room temperature. The reaction mixture was filtered through Celite using ethyl acetate as eluent, the solvents were removed *in vacuo*. The crude mixture obtained was a yellow oil and was used without further purification.

The crude product from the borylation, compound **11** (55 mg, 0.085 mmol), Pd(OAc)<sub>2</sub> (0.38 mg, 1.70 μmol), SPhos (1.4 mg, 3.4 μmol) and K<sub>2</sub>CO<sub>3</sub> (47 mg, 0.34 mmol) were mixed. 1,4-Dioxane (1 mL) and water (1 mL) were degassed and added under nitrogen atmosphere. The reaction mixture was heated to 80 °C and left stirring for 2 hours before cooling to room temperature. Water (20 mL) was added and the aqueous phase extracted by ethyl acetate (3 × 25 mL). The combined organic phases were dried with brine (25 mL) and over anhydrous Na<sub>2</sub>SO<sub>4</sub>, filtered and the solvents were removed *in vacuo*. The crude product was purified by silica gel column chromatography (*n*-pentane/ethyl acetate, 1:1, *R<sub>f</sub>* = 0.16) to obtain compound **14** as yellow solid (33 mg, 0.028 mmol, 33%).

**Synthesis of 5-(5-(4-(bis(2',4'-bis(hexyloxy)-[1,1'-biphenyl]-4-yl)amino)phenyl)-3-(((4*S*)-4-((3*S*,7*S*,8*S*,9*R*,10*R*,13*S*,14*R*,17*S*)-3,7-dihydroxy-10,13-dimethylhexadecahydro-1*H*-cyclopenta[*a*]phenanthren-17-yl)pentyl)oxy)methyl)thiophen-2-yl)furan-2-carbaldehyde (**15**)**

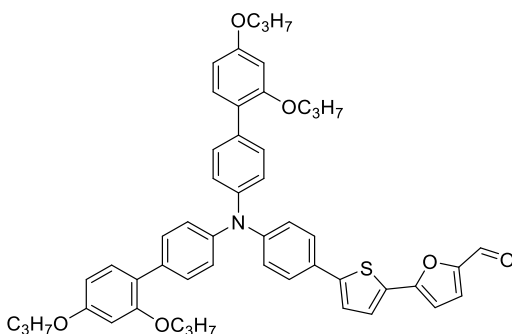


Compound **5** (133 mg, 0.151 mmol), PdCl<sub>2</sub>(CH<sub>3</sub>CN)<sub>2</sub> (0.8 mg, 3.0 μmol) and SPhos (5 mg, 12.0 μmol) were added to a Schlenk-tube before it was evacuated, and N<sub>2</sub>-atmosphere established. Dry 1,4-dioxane (0.3 mL) was used to dissolve the compounds and the reaction mixture was stirred at rt. before 4,4,5,5-tetramethyl-1,3,2-dioxaborolane (33 μL, 0.227 mmol) and dry triethylamine (0.2 mL) were added. The reaction mixture was heated to 80 °C and left stirring for 2.5 hours before cooling to room temperature. The

reaction mixture was filtered through Celite using ethyl acetate as eluent. The solvents were removed *in vacuo*, giving the crude material as a yellow oil.

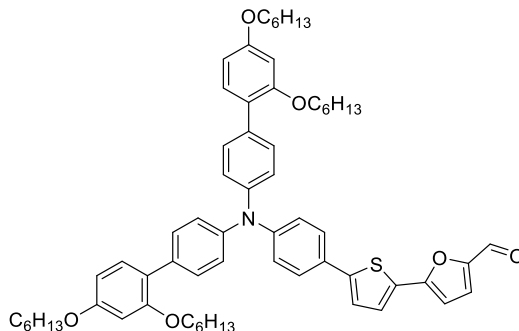
The crude product from the borylation, compound **11** (70 mg, 0.108 mmol), Pd(OAc)<sub>2</sub> (0.5 mg, 2.161 μmol), SPhos (1.8 mg, 4.3 μmol) and K<sub>2</sub>CO<sub>3</sub> (60 mg, 0.43 mmol) were mixed. 1,4-Dioxane (1 mL) and water (1 mL) were degassed and added under nitrogen atmosphere. The reaction mixture was heated to 80 °C and left stirring for 35 minutes before cooling to room temperature. Water (20 mL) was added and the aqueous phase extracted by ethyl acetate (4 × 25 mL). The combined organic phases were dried with brine (30 mL) and over anhydrous Na<sub>2</sub>SO<sub>4</sub>, filtered and the solvents were removed *in vacuo*. The crude product was purified by silica gel column chromatography (ethyl acetate, *R<sub>f</sub>* = 0.48) to obtain compound **15** as a yellow solid (46 mg, 0.034 mmol, 31%). HRMS (ESI<sup>+</sup>, *m/z*): found 1364.8512 (calcd. C<sub>88</sub>H<sub>118</sub>NO<sub>9</sub>S 1364.8527, [M+H]<sup>+</sup>).

#### Synthesis of 5-(5-(4-(bis(2',4'-dipropoxy-[1,1'-biphenyl]-4-yl)amino)phenyl)thiophen-2-yl)furan-2-carbaldehyde (**16**)



Compound **4** (373 mg, 0.53 mmol), PdCl<sub>2</sub>(CH<sub>3</sub>CN)<sub>2</sub> (4 mg, 16 μmol) and SPhos (13 mg, 32 μmol) were added to a Schlenk-tube before it was evacuated, and N<sub>2</sub>-atmosphere established. Dry 1,4-dioxane (1.5 mL) was used to dissolve the compounds and the reaction mixture was stirred at rt. before 4,4,5,5-tetramethyl-1,3,2-dioxaborolane (160 μL, 1.11 mmol) and dry triethyl amine (230 μL, 1.65 mmol) were added. The reaction mixture was heated to 110 °C and left stirring for 60 minutes before cooling to room temperature. The reaction mixture was filtered through Celite using ethyl acetate as eluent, the solvents were removed *in vacuo*. The crude mixture obtained was a yellow oil and was reacted without further purification.

The crude product from the borylation, compound **13** (57 mg, 0.22 mmol), Pd(OAc)<sub>2</sub> (2.4 mg, 11 μmol), SPhos (9 mg, 22 μmol) and K<sub>2</sub>CO<sub>3</sub> (122 mg, 0.88 mmol) were mixed. 1,4-Dioxane (4 mL) and water (4 mL) were degassed and added under nitrogen atmosphere. The reaction mixture was heated to 80 °C and left stirring for 16 hours before cooling to room temperature. Water (40 mL) was added and the aqueous phase extracted by dichloromethane (3 × 40 mL). The combined organic phases were dried over anhydrous Na<sub>2</sub>SO<sub>4</sub>, filtered and the solvents were removed *in vacuo*. The crude product was purified by silica gel column chromatography (*n*-pentane/dichloromethane, 1:4, *R<sub>f</sub>* = 0.13) to obtain compound **16** as a red solid (72 mg, 89 μmol, 41%). HRMS (ASAP<sup>+</sup>, *m/z*): found 806.3521 (calcd. C<sub>51</sub>H<sub>52</sub>NO<sub>6</sub>S 806.3515, [M+H]<sup>+</sup>).

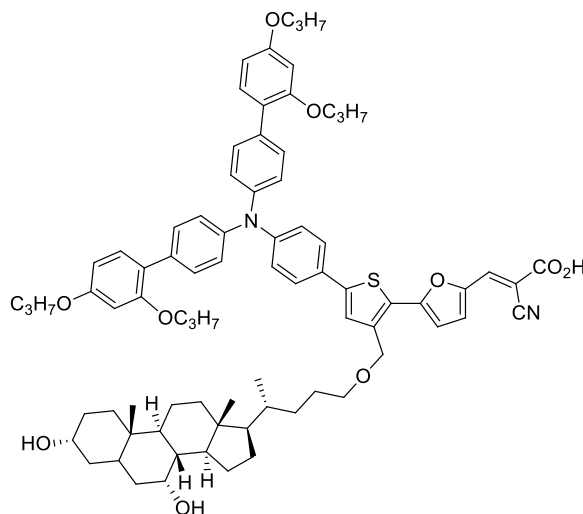
**Synthesis of 5-(5-(4-(bis(2',4'-bis(hexyloxy)-[1,1'-biphenyl]-4-yl)amino)phenyl)thiophen-2-yl)furan-2-carbaldehyde (17)**

Compound **5** (312 mg, 0.36 mmol), PdCl<sub>2</sub>(CH<sub>3</sub>CN)<sub>2</sub> (3 mg, 12 μmol) and SPhos (9 mg, 22 μmol) were added to a Schlenk-tube before it was evacuated, and N<sub>2</sub>-atmosphere established. Dry 1,4-dioxane (1 mL) was used to dissolve the compounds and the reaction mixture was stirred at rt. before 4,4,5,5-tetramethyl-1,3,2-dioxaborolane (110 μL, 0.75 mmol) and dry triethyl amine (150 μL, 1.10 mmol) were added. The reaction mixture was heated to 110 °C and left stirring for 60 minutes before cooling to room temperature. The reaction mixture was filtered through Celite using ethyl acetate as eluent, the solvents were removed *in vacuo*. The crude mixture obtained was a yellow oil and was reacted without further purification.

The crude product from the borylation, compound **13** (57 mg, 0.222 mmol), Pd(OAc)<sub>2</sub> (2.5 mg, 0.011 mmol), SPhos (9.1 mg, 0.022 mmol) and K<sub>2</sub>CO<sub>3</sub> (188 mg, 1.36 mmol) were mixed. 1,4-Dioxane (4 mL) and water (4 mL) were degassed and added under nitrogen atmosphere. The reaction mixture was heated to 80 °C and left stirring for 17 hours before cooling to room temperature. Water (40 mL) was added and the aqueous phase extracted by ethyl acetate (3 × 40 mL). The combined organic phases were dried with brine (40 mL) and over anhydrous Na<sub>2</sub>SO<sub>4</sub>, filtered and the solvents were removed *in vacuo*. The crude product was purified by silica gel column chromatography (CH<sub>2</sub>Cl<sub>2</sub>, R<sub>f</sub> = 0.39) to obtain compound **17** as a red solid (135 mg, 0.138 mmol, 40%). HRMS (ASAP+, *m/z*): found 974.5391 (calcd. C<sub>63</sub>H<sub>76</sub>NO<sub>6</sub>S 974.5393, [M+H]<sup>+</sup>).

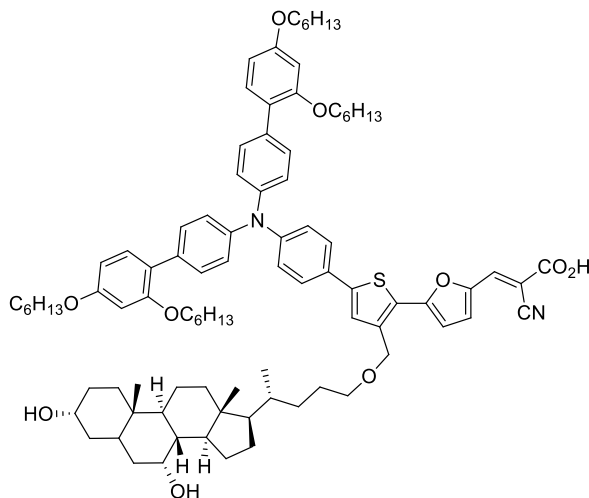


Synthesis of (*E*)-3-(5-(5-(4-(bis(2',4'-dipropoxy-[1,1'-biphenyl]-4-yl)amino)phenyl)-3-(((4*S*)-4-((3*S*,7*S*,8*S*,9*R*,10*R*,13*S*,14*R*,17*S*)-3,7-dihydroxy-10,13-dimethylhexadecahydro-1*H*-cyclopenta[*a*]phenanthren-17-yl)pentyl)oxy)methyl)thiophen-2-yl)furan-2-yl)-2-cyanoacrylic acid (Dye C<sub>3</sub>-CDCA)



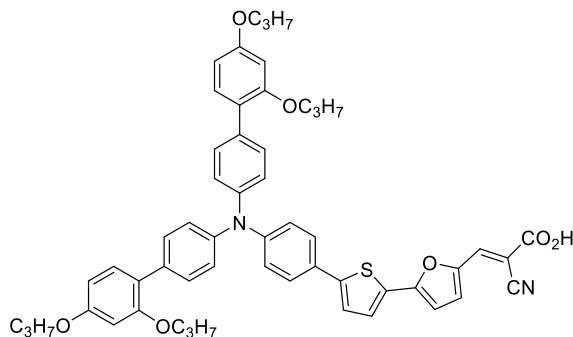
Compound **14** (32 mg, 0.027 mmol) and cyanoacetic acid (46 mg, 0.54 mmol) were dissolved in degassed acetonitrile (12 mL) and THF (2 mL) under nitrogen atmosphere. Piperidine (32  $\mu$ L, 27 mg, 0.321 mmol) was added and the reaction was heated to 80  $^{\circ}$ C for 2 hours before cooling to room temperature and quenched in HCl (1 M, 50 mL). Ethyl acetate (30 mL) was added and the organic phase was washed with water ( $3 \times 200$  mL), then dried with brine (30 mL) and over anhydrous Na<sub>2</sub>SO<sub>4</sub>, filtered and the solvents were removed *in vacuo*. The crude product was purified by silica gel column chromatography (gradient: 0-20% MeOH in ethyl acetate). The solvents were removed, the product redissolved in ethyl acetate and then filtered before complete removal of the solvents yielded sensitizer C<sub>3</sub>-CDCA as a dark solid (18 mg, 0.014 mmol, 54%), mp 153-154  $^{\circ}$ C (dec. 173  $^{\circ}$ C). HRMS (APPI-, *m/z*): found 1261.6573 (calcd. C<sub>79</sub>H<sub>93</sub>N<sub>2</sub>O<sub>10</sub>S 1261.6551, [M-H]).

Synthesis of (*E*)-3-(5-(5-(4-(bis(2',4'-bis(hexyloxy)-[1,1'-biphenyl]-4-yl)amino)phenyl)-3-(((4*S*)-4-((3*S*,7*S*,8*S*,9*R*,10*R*,13*S*,14*R*,17*S*)-3,7-dihydroxy-10,13-dimethylhexadecahydro-1*H*-cyclopenta[*a*]phenanthren-17-yl)pentyl)oxy)methyl)thiophen-2-yl)furan-2-yl)-2-cyanoacrylic acid (Dye C<sub>6</sub>-CDCA)

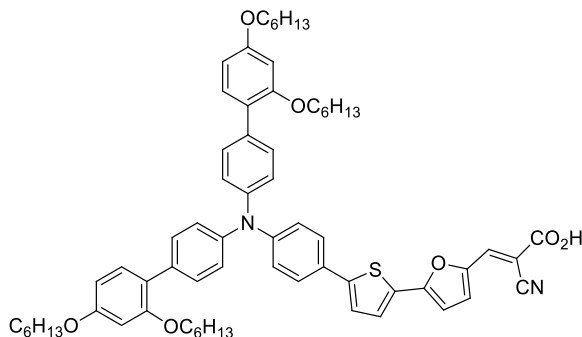


Compound **15** (45 mg, 0.033 mmol) and cyanoacetic acid (56 mg, 0.66 mmol) were dissolved in degassed acetonitrile (35 mL) and THF (5 mL) under nitrogen atmosphere. Piperidine (39  $\mu$ L, 34 mg, 0.396 mmol) was added and the reaction was heated to 80 °C for 1 hour before cooling to room temperature and quenched in HCl (1 M, 100 mL). Ethyl acetate (30 mL) was added and the organic phase was washed with water (3  $\times$  200 mL), then dried with brine (30 mL) and over anhydrous Na<sub>2</sub>SO<sub>4</sub>, filtered and the solvents were removed *in vacuo*. The crude product was purified by silica gel column chromatography (gradient: 0-30% MeOH in ethyl acetate). The solvents were removed, the product redissolved in ethyl acetate and then filtered before complete removal of the solvents yielded sensitizer C<sub>6</sub>-CDCA as a dark solid (45 mg, 0.031 mmol, 95%), mp 132-134 °C (dec. 163 °C).

**Synthesis of (*E*)-3-(5-(5-(4-(bis(2',4'-dipropoxy-[1,1'-biphenyl]-4-yl)amino)phenyl)thiophen-2-yl)furan-2-yl)-2-cyanoacrylic acid (Dye C<sub>3</sub>)**



Compound **16** (59 mg, 73  $\mu$ mol) and cyanoacetic acid (125 mg, 1.46 mmol) were dissolved in degassed acetonitrile (17 mL) under nitrogen atmosphere. Piperidine (87  $\mu$ L, 75 mg, 0.88 mmol) was added and the reaction was heated to 80  $^{\circ}$ C for 1 hour before cooling to room temperature and quenched in HCl (4 M, 30 mL). Dichloromethane (50 mL) was added and the organic phase was washed with water ( $4 \times 100$  mL), then dried over anhydrous Na<sub>2</sub>SO<sub>4</sub>, filtered and the solvents were removed *in vacuo*. The crude product was purified by silica gel column chromatography (gradient: 0-15% MeOH in CH<sub>2</sub>Cl<sub>2</sub>), the dye-containing fractions were washed with HCl (1 M,  $2 \times 30$  mL) to obtain sensitizer C<sub>3</sub> as a dark solid (58 mg, 66  $\mu$ mol, 91%), mp 125-127  $^{\circ}$ C (dec. 178  $^{\circ}$ C). HRMS (TOF MS ES<sup>+</sup>, *m/z*): found 873.3561 (calcd. C<sub>54</sub>H<sub>53</sub>N<sub>2</sub>O<sub>7</sub>S 873.3573, [M+H]<sup>+</sup>).

**Synthesis of (*E*)-3-(5-(5-(4-(bis(2',4'-bis(hexyloxy)-[1,1'-biphenyl]-4-yl)amino)phenyl)thiophen-2-yl)furan-2-yl)-2-cyanoacrylic acid (Dye C<sub>6</sub>)**

Compound **17** (110 mg, 0.11 mmol) and cyanoacetic acid (192 mg, 2.26 mmol) were dissolved in degassed acetonitrile (26 mL) under nitrogen atmosphere. Piperidine (134  $\mu$ L, 115 mg, 1.35 mmol) was added and the reaction was heated to 80 °C for 1 hour before cooling to room temperature and quenched in HCl (4 M, 50 mL). Dichloromethane (100 mL) was added and the organic phase was washed with water (4  $\times$  100 mL), then dried over anhydrous Na<sub>2</sub>SO<sub>4</sub>, filtered and the solvents were removed *in vacuo*. The crude product was purified by silica gel column chromatography (gradient: 0-20% MeOH in CH<sub>2</sub>Cl<sub>2</sub>), the dye-containing fractions were washed with HCl (1 M, 2  $\times$  20 mL) to obtain sensitizer C<sub>6</sub> as a dark solid (96 mg, 92  $\mu$ mol, 82%), mp 97-99 °C (dec. 142 °C). HRMS (ASAP+, *m/z*): found 997.5543 (calcd. C<sub>65</sub>H<sub>77</sub>N<sub>2</sub>O<sub>5</sub>S 997.5553, [M-CO<sub>2</sub>+H]<sup>+</sup>).

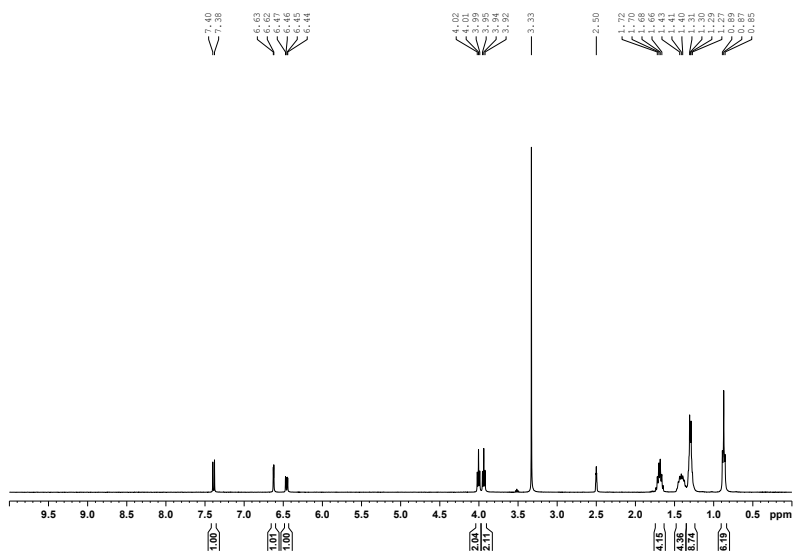
**NMR  
Compound 1**

Figure S4.  $^1\text{H}$  NMR spectrum for compound 1.

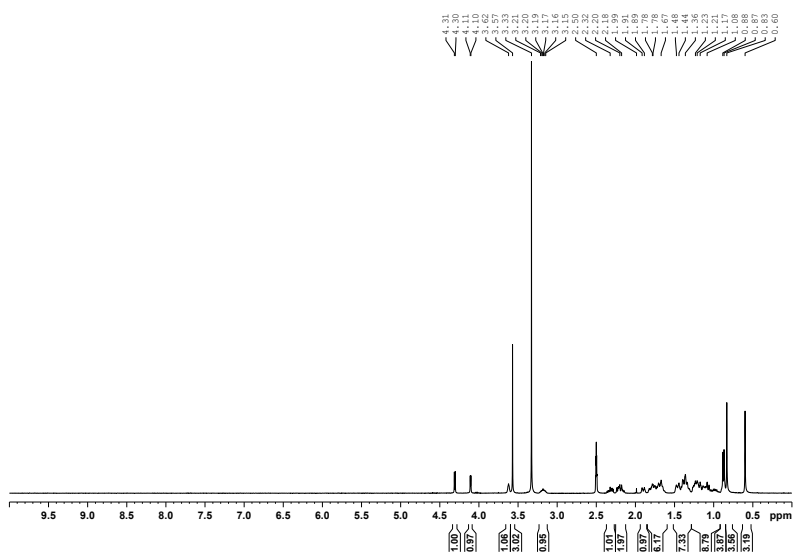
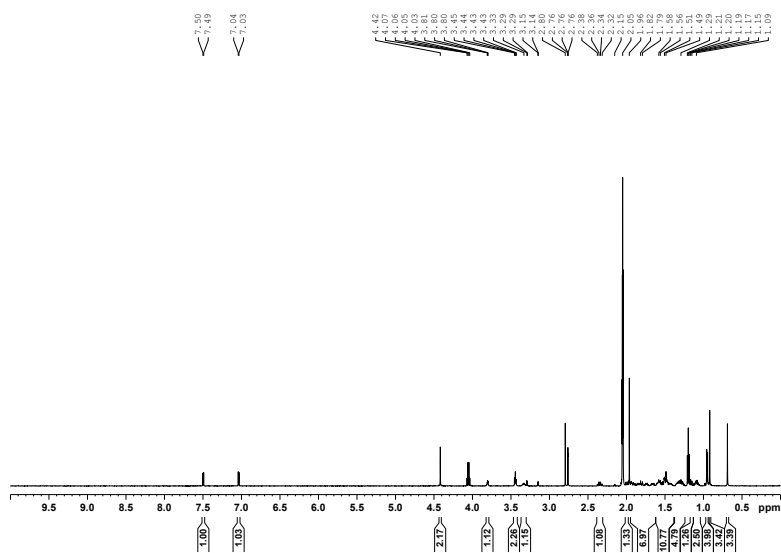
**Compound 6**

Figure S5.  $^1\text{H}$  NMR spectrum for compound 6.

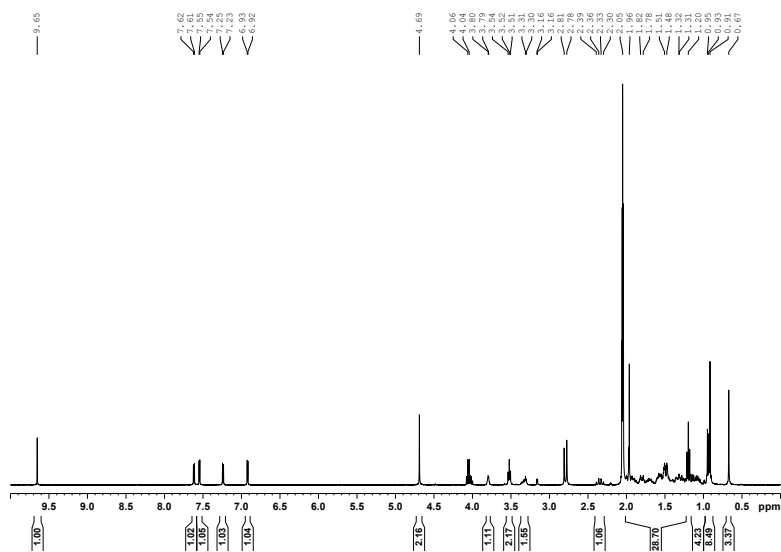




## Compound 9

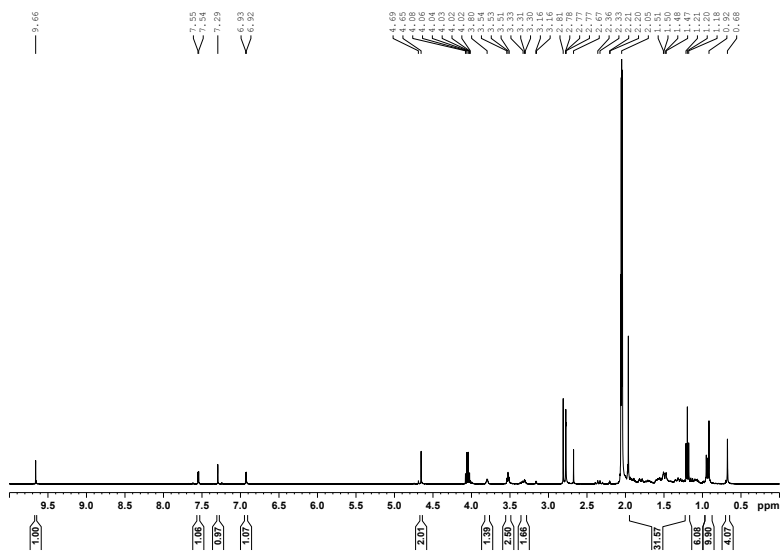
Figure S10.  $^1\text{H}$  NMR spectrum for compound 9.

## Compound 10

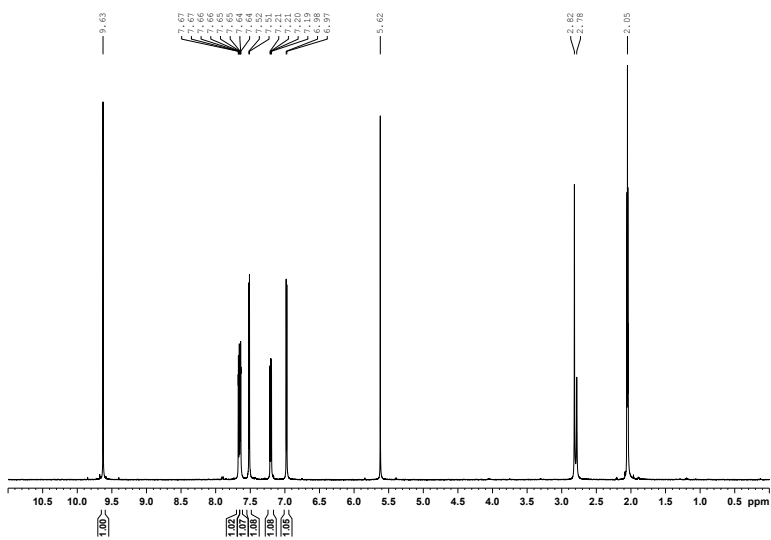
Figure S11.  $^1\text{H}$  NMR spectrum for compound 10.



## Compound 11

Figure S12.  $^1\text{H}$  NMR spectrum for compound 11.

## Compound 12

Figure S13.  $^1\text{H}$  NMR spectrum for compound 12.

## Compound 13

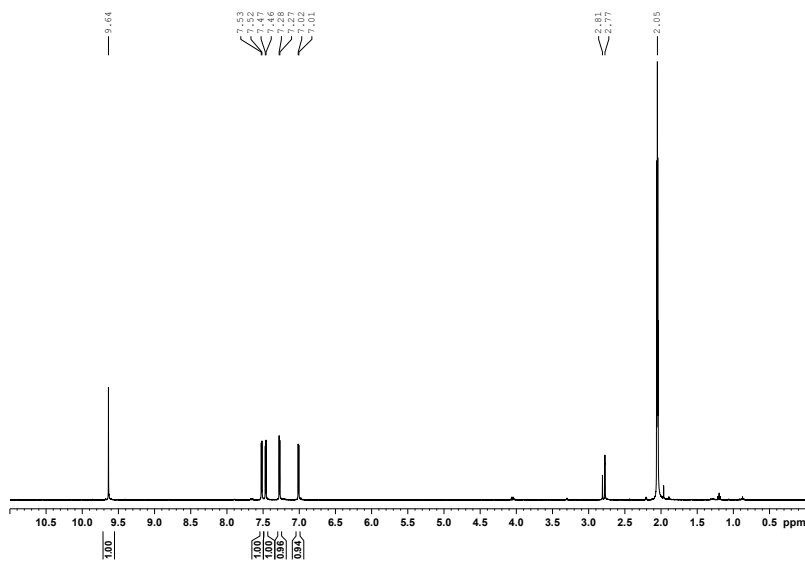


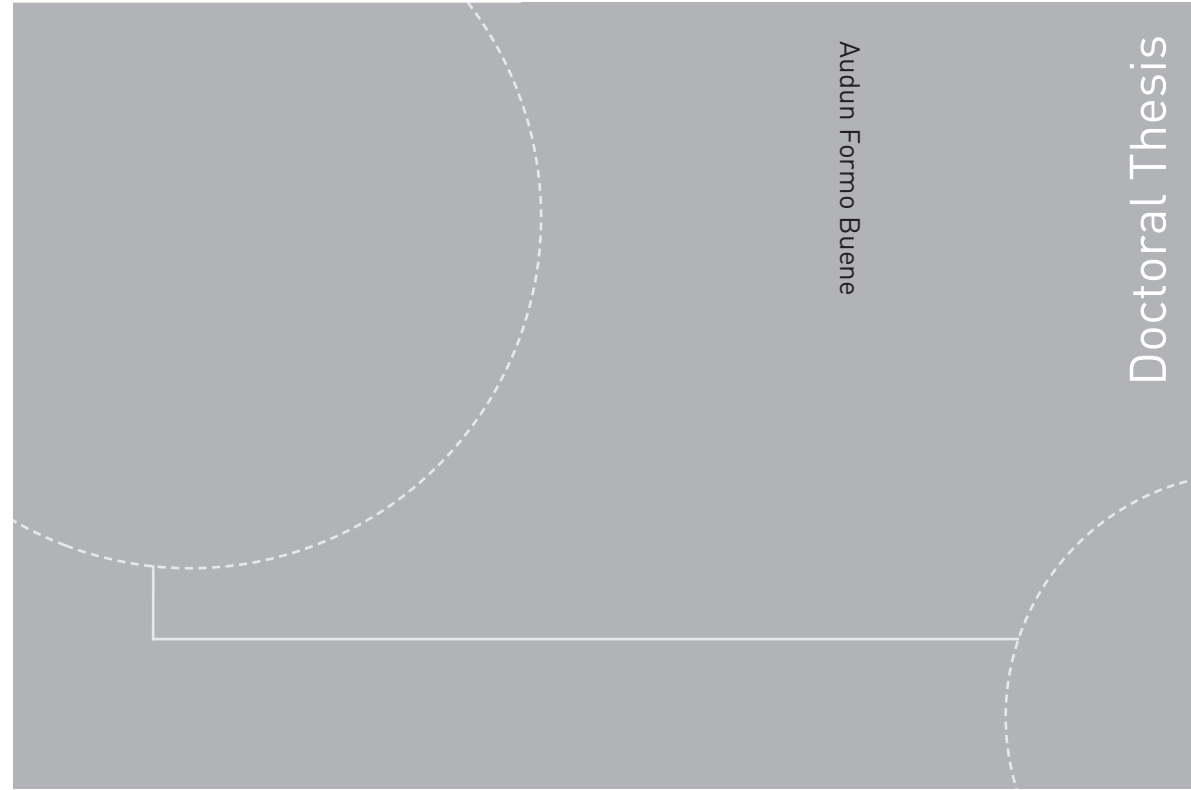
Figure S14.  $^1\text{H}$  NMR spectrum for compound 13.

## References

1. J.-H. Yum, T. W. Holcombe, Y. Kim, J. Yoon, K. Rakstys, M. K. Nazeeruddin and M. Grätzel, *Chem. Commun.*, 2012, **48**, 10727-10729.
2. Nazeeruddin, Md. K.; Grätzel, M.; Baranoff, E.; Kessler, F.; Yum, J.-H., Patent EP2492277A1. 2011.
3. L. Huang, Y. Sun, H. Zhu, Y. Zhang, J. Xu and Y.-M. Shen, *Steroids*, 2009, **74**, 701-706.
4. C. D'Amore, F. S. Di Leva, V. Sepe, B. Renga, C. Del Gaudio, M. V. D'Auria, A. Zampella, S. Fiorucci and V. Limongelli, *Journal of Medicinal Chemistry*, 2014, **57**, 937-954.
5. P. R. Parry, M. R. Bryce and B. Tarbit, *Org. Biomol. Chem.*, 2003, **1**, 1447-1449.
6. S.-H. Kim and R. D. Rieke, *The Journal of Organic Chemistry*, 2013, **78**, 1984-1993.



ISBN 978-82-326-4104-8 (printed version)  
ISBN 978-82-326-4105-5 (electronic version)  
ISSN 1503-8181



Doctoral theses at NTNU, 2019:254

**NTNU**  
Norwegian University of  
Science and Technology  
Faculty of Natural Sciences  
Department of Chemistry

 NTNU

Doctoral theses at NTNU, 2019:254

Audun Formo Buene

**Molecular Engineering and  
Photovoltaic Evaluation of  
Phenothiazine and Triarylamine Dyes  
for Dye-Sensitized Solar Cells**

 **NTNU**  
Norwegian University of  
Science and Technology

 **NTNU**  
Norwegian University of  
Science and Technology